Universitat
de les Illes Balears

DOCTORAL THESIS

2017

ON THE IMPORTANCE OF σ-/π-HOLE INTERACTIONS IN CHEMISTRY AND BIOCHEMISTRY

Antonio Bauzá Riera

Universitat
de les Illes Balears

DOCTORAL THESIS

2017

Doctoral Programme of Chemical Science and Technology

ON THE IMPORTANCE OF σ-/π-HOLE INTERACTIONS IN CHEMISTRY AND BIOCHEMISTRY

Antonio Bauzá Riera

Thesis Supervisor: Dr. Antonio Frontera
Thesis Supervisor: Dr. David Quiñonero

Doctor by the Universitat de les Illes Balears

Universitat de les Illes Balears

Dr Antonio Frontera Beccaría and Dr David Quiñonero Santiago, of University of Balearic Islands

WE DECLARE:

That the thesis entitled On the Importance of σ-/π-Hole Interactions in Chemistry and Biochemistry, presented by Antonio Bauzá Riera to obtain a doctoral degree, has been completed under our supervision.

For all intents and purposes, we hereby sign this document.

Signature

Dr. Antonio Frontera

Dr. David Quiñonero

Palma de Mallorca, 10/02/2017

This PhD thesis is composed by a compendium of scientific articles derived from the investigation carried out in our group. The complete list of references as well as the Impact Factor of the journals are shown below:

1. A. Bauzá, T. J. Mooibroek, A. Frontera, *Angew. Chem. Int. Ed*. **2013**, *52*, 12317–12321. (Impact Factor: 11.336)
2. A. Bauzá, T. J. Mooibroek, A. Frontera, *Chem. Commun.* **2014**, *50*, 12626–12629. (Impact Factor: 6.834)
3. A. Bauzá, A. Frontera, *Phys. Chem. Chem. Phys.* **2016**, *18*, 32155–32159 (Impact Factor: 4.449)
4. A. Bauzá, A. Frontera, *Crystals* **2016**, *6*, 26. (Impact Factor: 2.08)
5. A. Bauzá, T. J. Mooibroek, A. Frontera, *Chem. Commun.* **2015**, *51*, 1491–1493. (Impact Factor: 6.567)
6. A. Bauzá, T. J. Mooibroek, A. Frontera, *Nat. Commun.* **2017**, DOI: 10.1038/ncomms14522. (Impact Factor: 11.329)
7. A. Bauzá, D. Quiñonero, P. M. Deyà, A. Frontera, *Phys. Chem. Chem. Phys.* **2012**, *14*, 14061–14066. (Impact Factor: 3.829)
8. A. Bauzá, A. Frontera, *Angew. Chem. Int. Ed.* **2015**, *54*, 7340–7343. (Impact Factor: 11.709)
9. A. Bauzá, A. Frontera, *Phys. Chem. Chem. Phys.* **2015**, *17*, 24748–24753. (Impact Factor: 4.449)
10. A. Bauzá, A. Frontera, *ChemPhysChem* **2015**, *16*, 3625–3630. (Impact Factor: 3.138)

Other publications derived from this thesis:

1. A. Bauzá, T. J. Mooibroek, A. Frontera, *ChemPhysChem* **2015**, *16*, 2046–2517.
2. A. Bauzá, R. Ramis, A. Frontera, *Comp. Theor. Chem.* **2014**, *1038*, 67–70.
3. A. Bauzá, T. J. Mooibroek, A. Frontera, *Chem. Eur. J.* **2014**, *20*, 10245–10248.
4. E. C. Escudero-Adán, A. Bauzá, A. Frontera, P. Ballester, *ChemPhysChem* **2015**, *16*, 2530–2533.
5. A. Bauzá, T. J. Mooibroek, A. Frontera, *Phys. Chem. Chem. Phys.* **2014**, *16*, 19192–19197.
6. A. Bauzá, T. J. Mooibroek, A. Frontera, *Chem. Rec.* **2016**, *16*, 473–487.
7. A. Bauzá, A. Frontera, T. J. Mooibroek, *Phys. Chem. Chem. Phys.* **2016**, *18*, 1693–1698.
8. A. Bauzá, A. Frontera, T. J. Mooibroek, *Cryst. Growth Des.* **2016**, *16*, 5520–5524.
9. A. Bauzá, R. Ramis, A. Frontera, *J. Phys. Chem. A* **2014**, *118*, 2827–2834.
10. A. Bauzá, T. J. Mooibroek, A. Frontera, *ChemPhysChem* **2016**, *17*, 1608–1614.
11. A. Bauzá, A. Frontera, *Chem. Phys. Lett.* **2015**, *633*, 282–286.

Acknowledgements

First of all I would like to thank my PhD. supervisors, Dr. Antonio Frontera and Dr. David Quiñonero for their constant guidance throughout this thesis. This work could not have been possible without their persistence and passion for research, two key aspects of any scientist.

I would like to specially thank Dr. Pere Deyà for giving me the opportunity to join the research group and show me the world of Computational Chemistry. I would also like to thank other professors; Drs. Jeroni Morey, Antoni Costa, Carme Rotger, Neus Pinya, Biel Martorell and Rosa Gomila for the moments shared during my PhD journey.

Finally I would like to thank my family and friends for their constant support and the UIB for an Assistant Lecturer position contract.

List of abbreviations

ADME	Absorption, Distribution, Metabolism, and Excretion
A	Acceptor
Å	Ångström
BD*	Antibonding Orbital
AB	Antonio Bauzá
AF	Antonio Frontera
ARG	Arginine
ASP	Aspartate
AO	Atomic Orbital
a.u.	Atomic Units
AIM	Atoms in Molecules
BSSE	Basis Set Superposition Error
BLYP	Becke-Lee-Yang-Parr
BP86	Becke-Perdew
BCP	Bond Critical Point
BD	Bonding Orbital
S_N2	Bimolecular Nucleophilic Substitution
CCP	Cage Critical Point
CSD	Cambridge Structural Database
CTI	Centre de les Tecnologies de la Informació
Ch	Chalcogen
CI	Configuration Interactions
CBS	Complete Basis Set
ΔE	Interaction Energy without BSSE correction
ΔE_{BSSE}, ΔE_{CP}	Counterpoise Corrected Interaction Energy
CC	Coupled Cluster
CCSD(T)	Coupled Cluster with Singles, Doubles and Non Iteratively Triples Excitations
CP	Critical Point
CESCA	Centro de Supercomputación de Cataluña
CIF	Crystallographic Information File
DQ	David Quiñonero
°	Degrees
DFT	Density Functional Theory
$\nabla\rho$	Density Gradient
DGICYT	Dirección General de Investigación Científica y Técnica
E_{disp}	Dispersion Contribution
D3	Dispersion 3 Empirical Correction
D	Donor
D4R	Double 4-Ring
DLS	Dynamic Light Scattering
ECP	Effective Core Potential
ρ	Electron Density
El.R.	Electron-rich Atom
ESI-MS	Electron Spray Ionization-Mass Spectroscopy
E_{ee}	Electrostatic Contribution
ΔH	Enthalpy

E_{ex}	Exchange Contribution
D, R	Equilibirum Distance
FMN	Flavin Mononucleotide
FEDER	Fondo Europeo de Desarrollo Regional
MP4	Fourth Order Møller Plesset
GTO	Gaussian Type Orbitals
GGA	General Gradient Approximation
ΔG	Gibbs Free Energy
GLY	Glycine
IC_{50}	Half Maximal Inhibitory Concentration
E_{ind}	Induction Contribution
ICSD	Inorganic Crystal Structure Database
K	Kelvin
H	Hamiltonian Operator
HF	Hartree-Fock
Hlg	Halogen
HMTA	Hexamethylenetetramine
HIST	Histidine
HIV	Human Immunodeficiency Virus
MDM2	Human Murine Double Mutant 2
LYP	Lee-Yang-Parr
LDA	Local Density Approximation
pKa	Logarithmic Acid-Ionization Constant
LP	Lone Pair
GlcB	Malate Synthase
Q_{MK}	Merz-Kollman Charges
MINECO	Ministerio de Economía, Industria y Competitividad
MICINN	Ministerio de Ciencia e Innovación
MEP	Molecular Electrostatic Potential
MO	Molecular Orbital
$\alpha_{\|\|}$	Molecular Polarizability
NDI	Naphtalenediimide
NAO	Natural Atomic Orbital
NBO	Natural Bonding Orbital
NHO	Natural Hybrid Orbital
NKMO	Natural (semi-)Localized Molecular Orbital
NVO	Netherlands Organisation for Scientific Research
N_{imag}	Number of Imaginary Frequencies
TBAF	Tetrabutylammonium Fluoride
E_{total}	Total SAPT Energy
∠Tr–O–Tr	Tr-O-Tr angle
NMR	Nuclear Magnetic Resonance
TLCK	Nα-p-tosyl-lysyl chloromethylketone
TMEDA	N,N,N',N'-tetramethylethylenediamine
PBE	Perdew-Burke-Ernzerhof
PDKA	Phenil Diketoacid
PDE5	Phosphodiesterase Type 5
Pn	Pnicogen
PDB	Protein Data Bank

Q_{zz}	Quadrupole Moment
QM	Quantum Mechanics
QM-MM	Quantum Mechanics/Molecular Mechanics
RI-MP2	Resolution of the Identity MP2
RCP	Ring Critical Point
RY	Rydberg Atomic Orbital
MP2	Second Order Møller Plesset
$E^{(2)}$	Second-Order Interaction Energy
SER	Serine
STO-nG	Slater Type Orbital Basis
SAR	Structure-Activity Relationship
STAAR	Statistical Analysis of Aromatic Rings
SAPT	Symmetry Adapted Perturbation Theory
Symm, PG	Symmetry Point Group
SCF	Self Consistent Field
SI	Supporting Information
THF	Tetrahydrofuran
Tr	Tetrel
MP3	Third Order Møller Plesset
TJM	Tiddo Jonathan Mooibroek
®	Trademark
TR	Trypanothione Reductase
TYR	Tyrosine
Pnkp	T4 Polynucleotide kinase/Phosphatase
UIB	Universitat de les Illes Balears
UK	United Kingdom
UV-vis	Ultraviolet-Visible Spectroscopy
Ψ	Wavefunction
BTEMPO	(4-(benzoyloxy)-2,2,6,6-tetramethylpiperidinyl)-1-oxy

Abstract

This PhD. thesis is devoted to the study of "unconventional" noncovalent interactions, particularly σ-/π-hole interactions. The inner structure is composed by a *State of the art* (*Chapter 1*) which gives a general overview of this "non-classical" noncovalent chemistry, followed by three main chapters (*Chapters 2 to 4*), each one devoted to the analysis of a particular interaction. These chapters are: Tetrel bonding Interactions (*2*), Pnicogen bonding Interactions (*3*) and finally Aerogen bonding Interactions (*4*).

Chapter 1 collects a detailed introduction to focalize the main subject of this research, particularly on σ- and π-hole interactions, which are the main goal of this investigation. Their physical nature is explained as well as several experimental examples in order to put onto scene the vast potential of this family of interactions in fields such as supramolecular chemistry, molecular sensing and biological systems.

Chapters 2 to *4* are divided into a number of sections, involving several papers derived from our research. In these sections, the reader will find the same distribution for his/her comfort. First, an *Introduction* part where the background about the main issue is detailed, including previous results related with the topic. The second part gathers the *Computational methodology* used, followed by the *Results and discussion* section. Finally, the main *Conclusions* derived from our investigation are highlighted.

Chapter 2 is divided into four sections. First, the "rediscovery" of the tetrel bonding interaction, a term coined by our research group to describe the σ-hole interaction established between tetrel bearing compounds and electron-rich entities. Second, the role of sp^3 carbon atoms to act as tetrel bond donors in $ArCX_3$ (X = H and F) compounds is analyzed using a combination of the CSD (Cambridge Structural Database) as a useful source of experimental data and high level *ab initio* calculations. Finally, the last part of this chapter is devoted to study the impact of tetrel bonding interactions in two different fields; atmospheric chemistry and biological systems.

Chapter 3 is divided into four sections. First, the directionality of π-hole pnicogen bonding interactions involving the sp^2 nitrogen atom present in $-NO_2$ group is analyzed using the CSD (Cambridge Structural Database) and high level *ab initio* calculations. Second, the ability of the NO_3^- to behave as a Lewis acid when placed in the appropiate chemical context and establish π-hole antielectrostatic interactions with electron-rich guests is studied using both CSD and PDB (Protein Data Bank) databases. Finally, the study of the interaction between sp^3 pnicogen atoms and aromatic rings is analysed using the PDB (Protein Data Bank) database to support the results retrieved from *ab initio* calculations. These particular interactions are key in the mechanism of action of drugs used in the treatment of Leishmaniasis disease.

Chapter 4 is divided into three sections. First, aerogen bonding interactions involving Xe(VI) and Xe(IV) compounds are analysed and characterized as a novel

supramolecular force involving the σ-hole of the aerogen atom and electron-rich entities. In addition, π-hole bonding interactions involving Xe(IV) compounds are also described focusing on two derivatives; XeF_4 and $Xe(OTeF_5)_4$. Finally, the last section of the chapter is focused on the ability of Xe(VI) and Xe(IV) compounds to interact with aromatic moieties, thus establishing aerogen-π interactions.

Finally, *Chapter 5* assembles the main conclusions derived from this thesis.

At the end, all *Bibliographic sources* in reference to the subject are also included. Besides, a set of annexes that contains information about the *Computational methods* and the *Published articles* derived from this research can also be found.

Resumen

Esta tesis doctoral se enmarca dentro del estudio de las interacciones no covalentes denominadas "no convencionales", también conocidas como interacciones σ-/π-hole. Su estructura está compuesta por un primer capítulo dedicado al análisis del *Estado del arte* (*Capítulo 1*) el cual proporciona una visión general de la química supramolecular "no convencional", seguido de tres capítulos principales (*Capítulos 2 a 4*), cada uno dedicado al análisis de una interacción en concreto. Estos capítulos son: *Interacciones Tetrel bond* (*2*), *Interacciones Pnicogen bond* (*3*) y finalmente *Interacciones Aerogen bond* (*4*).

El *Capítulo 1* recoge una introducción detallada con el objetivo de presentar y focalizar el tema principal de esta investigación. Además de analizar los fundamentos físicos que sustentan la naturaleza de las interacciones σ-/π-hole, se exponen varios ejemplos experimentales con el fin de demostrar el vasto potencial de aplicación de dichas fuerzas no covalentes en campos tales como la química supramolecular, el reconocimiento molecular y la química biológica.

Los *Capítulos 2 a 4* incluyen varios trabajos derivados de nuestra investigación, los cuales poseen una distribución de secciones común para una lectura más cómoda por parte del lector. En primer lugar, una sección de *Introducción* donde se detallan los antecedentes relativos al tema de estudio, incluyendo resultados de investigaciones anteriores relacionadas con el tema. La segunda parte consta de la *Metodología computacional* utilizada, seguida de la sección de *Resultados y discusión*. Por último, se recogen las principales *Conclusiones* derivadas de nuestra investigación.

El *Capítulo 2* se divide en cuatro secciones. En primer lugar, el "redescubrimiento" de la interacción tetrel bond, término propuesto por nuestro grupo de investigación para describir la interacción σ-hole establecida entre compuestos que presentan átomos pertenecientes al grupo de los tetrels y bases de Lewis. En segundo lugar, el análisis de la direccionalidad de interacciones tetrel bond donde participan átomos de carbono con hibridación sp^3 en compuestos de tipo $ArCX_3$ (X= H y F), utilizando para ello un estudio teórico, a base de cálculos *ab initio* de alto nivel, y cristalográfico gracias al CSD (Cambridge Structural Database). Finalmente, la última parte de este capítulo se dedica a estudiar el impacto de las interacciones tetrel bond en dos campos diferentes; la Química Atmosférica y la Química Biológica.

El *Capítulo 3* se divide en cuatro secciones. En primer lugar, el análisis de la direccionalidad de las interacciones π-hole pnicogen bond que implican al átomo de nitrógeno sp^2 presente en el grupo $-NO_2$, utilizando la base de datos CSD (Cambridge Structural Database) y cálculos *ab initio* de alto nivel. En segundo lugar, la evaluación de la capacidad del anión NO_3^- de comportarse como un ácido de Lewis al encontrarse en un contexto químico apropiado. De esta manera, es posible establecer interacciones antielectrostáticas utilizando el π-hole generado sobre el átomo de nitrógeno. Dicha hipótesis es confirmada mediante el análisis de las bases de datos CSD y PDB (Protein Data Bank). Finalmente, el último trabajo se centra en el estudio de la interacción entre el σ-hole presente en átomos pertenecientes al grupo de los pnicogens con hibridación sp^3 y anillos aromáticos, utilizando la base

de datos PDB (Protein Data Bank) como soporte experimental de los resultados obtenidos mediante cálculos *ab initio*. Dichas interacciones son claves en el mecanismo de acción de fármacos relacionados con el tratamiento de la enfermedad Leishmaniasis.

El *Capítulo 4* se divide en tres secciones. En primer lugar, se analiza y caracteriza la interacción aerogen bonding que implica a compuestos de Xe(VI) y Xe(IV) como nueva fuerza supramolecular en la que participan el σ-hole presente en el átomo de aerogen y bases de Lewis. Además, se describen también interacciones π-hole presentes en compuestos de Xe(IV), concretamente XeF_4 y $Xe(OTeF_5)_4$. Por último, la tercera sección del capítulo se centra en la capacidad de los compuestos Xe(VI) y Xe(IV) para interactuar con anillos aromáticos, estableciendo así interacciones aerogen-π.

Finalmente, el *Capítulo 5* reúne las conclusiones principales derivadas de esta tesis.

En la sección de *Bibliografía* se incluyen todas las referencias bibliográficas relacionadas con el tema. Además, también se puede encontrar un conjunto de anexos que contienen información sobre los *Métodos computacionales* y los *Artículos publicados* derivados de esta investigación.

Resum

Aquesta tesi doctoral s'emmarca dins de l'estudi de les interaccions no covalents anomenades "no convencionals", també conegudes com interaccions σ-/π-hole. L'estructura general es troba formada per un primer capítol dedicat a l'anàlisi de *l'Estat de l'art* (*Capítol 1*) el qual proporciona una visió general de la química supramolecular "no convencional", seguit de tres capítols principals (*Capítols 2* a *4*), cada un d'ells dedicat a l'anàlisi d'una interacció en particular. Aquests capítols són: *Interaccions Tetrel bond* (*2*), *Interaccions Pnicogen bond* (*3*) i finalment *Interaccions Aerogen bond* (*4*).

El *Capítol 1* recull una introducció detallada amb l'objectiu de presentar i focalitzar el tema principal d'aquesta investigació. A més dels fonaments físics que componen la naturalesa de les interaccions σ-/π-hole, es recullen diversos exemples experimentals amb la finalitat de demostrar el vast potencial d'aplicació d'aquestes interaccions en camps de recerca com la química supramolecular, el reconeixement molecular i la química biològica.

Els *Capítols 2* a *4* inclouen diversos treballs derivats de la nostra investigació, els quals posseeixen una distribució de seccions comú per a una lectura més còmoda per part del lector. En primer lloc, una secció d'*Introducció* on es detallen els antecedents relatius al tema d'estudi, incloent resultats d'anteriors investigacions relacionades amb el tema. La segona part recull la *Metodologia computacional* utilitzada, seguida de la secció de *Resultats i discussió*. Finalment, es destaquen les principals *Conclusions* derivades de la nostra investigació.

El *Capítol 2* es divideix en quatre seccions. En primer lloc, el "redescobriment" de la interacció tetrel bonding, terme proposat pel nostre grup de recerca per descriure la interacció σ-hole establerta entre compostos que presenten àtoms pertanyents al grup dels tetrels i bases de Lewis. En segon lloc, l'anàlisi de la direccionalitat de les interaccions tetrel bond on participen àtoms de carboni amb hibridació sp^3 en composts del tipus $ArCX_3$ (X= H i F), utilitzant una *Metodología d'investigació* combinada formada per un estudi teòric mitjançant càlculs *ab initio* d'alt nivell i un estudi cristal·logràfic gràcies al CSD (Cambridge Structural Database). Finalment, la darrera part d'aquest capítol es dedica a estudiar l'impacte de les interaccions tetrel bond en dos camps diferents; la Química Atmosfèrica i la Química Biològica.

El *Capítol 3* es divideix en quatre seccions. En primer lloc, s'analitza la direccionalitat de les interaccions π-hole pnicogen bond on hi participa l'àtom de nitrogen sp^2 present en el grup $-NO_2$, utilitzant la base de dades CSD (Cambridge Structural Database) i càlculs *ab initio* d'alt nivell. En segon lloc, es va dur a terme una anàlisi de la capacitat del NO_3^- de comportar-se com un àcid de Lewis al estar localitzat en un contexte químic apropiat. D'aquesta manera, és possible establir interaccions antielectrostàtiques utilitzant el π-hole present a l'àtom de nitrogen. Aquesta hipòtesi va ser confirmada mitjançant l'anàlisi de les bases de dades CSD i PDB (Protein Data Bank). Finalment, l'últim treball es centra en l'estudi de la interacció entre el σ-hole present en àtoms que pertanyen al grup dels pnicogens amb hibridació sp^3 i anells aromàtics, utilitzant la base de dades PDB (Protein Data Bank) com a suport experimental dels resultats obtinguts mitjançant càlculs *ab initio*. Es va

poder demostrar que aquestes interaccions són claus en el mecanisme d'acció de fàrmacs relacionats amb el tractament de la malaltia Leishmaniasis.

El *Capítol 4* es divideix en tres seccions. En primer lloc, s'analitza i caracteritza la interacció aerogen bonding on hi participen compostos de Xe(VI) i Xe(IV) com una nova força supramolecular en la qual participen el σ-hole present a l'àtom d'aerogen i bases de Lewis. A més, es descriuen també interaccions π-hole presents en compostos de Xe(IV), concretament XeF_4 i $Xe(OTeF_5)_4$. Finalment, la tercera secció del capítol es centra en la capacitat dels compostos Xe(VI) i Xe(IV) per interactuar amb anells aromàtics, establint d'aquesta manera interaccions aerogen-π.

Finalment, al *Capítol 5* reuneix les conclusions principals derivades d'aquesta tesi.

A la secció de *Bibliografía* s'inclouen totes les referències bibliogràfiques relacionades amb el tema. A més, també es pot trobar un conjunt d'annexos que contenen informació sobre els *Mètodes computacionals* així com els *Articles publicats* derivats d'aquesta investigació.

Table of contents

Chapter 1

State of the art

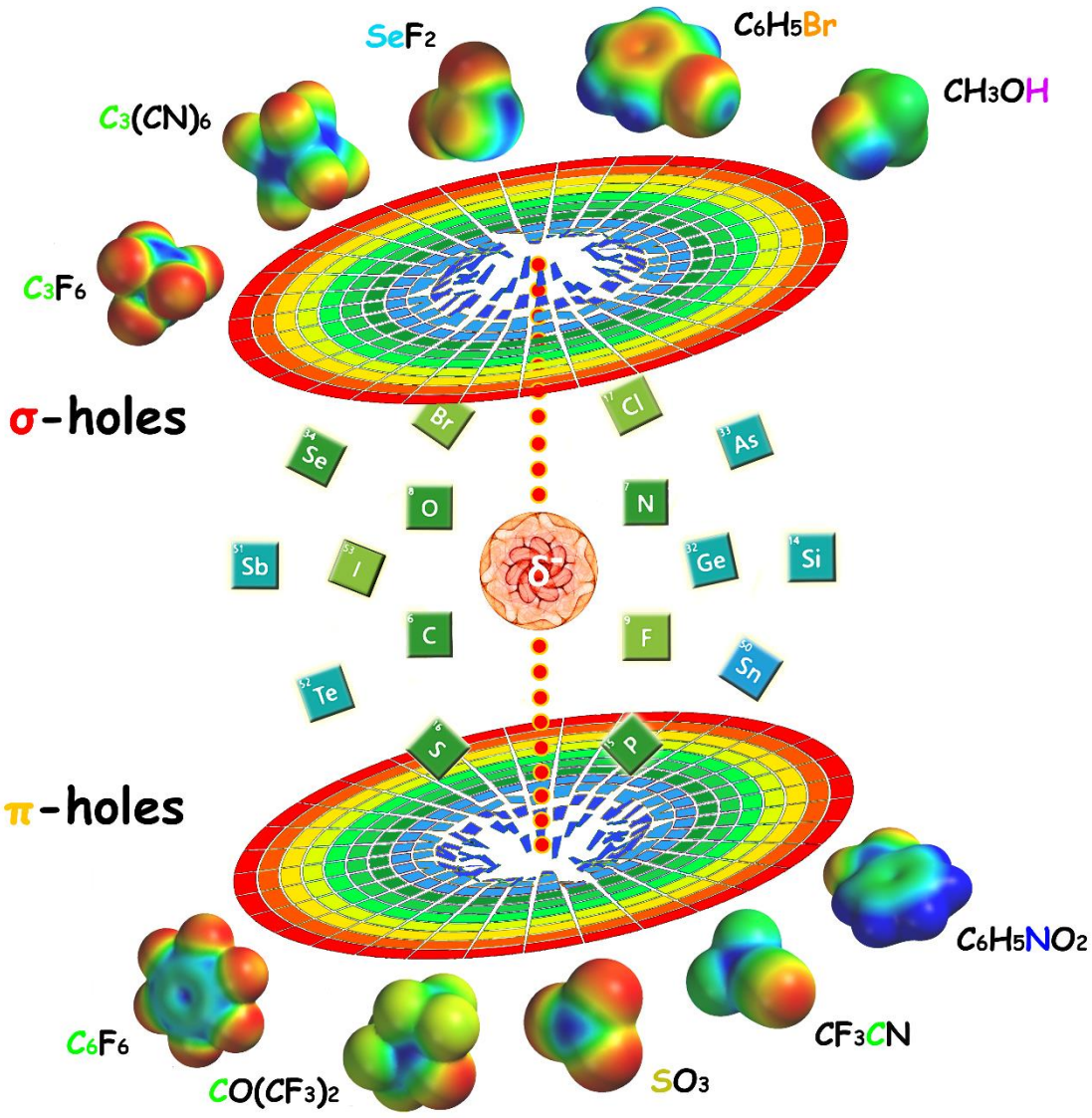

1.1 σ-/π-Hole chemistry

Supramolecular chemistry can be regarded as one of the most multidisciplinary fields of research. The rapid development of this discipline has been related to the increasing efficiency and success in the synthesis of structures of different sizes, shapes and functionalities. Supramolecular chemists rely on the comprehension of the noncovalent forces that are the basis of highly specific recognition, transport and regulation mechanisms. The orquestration of many biological and chemical processes is often controlled by an intricate combination of noncovalent interactions.[1] This is exemplified by the foundation of the life process itself, which is considered as the ultimate expression of function. Particularly in host-guest chemistry, interactions between targeted guests and rationally designed receptors govern the formation of assemblies of different shapes, sizes and affinities.[2] Therefore, a proper description of interactions between molecules is necessary for the understanding and progress of the supramolecular chemistry that relies on strong, directional interactions such as hydrogen bonding and halogen bonding, and less directional forces like ion pairing.

In this context, the halogen bonding interaction has been extensively analyzed in a series of studies using the Cambridge Structural Database.[3] In recent years the interest in halogen bonding has grown exponentially due to the recognition of its importance in biological systems and the design of new materials.[4] More recently, general σ-hole interactions including covalently-bonded atoms of Groups IV–VI have been also considered as an important addition to the cluster of well-known directional noncovalent interactions.[4c,5] As a natural consequence of the success of halogen bonding, the usefulness of the σ-hole bonding interactions involving these atoms in crystal engineering and supramolecular chemistry has been recently investigated, starting from a series of computational studies.[6] It was shown that covalently-bonded atoms of Groups IV–VI can posses regions (from two to four) of positive electrostatic potential on the extensions of their covalent bonds attributed to the anisotropies on the distribution of the electronic density.[7] The size and

---

[1] H. J. Schneider, *Angew. Chem. Int. Ed.* **2009**, *48*, 3924–3977.

[2] a) J. M. Lehn, *Supramolecular Chemistry Concepts and Perspectives*, Wiley-VCH, Weinheim, **1995**; b) A. S. Mahadevi, G. N. Sastry, *Chem. Rev.* **2016**, *116*, 2775–2825.

[3] P. Murrayrust, W. D. S. Motherwell, *J. Am. Chem. Soc.* **1979**, *101*, 4374–4376.

[4] a) P. Metrangolo, H. Neukirch, T. Pilati, G. Resnati, *Acc. Chem. Res.* **2005**, *38*, 386–395; b) P. Politzer, J. S. Murray, *ChemPhysChem* **2013**, *14*, 278–294; c) P. Politzer, J. S. Murray, T. Clark, *Phys. Chem. Chem. Phys.* **2013**, *15*, 11178–11189; d) L. P. Wolters, P. Schyman, M. J. Pavan, W. L. Jorgensen, F. M. Bickelhaupt, S. Kozuch, *WIREs Comp. Mol. Sci.* **2014**, *4*, 523–540; e) K. El Hage, V. Pandyarajan, N. B. Phillips, B. J. Smith, J. G. Menting, J. Whittaker, M. C. Lawrence, M. Meuwly, M. A. Weiss, *J. Biol. Chem*. **2016**, *291*, 27023–27041; f) P. Politzer, J. S. Murray, T. Clark, *Top. Curr. Chem.*, **2015**, *358*, 19–42.

[5] a) P. Politzer, J. S. Murray, T. Clark, *Phys. Chem. Chem. Phys.* **2010**, *12*, 7748–7757; b) K. E. Riley, J. S. Murray, J. Franfrlík, J. Rezáč, R. J. Solá, M. C. Concha, F. M. Ramos, P. Politzer, *J. Mol. Model.* **2011**, *17*, 3309–3318; c) B. V. Pandiyan, P. Deepa, P. Kolandaivel, *Mol. Phys.* **2016**, *114*, 3629–3642.

[6] a) J. S. Murray, P. Lane, T. Clark, P. Politzer, *J. Mol. Model.* **2007**, *13*, 1033–1038; b) J. S. Murray, P. Lane, P. Politzer, *Int. J. Quantum Chem.* **2007**, *107*, 2286–2292; c) J. S. Murray, P. Lane, P. Politzer, *J. Mol. Model.* **2009**, *15*, 723–729.

[7] a) S. C. Nyburg, C. H. Faerman, *Acta Crystallogr. B* **1985**, *41*, 274–279; b) P. Politzer, K. E. Riley, F. A. Bulat, J. S. Murray, *Comp. Theor. Chem.* **2012**, *998*, 2–8; c) T. N. G. Row, R. Parthasarathy, *J. Am. Chem. Soc.* **1981**, *103*, 477–479; d) N. Ramasubbu, R. Parthasarathy, *Phosphorus Sulfur* **1987**, *31*, 221–229.

magnitude of these σ-hole potentials are governed by the same factors as for the halogens, as detailed in this chapter.
An important and relatively unexplored group of noncovalent interactions can be classified as π-hole bonding. A π-hole is a region of positive electrostatic potential involving π-orbitals that are perpendicular to a portion of a molecular framework. In case that this portion is an aromatic π-system substituted with electron withdrawing groups (characterized by a positive electrostatic surface potential region perpendicular to the aromatic molecular plane), the interaction is known as either lone pair-π[8] or anion-π[9] depending on the nature of the electron donor. As a matter of fact, the anion-π interaction,[10] has been investigated by a plethora of theoretical studies [11] in addition to an increasing amount of experimental investigations.[12] Anion-π interactions have become noticeable players in fields as diverse as medicine, environmental chemistry and biochemical processes.[9a, 13] Furthermore, their application to the design of selective anion receptors and transport channels confirms their significance in the field of supramolecular chemistry.[14]

Other pioneering π-hole interactions that involve different types of molecular frameworks should be mentioned. For instance, the identification of π-hole interactions in crystal structures was carried out around 1973 by Bürgi and Dunitz in a series of studies where they analyse the trajectory along which a nucleophile attacks the π-hole present in a C=O group.[15] Closely related, the ability of guanosine to act as a π-hole was pointed out by Egli and co-workers in 1995, when they studied the crystal structure of Z-DNA.[16] Recently, the study of π-hole interactions has been extended to acyl carbons, [17] sulphur containing moieties, [18] RNO_2

[8] a) M. Egli, S. Sarkhel, *Acc. Chem. Res.* **2007**, *40*, 197–205; b) T. J. Mooibroek, P. Gamez, J. Reedijk, *CrystEngComm* **2008**, *10*, 1501–1515.
[9] a) A. Frontera, P. Gamez, M. Mascal, T. J. Mooibroek, J. Reedijk, *Angew. Chem. Int. Ed.* **2011**, *50*, 9564–9583; b) B. L. Schottel, H. T. Chifotides, K. R. Dunbar, *Chem. Soc. Rev.* **2008**, *37*, 68–83; c) C. Caltagirone, P. A. Gale, *Chem. Soc. Rev.* **2009**, *38*, 520–563.
[10] a) P. Gamez, T. J. Mooibroek, S. J. Teat, J. Reedijk, *Acc. Chem. Res.* **2007**, *40*, 435–444; b) B. P. Hay, V. S. Bryantsev, *Chem. Commun.* **2008**, *44*, 2417–2428.
[11] a) D. Quiñonero, C. Garau, C. Rotger, A. Frontera, P. Ballester, A. Costa, P. M. Deyà, *Angew. Chem. Int. Ed.* **2002**, *41*, 3389–3392; b) M. Mascal, A. Armstrong, M. D. Bartberger, *J. Am. Chem. Soc.* **2002**, *124*, 6274–6276; c) I. Alkorta, I. Rozas, J. Elguero, *J. Am. Chem. Soc.* **2002**, *124*, 8593–8598; d) D. Y. Kim, N. J. Singh, K. S. Kim, *J. Chem. Theory Comput.* **2008**, *4*, 1401–1407.
[12] a) B. L. Schottel, J. Bacsa, K. R. Dunbar, *Chem. Commun.* **2005**, *41*, 46–47; b) B. Han, J. Lu, J. K. Kochi, *Cryst. Growth Des.* **2008**, *8*, 1327–1334; c) M. Mascal, I. Yakovlev, E. B. Nikitin, J. C. Fettinger, *Angew. Chem. Int. Ed.* **2007**, *46*, 8782–8784; d) R. J. Götz, A. Robertazzi, I. Mutikainen, U. Turpeinen, P. Gamez, J. Reedijk, *Chem. Commun.* **2008**, *44*, 3384–3386; e) M. Albrecht, M. Müller, O. Mergel, K. Rissanen, A. Valkonen, *Chem. Eur. J.* **2010**, *16*, 5062–5069.
[13] a) C. Estarellas, A. Frontera, D. Quiñonero, P. M. Deyà, *Angew. Chem. Int. Ed.* **2011**, *50*, 415–418; b) S. Chakravarty, Z.-Z. Sheng, B. Iverson, B. Moore, *FEBS Lett.* **2012**, *586*, 4180–4185; c) D. D. Jenkins, J. B. Harris, E. E. Howell, R. J. Hinde, J. Baudry, *J. Comput. Chem.* **2013**, *34*, 518–522.
[14] a) R. E. Dawson, A. Hennig, D. P. Weimann, D. Emery, V. Ravikumar, J. Montenegro, T. Takeuchi, S. Gabutti, M. Mayor, J. Mareda, C. A. Schalley, S. Matile, *Nat. Chem.* **2010**, *2*, 533–538; b) N. Sakai, J. Mareda, E. Vauthey, S. Matile, *Chem. Commun.* **2010**, *46*, 4225–4237.
[15] a) H. B. Burgi, *Inorg. Chem.* **1973**, *12*, 2321–2325; b) H. B. Burgi, J. D. Dunitz, E. Shefter, *J. Am. Chem. Soc.* **1973**, *95*, 5065–5067; c) H. B. Burgi, J. D. Dunitz, J. M. Lehn, G. Wipff, *Tetrahedron* **1974**, *30*, 1563–1572.
[16] M. Egli, R. V. Gessner, *P. Natl. Acad. Sci. USA* **1995**, *92*, 180–184.
[17] P. Sjoberg, P. Politzer, *J. Phys. Chem.* **1990**, *94*, 3959–3961.

molecules,[19] XCN, XZO_2 (X = halogen, Z = pnicogen)[20]. Finally, it is also worth to mention the studies carried out by Grabowski and coworkers on the physical nature of π-hole interactions involving triel atoms.[21] The interplay between this novel interaction and pnicogen and tetrel bonding interactions has been analysed by the groups of Liu[22] and Yourdkhani.[23]

1.2 Physical nature of σ- and π-hole interactions

1.2.1. σ-Hole interactions

A σ-hole can be viewed as the region of positive electrostatic potential found on an (partially) empty anti-bonding σ* orbital, typically located along the vector of a covalent bond. This concept of a σ-hole was originally used to explain the unexpected interaction of an electronegative halogen atom (Hlg) with a negative site, wherein the electropositive potential is found on the halogen atom at the end of the X-Hlg vector (X can be any atom, although it is typically carbon).[5a, 24] It recently became clear that such electronic anisotropy is not unique to atoms of the halogen family due to the discovery of σ-holes on covalently-bonded atoms of the pnicogen (Pn) and chalcogen (Ch) families.[6, 25]

In analogy to hydrogen bonding, the atom on which the electropositive potential is located is commonly referred to as the donor atom.[26] Hence, σ-hole interactions can be written as X–D···A (where X can be any atom, D = donor atom and A = acceptor moiety; i.e. similar as hydrogen bonding).[26a] The magnitude of a σ-hole depends on two main factors: it becomes more positive when D is more polarizable (heavier atoms) and when X is more electron withdrawing.[5b, 27] Although σ-hole bonding is greatly influenced by electrostatic effects, other forces such as polarization and

---

[18] a) L. M. Azofra, I. Alkorta, S. Scheiner, *Theor. Chem. Acc.* **2014**, *133*, 1586, 8p; b) M. D. Esrafili, R. Nurazar, *Mol. Phys.* **2016**, *114*, 276–282; c) X. Guo, Y. -W. Liu, Q. -Z. Li, W. -Z. Li, J. -B. Cheng, *Chem. Phys. Lett.* **2015**, *620*, 7–12; d) D. Quiñonero, *Molecules* **2015**, *20*, 11632–11659.

[19] a) A. Bauzá, R. Ramis, A. Frontera, *J. Phys. Chem. A.* **2014**, *118*, 2827–2834; b) D. Quiñonero, A. Bauzá, G. Sánchez-Sanz, C. Trujillo, I. Alkorta, J. Elguero, *New. J. Chem.* **2016**, *40*, 9060–9072.

[20] a) G. Sánchez-Sanz, C. Trujillo, M. Solimannejad, I. Alkorta, J. Elguero, *Phys. Chem. Chem. Phys.* **2013**, *15*, 14310–14318; b) J. E. Del Bene, I. Alkorta, J. Elguero, *J. Phys. Chem. A.* **2013**, *117*, 6893–6903.

[21] a) S. L. Grabowski, *Molecules* **2015**, *20*, 11297–11316; b) S. L. Grabowski, *ChemPhysChem* **2015**, *16*, 1470–1479; c) S. L. Grabowski, *ChemPhysChem*, **2014**, *15*, 2985–2993.

[22] M.-X. Liu, H.-Y. Zhuo, Q.-Z. Li, C. Wen-Zuo, J.-B. Cheng, *J. Mol. Model.* **2016**, *22*, 1–7.

[23] S. Yourdkhani, T. Korona, N. L. Hadipour, J. *Comp. Chem.* **2015**, *36*, 2412–2428.

[24] a) T. Clark, M. Hennemann, J. S. Murray, P. Politzer, *J. Mol. Model.* **2007**, *13*, 291–296; b) T. Brinck, J. S. Murray, P. Politzer, *Int. J. Quantum Chem.* **1992**, *44*, 55–64; c) P. Auffinger, F. A. Hays, E. Westhof, P. S. Ho, *P. Natl. Acad. Sci. USA* **2004**, *101*, 16789–16794; d) P. Politzer, P. Lane, M. C. Concha, Y. Ma, J. S. Murray, *J. Mol. Model.* **2007**, *13*, 305–311.

[25] a) P. Politzer, J. S. Murray, *Practical Aspects of Computational Chemistry*, Springer, Heidelberg, **2009**; b) J. S. Murray, K. E. Riley, P. Politzer, T. Clark, *Aust. J. Chem.* **2010**, *63*, 1598–1607.

[26] a) E. Arunan, G. R. Desiraju, R. A. Klein, J. Sadlej, S. Scheiner, I. Alkorta, D. C. Clary, R. H. Crabtree, J. J. Dannenberg, P. Hobza, H. G. Kjaergaard, A. C. Legon, B. Mennucci, D. J. Nesbitt, *Pure Appl. Chem.* **2011**, *83*, 1637–1641; b) G. R. Desiraju, P. S. Ho, L. Kloo, A. C. Legon, R. Marquardt, P. Metrangolo, P. Politzer, G. Resnati, K. Rissanen, *Pure Appl. Chem.* **2013**, *85*, 1711–1713.

[27] J. S. Murray, P. Lane, T. Clark, K. E. Riley, P. Politzer, *J. Mol. Model.* **2012**, *18*, 541–548.

dispersion contributions also play an important role in the structure and energetic stability of σ-hole bonded complexes.[7b, 28]

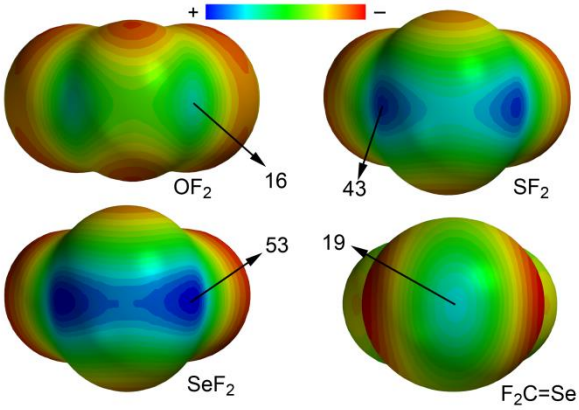

Figure 1. Molecular electrostatic potential of representative chalogen bonding donor molecules at the B3LYP/6-31+G* level of theory. Energies at the σ-holes are given in kcal/mol.

Any enhancement of the polarizability increases the magnitude of the σ-hole and strengthens the resulting σ-hole complex. The atomic polarizabilities of atoms belonging to groups IV–VII are gathered in Table 1. It can be observed that the values are very modest for atoms of the second row and they increase significatly on going from row 2 to 5. To illustrate this trend, the molecular electrostatic potential surface plots of several YF_2 molecules (Y = O, S and Se) and F_2C=Se are shown in Figure 1. Two σ-holes are present for the YF_2 molecules on the extensions of each covalent Y-F bond. The MEP value at the σ-hole of the SeF_2 molecule is the largest due to the larger polarizability of Se (five times more than O, see Table 1). Interestingly, in F_2C=Se a single σ-hole is observed along the C=Se bond (in addition to a π-hole above and below the C atom). Chalcogen bonding interactions involving a single σ-hole have been studied in C=S/Se and P=S/Se derivatives.[29]

Table 1. Atomic polarizabilities (a.u.)[a] and [van der Waals radii] (Å)[30] for some elements of groups IV, V, VI and VII.

	Group IV (tetrel)	Group V (pnicogen)	Group VI (chalcogen)	Group VII (halogen)
Row 2	**C**	**N**	**O**	**F**
	11.5 [1.70]	7.1 [1.55]	4.9 [1.52]	3.4 [1.47]
Row 3	**Si**	**P**	**S**	**Cl**
	38.1 [2.10]	25.0 [1.80]	19.3 [1.80]	14.3 [1.75]
Row 4	**Ge**	**As**	**Se**	**Br**
	40.3 [2.00]	29.7 [1.85]	25.4 [1.90]	20.5 [1.85]
Row 5	**Sn**	**Sb**	**Te**	**I**
	55.6 [2.17]	43.3 [2.00]	38.3 [2.06]	32.3 [1.98]

[a]Computed at the MP2/aug-cc-pVTZ (row 2–4) and MP2/aug-cc-pVTZ-

[28] A. J. Stone, *J. Am. Chem. Soc.* **2013**, *135*, 7005–7009.

[29] A. Bauzá, I. Alkorta, A. Frontera, J. Elguero, *J. Chem. Theory Comput.* **2013**, *9*, 5201–5210.
[30] A. Bondi, *J. Phys. Chem.* **1964**, *68*, 441–451.

PP (row 5) level of theory.

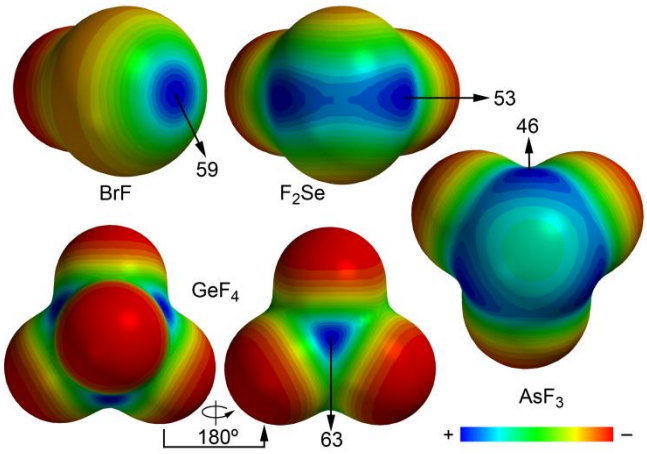

Figure 2. Molecular electrostatic potential surfaces of representative halogen (BrF), chalcogen (SeF_2), pnicogen (AsF_3) and tetrel (GeF_4) bond donors at the B3LYP/6-31+G* level of theory. Energies at the σ-holes are given in kcal/mol.

The ability of a σ-hole to act as electron-deficient host for an electron-rich guest molecule depends not only on the magnitude of the electropositive potential, but also on its steric environment. Indeed, while the value of MEP at the σ-hole is similar in representative compounds of the same row (see Figure 2, BrF, SeF_2, AsF_3 and GeF_4), the σ-holes are sterically more accessible with lower valence, i.e.: BrF>SeF_2>AsF_3>GeF_4. This steric hinderance is particularly relevant in the case of carbon, which is the smallest tetrel atom (see Table 1). Thus, in a sp^3 hybridized electron-deficient C atom, such as C_2F_6 (see Figure 3, left) there is only a very limited space available for the electron-rich guest molecule to nest itself. In addition, the negative electrostatic potential at van der Waals surface of the interacting guest would be very close to possible negative electrostatic potential belts of (in this example) F. In small rings such as hexafluorocyclopropane (C_3F_6, see Figure 3, right), the σ-hole on C is more exposed due to the small FCCF dihedral angle.

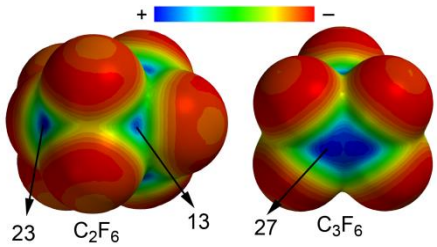

Figure 3. Molecular electrostatic potential surface of hexafluoroethane (left) and hexafluorocyclopropane (right) at the B3LYP/6-31+G* level of theory. Energies at the σ-holes are given in kcal/mol.

It is worth pointing out that in some cases the σ-bond donor can also bear lone pair electrons, meaning that it can act concurrently as the σ-bond donor and acceptor. Such 'like-like' interactions have been pointed out for atoms of groups V–VII (in

particular sulphur and phosphorus),[4c,7c] but could in principle also occur with tetrel atoms (i.e. a carbene).

1.2.2 π-Hole interactions

A π-hole can be understood as the region of positive electrostatic potential found on an (partially) empty (anti-bonding) π(*) orbital, typically located perpendicular to a molecular framework. Depending on the nature of the electron-rich partner and the characteristics of the molecular fragment, π-hole interactions are known by other names or sub-classes.

Politzer *et al.*[5a] used π-hole nomenclature to describe the depletion of charge density of unoccupied π-type orbitals on the central atom in SO_2 and similar molecules. In the particular case of group III elements the interaction has been termed triel bonding by Grabowski.[21b] In this type of π-hole interaction the electron depletion is located on a single atom (similar to σ-holes) and usually appears in the literature using the name of the group, for instance pnicogen/chalcogen π-hole interaction. Several studies have appeared that report on π-hole interactions involving SO_3, XNO_2, $XONO_2$, etc.[18,19,20] Shown in Figure 4 are the MEP surfaces of four representative planar molecules where the π-hole is located over the central atom belonging to the second (F_2**C**O and F**N**O_2) or third (F_2**Si**O and F**P**O_2) row of the periodic table. Similarly to the behavior described above for the σ-hole bonding, the MEP at the π-hole is significantly more positive as the bond donor atom is increasingly polarizable (heavier atoms). This is especially important going from elements of row 2 to elements of row 3–5. In addition, the π-hole is more accessible (more extended) in heavier (typically also larger) atoms (see Figure 5).

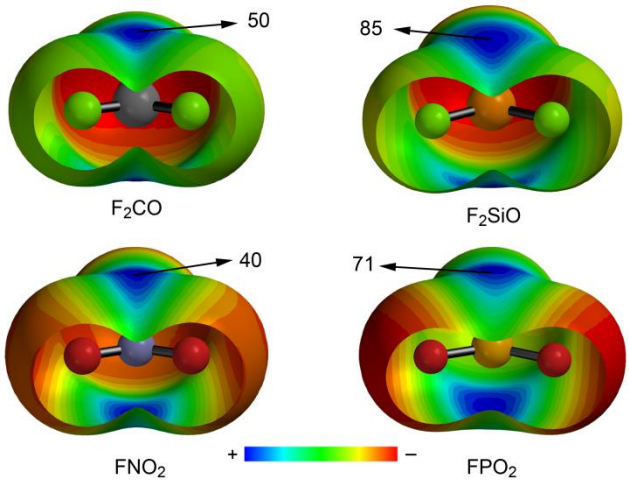

Figure 4. Molecular electrostatic potential of representative tetrel (F_2CO and F_2SiO), and pnicogen (FNO_2 and FPO_2) bond donors at the B3LYP/6-31+G* level of theory. Energies at the π-holes are given in kcal/mol.

Since the second row atoms of groups VI and VII do not participate in π-hole bonding, the MEP surfaces of four representative π-hole donor molecules of rows 3 and 4 are represented in Figure 5. It can be observed that all compounds exhibit

similar electrostatic potential values, indicating that the ability of S/Cl and Se/Br to participate in π-hole bonding interactions is similar. Interestingly, the results derived from the MEP values shown in Figures 4 and 5 clearly indicate that the π-hole potentials decrease on going from Si to Cl (85 to 53 kcal/mol) in agreement with the atomic polarizability of the π-hole donor.

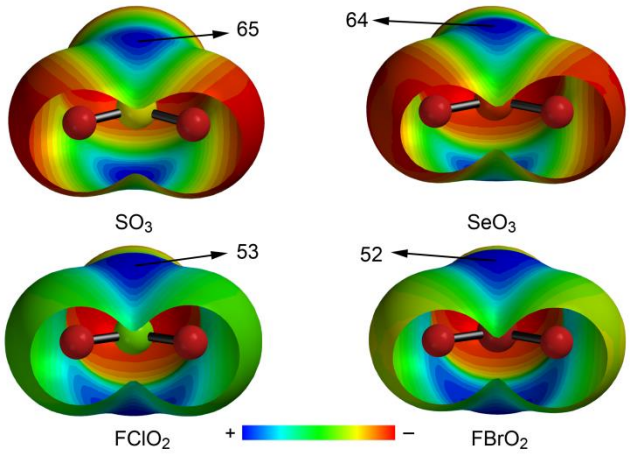

Figure 5. Molecular electrostatic potential of representative chalcogen (SO_3 and SeO_3), and halogen ($FClO_2$ and $FBrO_2$) bond donors at the B3LYP/6-31+G* level of theory. Energies at the π-holes are given in kcal/mol.

When the molecular framework is an aromatic ring the interactions are commonly referred to as anion-π or lone pair-π interactions (depending on whether the electron-rich guest is anionic or neutral). Anion/lone pair-π interactions have attracted much attention in recent years and several reviews have been published describing their physical nature.[8,9,10,31] In addition, several partition energy schemes have been used to decompose the total interaction energy into individual terms.[32] The general conclusion is that electrostatic forces and ion-induced polarization dictate the stability of anion/lone pair-π interactions.[33] The electrostatic term is explained by means of the permanent quadrupole moment (Q_{zz}) of the arene, which is the first non-zero multipole moment in symmetric arenes (see Figure 6A). The Q_{zz} of benzene substituted with electron withdrawing groups is positive and, consequently, the electrostatic charge-quadrupole interaction between an anion and an aromatic ring is attractive.

On the other hand, the ion-induced polarization of the π-system by the anion is also important, inducing a dipole on it (see Figure 6B). Therefore, the polarization contribution to the total interaction energy derives from the interaction of the anion with the induced dipole.[32,33] The electrostatic term is governed by the magnitude of the Q_{zz} and the polarization term by the magnitude of the molecular polarizability parallel to the main symmetry axis (denoted as $\alpha_{||}$) in symmetric arenes (or

[31] a) A. Frontera, D. Quiñonero, P. M. Deyà, *WIREs Comput. Mol. Sci.* **2011**, *1*, 440–459; b) A. Frontera, *Coord. Chem. Rev.* **2013**, *257*, 1716–1727; c) J. J. Fiol, M. Barceló-Oliver, A. Tasada, A. Frontera, À. Terrón, Á. García-Raso, *Coord. Chem. Rev.* **2013**, *257*, 2705–2715.

[32] a) D. Kim, P. Tarakeshwar, K. S. Kim, *J. Phys. Chem. A.* **2004**, *108*, 1250–1258; b) D. Y. Kim, N. J. Singh, J. W. Lee, K. S. Kim, *J. Chem. Theory Comput.* **2008**, *4*, 1162–1169.

[33] a) C. Garau, A. Frontera, D. Quiñonero, P. Ballester, A. Costa, P. M. Deyà, *ChemPhysChem* **2003**, *4*, 1344–1348; b) D. Quiñonero, C. Garau, A. Frontera, P. Ballester, A. Costa, P. M. Deyà, *Chem. Phys. Lett.* **2002**, *359*, 486–492; c) A. Bauzá, P. M. Deyà, A. Frontera, D. Quiñonero, *Phys. Chem. Chem. Phys.* **2014**, *16*, 1322–1326.

perpendicular to the ring plane in asymmetric arenes, denoted as α_{zz}), which are inherent properties of the π-system. In contrast to the intuitive view where the substituent induces changes in the aryl π-system, Wheeler and Houk propose a model where substituent effects in these systems can be attributed mainly to direct interactions between the anion and local C-Y dipoles.[34] A similar explanation has been provided for π-acidic azines.[35]

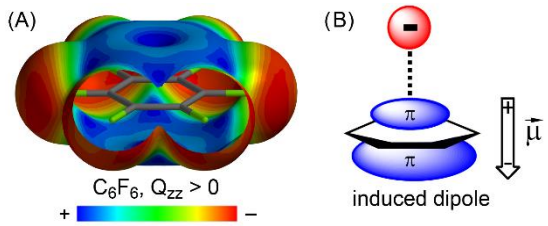

Figure 6. (A) Molecular electrostatic potential of hexafluorobenzene at the B3LYP/6-31+G* level of theory. (B) Schematic representation of the ion-induced dipole.

The comprehension that anion/lone pair-π interactions are governed by electrostatic and induced polarization forces is essential to understand the dual binding mode exhibited by arenes with small quadrupole moments.[36] For instance, 1,3,5-trifluorobenzene (Q_{zz} = 0.57 B) and *s*-triazine (Q_{zz} = 0.90 B) are able to interact with both anions and cations because the electrostatic term is negligible and the interaction is thus dominated by the polarization term, which is always attractive. Similarly, the anion-π interaction energy of benzene with chloride is very small (2.4 kcal/mol), due to the compensating effect between the electrostatic (unfavorable) and ion-induced polarization (favorable) forces that approximately cancel each other out.[37]

1.3. Exploitation of σ-/π-hole interactions

To date, a great deal of experimental and theoretical work has provided strong and reliable evidence of the importance of the σ-/π-hole bonding interactions. In the following sub-sections, several experimental and theoretical examples that demonstrate the potential use and importance of these interactions are shown.

1.3.1. σ-Hole interactions

1.3.1.1. Halogen bonding

[34] S. E. Wheeler, K. N. Houk, *J. Phys. Chem. A.* **2010**, *114*, 8658–8664.
[35] S. E. Wheeler, J. W. G. Bloom, *Chem. Commun.* **2014**, *50*, 11118–11121.
[36] a) C. Garau, D. Quiñonero, A. Frontera, P. Ballester, A. Costa, P. M. Deyà, *Org. Lett.* **2003**, *5*, 2227–2229; b) C. Garau, A. Frontera, D. Quiñonero, P. Ballester, A. Costa, P. M. Deyà, *J. Phys. Chem. A.* **2004**, *108*, 9423–9427.
[37] a) C. Garau, D. Quiñonero, A. Frontera, P. Ballester, A. Costa, P. M. Deyà, *New J. Chem.* **2003**, *27*, 211–214; b) D. Quiñonero, A. Frontera, C. Garau, P. Ballester, A. Costa, P. M. Deyà, *ChemPhysChem* **2006**, *7*, 2487–2491.

A wide number of studies[38] have been devoted to the analysis of solid-state architectures with halogen bonding as the predominant intermolecular interaction that governs their stability. A clear evidence to illustrate the dominant role of halogen bonding interactions in solid state chemistry is related to the bis(N-heterocycle)diacetylene unit. Two examples are worth to be mentioned, involving ditopic iodo donors[39] and bifunctional molecules (both of them containing halogen bond donor and acceptor moieties),[40] forming a chain-like structure.[41] The formation of chain-like structures is useful in the preparation of materials with conducting and magnetic properties as well as noncentrosymmetric crystals capable of second harmonic generation in optical devices. In this regard, Metrangolo and Resnati *et al.*[42]and van der Boom *et al.*[43] demonstrated the formation of a 1D chain in a helical disposition using dibromopyridinium helices and stilbazole-based helices, respectively.

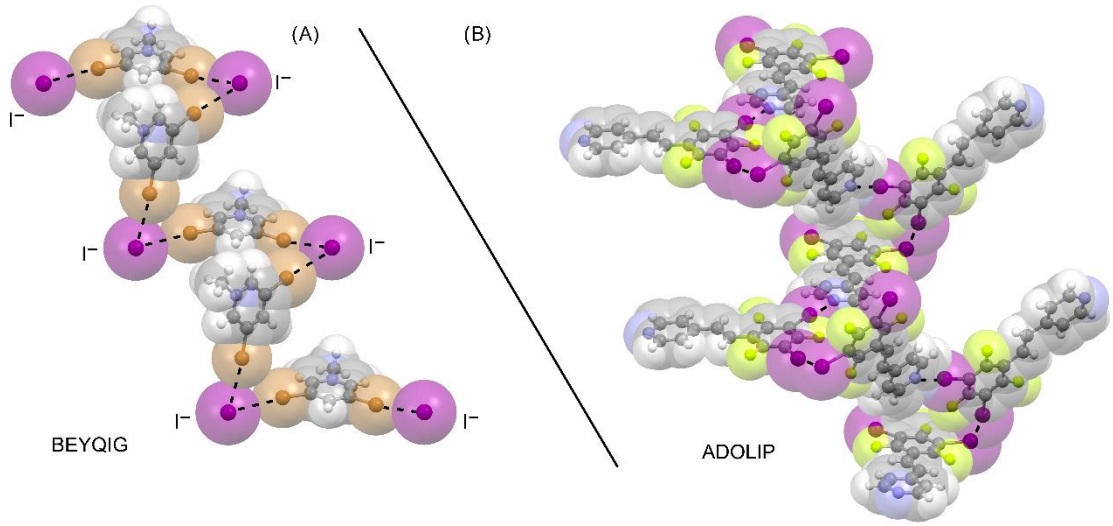

Figure 7. Crystal structures of halogen bonding helices: (A) Metrangolo and Resnati's helix formed via Br···I⁻ halogen-bonding interactions in *N*-methyl-3,5-dibromopyridinium iodide[42] and (B) van der Boom's helix formed via I···I and N···I halogen bonds in the iodo-substituted stilbazole.[43] The CSD reference codes are also indicated.

[38] a) O. Dumele, B. Schreib, U. Warzok, N. Trapp, C. A. Schalley, F. Diederich, *Angew. Chem. Int. Ed.* **2017**, *56*, 1152–1157; b) F. Pan, N. K. Beyeh, R. H. A. Ras, K. Rissanen, *Cryst. Growth & Des.* **2016**, *16*, 6729–6733; c) S. T. Nguyen, A. L. Rheingold, G. S. Tschumper, D. L. Watkins, Cryst. *Growth & Des.* **2016**, *16*, 6648–6653; d) F. Fernández-Palacio, M. Poutanen, M. Saccone, A. Siiskonen, G. Terraneo, G. Resnati, O. Ikkala, P. Metrangolo, A. Priimagi, *Chem. Mater.* **2016**, *28*, 8314–8321; e) G. Kawaguchi, M. Maesato, T. Komatsu, T. Imakubo, A. Kiswandhi, D. Graf, H. Kitagawa, *Chem. Mater.* **2016**, *28*, 7276–7286; f) P. S. Salini, K. Shinaj, M. Hariharan, Cryst. *Growth & Des.* **2016**, *16*, 5822–5830.

[39] A. Crihfield, J. Hartwell, D. Phelps, R. B. Walsh, J. L. Harris, J. F. Payne, W. T. Pennington, T. W. Hanks, *Cryst. Growth Des.* **2003**, *3*, 313–320.

[40] T. Shirman, J. F. Lamere, L. J. W. Shimon, T. Gupta, J. M. L. Martin, M. E. Van Der Boom, *Cryst. Growth Des.* **2008**, *8*, 3066–3072.

[41] a) R. Gajda, A. Katrusiak, *Acta Crystallogr. B* **2007**, *63*, 896–902; b) C. B. Aakeroy, J. Desper, B. A. Helfrich, P. Metrangolo, T. Pilati, G. Resnati, A. Stevenazzi, *Chem. Commun.* **2007**, *43*, 4236–4238; c) A. K. Przybył, M. J. Kubicki, *Chem. Crystallogr.* **2012**, *42*, 685–690.

[42] T. A. Logothetis, F. Meyer, P. Metrangolo, T. Pilati, G. Resnati, *New J. Chem.* **2004**, *28*, 760–763.

[43] A. C. B. Lucassen, T. Zubkov, L. J. W. Shimon, M. E. Van Der Boom, *CrystEngComm* **2007**, *9*, 538–540.

Related to this, the continuos search on the formation of 2D sheet-like structures based on halogen bonding interactions unveiled novel supramolecular synthon, namely, the X_3 (X = Br or I) synthon, in which three halogen bonds form a trimeric unit with interactions reminiscent of type II contacts.[44] In the case of trihalomesitylenes, this synthon is propagated in a 2D sheet throughout the self-assembled crystal structure.[45] In addition, due to their biological implications, the formation of β-sheet-like structures is also a desirable goal that can be achieved using a combination of halogen bonding and hydrogen bonding interactions, as shown by Samai and Biradha in their study of bis((4-halophenyl)amido)alkanes.[46] They showed that iodo-substituted structures were more susceptible to the formation of bifurcated halogen bonds as these help to stabilize the neighboring chains. Cocrystallization of these halo-substituted bis(amido)alkanes resulted in the observation of synthon modularity between the cocrystal structures and those of the parent crystals.

A leap forward on the study of these 1D chains and 2D sheets is the utilization of halogen bonding interactions as building blocks of higher order 3D assemblies, such as discrete capsules, cages and supramolecular networks.[47] An interesting example published by Aakeröy *et al.*[48] demonstrates that halogen bonding interactions can indeed be used to self-assemble two supramolecules, a tetraiodo-functionalized calix[4]arene halogen bond donor and a tetrapyridyl-functionalized cavitand halogen bond acceptor, into a capsule via four halogen bonds (see Figure 8).

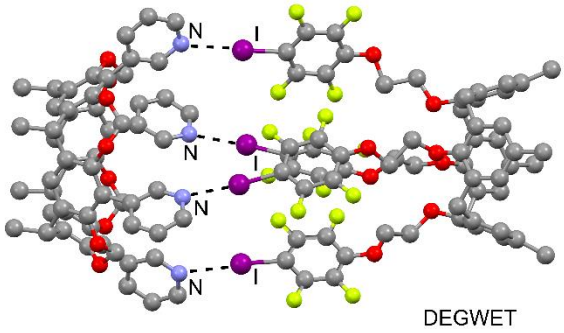

Figure 8. Aakeröy's molecular capsule formed by a tetraiodo-functionalized calix[4]arene and a tetrapyridyl-functionalized cavitand self-assembled via four concurrent N···I halogen bonds.[48] The CSD reference code is indicated.

In this context, the use of inorganic iodine and the (4-(benzoyloxy)-2,2,6,6-tetramethylpiperidinyl)- 1-oxy (BTEMPO) free radical species as starting materials for cocrystallization resulted in the formation of an anionic 3D cage network constructed from iodine and I_5^- via multiple halogen bonds and templated by

[44] L. C. Gilday, S. W. Robinson, T. A. Barendt, M. J. Langton, B. R. Mullaney, P. D. Beer, *Chem. Rev.* **2015**, *115*, 7118–7195.
[45] E. Bosch, C. L. Barnes, *Cryst. Growth Des.* **2002**, *2*, 299–302.
[46] S. Samai, K. Biradha, *CrystEngComm* **2009**, *11*, 482–492.
[47] M. J. Bojdys, M. E. Briggs, J. T. A. Jones, D. J. Adams, S. Y. Chong, M. Schmidtmann, A. I. Cooper, *J. Am. Chem. Soc.* **2011**, *133*, 16566–16571.
[48] C. B. Aakeroy, A. Rajbanshi, P. Metrangolo, G. Resnati, M. F. Parisi, J. Desper, T. Pilati, *CrystEngComm* **2012**, *14*, 6366–6368.

$(BTEMPO)_2^{2+}$ dimers.[49] The authors proposed a mechanism for this observation confirmed by UV-vis spectroscopy and ESI-MS: an initial halogen bond complex was formed between I_2 and BTEMPO radical followed by Mulliken inner charge transfer and a subsequent charge separation reaction. Consequently, the pentaiodide was formed, presumably stabilized by the amphoteric nature of iodine.

Another interesting example was studied by Goldberg *et al.*,[50] which take advantatge from the formation of halogen bonds in the construction of molecular scaffolds based on the asymmetric functionalization of tetraarylporphyrin to afford impressive chiral architectures. Similarly, in their search for novel porous materials without metals, Rissanen and co-workers have taken advantatge of halogen bonding interactions as a means toward preparing such structures.[51]

Recently, the same authors reported a flexible structural framework that was able to accommodate solvent guests in nanosized channels via an induced fit mechanism.[52] This framework was constructed from hexamethylenetetramine (HMTA) and N-iodosuccinimide bonded by $(OC-)_2N-I\cdots N$ halogen bonds. Due to the "breathing" nature of the framework, three distinct solvent-dependent structural topologies were observed via single-crystal X-ray diffraction analysis. The first displayed ovoid channels which include toluene and chloroform molecules, the second exhibited spherical channels containing nitromethane or acetonitrile, and finally, the last structure formed a square-grid motif with the largest relative channel volume of the three structures containing either dichloromethane or tetrachloromethane.

These results provide interesting opportunities for the construction of metal-free organic host structural frameworks, able to capture and accommodate small solvent guests. Lastly, due to their potential applications in materials chemistry, biomedicine, and nanotechnology, dendrimers have attracted much attention in recent years, and halogen bonding interactions have been incorporated into such structures.[53] Metrangolo *et al.*[54] reported the synthesis of DAB-dendr-$(NH\text{-}C_6F_4I)_2$ 2, a poly(propylenimine) dendrimer functionalized with four iodotetrafluorophenyl halogen bond donor groups. Crystallization of the dendrimer with bis(4-pyridyl)ethylene resulted in the self-assembly of a 1:2 supramolecular adduct propagated into large 2D square networks with unprecedented 5-fold interpenetration. This work was extended with the self-assembly of polymers up to the millimeter length via halogen bonding interactions. This research paves the way for new designing tools of dendrimers and polymers with novel shapes and functionalities using σ-hole interactions.

---

[49] X. Pang, H. Wang, X. R. Zhao, W. J. Jin, *Dalton Trans.* **2013**, *42*, 8788–8795.
[50] a) S. Muniappan, S. Lipstman, I. Goldberg, *Chem. Commun.* **2008**, *44*, 1777–1779; b) H. M. Titi, R. Patra, I. Goldberg, *Chem. Eur. J.* **2013**, *19*, 14941–14949.
[51] a) K. Raatikainen, J. Huuskonen, M. Lahtinen, P. Metrangolo, K. Rissanen, *Chem. Commun.* **2009**, *45*, 2160–2162; b) K. Raatikainen, K. Rissanen, *Cryst. Growth Des.* **2010**, *10*, 3638–3646; c) K. Raatikainen, K. Rissanen, *CrystEngComm* **2011**, *13*, 6972–6977.
[52] K. Raatikainen, K. Rissanen, *Chem. Sci.* **2012**, *3*, 1235–1239.
[53] P. Metrangolo, F. Meyer, T. Pilati, D. M. Proserpio, G. Resnati, *Cryst. Growth Des.* **2008**, *8*, 654–659.
[54] N. Houbenov, R. Milani, M. Poutanen, J. Haataja, V. Dichiarante, J. Sainio, J. Ruokolainen, G. Resnati, P. Metrangolo, O. Ikkala, *Nat. Commun.* **2014**, *5*, 4043.

An in depth analysis of the PDB reveals hundreds of examples of halogen bonding interactions within protein-ligand complexes, and in many cases the presence of the halogen bonds resulted in higher binding affinity and activity of the ligand toward the protein's active site. A nice example that illustrates this is provided by Arnold and co-workers,[55] who have demonstrated that halogenation of HIV reverse transcriptase inhibitors (a key enzyme used by HIV to generate new viral particles) resulted in a potent inhibitor, stabilized by an halogen bond between the iodine atom and the carbonyl oxygen of TYR188.

Another example is the work carried out by Lemke *et al.*,[56] who have developed a potent inhibitor of the hepatitis C virus NS_3-NS_4A protease that is currently undergoing phase III clinical trials for the treatment of the virus. The crystal structure of the ligand bound within NS_3-NS_4A protease shows the presence of a Br···O halogen bond formed between the ligand and the backbone carbonyl oxygen of ASP79. Furthermore, both kinetic studies and SARs support the role of the halogen bonding interaction in improving the efficacy of the inhibitor molecule; the association constant increased 3.6-fold relative to that of the protic analogue. The bromine atom was also shown to improve drug absorption, distribution, metabolism, and excretion (ADME) properties, which highlights the additional advantages of incorporating halogen bond donor elements within drug molecules.

The structure of the protic analogue indicates that it binds in a similar way, but caused a small change in the protein conformation. Halogenation has also been shown to increase the efficacy of a ligand inhibitor through formation of a halogen bond, as showed by Carpenter *et al.*,[57] who reported the halogenated benzimidazole carboxamide inhibitor of integrin-α4β1. The IC_{50} data follow the expected trend of F > Cl ≈ H ≈ CH_3 > Br > I, which reflects the predicted halogen bond strength. The same trend was also observed in a series of halogen-substituted 1,4-benzodiazepine-2,5-dione ligands, designed as anticancer drugs for targeting the p_{53} pathway, that bind to the p_{53} binding site of human murine double mutant 2 (MDM2). The crystal structure of the iodo-substituted ligand bound to MDM2 (PDB entry 1T4E) reveals the presence of a halogen bond between the iodine atom and the backbone oxygen of GLY72 (see Figure 9A).[58] Replacement of the iodine atom with bromine or chlorine resulted in a decrease in binding affinity and 2-fold and 4-fold increases in IC_{50}, respectively.[59]

---

[55] a) D. M. Himmel, K. Das, A. D. Clark, S. H. Hughes, A. Benjahad, S. Oumouch, J. Guillemont, S. Coupa, A. Poncelet, I. Csoka, C. Meyer, K. Andries, C. H. Nguyen, D. S. Grierson, E. J. Arnold, *J. Med. Chem.* **2005**, *48*, 7582–7591; b) A. Benjahad, J. Guillemont, K. Andries, C. H. Nguyen, D. S. Grierson, *Bioorg. Med. Chem. Lett.* **2003**, *13*, 4309–4312.

[56] M. Llinàs-Brunet, M. D. Bailey, N. Goudreau, P. K. Bhardwaj, J. Bordeleau, M. Bös, Y. Bousquet, M. G. Cordingley, J. Duan, P. Forgione, M. Garneau, E. Ghiro, V. Gorys, S. Goulet, T. Halmos, S. H. Kawai, J. Naud, M. -A. Poupart, P. W. J. White, *J. Med. Chem.* **2010**, *53*, 6466–6476.

[57] R. D. Carpenter, A. Natarajan, E. Y. Lau, M. Andrei, D. M. Solano, F. C. Lightstone, S. J. DeNardo, K. S. Lam, M. J. Kurth, *Cancer Res.* **2010**, *70*, 5448–5456.

[58] B. L. Grasberger, T. Lu, C. Schubert, D. J. Parks, T. E. Carver, H. K. Koblish, M. D. Cummings, L. V. LaFrance, K. L. Milkiewicz, R. R. Calvo, D. Maguire, J. Lattanze, C. F. Franks, S. Zhao, K. Ramachandren, G. R. Bylebyl, M. Zhang, C. L. Manthey, E. C. Petrella, M. W. Pantoliano, I. C. Deckman, J. C. Spurlino, A. C. Maroney, B. E. Tomczuk, C. J. Molloy, R. F. Bone, *J. Med. Chem.* **2005**, *48*, 909–912.

[59] D. J. Parks, L. V. LaFrance, R. R. Calvo, K. L. Milkiewicz, V. Gupta, J. Lattanze, K. Ramachandren, T. E. Carver, E. C. Petrella, M. D. Cummings, D. Maguire, B. L. Grasberger, T. Lu, *Bioorg. Med. Chem. Lett.* **2005**, *15*, 765–770.

Zhu and co-workers have used halogen bonds in ligand optimization, designing a series of potent halogenated inhibitors of phosphodiesterase type 5 (PDE5).[60] Using a combined QM-MM computational modelling approach, the strength of the halogen bond formed between the ligand halogen atom and the TYR612 phenol oxygen was calculated and compared to the observed IC_{50} values. A strong correlation was observed (a 7-fold decrease in IC_{50} with the iodo ligand compared to the protic ligand), which demonstrated the crucial role of the halogen bonding interaction in enhancing the ligand binding affinity and efficacy. The presence of this interaction was confirmed by analysis of the crystal structure of PDE5 with the fluoro, chloro, and bromo ligands. Very recently, the authors undertook a more comprehensive study of the strength of the halogen bond interaction in the same series of halogenated ligands.[61] Using a combination of thermodynamic, X-ray crystallographic data and DFT calculations, the contribution to the ligand binding affinity from the Hlg···O halogen bond was shown to be −1.6, −3.1, and −5.6 kJ/mol for X = Cl, Br and I, respectively.

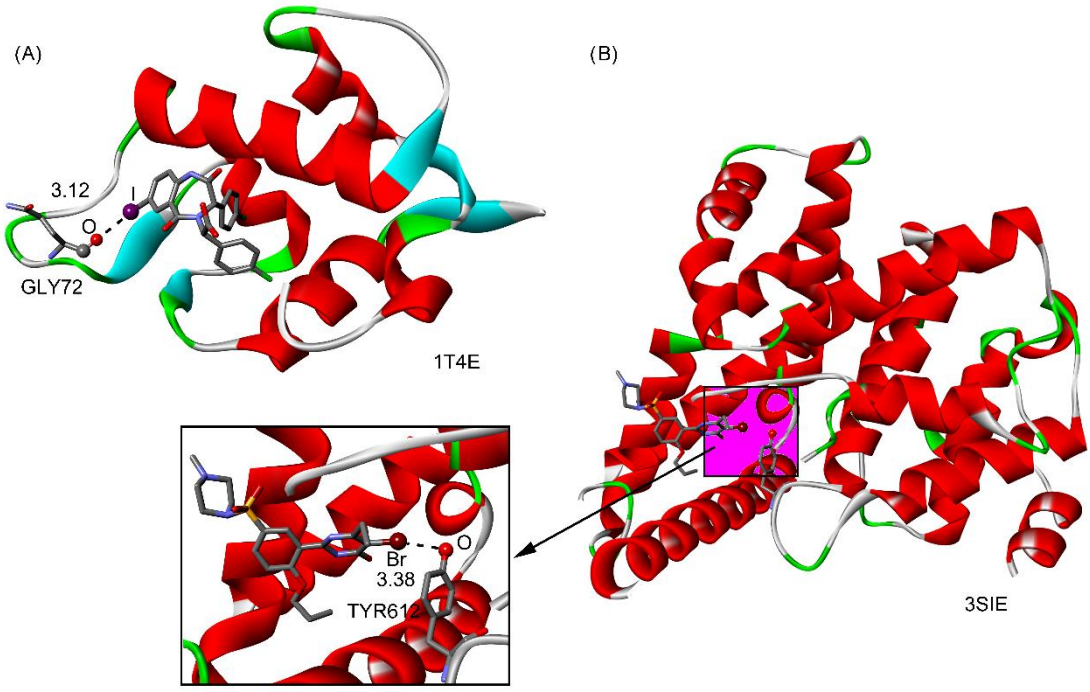

Figure 9. Halogenated ligands targeting MDM2. (A) Crystal structure of a iodo-substituted ligand within the MDM2 active site, interacting with GLY72 via halogen bonding interaction.[58] (B) Crystal structure of a bromo-substituted ligand interacting with the phenolic oxygen of TYR612.[60] Distances in Å. The PDB reference codes are also indicated.

1.3.1.2. Chalcogen bonding

[60] Z. Xu, Z. Liu, T. Chen, T. Chen, Z. Wang, G. Tian, J. Shi, X. Wang, Y. Lu, X. Yan, G. Wang, H. Jiang, K. Chen, S. Wang, Y. Xu, J. Shen, W. Zhu, *J. Med. Chem.* **2011**, *54*, 5607−5611.
[61] J. Ren, Y. He, W. Chen, T. Chen, G. Wang, Z. Wang, Z. Xu, X. Luo, W. Zhu, H. Jiang, J. Shen, Y. Xu, *J. Med. Chem.* **2014**, *57*, 3588−3593.

Most studies on the chalcogen bonding interaction are devoted to the analysis of the attractive interaction between S or Se with an electronegative atom like N or O.[62] Their strength is comparable to, -and occasionally surpasses that of- hydrogen bonds. For instance, the binding energy of the $FHS\cdots NH_3$, complex is 8 kcal/mol.[63] Particularly, the σ-hole interaction between a divalent sulfur (S) and an oxygen (O) atom has attracted interest because it plays an important role in the structure and biological activity of some organo-sulfur compounds [64] and likely regulates enzymatic functions.[65]

Related to this, the group of Iwaoka and coworkers[66] suggested that nonbonding S···O interactions may stabilize folded protein structures. In addition, the structural features of intra- and intermolecular S···O interactions were originally analyzed by Rosenfield *et al.*[67] in the surrounding environments of a divalent S atom (Y-S-Z) in organic and inorganic crystals. They showed that a nucleophilic O atom tends to approach the S atom from the backside of S-Y and S-Z bonds (the σ-hole directions). The relative directional preference of the S···O interactions to the O atom was studied in detail by Kucsman and Kapovits.[68] For intramolecular 1,4- and 1,5-type S···O=C interactions it was shown that the S atom tends to lie in the direction of the O lone pairs. Therefore the stabilization mechanism of the typical S···O=C interaction was described as $n \rightarrow \sigma^*$ orbital interaction.

Iwaoka *et al.*[62f] have suggested that the structural features of S···O=C interactions depend on the type of carbonyl groups involved and that such interactions may control protein folding to some extent. Hobza and collaborators showed the dominant role of chalcogen noncovalent bonding in the crystal packing of 2D/3D aromatics.[62h] Taking advantage of the strong ability of thiaboranes to form chalcogen bonds, they designed and synthesized a phenyl substituted thiaborane which they analyzed with X-ray crystallography. As is shown in Figure 12, S-π type chalcogen bonds are present in the crystal structure of their thiaborane. Theoretical calculations revealed that the most stable binding motif in the crystal structure of 12-Ph-*closo*-1-$SB_{11}H_{10}$ corresponds to a very strong B-S···π chalcogen bond

---

[62] a) A. Bauzá, D. Quiñonero, P. M. Deyà, A. Frontera, *CrystEngComm* **2013**, *15*, 3137–3144; b) M. Iwaoka, N. Isozumi, *Molecules* **2012**, *17*, 7266–7283; c) G. Sánchez-Sanz, C. Trujillo, I. Alkorta, J. Elguero, *ChemPhysChem* **2012**, *13*, 496–503; d) P. Sanz, O. Mó, M. Yáñez, *Phys. Chem. Chem. Phys.* **2003**, *5*, 2942–2947; e) M. H. Esseffar, R. Herrero, E. Quintanilla, J. Z. Dávalos, P. Jiménez, J. -L. M. Abboud, M. Yáñez, O. Mó, *Chem. Eur. J.* **2007**, *13*, 1796–1803; f) M. Iwaoka, S. Takemoto, S. Tomoda, *J. Am. Chem. Soc.* **2002**, *124*, 10613–10620; g) L. M. Azofra, S. Scheiner, *J. Chem. Phys.* **2014**, *140*, 034302, 10p; h) J. Fanfrlík, A. Přáda, Z. Padělková, A. Pecina, J. Macháček, M. Lepšík, J. Holub, A. Růžička, D. Hnyk, P. Hobza, *Angew. Chem. Int. Ed.* **2014**, *53*, 10139–10142; i) U. Adhikari, S. Scheiner, *Chem. Phys. Lett.* **2012**, *532*, 31–35.

[63] V. Nziko, S. Scheiner, *J. Phys. Chem. A.* **2014**, *118*, 10849–10856.

[64] a) F. T. Burling, B. M. Goldstein, *J. Am. Chem. Soc.* **1992**, *114*, 2313–2320; b) Y. Nagao, T. Hirata, S. Goto, S. Sano, A. Kakehi, K. Iizuka, M. Shiro, *J. Am. Chem. Soc.* **1998**, *120*, 3104–3110; c) S. Wu, A. Greer, *J. Org. Chem.* **2000**, *65*, 4883–4887.

[65] a) J. C. Taylor, G. D. Markham, *J. Biol. Chem.* **1999**, *274*, 32909–32914; b) W. Brandt, A. Golbraikh, M. Tager, U. Lendeckel, *Eur. J. Biochem.* **1999**, *261*, 89–97.

[66] a) M. Iwaoka, S. Takemoto, M. Okada, S. Tomoda, *Chem. Lett.* **2001**, *30*, 132–133; b) M. Iwaoka, S. Takemoto, M. Okada, S. Tomoda, *Bull. Chem. Soc. Jpn.* **1977**, *99*, 4860–4862.

[67] R. E. Rosenfield, R. Parthasarathy, J. D. Dunitz, *J. Am. Chem. Soc.* **1977**, *99*, 4860–4862.

[68] A. Kucsman, I. Kapovits, 'Nonbonded Sulfur-Oxygen Interaction in Organic Sulfur Compounds', in: *Organic Sulfur Chemistry*, Elsevier, Amsterdam, **1985**, pp. 191–245.

exceeding –8 kcal/mol. A combined experimental and theoretical study by Mó and coworkers[62e] suggested that chalcogen-chalcogen interactions are relevant in the reaction of dimethyldisulfide and its protonated form to yield methanethiol and a dimethyldithiosulfonium ion. Sánchez-Sanz *et al.*[62c] have studied theoretically a series of HTeXH (X = O, S, Se and Te) monomers and homodimers by means of high level *ab initio* calculations. Due to the axial chirality present in the momomer, the dimers can exist as the homo and heterochiral isomers. Their computations suggest that hydrogen bonds and chalcogen-chalcogen interactions are the reason for chiral discrimination.

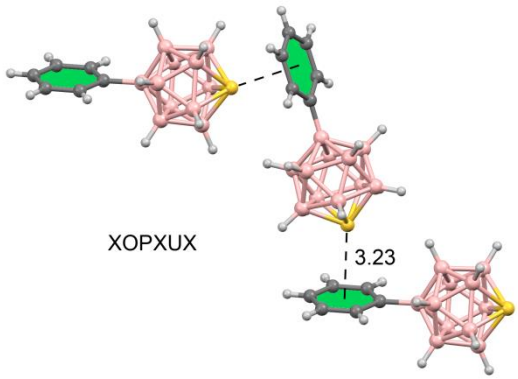

Figure 12. Partial view of the X-ray packing of the phenylsubstituted thiaborane reported by Hobza and collaborators[62h] where the chalcogen-π interaction is shown. The CSD reference code is indicated. Distance in Å.

Related to this, chalcogen bonding between tetravalent SF_4 and amines has been studied theoretically by Nziko and Scheiner.[63] In particular, the N···S chalcogen bond between SF_4 and a series of alkyl and arylamines was examined by means of *ab initio* calculations. They have demonstrated that this noncovalent bond is strong with an interaction energy that ranges from –7 kcal/mol for NH_3 to –14 kcal/mol for trimethylamine. As expected, the strength mostly derives from charge transfer from the N lone pair into the σ*(S-F) antibonding orbitals involving the two equatorial F atoms, one of which is disposed directly opposite the N atom. The authors even propose that the N···S bonding interaction in the dimethylamine···SF_4 complex should be described as a weak covalent bond due to the shortness of the bond and strength of the interaction. As a matter of fact, it has been experimentally shown that sulfur tetrafluoride and triethylamine react at low temperatures to form a 1:1 adduct that has been unambiguously characterized by means of X-ray crystallography[69] (see Figure 13). It is only stable at low temperature and proves the Lewis acid property of SF_4 towards organic Lewis bases. The S-N bond has a length of 2.384(2) Å and it is an archetypical example of a dative N → S^{IV} bond.

[69] J. T. Goettel, P. Chaudhary, P. Hazendonk, H. P. A. Mercier, M. Gerken, *Chem. Commun.* **2012**, *48*, 9120–9122.

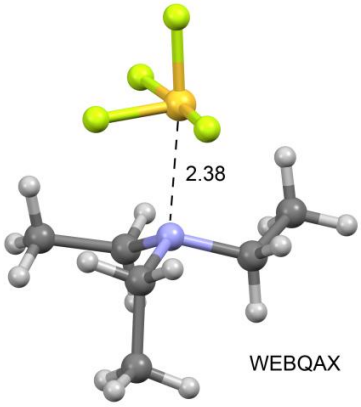

Figure 13. X-ray structure of the 1:1 adduct between SF_4 and triethylamine where the N → S(IV) interaction is shown.[69] The CSD reference code is indicated and distance is in Å.

1.3.1.3. Pnicogen bonding

The strength of pnicogen bonding interactions is similar to standard hydrogen bonds.[70] For example, the binding energy in the $FH_2P\cdots NH_3$ complex (–7.0 kcal/mol) greatly exceeds that of the paradigmatic hydrogen bonding water dimer (–3.2 kcal/mol).[71] Interestingly di- or tri-halogenation of H_3P does not increase the binding energy, in marked contrast to hydrogen bonds. The pnicogen bonding interaction is very strong when the electron-rich atom is an anion.[29] For a given electron-withdrawing substituent, chalcogen and halogen bonds show similar strength to the pnicogen bond. Experimentally, several analyses of crystal structures provide evidence for the existence of "like–like" pnicogen bonds of the N···N,[72] P···P[73] and As···As[74] varieties. The P···N bond variety has been noted in several systems.[75] For instance, in the solid state 1,4-dimethylpiperazine[76] forms a ditopic complex with PBr_3 exhibiting a short intermolecular P···N distance of 2.80 Å (see Figure 14A), close to the theoretical value.[77] When employing the better chelator N,N,N',N'-tetramethylethylenediamine (TMEDA), $(TMEDA)PBr_3$ is obtained (Figure 14B) where two P–Br covalent bonds have been replaced by two P-N covalent bonds (P–N distances: 2.03 and 1.94 Å).[76]

[70] S. Zahn, R. Frank, E. Hey-Hawkins, B. Kirchner, *Chem. Eur. J.* **2011**, *17*, 6034–6038.
[71] B. E. Rocher-Casterline, L. C. Ch'ng, A. K. Mollner, H. Reisler, *J. Chem. Phys.* **2011**, *134*, 211101, 4p.
[72] P. Batail, D. Grandjean, F. Dudragne, C. Michaud, *Acta Crystallogr. B* **1975**, *B34*, 1367–1372.
[73] a) P. Kilian, A. M. Z. Slawin, J. D. Woollins, *Chem. Eur. J.* **2003**, *9*, 215–222; b) M. R. Sundberg, R. Uggla, C. Viñas, F. Teixidor, S. Paavola, R. Kivekäs, *Inorg. Chem. Commun.* **2007**, *10*, 713–716; c) A. C. Marr, M. Nieuwenhuyzen, C. L. Pollock, G. C. Saunders, *Organometallics* **2007**, *26*, 2659–2671; d) C. Ganesamoorthy, M. S. Balakrishna, J. T. Mague, H. M. Tuononen, *Inorg. Chem.* **2008**, *47*, 7035–7047; e) S. Bauer, S. Tschirschwitz, P. Lönnecke, R. Frank, B. Kirchner, M. L. Clarke, E. Hey-Hawkins, *Eur. J. Inorg. Chem.* **2009**, *2009*, 2776–2788; f) M. Bühl, P. Kilian, J. D. Woollins, *ChemPhysChem* **2011**, *12*, 2405–2408.
[74] E. V. Avtomonov, K. Megges, S. Wocadlo, J. Lorberth, *J. Organomet. Chem.* **1996**, *524*, 253–261.
[75] a) S. B. Bushuk, F. H. Carré, D. M. H. Guy, W. E. Douglas, Y. A. Kalvinkovskya, L. G. Klapshina, A. N. Rubinov, A. P. Stupak, B. A. Bushuk, *Polyhedron* **2004**, *23*, 2615–2623; b) S. Tschirschwitz, P. Lönnecke, E. Hey-Hawkins, *Dalton Trans.* **2007**, *37*, 1377–1382.
[76] G. Müller, J. Brand, S. E. Jetter, F. Chemie, U. Konstanz, D. Konstanz, *Z. Naturforsch.* **2001**, *56b*, 1163–1171.
[77] S. Scheiner, *Chem. Phys.* **2011**, *387*, 79–84.

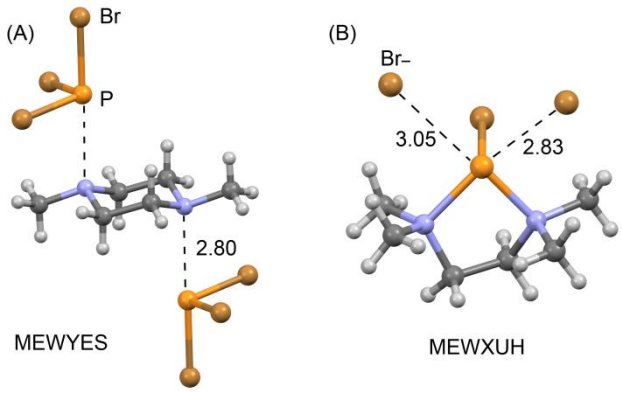

Figure 14. X-ray structures of the complexes between PBr_3 and 1,4-dimethylpiperazine (A) or TMEDA (B).[76,77] The CSD reference codes are indicated. Distances in Å.

The interaction between π-electrons of arenes and the heavier pnicogen atoms (As, Sb and Bi) has been known for a long time, but its study in the context of supramolecular chemistry is more recent.[78] Investigations by Johnson *et al.* have highlighted the potential use of this weak interaction to regulate self-assembly processes to form macrocycles.[79] Mainly using X-ray analysis[80] it has been demonstrated that post-transition metals with stereochemically active lone pairs, such as heavier pnicogens in low oxidation states, yield stable complexes with arenes (see Figure 15 for two representative examples).

[78] M. M. Watt, M. S. Collins, D. W. Johnson, *Acc. Chem. Res.* **2013**, *46*, 955–966.
[79] a) W. J. Vickaryous, R. Herges, D. W. Johnson, *Angew. Chem. Int. Ed.* **2004**, *43*, 5831–5833; b) W. J. Vickaryous, E. R. Healey, O. B. Berryman, D. W. Johnson, *Inorg. Chem.* **2005**, *44*, 9247–9252; c) V. M. Cangelosi, A. C. Sather, L. N. Zakharov, O. B. Berryman, D. W. Johnson, *Inorg. Chem.* **2007**, *46*, 9278–9284; d) V. M. Cangelosi, L. N. Zakharov, S. A. Fontenot, M. A. Pitt, D. W. Johnson, *Dalton Trans.* **2008**, *37*, 3447–3453; e) V. M. Cangelosi, L. N. Zakharov, J. L. Crossland, B. C. Franklin, D. W. Johnson, *Cryst. Growth Des.* **2010**, *10*, 1471–1473; f) N. R. Lindquist, T. G. Carter, V. M. Cangelosi, L. N. Zakharov, D. W. Johnson, *Chem. Commun.* **2010**, *46*, 3505–3507; g) M. A. Pitt, L. N. Zakharov, K. Vanka, W. H. Thompson, B. B. Laird, D. W. Johnson, *Chem. Commun.* **2008**, *44*, 3936–3938; h) V. M. Cangelosi, M. A. Pitt, W. J. Vickaryous, C. A. Allen, L. N. Zakharov, D. W. Johnson, *Cryst. Growth Des.* **2010**, *10*, 3531–3536; i) W. J. Vickaryous, L. N. Zakharov, D. W. Johnson, *Main Group Chem.* **2006**, *5*, 51–59; j) V. M. Cangelosi, L. N. Zakharov, D. W. Johnson, *Angew. Chem. Int. Ed.* **2010**, *49*, 1248–1251; k) V. M. Cangelosi, T. G. Carter, J. L. Crossland, L. N. Zakharov, D. W. Johnson, *Inorg. Chem.* **2010**, *49*, 9985–9992; l) S. A. Fontenot, V. M. Cangelosi, M. A. W. Pitt, A. C. Sather, L. N. Zakharov, O. B. Berryman, D. W. Johnson, *Dalton Trans.* **2011**, *40*, 12125–12131.
[80] a) W. Frank, J. Schneider, S. Müller-Becker, *J. Chem. Soc. Chem. Commun.* **1993**, 799–800; b) D. Mootz, V. Händler, *Z. Anorg. Allg. Chem.* **1986**, *533*, 23–29.

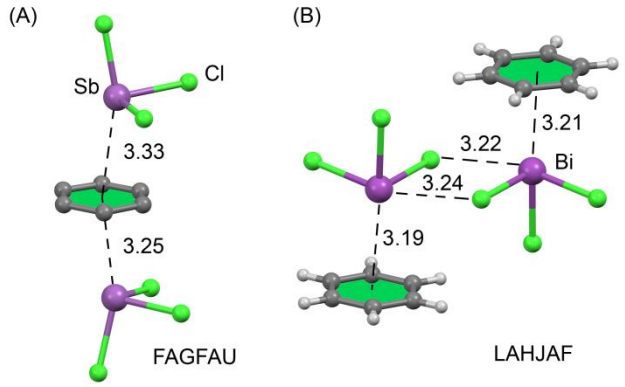

Figure 15. X-ray structures of the complexes between benzene and $SbCl_3$ (A) or $BiCl_3$ (B). The CSD reference codes are indicated. Distances in Å.[80]

Several examples of pnicogen derivatives interacting with aromatic moieties have been found in the Protein Data Bank, confirming the presence of these interactions in biological systems and their potential use as effective enzyme inhibitors (by means of the σ-hole-π(arene) interaction involving pnicogen atoms). Interestingly, it has been proposed that Sb(III) plays an important role in the inhibition mechanism of trypanothione reductase (TR), which involves an Sb-π interaction with TRP231.[81] Consequently, the current treatment of leishmaniasis relies on antimony based drugs: meglumine antimoniate (Glucantime) and sodium stibogluconate (Pentostam).[82] Furthermore, the crystal structures of TR (from Leishmania infantum) and its complex with NADPH and Sb(III) were reported in 2009[82] and curiously, the Sb(III) is present in the catalytic cleft and coordinated by one threonine residue (THR335) and the two redox-active catalytic cysteine residues (CYS52 and CYS57). Therefore, the inhibition mechanism is caused by the disulfur brigde breaking due to the complexation of the Sb(III), which reduces the redox ability of the enzyme.

Another useful example involves the interaction of an Sb(III) moiety with the FAD cofactor, which also plays a remarkable role in the stabilization of the Sb(III) coordination site.[82] Thus, this interaction contributes to the tight binding of the inhibitor to the active site. Interestingly, Sb(V)-containing compounds are less toxic than their trivalent analogues, although Sb(V) has to be activated by conversion to the trivalent form Sb(III) to exert its action against the parasite.[83]

Trujillo and collaborators[84] have reported a computational study of the intramolecular pnicogen bonding in 1,8-bis-substituted naphthalene derivatives (see Figure 16). These molecules are structurally related to Proton Sponge® (1,8-bis(dimethylamino)naphthalene). By means of in silico isodesmic reactions they demonstrate that some 1,8-bis-substituted derivatives are more stable than the monosubstituted ones due to intramolecular pnicogen-pnicogen interactions.

[81] H. Zhu, P. Smith, L. K. Wang, S. Shuman, *Virology* **2007**, *366*, 126–136.
[82] P. Baiocco, G. Colotti, S. Franceschini, A. Ilari, *J. Med. Chem.* **2009**, *52*, 2603–2612.
[83] L. G. Goodwin, J. E. Page, *Biochem. J.* **1943**, *37*, 198–209.
[84] G. Sánchez-Sanz, C. Trujillo, I. Alkorta, J. Elguero, *Phys. Chem. Chem. Phys.* **2014**, *16*, 15900–15909.

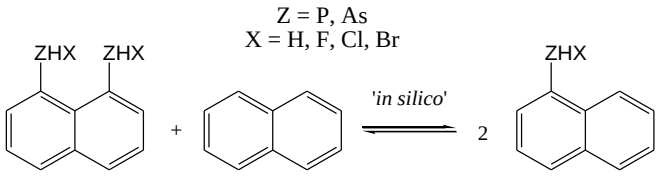

Figure 16. Isodesmic in silico reactions of phosphorus and arsenic analogues of Proton Sponge® reported by Trujillo *et al.*[84]

1.3.1.4. Tetrel bonding

The interaction where atoms of group IV act as Lewis acid[85] has been named 'tetrel bonding' by several groups in 2013/2014.[5c, 86] Such interactions involving Si, Ge and Sn were explored before that, while 'noncovalent carbon bonding' is a more recent subject of enquiry. Alkorta *et al.*[87] studied molecular complexes between silicon derivatives (SiX_4, X = halogen) and electron-rich groups (NH_3, H_2O, etc.) and have also analyzed this interaction in aminopropylsilanes.[88] Other research groups have also described this interaction in complexes involved in S_N2 processes for the elements of group IV.[5c,89] Mani and Arunan[90] performed a comprehensive theoretical study for the tetrel bonding in the complexes of methanol as the tetrel bond donor with the Lewis bases Y = H_2O, H_2S, HF, HCl, HBr, ClF, LiF, LiCl, LiBr, NH_3, and PH_3, and the results demonstrated that the methyl groups bonded to electron-withdrawing substituents participate in the formation of tetrel bonding. The existence of tetrel bonding was further validated with experimental charge density analysis and a large number of X-ray characterized crystal structures exhibiting tetrel bonding interactions in the solid state.[91] Single-electron tetrel bonding interaction with radical species as electron donors has been also reported.[92]

---

[85] A. Bundhun, P. Ramasami, J. S. Murray, P. Politzer, *J. Mol. Model.* **2013**, *19*, 2739–2746.

[86] a) S. J. Grabowski, *Phys. Chem. Chem. Phys.* **2014**, *16*, 1824–1834; b) A. Bauzá, T. J. Mooibroek, A. Frontera, *Chem. Eur. J.* **2014**, *20*, 10245–10248; c) A. Bauzá, R. Ramis, A. Frontera, *Comp. Theor. Chem.* **2014**, *1038*, 67–70.

[87] I. Alkorta, I. Rozas, J. Elguero, *J. Phys. Chem. A* **2001**, *105*, 743–749.

[88] I. Alkorta, *J. Organomet. Chem.* **2001**, *625*, 148–153.

[89] a) C. J. Levy, R. J. Puddephatt, *J. Am. Chem. Soc.* **1997**, *119*, 10127–10136; b) J. Langer, S. Matejcik, E. Illenberger, *Phys. Chem. Chem. Phys.* **2000**, *2*, 1001–1005; c) J. Mikosch, S. Trippel, C. Eichhorn, R. Otto, U. Lourderaj, J. X. Zhang, W. L. Hase, M. Weidemüller, R. Wester, *Science* **2008**, *319*, 183–186; d) M. Sohail, R. Panisch, A. Bowden, A. R. Bassindale, P. G. Taylor, A. A. Korlyukov, D. E. Arkhipov, L. Male, S. Callear, S. J. Coles, M. B. Hursthouse, R. W. Harrington, W. Clegg, *Dalton Trans.* **2013**, *42*, 10971–10981.

[90] D. Mani, E. Arunan, *Phys. Chem. Chem. Phys.* **2013**, *15*, 14377–14383.

[91] S. P. Thomas, M. S. Pavan, T. N. Guru Row, *Chem. Commun.* **2014**, *50*, 49–51.

[92] Q. Li, X. Guo, X. Yang, W. Li, J. Cheng, H.-B. Li, *Phys. Chem. Chem. Phys.* **2014**, *16*, 11617–11625.

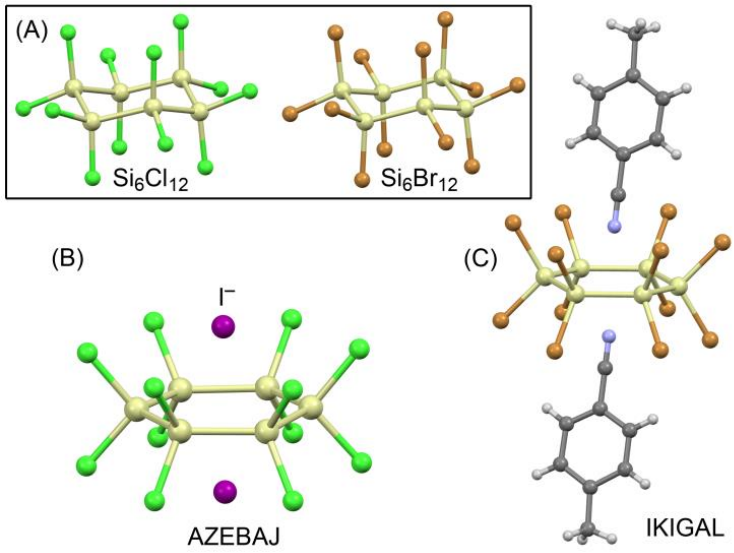

Figure 17. X-ray structures of fluoride encapsulated into silicon (A) and germanium (B) hexahedral [4^6] cages. The CSD reference codes are indicated.[93, 94]

An important experimental work has shown that tetrel bonding interactions induce planarity in five and six membered silicon rings. The formation of these interesting and unexpected "inverse sandwich" complexes in perhalogenated cyclohexasilanes[93] (Si_6Cl_{12} and Si_6Br_{12} X-ray structures are shown in Figure 17A) interacting with anions or lone pair donor molecules (see Figure 17B and C, respectively) is due to the formation of six concurrent tetrel bonds. The same behaviour has been observed in perchlorocyclopentasilane.[94]

Another experimental evidence that emphasizes the importance of the tetrel bonding was reported by Taylor *et al.*[95] The synthesis of spherosilicates is significantly improved using n-butylammonium fluoride (TBAF) as a catalyst. Interestingly, a new class of cage compound was obtained showing a fluoride ion perfectly centered within the octasilsesquioxane cage (see Figure 18A).[96] The ^{19}F chemical shift of this encapsulated F^- anion resembles that of a naked uncoordinated F^- anion. These fluoride-encapsulating cages can be seen as models of the environment that may exist in certain zeolites that are stabilized by fluoride anions (F^- may also template formation of such zeolites).[97] This type of encapsulated compound has also been reported for germanium-based T8 cages (see Figure 18B).[98]

[93] a) X. Dai, D. L. Schulz, C. W. Braun, A. Ugrinov, P. Boudjouk, *Organometallics* **2010**, *29*, 2203–2205; b) X. Dai, S.-B. Choi, C. W. Braun, P. Vaidya, S. Kilina, A. Ugrinov, D. L. Schulz, P. Boudjouk, *Inorg. Chem.* **2011**, *50*, 4047–4053.
[94] J. Tillmann, F. Meyer-Wegner, A. Nadj, J. Becker-Baldus, T. Sinke, M. Bolte, M. C. Holthausen, M. Wagner, H.-W. Lerner, *Inorg. Chem.* **2012**, *51*, 8599–8606.
[95] P. G. Taylor, A. R. Bassindale, Y. El Aziz, M. Pourny, R. Stevenson, M. B. Hursthouse, S. J. Coles, *Dalton Trans.* **2012**, *41*, 2048–2059.
[96] A. R. Bassindale, M. Pourny, P. G. Taylor, M. B. Hursthouse, M. E. Light, *Angew. Chem. Int. Ed.* **2003**, *42*, 3488–3490.
[97] a) G. van de Goor, C. C. Freyhardt, P. Behrens, *Z. Anorg. Allg. Chem.* **1995**, *621*, 311–322; b) P. Caullet, J. L. Guth, J. Hazm, J. M. Lamblin, H. Gies, *Eur. J. Sol. State Inorg.* **1991**, *28*, 345–361.
[98] L. A. Villaescusa, P. Lightfoot, R. E. Morris, *Chem. Commun.* **2002**, *38*, 2220–2221.

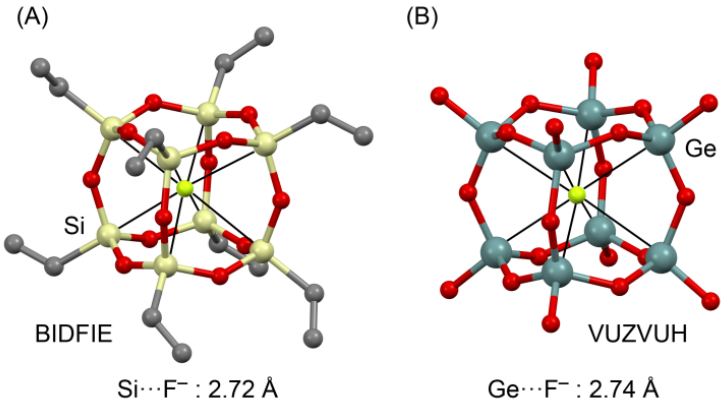

Figure 18. X-ray structures of fluoride encapsulated into silicon (A) and germanium (B) hexahedral cages.[95] The CSD reference codes are indicated.

A fascinanting experimental finding that corroborates the importance of noncovalent tetrel bonding interactions in the solid state is the encapsulation of tetramethylammonium fluoride salt into octadecasil.[99] The topology is defined by rhombododecahedral [$4^6 6^{12}$] cages, which are connected by hexahedral [4^6] cages, usually denoted as double 4-rings (D4R), see Figure 19. Interestingly, the octadecasil structure is acting as a ditopic carcerand, where the fluoride guest is confined by the D4R unit establishing eight simultaneous tetrel bonds and the counterion is located in the interior of the rhombododecahedral cages establishing a large number of C–H···O interactions. The oxygen atoms of the D4R units are pointing toward the exterior of the cage and concurrently toward the interior of the [$4^6 6^{12}$] cage facilitating both tetrel bonding interactions in the former and the hydrogen bonding interaction in the latter.

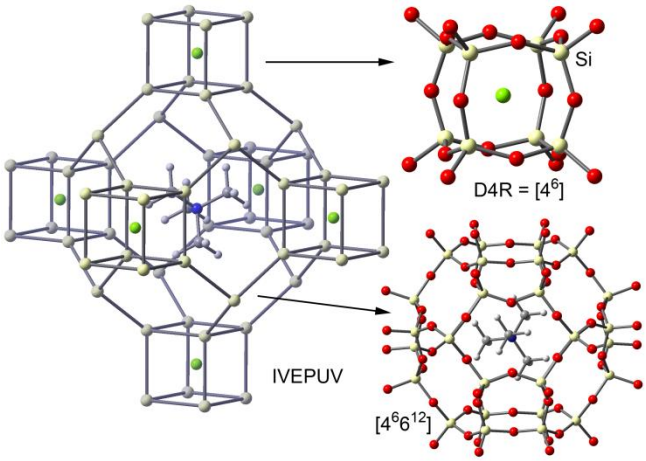

Figure 19. Partial view of the X-ray structure of TMA^+F^--octadecasil, showing D4R units with the guest fluoride and the [$4^6 6^{12}$] cage with tetramethylammonium ion. For clarity, the oxygen atoms have been omitted in the representation shown in the left.[99]

[99] X. Yang, *Mater Res. Bul.* **2006**, *41*, 54–66.

A tetrel complex with an sp^3 hybridized tetrel atom can be seen as the advent, [X⁻···TrY_4], or aftermath, [$XTrY_3$···Y⁻], of an S_N2 nucleophilic attack of X⁻ on TrY_4, while the transition state is the hypervalent species [$XTrY_4$]⁻.[89a, 89b, 89d, 100] Si and also Ge[101] tetrel atoms are well-known to form stable hypervalent adducts with nucleophiles and bidentate 'ligands'.[102] Hypervalent carbon has only been isolated in the context of a geometrically confined scaffold (see Figure 20A).[103]

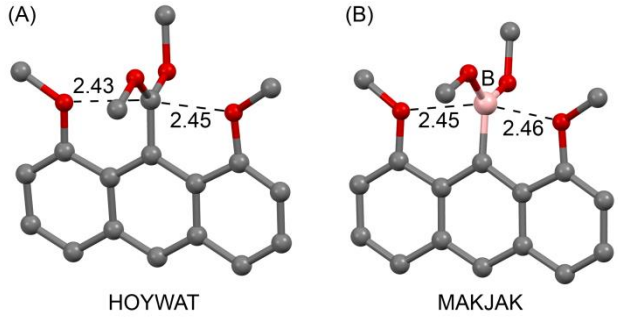

Figure 20. (A) X-ray structure of a hypervalent carbon atom interacting with two OMe groups at the 1,8-position of the anthracene skeleton. The ClO_4^- counterion and hydrogen atoms have been omitted for clarity. (B) X-ray structure of the equivalent compound with boron. The CSD reference codes are indicated. Distances in Å.

This implies that noncovalent tetrel bonding with sp^3 hybridized Tr-atoms (avoiding traditional hypervalent adducts) is more likely for carbon (over Si, Ge and Sn). Nevertheless, 'noncovalent carbon bonding' remains the least studied tetrel bonding interaction.[86b,90,104] One possible explanation for this lack of studies could be the relatively small size of carbon (see Table 1), leading to only a very limited amount of space available for any electron-rich guest molecule to interact with any potential σ-hole on C.

However, several examples found in the CSD highlight the ability of cyclopropanic rings to establish σ-hole noncovalent interactions with electron-rich atoms (El.R.). Two examples are shown in Figure 21, involving oxygen and nitrogen atoms as lone pair donors. It can be clearly observed that the intermolecular distances lay within the sum of the van der Waals radii, confirming the hydrophobic electrophilic bowl formed by 1,1',2,2'-tetracyano cyclopropane derivatives as a new and synthetically accessible supramolecular synthon.

---

[100] a) S. C. A. H. Pierrefixe, S. J. M. van Stralen, J. N. P. van Stralen, C. Fonseca Guerra, F. M. Bickelhaupt, *Angew. Chem. Int. Ed.* **2009**, *48*, 6469–6471; b) S. C. A. H. Pierrefixe, J. Poater, C. Im, F. M. Bickelhaupt, *Chem. Eur. J.* **2008**, *14*, 6901–6911.

[101] E. K. Lermontova, A. A. Selina, S. S. Karlov, A. V. Churakov, J. A. K. Howard, Y. F. Oprunenko, M. Y. Antipin, J. Sundermeyer, G. S. Zaitseva, *J. Organomet. Chem.* **2006**, *691*, 5710–5724.

[102] a) R. R. Holmes, *Chem. Rev.* **1996**, *96*, 927–950; b) G. P. Schiemenz, *Z. Anorg. Allg. Chem.* **2002**, *628*, 2597-2604; c) P. D. Prince, M. J. Bearpark, G. S. McGrady, J. W. Steed, *Dalton Trans.* **2008**, *37*, 271–282; d) P. Gualco, M. Mercy, S. Ladeira, Y. Coppel, L. Maron, A. Amgoune, D. Bourissou, *Chem. Eur. J.* **2010**, *16*, 10808–10817; e) D. Kost, I. Kalikhman, *Acc. Chem. Res.* **2009**, *42*, 303–314; f) W. Levason, G. Reid, W. Zhang, *Coord. Chem. Rev.* **2011**, *255*, 1319–1341.

[103] a) M. Yamashita, Y. Yamamoto, K.-Y. Akiba, D. Hashizume, F. Iwasaki, N. Takagi, S. Nagase, *J. Am. Chem. Soc.* **2005**, *127*, 4354–4371; b) K.-Y. Akiba, Y. Moriyama, M. Mizozoe, H. Inohara, T. Nishii, Y. Yamamoto, M. Minoura, D. Hashizume, F. Iwasaki, N. Takagi, K. Ishimura, S. Nagase, *J. Am. Chem. Soc.* **2005**, *127*, 5893–5901.

[104] a) A. Bauzá, T. J. Mooibroek, A. Frontera, *Phys. Chem. Chem. Phys.* **2014**, *16*, 19192–19197; b) F. H. Allen, *Acta Crystallogr. B* **2002**, *58*, 380–388.

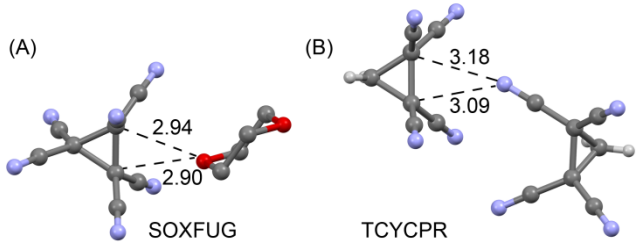

Figure 21. X-ray structures of 1,1',2,2'-tetracyano cyclopropane derivatives interacting with electron-rich atoms. The CSD reference codes are indicated. Distances in Å.

Finally, it is also worth to emphasize the ability of cubane substituted with electron withdrawing groups as carbon bond donor moieties. Cubanes substituted with nitro groups present significant noncovalent carbon bonding interactions (O···C) that have a critical influence on their solid state packing (see Figure 22).

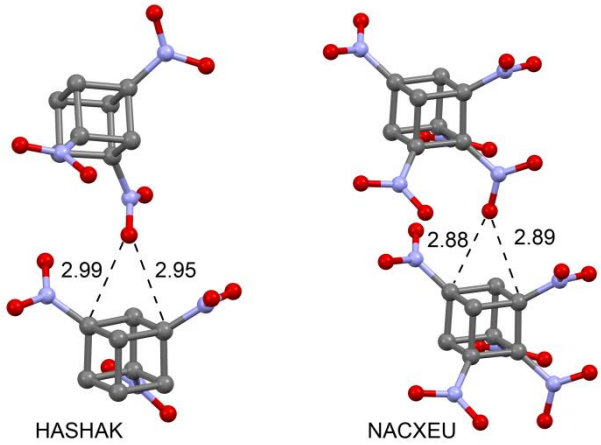

Figure 22. X-ray structures of nitrocubanes exhibiting carbon bonding interactions. The CSD reference codes are indicated. Distances in Å.

Since carbon is the most abundant tetrel atom in Nature and appears to be capable of establishing intermolecular interactions similar in energy as hydrogen bonding, this hints at a particularly promising future for this type of tetrel bonding interaction that might be used as a powerfull tool in fields such as enzyme chemistry and molecular recognition.

1.3.2. π-Hole interactions

1.3.2.1. π-Hole interactions with diatomic π-systems

The oldest known π-hole interactions involve diatomic π-systems such as carbonyl compounds. For example, the canonical trajectory along which a nucleophile attacks the π-hole of the carbon atom in a carbonyl group has been uncovered by Bürgi and Dunitz.[15] Moreover, π-hole interactions involving amides are known to persist in

protein structures.[105] Recently, several theoretical manuscripts have appeared in the literature devoted to the study of π-hole interactions in small molecules.[18,19,20] Most of them are focused on the analysis of the interaction between the unpopulated π*-orbital on a tetrel, pnicogen or chalcogen atom and an electron-rich moiety.

A recent example of a π-hole interaction where a tetrel atom is part of the diatomic π-system comes from Guo *et al.*[106] They performed an *ab initio* study of complexes between F_2XO (X = C and Si) and HCN, to investigate the competition between π-hole interactions and hydrogen bonds. Both types of interactions become stronger for X = Si, and they found that the π-hole interaction is much stronger than the hydrogen bond. Moreover, the importance of anion···π-hole interactions between PF_6^- and malonate has been found crucial to rationalize the crystal packings of copper(II)-malonate [107] and copper(II) N,N'-bis(1-pyridin-2-yl-ethylidene)-2,2-dimethylpropane-1,3-diamine complexes.[108]

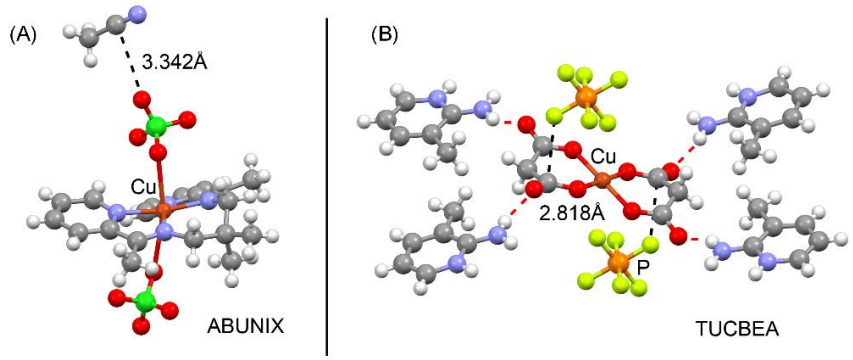

Figure 23. X-ray fragments of two selected structures exhibiting tetrel π-hole interactions. The CSD codes are indicated. Distances in Å.

Other π-hole complexes involving tetrel atoms have been also highlighted by Khan *et al.*,[108] remarking the ability of malonate derivatives to establish this type of interactions when a transition metal is present. In Figure 24 a representative number of hits are shown and most of them are characterized by short X⁻···CO distances (in some cases considerably shorter than the sum of van der Waals radii). This considerably amount of structures exhibiting interactions between anions and the π-hole of a carboxylate group coordinated to a transition-metal gives relevance to the anion-π-hole binding mode and can be exploited as new supramolecular synthon in chemistry. Indeed, in case of malonate such structures represent a unique electrophilic bowl that can accommodate a range of electron-rich molecules.

[105] a) P. H. Maccallum, R. Poet, E. J. Milnerwhite, *J. Mol. Biol.* **1995**, *248*, 374–384; b) G. J. Bartlett, A. Choudhary, R. T. Raines, D. N. Woolfson, *Nat. Chem. Biol.* **2010**, *6*, 615–620; c) M. Harder, B. Kuhn, F. Diederich, *ChemMedChem* **2013**, *8*, 397–404.
[106] X. Guo, L. Cao, Q. Li, W. Li, J. Cheng, *J. Mol. Model.* **2014**, *20*, 2493–2498.
[107] M. Mitra, P. Manna, A. Bauzá, P. Ballester, S. K. Seth, S. Ray Choudhury, A. Frontera, S. Mukhopadhyay, *J. Phys. Chem. B* **2014**, *118*, 14713–14726.
[108] S. Khan, S. Chattopadhyay, A. A. Masum, M. M. Islam, M. G. B. Drew, A. Bauzá, A. Frontera, *Polyhedron* **2017**, *123*, 334–343.

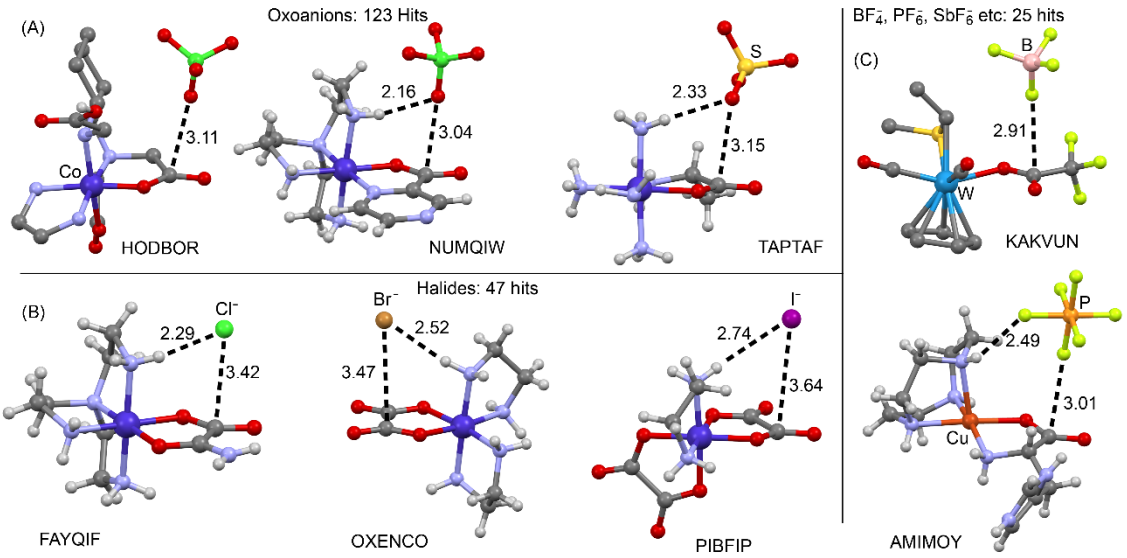

Figure 24. CSD search performed by Khan *et al.*[108] showing the ability of malonate moieties to establish π-hole bonding interactions with (A) Oxoanions, (B) Halides and (C) other anionic entities. Distances in Å. The CSD reference codes are also indicated.

Del Bene *et al.*[109] have analyzed the properties of complexes $H_2C{=}(X)P{\cdots}PXH_2$ (for X = F, Cl, OH, CN, NC, CCH, H, CH_3 and BH_2) focusing their attention to the P···P pnicogen bonding at σ-holes and π-holes. Several types of complexes were found on the potential surfaces and one of them involves charge transfer from the P lone pair of the PXH_2 molecule into the π-hole of the $H_2C{=}PX$ molecule (π* P=C orbital). Pnicogen π-hole bonding has also been analyzed recently in the solid state that involves the central nitrogen atom of azides. Three new dinuclear mixed valence Co(II/III) complexes were synthesized and characterized by X-ray crystallography by Hazari *et al.*[110] The π-hole pnicogen bonding interaction was observed only in the complex where the azide ligand was coordinated at both ends to transition metals. Combining theoretical calculations and a CSD search the authors explained the counter intuitive electron acceptor ability of the $\mu_{1,3}$-azido ligand due to the presence of a π-hole at the central N atom.

[109] J. E. Del Bene, I. Alkorta, J. Elguero, *J. Phys. Chem. A* **2013**, *117*, 11592–11604.
[110] A. Hazari, L. K. Das, R. M. Kadam, A. Bauzá, A. Frontera, A. Ghosh, *Dalton Trans.* **2015**, *44*, 3862–3876.

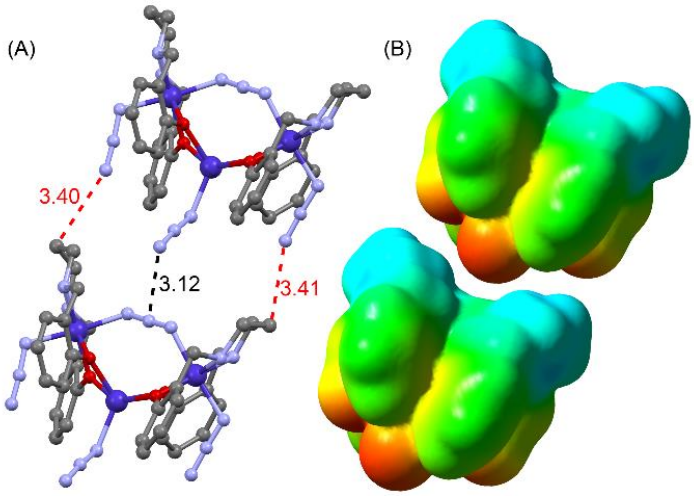

Figure 25. (A) X-ray crystal structure of WOWLOL showing π-hole pnicogen bonding interactions. Ancillary hydrogen bonding interactions are depicted in red dashed lines. (B) MEP surface plots of two complementary Co(II/III) units synthesized by Hazari *et al.*[110] Distances in Å.

Regarding chalcogen π-hole bonding, noncovalent interactions in dimers and trimers of SO_3 and CO have been studied by Azofra *et al.*[18] by means of high level *ab initio* calculations. The SO_3···CO heterodimer forms a complex in which the C lone pair of CO interacts with the π*(SO) antibonding orbital via the π-hole lying directly above the S atom of SO_3. The binding energy of this complex is 4.3 kcal/mol and the interaction is dominated by Coulombic attraction. A strong chalcogen bond between SO_3 molecules is the dominant feature of the $(SO_3)_2$···CO trimer, supplemented by an S···C chalcogen bond.

1.3.2.2. π-Hole interactions with conjugated π-systems

1.3.2.2.1. Lone pair-π interactions

The attractive interaction between a lone pair of electrons and the electron-deficient π-conjugate of an extended aromatic system is known as the lone pair (lp)-π interaction. The first experimental reports of lp-π interactions involve the X-ray structure of Z-DNA (see Figure 26).[16, 111]

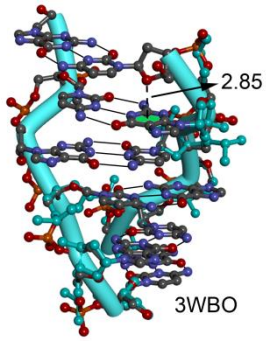

Figure 26. Short lp-π interaction (indicated as dashed line) in the Z-DNA (PDB ID 3WBO).[16,111] Distance in Å.

[111] S. Sarkhel, A. Rich, M. Egli, *J. Am. Chem. Soc.* **2003**, *125*, 8998–8999.

More recently, Sankararamakrishnan and collaborators have systematically analyzed the Protein Data Bank and, among hundreds of high-resolution protein structures, they have identified eighteen structures where an attractive lp-π interaction between a water oxygen atom and an aromatic residue in the protein likely exists.[112] Similarly, Gamez and co-workers have analyzed thousands of crystal structures in the CSD and have identified numerous potential examples of lp-π interactions in which electron-rich atoms (halogens, oxygen, and nitrogen) approach aromatic centers with a distance of less than 4 Å.[8b, 113]
The lp-π interaction between electron-rich atoms and electron-deficient aromatic rings has also been indirectly observed in solution for several different organic compounds on the basis of NMR equilibrium constant measurements.[114] For instance oxygen-arene interactions in triptycene derivatives have been reported by Gung *et al.*[114b] (see Figure 27).

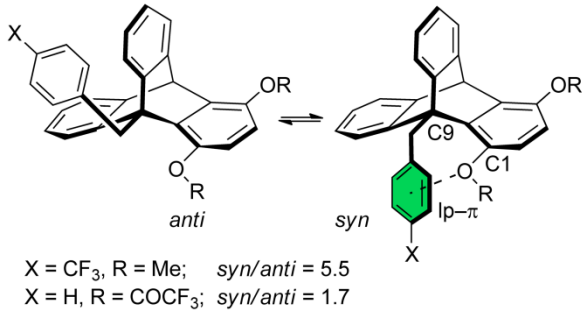

Figure 27. Triptycenes derivatives synthesized by Gung *et al.*.[114b]

They have synthesized C1 and C9 substituted triptycenes (R_{C1} = MeO, HCOO, MeCOO, CF_3COO, etc. and R_{C9} = $pXC_6H_4CH_2$; X = Me, H, F, CN, CF_3) to measure lp-π interactions in the off-center configuration. The ratios of the *syn* and *anti* conformers were determined by low-temperature NMR spectroscopy. The lp-π interaction is only possible in the *syn* conformer allowing the estimation of the free energy of the interaction from the *syn*/*anti* ratio. The triptycene derivative with X = H and R = CF_3 is the only compound that shows a slightly repulsive interaction (0.08 kcal/mol). Conversely, the compound with X = CF_3 and MeO substituent at C1 exhibits an attractive interaction (−0.47 ± 0.05 kcal/mol). All other combinations showed negligible attractive interactions likely due to the very low acidity of the arene (absence of π-hole).

Interestingly, similar research on lp-π interactions in solution using the triptycene scaffold was continued by the same group[114d] who reported additional investigations using aromatic rings with a wide range of substituents. A single

[112] A. Jain, V. Ramanathan, R. Sankararamakrishnan, *Protein Sci.* **2009**, *18*, 595–605.
[113] T. J. Mooibroek, P. Gamez, *CrystEngComm* **2012**, *14*, 1027–1030.
[114] a) C. C. Forbes, A. M. Beatty, B. D. Smith, *Org. Lett.* **2001**, *3*, 3595–3598; b) B. W. Gung, X. Xue, H. J. Reich, *J. Org. Chem.* **2005**, *70*, 7232–7237; c) W. B. Motherwell, J. Moïse, A. E. Aliev, M. Nic, S. J. Coles, P. N. Horton, M. B. Hursthouse, G. Chessari, C. A. Hunter, J. G. Vinter, *Angew. Chem. Int. Ed.* **2007**, *46*, 7823–7826; d) B. W. Gung, Y. Zou, Z. Xu, J. C. Amicangelo, D. G. Irwin, S. Ma, H.-C. Zhou, *J. Org. Chem.* **2008**, *73*, 689–693; e) R. Annunziata, M. Benaglia, F. Cozzi, A. Mazzanti, *Chem. Eur. J.* **2009**, *15*, 4373–4381; f) T. Korenaga, T. Shoji, K. Onoue, T. Sakai, *Chem. Commun.* **2009**, *45*, 4678–4680; g) M. Benaglia, F. Cozzi, M. Mancinelli, A. Mazzanti, *Chem. Eur. J.* **2010**, *16*, 7456–7468.

crystal was obtained for one of the model compounds, confirming the existence of the lp-π interaction in the solid state (see Figure 28). The crystal structure confirms that the *syn* conformation is the preferred arrangement, where the methoxy oxygen atom of the methoxymethyl group is situated near the center of the pentafluorophenyl ring.

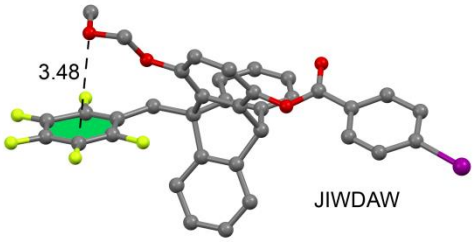

Figure 28. X-ray structure of a triptycene derivative exhibiting a lp-π interaction. The CSD reference code is indicated.[114d] Distance in Å.

Annunziata *et al.*[114e] have synthesized some model systems containing (fluoro)aromatic and pyridine or benzene residues arranged in an edge-to-face disposition (see Figure 29).

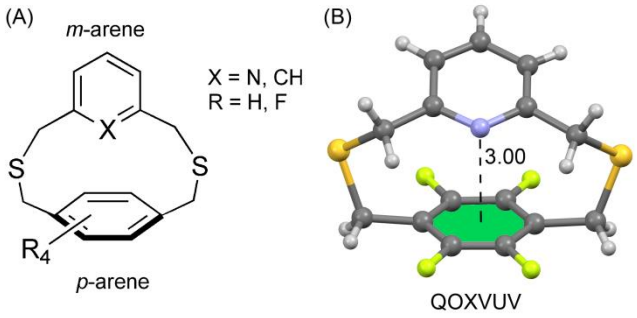

Figure 29. (A) [3,3]metaparacyclophane model systems reported by Annunciata *et al.* (B) X-ray structure of the pyridine derivative exhibiting a lp-π interaction.[114e] The CSD reference code is indicated. Distance in Å.

Their investigation of the structures and stereodynamic behavior showed a favorable interaction between an "edge" ring featuring a pyridine nitrogen lone pair and a perfluorinated "face" ring. These minimalistic model systems based on the [3,3]metaparacyclophane skeleton are useful to study the effect of fluorination of the "face" ring on the edge-to-face interaction with the nitrogen lone pair of pyridine. By means of density functional theory calculations, the authors established that in their more stable conformation the model systems adopt a tilted edge-to-face disposition with the rim of the *meta*-substituted ring pointing towards the face of the *para*-substituted ring. Topomerization occurs by flipping of the *meta*-substituted ring, a process that involves the formation of an intermediate featuring an orthogonal edge-to-face disposition of the arenes. The variation in the energy barrier as a function of the substitution of the *para*-substituted ring (fluorinated or not) could be rationalized well by the formation of a lp-π interaction in the cases of model systems presenting the Py···π interaction but not in the cases of models featuring the C–H···π interaction (phenyl instead of pyridine).

An extension of aforementioned investigation concerns the use of four thiophene- and furan-containing [3,3]meta(heterocyclo)paracyclophanes (see Figure 30A) instead of pyridine to study the intramolecular lp-π interaction between O/S atoms and tetra-H- or tetra-F-substituted benzenes.[114g]

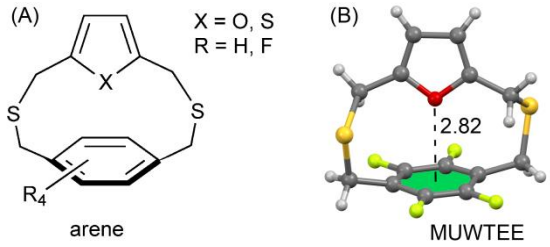

Figure 30. (A) [3,3]metaparacyclophane model systems reported by Cozzi and coworkers.[114g] (B) X-ray structure of the furane derivative exhibiting a O-π interaction. The CSD reference code is indicated. Distance in Å.

A complete conformational analysis (combining DFT calculations and variable-temperature NMR techniques) was used to demonstrate the different conformational preferences and types of isomerization processes depending on the nature of the heterocycle. For thiophene, the isomerization pathway ring-flip process passes through an edge-to-face arranged transition state in which the sulfur atom points toward the center of the six-membered aromatic ring. The energy barrier to the ring-flip process for the thiophene was higher by 2.4 kcal/mol in the case of the perfluorinated benzene. This difference was due to the different stability of the ground state depending on the electronic nature of the aromatic ring (H- and F-substituted). On the contrary, the furan-derived adducts adopt a perpendicular edge-to-face disposition of the rings in the ground state with the oxygen atom pointing toward the benzene platform, as confirmed by X-ray crystallography (see Figure 30B), likely due to the smaller van der Waals radius of the oxygen atom.

Inspired by their previous work[115] where an intermolecular oxygen lp-π interaction was described in the crystal packing of a chiral amino alcohol (see Figure 31A), Korenaga *et al.*[114f] have demonstrated experimentally the existence of unprecedented intermolecular lp-π interactions between alcoholic oxygen and the C_6F_5 group in $CDCl_3$ solution. Since the O-π interaction alone is too weak to detect in organic solution, the complexation was assisted by N···H-OR hydrogen bonds (see Figure 31) To confirm the existence of the lp-π interaction in solution, the authors synthesized a simplified interaction system combining N,N'-dimethyl-2-arylethylamine and MeOH as the evaluation model for the interaction. For the aromatic moiety, the authors used six different aryl groups. The C_6F_5-containing complex is stabilized by the combined effects of O-π interaction and hydrogen bonding and the other complexes studied were controlled exclusively by the hydrogen bond. The interaction energies dominated by the hydrogen bond should be proportional to the basicity of amines, which decreases with increasing the electron-withdrawing ability of the aryl group in the model system. If both the hydrogen bonding and O-π interaction exist in the complex, the interaction energy would consist of the sum of the hydrogen bonding and lp-π interaction energies and

[115] T. Korenaga, H. Tanaka, T. Ema, T. Sakai, *J. Fluorine Chem.* **2003**, *122*, 201–205.

should be larger than that expected by the inductive effect of the aryl group. The values of ΔH between six different model systems (arene = C_5F_6, 3,4,5-$C_6F_3H_2$, p-CF_3-C_6H_4, p-F-C_6H_4, C_6H_5, p-MeO-C_6H_4) and MeOH in $CDCl_3$ were estimated by NMR titration. Interestingly, the relationship between ΔH and Taft's σ* value (index of the inductive effect) of aryl groups showed a good correlation, but not in the case of the C_6F_5-containing complex: there the interaction is stronger than predicted by the σ* value. This finding strongly suggests that an attractive interaction different from hydrogen bonding exists in the C_6F_5-containing complex.

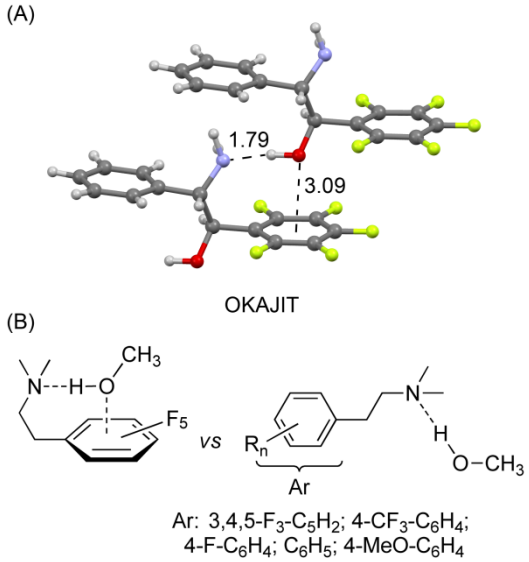

Figure 31. (A) X-ray structure of the pyridine derivative exhibiting a lp-π interaction. The CSD reference code is indicated. Distances in Å. (B) N,N-dimethyl-2-arylethylamine model systems reported by Korenaga *et al.*[114f]

The lone pair-π interaction between H_2O and hexafluorobenzene has been recently investigated by Amicangelo *et al.*[116] using matrix isolation infrared spectroscopy and quantum chemical calculations. Co-deposition of water with hexafluorobenzene in a nitrogen matrix at 17K followed by annealing to 30K, showed the presence of multiple new peaks in the infrared spectrum that are shifted from the water and hexafluorobenzene parent absorptions. These peaks only appear when both molecules are present and were assigned to distinct structures of a 1:1 $H_2O{\cdot}C_6F_6$ complex (see Figure 32).

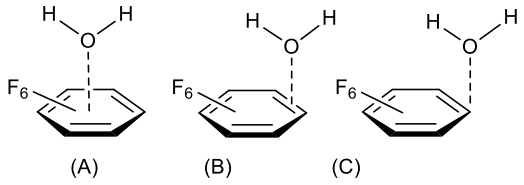

Figure 32. Structural minima obtained for the $H_2O{\cdot}C_6F_6$ complex

[116] J. C. Amicangelo, D. G. Irwin, C. J. Lee, N. C. Romano, N. L. Saxton, *J. Phys. Chem. A* **2013**, *117*, 1336–1350.

Very interestingly, similar experiments were performed with D_2O and HDO and the corresponding infrared peaks for the structures of the $D_2O{\cdot}C_6F_6$ and $HDO{\cdot}C_6F_6$ complexes have also been observed. Theoretical calculations were also carried out by the authors at several levels of theory, locating three different minima, all of which involve the lone pair-π interaction between the H_2O and the C_6F_6 ring with different relative orientations (see Figure 32). The three orientations correspond to a η^6, η^3 and η^1 O-π interaction modes. Vibrational frequencies for the each of the structures were calculated supporting the assignments of the observed new peaks in the infrared spectra to the structures of the H_2O-C_6F_6 complex and the theoretical frequency shifts were in good quantitative agreement with the experimentally observed frequency shifts.

1.3.2.2.2. Anion-π interactions

The main aim of this section is to highlight the most recent and especially relevant advances in this field since there is a continuous and increasing interest for investigating anion-π interactions in several fields like supramolecular chemistry, catalysis and enzymatic chemistry. As previously mentioned, there are excelent reviews in the literature that describe previous work on anion-π interactions.[9, 10, 31]

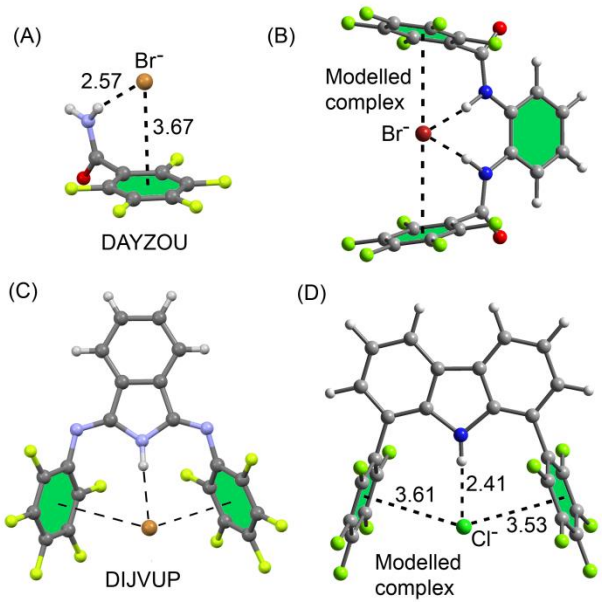

Figure 33. (A) Partial view of the X-ray crystal structure reported by Giese *et al.*[117] showing the pentafluorobenzamide and the interacting bromide. The CSD code is indicated. (B) Modelled binding motif for the interaction of bromide with a receptor containing two pentafluorobenzamide moieties. (C) Partial view of the X-ray crystal structure reported by Meyer's group[118] showing the 1,3-bis(pentafluorophenyl-imino) isoindoline and the interacting bromide. The CSD code is indicated. (D) Modelled binding motif 1,8-bis(pentafluorophenyl)-9H-carbazole interacting with chloride. Distances in Å.

[117] M. Giese, M. Albrecht, T. Krappitz, M. Peters, V. Gossen, G. Raabe, A. Valkonen, K. Rissanen, *Chem. Commun.* **2012**, *48*, 9983–9985.
[118] A. Bretschneider, D. M. Andrada, S. Dechert, S. Meyer, R. A. Mata, F. Meyer, *Chem. Eur. J.* **2013**, *19*, 16988–17000.

Giese *et al.*[117] have studied the binding of a series of anions with neutral π-acceptors by means of simultaneous hydrogen bonding and anion-π interactions both in the solid state and in solution. The receptors are based on pentafluorobenzamides (see Figure 33), and one model anion-π complex was also characterized by X-ray spectroscopy. In solution the enhanced ability of the receptors functionalized with electron-poor systems to bind anions is explained by a cooperative effect of N-H···anion and anion-π interactions. In part, the enhanced affinity stems from the increased acidity of the amide proton by the electron-withdrawing C_6F_5-unit. Using a similar strategy, Meyer's group[118] has designed and synthesized pre-organized anion traps for exploiting anion-π interactions based on 1,3-bis(pentafluorophenyl-imino) isoindoline (Figure 33C) and 3,6-di-*t*-butyl-1,8-bis(pentafluorophenyl)-9H-carbazole (Figure 33D) in various solvents. Both neutral receptors provide a central N-H···X-hydrogen bond that guides the halide anion into a pre-organized clamp formed by the two electron-deficient C_6F_5-units.

In solution, association constants up to 960 M^{-1} have been determined by NMR spectroscopy. Moreover, crystal structures of host-guest complexes confirm that in all cases the guest is located in the cleft between the perfluorinated flaps. A detailed computational analysis of the host-guest complexes using an energetic decomposition of the ring-anion interactions reveals that the contribution of the anion-π interactions to the stabilization of these complexes is ~50% of the total energy. Wang and Wang[119] have systematically studied anion-π interactions by using an electron-deficient and neutral macrocyclic host, i.e. tetraoxacalix[2]arene-[2]triazine (see Figure 34).

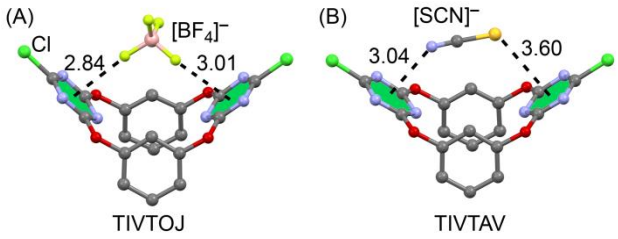

Figure 34. Crystal structures of the complexes between tetraoxacalix[2]arene[2]triazine host and BF_4^- (A) and SCN^- (B) guests reported by Wang and Wang.[119] The CSD reference codes are indicated. Distances in Å.

By means of several experimental techniques (Electrospray Ionization-Mass Spectrometry, fluorescence titration and X-ray crystallography) the authors demonstrated the formation of 1:1 host-guest complexes with four polyatomic anions (NO_3^-, BF_4^-, PF_6^-, SCN^-) in the gaseous phase, in solution and in the solid state. The X-ray structures of two representative complexes (BF_4^- and SCN^-) are shown in Figure 34 (A and B, respectively). The association constants for the formation of anion-π complexes in acetonitrile are very high, ranging from 239 to 16,950 M^{-1}. The geometries of the complexes in the solid state show that two opposed electron-deficient aromatic rings of the host interact with the anionic guests through cooperative anion-π and lp-π interactions.

[119] D. X. Wang, M. X. Wang, *J. Am. Chem. Soc.* **2013**, *135*, 892–897.

Using a similar strategy, He *et al.*[120] have recently investigated the stability of size-regulable vesicles based on anion-π interactions using tetraoxacalix[2]arene-[2]triazine as a functionalization platform. They have synthesized a series of new amphiphilic anion receptors that self-assemble into stable vesicles in a mixture of THF and water, with the surface of the vesicles engineered by electron-deficient cavities. Remarkably, the anions are able to influence the size of self-assembled vesicles selectively, following the order of $F^- < ClO_4^- < SCN^- < BF_4^- < Br^- < Cl^- < NO_3^-$, as revealed by Dynamic Light Scattering (DLS) experiments. This order of selectivity agrees with the binding strength of anions with tetraoxacalix-[2]arene[2]triazine, suggesting that the anion-π interaction might prevail over other possible weak interactions and could thus be responsible for this selectivity. Moreover, the chloride permeation process across the membrane of the vesicles was also studied using fluorescent experiments showing the potentiality of tetraoxa-calix[2]arene[2]triazine as new models to construct functional vesicles.

Schneebeli *et al.*[121] have reported interesting anion-π recognition systems in molecular triangular prisms formed by naphthalenediimide moieties (see Figure 35). The electronic communication among the naphthalenediimide units leads to an unusually large number of individually accessible redox states in the triangular prisms, opening the door to potential applications in the field of molecular electronics. The ability of the electron-deficient cavity of the molecular prism to encapsulate the linear I_3^- anion is shown by the X-ray crystallography solid state architecture depicted in Figure 35. Very interestingly, the inclusion of I_3^- anions induces π-π stacking of the chiral prisms into supramolecular helices, providing a unique example of anion-induced self-assembly with potential applications as ion-channels.

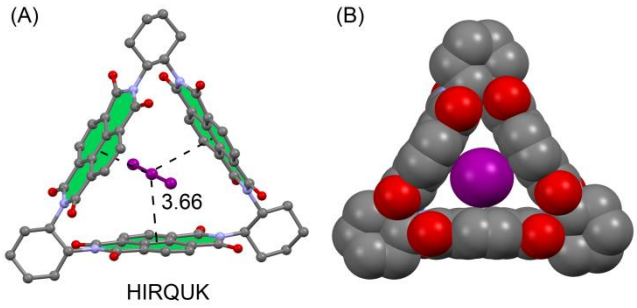

Figure 35. Two views in ball and stick (A) and space filling (B) of the crystal structure of the triangular prism complexed to I_3^- reported by Stoddart and coworkers.[121] The CSD reference code is indicated. Distances in Å.

The strong π-hole electrostatic potential of heteroaromatic ligands upon its coordination to transition metals has been used by Chifotides *et al.*[122] to generate supramolecular architectures with 3,6-bis(2-pyridyl)-*s*-tetrazine cavities where anion-π interactions participate in the remarkable stability of Fe(II) metallacycles in solution. This comprehensive investigation showed that anion-π interactions are the

[120] Q. He, Y. Han, Y. Wang, Z.-T. Huang, D.-X. Wang, *Chem. Eur. J.* **2014**, *20*, 7486–7491.
[121] S. T. Schneebeli, M. Frasconi, Z. Liu, Y. Wu, D. M. Gardner, N. L. Strutt, C. Cheng, R. Carmieli, M. R. Wasielewski, J. F. Stoddart, *Angew. Chem. Int. Ed.* **2013**, *52*, 13100–13104.
[122] H. T. Chifotides, I. D. Giles, K. R. Dunbar, *J. Am. Chem. Soc.* **2013**, *135*, 3039–3055.

main driving force in the formation of self-assembled metallacycles. Combining several technics, like cyclic voltammetry, NMR and mass spectroscopy and X-ray crystallography, they demonstrated that the anion occupies the π-acidic cavities, templating and controlling the nuclearity of the cages. That is, $[BF_4]^-$ and $[ClO_4]^-$ anions generate molecular squares (see Figure 36A) and $[SbF_6]^-$, $[AsF_6]^-$ and $[PF_6]^-$ anions template molecular pentagons (see Figure 36B) establishing close π-hole contacts with the *s*-tetrazine rings. NMR, cyclic voltammetry and mass spectroscopy studies also demonstrate that the molecular assemblies (squares and pentagons) persist in solution.

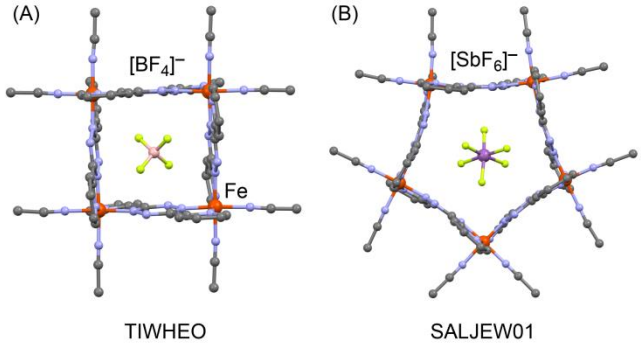

Figure 36. Anion-templated X-ray structures of a molecular square (A) and a molecular pentagon (B) reported by Chifotides *et al*.[122] The CSD reference codes are indicated. Distances in Å.

Ballester and coworkers have carried out several investigations devoted to the experimental quantification of anion-π interactions in solution using neutral host-guest model systems.[123] They have reported several examples of neutral molecular receptors that bind anions in solution as a combination of anion-π interactions and hydrogen bonding.[124] The strength of the anion-π interaction is indirectly detected as a modulation of the dominating hydrogen bonding interaction. The dissection of the energy contribution of the anion-π interaction to the overall binding is complex and requires the use of appropriate reference systems. They have designed a model system based on a series of "four wall" aryl-extended calix[4]pyrrole receptors containing deep aromatic cavities with fixed walls (see Figure 37A, for the X-ray structure of the nitro-derivative as example). The formation of four concurrent hydrogen bonds between the anion and the NH groups of the calix[4]pyrrole scaffold fixes the halide in the aromatic cavity, above the planes of the π-systems of the four meso-aryl substituents, as probed using ^{1}H NMR spectroscopy.

Different *para*-substituents in the aromatic rings were utilized to fine tune the π-hole electrostatic potential. The magnitude of the association constant was increased with the electron-withdrawing ability of the *para*-substituent. The difference in free energy (ΔΔG, see Figure 37) of binding between different complexes provides a direct measurement of the relative anion-π interaction energy. Using this approach, they estimated a maximum contribution of −4.4 kcal/mol for

[123] P. Ballester, *Acc. Chem. Res.* **2013**, *46*, 874–884.
[124] a) G. Gil-Ramírez, E. C. Escudero-Adán, J. Benet-Buchholz, P. Ballester, *Angew. Chem. Int. Ed.* **2008**, *47*, 4114–4118; b) L. Adriaenssens, G. Gil-Ramírez, A. Frontera, D. Quiñonero, E. C. Escudero-Adán, P. Ballester, *J. Am. Chem. Soc.* **2014**, *136*, 3208–3218.

the four chloride-π interactions to the overall binding free energy that corresponds to the *para*-nitroaryl substituted receptor. This is likely an underestimation of the anion-π contribution because the reference system used was octamethylcalix[4]pyrrole, which provides four additional C-H···Cl interactions (see Figure 37B) that are not present in the meso-aryl-substituted receptors. Therefore, the contribution of –4.4 kcal/mol likely means that each anion-π interaction is 1.1 kcal/mol more favorable than each C-H···Cl$^-$ interaction that is established in the reference complex. In any case the small interaction energy measured for the anion-π interaction is unsurprising given the large anion-arene distance (4.38 Å, see Figure 37A) that is approximately 1 Å longer that the ideal one for a Cl$^-$-π interaction.[9a]

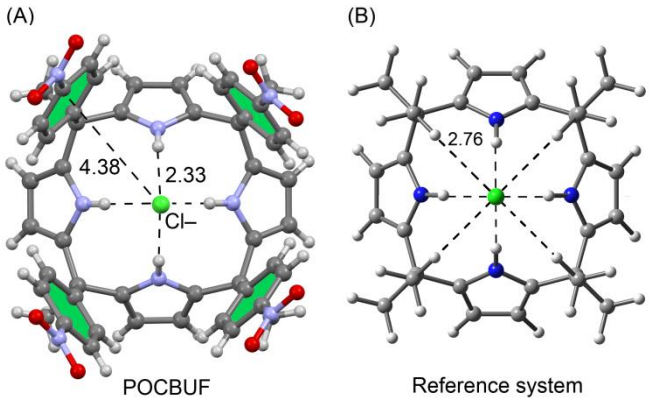

Figure 37. (A) X-ray structure of a four wall calix[4]pyrrole, the CSD reference code is indicated. (B) The receptor used by Ballester's group[124a] as reference for the estimation of chloride-π interactions. Distances in Å.

The performance of chloride-selective electrodes based on "two-wall" aryl-extended calix[4]pyrroles and multiwall carbon nanotubes has been recently reported by Ballester's and Blondeau's groups.[125] The anion-π interactions were shown to significantly affect the selectivity of the electrodes. Calix[4]pyrrole, bearing a *p*-nitro withdrawing group on each of the meso phenyl rings, afforded sensors that display anti-Hofmeister behavior against the lipophilic salicylate and nitrate anions. The sensors delivered excellent results in the direct detection of chloride in bodily fluids. Remarkably, this investigation is a demonstration that anion-π interactions can have very significant effects in functional devices.

Zhao *et al.* reported in 2013 for the first time experimental evidence suggesting that anion-π interactions contribute to the catalysis of the Kemp elimination reaction by π-acidic naphthalene diimides (NDI) leading to conceptually innovative design strategies to stabilize anionic transition states.[126] Subsequent studies[127] with modified, sulfur-containing NDI catalysts confirmed the general validity of increasing transition-state stabilization with increasing π-acidity with regard to the Kemp elimination. Moreover, computational simulations are in excellent agreement

[125] J. Sabek, L. Adriaenssens, T. Guinovart, E. J. Parra, F. X. Rius, P. Ballester, P. Blondeau, *Chem. Eur. J.* **2015**, *21*, 448–454.
[126] Y. Zhao, Y. Domoto, E. Orentas, C. Beuchat, D. Emery, J. Mareda, N. Sakai, S. Matile, *Angew. Chem. Int. Ed.* **2013**, *52*, 9940–9943.
[127] Y. Zhao, C. Beuchat, Y. Domoto, J. Gajewy, A. Wilson, J. Mareda, N. Sakai, S. Matile, *J. Am. Chem. Soc.* **2014**, *136*, 2101–2111.

with experimental results, confirming that the stabilization of the anionic transition states (but not the neutral ground states) increases with the π-acidity of the catalysts, i.e., the existence of what can be called 'anion-π catalysis'. Matile's group has applied this concept to enolate chemistry.[128] They have covalently attached a malonate moiety to an NDI (see Figure 38) and by means of ^{1}H NMR spectroscopy they have measured the acidity of the hydrogen atoms of free diethyl malonate and the corresponding ones upon its attachment to the naphthalene diimide.

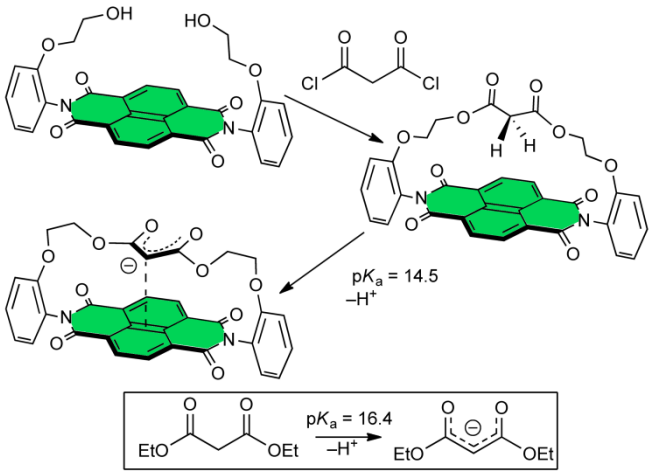

Figure 38. Schematic representation of π-acidic naphthalene diimides covalently bonded to malonate as reported by Matile *et al.*[128]

As a result, the chemical shift of the acidic hydrogen atoms in free diethylmalonate is reduced by 1.6 ppm due to their exposure to the naphthalene ring current causing the upfield shift. This direct experimental evidence for the fixed covalent positioning of the malonate above the π-acidic surface is very important because it assures that any changes in acidity can be unambiguously attributed to the stabilization of the enolate by anion-π interactions. In fact, ^{1}H NMR titrations evidence that the anion-π interaction stabilizes the enolate by almost two pK_a units. Remarkably, the addition of these anion-π-stabilized reactive enolate intermediates to enones and nitroolefins occurs with significant transition-state stabilizations (up to 11 kJ/mol).[128] Moreover, anionic cascade reactions that cover aldol condensation, elimination and transesterification also accelerate on π-acidic surfaces.

Significant evidence that illustrates the importance of anion-π interactions in biological systems is the development of new software capable to search anion-π contacts in the PDB and related biological databases. In this respect, the STAAR (statistical analysis of aromatic rings) program[13c] can identify anion-π interactions in a large structural database of biomolecules. A pioneering work on the study of anion-π interaction in biomolecular recognition was published in 2012 by Chakravarty *et al.*[13b] Their examination of high-resolution structures of proteins and nucleic acids indicated the presence of anion-π interactions in protein/nucleic acid loops (often involving conserved/coevolving sites in proteins). These findings suggest that this interaction plays an important role in macromolecular folding and

[128] Y. Zhao, N. Sakai, S. Matile, *Nat. Commun.* **2014**, *5*, 3911, 5p.

function. Finally, it is also worth to mention the work carried out in our group devoted to the analysis of cooperativity effects in anion-π interactions involving biomolecules.[129]

Frontera and coworkers[13a] have also studied the important role of anion-π interactions in the active site of the urate oxidase enzyme. The inhibition of this enzyme by cyanide ions is caused by the existence of an anion-π interaction between the anionic inhibitor and the π-electron-deficient enzymatic substrate (uric acid). They demonstrated using high level *ab initio* calculations that the anion-π interaction between the inhibitor and the substrate in a model of the active site is energetically favorable. This was the first example where the presence of an anion-π interaction between an inhibitor and an enzymatic substrate was proposed to be crucial in the inhibition of an enzyme and extended the relevance of this interaction to an important field such as enzyme chemistry. This was further confirmed by Estarellas *et al*.[130] who demonstrated the relevance of anion-π interactions in flavoproteins: either participating in the regioselective chlorination at the 7 position of tryptophan by the tryptophan 7-halogenase or inhibiting the FMN-dependent nitroreductase by means of an acetate···FMN π-hole interaction.

Furthermore, our group[131] have analyzed the importance of anion-π interactions in the mechanism of sulfide:quinone oxidoreductase, which is a flavin-dependent enzyme that plays a physiological role in two important processes (sulfide detoxification and sulfide-dependent respiration). Two mechanisms of action for this enzyme have been proposed[131] that involve a common anionic intermediate that is stabilized by an anion-π interaction. These suggestions were backed by analysis of the X-ray structures of succinate dehydrogenates available in the Protein Data Bank (PDB) and using DFT calculations.

Our group[132] have also studied long-range effects in anion-π interactions and their crucial role in the inhibition mechanism of *mycobacterium tuberculosis* malate synthase. In this enzyme a catalytic Mg^{2+} unit is located at the bottom of the cavity, and plays a very important role. Recently, the development of effective antituberculosis drugs based on phenyldiketo acids (PDKAs) has been reported.[133] Interestingly, all the crystal structures of malate synthase-inhibitor complexes exhibit close contact between the carboxylate of ASP633 and the face of the aromatic ring of the inhibitor (see Figure 39). Remarkably, the replacement of the phenyl ring in PDKA by aliphatic moieties yields inactive inhibitors, suggesting that the aromatic moiety is crucial for inhibition. However, the aromatic ring of PDKA is not electron-deficient, and consequently, the anion-π interaction is expected to be very weak (dominated only by polarization effects). Combining an analysis of the recent X-ray structures of GlcB-PDKA complexes retrieved from the PDB and computational *ab initio* studies our group[135] demonstrated the prominent role of the Mg^{2+} ion in the active site, which promotes long-range enhancement of the anion-π interaction.

---

[129] X. Lucas, A. Bauzá, A. Frontera, D. Quiñonero, *Chem. Sci.* **2016**, *7*, 1038–1050.
[130] C. Estarellas, A. Frontera, D. Quiñonero, P. M. Deyà, *Chem. Asian J.* **2011**, *6*, 2316–2318.
[131] A. Bauzá, D. Quiñonero, P. M. Deyà, A. Frontera, *Chem. Asian J.* **2013**, *8*, 2708–2713.
[132] A. Bauzá, D. Quiñonero, P. M. Deyà, A. Frontera, *Chem. Eur. J.* **2014**, *20*, 6985–6990.
[133] I. V. Krieger, J. S. Freundlich, V. B. Gawandi, J. P. Roberts, V. B. Gawandi, Q. Sun, J. L. Owen, M. T. Fraile, S. I. Huss, J.-L. Lavandera, T. R. Ioerger, J. C. Sacchettini, *Chem. Biol.* **2012**, *19*, 1556–1567.

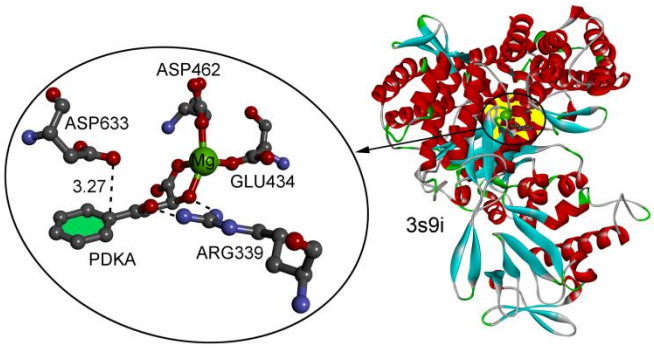

Figure 39. X-ray structure of the PDB ID 3S9I is represented and the anion-π interaction observed in the active site between ASP633 and the PDKA inhibitor is highlighted. Distance in Å.

One of the latest examples where the anion-π interaction has been exploited was reported by Stoddart's group.[134] They have synthesized a remarkably electron-poor cavity, namely Blue-Cage^{6+}. It is a macrobicyclic cyclophane composed of six pyridinium rings fused with two central triazines and bridged by three paraxylylene units. It is a powerful receptor for trapping polycyclic aromatic hydrocarbons and anions (see Figure 40). The presence of either PF_6^- or coronene inside the cavity (establishing anion-π or π-π interactions respectively) is supported by X-ray crystallography.

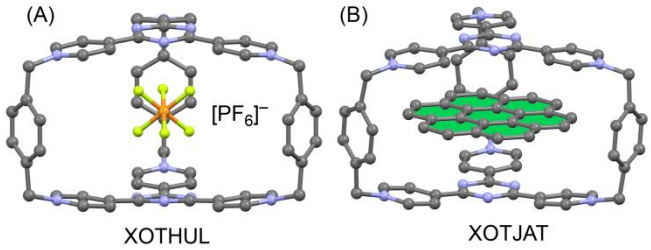

Figure 40. Crystal structures of the complexes between Blue-Cage^{6+} host and PF_6^- (A) and coronene (B) guests reported by Stoddart and coworkers.[134] The CSD reference codes are indicated.

1.4. Concluding remarks

In this chapter the physical nature of the intermolecular bonding interaction that can exist between electron-rich entities (anionic or charge neutral) and σ-/π-hole donor systems has been discussed. The selection of experimental studies together with the overview of CSD/PDB surveys highlights the ability of σ- and π-hole interactions to influence the molecular structure and function of both artificial and Natural systems. While some σ-/π-holes have been known for years (e.g. halogens, carbonyls, electron-deficient aromatics), others have only been marked as potential supramolecular synthons in the past decade or so (e.g. tetrel bonding). The main aim of this thesis is to point out that 'unconventional' σ-hole and π-hole interactions are fundamentally similar to 'conventional' ones, and might thus be equally useful.

[134] N. Hafezi, J. M. Holcroft, K. J. Hartlieb, E. J. Dale, N. A. Vermeulen, C. L. Stern, A. A. Sarjeant, J. F. Stoddart, *Angew. Chem. Int. Ed.* **2015**, *54*, 456–461.

Chapter 2

Tetrel bonding Interactions

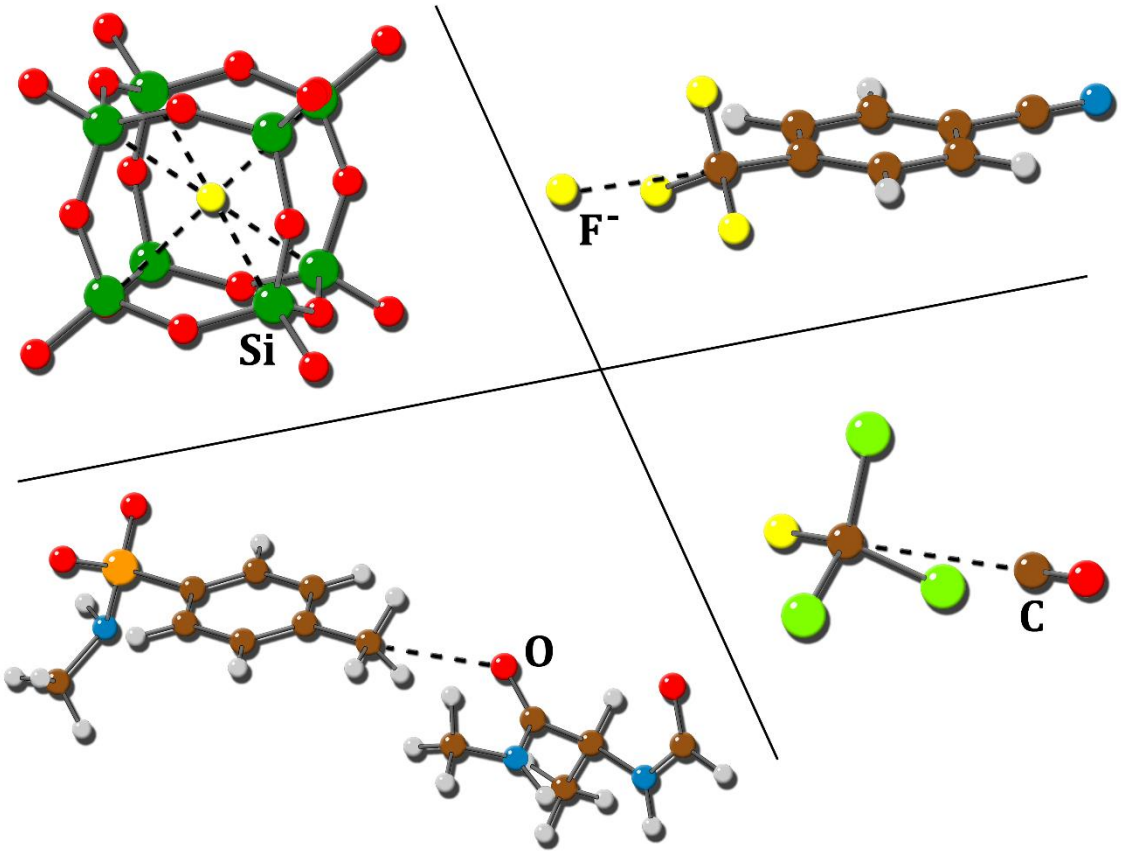

2.1 Preface and Objectives

This chapter is devoted to the study of σ-hole interactions where tetrel atoms act as Lewis acid compounds. The chapter is divided into four sections: firstly *section 2.2.* empasses the "rediscovery" of a new supramolecular bond, the tetrel bonding interaction. This term was simultaneously coined by our research group and others,[86a,87,88,90] paving the way for the re-naissance of a novel noncovalent force. In addition to the theoretical calculations presented, a CSD search was performed, remarking the importance of this interaction in solid state chemistry. Secondly, in *section 2.3.* the directionality of tetrel bonding interactions involving sp^3 carbon atoms is analyzed using a combined theoretical and crystallographic study by means of the CSD. These results highlight the strong directionality of the interaction, as well as energetic similarities between tetrel bonding and CH-π interactions. Thirdly, in *section 2.4.* the role of carbon···carbon interactions involving atmospheric gases such as CO_2 and CFC molecules has been investigated using high level *ab initio* calculations. In addition, cooperative effects between hydrogen and tetrel bonding interactions are also analysed. Finally, in *section 2.5.* the importance of tetrel bonding interactions in biological systems is evaluated using a combined theoretical and PDB study. Particularly, the ability of Zn-porphirines to establish this type of interaction remarks the influence of tetrel bonding interactions in the stabilization of protein-ligand complexes involving the heme group.

The main objectives of this chapter are listed below:

- Understanding in a proper way the physical nature and stability properties of the tetrel bonding interaction.

- Analysing the directionality features of the tetrel bonding interaction involving sp^3 carbon atoms, which are part of a vast quantity of substrates in organic chemistry.

- Evaluating the role of tetrel bonding interactions in the fields of atmospheric chemistry and biological systems.

2.2. Tetrel bonding interaction: a rediscovered supramolecular force?

2.2.1. Abstract

A tetrel bond is a directional noncovalent interaction between a covalently bonded atom of Group IV and a negative site, for example, the lone pair of a Lewis base or an anion. It involves a region of positive electrostatic potential (σ-hole), and energetically, they are comparable to hydrogen bonds and other σ-hole-based interactions.

2.2.2. Introduction

Noncovalent bonding interactions are crucial in many chemical and biological phenomena and they have been intensively investigated for many years.[135] The hydrogen bond (AH···D) is probably the most studied and analyzed noncovalent interaction, where A (acceptor) can be basically any atom more electronegative than H and D (donor) can be any entity with the ability to act as an electron donor (lone pair, π-system, anion, etc.).[136] Among many interactions, those involving halogen, chalcogen and pnicogen atoms have attracted considerable attention in recent years and they are increasingly being recognized by scientists and used in supramolecular chemistry, crystal engineering and biochemistry.[70, 137] These interactions are moderately strong and directional basically due to the localization of a positive region on the extension of the covalent bonds (σ-hole) in the acceptor molecule. This class of interactions has been also observed for the group IV of elements. For instance, Si···N contacts have been described in the solid state structure of $Si(ONMe_2)_4$ and related compounds by Mitzel *et al.*[138,139] and Si···halide contacts have been described in perhalocyclohexasilane compounds.[140] Moreover, group IV interactions have been recently included as a subgroup of a general definition of σ-hole bonding interactions by Politzer and coworkers.[4c]

In this manuscript we coin the term *tetrel bonding* for describing the tendency of heavier tetrel atoms (Tr) to interact with anions or lone pair possessing atoms (group IV of elements are also referred to as tetrels). The binding features and structural properties of tetrel bonding are discussed, several fascinating X-ray structures are selected to illustrate the importance of this interaction, and a survey of the Cambridge Structure Database (CSD) suggests that the tetrel bonding is

---

[135] a) *Encyclopedia of Supramolecular Chemistry*, New York, **2004**; b) K. Ariga, T. Kunitake, *Supramolecular Chemistry-Fundamentals and Applications*, Springer-Verlag, Heidelberg, **2006**; c) *Supramolecular Chemistry: From Molecules to Nanomaterials*, John Wiley & Sons, Chichester, **2012**.

[136] E. Arunan, G. R. Desiraju, R. A. Klein, J. Sadlej, S. Scheiner, I. Alkorta, D. C. Clary, R. H. Crabtree, J. J. Dannenberg, P. Hobza, H. G. Kjaergaard, A. C. Legon, B. Mennucci, D. Nesbitt, *J. Pure Appl. Chem.* **2011**, *83*, 1619–1636.

[137] a) A. Priimagi, G. Cavallo, P. Metrangolo, G. Resnati, *Acc. Chem. Res.* **2013**, *46*, 2686–2695; b) S. Scheiner, *Acc. Chem. Res.* **2013**, *46*, 280–288.

[138] N. W. Mitzel, U. Losehand, *Angew. Chem. Int. Ed.* **1997**, *36*, 2807–2809.

[139] N. W. Mitzel, A. J. Blake, D. W. H. Rankin, *J. Am. Chem. Soc*. **1997**, *119*, 4143–4148.

[140] S.-B. Choi, B.-K. Kim, P. Boudjouk, D. G. Grier, *J. Am. Chem. Soc*. **2001**, *123*, 8117–8118.

common in X-ray structures. The tetrel bonding is expected to be an effective and reliable instrument in crystal engineering, supramolecular chemistry, biochemistry, etc. As far as our knowledge extends, this term has not been used before to describe this interaction that has been scarcely studied in the literature.

Recently, P. G. Taylor *et al.*[95] have reported that the synthesis of spherosilicates is significantly improved using n-butylammonium fluoride (TBAF) as a catalyst. Interestingly, during the reaction work-up a new class of cage compound was obtained showing a fluoride ion perfectly centred within the octasilsesquioxane cage (see Figure 41).[96] Using NMR data the authors conclude that it essentially resembles a "naked" uncoordinated fluoride ion. These fluoride-encapsulated octasilsesquioxane cages can be used as small models for studying the environment that exist in zeolites. It is well known that fluoride anions act as templates in zeolite synthesis and also act as a stabilizing agents for the zeolite building unit via electron density transfer into the framework of silicon atoms.[97] This type of encapsulated compounds have been also reported for germanium based T8 cages.[98]

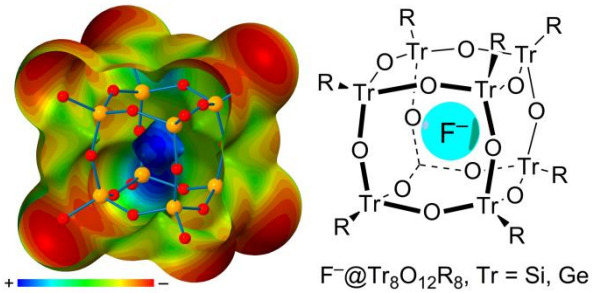

Figure 41. Right: Schematic representation of a F^- encapsulated inside a $Tr_8O_{12}R_8$ cage. Left: MEPS of $SiO_{12}(OH)_8$ cage.

2.2.3. Theoretical methods and CSD search criteria

The geometries of the complexes reported in this study have been optimized at the RI-MP2/aug-cc-pVDZ level of theory by means of the TURBOMOLE 6.4 software.[141] The interaction energies were calculated with correction for the basis set superposition error (BSSE) by using the Boys-Bernardi counterpoise technique.[142] Either C_{2v} or D_{4h} symmetry groups were imposed for the optimization of the complexes. The minimum nature of complexes **1–15** has been confirmed by performing frequency calculations at the same level of theory. All complexes apart from **2** and **3** are true minimum (N_{Imag} = 0). Complexes **2** and **3** have one negative frequency that corresponds to a transition state connecting the bifurcated tetrel-bonded complex with the two equivalent single complexes. The MEP values where computed at the MP2/aug-cc-pVDZ level of theory using Gaussian 09 software package.[143] The MEP surfaces were plotted using Spartan'10, v1.10.[144]

[141] R. Ahlrichs, M. Bär, M. Hacer, H. Horn, C. Kömel, *Chem. Phys. Lett.* **1989**, *162*, 165–169.
[142] S. B. Boys, F. Bernardi, *Mol. Phys.* **1970**, *19*, 553–566.
[143] Gaussian 09, Revision B.01, M. J. Frisch, G. W. Trucks, H. B. Schlegel, G. E. Scuseria, M. A. Robb, J. R. Cheeseman, G. Scalmani, V. Barone, B. Mennucci, G. A. Petersson, H. Nakatsuji, M. Caricato, X. Li, H. P. Hratchian, A. F. Izmaylov, J. Bloino, G. Zheng, J. L. Sonnenberg, M. Hada, M. Ehara, K. Toyota, R. Fukuda, J. Hasegawa, M. Ishida, T. Nakajima, Y. Honda, O. Kitao, H. Nakai, T. Vreven, J. A. Montgomery, Jr., J. E. Peralta, F. Ogliaro, M. Bearpark, J. J. Heyd, E. Brothers, K. N. Kudin, V. N. Staroverov, R. Kobayashi, J.

The Cambridge Structure Database (CSD, version 5.34, November 2012, including three updates) was inspected using ConQuest (version 1.15). Only intermolecular distances were considered and powder structures were omitted from the search. Two queries were drawn to retrieve initial datasets containing tetravalent tetrel atoms (Tr = Si, Ge, Sn) and an electron-rich atom (El.R. = a halogen atom or a charge neutral oxygen atom). The intermolecular Tr ···El.R. distance (*d*) was set to the sum of their respective van der Waals radii + 2.5 Å. These data were then binned with 0.05 Å intervals and the hit fraction (i.e. $N_{d\ -\ d+0.05Å}/N_{total} \times 100\%$) plotted as a function of *d*. As these plots were overcrowded by the data at longer distances, the cut-off distance of the plots used was set to $\Sigma_{vdWaals+0.5}$ Å (when there were few data points the resolution used was 0.1 Å). Integration to assess overlap of van der Waals shells was performed until the nearest data point of the data binned with 0.05 Å increments.

For the distances involving R_4**Si**···Hlg (See Figure S1), the majority of data is found above the $\Sigma_{vdWaals}$ benchmark, yet small peaks are observed at shorter distances (e.g., centred around 3 Å for Cl). For the distances involving R_4Si···**F**, these data come from cage-like structures such as the one shown in Figure 41 (BIDFIE, BIDFOK, CANCUR, IVEPUV, OJUYIB, WAVYAV, WAVYEZ, WAVYID, WAVYOJ, and WIJPUB). For R_4Si···**Cl** most data stem from Si_6Cl_{12}···Cl interactions (NENLOH, LECXAU, and LECXIC) and two originate from QOMBID (see also Figure 43). For R_4Si···**Br** most data originate from the Si_6Br_{12}···Br interactions in AZEBEN and one is found in FUFXAF10. For R_4Si···**I** most data involve a Si_6Hlg_{12}···I interaction (AZEBAJ and AZEBIR) and one was found within OYOMOZ (see also Figure 43).

2.2.4. Results and discussion

We have computed the interaction energies of fluoride complexes with $Tr_8O_{12}(OH)_8$ cages (Tr = Si, Ge and Sn), see section 2.2.3. for computational details. It can be observed that the binding energies are very large and negative indicating a strong interaction. Consistent with related σ-hole based interactions, the binding energy becomes more favourable toward the heavier tetrels. Since the fluoride establishes eight tetrel bonding interactions simultaneously the charge transfer is very large (> 50% of the charge). In terms of energetic features, each individual F^-···Tr interaction ranges 11–15 kcal/mol. The optimized Si and Ge complexes are shown in Figure 42

Normand, K. Raghavachari, A. Rendell, J. C. Burant, S. S. Iyengar, J. Tomasi, M. Cossi, N. Rega, J. M. Millam, M. Klene, J. E. Knox, J. B. Cross, V. Bakken, C. Adamo, J. Jaramillo, R. Gomperts, R. E. Stratmann, O. Yazyev, A. J. Austin, R. Cammi, C. Pomelli, J. W. Ochterski, R. L. Martin, K. Morokuma, V. G. Zakrzewski, G. A. Voth, P. Salvador, J. J. Dannenberg, S. Dapprich, A. D. Daniels, Ö. Farkas, J. B. Foresman, J. V. Ortiz, J. Cioslowski, D. J. Fox, Gaussian, Inc., Wallingford CT, 2009.

[144] Y. Shao, L.F. Molnar, Y. Jung, J. Kussmann, C. Ochsenfeld, S.T. Brown, A.T.B. Gilbert, L.V. Slipchenko, S.V. Levchenko, D.P. O'Neill, R.A. DiStasio Jr., R.C. Lochan, T. Wang, G.J.O. Beran, N.A. Besley, J.M. Herbert, C.Y. Lin, T. Van Voorhis, S.H. Chien, A. Sodt, R.P. Steele, V.A. Rassolov, P.E. Maslen, P.P. Korambath, R.D. Adamson, B. Austin, J. Baker, E.F.C. Byrd, H. Dachsel, R.J. Doerksen, A. Dreuw, B.D. Dunietz, A.D. Dutoi, T.R. Furlani, S.R. Gwaltney, A. Heyden, S. Hirata, C-P. Hsu, G. Kedziora, R.Z. Khalliulin, P. Klunzinger, A.M. Lee, M.S. Lee, W.Z. Liang, I. Lotan, N. Nair, B. Peters, E.I. Proynov, P.A. Pieniazek, Y.M. Rhee, J. Ritchie, E. Rosta, C.D. Sherrill, A.C. Simmonett, J.E. Subotnik, H.L. Woodcock III, W. Zhang, A.T. Bell, A.K. Chakraborty, D.M. Chipman, F.J. Keil, A.Warshel, W.J. Hehre, H.F. Schaefer, J. Kong, A.I. Krylov, P.M.W. Gill, M. Head-Gordon, *Phys. Chem. Chem. Phys.* **2006**, *8*, 3172–3191.

and the related X-ray structures retrieved from the CSD are also shown for comparison purposes. The energetic results gathered in Table 2 are in disagreement with experimental results, which suggest that the interaction of F^- with the Si atoms is almost negligible. This is based on the fact that fluoride ion makes very little difference to the structure. That is, the mean separation between the silicon atoms on opposite vertices of the cube is only slightly shorter in the fluoride encapsulated cage (5.306 Å) than in the free structure (5.381 Å) and the Si···F separation in these type of fluoride cages is ~2.65 Å, which is much longer than that of a full Si–F covalent bond (1.709 Å). This is certainly true in terms of covalent bonding (the absence of any measurable Si–F coupling has been used to confirm the low degree of silicon–fluoride interaction).

However in terms of noncovalent bonding, the reported changes on the ^{29}Si and ^{19}F NMR spectra along with structural changes (the Si atoms approximate to the F^- upon binding) are in agreement with a moderately strong noncovalent interaction, as those observed in Table 2. Moreover, the molecular electrostatic potential (MEP) surface mapped onto the van der Waals surface shows a small region of positive potential in the center of the cage (see Figure 41).

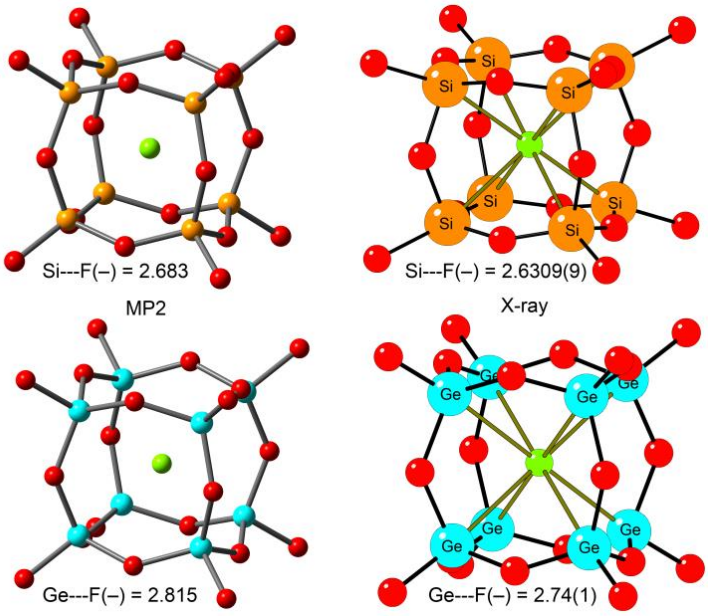

Figure 42. RI-MP2/aug-cc-pVDZ $F^-@Tr_8O_{12}(OH)_8$ optimized complexes and the equivalent X-ray structures. Distances in Å.

Table 2. Interaction energies without and with the basis set superposition error (ΔE and ΔE_{CP} in kcal/mol, respectively), and equilibrium distances (R_e, Å) for $F^-@Tr_8O_{12}(OH)_8$ complexes at the RI–MP2/aug-cc-pVDZ level of theory.

Complex	ΔE	ΔE_{CP}	$\Delta E_{CP}/8$	R_e
$F^-@Si_8O_{12}(OH)_8$	–98.0	–89.3	–11.2	2.683
$F^-@Ge_8O_{12}(OH)_8$	–116.8	–108.9	–13.6	2.815
$F^-@Sn_8O_{12}(OH)_8$	–124.8	–119.1	–14.8	3.113

An interesting experimental finding that nicely illustrates the importance of noncovalent tetrel bonding interaction is the formation of a crystalline chloride bridged disiloxane.[145] The X-ray structure is shown in Figure 43 (QOMBID, top) and the bifurcated tetrel bond was defined by the original authors as a dative bond to each of the silicon centers. This is confirmed by reference to the Si-Cl distances, 2.887 and 2.731 Å, respectively, which are both substantially longer than normal covalent Si-Cl bonds (2.05 ± 0.03 Å)[145] and significantly shorter than the sum of the corresponding van der Waals radii. Furthermore, in Figure 43 (bottom) we show the X-ray structures of two binuclear pentacoordinate silicon complexes of diketopiperazine. By means of variable-temperature NMR spectroscopy and X-ray crystallography experiments the S_N2 reaction mechanism has been studied for five differently substituted analogous structures (X = F, Cl, OTf, Br, and I).[146] Two extreme cases are shown in Figure 43, a covalent bond (F-Si, OYOMIZ) is observed for a very poor leaving group (F^-) and a tetrel bond (I···Si, OYOMOZ) is clearly formed for a good leaving group (I^-).

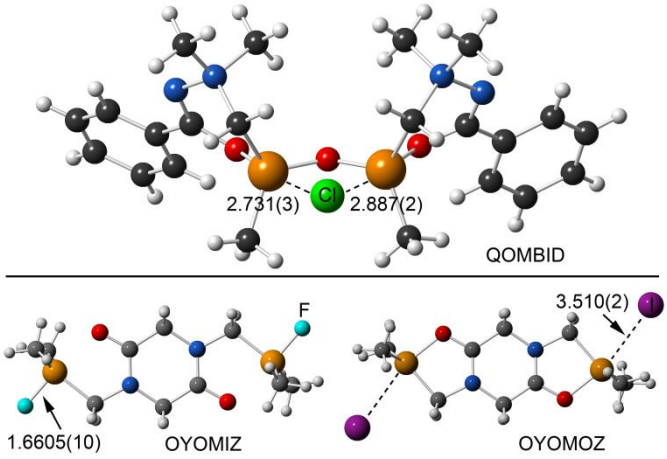

Figure 43. X-ray fragments of CSD structures QOMBID, OYOMIZ and OYOMOZ. Distances in Å.

We have studied computationally the tetrel bonded complexes of perfluorodisiloxane, as a theoretical model of the experimental structure described above (QOMBID, see Figure 43), with halides. In addition we have extended our study to perfluorodigermoxane and perfluorodistannoxane in order to analyze the influence of the tetrel atom on the interaction strength. In addition to the anionic donors (F^-, Cl^- and Br^-) we have also included in the study neutral donor molecules (H_2O and H_2S), as represented in Figure 44 (top). Previously to the optimization of the complexes we have calculated the MEP surfaces of the F_3Tr-O-TrF_3 (Tr = Si, Ge and Sn) molecules. The three surfaces are very similar and we have only represented the one obtained for F_3Si-O-SiF_3 in Figure 44 (bottom). It can be observed the presence of four equivalent σ-holes at one side of the molecule (Figure 44, bottom left) and other two σ-holes at both ends of the molecule (Figure 44, bottom middle). These six σ-holes are almost isoenergetic. Opposite to the four equivalent σ-holes, the most positive part of the MEP is found as a consequence of

[145] I. Kalikhman, O. Girshberg, L. Lameyer, D. Stalke, D. Kost, *J. Am. Chem. Soc*. **2001**, *123*, 4709–4716.
[146] S. Muhammad, A. R. Bassindale, P. G. Taylor, L. Male, S. J. Coles, M. B. Hursthouse, *Organometallics* **2011**, *30*, 564–571.

the superposition of two σ-holes along the bisectrix of the Si-O-Si angle (obtuse part). The MEP value at this point is 37 kcal/mol for Si, 41 kcal/mol for Ge and 45 kcal/mol for Sn. Therefore the σ-hole becomes more positive toward the heavier tetrels.

The binding energies and equilibrium distances for the anionic complexes **1**–**9** are gathered in Table 3. The energies are very large in fluoride complexes due to the partial covalent bond as suggested by the very short equilibrium distances. The energetic features of complexes involving Cl^- and Br^- are more modest and comparable to the explained above for the $Tr_8O_{12}(OH)_8$ cages. As predicted by the MEP surfaces, the energies are more favourable for the heavier tetrels and the charge transfer is very important (47–66%). It is interesting to note the variation of the Tr-O-Tr angle that increases on going from fluoride to bromide and decreases on going from Si to Sn to facilitate the simultaneous interaction with both tetrel atoms. The strong interaction energies observed for F^- complexes suggest that the observation of this interaction in solution would be difficult for this anion (S_N2 reaction will likely occur), however it would be possible for the higher halides.

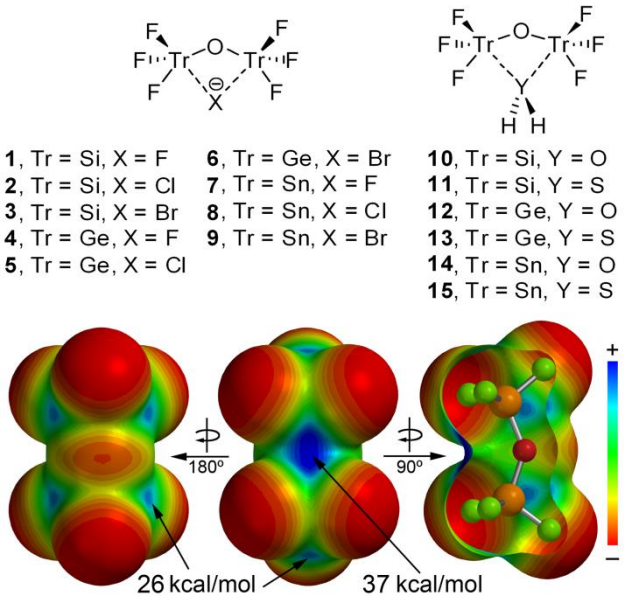

Figure 44. Top. complexes **1**-**15**. Bottom: MEP of the F_3Tr-O-TrF_3 molecules.

Table 3. Interaction energies without and with the BSSE (ΔE and ΔE_{CP} in kcal/mol, respectively), equilibrium distances (R_e, Å), Tr-O-Tr angle and Merz-Kollman charges (Q_{MK}, e) for complexes **1**–**9** at the RI-MP2/aug-cc-pVDZ level of theory.

Complex	ΔE	ΔE_{CP}	R_e	∠Tr-O-Tr	Q_{MK}
1	–89.7	–83.6	1.917	109.6	–0.43
2	–38.9	–34.0	2.497	125.0	–0.45
3	–28.9	–24.0	2.726	130.1	–0.49
4	–103.9	–96.5	1.994	108.3	–0.48
5	–57.6	–51.5	2.490	119.3	–0.40
6	–47.7	–41.7	2.662	122.3	–0.38
7	–121.0	–115.7	2.147	108.0	–0.53
8	–80.6	–75.4	2.621	117.0	–0.40
9	–72.2	–66.8	2.774	119.3	–0.34

The binding energies and equilibrium distances for the neutral complexes **10–15** are summarized in Table 4. The energies are obviously less favourable than those computed for the anionic complexes due to different electrostatic nature of the donor atom. The equilibrium distances are longer and consequently the Tr-O-Tr angle considerably increases with respect to the anionic complexes to facilitate the interaction of the lone pairs of the O/S atoms with the σ-holes. The interaction energies of the water complexes are considerable more favorable than the H_2S ones and the equilibrium distances shorter, in line with the higher basicity of the oxygen atom. The geometries of some representative complexes are shown in Figure 45. In all complexes the X⁻···Tr-F angle is close to 180°, indicating that the interaction is highly directional, similarly to the halogen bonding interaction.

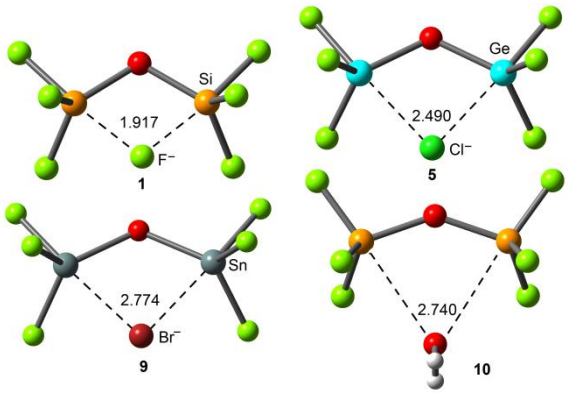

Figure 45. RI-MP2/aug-cc-pVDZ optimized geometries of some representative F_3Tr-O-TrF_3 complexes. Distances in Å.

Table 4. Interaction energies without and with the BSSE (ΔE and ΔE_{CP} in kcal/mol, respectively), equilibrium distances (R_e, Å) and Tr-O-Tr angle for complexes **10–15** at the RI-MP2/aug-cc-pVDZ level of theory.

Complex	ΔE	ΔE_{CP}	R_e	∠Tr–O–Tr
10	–9.3	–6.2	2.740	140.5
11	–2.8	–1.1	3.748	147.5
12	–15.2	–9.9	2.487	127.2
13	–3.3	–1.2	3.647	136.8
14	–24.3	–19.1	2.521	121.4
15	–8.3	–4.6	3.159	135.2

Finally, we would like to highlight the solid state structure of tetramethylammonium fluoride octadecasil that has been elucidated based on powder X-ray diffraction data.[99] The topology is defined by rhombododecahedral [$4^6 6^{12}$] cages, which are linked together by hexahedral [4^6] cages, commonly referred to as double 4-rings (D4R), see Figure 46. Interestingly, the octadecasil structure is acting as a ditopic carcerand, where the fluoride guest is confined in the D4R unit forming eight tetrel bonds and the counterion is located in the interior of the rhombododecahedral cages forming a large number of C–H···O interactions. The oxygen atoms of the D4R units are pointing toward the exterior of the cage and concurrently toward the interior of the [$4^6 6^{12}$] cage facilitating both tetrel bonding interactions in the former and the hydrogen bonding interaction in the latter.

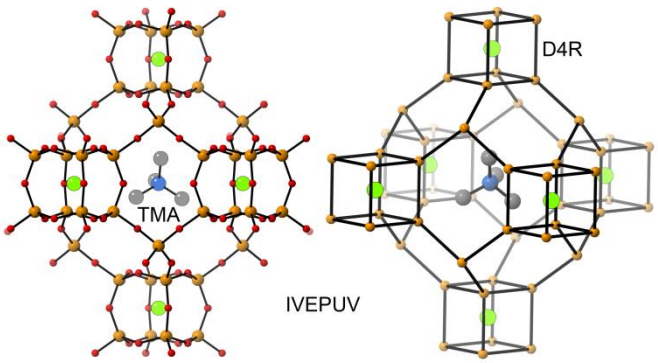

Figure 46. Partial view of the X-ray structure of TMA^+F^--octadecasil, showing D4R units with the guest fluoride and the [$4^6 6^{12}$] cage with tetramethylammonium ion. For clarity, the oxygen atoms have been omitted in the representation shown in the right.

2.2.5. CSD survey

The Cambridge Structure Database was inspected to assess whether tetrel bonding could be a generally occurring interaction within crystal structures (see SI for details). Table 5 lists some numerical data of intermolecular distances (d) between a tetravalent tetrel atom (Tr; Si, Ge, Sn) and an electron-rich atom (El.R.; O^0, F, Cl, Br, I) where $d = \Sigma_{vdWaals+0.5}$ Å. The amount of data where overlap of van der Waals shells was observed is listed separately and, for comparison, also expressed as percentage of the total amount of data. The fraction of van der Waals overlap seems to increase in the order Si < Ge < Sn and O ≤ F < Cl ≤ Br < I. The data for $R_4Si\cdots F$ seems an exception and manual inspection of the data revealed that about 1/3 of the cases of van der Waals overlap are found within (engineered) cage structures such as the one shown in Figure 41.[147] As a typical example, Figure 47 shows plots of the frequency count *vs.* the intermolecular $R_4Tr\cdots Cl$ distance; *idem* plots for the rest of the data given in Table 5 can be found in the supporting information and reveal similar features.

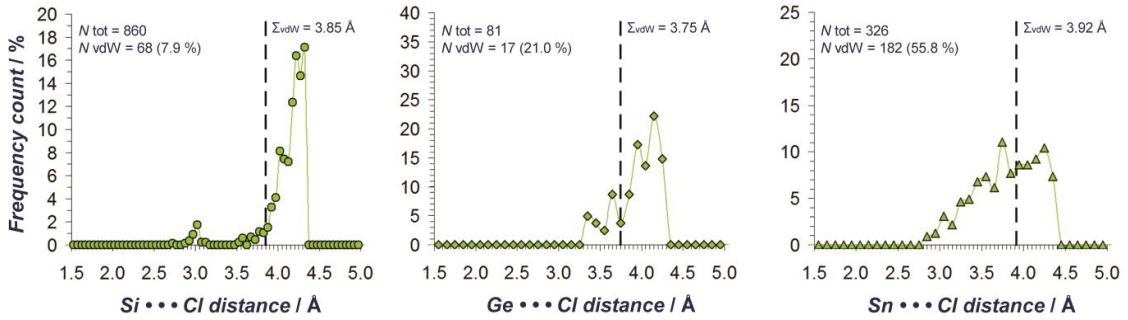

Figure 47. Plots of the frequency count (in %) as a function of the $R_3Tr\cdots Cl$ distance (in Å) for Tr = Si (left, green spheres); Ge (centre, green diamonds); and Sn (right, green triangles). The solid green lines are added as a guide to the eye and the vertical dashes black lines indicate the sum of the van der Waals radii of Tr and Cl. The inset numbers represent the total amount of data (N_{tot}) and the absolute and relative mount of data displaying van der Waals overlap.

[147] See CSD refcodes BIDFIE, BIDFOK, CANCUR, IVEPUV, OJUYIB, WAVYAV, WAVYEZ, WAVYID, WAVYOJ, and WIJPUB.

For the distances involving $R_4Si\cdots Cl$ (Figure 47, left), the majority of data is found above the $\Sigma_{vdWaals}$ benchmark, yet a small peak is observed centred around 3 Å. Such peaks are also present for the other halides as the interacting atom (not for oxygen, see SI for details). These Si···Hlg data are about 0.8 Å within the sum of the van der Waals radii of the elements involved. This means that these interactions are very significant, yet not as strong as a conventional Si–Hlg bond ($\Sigma_{vdWaals}$ -Si-Hlg < 1.76 Å). Such peaks were not found for $R_4Ge\cdots Cl$ (centre) and $R_4Sn\cdots Cl$ (right), but the relative amount of overlap of van der Waals shells clearly increases in the order Si < Ge < Sn. For $R_4Sn\cdots Cl$, more than half of the data actually is found within the ΣvdWaals benchmark (3.92 Å) and a number of short distances are found around 3 Å. The CSD data presented above clearly suggests that noncovalent interactions with the tetravalent tetrel entities investigated are rather common within the CSD (16% of all the data involve overlap of van der Waals shells). It must be stressed that the majority of these data are mere accidental occurrences rather than engineered. Actually, the very short (and relatively rare) Tr···El.R. distances highlighted in this paper imply that the strength of tetrel bonding can be significantly tweaked. Clearly this presents an opportunity for (supramolecular) chemists to further explore the potential of this novel interaction.

Table 5. Numerical overview of data retrieved from the Cambridge Stucture Database involving tetravalent Tetrel atoms and charge neutral Oxygen or a Halogen atom.

	R_4Si		R_4Ge		R_4Sn	
El.R:	Ntot[a]	NvdW[b]	Ntot[a]	NvdW[b]	Ntot[a]	NvdW[b]
O^0	3,449	118 (5.5 %)	626	177 (28 %)	678	293 (43 %)
F	1,030	143 (14 %)	48	2 (4.2 %)	109	35 (32 %)
Cl	860	68 (7.9 %)	81	17 (21 %)	326	182 (56 %)
Br	151	16 (11 %)	8	3 (38 %)	45	50 (44 %)
I	102	28 (28 %)	9	4 (44 %)	25	16 (64 %)

[a]Number of data with intermolecular distances ≤ the sum of the van der Waals radii of Tr+El.R.

[b]Number of data with intermolecular distances ≤ the sum of the van der Waals radii of Tr+El.R.+0.5Å.

2.2.6. Conclusions

In conclusion, in this manuscript we propose the use of tetrel bonding to refer to the noncovalent interaction between tetrel atoms acting as Lewis acids and any entity with the ability to act as an electron donor (lone pair, anion, etc.). Tetrel bonds have, as a minimum, comparable strength to hydrogen bonds and other σ-hole based interactions, they are highly directional and might act as a new possible molecular linker. The tetrel bonding interaction is expected to be involved in new effective and reliable instruments for crystal engineering, supramolecular chemistry and catalysis.

2.2.7. Acknowledgements

This work was funded by the MINECO of Spain (CONSOLIDER-Ingenio 2010 project CSD2010-0065, and project CTQ2011-27512, FEDER funds) and the Govern Balear (project 23/2011, FEDER funds). TJM acknowledges the School of Chemistry of the University of Bristol (UK).

2.2.8. Supporting information

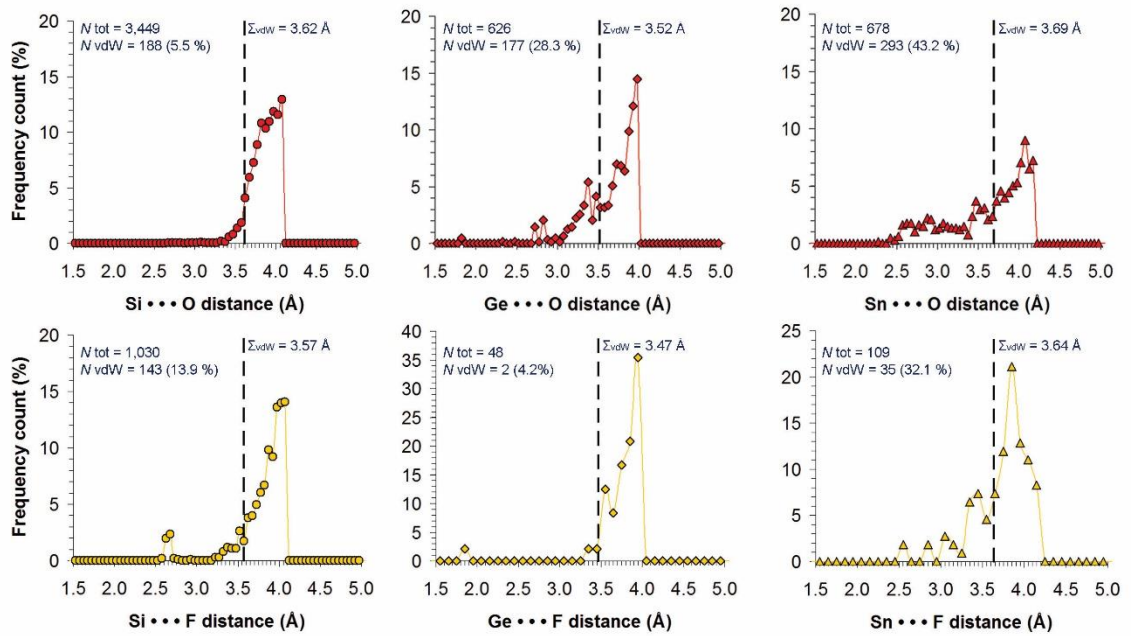

Figure S1. Plots of the frequency count (in %) as a function of the $R_3Tr\cdots El.R.$ distance (in Å) for Tr = Si (left, spheres); Ge (centre, diamonds); and Sn (right, triangles) and El.R. = O^0 (red); F (orange); Cl (green); Br (brown); I (purple). The solid lines are added as a guide to the eye and the vertical dashes black lines indicate the sum of the van der Waals radii of Tr+Cl. The inset numbers represent the total amount of data (N_{tot}) and the absolute and relative mount of data displaying van der Waals overlap. The small features around 1.8 Å for $R_3Ge\cdots O$ and $R_3Ge\cdots F$ are artefacts (covalent bonds mistaken for intermolecular contacts by ConQuest).

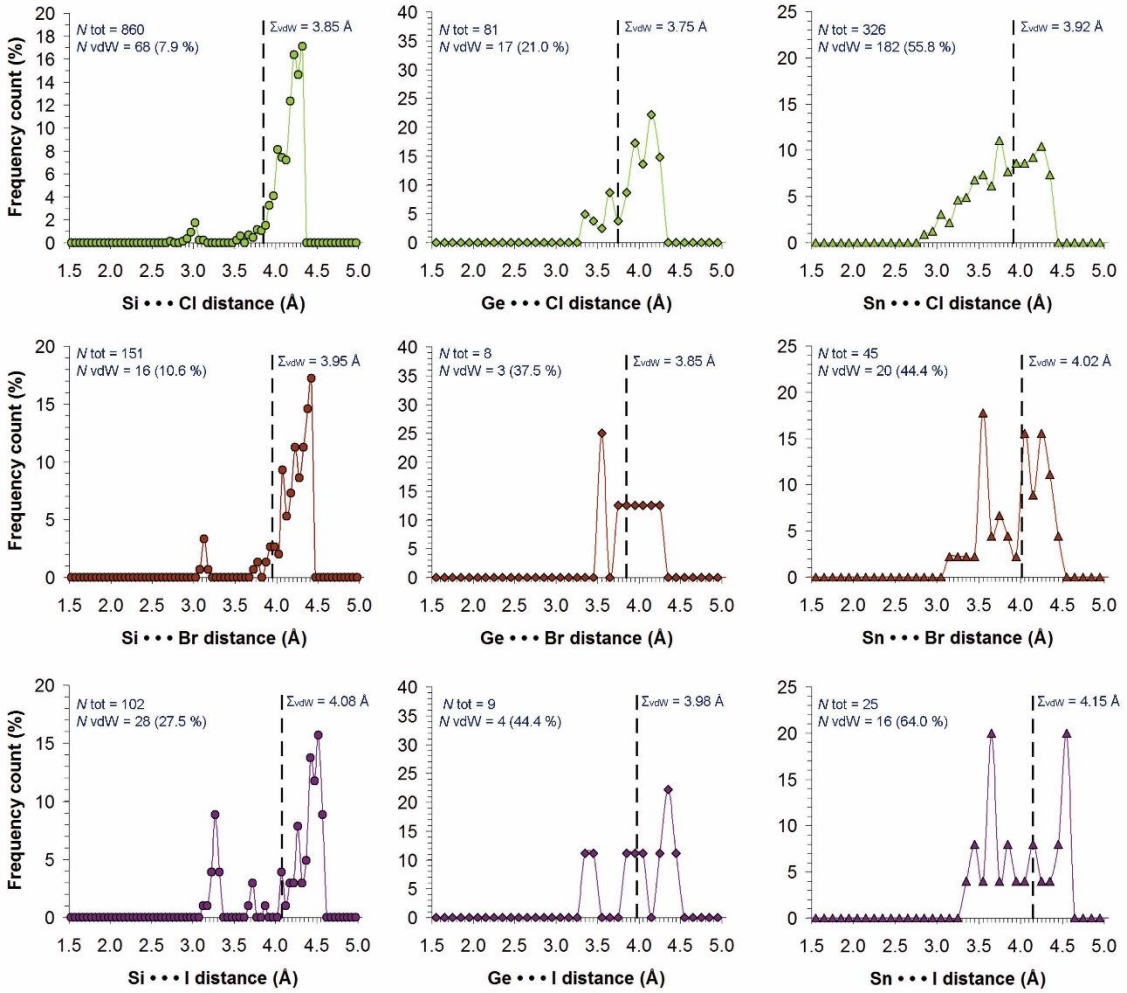

Figure S1 (cont). Plots of the frequency count (in %) as a function of the $R_3Tr\cdots El.R.$ distance (in Å) for Tr = Si (left, spheres); Ge (centre, diamonds); and Sn (right, triangles) and El.R. = O^0 (red); F (orange); Cl (green); Br (brown); I (purple). The solid lines are added as a guide to the eye and the vertical dashes black lines indicate the sum of the van der Waals radii of Tr+Cl. The inset numbers represent the total amount of data (N_{tot}) and the absolute and relative mount of data displaying van der Waals overlap. The small features around 1.8 Å for $R_3Ge\cdots O$ and $R_3Ge\cdots F$ are artefacts (covalent bonds mistaken for intermolecular contacts by ConQuest).

2.3. Noncovalent sp^3 carbon bonding with $ArCF_3$ is analogous to CH-π interactions.

2.3.1. Abstract

A combined CSD and *ab initio* study reveals that the interaction between the sp^3 C-atom in *para*-substituted $ArCF_3$ and electron-rich atoms is weak (<5 kcal/mol), somewhat directional, and thus comparable to CH-π interactions.

2.3.2. Introduction

Supramolecular chemistry and much of biology is concerned with intermolecular attractions that are reversible in the ambient temperature regime.[1,148] The sharing of a hydrogen atom (H) between a donor (D) and acceptor (A) entity, D–H···A hydrogen bonding,[149] is a particularly well established supramolecular binding motif varying in strength from very weak (~1 kcal/mol)[150] to very strong (~40 kcal/mol).[151] The bottom of the H-bonding spectrum consists of weakly polarized D–H entities (e.g. aliphatic or aromatic CH) and mildly electron-rich acceptor moieties (e.g. π-electrons).[152] While a single interaction is energetically unimpressive, when several weak hydrogen bonds work together they can stabilize protein structures[153] and contribute to the binding of proteins to ligands such as carbohydrates.[154]

Over the years, many other weak intermolecular forces have been identified as potentially relevant in (bio)chemical machineries: halogen bonding, π-π stacking, carbonyl-carbonyl, cation-π, anion-π and lone pair-π interactions.[155] Given this abundance of supramolecular synthons one may wonder what other electron-poor/rich entities Nature has to offer. Or better yet, which ones we might design ourselves.
Recent theoretical explorations have suggested that the chalcogen, pnicogen and tetrel atoms in their sp^3 hybridized form can be made electron-poor enough to

---

[148] H. J. Schneider, A. Yatsimirski, *Principles and Methods in Supramolecular Chemistry*, Wiley, Chichester, **2000**.
[149] G. R. Desiraju, *Angew. Chem. Int. Ed.* **2011**, *50*, 52–59.
[150] G. R. Desiraju, T. Steiner, *The Weak Hydrogen Bond in Structural Chemistry and Biology*, Oxford Univ. Press, Oxford, **1999**.
[151] J. W. Larson, T. B. McMahon, *Inorg. Chem*. **1984**, *23*, 2029–2033.
[152] a) M. Nishio, Y. Umezawa, J. Fantini, M. S. Weiss, P. Chakrabarti, *Phys. Chem. Chem. Phys*. **2014**, *16*, 12648–12683; b) M. Nishio, Y. Umezawa, K. Honda, S. Tsuboyamad, H. Suezawae, *CrystEngComm* **2009**, *11*, 1757–1788; c) M. Nishio, M. Hirota, Y. Umezawa, *The C–H/π Interaction: Evidence, Nature, Consequences*, Wiley-VCH: New York, **1998**.
[153] a) U. Samanta, D. Pal, P. Chakrabarti, *Proteins* **2000**, *38*, 288–300; b) M. J. Plevin, D. L. Bryce, J. Boisbouvier, *Nature Chem*. **2010**, *2*, 466–471; c) M. Brandl, M. S. Weiss, A. Jabs, J. Sühnel, R. Hilgenfeld, *J. Mol. Biol.* **2001**, *307*, 357–377.
[154] a) F. A. Quiocho, N. K. Vyas, *Nature* **1984**, *310*, 381–386; b) N. K. Vyas, M. N. Vyas, F. A. Quiocho, *Science* **1988**, *242*, 1290–1295; c) M. Nishio, *Phys. Chem. Chem. Phys*. **2011**, *13*, 13873–13900; d) Z. R. Laughrey, S. E. Kiehna, A. J. Riemen, M. L. Waters, *J. Am. Chem. Soc.* **2008**, *130*, 14625–14633; e) N. P. Barwell, A. P. Davis, *J. Org. Chem.* **2011**, *76*, 6548–6557.
[155] a) P. V. Hobza, K. Müller-Dethlefs, *Noncovalent Interactions: Theory and Experiment*, RSC publishing, **2010**; b) *Supramolecular Systems in Biomedical Fields*, RSC publishing, **2013**.

accommodate an electron-rich guest.[4c,5a,25b,85,86a,156,157] Surprisingly few studies have been dedicated to study the most abundant of these nuclei, namely R_4C.[90] It has recently been calculated that strong complexes (up to –42.3 kcal/mol) are formed between electron-rich entities and derivatives of small cycloalkane rings containing four cyano groups in the 1,1',2,2' positions.[86b] Moreover, this interaction was found to be highly directional by means of a thorough statistical evaluation of the Cambridge Structure Database (CSD).

In analogy to strong and weak hydrogen bonding, we wondered if perhaps weak noncovalent bonding with sp^3 hybridized carbon could have some relevance. Our approach was to conduct a rigorous statistical survey of the CSD together with quantum mechanical computations on the RI-MP2/def2-TZVP level of theory. For the present study we considered the (*para*-substituted) *α,α,α*-trifluorotoluene and for comparison regular (*para*-substituted) toluene (see Figure 48). Both these entities are very common in the CSD.

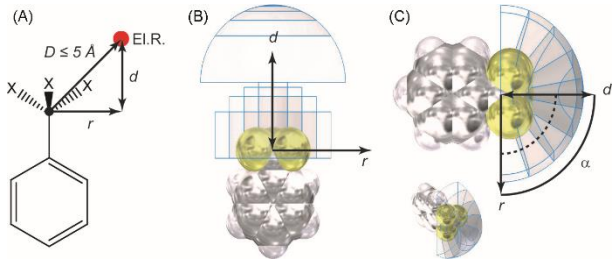

Figure 48. (A) Query used to inspect the CSD for intermolecular interactions between an electron-rich atom (El.R., N, P, As, O, S, Se, Te, F, Cl, Br, I or At) and (*para*-substituted) -C_6H_4-CX_3, where X = F, or H; (B-C) illustrations of the method used to assess directionality with X = F as example.

2.3.3. Theoretical methods and CSD search criteria

The energies of all complexes included in this study were computed at the RI-MP2/def2-TZVP level of theory. Since the estimated $[PhCF_3\cdots F]^-$ interaction energy is very weak (–0.6 kcal/mol) and it is in the limit of the accuracy of the theoretical method (RI-MP2/def2-TZVP), we have validated this energetic value using a higher level of theory. We have computed the interaction energy using a coupled cluster with single, double and triple excitations, CCSD(T),[158] and the same basis set. As a result, the interaction energy is –0.8 kcal/mol, in sharp agreement with the value computed at the RI-MP2/def2-TZVP level of theory. The calculations have been performed by using the program TURBOMOLE version 6.4.[141]

An illustration of the query used to obtain datasets from the CSD is shown in Figure 48A. An entry was considered a hit when the *inter*molecular distance (*D*) between the carbon atom of the -CX_3 moiety (X = F, H) and any electron-rich atom (red, El.R. = N, P, As, O, S, Se, Te, F, Cl, Br, I or At) was ≤ 5 Å. These data are thus located within a sphere with a radius of 5Å, centred on the sp^3 C-atom. The distance *d* signifies the spatial separation between El.R. and an imaginary plane that is perpendicular to the

[156] T. Clark, *WIREs Comp. Mol. Sci.* **2013**, *3*, 13–20.
[157] A. Bauzá, T. J. Mooibroek, A. Frontera, *Angew. Chem. Int. Ed.* **2013**, *52*, 12317–12321.
[158] J. A. Pople, M. Head-Gordon, K. Raghavachari, *J. Chem. Phys.* **1987**, *87*, 5968–5975.

aryl ring plane and runs through the sp^3 C-atom. Using *D*, *d*, and Pythagoras's theorem, the parallel displacement parameter *r* could be computed. The angle *α* between the aryl ring, the sp^3 C-atom and El.R. was measured as well. Illustrated in Figure 48B-C is the method used to assess directionality, this method has been very successful in establishing the directional character of other weak intermolecular interactions.[159]

The parameter *P*(*x*) signifies the distribution of the data along some metric parameter *x*, that has been corrected for the volume occupied by the host and for a random scattering of data. When $P \neq 1$, a *non-accidental clustering* of data is established and $P > 1$ is indicative of an attractive interaction. For this study, *P* has been made dependant on both *r* and *α* (see Figure 48A and B). The data for *P*(*r*) was limited to data with $\alpha \geq 90°$, so that the hits are located within a hemisphere centred at CX_3. The data for *P*(*α*) was limited to data contained within spherical cones that were truncated 2Å above and below the aryl ring plane (Figure 48C only illustrates bodies with *α* in between 90 and 180°). As an example equation 1 details how *P*(*r*) was obtained.

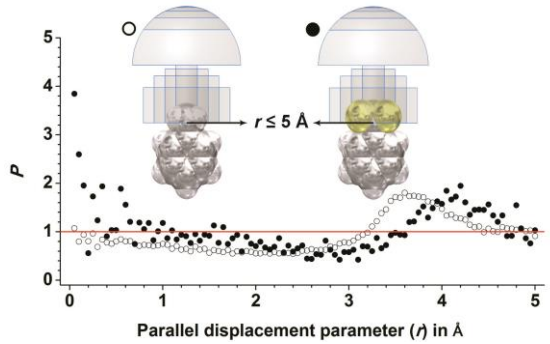

Figure 49. Directionality plots of *P vs. r* for $PhCX_3\cdots$El.R. with X = H (○, N_{tot} = 88,305) and X = F (●, N_{tot} = 4,631). Data used were limited to $\alpha \geq 90°$.

2.3.4. Results and discussion

The *P* versus *r* plots for $PhCH_3$ (empty circles) and $PhCF_3$ (black circles) are shown in Figure 49. For both central groups, $P > 1$ at longer *r*-values ($r \approx 3.6$ Å for $PhCH_3$ and 4.2 Å for $PhCF_3$), indicating hydrogen bonding to the H-atoms *ortho* to the CX_3 moiety (and possibly also halogen bonding to F). At intermediate *r*-values *P* is below unity, indicating a relative depletion of data. Interestingly, with $r \leq 1.0$-0.5 Å the *P*-values seem to increase slightly to about 1 for $PhCH_3$ and above 1 for $PhCF_3$. These data indicate that the interaction between El.R. and both $PhCX_3$ groups is slightly directional linearly (e.g. *α* close to 180°), but more so when X = F. A very similar pattern emerges from the *P* versus *α* plots shown in Figure 50.

[159] a) T. J. Mooibroek, P. Gamez, *CrystEngComm* **2013**, *15*, 1802–1805; b) T. J. Mooibroek, P. Gamez, *CrystEngComm* **2013**, *15*, 4565–4570; c) K. E. Ranaghan, J. E. Hung, G. J. Bartlett, T. J. Mooibroek, J. N. Harvey, D. N. Woolfson, W. A. van der Donk, A. Mulholland, *Chem. Sci*. **2014**, *5*, 2191–2199.

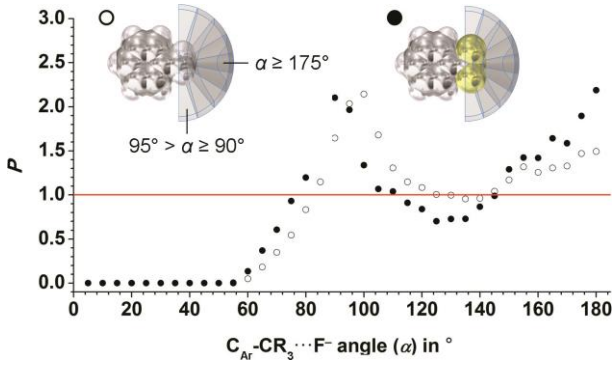

Figure 50. Directionality plots of *P vs.* α for $PhCX_3\cdots$El.R. with X = H (○, N_{tot} = 53,232) and X = F (●, N_{tot} = 3,037). Data used were limited to data 2 Å above or below the aryl plane.

That is; $P \geq 1$ around $\alpha \approx 90\text{-}100°$ (hydrogen and perhaps halogen bonding); and $P \geq 1$ at $\alpha > 150°$ (some linear directionality of the $PhCX_3\cdots$El.R. interaction).
It was further assessed how exactly the data is distributed within the data characterized by $r \leq 1$ Å. Thus, the cumulative hit fraction was plotted as a function of the van der Waals corrected $PhR_3C\cdots$El.R. distance, as is shown in Figure 51. From these data it is clear that hardly any overlap of van der Waals shells is present between El.R. and the sp³ C-atom in $PhCF_3$ (0.42 %, black circles). For $PhCH_3$ this is 6.62% (open circles). Both these values can be considered as very low and comparable to weak CH-π interactions where typically > 10% van der waals overlap is observed.[160] It can be noted however that the feature for $PhCF_3$ is much steeper than that for $PhCH_3$, meaning that the data for $PhCF_3$ is grouped more.

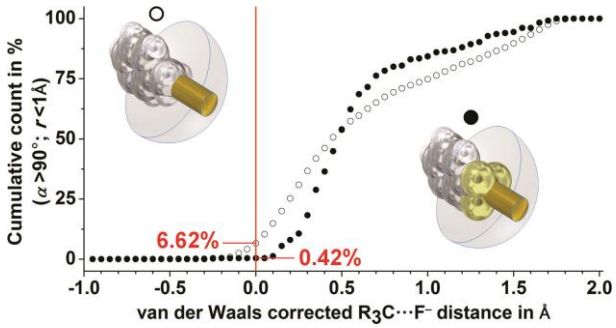

Figure 51. Assesment of overlapping van der Waals shells for data with $\alpha \geq 90°$ and $r \leq 1$ Å in $PhCX_3\cdots$El.R. pairs with X = H (○, N_{tot} = 2,888) and X = F (●, N_{tot} = 236).

In order to relate the above findings from crystal structure data to energetic values, the association of a F^- anion with $PhCX_3$ (X = H, F) was examined in some detail on the MP2/def2-TZVP level of theory, as is illustrated in Figure 52 (see SI for details).
First, the energetic minimum (E_{min}, blue dot in Figure 52A) along the ArC–CX_3 bond was computed for both central groups. To mimic the crystallographic data obtained as a function of *r*, the F^- anion was then moved away from this origin within the xz-plane π (see Figure 52A-B).

[160] T. J. Mooibroek, P. Gamez, *CrystEngComm* **2012**, *14*, 8462–8467.

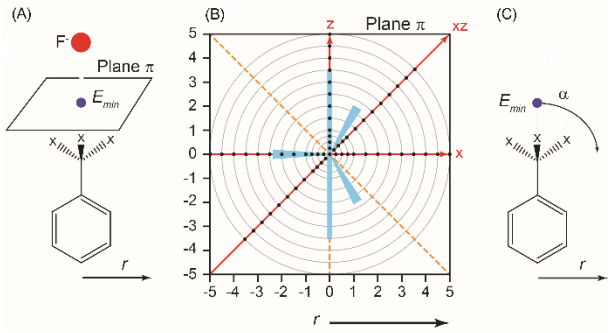

Figure 52. Illustrations of geometries calculated. See text for details.

The concentric grey circles in Figure 52B represent the *r* increments used, and the black dots denote the geometry of actual calculations. These computations were located on the x, z, and xz-axes that are represented by a solid red line. The data along the rest of the x, z, and xz-axes (orange stripped lines) were obtained by virtue of symmetry. The datasets thus obtained represent the energy landscape of plane π, which can be expressed as $E(r)$. In an attempt to simulate the CSD data as a function of α, the F^- anion was moved away from the origin with regular α-intervals, while keeping the F^- anion in-plane with the aryl ring and keeping the sp^3 C···F^- distance constant (to avoid the $PhCF_3$ complexes to converge with unreasonably large F···F^- distances). These data can thus be expressed as $E(\alpha)$.

In Figure 53 the energy landscapes are shown computed at the RI-MP2/def2-TZVP level of theory, which were obtained for the $[PhCX_3\cdots F]^-$ molecule pairs within the xz-plane centred at E_{min} for X = H (left) and X = F (right). The colour codes represent values relative to E_{min}. For the $[PhCH_3\cdots F]^-$ pair, E_{min} = –11 kcal/mol (D = 2.77 Å), positioning the F^- anion directly above the CH_3 hydrogens seems most favourable and the computed energy is above E_{min} only at r > 1.5 Å. For the $[PhCF_3\cdots F]^-$ interaction, E_{min} = –0.6 kcal/mol (D = 3.06 Å; –0.8 kcal/mol at the CCSD(T)/def2-TZVP level of theory) and moving the F^- anion away from this small minimum is energetically unfavourable in all directions and at all values for r. This is also reflected in the E versus r plots shown in Figure 54, where E is the average energy computed at a certain r-value (see also Figure 52B).

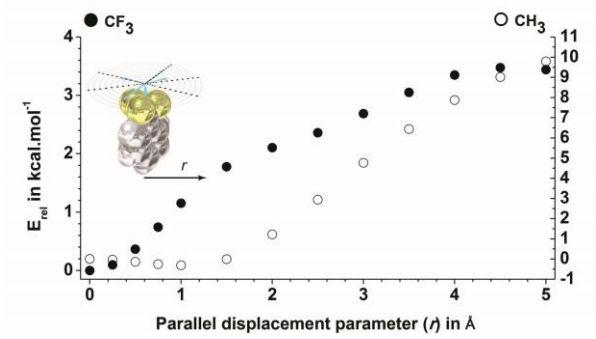

Figure 54. E_{rel} *vs. r* plots of computed geometries for the interaction of F^- with $PhCH_3$ (open circles) $PhCF_3$ (black circles).

Indeed, the energy penalty of moving F^- along *r* becomes apparent above 1.5 Å for $PhCH_3$ (open spheres) and above 0.2 Å for $PhCF_3$ (black spheres). These data imply that the energy-well above $PhCH_3$ is largest but wide (e.g. stronger but less directional), while for $PhCF_3$ it is smallest but very narrow (e.g. weaker but more directional). This is consistent with the *P*(*r*) plots (Figure 49) and the analysis of v/d Waals overlap (Figure 51).

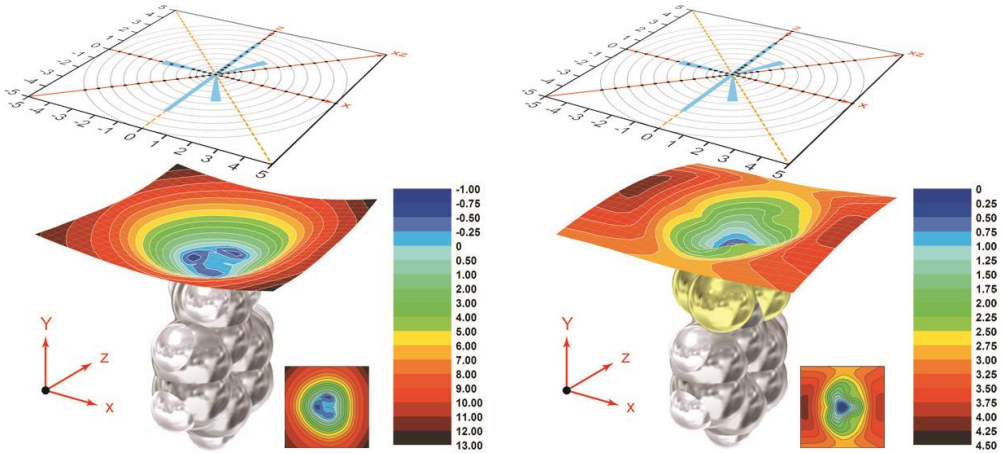

Figure 53. Illustrations of energy landscapes derived from the calculated energies (RI-MP2/def2-TZVP) by moving F^- in the plane π (see Figure 52B) above $PhCH_3$ (left) or $PhCF_3$ (right). Color codes are relative to E_{min} (along the y-axis), which is –11 kcal/mol for $[PhCH_3\cdots F]^-$ and –0.6 kcal/mol for $[PhCF_3\cdots F]^-$.

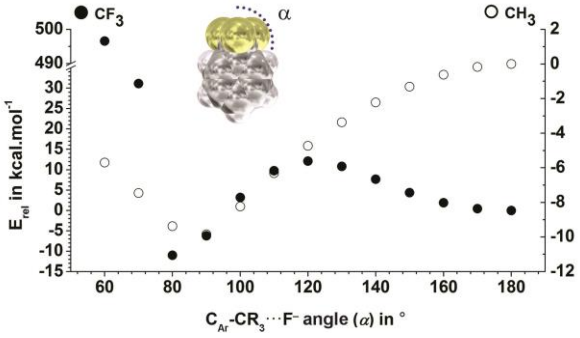

Figure 55. E_{rel} *vs.* α plots of computed geometries for the interaction of F^- with$PhCH_3$ (open circles) $PhCF_3$ (black circles).

From the $E(\alpha)$ plots shown in Figure 55, it is clear that the F^- anions prefer to interact with the H-atoms *ortho* to the CX_3 groups (i.e. around $\alpha = 80°$). At smaller α-values steric repulsion takes over and the energies become large and positive. Apparently, the sp^3 H-atoms in $PhCH_3$ provide a smooth electropositive surface so that the transition from $\alpha = 190°$ to 90° is without a barrier. In contrast, the electronegative belts around the F-atoms create a small energetic hill in moving from the local minimum at $\alpha = 180°$ to the one in $\alpha = 80°$. These computations imply that there is no real energy-well above $PhCH_3$, while there is a small but very narrow energy-well above $PhCF_3$ (i.e. the interaction is weak but directional). Introducing electron withdrawing substituents in the *para*-position of $PhCF_3$ significantly

increased the interacting energy with F^-: from –2.3 kcal/mol for *p*-fluoro- to –6.6 kcal/mol for *p*-nitro substitution ($F<CF_3<CN<NO_2$, see Figure S2 for the whole set of energies).

2.3.5. Conclusions

Electron-rich entities (El.R.) seem to have a preference for interacting with the aromatic H-atoms of (*para*-substituted) $PhCH_3$ or $PhCF_3$ entities. However, the interaction with the aliphatic H-atoms in $PhCH_3$ or the small electropositive region in between the three F-atoms in $PhCF_3$ is energetically favourable as well: E_{min} = –11 and –0.6 kcal/mol respectively with El.R. = F^- (and up to –6.6 kcal/mol with *p*-NO_2PhCF_3). For the larger $PhCH_3\cdots F^-$ interaction, distortion from the linear conformation seems to go without energy penalty. This suggests that this conformation is not at the bottom of an energy-well; hence this type of interaction is hardly directional, as indeed observed in our CSD analysis. In contrast, the small $PhCF_3\cdots F^-$ interaction is located in a very narrow energy-well and any distortion from linearity thus comes with an energy penalty. As a result, this interaction is more directional, as confirmed by our analysis of the CSD.

The estimated –0.6 to –6.6 kcal/mol for an $[ArCF_3\cdots F]^-$interaction is comparable to weak CH-π interactions, which are generally accepted as a small but important supramolecular interaction.[152] Moreover, $-CF_3$ groups and electron-rich atoms occur frequently in Nature. This implies that noncovalent carbon bonding might turn out to be as abundant and functionally relevant as weak CH-π interactions.

2.3.6. Notes

$$P(r) = \frac{N_r}{N_{total}} \div \frac{V_r^{free}}{V_{total}^{free}} \qquad \text{Equation 1}$$

N_r = the number of hits in between two *r*-values; N_{total} = the total number of hits; V_r^{free} = the volume of a 5 Å high and wide hemisphere in between two *r*-values minus the volume of the host in between these two *r*-values (hence the free volume); V_{total}^{free} is the volume of a 5 Å high and wide hemisphere minus the volume of the host in that hemisphere.

2.3.7. Supporting information

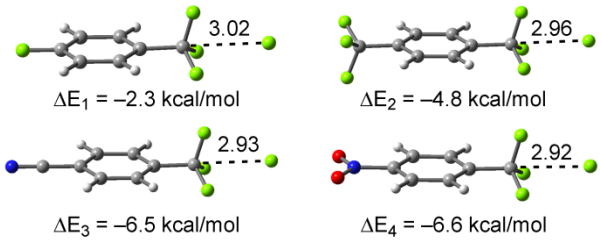

Figure S2. RI-MP2/def2-TZVP optimized $[p\text{-}XC_6H_4CF_3\cdots F]^-$ complexes, interaction energies and equilibrium distances (Å).

2.4. Theoretical study on σ- and π-hole carbon···carbon bonding interactions: Implications in CFC chemistry.

2.4.1 Abstract

In this manuscript the ability of CO_2 and several CFCs to establish noncovalent carbon···carbon interactions (termed as noncovalent carbon···carbon bonding) with atmospheric gases CO, ethene and ethyne has been studied at the RI-MP2/def2-TZVPD level of theory. We have used several CFCs ($CFCl_3$, CF_3Cl, CF_2Cl_2 and CH_3F) and the CO_2 molecule as σ- and π-hole carbon bond donors (electron-poor carbon atom). As electron-rich moieties we have used CO, ethene and ethyne (electron-rich carbon atom bearing molecules). We have also used Bader's theory of "Atoms in molecules" to further analyse and characterize the noncovalent interactions described herein. Finally, we have analyzed possible cooperativity effects between the noncovalent carbon···carbon bonding and hydrogen bonding interactions in case of ethyne.

2.4.2. Introduction

Noncovalent interactions are fairly recognized as key players in modern chemistry.[161] Actually, supramolecular chemists rely on their proper comprehension and rationalization in order to achieve progress in fields such as, molecular recognition[1] and materials science.[79a] Hydrogen bonding, and more recently, halogen bonding[162] are examples of well-known σ-hole interactions that play an important role in many chemical and biological environments.[3] For instance, hydrogen bonding interactions are main driving forces in enzyme chemistry and protein folding.[163] Consequently, both noncovalent forces have been widely studied from theoretical and experimental perspectives.[164,4a] Their similarities in both strength and directionality features stimulated a series of studies using the Cambridge Structural Database (CSD) in order to shed light into the impact of these interactions in crystal structures.[165,166]

Related to this, σ-hole interactions involving elements of Groups IV–VI have also earned recognition among the scientific society as an important addition to the family of well-established directional noncovalent interactions.[5a,5b,157] Recently, it was demonstrated that atoms of Groups IV–VI (from tetrels to chalcogens) when covalently bonded are able to establish attractive interactions with electron-rich entities through their positive electrostatic potential regions, which are attributed to the anisotropies of the electronic density distribution on the extensions of their covalent bonds.[7] It was also shown that the factors that rule the σ-hole potentials are the same across Groups IV–VI.

---

[161] C. A. Hunter, J. K. M. Sanders *J. Am. Chem. Soc.* **1990**, *112*, 5525–5534.
[162] S. J. Grabowski, *Chem. Rev.* **2011**, *111*, 2597–2625.
[163] Y. Bai, T. R. Sosnick, L. Mayne, S. W. Englander, *Science* **1995**, *269*, 192–197.
[164] A .C. Legon, D. J. Millen, *Acc. Chem. Res.* **1987**, *20*, 39–46.
[165] G. A. Cavallo, P. Metrangolo, R. Milani, T. Pilati, A. Priimagi, G. Resnati, G. Terraneo, *Chem. Rev.* **2016**, *116*, 2478–2601.
[166] T. Steiner, *Angew. Chem. Int. Ed.* **2002**, *41*, 48–76.

As a natural consequence of the scientific curiosity over the σ-hole chemistry a novel and relatively unexplored group of noncovalent interactions emerged, named π-hole bonding. A π-hole is a region of positive electrostatic potential that is perpendicular to a portion of a molecular framework.[27] Two pioneering works that exemplify the impact of π-hole interactions in chemical and biological systems should be emphasized. Firstly, Bürgi and Dunitz studied the trajectory along which a nucleophile attacks the π-hole of a C=O group[15] and, secondly, Egli and co-workers studied and rationalized the ability of guanosine to behave as a π-hole donor in the crystal structure of Z-DNA.[16] More recently, the study of π-hole interactions has been extended to acyl carbons[17] and other entities involving pnicogen[19a,167,168,169] and chalcogen bearing compounds.[18a,170]

Haloalkanes have been widely used in industry as refrigerant agents, propellants and cleaning solvents until the 1970s.[171] Related to this, chlorofluorocarbons (CFCs) are a family of haloalkane compounds mostly formed by hydrocarbons, particularly alkanes, covalently bonded with halogens such as chlorine or fluorine. Nowadays, they are well known to play a key role in the depletion process of the ozone layer, which is a vital natural defense against the incoming UV radiation.[172] Several theoretical studies have been devoted to analyse the interaction between CFCs and ozone, carbon dioxide and nitrogen oxide molecules, as well as sulphur containing compounds.[173,174,175] While CFCs are considered as an important source of carbon atoms,[176] it is intriguing whether they can undergo carbon bonding interactions with other atmospheric gases, such as carbon monoxide or ethene and ethyne molecules.[177,178] In this regard, we propose to coin the term dicarbon bond, since both the electron donor and acceptor are carbon atoms, thus resembling the concept of dihydrogen bond.[179] The concept of carbon···carbon interactions involving sp and sp^2 carbons has been previously studied by Remya and coworkers.[180]

In this study, our purpose is to investigate the ability of CFCs and CO_2 moieties to establish σ- and π-hole noncovalent carbon···carbon bonding interactions. In order to achieve this goal, we have used several CFCs ($CFCl_3$, CCl_3F, CH_3F and CF_2Cl_2) as σ-hole carbon bond donor entities. We have used CO, ethene and ethyne as electron-rich moieties (see Figure 56). Particularly, in CO_2 π-hole complexes, we have

---

[167] A. Bauzá, T. J. Mooibroek, A. Frontera, *Chem. Commun*. **2015**, *51*, 1491–1493.
[168] A. Bauzá, A. Frontera, T. J. Mooibroek, *Cryst. Growth Des.* **2016**, *16*, 5520–5524.
[169] A. Bauzá, T. J. Mooibroek, A. Frontera, *ChemPhysChem* **2016**, *17*, 1608–1614.
[170] L. M. Azofra, I. Alkorta, S. Scheiner, *Phys. Chem. Chem. Phys.* **2014**, *16*, 18974–18981.
[171] A. Chatterjee, T. Ebina, T. Iwasaki, F. Mizukami, *J. Mol. Struct*. **2003**, *630*, 233–242.
[172] J. E. Lovelock, R. J. Maggs, R. A. Rasmussen, *Nature* **1972**, *237*, 452–453.
[173] B. G. de Oliveira, R. C. M. Ugulino de Araújo, E. S. Leite, M. N. Ramos, *Int. J. Quantum Chem.* **2011**, *111*, 111–116.
[174] K. S. Diao, F. Wang, H. J. Wang, *J. Mol. Struct.* **2009**, *913*, 195–199.
[175] L. Ai, J. Liu, *J. Mol. Model.* **2014**, *20*, 2179, 10p.
[176] K. S. Diao, F. Wang, H. J. Wang, *Environ. Contam. Toxicol.* **2010**, *84*, 170–174.
[177] J. G. Calvert, R. Atkinson, J. A. Kerr, S. Madronich, G. K. Moortgat, T. J. Wallington *et al., The Mechanisms of Atmospheric Oxidation of the Alkenes*, Oxford University Press, New York, **2000**.
[178] a) M. P. Fraser, G. R. Cass, B. R. Simoneit, *Environ. Sci. Technol.* **1998**, *32*, 2051–2060; b) A. C. Aikin, J. R. Herman, E. J. Maier, C. J. McQuillan, *J. Geophys. Res.* **1982**, *87*, 3105–3118; c) Y. Xiaoi, D. J. Jacob, S. Turquety, *J. Geophys. Res.* **2007**, *112*, D12305.
[179] R. Custelcean, J. E. Jackson, *Chem. Rev.* **2001**, *101*, 1963–1980.
[180] K. Remya, C. H. Suresh, *Phys. Chem. Chem. Phys.* **2015**, *17*, 18380–18392.

explored two different orientations (parallel and perpendicular) between both donor and acceptor molecules. Finally, we have also used the Bader's theory of "Atoms in molecules" to further describe and rationalize the interactions described above.

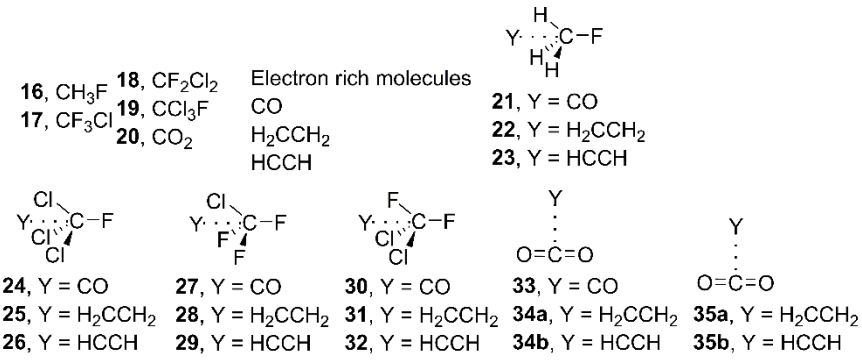

Figure 56. Compounds **16**–**20** and complexes **21**–**35** used in this study. For complexes **34** and **35** two possible orientations were considered; parallel (denoted as **a**) and perpendicular (denoted as **b**).

2.4.3. Theoretical methods

The energies of all complexes included in this study were computed at the RI-MP2/def2-TZVPD level of theory by means of the program TURBOMOLE version 7.0.[141] Single point calculations at the CCSD(T)/def2-TZVP level of theory have been performed in order to give reliability to the RI-MP2 method. The MEP (Molecular Electrostatic Potential) calculations have been performed at the MP2/def2-TZVP level of theory by means of the Gaussian 09 calculation package.[143] Frequency calculations have been performed at the RI-MP2/def2-TZVPD level of theory and in all cases a true minima have been found. Moreover, all carbon···carbon complexes correspond to global minima apart from complex **23** that is a local minimum. The global minimum corresponds to an H-bonded complex CH_3F···HCCH. The Bader's "Atoms in molecules" theory has been used to study the interactions discussed herein by means of the AIMAll calculation package.[181] The calculations for wavefunction analyses were carried out at the MP2/def2-TZVP level of theory.

2.4.4. Results and discussion

2.4.4.1. MEP study

As a preliminary study, we have computed the molecular electrostatic potential (MEP) surface of compounds **16** to **20** (see Figure 57). As it can be observed, for compounds **16** to **19** the MEP surface showed the presence of a positive potential area located at the outermost region of the carbon atom, opposite to the C-X bond (σ-hole). Consequently, an attractive interaction with electron-rich entities is expected. In addition, the MEP value of the σ-hole is more positive for compounds **16** and **17**, thus expecting a stronger binding upon complexation from an

[181] AIMAll (Version 13.05.06), T. A. Keith, TK Gristmill Software, Overland Park KS, USA, **2013**.

electrostatic perspective. Moreover, the MEP values become less positive ongoing from compound **17** to **19**, due to the difference in electronegativity between chlorine and fluorine atoms. In case of compound **20**, a positive potential region is observed on the tip of the carbon atom, perpendicularly located over the molecular plane (π-hole). The MEP value obtained is the most positive among compounds **16** to **20**, thus expecting a stronger binding for π-complexes over the σ-hole set. Finally, among the electron donors, the most negative MEP value corresponds to the ethene molecule, thus expecting a slightly stronger binding over the other CO and ethyne molecules.

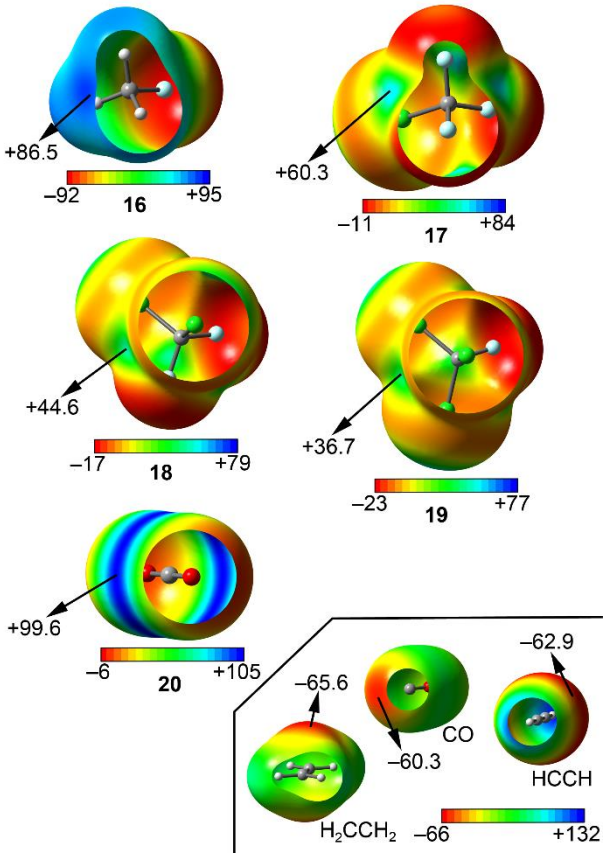

Figure 57. MEP (Molecular Electrostatic Potential) surfaces for compounds **16** to **20** and electron-rich molecules H_2CCH_2, CO and HCCH. Energy values in kJ/mol.

2.4.4.2. Energetic study

The interaction energies and equilibrium distances obtained for complexes **21** to **35** (see Figure 58) studied herein are summarized in Table 6. The examination of the results indicates that the interaction energy values are weak but attractive in all cases, ranging from −11 to −4 kJ/mol. Among the σ-hole complexes studied (**21**–**32**) the $CFCl_3$ and CF_2Cl_2 ones (**24**–**26** and **30**–**32**, respectively) present stronger interaction energies, conversely to the MEP analysis that shows more positive values at the σ-hole of CH_3F and CF_3Cl molecules, likely due to the greater polarizability of chlorine *vs.* fluorine. Moreover, $CFCl_3$ and CF_2Cl_2 complexes present larger equilibrium distance values than those involving CH_3F and CF_3Cl molecules.

On the other hand, for CH_3F and CF_3Cl complexes (**21**–**23** and **27**–**29**, respectively) comparable interaction energy values were obtained.

For π-complexes involving CO_2 (**33** to **35b**) the binding energy values are similar to those obtained for CCl_3F and CF_2Cl_2 complexes. For some complexes we have computed the interaction energies at a higher level of theory in order to validate the computational method used herein. The values in parenthesis summarized in Table 6 correspond to the interaction energies at CCSD(T)/def2-TZVPD level of theory, which are in good agreement with the MP2 values.

The σ-hole CFC complexes with ethene (**22**, **25**, **28**, **31**) are more favourable than the complexes with ethyne, in agreement with the MEP values shown in Figure 57, which indicate that ethene is slightly more π-basic than ethyne. In addition, complexes involving the CO molecule achieved the lowest binding energy values of the set, also in agreement with the MEP analysis. For π-hole complexes **33** to **35** the parallel orientation presents larger binding energy values than the perpendicular one, likely due to major overlap between the π-systems of CO_2 and ethene/ethyne molecules. Moreover, the CO_2···ethene π-hole complexes **34a,b** are more favourable than the ethyne ones **35a,b**.

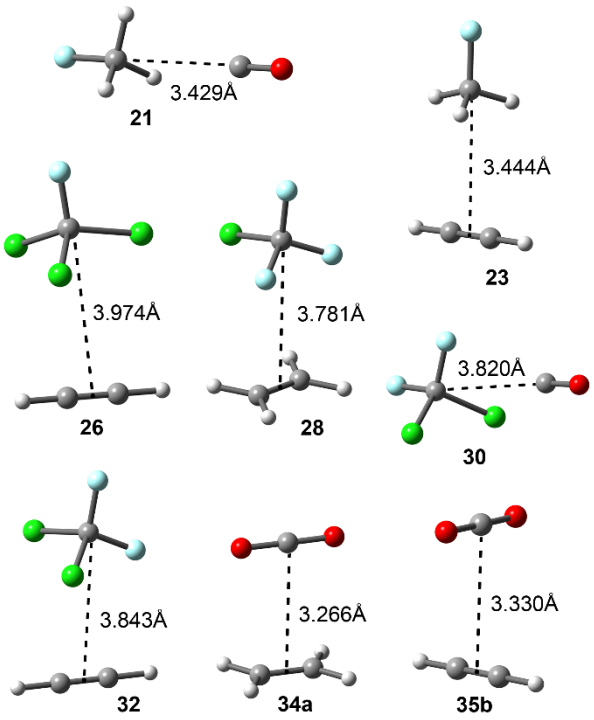

Figure 58. Optimized geometries of some representative complexes at the RI-MP2/def2-TZVPD level of theory.

Table 6. Interaction energies (ΔE, kJ/mol), equilibrium distances (R, Å) and symmetry point group used (Symm) at the RI-MP2/def2-TZVPD level of theory for complexes **21** to **35**.

Complex	ΔE[a]	R[b]	Symm
21 ($OC:CH_3F$)	−4.3	3.429	C_{3v}
22 ($H_2CCH_2:CH_3F$)	−7.0 (−6.7)	3.452	C_s
23 ($HCCH:CH_3F$)	−6.2	3.444	C_s
24 ($OC:CCl_3F$)	−4.8 (−4.3)	3.922	C_{3v}
25 ($H_2CCH_2:CCl_3F$)	−10.8	3.937	C_s
26 ($HCCH:CCl_3F$)	−8.6	3.974	C_s
27 ($OC:CClF_3$)	−4.1 (−4.0)	3.748	C_s
28 ($H_2CCH_2:CClF_3$)	−7.6	3.781	C_s
29 ($HCCH:CClF_3$)	−6.3 (−5.5)	3.802	C_s
30 ($OC:CCl_2F_2$)	−4.5	3.820	C_s
31 ($H_2CCH_2:CCl_2F_2$)	−9.4 (−8.2)	3.830	C_s
32 ($HCCH:CCl_2F_2$)	−7.8	3.843	C_s
33 ($OC:CO_2$)	−5.4	3.240	C_{2v}
34a ($H_2CCH_2:CO_2$)	−9.2	3.266	C_{2v}
34b ($H_2CCH_2:CO_2$)	−8.8	3.252	C_{2v}
35a ($HCCH:CO_2$)	−9.8	3.210	C_{2v}
35b ($HCCH:CO_2$)	−6.1	3.330	C_{2v}

[a]Values in parenthesis correspond to the CCSD(T)/def2-TZVPD level of theory.
[b]For complexes involving ethene and ethyne distances were measured from the C-C bond centroid.

2.4.4.3. AIM analysis

We have used the Bader's theory of "Atoms in molecules" to characterize the noncovalent carbon···carbon bond complexes described above. The distribution of critical points (CPs) and bond paths for some representative complexes is shown in Figure 59. For σ-hole complexes involving the CH_3F moiety (**21** to **23**) it can be noticed the presence of a bond CP (red sphere) and bond path (dashed line) connecting both carbon atoms. In addition, in case of complex **22** two symmetrically distributed bond CPs connect the π-system of ethene (both C atoms) to the carbon atom of the CH_3F moiety, consequently a supramolecular ring is formed and a ring CP is created.

On the other hand, for complexes involving the CO_2 moiety (**33**, **34b** and **35b**) the interaction is characterized by the presence of a bond CP and bond path connecting the carbon atom of CO_2 to either the carbon atom of CO or the bond critical point of the CC bond of ethene/ethyne Moreover, in complex **34a** where the CO_2 and the ethene portions are parallel disposed, it can be noticed the presence of two symmetrically distributed bond CPs connecting both C atoms of the ethene to the central C atom of the CO_2, forming a supramolecular ring and its corresponding ring CP. The values of the Laplacian are all positive, as in common in closed shell calculations. Finally, additional AIM analyses are included in the SI (see Figure S3). In these complexes the bond paths that characterize the interaction connect the carbon atoms of the electron-rich molecules to the halogen atoms of the CFCs.

2.4.4.4. Noncovalent carbon···carbon bonding *vs.* H-bonding

This manuscript is devoted to the ability of CFCs to establish noncovalent carbon···carbon bonding with other atmospheric gases. It should be mentioned that the most favourable binding mode between CH_3F and ethyne is the formation of a hydrogen-bonded complex by means of a HCC–H···FCH_3 interaction. The interaction energy of the global minimum is –8.8 kJ/mol while the carbon···carbon complex **23** is –6.2 kJ/mol. We have also analysed possible cooperativity effects between both interactions. Particularly, we have computed the binding energies of ethyne interacting with two CH_3F molecules either forming two hydrogen bonds (ΔE_5, complex **36**) or two noncovalent carbon···carbon bonds (ΔE_6, complex **37**). It can be observed that the hydrogen bonding complex is approximately 5 kJ/mol more favourable than the noncovalent carbon···carbon complex.

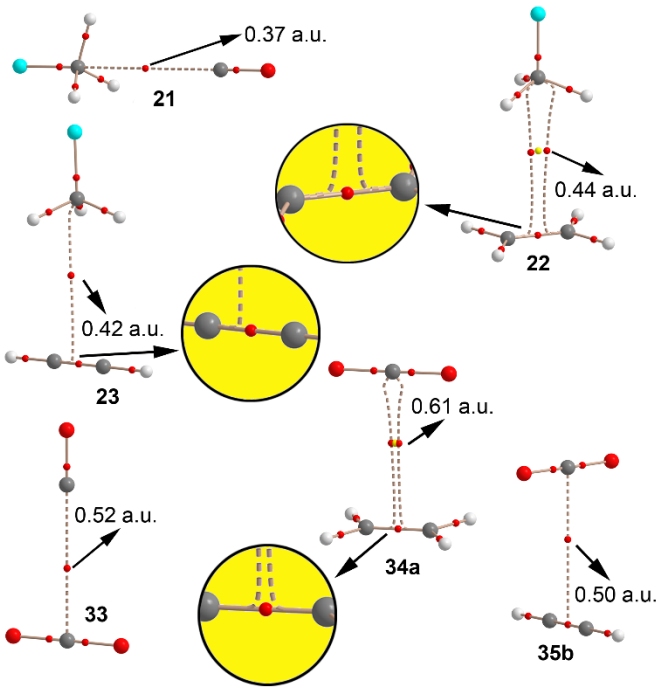

Figure 59. Distribution of critical points and bond paths in complexes **21**, **22**, **23**, **33**, **34a** and **35b**. Bond and ring critical points are represented by red and yellow spheres, respectively. The bond paths connecting bond critical points are also represented. The value of the density at the bond critical point (10^2 x ρ) is also indicated.

More interestingly, the H-bonded complex **36** has enhanced the ability to interact with additional CH_3F molecules forming noncovalent carbon···carbon bonding interactions (ΔE_7 = –19.8 kJ/mol) to form complex **38**. Similarly, the noncovalent carbon···carbon bonded complex **37** forms stronger H-bonding interactions (ΔE_8 = –24.7 kJ/mol) than ethyne alone (ΔE_5 = –16.5 kJ/mol). Therefore, strong cooperativity effects are found between both interactions in the formation of complex **38**. This mutual influence between the interactions is further confirmed by the AIM analysis. The charge density at the bond CP is usually related to the interaction strength.[182] It can be observed that the values of ρ(r) at the bond CPs

[182] *Computational Chemistry: Reviews of Current Trends*, *Vol. 4*, World Scientific, Singapore, **1996**.

that characterize the H-bonding and noncovalent carbon···carbon bonding interactions in complex **38** are greater than the corresponding values in complexes **36** and **37**, thus confirming the mutual reinforcement of both interactions, in agreement to the energetic study.

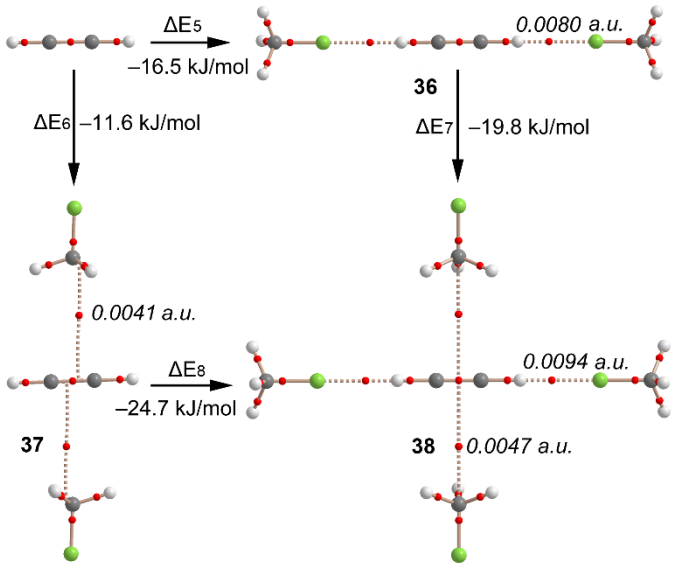

Figure 60. Distribution of critical points and bond paths in complexes **36**–**38**, along with the binding energies. The value of the density at the bond critical point is also indicated in italics.

2.4.5. Conclusions

The results reported in this manuscript highlight the ability of CFCs and CO_2 molecules to establish weak interactions (noncovalent carbon···carbon bonds) with CO, ethene and ethyne molecules acting as electron donors, which are present in the higher layers of the atmosphere. The results presented herein provide new insights on how these molecules interact with each other and may be important in the field of atmospheric chemistry. We have successfully used the Bader's theory of "Atoms in molecules" to characterize the noncovalent carbon···carbon bond complexes described above. Finally, favourable cooperativity effects between noncovalent carbon···carbon and hydrogen bonding interactions have been demonstrated energetically and using the AIM theory.

2.4.6. Acknowledgements

AB and AF thank the DGICYT of Spain (projects CTQ2014-57393-C2-1-P and CONSOLIDER INGENIO 2010 CSD2010-00065, FEDER funds). We thank the CTI (UIB) for computational facilities.

2.4.7. Supporting information

In Figure S3 the distribution of critical points (CPs) and bond paths for some additional complexes is shown. As it can be observed, for complexes **24** and **30** where a CO molecule acts as electron donor three symmetrically distributed bond CPs (red spheres) connect the halogen and carbon atoms. In addition, a cage CP emerges and further characterizes the interaction. On the other hand, in complexes **26** and **28** it can be noticed three bond CPs that connect the halogen atoms with the carbon atoms of the π-system.

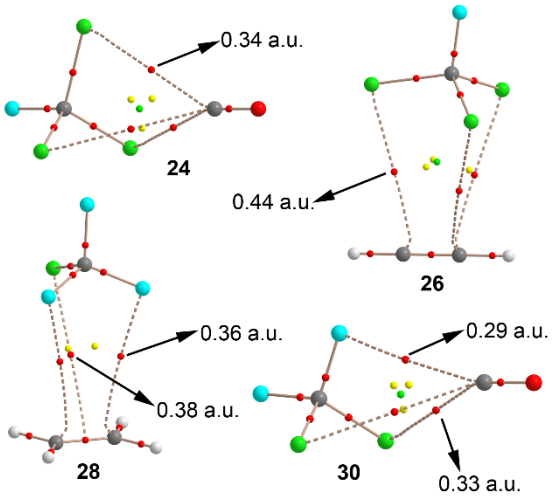

Figure S3. Distribution of critical points and bond paths in complexes **24**, **26**, **28** and **30**. Bond, ring and cage critical points are represented by red, yellow and green spheres, respectively. The bond paths connecting bond critical points are also represented. The value of the density at the bond critical point (10^2 x ρ) is also indicated.

2.5. $RCH_3\cdots O$ interactions in biological systems: are they trifurcated H-bonds or noncovalent carbon bonds?

2.5.1. Abstract

In this manuscript we combine high level *ab initio* calculations on some model systems (XCH_3 σ-hole/H-bond donors) and a PDB survey to distinguish between trifurcated H-bonds and noncovalent carbon bonds in $XCH_3\cdots O$ complexes (X = any atom or group). Recently, it has been demonstrated both experimentally and theoretically the importance of noncovalent carbon bonds in the solid state. When an electron-rich atom interacts with a methyl group, the role of the methyl group is commonly viewed as a weak H-bond donor. However, if the electron-rich atom is located equidistant from the three H atoms, the directionality of each individual H-bond in the trifurcated binding mode is poor. Therefore, the $XCH_3\cdots O$ interaction could be also defined as a tetrel bond (C···O interaction). In this manuscript we shed light into this matter and demonstrate the importance of $XCH_3\cdots O$ noncovalent carbon bonding interactions in two relevant protein-substrate complexes retrieved from the PDB.

2.5.2. Introduction

Supramolecular chemistry is a multidisciplinary field of research that develops very fast and has a deep impact[1,148] in the scientific community. Undoubtedly, the comprehension of the great deal of noncovalent forces, which are the basis of highly specific recognition, is crucial for the chemists working in this discipline. For instance, interactions between hosts and guests govern the creation of assemblies with high affinities even in highly competitive media.[2,183,184,185] For this reason, the correct description and understanding of noncovalent interactions between molecules is essential for being successful in this field of research. In general, strong and highly directional interactions such as hydrogen bonding and σ-hole bonding[3,4a,4b,5a,157,186,187,188,189,190,191] and less directional forces like ion pairing are used for this purpose.

The allocation of a hydrogen atom between a donor (D) and acceptor (A) moiety, D-H···A hydrogen bonding,[149] is a particularly well studied and established supramolecular interaction ranging in strength from very weak (~1 kcal/mol)[150] to very strong (~40 kcal/mol).[151] The weakest H-bonding interactions are established between weakly polarized D–H bonds (e.g. aliphatic CH) and mildly electron-rich H-

[183] F. Vögtle, *Supramolecular Chemistry: an Introduction*, Wiley, New York, **1993**.
[184] P. D. Beer, P. A. Gale, D. K. Smith, *Supramolecular Chemistry*, Oxford University Press, Oxford, **1999**.
[185] J. W. Steed, J. L. Atwood, *Supramolecular Chemistry*, Wiley, Chichester, **2000**.
[186] H. Destecroix, H. C. M. Renney, T. J. Mooibroek, T. S. Carter, P. F. N. Stewart, M. P. Crump, A. P. Davis, *Angew. Chem. Int. Ed*. **2015**, *54*, 2057–2061.
[187] P. Murray-Rust, W. C. Stallings, C. T. Monti, R. K. Preston, J. P. Glusker, *J. Am. Chem. Soc.* **1983**, *105*, 3206–3214.
[188] N. Ramasubbu, R. Parthasarathy, P. Murray-Rust, *J. Am. Chem. Soc*. **1986**, *108*, 4308–4314.
[189] A. Bauzá, T. J. Mooibroek, A. Frontera, *ChemPhysChem* **2015**, *16*, 2496–2517.
[190] A. Bauzá, T. J. Mooibroek, A. Frontera, *Chem. Rec.* **2016**, 16, 473–487.
[191] A. Bauzá, A. Frontera, *ChemPhysChem* **2015**, *16*, 3108–3113.

acceptor moieties (e.g. alkene π-electrons).[152] While a single interaction is energetically insignificant, when several weak H-bonds coexist they can stabilize protein structures[153] and contribute to the binding of proteins to carbohydrates.[154]

Apart from this weak bonding interaction, recent theoretical explorations have suggested that pnicogen and tetrel atoms in their sp^3 hybridized form can act as electron-poor entities suitable to accommodate an electron-rich guest.[4c,5a,25b,85,86a,156,157] Surprisingly few studies have been dedicated to study the most abundant of these atoms, namely the carbon atom. As a matter of fact, it has recently been reported that strong complexes are formed between electron-rich entities and 1,1,2,2-tetracyanocyclopropane.[86b,192,193] Moreover, the ability of the carbon atom in a methyl group or in an aliphatic chain (sp^3 hybridized) to participate in σ-hole interactions (as σ-hole donor, i.e. electron acceptor) has been explored by Mani and Arunan.[90] They demonstrated that the carbon atom in fact could act as an electrophilic centre which can noncovalently bond with electron-rich entities leading to noncovalent carbon bonding, following a nomenclature analogous to other σ-hole interactions.

The theoretical predictions were confirmed experimentally by Guru Row's group,[91] thus validating the existence of this type of bonding by means of X-ray charge density analysis. Electron density topologies in two prototypical crystal structures with potential carbon bonding motifs (R_3N^+-CH_3···O/Cl) were reported and revealed two distinct features of bond paths. That is, for the X-ray structure with the R_3N^+-CH_3··· Cl motif, the bond path revealed a C-H···Cl hydrogen bond and for the other motif the bond path connected the electron-rich oxygen atom with the -CH_3 carbon atom and, remarkably, no other bond paths connected the oxygen atom to the C-H hydrogen atoms. More recently, cooperativity effects involving carbon bonding interactions and other noncovalent interactions have been analyzed in several theoretical studies.[18c,194,195]

The presence of methyl groups is abundant in many biologically relevant ligands and electron-rich O atoms are ubiquitous in proteins. Therefore, we wondered if perhaps weak noncovalent bonding with sp^3 hybridized carbon could have some relevance in ligand-protein complexes. Our approach was to conduct a rigorous statistical survey of the PDB together with quantum mechanical computations on the RI-MP2/aug-cc-pVTZ level of theory on some model systems. For the present theoretical study we considered the sp^3 C-atom in several exemplifying molecules (**39–41**, see Figure 61) and computed their complexes with the electron-rich O atom of two molecules (formaldehyde and HO-) In addition, using the Bader's theory of "Atoms in molecules"[196] we have analyzed the bond path connecting the O atom with the CH_3 group in several complexes with the purpose to differentiate the hydrogen bonding to the carbon bonding. From the PDB search we analyze the impact of the X–CH_3···O interactions in biologically relevant protein-ligand complexes.

[192] A. Bauzá, T. J. Mooibroek, A. Frontera, *Phys. Chem. Chem. Phys*. **2016**, *18*, 1693–1698.
[193] E. C. Escudero-Adán, A. Bauzá, A. Frontera, P. Ballester, *ChemPhysChem* **2015**, *16*, 2530–2533.
[194] M. Solimannejad, M. Orojloo, S. Amani, *J. Mol. Model.* **2015**, *21*, 183, 7p.
[195] M. Marín-Luna, I. Alkorta, J. Elguero, *J. Phys. Chem. A* **2016**, *120*, 648–656.
[196] R. F. W. Bader, *Chem. Rev*. **1991**, *91*, 893–928.

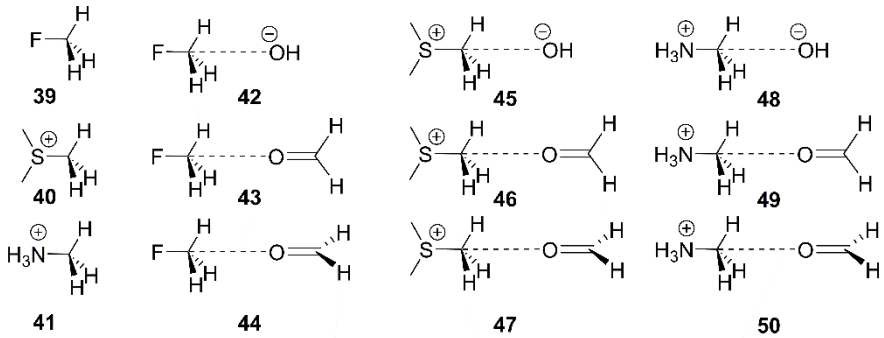

Figure 61. Compounds and complexes **39–50** studied in this work.

2.5.3. Theoretical methods

The geometries of the complexes studied herein have been fully optimized at the RI-MP2/aug-cc-pVTZ level of theory. The calculations have been performed by using the program TURBOMOLE version 7.0.[141] The interaction energies were calculated with correction for the basis set superposition error (BSSE) by using the Boys-Bernardi counterpoise technique.[142] The C_s symmetry point group has been used in the optimization of the complexes. The minimum nature of the complexes has been confirmed by carrying out frequency calculations. For the theoretical analysis of the noncovalent interactions present in PDB structures 4NSY and 4U14 the BP86-D3/aug-cc-pVTZ level of theory was used and the position of the hydrogen atoms present in these structures was optimized prior to the evaluation of the binding energy values.

For the heteroatoms we have used the crystallographic coordinates. We have used the DFT-D functional with the latest available correction for dispersion (D3).[197] The Bader's "Atoms in molecules" theory has been used to study the interactions discussed herein by means of the AIMAll calculation package.[181] Finally, the partitioning of the interaction energies into the individual electrostatic, induction, dispersion and exchange-repulsion components was carried out with the symmetry adapted intermolecular perturbation theory approach DFT-SAPT at the BP86/aug-cc-pVTZ level of theory using the aug-cc-pVQZ basis set for the MP2 density fitting[198] by means of the MOLPRO program.[199,200]

---

[197] S. Grimme, J. Antony, S. Ehrlich, H. A. Krieg, *J. Chem. Phys.* **2010**, *132*, 154104, 19p.
[198] A. Heβelmann, G. Jansen, *Phys. Chem. Chem. Phys*. **2003**, *5*, 5010–5014.
[199] H. -J. Werner, P. J. Knowles, G. Knizia, F. R. Manby, M. Schütz, *WIREs Comput. Mol. Sci*. **2012**, *2*, 242–253.
[200] MOLPRO, version 2012.1, a package of ab initio programs, H.-J. Werner, P. J. Knowles, G. Knizia, F. R. Manby, M. Schütz, P. Celani, W. Györffy, D. Kats, T. Korona, R. Lindh, A. Mitrushenkov, G. Rauhut, K. R. Shamasundar, T. B. Adler, R. D. Amos, A. Bernhardsson, A. Berning, D. L. Cooper, M. J. O. Deegan, A. J. Dobbyn, F. Eckert, E. Goll, C. Hampel, A. Hesselmann, G. Hetzer, T. Hrenar, G. Jansen, C. Köppl, Y. Liu, A. W. Lloyd, R. A. Mata, A. J. May, S. J. McNicholas, W. Meyer, M. E. Mura, A. Nicklaß, D. P. O'Neill, P. Palmieri, D. Peng, K. Pflüger, R. Pitzer, M. Reiher, T. Shiozaki, H. Stoll, A. J. Stone, R. Tarroni, T. Thorsteinsson, M. Wang.

2.5.4. Results and discussion

2.5.4.1. Preliminary MEP analysis

We have firstly computed the molecular electrostatic potential (MEP) mapped onto the van der Waals surface in very simple compounds (XCH_3) to explore the existence/absence of a σ-hole in the carbon atom (along the extension of the X-C bond) and to compare its electrostatic potential to that measured along the C-H bonds of the methyl group. In particular we have computed the MEP surfaces of fluoromethane, dimethylether, dimethylthioether, DMF, acetonitrile and methylamine and the results are shown in Figure 62. In fluoromethane and dimethylether an evident σ-hole is observed (see Figure 62A, B) in the C atom with a MEP value that is comparable to that observed in the H atoms. Therefore either the carbon or hydrogen bonding interactions should be equally favored, at least electrostatically, in both molecules.

For the DMF and acetonitrile molecules, a perfectly defined σ-hole is not observed, however both molecules present a significantly positive value of MEP at the C atom. Finally, the methylamine and dimethylthioether molecules (see Figure 62D, E) do not present a σ-hole at the C atom, although the electrostatic potential is slightly positive. Consequently, both molecules are better H-bond donors than carbon bond donors in terms of electrostatic effects.

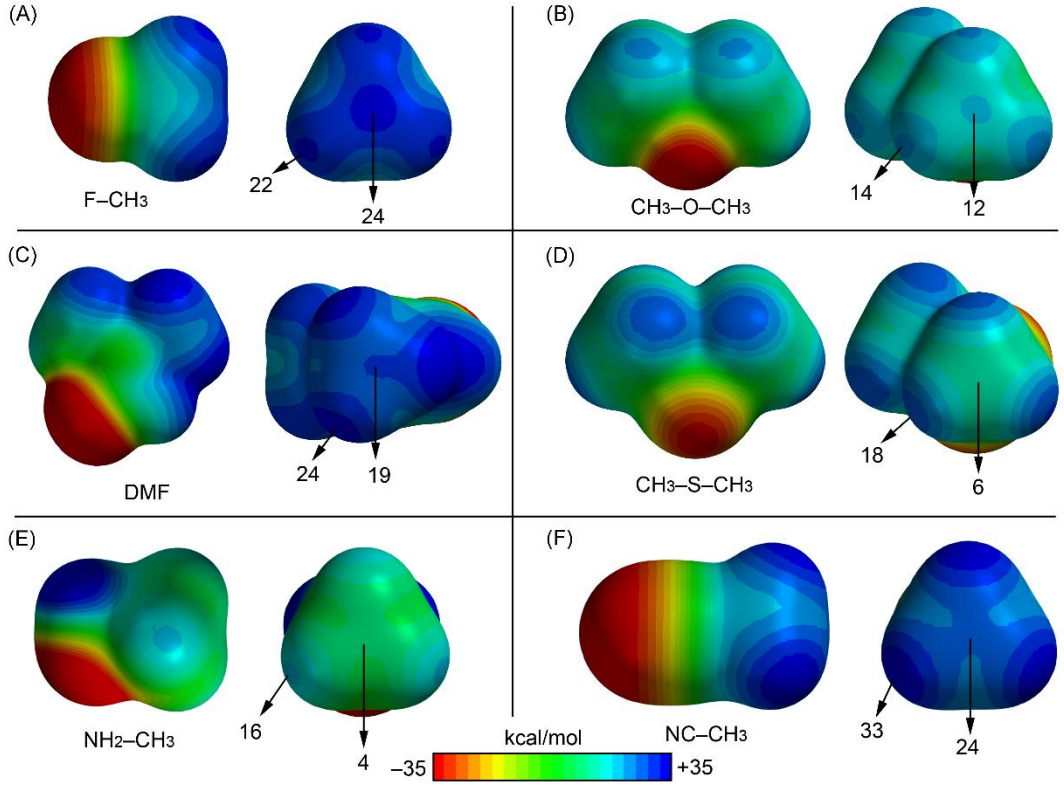

Figure 62. MEP surfaces of fluoromethane (A), dimethylether (B), DMF (C), dimethylthioether (D), methylamine (E) and acetonitrile (F). The MEP values at selected points are indicated.

2.5.4.2. Energetic and geometric results

Table 7 reports the interaction energies and equilibrium distances of the optimized complexes **42**–**50** (see Figures 61 and 63) computed at the RI-MP2/aug-cc-pVTZ level of theory. In complexes **45** and **48**, where the OH^- anion interacts with charged carbon bond donors the noncovalent complex was not found, instead a nucleophilic S_N2 reaction occurs in the optimization. In formaldehyde complexes, we have studied the influence of the orientation of the lone pairs of the O atom on the interaction energy and equilibrium distance. At this point, it should be commented that we have used two charged carbon bond donors for the following reasons. First, the utilization of trimethylsulfonium was chosen to mimic the SAM cofactor (important in methyl transfer enzymatic processes). Second, we have used methanaminium because at physiological conditions the amine groups are likely protonated.

From the inspection of the results summarized in Table 7 and Figure 63, several points are worthy to discuss. First, in the fluoromethane complexes, the interaction energy with the charged OH^- guest is large and negative (–12.9 kcal/mol) and it is modest for the complex with the neutral formaldehyde guest (–1.9 kcal/mol). Interestingly, the carbon bonding complexes (or trifurcated hydrogen bonded) are found to be minima on the potential hypersurface. Moreover, the orientation of the oxygen lone pairs in the formaldehyde in its complexes with fluoromethane does not influence either the interaction energy or the equilibrium distance (complexes **43** and **44**). Second, the trimethylsulfonium and methanaminium complexes with neutral formaldehyde present large interaction energies, being more favorable with the protonated amine. Third, the interaction energies are identical for both orientations of formaldehyde; however in the case of trimethylsulfonium the C···O equilibrium distance is longer in complex **46** than in **47** and the S-C····O angle is smaller (172.0° in **46** and 178.6° in **47**, see Figure 63B). This behavior is not observed in methanaminium complexes **49** and **50** and both present almost identical geometric and energetic features.

Table 7. Interaction energies (BSSE corrected, ΔE_{BSSE}, kcal/mol) and equilibrium distances (R_1 and R_2, Å) for complexes **42**–**50** at the RI-MP2/aug-cc-pVTZ level of theory.

Complex	ΔE_{BSSE}	R_1 (C···O)	R_2 (C···H)
42	–12.9	2.654	2.521
43	–1.9	2.993	2.829
44	–1.9	2.993	2.830
45	–1	–1	–1
46	–8.5	2.822	2.502
47	–8.5	2.803	2.665
48	–1	–1	–1
49	–9.7	2.746	2.600
50	–9.7	2.746	2.614

[1] S_N2 attack.

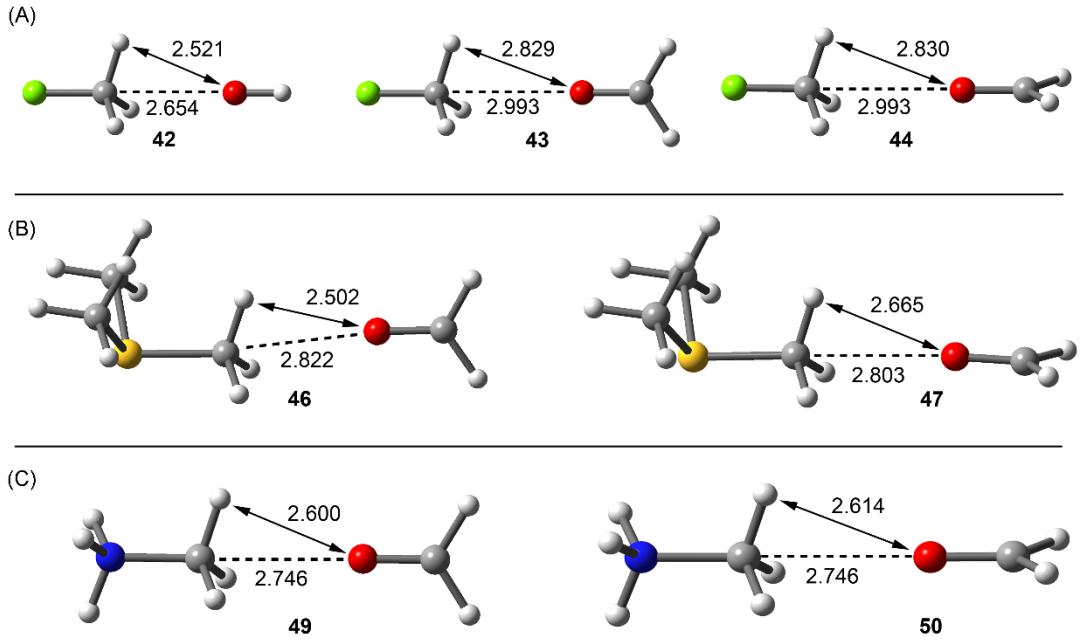

Figure 63. RI-MP2/aug-cc-pVTZ optimized complexes of fluoromethane (A), trimethylsulfonium (B) and methanaminium (C). Distances in Å.

2.5.4.3. AIM analysis

We have used the Bader's theory of "Atoms in molecules" (AIM) to characterize the noncovalent bonds in complexes **42**–**50** and also to differentiate the type of interaction (carbon or hydrogen bonding). A bond critical point (CP) and a bond path connecting two atoms is an unambiguous evidence of interaction. The AIM distribution of critical points and bond paths computed for the complexes is shown in Figure 64. In all CH_3F complexes (Figure 64A), the interaction is characterized by the presence of a bond CP that connects the O atom with the carbon atom, thus confirming the carbon bonding nature of this interaction. The value of ρ at the bond CP that emerges upon complexation is larger in complex **42** than in either complex **43** or **44**, in agreement with the interaction energies and equilibrium distances. In trimethylsulfonium complex **47**, where the S-C···O angle is close to 180°, the AIM analysis shows a bond CP and bond path unambiguously connecting the C and O atoms. In complex **46**, where the S-C···O angle is 172°, the bond path presents a different trajectory and, at first sight, seems to connect the O atom of formaldehyde to the C-H bond critical point. However, a closer look evidences that the bond path suddenly deviates when it reaches the C-H bond critical point and finally connects to the C atom.

The distribution in methanaminium complexes **49** and **50** (see Figure 64C) clearly shows a bond CP and bond path connecting the C and O atoms, thus confirming the carbon bonding nature of the interaction. In all cases, the Laplacian of ρ at the bond CP that connects the O and C atoms is positive, as is common in closed shell interactions. Interestingly, for the whole series of complexes the value of ρ strongly correlates with the interaction energies. Therefore the value of ρ can be used as a measure of bond order is this type of noncovalent bonding.

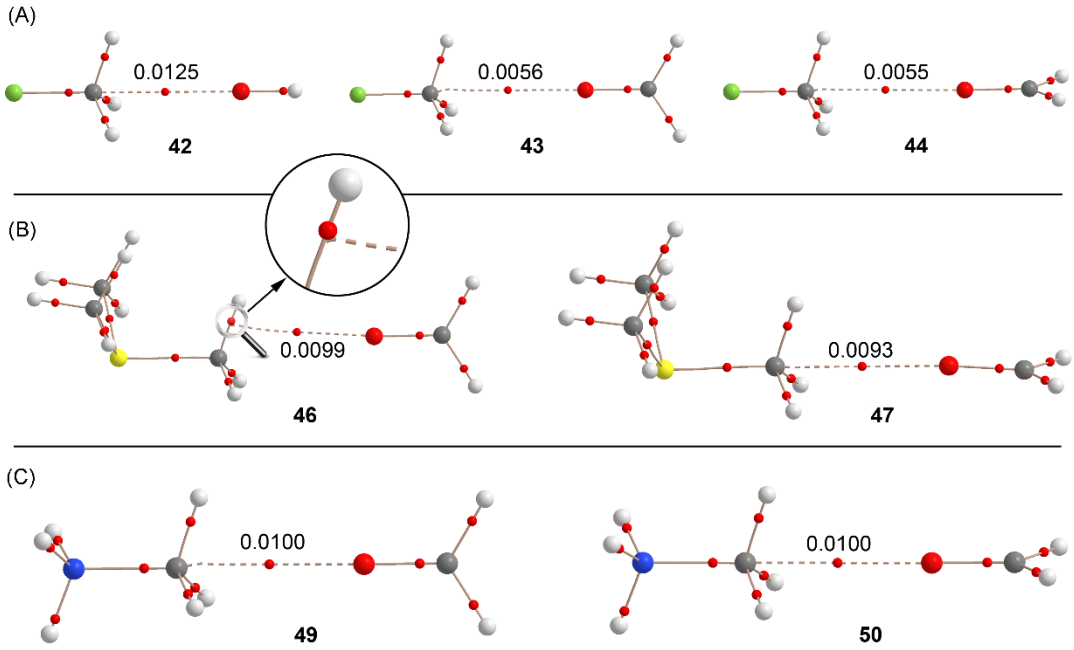

Figure 64. Distribution of critical points (red spheres) and bond paths for complexes of fluoromethane (A), trimethylsulfonium (B) and methanaminium (C) at the RI-MP2/aug-cc-pVTZ level of theory. The value of the charge density (ρ) at the bond critical points that emerge upon complexation is indicated in a.u.

We have also analyzed the effect of the X–C···O angle on the interaction to find the value that causes a change from carbon bonding to hydrogen bonding. For this study we have progressively changed the F–C···O angle (α) starting from 180° and moving the O atom in two opposite directions (see Figure 65A): (i) toward a single H atom (α < 180° values) and (ii) toward the middle of two H atoms (α > 180° values). In each point we have optimized the geometry and we have just frozen the angle to the desired value. Moreover, we have analyzed the distribution of critical points in order to find the value of α where the interaction changes from carbon to hydrogen bonding. In case that the OH^- moves to a single C-H bond (Figure 65B), the interaction rapidly changes from carbon bonding to hydrogen bonding; therefore the critical angle is close to 170°. This result agrees with the behavior observed for complex **46** (see Figure 64) that presents an S-C···O angle of 172° and the bond path trajectory reveals that it is in the borderline between both interactions.

When the OH^- moves to the opposite direction (toward the middle of two C-H bonds) the behavior is different: for α = 190° a bond path connects the C and O atoms similarly to fully optimized complex **42**. Curiously, for α = 200° and 210° two bond paths connect the C and O atoms, forming a bifurcated carbon bonding. As a consequence, a ring CP (yellow sphere) is also generated. Finally at 220° the carbon bonding changes to a bifurcated hydrogen bonding interaction.

This analysis is useful to define the search criteria of carbon bonding complexes in X-ray structure databases (CSD, PDB, etc.). Since the H atoms bonded to C are usually not experimentally located, there exists some uncertainty regarding their real position in the CH_3 group. Therefore, it is recommended to use a tight criterion

regarding the X-C···O angle (i.e. α > 170°) while searching for this type of noncovalent carbon bonding X-ray structures.

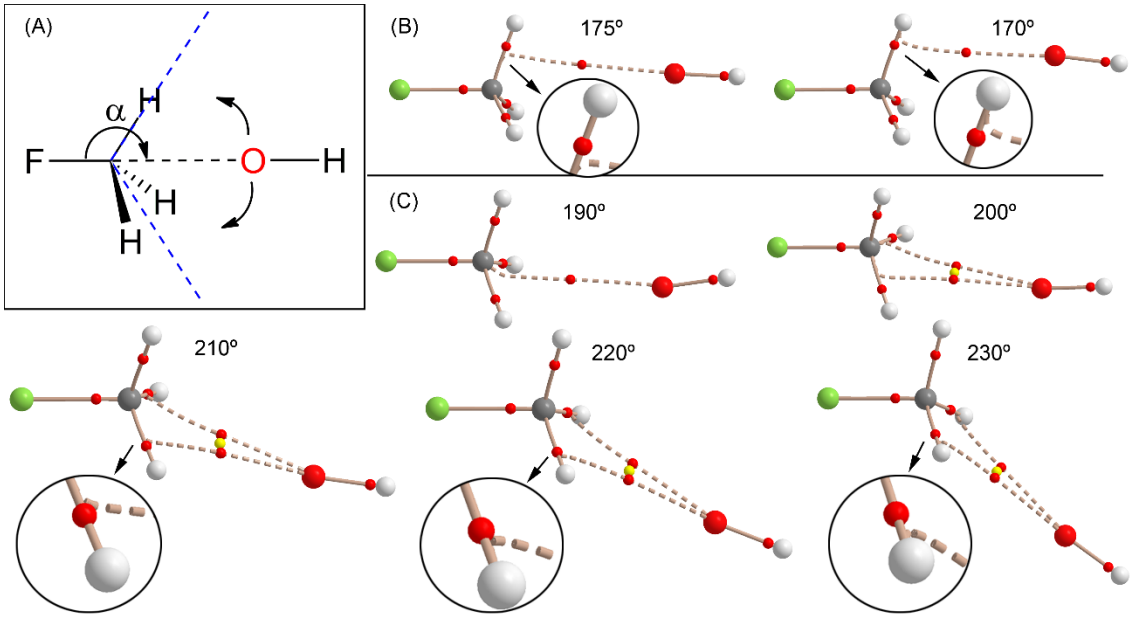

Figure 65. (A) Schematic representation of the angle and both directions. (B) Distribution of critical points (red spheres) and bond paths for complexes of fluoromethane with OH^- using F-C···O angles < 180° at the RI-MP2/aug-cc-pVTZ level of theory. (C) Same as (B) but using angles α > 180°.

2.5.4.4. PDB search

We have explored the PDB in order to evidence the importance of carbon bonding interactions in biologically relevant molecules. The following criteria have been used for the search. (i) The CH_3 donor group belongs to the ligand and the O atom is part of the protein; (ii) C···O distance (*d*) shorter than 3.2 Å and the X-C···O angle (A) > 170°; (iii) only X-ray solid state structures were considered (no NMR resolved); (iv) resolution factor < 10 Å. The search was performed using the freely available Relibase software.[201] As a result, we have found 459 protein-ligand complexes exhibiting this type of bonding (see SI for the full list of hits and their geometrical features, Table S1). The histograms plots for the angle and distance are represented in Figure 66. It should be emphasized the importance of this result since we have found a large number of hits, taking into consideration the tight geometric criteria used and that only one electron-rich element has been used in the search (O). Therefore, the carbon bonding interaction in general has a bright future in this field and it will likely become a prominent player for explaining some biological processes, either controlling or fine tuning the binding of substrates to enzymes.

In the original manuscripts where the protein-ligand complexes were reported the X-CH_3···O interaction was either overlooked or considered as a hydrogen bonding by the original authors. We have selected two examples from this search to further illustrate the importance of this interaction.

[201] https://www.ccdc.cam.ac.uk/Community/freeservices/Relibase/ (accessed on 25 January 2016).

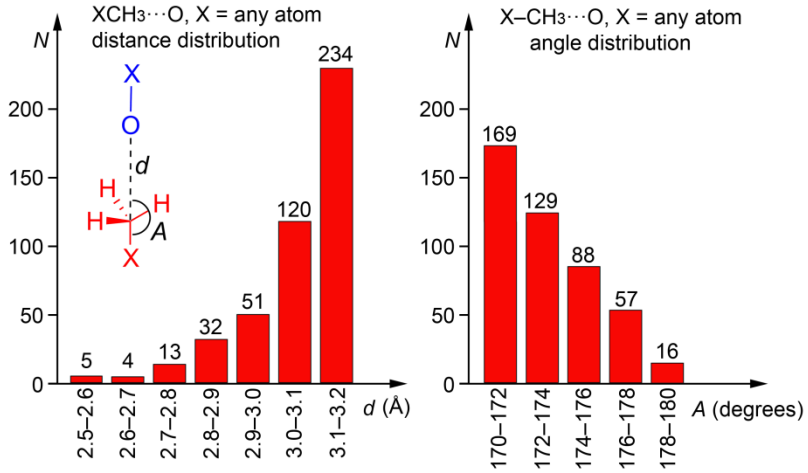

Figure 66. Histograms obtained directly from the Relibase software. Distance distribution is shown on the left and the angle distribution on the right of the figure. Inset figure: definition of d and A parameters, the protein is represented in blue and the ligand in red.

For the first example[202] we have selected a very well resolved X-ray structure (PDB ID: 4NSY, resolution 1.1 Å. see Figure 67A) that is a covalent complex between a trypsin-type serine protease (lysyl endoproteinase, LysC) and its inhibitor Nα-p-tosyl-lysyl chloromethylketone (TLCK). Chloromethyl ketones such as TLCK (Figure 67B) are well known covalent inhibitors of cysteine and serine proteases.[203] Two covalent bonds are formed with serine proteases, each one to the active-site serine and histidine. Similarly, in LysC enzyme, the TLCK inhibitor is attacked by SER194 and by nucleophilic substitution of the Cl atom by HIS57. This covalently bonded inhibitor interacts with the other subunit by means of a noncovalent carbon bonding interaction (see Figure 67A). We have constructed a model to evaluate energetically this interaction. We have substituted the SER193 and HIS47 that are covalently bonded to the inhibitor by C-H bonds in order to keep the size of the system computationally approachable. The model also includes the alanine residue and part of the peptide backbone (see Figure 67C). The interaction energy is –1.8 kcal/mol that is similar to that obtained for neutral complexes **43** and **44** (see Table 7). Remarkably, the distribution of CPs shows a bond critical point and a bond path connecting the O atom of the amide group to the carbon atom of the inhibitor, thus confirming the existence of the carbon bonding interaction in 4NSY.

The second example we have selected[204] corresponds to the structure of a M3 muscarinic acetylcholine receptor bound to tiotropium (PDB ID: 4U14, resolution 2.5 Å. see Figure 68A). Tiotropium is a muscarinic receptor antagonist (anticholinergic bronchodilator) used in the management of chronic obstructive pulmonary disease.[205] The presence of a dimethylammonium group in the structure ensures their ability to form electrostatically assisted carbon (or hydrogen) bonding interactions using the R_3N^+-CH_3 groups. As a matter of fact, an aspartate residue of the active site is very close to a carbon atom belonging to one of both methyl groups

[202] P. Asztalos, A. Müller, W. Hölke, H. Sobek, M. G. Rudolph, *Acta Cryst.* **2014**, *D70*, 1832–1843.
[203] J. Drenth, *Biochem.* **1976**, *15*, 3731–3738.
[204] T. S. Thorsen, R. Matt, W. I. Weis, B. K. Kobilka, *Struct.* **2014**, *22*, 1657–1664.
[205] M. Kato, K. Komamura, M. Kitakaze, *Circ. J.* **2006**, *70*, 1658–1660.

(2.935 Å) with an almost linear N–C···O angle (177.4°). We have used a theoretical model derived from the crystallographic coordinates that includes the antagonist and the aspartate bonded to a fragment of the peptide backbone. The AIM analysis confirms the existence of a carbon bonding interaction (see bond path in Figure 68A). The ASP147 residue is likely deprotonated in the X-ray structure, since both C–O distances are very similar (1.248 and 1.250 Å). In any case we have evaluated the interaction energy considering both possibilities. The interaction energy of the carbon bonding complex using the protonated ASP147 is –9.0 kcal/mol. Moreover, the value of the density at the bond critical point is ρ = 0.0093 a.u. These values strongly agree with those previously computed for methanaminium, see Table 7 and Figure 64 (complexes **49** and **50**). Considering the deprotonated ASP147, the interaction energy is very large (–73.9 kcal/mol) due to the strong electrostatic contribution. Therefore this charge assisted carbon bonding interaction has a strong influence on the binding of tiotropium in the muscarinic acetylcholine receptor.

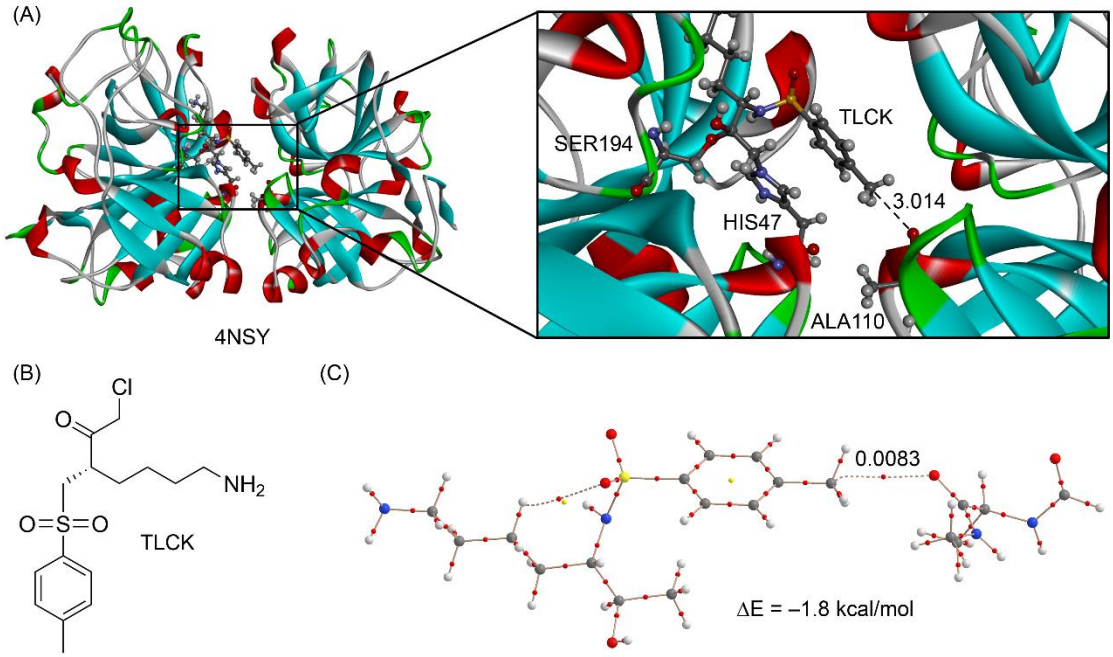

Figure 67. (A) X-ray structure of 4NSY with indication of the carbon bonding interaction (distance in Å). (B) Chemical drawing of the TLCK. (C) AIM distribution of critical points of a model derived from the X-ray coordinates. The value of the density (ρ) at the BCP is also given in a.u.

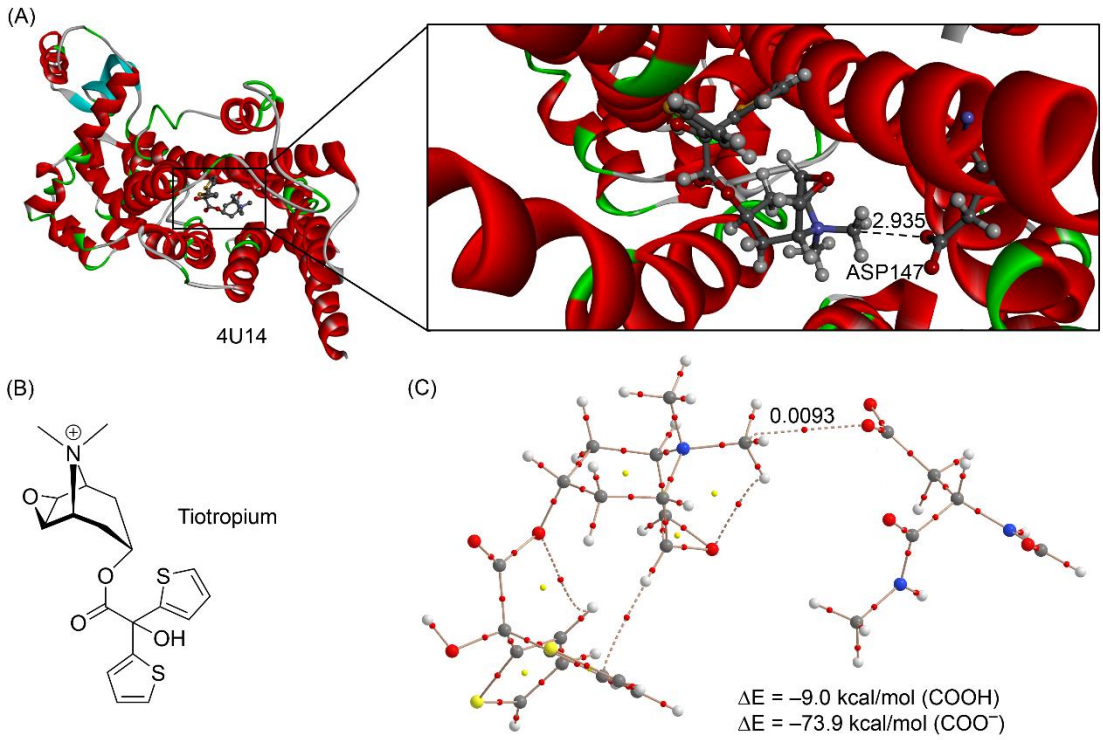

Figure 68. (A) X-ray structure of 4U14 with indication of the carbon bonding interaction (distance in Å). (B) Chemical drawing of the tiotropium antagonist. (C) AIM distribution of critical points of a model retrieved from the X-ray coordinates. The value of the density (ρ) at the BCP is also given in a.u.

2.5.4.5. NBO analysis

To study if orbital effects are important to explain the carbon bonding interactions described above, we have performed natural bond orbital (NBO) calculations focusing our attention on the second order perturbation analysis, due to its usefulness to study donor-acceptor interactions.[206] We have carried out the NBO calculations for complex **42** and for the theoretical model used to characterize the interaction in the PDB ID 4U14 (see Figure 68C). The results of the second order perturbation analysis are summarized in Table 8. For complex **42** we have found an important orbital contribution that consist in the interaction of the lone pair orbital (LP) of the donor with the C-F antibonding orbital (BD*) of the acceptor. This interaction is significant (3.5 kcal/mol) since it accounts for approximately the 27% of the total interaction energy and further confirms that the interaction in complex **42** is with the σ-hole of the carbon atom. Moreover the expected LP→BD*(C-H) orbital contribution that is typical of a hydrogen bond is less than 0.1 kcal/mol. Similarly in the PDB 4U14 we have found an interesting LP(O)→BD*(C-N) contribution that is also 2.0 kcal/mol and that the LP(O)→BD*(C-H) interaction is less than 0.1 kcal/mol in sharp agreement with the AIM analysis commented above.

[206] F. Weinhold, C. R. Landis, *Valency and Bonding: A Natural Bond Orbital Donor-Acceptor Perspective*, Cambridge University Press, Cambridge, UK, **2005**.

Table 8. Donor and acceptor NBOs with indication of the second-order interaction energy $E^{(2)}$ and donor and acceptor orbitals for complexes **42** and PDB ID 4U14. Energy values are in kcal/mol.

Complex	Donor[1]	Acceptor	$E^{(2)}$
42	LP (O)	BD* (C-H)	<0.1
	LP(O)	BD* (C-F)	3.5
4U14	LP (O)	BD* (C-H)	<0.1
	LP(O)	BD* (C-N)	2.0

[1]LP stands for lone pair orbital and BD* for antibonding orbital.

2.5.4.6. SAPT analysis

In Table 9 we summarize the DF-DFT-SAPT energy values relative to some of the carbon bonding complexes showed above in order to know the relative importance of the electrostatic contribution to the total interaction energies, especially those involving charged carbon bonding donors. The total SAPT interaction energies for these three complexes are similar to those obtained using the RI-MP2/aug-cc-pVTZ level of theory (see Table 7) giving reliability to the partition method and the level of theory used to compute the SAPT. The energetic contributions (Table 9) indicate that the cationic complexes **47** and **50** are clearly dominated by the electrostatic term. Moreover, the contributions of induction and dispersion terms are also important. In the neutral complex **44** the electrostatic and dispersion terms equally contribute to the total interaction energy.

Table 9. SAPT interaction energies (E_{total}, kcal/mol) and their partitioning into the electrostatic, exchange, induction, dispersion and contributions (E_{ee}, E_{ex}, E_{ind}, E_{disp}, respectively, kcal/mol) at the BP-86/aug-cc-pVTZ level of theory using the DF-DFT-SAPT approach.

Complex	E_{ee}	E_{ex}	E_{ind}	E_{disp}	E_{total}
44	–1.8	2.1	–0.2	–1.6	–1.5
47	–8.3	4.4	–1.3	–2.4	–7.6
50	–9.5	4.8	–1.7	–2.3	–8.7

To further demonstrate the importance of electrostatic forces in the interaction energies of compounds **47** and **50**, we have computed the carbon bonding interaction of their equivalent neutral complexes where methylamine and dimethylthioether are used as carbon bond donors. The results are gathered in Figure 69 and it can be observed that the interaction energies are very small (–0.7 kcal/mol for **51** and –1.1 kcal/mol for **52**) in agreement with the MEP surfaces of methylamine and dimethylthioether shown in Figure 62. Moreover, it is worthy to emphasize the localization of the minima corresponding to the carbon bonding complexes **51** and **52** (see Figure 69) on the potential surface, since the MEP value at the H-atoms is considerably more positive than that at the C atom in both neutral molecules.

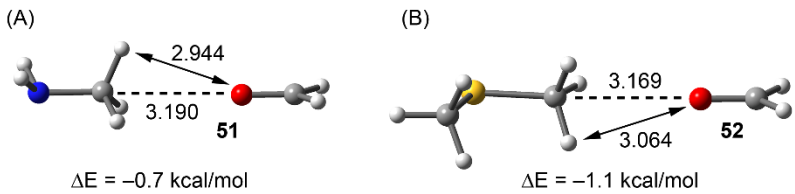

Figure 69. RI-MP2/aug-cc-pVTZ optimized complexes end interaction energies of methylamine (A) and dimethylthioether (B). Distances in Å.

2.5.5. Conclusions

In this manuscript we have analyzed the dual ability of the methyl group (XCH_3) to act as either hydrogen bond or carbon bond donor in complexes with electron-rich oxygen atoms by means of high level *ab initio* calculations and using the Bader's theory of "Atoms in molecules". For X-C···O complexes exhibiting angles close to linearity, a carbon bonding interaction instead of a hydrogen bonding is established as confirmed by AIM and NBO analyses. The importance of electrostatic and dispersion contributions to the interaction energy of the carbon bonding complexes has been shown using the SAPT partition scheme. We have demonstrated the importance of latter interactions in biological systems by examining the PDB and illustrated in two selected examples. Since $-CH_3$ groups are commonplace, noncovalent carbon bonding involving this group might turn out to be as functionally relevant as other σ-hole and hydrogen bonding interactions.

2.5.6. Acknowledgements

We thank CONSOLIDER-Ingenio 2010 (project CSD2010-0065) and the MICINN of Spain (project CTQ2014-57393-C2-1-P FEDER funds). We thank the CTI for computational facilities.

2.5.7. Supporting information

Table S1. Results from the PDB search. Distances in Å. Angles in degrees.

LIG ID	Ligand position	PDB-ID	Distance	Angle
17	202-B	3UCB	2.93	172.0
133	246	1GJ8	2.90	174.1
282	2001-X	2RBZ	2.96	171.1
372	303-A	4GR9	3.01	177.2
592[a]	1224-A	4AWQ	3.11	170.2
861	201-D	4GGQ	3.19	171.4
0HK[a]	2000-A	4DAJ	2.81	170.2
0JZ	6002-B	3G60	3.17	174.7
0MS	601-B	4DYP	2.93	172.1
17E[a]	502-F	4R85	3.20	170.3
1EU	2-A	3FV5	3.12	174.5
2KT	524-B	3TDF	2.87	174.1
2L0	301-H	4NO9	2.94	177.7

LIG ID	Ligand position	PDB-ID	Distance	Angle
2NR	1001-A	4NW5	3.18	173.5
2OY[a]	301-B	4NSY	3.01	171.5
2VA	901	1WNZ	3.16	177.6
30B	500-D	3KEE	3.09	172.4
3BV[a]	201-b	4QWL	3.00	172.0
3G4	2007-D	3G49	2.72	170.4
3PK	501-A	4K7R	3.16	171.4
41Z	401-A	4XJT	2.78	171.7
4MB	1603	2HDS	3.10	170.2
5MC[a]	501-C	4JNP	3.17	170.6
6HE	154-A	2EKT	3.19	173.0
7DE	102	1Y2J	3.17	174.4
ACE-LEU-ALA-DCL-POL	1-c	4Y74	3.09	177.7
ACE-XXXLXLXX-MLU-GLY	1-C	5AH4	3.09	173.4
ACM	360-A	3IDS	3.16	175.0
ACT[a]	1722-C	4AJ9	3.12	171.1
ACY[a]	1643-A	2WQ8	3.03	172.0
ADN	300	1MRJ	2.87	175.3
AITLIFI	1-D	2GRM	3.19	171.7
ARTMQTARKSTG AKAP	1-C	2V1D	2.52	175.4
ARTX	1-B	3MEA	3.16	172.9
ARTXQTA	1-D	2GFA	3.20	176.5
ASP-PLP	414-C	1GCK	2.84	178.2
AVI	401-A	4PIN	3.04	172.9
B12[a]	1801-D	3KOX	3.19	170.4
B35	449-A	3H0B	3.12	170.1
BB2	194-D	3M6R	3.15	175.8
BCL[a]	852	1Z9J	3.19	170.8
BCR[a]	514-c	4TNI	3.09	170.0
BET	264-A	3T27	2.92	176.3
BOG	705-C	4RRY	3.10	171.9
BTM	406-A	4LTZ	3.09	173.1
BU3	1030-G	3SE9	2.79	170.6
CAC	1301	1TYE	3.00	172.1
CL1[a]	1226-B	3LW5	2.85	170.3
CLA[a]	606-C	2BHW	2.83	170.1
CLR	253-A	3GKI	3.18	170.8
CNO	801	1K0Y	2.95	170.6
COH[a]	154-X	205T	3.17	174.7
CRT	103-F	3WMO	3.15	171.2
CWB	1207-A	2YME	3.10	170.7
CXE	503-D	4MLB	3.10	177.4
CYC[a]	255-P	1HA7	3.13	170.5
D2B	187-A	3NXO	3.18	173.2
DDJ	801-A	3VLJ	3.04	171.1

LIG ID	Ligand position	PDB-ID	Distance	Angle
DMA[a]	998-B	3KEF	2.94	173.0
DMS[a]	103	2OHM	2.87	170.4
DTM	187	1MVT	3.16	174.3
EKRVASSVFITLA PP	6-K	4P3W	3.12	172.2
EMC	451-A	1EMS	3.05	170.5
ENB	145	2D2D	2.77	174.4
EOH	401-A	4MUL	3.16	174.8
EP	1001	1TVK	2.82	176.1
FAD[a]	7202	2PD7	2.96	171.4
FMN	400-D	4LAF	3.08	171.2
FOK[a]	2	1AB8	2.92	171.3
G39	501-A	4GZT	2.65	177.1
GEA	3990	1D8T	3.12	172.4
GLY-TYR-GLU	756-F	3SV1	3.00	171.4
GPP	903-H	1H48	3.01	176.1
GPRV	1-J	2FFD	3.11	173.0
HEA[a]	559-A	3EHB	3.20	171.7
HEB[a]	201-A	4I0V	3.05	172.0
HEEAVSVDRVL	1-C	3LN5	3.01	172.7
HEM[a]	1001-A	2YYW	3.16	170
IM1	400	1TCW	3.20	170.4
IPA	1423-A	2WGE	3.16	170.7
IRC	410-A	3O3N	3.01	173.2
IZN[a]	400-D	4ALX	3.10	170.9
JUS	1257-G	4BNN	2.97	172.2
KLTPLCVTL	1-C	2X4O	3.19	177.5
KMIDFATLSKLKK KYQIILD	461-C	3OWT	3.10	172.7
L1G	1506-A	2C0I	3.14	176.7
LAC	398-C	2PI1	2.62	174.1
LDA[a]	504-B	2R4O	3.18	170.1
LLFNILGGWV	1-P	3MRN	3.08	173.6
LN5	500-B	3I4A	3.09	171.0
LVEALYLVCGERG G	1-C	1JK8	3.19	172.4
M8E	368-A	3DZ6	3.13	171.9
MBV	1207-A	1HE3	2.44	171.1
MD4	301-A	4WV9	3.14	172.6
MER	401-A	2ZD8	3.17	176.9
MGR	200-A	3BQZ	2.30	171.6
MHZ	368-A	1I79	3.06	173.2
MLK	301-A	3SH1	2.81	172.7
MNH	154-X	2O5Q	3.14	171.3
MNR[a]	154-X	2O5M	3.16	170.9
MPD[a]	3-D	3DCX	3.07	170.2
MRD	304-C	3NO6	3.12	173.4
MUR	1670-A	3ZFZ	2.76	171.6

LIG ID	Ligand position	PDB-ID	Distance	Angle
NAG[a]	1694-A	2IUF	3.18	171.5
NAG-NAG[a]	606-C	4MIV	2.89	171.0
NAG-NAG-BMA	5158-C	3I26	3.18	176.7
NAG-NAG-BMA-MAN	2006-A	4G1E	3.06	171.7
NAG-NAG-FUL	608	1MAA	3.15	171.1
NDG-NAG-BMA-MAN-MAN-MAN-MAN-MAN	1-C	1O7D	2.77	170.2
NTE	201-A	3VAU	3.18	172.0
NVW	901-A	3W5E	3.12	177.1
NZF	1501-A	4FNZ	2.83	172.8
OLO	800	4ERK	3.15	172.4
P68	501-H	4MY1	2.95	177.1
PDA	401-X	4ZU8	3.17	174.2
PDS	902	2I0E	3.09	174.5
PE5	534-B	2YEQ	3.04	172.1
PFNVDDVLKFTFTGEK	195-K	2HZS	3.18	170.7
PFNVDDVLKFTFTGEKH	195-L	2HZS	3.19	171.6
PGO	1602	1IWP	3.11	171.5
PHE-HIS-PRO-ACE-NH2	1-P	1MCJ	3.13	175.2
PLP[a]	1430-B	2X5F	3.17	171.6
PSC	303-O	3X2Q	3.10	172.6
PTT[a]	801	1B25	2.50	171.1
PVKKPKIRR	297-B	4WV6	2.87	177.5
PWK	201-B	4PWK	2.76	170.7
PYR-SMM	68-A	3EP7	3.10	173.0
QO9	556-A	3QO9	3.13	174.0
R19[a]	800-B	1O6R	3.03	170.2
RVB	451-B	3RV7	3.09	171.1
SAV	1167-A	3CJF	3.03	175.1
SAZ	709	1YYR	3.05	175.2
SIA	782	1YAJ	3.11	170.1
SLLMWITQV	1-F	3GJF	3.13	177.3
SMM	368-A	3DZ3	2.99	170.5
SZ8	8-A	3RXK	3.11	171.4
T9N	1296-C	4BCN	2.84	172.5
TCU	1257-A	4BNM	2.97	170.1
TSHKLVQLLTT	629-B	3H0A	3.12	171.3
TSSKIYDNKNQLIADL	51-A	2C5W	2.97	174.3
TZZ	901	2D2H	3.15	175.9
UQ1	614	1PRC	2.81	170.3
V55	1251-D	2VSU	3.13	171.5
WYQ	701-A	3V94	2.95	171.2
XRS	301-A	3ZDH	3.01	171.1

LIG ID	Ligand position	PDB-ID	Distance	Angle
XRX	301-J	3ZDG	3.16	170.6
YLVTSV	2838-B	4G69	3.13	171.1
ZGA	301-B	3VJE	3.17	173.6
ZZC	401-A	2WOD	3.19	171.3

[a]For these ligands only one entry is shown. More details can be found in *Crystals* **2016**, *6*, 26.

Chapter 3

Pnicogen bonding Interactions

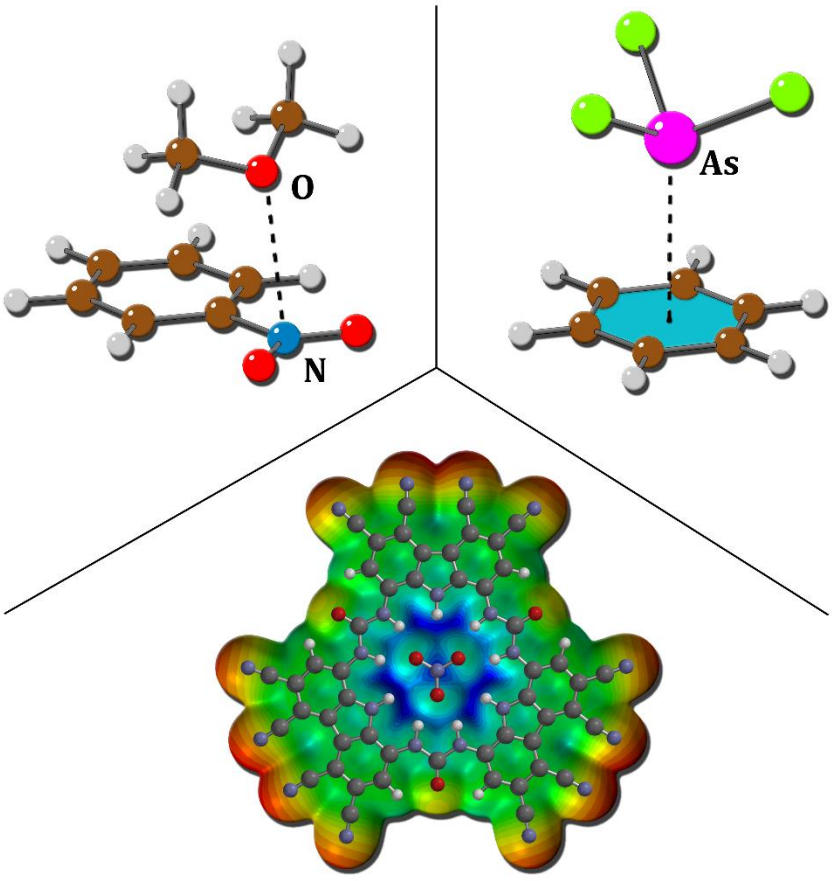

3.1. Preface and Objectives

This chapter is devoted to the study of σ- and π-hole interactions involving pnicogens. The chapter is divided into three sections: firstly *section 3.2.* analyzes the directionality of π-hole interactions involving the nitro group and electron-rich moieties. This study is supported by an statistical analysis of the CSD. Secondly, *section 3.3.* reveals an uncommon and novel behavior of a well know anion, that is, NO_3^- can behave as Lewis acids in the proper chemical context, thus opening the door to a new interpretation of the role that anions play in chemical processes. A variety of supportting evidences were found, both in the CSD and PDB databases. Finally, *section 3.4.* is devoted to the study of the interaction between sp^3 pnicogen atoms and aromatic moieties, named pnicogen-π interactions. In addition, several experimental examples are highlighted, particularly in the field of biological chemistry.

The main objectives of the chapter are listed below:

- Study the directionality of π-hole interactions involving the nitro group using the CSD as a reliable source of experimental data.

- Unveil the potential of NO_3^- to behave as a Lewis acid center in solid state chemistry, including both PDB and CSD database analyses.

- Analyse the interaction between a pnicogen sp^3 atom and an aromatic system as well as its biological implications using the PDB database.

3.2. Directionality of π-holes in nitro compounds.

3.2.1. Abstract

A statistical survey of the Cambridge Structural Database reveals that the interaction between the π-hole of nitro groups and electron-rich atoms is somewhat directional. High level *ab initio* computations indicate energies up to –6.6 kcal/mol.

3.2.2 Introduction

Intermolecular interactions determine how molecules interact with one another and are thus fundamental to inquiries in areas like supramolecular chemistry and molecular biology.[1,148] It is well-appreciated that even weak interactions (e.g. hydrogen bonding involving C-H) can bear functional relevance, especially when several such forces work in concert.[166,153c] This begs the question what weak interactions can be identified as possibly functionally relevant. Hydrogen (H) and halogen (Hlg) bonding are by far the best established intermolecular forces.[207] The regions of electropositive potential on R-H or R-Hlg (Figure 70A and B, phenol and bromobenzene, respectively) can be described as an unpopulated σ* antibonding orbital along the R–H/Hlg vector.[207b,c] These 'σ-holes' have also been identified on atoms that belong to the oxygen, nitrogen and carbon families, and their binding to electron-rich entities is referred to as Chalcogen-,[62f,208] Pnicogen-,[70,73a,209] and Tetrel-bonding[86a,86b,157,210] respectively.

In analogy to the σ-hole, a π-hole can be seen as an electropositive potential located on an unpopulated π*-orbital. The best-known π-hole interactions involve carbonyl compounds (e.g. Figure 70C: *p*-quinone): Bürgi and Dunitz[15] uncovered the trajectory along which a nucleophile attacks the π-hole of a carbonyls' C atom, and π-hole interactions involving amides are known to persist in protein structures.[105] Aromatic rings bearing electron withdrawing substituents such as hexafluorobenzene (Figure 70D) can also function as a π-hole.[113,211] Interactions involving such π-acidic aromatic rings are generally referred to as anion- or lone pair-π interactions.[9a]

---

[207] a) *Hydrogen Bonding: New Insights*, Springer, Heidelberg, **2006**; b) M. Erdélyi, *Chem. Soc. Rev*. **2012**, *41*, 3547–3557; c) G. Cavallo, P. Metrangolo, T. Pilati, G. Resnati, M. Sansotera, G. Terraneo, *Chem. Soc. Rev*. **2010**, *39*, 3772–3783.
[208] a) D. B. Werz, R. Gleiter, F. Rominger, *J. Am. Chem. Soc.* **2002**, *124*, 10638–10639; b) P. Sanz, O. Mó, M. Yáñez, *Phys. Chem. Chem. Phys*. **2003**, *5*, 2942–2947.
[209] a) S. Scheiner, *J. Chem. Phys*. **2011**, *134*, 094315, 9p; b) J. E. Del Bene, I. Alkorta, G. Sánchez-Sanz, J. Elguero, *J. Phys. Chem. A* **2012**, *116*, 9205–9213.
[210] A. Bauzá, T. J. Mooibroek, A. Frontera, *Chem. Commun.* **2014**, *50*, 12626–12629.
[211] T. J. Mooibroek, P. Gamez, *CrystEngComm* **2012**, *14*, 3902–3906.

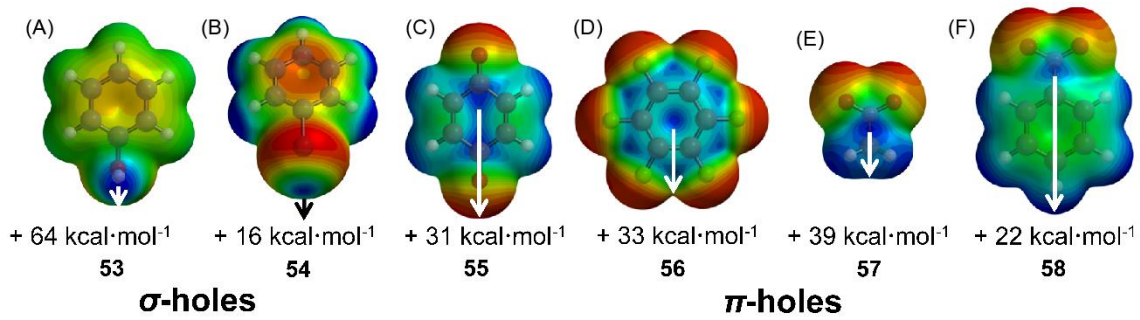

Figure 70. Some σ-and π-holes with their electropositive potential (MP2/6-311+G**).

A recent theoretical study revealed that a π-hole can also be found on a nitro group.[19a] Association of this π-hole with electron-rich entities (ElR, e.g. H_2O, Cl^-) was estimated to vary in strength between –0.5 and –27.9 kcal/mol. Figure 70E and F illustrates the π-holes in nitromethane and nitrobenzene respectively. One might thus wonder if the 'NO_2π···ElR' interaction bears any functional relevance. A first step in answering this question is to establish whether this intermolecular force actually is directional. Analysis of the data compiled within the Cambridge Structural Database (CSD)[104b] has proven to be an exquisite tool in revealing the directional nature of traditional and non canonical intermolecular forces. We thus set out to evaluate the CSD using a methodology that is particularly apt for ascertaining the directional character of weak intermolecular forces.[211,113]

3.2.3. Computational methods

The energies of all complexes included in this study were computed at the RI-MP2/def2-TZVPD//BP86-D3/def2-TZVPD level of theory. The calculations have been performed by using the program TURBOMOLE version 6.4. The MEP calculations have been performed at the MP2/6-311+G** level of theory using the Spartan v.10 program. The C_s symmetry point group was imposed during the optimization process. The interaction energies were calculated with correction for the basis set superposition error (BSSE) by using the Boys-Bernardi counterpoise technique.

3.2.4. Results and discussion

Aliphatic and aromatic C-NO_2 compounds are abundant within the CSD: there are 900 Crystallographic Information Files (CIFs) containing nitromethane, and 14,227 CIFs containing an aromatic nitro compound where the NO_2 moiety is flanked by two *ortho*-H's (this allows the NO_2 and C_6H_2 moieties to be relatively coplanar). Illustrated in Figure 71A is the query used to obtain initial datasets from the CSD.

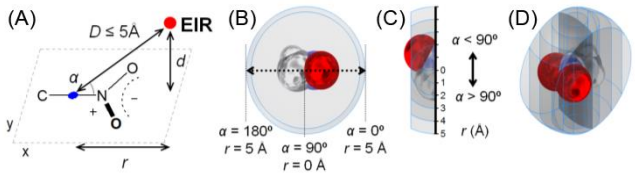

Figure 71. Illustrations of the method used to analyse directionality of intermolecular interactions between an electron-rich atom (El.R., N, P, As, O, S, Se, Te, F, Cl, Br, I or At) and a nitro group (in this illustration nitromethane).

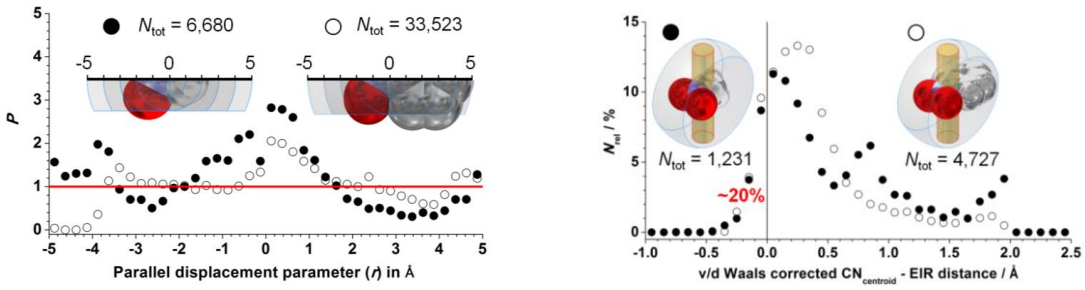

Figure 72. Analysis of the directional nature of CNO_2 π-holes. Left: directionality plots of *P vs. r* for $CH_3NO_2\cdots$ElR (●, N_{tot} = 6,680) and $C_6H_2NO_2\cdots$ElR (○, N_{tot} = 33,523) of the data characterized by $D \leq 5$ Å and $y \pm 2$ Å; Right: $N_{relative}$ *vs.* v/d Waals corrected $CN_{centroid}$-ELR distance (assuming $(v^{dWC}+v^{dW}N)/2$ = 1.625 Å) for $CH_3NO_2\cdots$ElR (●, N_{tot} = 1,231) and $C_6H_2NO_2\cdots$ElR (○, N_{tot} = 4,727) of the data characterized by $D \leq 5$ Å and $r \pm 1$ Å.

An entry was considered a hit when the *inter*molecular distance (*D*) between the C–N centroid (blue) and any electron-rich atom (red, ElR = N, P, As, O, S, Se, Te, F, Cl, Br, I or At) was ≤ 5 Å. The initial dataset is thus confined within a sphere with a radius of 5Å, centred on the C–N centroid. The spatial separation (*d*) between ElR and the CNO_2 plane was also retrieved from the CSD. The xy coordinates relative to this plane were determined as described elsewhere.[159c] By virtue of Pythagoras's theorem, the parallel displacement parameter *r* could be derived from *D* and *d*. The $CN_{centroid}$-N-ElR angle (α) was measured as well.

For this study, only the data characterized by $y = \pm 2$ Å was considered, which are therefore located within the 4 Å wide spherical segment illustrated in Figure 71B-D. The data can thus be characterized by the parallel displacement (*r*) within this spherical segment, either towards the NO_2 group ($\alpha < 90°$) or towards the atoms attached to C ($\alpha > 90°$). To analyse directionality, we applied a method described in detail elsewhere.[113,211,159] This method entails computing the parameter *P*(*r*), which signifies the distribution of the data along *r* that has been corrected for the volume occupied by the host and for a random scattering of data. When $P \neq 1$, a *non-accidental clustering* of data is established and $P > 1$ is indicative of an attractive interaction.

The *P* versus *r* plots for CH_3NO_2 (black circles) and $C_6H_2NO_2$ (open circles) are shown in the left hand side of Figure 72. For both 'hosts', $P > 1$ around $r = 0$, indicating some directionality of the π-hole. The *P*-values of 2–3 are similarly to those observed for C-H$\cdots\pi^{phenyl}$ hydrogen bonding.[160] In the case of CH_3NO_2, the

observed clustering is spread out over the region ranging from r = –1 to +1 Å. It is likely that CH···ElR hydrogen bonding also contributes to the observed distribution. The clustering observed for aromatic NO_2 is spread out over the region r = 0 to +1 Å, and hydrogen bonding cannot contribute in this case. It was further assessed how exactly the data is distributed within the data characterized by $-1 > r < 1$Å. Thus, the relative hit fraction was plotted as a function of the van der Waals corrected $CN^{centroid}$···ElR distance, as is shown in the right hand side of Figure 72. For both central groups roughly 20% van der Waals overlap is present. These two plots together indeed show that a nitro moiety can be a directional π-hole donor.

We have analysed theoretically (see SI for details) several representative complexes between electron-rich moieties and nitrobenzene (Figure 73A; a similar study with nitromethane is reported elsewhere).[19a] The interaction energies and some geometric features of the complexes are gathered in Table 10.

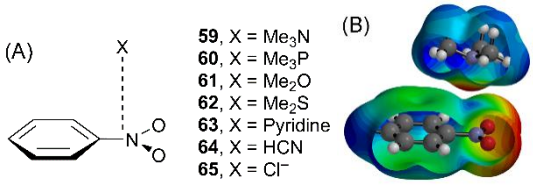

Figure 73. (A) Complexes **59–65** studied in this work. (B) Pictorial representation of the complementarity of the MEP surfaces of nitrobenzene and trimethylamine.

Table 10. BSSE corrected interaction energies (ΔE_{BSSE}, kcal/mol) and equilibrium distances from the electron-rich atom to the N (D_N) and C (D_C) atoms of the C–NO_2 moiety (in Å) of complexes **59–65** at the RI-MP2/def2-TZVPD//BP86-D3/def2-TZVPD level of theory.

Complex	ΔE_{BSSE}	D_N	D_C
59	–6.2	2.770	2.932
60	–4.3	3.636	3.547
61	–4.4	2.825	2.931
62	–4.7	3.416	3.448
63	–4.7	2.956	3.001
64	–2.3	3.181	3.191
65	–6.6	3.204	3.047

The interaction energies are similar for nearly all complexes ranging from –2.3 to –6.6 kcal/mol and the most favourable one corresponds to chloride complex **65**. The π-hole in nitrobenzene is located along the C–N bond and close to the nitrogen atom (see Figure 70F and 73B). We have included both ElR···N and ElR···C distances (denoted as D_N and D_C respectively) in Table 10. All complexes exhibit similar D_N and D_C distances and in all cases the electron-rich atom is located over the C–N bond, in agreement with the MEP analysis. The interaction energy is modest in complex **64** due to the low basicity of the sp-hybridized nitrogen atom of the HCN molecule.

The optimized geometries of some complexes are shown in Figure 74, including the "Atoms in molecules"[196,212] distribution of critical points computed for complexes **59** (lone pair donor ElR) and **65** (anionic ElR). The optimized geometries and critical point distribution for the rest of complexes are included in the SI. It can be clearly observed in Figures 74 and S4 that the position of the ElR atom of the interacting molecule coincides with the location of the π-hole in all complexes, indicating that the interaction is basically electrostatic in nature.

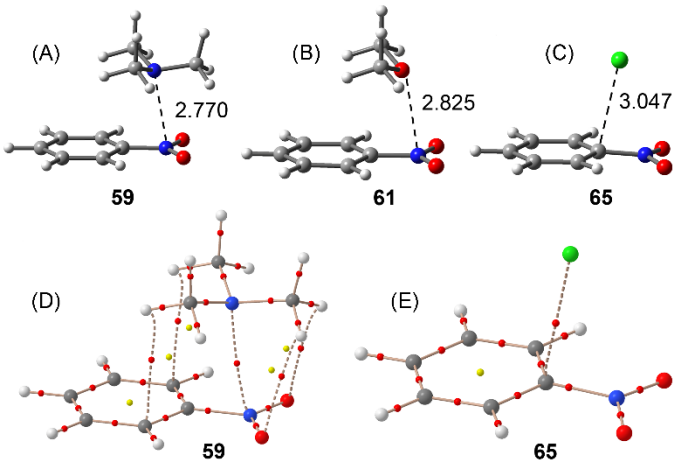

Figure 74. (A-C) Optimized π-hole complexes **59**, **61** and **65** studied in this work. (D, E) Distribution of critical points in complexes **59** and **65** (bond and ring critical points are represented by red and yellow spheres, respectively). Bond paths connecting bond critical points are represented. Distances in Å.

The AIM analysis of **59** is complicated since it shows five bond critical points symmetrically distributed. One bond critical point (ρ = 1.54×10^2 a.u.) connects both nitrogen atoms characterizing and confirming the π-hole interaction. In addition, two bond critical points (ρ = 0.62×10^2 a.u.), which connect two hydrogen atoms of trimethylamine to two carbon atoms of the ring, reveal the presence of two C-H/π interactions. Moreover, two additional bond critical points (ρ = 0.70×10^2 a.u.) connecting two hydrogen atoms to the oxygen atoms of the nitro group, reveal the presence of two C–H···O interactions. The charge density computed at the bond critical point that connects both nitrogen atoms is considerably greater than the ones measured at the other bond critical points (1.54×10^2 a.u. *vs.* ~0.66×10^2 a.u.). Therefore, the complexation is dominated by the π-hole interaction with some contribution of the other two. In complex **65** the distribution shows a single bond critical point that connects the Cl^- to the carbon atom, instead of the nitrogen atom, confirming the interaction.

3.2.5. Conclusions

In conclusion, we have demonstrated that the nitro group in nitromethane and nitrobenzene is able to interact favourably with electron-rich molecules by means of

[212] a) R. F. W. Bader, *Atoms in Molecules: A Quantum Theory*, Oxford University Press, USA, **1994**; b) R. F. W. Bader, *Atoms in Molecules. Encyclopaedia of Computational Chemistry*,John Wiley & Sons, Chichester, **1998**, vol. 1, pp. 64–86.

the π-hole that is located above and below the C-N bond. The interaction is characterized by the presence of a bond critical point that connects the ElR atom to the C-N bond. More importantly, the statistical survey of the CSD study reveals that the interaction between the π-hole of nitro groups and electron-rich atoms is directional. Nitro groups are widespread amongst small organic molecules and (at date) the Protein Data Bank (PDB) contains 380 ligands that bear an -NO_2 moiety. It is thus reasonable to anticipate an experimental study unveiling the functional relevance of this novel π-hole interaction.

3.2.6. Acknowledgements

AB and AF thank MINECO of Spain (projects CTQ2011-27512/BQU and CSD2010-00065, FEDER funds) for financial support.

3.2.7. Supporting Information

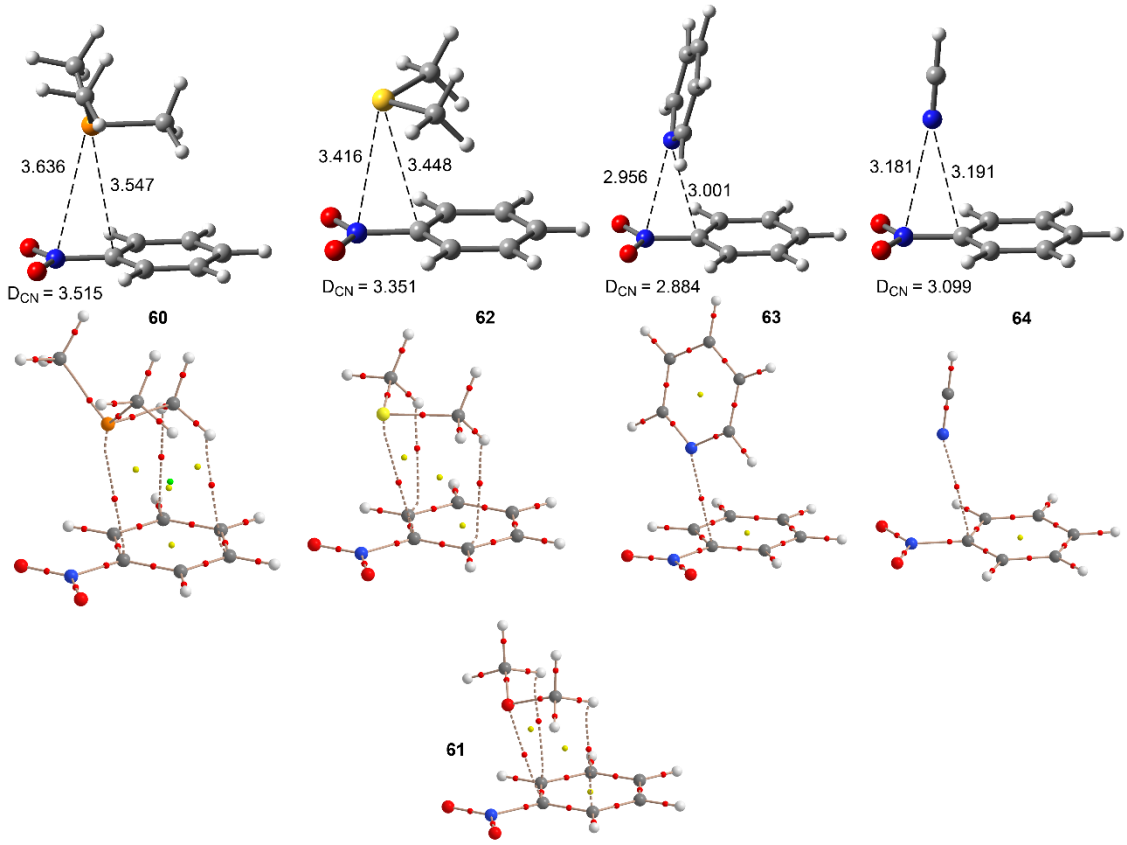

Figure S4 Top: optimized π-hole complexes **60** and **62–64** with distances in Å (D_{CN} stands for the distance measured from the interacting atom to the C–N centroid). Middle and bottom: distribution of critical points in the complexes, together with paths connecting bond critical points. Bond and ring critical points are represented by red and yellow spheres, respectively.

3.3. NO_3^- anions can act as Lewis acid in the solid state.

3.3.1. Abstract

Identifying electron donating and accepting moieties is crucial to understanding molecular aggregation, which is of pivotal significance to biology. Anions such as NO_3^- are typical electron donors. However, computations predict that the charge distribution of NO_3^- is anisotropic and minimal on nitrogen. Here we show that when the nitrate's charge is sufficiently dampened by resonating over a larger area, a Lewis acidic site emerges on nitrogen that can interact favorably with electron-rich partners. Surveys of the Cambridge Structural Database and Protein Data Bank reveal geometric preferences of some oxygen and sulfur containing entities around a nitrate anion that are consistent with this 'π-hole bonding' geometry. Computations reveal donor-acceptor orbital interactions that confirm the counterintuitive Lewis π-acidity of nitrate.

3.3.2. Introduction

Molecular recognition phenomena are of pivotal significance in biology and define the field of supramolecular chemistry.[2,185,213,214] Well-known intermolecular forces include hydrogen and halogen bonding. Both have recently been contextualized as instances of 'σ-hole bonding'.[4c,156,215] A σ-hole can be seen as a region of electropositive potential on a molecule that is roughly located on the unpopulated σ* antibonding orbital of a covalent bond. Typical examples of such σ-holes can be found along the O–H/C–Br vectors in phenol or bromobenzene.[167]

In analogy, a π-hole can be seen as a region of electropositive potential on a molecule that is roughly located on an unpopulated π* antibonding orbital of a π bond, e.g. on carbonyls or π-acidic aromatics like hexafluorobenzene.[27,190,167,189] It is known that π-holes in nitro-compounds such as nitrobenzene (Figure 75) can be directional in the solid state.[167,168] The magnitude of such π-holes can be enhanced when the negative charge is diluted over a larger area, e.g. if the O-atoms interact with water or NaCl (Figure 75B and C). We wondered to what extend this rationale applies to nitrate anions and if perhaps this anion might function as a π-hole to enable so-called (pseudo)anti-electrostatic interactions.[216,217] This seems counterintuitive, yet the charge distribution in naked NO_3^- is anisotropic and reminiscent of a π-hole (Figure 75D).[218] Dampening the charge with water further exposes the π-hole (Figure 75E), and the potential even becomes positive at +25 kcal/mol in charge-neutral [$LiNO_3 \cdot 2H_2O$] (Figure 75F). We found that such an exposed π-hole on NO_3^- can form complexes with electron-rich partners with

[213] H. J. Schneider, *Supramolecular Systems in Biomedical Fields*, RSC Publishing, Cambridge, **2013**.
[214] P. J. Cragg, *Supramolecular Chemistry: From Biological Inspiration to Biomedical Applications*, Springer, Dordrecht, **2010**.
[215] P. Politzer, J. S. Murray, P. Lane, *Int. J. Quantum Chem.* **2007**, *107*, 3046–3052.
[216] F. Weinhold, R. A. Klein, *Angew. Chem. Int. Ed.* **2014**, *53*, 11214–11217.
[217] A. Bauzá, A. Frontera, T. J. Mooibroek, J. Reedijk, *Crystengcomm* **2015**, *17*, 3768–3771.
[218] C. E. Housecrof, A. G. Sharpe, *Inorganic Chemistry*, Prentice Hall, Harlow, **2005**.

calculated energies of up to –31.6 kcal/mol. Statistical evaluations of the Cambridge Structural Database (CSD) and the Protein Data Bank (PDB) indeed reveal some geometric preferences consistent with this 'π-hole bonding' geometry. Several examples lifted from these databases are highlighted, where the Lewis acidity of NO_3^- seems evident.

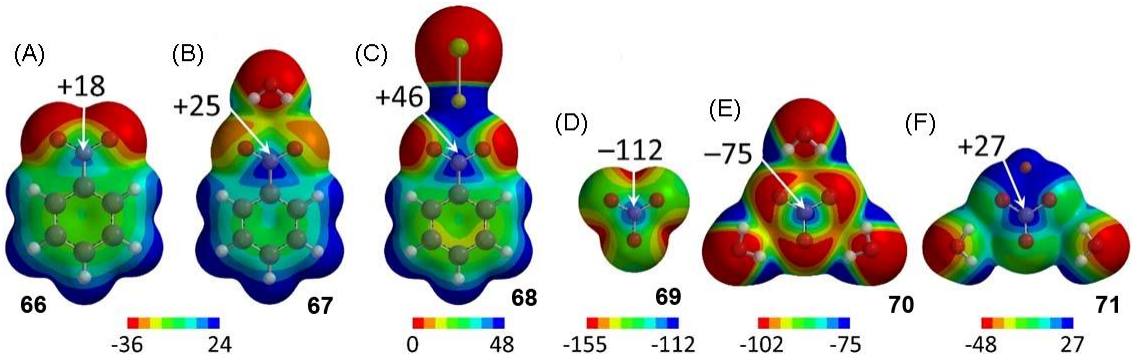

Figure 75. Some Molecular Electrostatic Potential maps (MEPs) of nitrobenzene and nitrate. Molecular Electrostatic Potential maps (MEPs) of nitrobenzene (A) interacting with water (B) and NaCl (B) and NO_3^- (D) interacting with 3 water molecules (E) or one Li^+ and two water molecules (F). Geometries were optimized with DFT/BLYP/6–31G* and MEPs and energetic values (in kcal/mol) generated at the MP2/6–311+G** level of theory. The color codes of the MEPs represent more negative (red) to more positive (blue) potentials in between: +36 and +24 (A, B); 0 and +48 (C); –155 and –122 (D); –102 and –75 (E); –48 and +27 (F).

3.3.3. Computational methods and PDB/CSD search criteria

The energies of all complexes included in this study were computed at the BP86-D3/def2-TZVP level of theory. The calculations have been performed by using the program TURBOMOLE version 7.0.[141] For the calculations we have used the BP86 functional with the latest available correction for dispersion (D3).[197] The optimization of the molecular geometries has been performed imposing the C_{3v} symmetry point group. The Bader's "Atoms in molecules" theory has been used to study the interactions discussed herein by means of the AIMAll calculation package.[181] The CSD (version 5.37 (Nov. 2015 including two updates) was inspected using ConQuest (version 1.18) on the 3rd of April 2016. The PDB was inspected with the online Query Sketcher of Relibase version 3.2.1 on the 2nd of March 2016. For the CSD search, a subset of data was first created containing uncoordinated nitrate anions (9,439 crystallographic information files; CIFs). All searches of the CSD were limited to high quality structure ($R \leq 0.1$) and powder structures and structures containing errors were omitted.

3.3.4. Results and discussion

3.3.4.1. Computational models

In order to further evaluate a possible π-hole on NO_3^- computationally, we designed tris urea based receptors that fully surround a nitrate anion with hydrogen bond

donors (Figure 76 **72a**, related [2+2] macrocycles are known).[219,220] This might mimic nitrate anions in crystal structures, which are typically enclosed by several (charge assisted) hydrogen bonds and/or charge compensated by coordination to a metal ion. In the anionic complexes **72** (Figure 72B), the π-hole region represents a relative electron depletion and is positive at +25 kcal/mol in the anionic species **72c**.

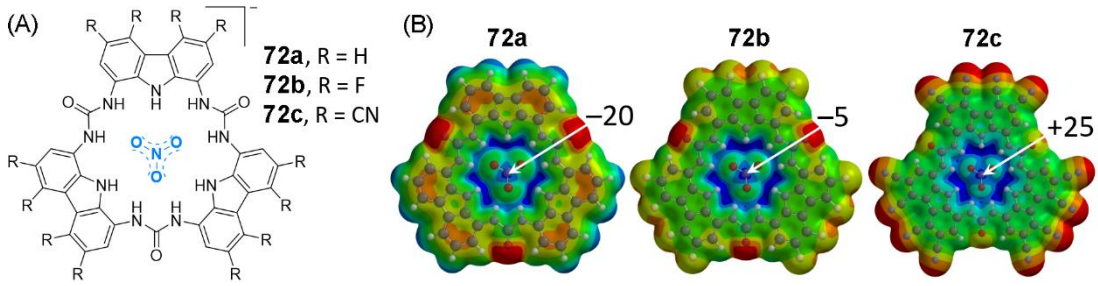

Figure 76. Nitrate complexes with trisurea macrocycles. (A) schematic drawing of **72**. (B) MEPs of **72a**, **72b** and **72c**. Geometries were optimized with DFT/BLYP/6-31G* and MEPs and energetic values (in kcal/mol) generated at the B3LYP/6-31G* level of theory. The color codes of the MEPs represent more negative (red) to more positive (blue) potentials in between:-80 and -18 (**72a**); -72 and -1 (**72b**); -80 and +35 (**72c**).

Next, we computed some complexes of **72** with electron-rich partners and found that complexes $[72c\cdots NCCH_3]^-$ and $[72c\cdots Cl]^{2-}$ gave interaction energies of –7.7 and –31.6 kcal/mol respectively (see Supplementary Note 1 and Table S2 for details). These values are in the range of weak to strong hydrogen bonding.[166] An "Atoms in molecules" (AIM) analysis[221] revealed a single bond critical point between the nitrate N-atom and N/Cl of the interacting partner (see Figures S5 and S6).

3.3.4.2. Database analyses

Encouraged by these computational predictions we wondered if there might be any experimental evidence for π-hole bonding with NO_3^- within the crystal structures deposited in the Cambridge Structural Database (CSD)[222] and the Brookhaven Protein Data Bank (PDB).[223] More in particular we were interested in ascertaining any possible directional behavior[113] of this interaction. We limited our inquiries to uncoordinated nitrate anions to simplify our analysis. Also, if uncoordinated nitrate can act as Lewis acid, it is likely that coordinated nitrate will do so as well (and likely even more so). Initial datasets were retrieved by limiting the $^-O_3N\cdots$El.R. distance to 5 Å (El.R. = some electron-rich atom). The data are thus confined within a sphere with 5 Å radius but will -due to symmetry- be represented as contained within a 5 Å high and 10 Å wide hemisphere. The interacting entities considered here are H_2O,

[219] N. Ahmed, I. Geronimo, I. C. Hwang, N. J. Singh, K. S. Kim, *Chem. Eur. J.* **2011**, *17*, 8542–8548.
[220] N. Ahmed, V. Suresh, B. Shirinfar, I. Geronimo, A. Bist, I. C. Hwang, K. S. Kim, *Org. Biomol. Chem.* **2012**, *10*, 2094–2100.
[221] R. F. W. Bader, *Acc. Chem. Res.* **1985**, *18*, 9–15.
[222] C. R. Groom, I. J. Bruno, M. P. Lightfoot, S. C. Ward, *Acta Crystallogr. B72* **2016**, 171–179.
[223] H. M. Berman, J. Westbrook, Z. Feng, G. Gilliland, T. N. Bhat, H. Weissig, I. N. Shindyalov, P. E. Bourne, *Nucleic Acid Res.* **2000**, *28*, 235–242.

O=X (X = any atom for the CSD data and only C for the PDB data) and S (CSD) / S–C (PDB). Further details of the methods employed can be found in sections 3.3.3 and 3.3.7. (*vide supra*).

Shown in Figure 77 are the distributions in three dimensional space of O-atoms in H_2O (left), O=X/C (middle), and of S-atoms (right) around a nitrate anion as found within the CSD (top) and the PDB (bottom). These distributions are remarkably similar in both databases. Water molecules seem to cluster near the O-atoms and are relatively in-plane with NO_3^-, suggesting that hydrogen bonding dominates. On the other hand sp^2-hybridized O-atoms and S-atoms tend to cluster perpendicular to the NO_3^- plane, above/below the nitrate's N atom. This clustering is consistent with a π-hole bonding geometry. 4D density plots (Figure S9) further confirm these trends and directionality plots clearly indicate that NO_3^- π-hole bonding is about as directional as NH···π^{aryl} hydrogen bonding (Figure S10).[86b,113,211,167,210] Also, significant amounts of data directly above/below N (13 – 21%) consist of overlapping van der Waals shells (Figure S11).

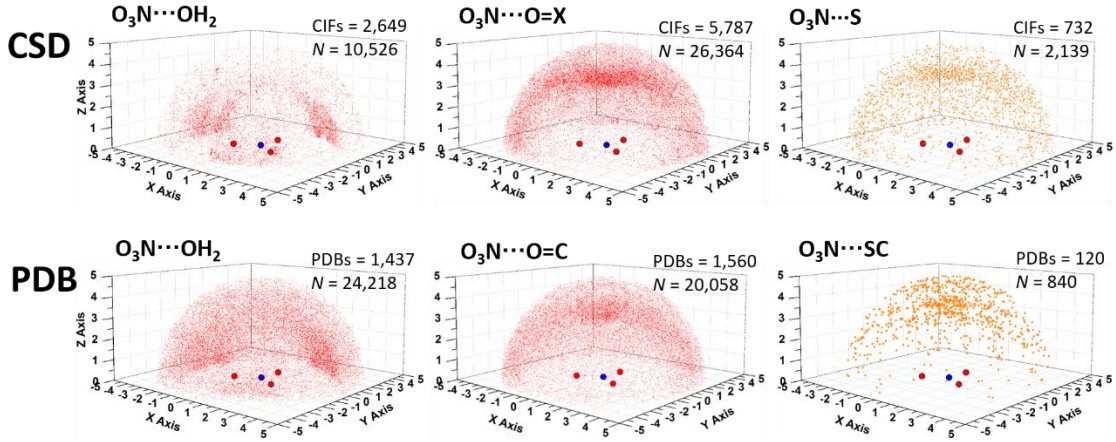

Figure 77. Database analyses. Distribution of the O- or S-atoms (belonging to water (left), OX/OC (middle), or S/SC (right) entities around an uncoordinated nitrate anion as found within the CSD (top) and PDB (bottom) and contained by the parameter ^{nitrate}N···O/S ≤ 5 Å. X = any atom.

3.3.4.3. Concrete examples

Finally, we selected several examples of crystal structures displaying short O_3N···El.R. distances and geometries consistent with a π-hole interaction (El.R. = 'electron-rich atom'). Shown in Figure 78 (top) are charge-neutral selections of the small salts EVIKEA,[224] ORUHOZ[225] and BIDHAX[226] lifted from the CSD. In all these instances the $^-O_3$N···El.R. distances are within the sum of the van der Waals radii of the elements involved and the nitrate anion is concurrently entrenched in a hydrogen bonding pocket (not shown).

[224] Q. Wang, Z. -Y. Fu, X. Li, L. M. Yu, *Acta Crystallogr. E* **2011**, *67*, O1671–U1543.
[225] T. J. Siciliano, M. C. Deblock, K. M. Hindi, S. Durmus, M. J. Panzner, C. A. Tessier, W. J. Youngs *J. Organomet. Chem.* **2011**, *696*, 1066–1071.
[226] G. B. Jameson, E. Blazso, N. Seferiadis, H. R. Oswald *Acta Crystallogr. B* **1982**, 38, 2272–2274.

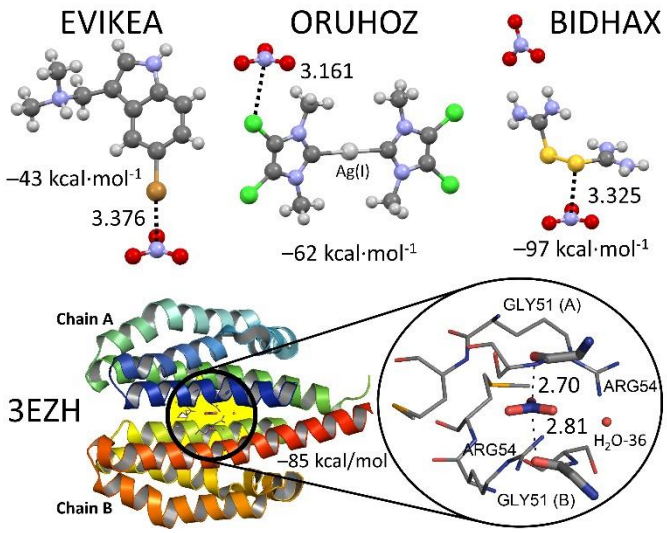

Figure 78. Examples of crystal structures exhibiting nitrate π-hole interactions. Top: three structures found in the CSD. Bottom: example lifted from the PDB with a zoom-in of the nitrate ligand's binding pocket (residues ≤ 4 Å displayed). All these selected fragments were computed at the BP86-D3/def2-TZVP level of theory leading to the indicated energies (dominated by charge compensation). Colour code: carbon = grey, hydrogen = white, nitrogen = blue, oxygen = red, sulphur = yellow, chloride = green, bromide = brown and silver = light grey.

Protein structure 3EZH[227] (Figure 78, bottom) consists of two isostructural chains (A and B) that are stuck together surrounding a central nitrate ligand. The NO_3^- anion is H-bonded to two arginine residues (ARG54) with N···N distances of about 3 Å. In addition, the carbonyl O-atoms of two glycine residues (GLY51) appear to interact with the nitrate ligand's π-hole. Indeed, the interatomic N···O distances (2.70 and 2.81 Å) are well within the van der Waals benchmark for N+O (3.07 Å).

The AIM analyses of these four examples revealed a clear bond critical point between the nitrate's N atom and the interacting electron donor for both EVIKEA and 3EZH (Figure S12). A Natural Bond Orbital analysis (with a focus on second order perturbation)[206] for each example revealed electron donation from a lone pair of electrons (LP) into an unoccupied orbital of the nitrate anion (e.g., 0.35 kcal/mol for the LP(C=O)→π*(NO_3^-) in 3EZH, see SI for details). This confirms that the NO_3^- anion can act as a Lewis acid in these examples.

3.3.5. Concluding remarks

The above computations, database analyses and examples clearly point out that a genuine π-hole might persist on a nitrate anion and that NO_3^- may thus act as a Lewis acid to form formally (pseudo)anti-electrostatic interactions in the solid state. One naturally wonders what other anions might be capable of displaying such behavior (using other atoms than hydrogen). It occurred to us that nitrate actually has a rather unique set of properties that set it apart from other common anions in this respect: NO_3^- is fairly polarized and further polarizable, not so charge-dense, and nitrate is flat, rendering the π-hole sterically accessible (see Supplementary

[227] J. Cheung, W. A. Hendrickson, *Structure* **2009**, *17*, 190–201.

note 3 in section 3.3.7.5. for a discussion of possible candidates). As nitrate anions are very common in chemistry and biology, we anticipate that our finding may serve as a (retrospective) guide to interpret chemical data where nitrate anions are involved. For example orthonitrate formation,[228,229] cases where NO_3 anions may be a structural determinant (as in 3EZH), or in transport phenomena involving this ubiquitous anion.[230,231]

3.3.6. Acknowledgements

AF and AB thank the MINECO of Spain (projects CTQ2014-57393-C2-1-P and CONSOLIDER INGENIO 2010 CSD2010-00065, FEDER funds) for funding. We also thank the "Centre de Tecnologies de la Informació" (CTI) at the UIB for computational facilities. T.J.M. partially conducted the work with funds from the research program 'VIDI' with project number 723.015.006, which is financed by the Netherlands Organisation for Scientific Research (NWO).

3.3.7. Supporting information

3.3.7.1. Supplementary note 1

For our initial calculations the cyanamide cation seemed an ideal candidate for two reasons: its positive charge would complement the negative charge in 7**2** while leaving some electron density on N, and its C_3v symmetry renders the computations more economical.

As is summarized in entries 1–3 in Table S2, the complexation energies for all three cyanamide structures are negative and fairly large (comparable to hydrogen bonding). This large enthalpy might depend significantly on simple charge compensation. As a matter of fact, the interaction energy of host **72a** with the cyanamide molecule flipped 180 degrees (so that the $-NH_3^+$ and nitrile N-atoms switch position, i.e. [7**2a**···N^+H_3–C≡N], not shown in the table) is –47.7 kcal/mol. This is nearly identical to the interaction energy of complex [7**2a**···N≡C–N^+H_3] (entry 1, –48.8 kcal/mol), thus confirming that the nature of the interaction is predominantly charge compensation. Interestingly, the least stable of these complexes involves **72c**, which actually had a positive potential on the nitrate's N-atom (see Figure 76b). This implies that the energy gain of charge compensation is largely counteracted by repulsion between the π-hole and the cyanamide cation.

Next we considered the charge neutral species acetonitrile and hydrogen cyanide as electron-rich partners for the π-hole in **72c** (entries 4 and 5 in Table S2). Interestingly, the estimated binding enthalpies of these 'pseudo anti-electrostatic'

[228] D. Trinschek, M. Jansen, *Angew. Chem. Int. Ed.* **1999**, *38*, 133–135.
[229] M. Jansen, *Angew. Chem. Int. Ed.* **1979**, *18*, 698–698.
[230] P. A. Gale, *Accounts Chem. Res.* **2011**, *44*, 216–226.
[231] H. Valkenier, L. W. Judd, H. Li, S. Hussain, D. N. Sheppard, A. P. Davis, *J. Am. Chem. Soc.* **2014**, *136*, 12507–12512.

complexes are negative and in the order of weak hydrogen bonding (up to –7.7 kcal/mol for [**72c**···N≡CCH_3]$^-$).
Stimulated by these findings, we wondered how cyanide, chloride and BF_4^- anions would interact with the π-hole in **72c** and if perhaps truly 'anti-electrostatic' complexes might be obtained. To our surprise these complexes (entries 6, 7 and 8 in Table S2) converged with their initial C_{3v} symmetry intact to give quite large and negative energies: –20.7 kcal/mol for [**72c**···NC]$^{2-}$, –31.6 kcal/mol for [**72c**···Cl]$^{2-}$ and –8.2 kcal/mol for [**72c**···BF_4]$^{2-}$. Such enthalpies are comparable to medium to strong hydrogen bonding. Unsurprisingly, when considering **72a** as partner to these anions (entries 9, 10 and 11 in Table S2), the computed enthalpies were fairly large but positive.

An "Atoms in molècules" analysis of all complexes (see Figures S5 and S6) indicate a single bond critical point between the nitrate's N-atom and the interacting electronegative atom.

Table S2. Overview of some characteristics of complexes involving **72** with C_{3v} symmetry as computed with the DFT paradigm at the BP86-D3/def2-TZVP level of theory.

Entry	**Host**	**Guest**	**Complex**	**ΔE (kcal/mol)**	**Distance (Å)**	**10^2 x ρ (a.u.)**
1	**72a**	$^+NH_3CN$	**73**	-48.8	2.719	1.28
2	**72b**		**74**	-40.2	2.783	1.11
3	**72c**		**75**	-22.4	2.972	0.73
4		CH_3CN	**76**	-7.7	2.867	1.00
5		HCN	**77**	-5.7	2.920	0.89
6		N≡C$^-$	**78**	-20.7	2.649	1.70
7		Cl$^-$	**79**	-31.6	2.943	1.43
8		BF_4^-	**80**	-8.2	2.472	1.75
9	**72a**	N≡C$^-$	**81**	+22.3	2.728	1.45
10		Cl$^-$	**82**	+14.7	2.997	1.28
11		BF_4^-	**83**	+28.6	2.604	1.27

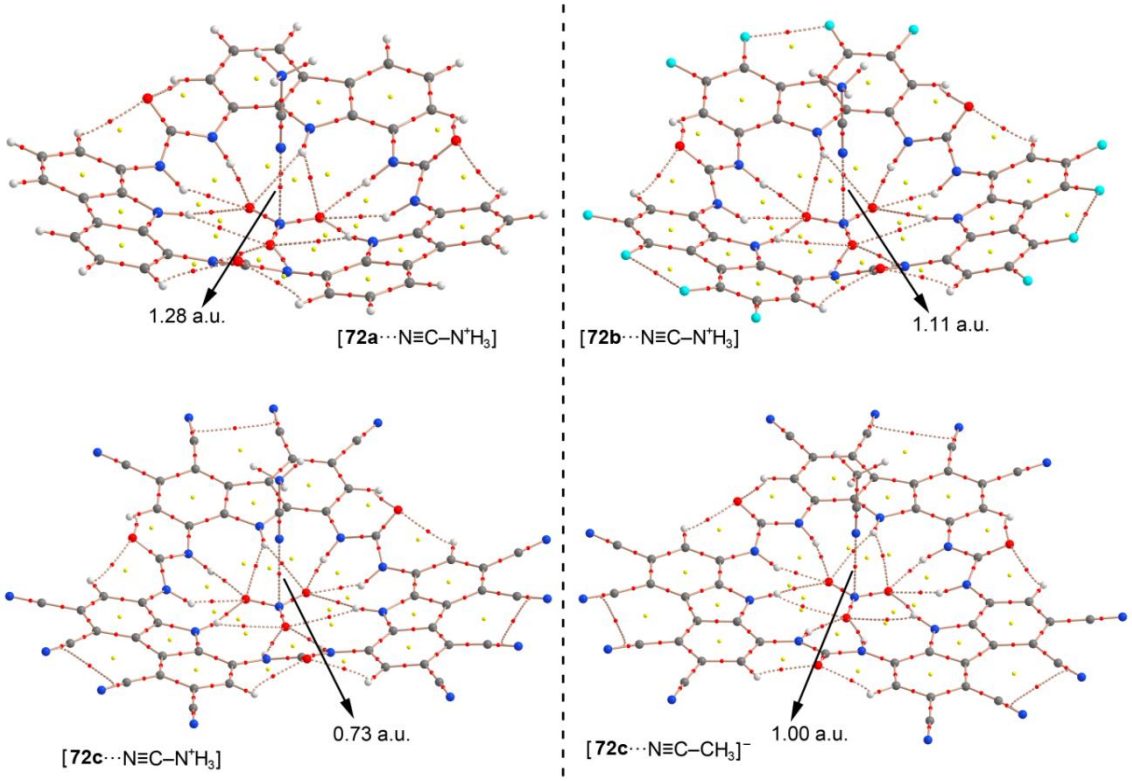

Figure S5. Renderings of "Atoms in molècules" analyses of the complexes corresponding to entries **1** to **4** (Table S2). The charge density values (10^2 x ρ, a.u.) at the bond CPs that characterize the π-hole interaction are given.

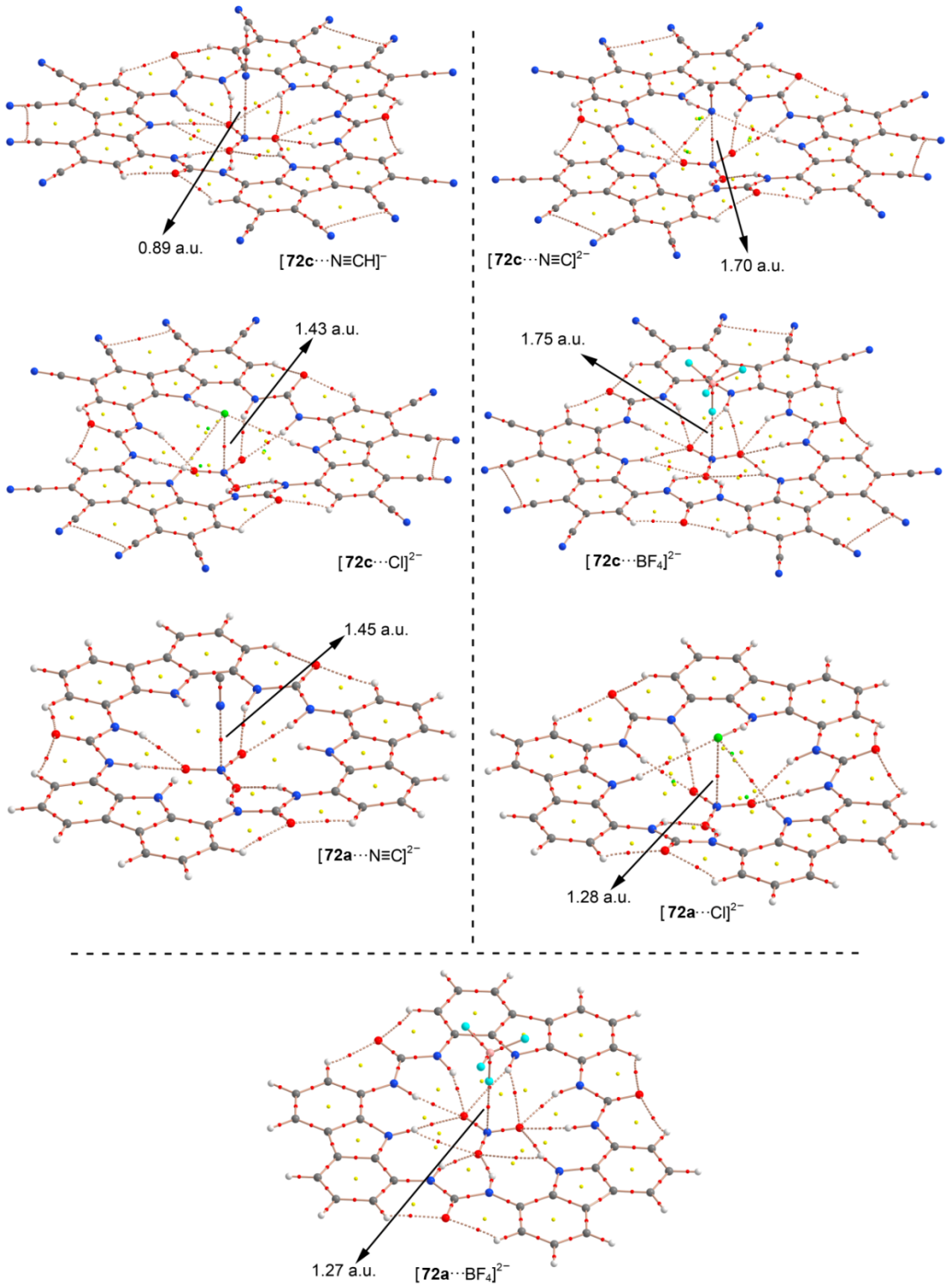

Figure S6. Renderings of "Atoms in molècules" analyses of the complexes corresponding to entries **5** to **11** (Table S2). The charge density values (10^2 x ρ, a.u.) at the bond CPs that characterize the π-hole interaction are given.

3.3.7.2. Queries used to retrieve data from the CSD and PDB

The N-O bonds were set to 'any type'. All covalent bond distances and selected triatomic angles were collected to reconstruct the average models (one for the PDB data and one for the CSD data) used for accessing directionality (see below). The interatomic distance between the interacting atom (O in O=C or OH_2; S in S, SC or SCC; or F, Cl, Br, I, At, O, S, Se, Te, N, P or As in El.R. ('electron-rich') and the nitrate's N-atom (**e**, highlighted in red in Figure S7) was set as ≤ 5 Å so that the data was confined within a 10 Å diameter sphere centred on N. In the PDB study the NO_3 central unit was marked as a ligand and the interacting atom(s) were marked as part of a protein, or in the case of water the interacting O was specified as water.

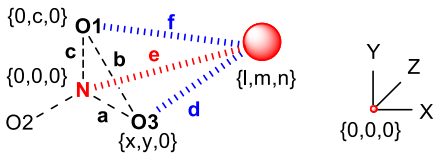

Figure S7. Query used for PDB and CSD search.

3.3.7.2.1. Deriving XYZ coordinates and *r*

The interatomic distances between the interacting atom and O1 and O3, as well as the O1-O3 distance were also collected (set to ≤ 8 Å in the PDB search and left unspecified for the CSD search). The triangle formed by O1-N-O3 was chosen as the base, and the interacting atom as the tip of a tetrahedron (see Figure S7) so that Cartesian Coordinates {X,Y,Z} of all the atoms could be derived as follows: the N-atom was taken as the centre {0,0,0}, O1 as {0,*c*,0}, O3 as {*x*,*y*,0}, and the interacting atom at {*l*,*m*,*n*}. Distances *a*-*f* were measured, from which *y*, *x*, *m*, *l* and *n* can be derived using equations 2 to 6 respectively.

$$y = \frac{a^2 + c^2 - b^2}{2c} \qquad \text{Equation 2}$$

$$x = \sqrt{a^2 - y^2} \qquad \text{Equation 3}$$

(X-value) $$m = \frac{c^2 + e^2 - d^2}{2c} \qquad \text{Equation 4}$$

(Y-value) $$l = \frac{a^2 + e^2 - f^2 - 2my}{2x} \qquad \text{Equation 5}$$

(Z-value) $$n = \sqrt{e^2 - m^2 - l^2} \qquad \text{Equation 6}$$

Thus, the distance between the interacting atom and the plane defined by O1-N-O3 is *n*, i.e. the Z-value. With this and the N⋯interacting atom distance (*e*) the parallel displacement parameter (*r*) could be derived according to equation 7:

$$r = \sqrt{e^2 - n^2} \qquad \text{Equation 7}$$

With this procedure the sign of *n* (i.e. the Z-axis) is always positive, meaning that data in one half of the sphere were reflected to the other half of the sphere to obtain the data within a 5 Å high and 10 Å wide hemisphere.

To obtain all {X,Y,Z} coordinates of the average models, it was assumed that O2 was coplanar with O1-N-O3. The averages of relevant distances and angles were then used together with the rules of sine and cosine to obtain the {*X*,*Y*,*X*} coordinates. The relative standard deviations of the parameters used were typically below 5%. A numerical overview of the data retrieved is shown in Table S3.

Table S3. Numerical overview of the data

DB:	CU:	Partner:	$N_{struct.}$	N_{total}	$N_{r\leq1}$	$N_{\leq vdW@r\leq1}$	$N_{r3\text{-}4}$	$N_{vdW@r\leq3\text{-}4}$
PDB	NO_3	N⋯O=C	1,560	20,058	1,296	266 (20.5%)	5,940	1,180 (19.9%)
PDB	NO_3	N⋯OH_2	1,437	24,218	430	86 (19.5%)	12,086	7,312 (60.5%)
PDB	NO_3	N⋯SC	120	840	168	36 (21.4%)		
PDB	NO_3	N⋯SCC	56	354	48	0 (0.0%)		
CSD	NO_3	N⋯ElR[a]	7,995	117,638[a]	5,540	494 (8.9%)	47,850	28 (0.06%)
CSD	NO_3	N⋯O=X	5,787	26,364	1,937	327 (16.9%)		
CSD	NO_3	N⋯OH_2	2,649	10,526	91	11 (12.0%)	7,406	2 (0.03%)
CSD	NO_3	N⋯S	732	2,139	167	22 (13.2%)		

[a]'ElR' stands for 'electron-rich and the data consists of ElR = N (89,845), O (53,504), F (433), P (470), S (2,071), Cl (999), As (33), Se (33), Br (186), Te (21) and I (43).

3.3.7.2.2. Rendering 4D plots and analysis of directionality

Four dimensional (4D) density plots were generated by first binning the data (using a custom build Excel spreadsheet, available on request) in 405 volumes {X [9 x $^{10}/_{9}$ Å], Y [9 x $^{10}/_{9}$ Å], Z [5 x $^{5}/_{5}$ Å]}. The percentage of the total that each volume contains was computed by dividing the number of data in a certain volume by the total amount of data. This density information was projected onto the centre of each volume using Origin Pro 8. The size and colour of the spheres in the resulting plots are a visual representation of the density of data, whereby red and large is denser, empty and small is less dense.

The average {X,Y,Z} coordinates of the atoms of nitrates found within the CSD or the PDB, together with the standard van der Waals radii for N (1.55 Å) and O (1.52 Å) were used to generate a model as a single body 'part' file (.ipt) using Autodesk Inventor® Professional 2016 (by using mm instead of Å). Similarly, a hemisphere was created with a radius of 5 mm. Derived from this hemisphere were bodies where the volume above the base with basal radius (representative for *r*) was trimmed, i.e. 'cylindrically trimmed hemispheres'. The NO_3 model, the hemisphere

and the cylindrically trimmed hemispheres were collected in an assembly file (.iam), properly alighted, as is illustrated in Figure S8 with (cylindrically trimmed) hemispheres of 1, 2, 3, 4 and 5 mm basal radius.

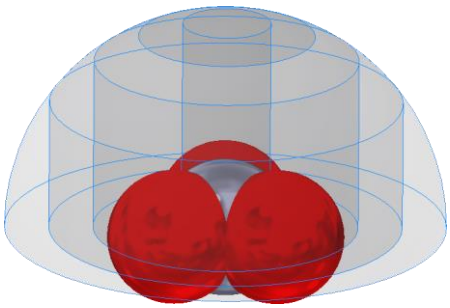

Figure S8. Nitrate model and the volumes used to access directionality.

Using the 'Analyse Interference' option in Autodesk Inventor® Professional 2016 the interfering volumes between the model and the cylindrically trimmed hemispheres could be determined. The volume difference between two such interfering volumes of incremental **r**-values, say $\mathbf{r}_a$ and $\mathbf{r}_b$, thus represent the volume that the model occupies in between two values of **r**, i.e. V_{model}. Similarly, the interfering volume between two cylindrically trimmed hemispheres could be derived as a function of **r**, from which the volume in between two **r**-values as found within the hemisphere could be derived, i.e. $V_{\text{no model}}$. The actual free volume in between two **r**-values that a 'host' can occupy, i.e. V_{free}^{r}, is thus given $V_{\text{no model}} - V_{\text{model}}$. The total freely accessible volume, V_{free}^{total}, is naturally given the volume of the hemisphere minus the volume of the model in the hemisphere. The random (or volume) distribution as a function of ***r***, i.e. D_{chance}^{r}, is thus given by:

$$D_{chance}^{r} = \frac{V_{free}^{r}}{V_{free}^{total}} \qquad \text{Equation 8}$$

The actual distribution of the data, D_{data}^{r}, is naturally given by:

$$D_{data}^{r} = \frac{N^{r}}{N^{total}} \qquad \text{Equation 9}$$

Thus, the change corrected distribution of data, $P(r)$ is given by:

$$P(r) = \frac{D_{data}^{r}}{D_{chance}^{r}} \qquad \text{Equation 10}$$

For an accidental distribution, P should be unity across all ***r***-values; a P-value greater than unity is thus evidence of positive clustering (suggesting a favourable interaction), while P-values smaller than unity reflect a depletion of data (suggesting an unfavourable interaction).

3.3.7.2.3. 4D plots and plots to evaluate directionality

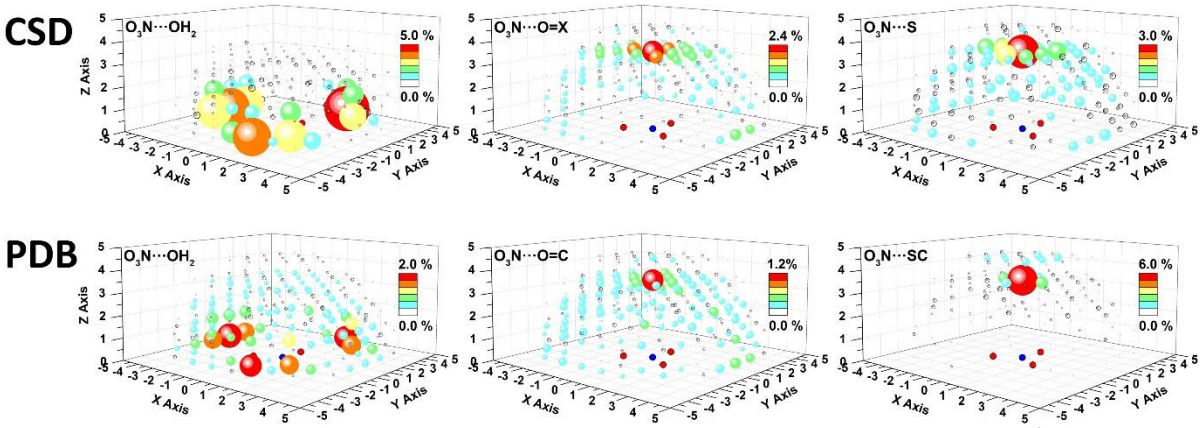

Figure S9. Four dimensional (4D) density plots of the CSD/PDB data found within the 10 Å wide and 5 Å high hemisphere.

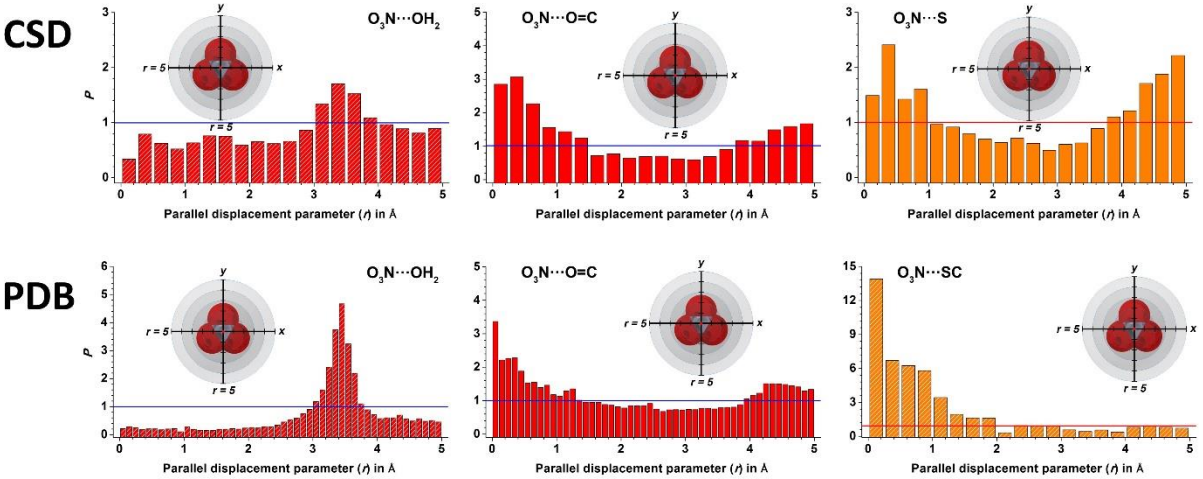

Figure S10. Directionality plots $P(r)$ of the data CSD/PDB data found within the 10 Å wide and 5 Å high hemisphere.

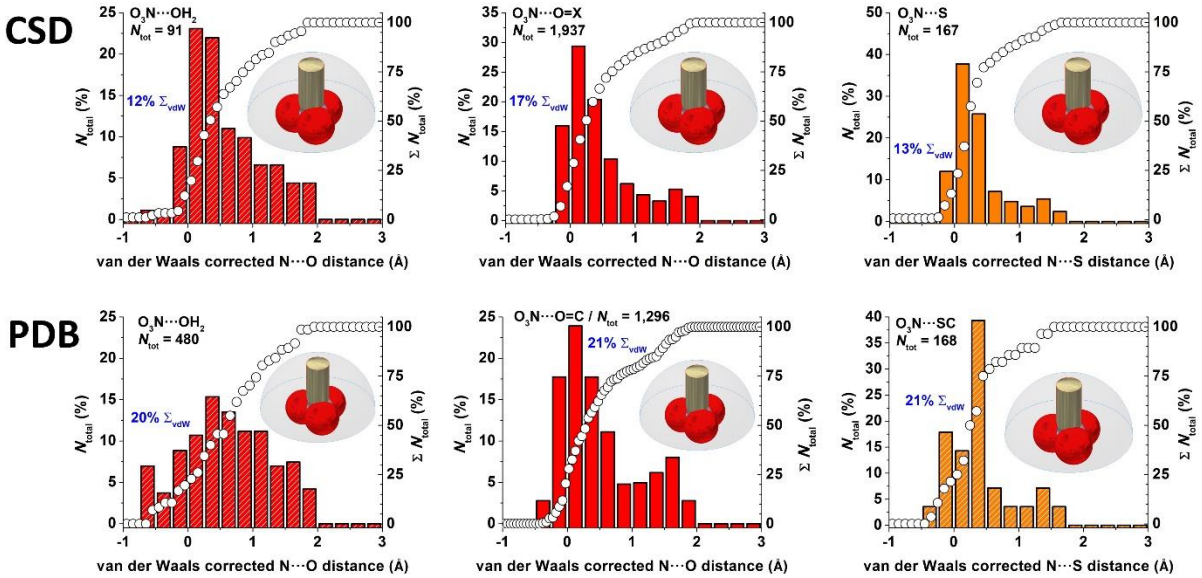

Figure S11. Distribution of the van der Waals corrected ^{nitrate}N···O/S distances within a spherical segment with base radius of 1 Å located within the 10 Å wide and 5 Å high hemisphere studied herein (gold in inset figures).

3.3.7.3. AIM and NBO analysis

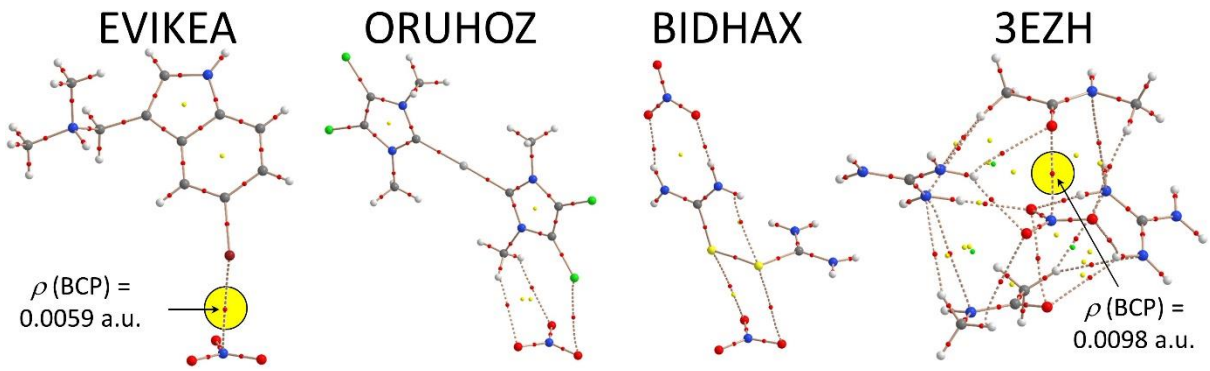

Figure S12. Renderings of "Atoms in molecules" analyses of the computed fragments of EVIKEA, ORUHOZ and BIDHAX (see also Figure 78).

3.3.7.4. Supplementary note 2

The Natural Bond Orbital analysis (with a focus on second order perturbation) revealed the following donor-acceptor interactions:

EVIKEA, $LP_{Br} \rightarrow LP^*_N$, $E^{(2)}$ = 0.51 kcal/mol;
ORUHOZ, $LP_{Cl} \rightarrow \pi^*_{NO3}$, $E^{(2)}$ = 0.24 kcal/mol;
BIDHAX, $LP_S \rightarrow \pi^*_{NO3}$, $E^{(2)}$ = 0.12 kcal/mol, $LP_{S-S} \rightarrow Ry^*_N$, $E^{(2)}$ = 0.24 kcal/mol;
3EZH, $LP_{C=O} \rightarrow \pi^*_{NO3}$, $E^{(2)}$ = 0.34 kcal/mol, $LP_{C=O} \rightarrow Ry^*_N$, $E^{(2)}$ = 0.13 kcal/mol.

3.3.7.5. Supplementary note 3

After some deliberation we could not think of a single (common) anion with the combined properties of NO_3^-, i.e.: fairly polarized and further polarizable, not so charge-dense, and flat, i.e. π-hole is sterically accessible. The halides are easily dismissed (point charge) and most other common anions are not flat and sterically too crowded to allow the approach of a Lewis base (e.g. ClO_3^-, BrO_3^-, ClO_4^-, BrO_4^-, BF_4^-, PF_6^-). Anions with two or more charges such as CO_3^{2-} are likely too charge dense. Flat anions such as NO_2^-, N_3^- and CN^- do not seem to be polarized enough and thus also too charge dense, i.e. the maximum potentials are respectively –132, –142 and –145 kcal/mol versus –110 kcal/mol for NO_3^- (MP2/6-311+G**). They are also intrinsically more charge dense with an atom over charge ratio of 3 (NO_2^-, N_3^-) or 2 (CN^-) versus 4 of nitrate.

We also contemplated trifluoroacetate but the maximum potentials (maximum actually lies on the σ-hole of $-CF_3$) are sterically less accessible. A promising candidate might be the rare FCO_2^- (similar MEP as nitrate, only one structure in the CSD and none in the PDB), but this anion is very likely to decomposes to F^- and CO_2. I_3^- (and possibly Hlg_3^- generally) can act as a halogen bond donor but is also prone to decomposition into I^- and I_2 (P. H. Svensson, L. Kloo, *Chem. Rev.* **2003**, *103*, 1649–1684; at the MP2/6-311+G** level of theory two latent σ-holes are present on I_3^- (–76 kcal/mol), Br_3^- (–87 kcal/mol) and Cl_3^- (–97 kcal/mol)).

3.4. Pnicogen-π complexes: theoretical study and biological implications.

3.4.1. Abstract

The energetic and geometric features of pnicogen-π complexes involving different types of aromatic rings (benzene, trifluorobenzene, hexafluorobenzene and *s*-triazine) and the heavier pnicogens (ECl_3, E = As, Sb, Bi) are investigated using theoretical methods (*ab initio* and DFT-D3). We have analyzed how the interaction energy is affected by the π-acidity of the aromatic moieties and the pnicogen used. In addition, we have found several examples in the Protein Data Bank where pnicogen-π interactions are present. This likely indicates the potential use of this interaction in the design and synthesis of potential inhibitors of enzymatic reactions. Moreover, in order to know the reliability of the latest version of dispersion termed corrected DFT-D3, we have also compared the energies obtained using the *ab initio* MP2 method with those obtained using BP86-D3.

We have also computed and analyzed the dispersion contribution to the total interaction energy in order to know if it is crucial for the favourable binding. This allows a better understanding of the physical nature of the interaction. Finally, we have used the Bader's theory of "Atoms in molecules" to demonstrate that the electron density computed at the bond critical point that emerges upon complexation can be used as a measure of bond order in this noncovalent interaction.

3.4.2. Introduction

The rational use of noncovalent interactions is crucial in modern chemistry[1] and, among others, interactions involving aromatic rings are extremely important in many fields.[232] For instance, ion-π,[9b,9c,10a,31a,233] π-π stacking,[234] lp-π[8b] and C-H/π[153b] interactions participate in important chemical and biological processes including molecular recognition, crystal engineering and enzymatic mechanisms. In addition, the importance of the π-interaction of arenes with heavier pnicogens (As, Sb and Bi) has also been known for a long time, but its study in the context of supramolecular chemistry is more recent.[78] As a matter of fact, the important work developed by Johnson's group in last years highlights the potential use of this weak interaction to control self-assembly processes that yield to the formation of macrocycles.[79]

Mainly using X-ray analysis,[79,80] it has been demonstrated that post-transition metals with stereochemically active lone pairs, such as heavier pnicogens in low

[232] a) L. M. Salonen, M. Ellermann, F. Diederich, *Angew. Chem. Int. Ed.* **2011**, *50*, 4808–4842; b) E. A. Meyer, R. K. Castellano, F. Diederich, *Angew. Chem. Int. Ed.* **2003**, *42*, 1210–1250.
[233] a) J. C. Ma, D. A. Dougherty, *Chem. Rev.* **1997**, *97*, 1303–1324; b) P. B. Crowley, A. Golovin, *Proteins* **2005**, *59*, 231–239; c) A. Robertazzi, F. Krull, E. -W. Knapp, P. Gamez, *CrystEngComm*, **2011**, *13*, 3293–3300.
[234] a) K. Muller-Dethlefs, P. Hobza, *Chem. Rev*. **2000**, *100*, 143–168; b) S. K. Burley, G. A. Petsko, *Science* **1985**, *229*, 23–28; c) J. T. Stivers, Y. L. Jiang, *Chem. Rev.* **2003**, *103*, 2729–2759.

oxidation state, produce stable arene complexes. For instance the binding enthalpies between $SbCl_3$ and neutral aromatic rings have been recently measured, ranging 5–10 kcal/mol. These values are in the typical range of noncovalent weak interactions.[235] The attractive origin of this interaction can be explained using two opposite points of view, which have been proposed in the literature. On one hand, it can be described as an electrostatic interaction between a Lewis acid (main group metalloid) and a π-base (arene ring) interaction.[235] These donor(π)-acceptor(As) orbital interactions are also known as "Menshutkin complexes". On the other hand, the interaction can be also described as an electron transfer between the pnicogen atom and the arene. In the latter description the interaction is identical to a lp-π interaction, which generally occurs between an arene and a Lewis base. This description has been recently proposed for supramolecular architectures based on As-π interactions.[236] It should be also noted that Auer *et al.* have demonstrated that dispersion forces are important in this type of interaction since standard DFT methods are not well suited for the quantitative description of the bonding between bismuth and arenes.[237]

The aim of this study is to investigate the geometric and energetic features of pnicogen-π complexes between aromatic moieties and ECl_3 neutral molecules. In order to shed light to the nature of the interaction, we have used four different arenes, ranging from electron-rich to electron-poor. In case that the origin of the interaction is the Lewis acidity of the pnicogen, the formation of the complexes should be favoured in electron-rich arenes. In contrast, if the interaction is equivalent to an lp-π interaction, the formation of the complexes should be favoured in electron-poor arenes. In addition, as previous works demonstrate that dispersion is important in this interaction, the latest version of the empirical dispersion correction, termed corrected DFT-D3, has been used to carry out the calculations and the geometries and energies have been compared to those obtained using the *ab initio* MP2 method. Furthermore, the "Atoms in molecules" (AIM)[238] analysis allows us to demonstrate that the electron density at the cage critical points that characterize the pnicogen bond can be used as a measure of bond order. Finally, we have analyzed the protein database (PDB) in order to provide evidence of the importance of pnicogen-π complexes in some biological systems.

3.4.3. Theoretical Methods

The geometry of all the complexes included in this study was optimized at the BP86-D3/def2-TZVPD level of theory and imposing C_{3v} symmetry point group within the program TURBOMOLE version 5.10.[141] For comparison purposes some complexes have been also computed at the MP2/def2-TZVPD. The interaction energies were calculated with correction for the basis set superposition error (BSSE) by using the Boys-Bernardi counterpoise technique.[142] The calculation of the wavefunction to

[235] A. Schier, H. Schmidbaur, *Organometallics* **2008**, *27*, 2361–2395.
[236] J. Zukerman-Schpector, A. Otero-de-la-Roza, V. Lauña, E. R. T. Tiekink, *Chem. Commun*. **2011**, *47*, 7608–7610.
[237] A. A. Auer, D. Mansfeld, C. Nolde, W. Schneider, M. Schurmann, M. Mehring, *Organometallics* **2009**, *28*, 5405–5411.
[238] R. W. F. Bader, *Atoms in Molecules. A Quantum Theory*, Clarendon, Oxford, **1990**.

perform the "Atoms in molecules" (AIM) analysis was computed at the same level of theory. The calculation of AIM properties was done using the AIM2000 program.[239]

3.4.4. Results and Discussion

3.4.4.1. Preliminary considerations

In Figure 79 the Molecular Electrostatic Potential (MEP) surfaces of the arenes are represented including the values of quadrupole moments (Q_{zz}) retrieved from the literature.[33b,240] On going from benzene to hexafluorobenzene, it can be observed a progressive change from red to blue colour above the ring and a change in the sign of the quadrupole moment from negative to positive. This gradual change of the π-basicity (or π-acidity) of the arene is useful to analyze the physical nature of the pnicogen-π interaction, as is explained below. We have also included *s*-triazine in this study, because, notwithstanding it has a Q_{zz} value like trifluorobenzene, it presents a peculiar distribution of the MEP above the ring that facilitates a dual behaviour. That is, depending on the relative orientation of the ECl_3 molecule with respect to the position of the aromatic nitrogen atoms, one of the proposed mechanisms of binding will be favoured. Therefore it is a good candidate for analyzing the physical nature of the pnicogen-π interaction. In addition, the use of a heteroaromatic ring allows us to compare the strength of the interaction with respect to carboaromatic rings. The MEP surface obtained for the three ECl_3 molecules (in Figure 79 only the $AsCl_3$ is indicated as model) is identical and the MEP value at the position of the lone pair is positive, indicating the presence of a σ-hole at this position, resembling the heavier halogens. Therefore, from this preliminary result, based only on electrostatic considerations, in the pnicogen-π interaction the ECl_3 acts as a Lewis acid and it can not be defined as an lp-π interaction.

In previous studies, it has been argued that the polarization of the π-cloud of the arene induced by the permanent dipole of the ECl_3 molecule is important.[236] Moreover, it has been also proposed that dispersion effects are important in this type of interaction,[237] mostly to explain the fact that the heavier pnicogens have more favourable interaction energies. Another possibility can be related to the polarization of the ECl_3 molecule, since the heavier pnicogens are more polarizable, as is indicated by the molecular polarizabilities computed for $AsCl_3$, $SbCl_3$ and $BiCl_3$ (see Figure 79). This issue is further analyzed below.

[239] F. Biegler-König, J. Schönbohm, D. Bayles, *J. Comput. Chem*. **2001**, *22*, 545–559.
[240] a) M. R. Battaglia , A. D. Buckingham, J. H. Williams, *Chem. Phys. Lett.* **1981**, *78*, 421–423; b) J. Vrbancich, G. L. D. Ritchie, *J. Chem. Soc. Faraday Trans. II* **1979**, *76*, 648–655.

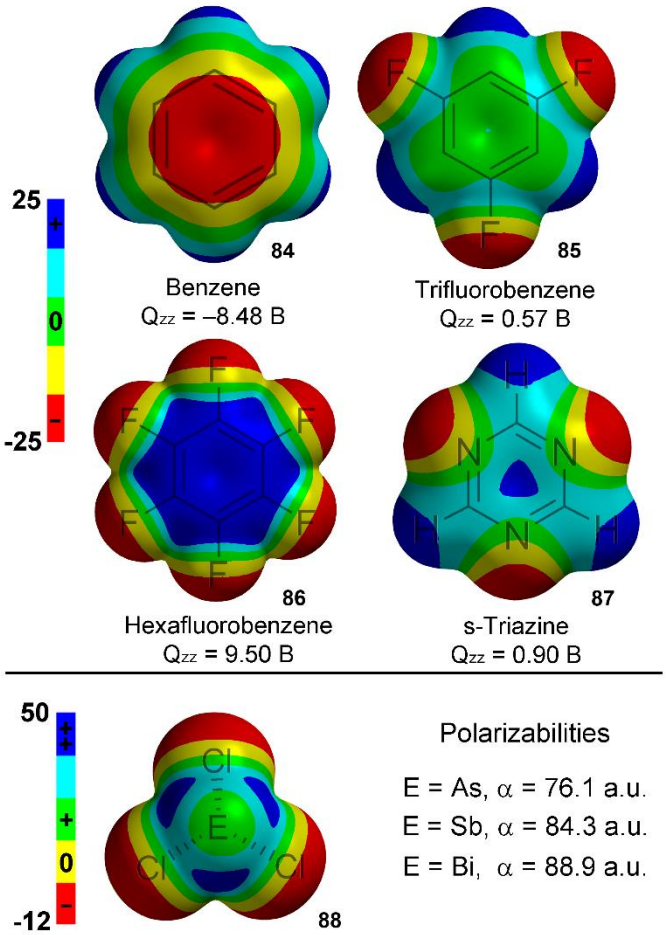

Figure 79. Top: MEP surfaces of benzene, trifluorobenzene and hexafluorobenzene. Down, MEP surface of $AsCl_3$ as a model of ECl_3 molecule and molecular polarizabilities.

3.4.4.2. Energetic and geometric results

In Table 11 we summarize the binding energies without and with the basis set superposition error (BSSE) correction and equilibrium distances (R_e) for complexes **89–97** (see Figure 80) at the BP86-D3/def2-TZVPD level of theory. For trifluorobenzene, we have studied two different orientations, one with the chloride atoms of the ECl_3 molecule located above the aromatic C-H bonds and the other above the C-F bonds. The computed interaction energies are identical for both orientations; therefore only one set is included in Table 11. As aforementioned, for *s*-triazine complexes we have also computed two orientations, one denoted as "**a**" where the chlorine atoms of the ECl_3 molecule are located above the aromatic C–H bonds (see Figure 81), and the other denoted as "**b**" where the chlorine atoms are located above the aromatic nitrogen atoms.

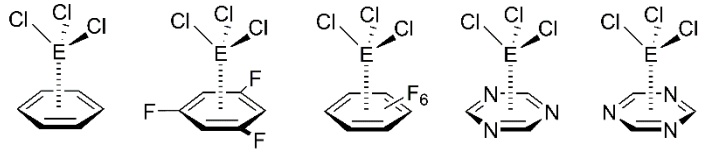

89, E = As **92**, E = As **95**, E = As **98a**, E = As **98b**, E = As
90, E = Sb **93**, E = Sb **96**, E = Sb **99a**, E = Sb **99b**, E = Sb
91, E = Bi **94**, E = Bi **97**, E = Bi **100a**, E = Bi **100b**, E = Bi

Figure 80. Pnicogen-π bonding complexes **89–100**

Table 11. Interaction energies without and with the BSSE correction (E and E_{BSSE}, kcal/mol), dispersion energy (E_{disp}, kcal/mol) equilibrium distances (R_e, Å), and the charge density at the cage CP (ρ, a.u.) at the BP86-D3/def2-TZVPD level of theory for complexes **89** to **100**.

Complex	E	E_{BSSE}[a]	E_{disp}	R_e	10^2 x ρ
89 (BEN + $AsCl_3$)	-7.1 (-9.9)	-6.5 (-6.9)	-5.2	3.210	0.478
90 (BEN + $SbCl_3$)	-6.4	-6.1	-3.6	3.446	0.440
91 (BEN + $BiCl_3$)	-8.7	-8.4	-3.8	3.328	-
92 (TFB + $AsCl_3$)	-5.2 (-7.8)	-4.6 (-4.7)	-5.1	3.285	0.420
93 (TFB + $SbCl_3$)	-3.9	-3.6	-3.6	3.552	0.365
94 (TFB + $BiCl_3$)	-4.9	-4.6	-4.0	3.474	-
95 (HFB + $AsCl_3$)	-3.8 (-6.4)	-3.2 (-3.4)	-5.0	3.383	0.340
96 (HFB + $SbCl_3$)	-2.1	-1.8	-3.2	3.851	0.195
97 (HFB + $BiCl_3$)	-2.2	-1.9	-3.7	3.860	-
98a (TAZ + $AsCl_3$)	-3.3 (-5.7)	-2.9 (-3.4)	-4.1	3.459	0.303
99a (TAZ + $SbCl_3$)	-2.6	-2.2	-3.1	3.713	0.271
100a (TAZ + $BiCl_3$)	-3.3	-2.9	-3.5	3.667	-
98b (TAZ + $AsCl_3$)	-2.9 (-5.2)	-2.5 (-3.0)	-3.9	3.412	0.272
99b (TAZ + $SbCl_3$)	-2.3	-1.9	-3.0	3.663	0.243
100b (TAZ + $BiCl_3$)	-2.8	-2.3	-3.4	3.607	-

[a]Values in parenthesis are computed at the MP2/def2-TZVPD level of theory

From the results gathered in Table 11, some interesting issues arise. First, the computed interaction energies obtained for benzene complexes are more favourable than the rest of arenes, indicating that electron-rich arenes favour the pnicogen-π interaction. The interaction strength progressively decreases as the quadrupole of the arene becomes more positive. In line with the energetic results, the equilibrium distances are shorter for benzene complexes than for the rest of arenes. This result clearly corroborates the postulation derived from the MEP results (vide supra). That is, the pnicogen-π interaction is better described as an electron donation from the arene to the ECl_3 molecule that acts as a Lewis acid. Second, in agreement with previous calculations, the interaction energy of the heaviest pnicogen with benzene (complex **91**) is the most favourable. Moreover, for *s*-triazine and 1,3,5-trifluorobenzene complexes, As and Bi complexes give very similar interaction energies. This likely means that the strengthening of the interaction observed in complex **91** (–8.4 kcal/mol, $Cl_3Bi\cdots$BEN) is due to electrostatic effects. This is confirmed by the small interaction energy obtained for complex **97** (–1.9 kcal/mol, $Cl_3Bi\cdots$HFB), which is significantly more positive than complex **95** (–3.2 kcal/mol, $Cl_3As\cdots$HFB).

In HFB complexes, the possible lp-π nature of the interaction may be enhanced because the arene is π-acidic. It is well-known that strong relativistic effects occur in bismuth.[241] Accordingly, the energies of all of the n*s* orbitals in bismuth are substantially lower than those of arsenic and antimony. The *p*-orbital energies are also lower but the difference is smaller than that of the *s*-orbitals.[242] The lower energy of the valence 6*s* orbital implies that the $6s^2$ lone pair of electrons is less readily available for bonding, making bismuth(III) a significantly weaker Lewis base than the lighter pnicogens,[243] and therefore the lp-π interaction would be considerably unfavoured with respect to As, in agreement with the interaction energies of complexes **95** and **97**. Apart from complex **97**, the equilibrium distances obtained for $BiCl_3$ complexes are shorter than SbCl-π complexes. The Bi atom has a smaller atomic radius than Sb due to a double effect: the orbital contraction due to relativistic effects[244] and the further contraction caused by the less effective screening provided by occupied *f*-orbitals.[245]

The results obtained for *s*-triazine complexes support the idea that the ECl_3 molecule acts as a Lewis acid in the pnicogen-π interaction. The best fitting of both MEP surfaces (*s*-triazine and the ECl_3 molecule) shown in Figure 79 is achieved if the chlorine atoms lie over the C–H bonds. The results gathered in Table 11 confirm this issue, since the "**a**" complexes are more favourable than "**b**" complexes.

Finally, we have also included in Table 11 the interaction energies computed using the *ab initio* MP2/def2-TZVPD level of theory for $AsCl_3$ complexes. It can be observed a very good agreement between the energetic results computed at MP2 and BP86-D3 levels of theory. This result gives reliability to the DFT method in combination with latest dispersion correction developed by Grimme *et al.*[197]

3.4.4.3. Dispersion effects

It has been previously described in the literature the importance of dispersion in the pnicogen-π interaction involving bismuth. In fact, the density functional theory (without dispersion correction) is not well suited for the quantitative description of the bonding between pnicogen and arenes, since for several functionals a very shallow minimum is found.[237] We have examined dispersion effects in the systems reported herein. The dispersion contribution is included in Table 11. It can be observed that the dispersion is very important in all complexes, especially in those involving π-acidic arenes, since it overcomes the unfavourable electrostatic interaction. It has been also proposed that the higher ability of heaviest pnicogen to interact with benzene is due to dispersion effects. However the results reported herein do not agree with this explanation, since the dispersion contribution is higher in $AsCl_3$ complex **89** than in either $SbCl_3$ or $BiCl_3$ complexes **90** or **91**. Therefore a likely explanation for higher ability of Bi to form pnicogen-π complexes is that it is

[241] *Biological Chemistry of Arsenic, Antimony and Bismuth*, John Wiley & Sons, Ltd., Chichester, **2010**.
[242] J. S. Thayer, *J. Chem. Ed.* **2005**, *82*, 1721–1729.
[243] W. Kutzelnigg, *Angew. Chem. Int. Ed.* **1984**, *23*, 272–295.
[244] K. C. H. Lange, T. Klapötke, *The Chemistry of Organic Arsenic, Antimony and Bismuth*, John Wiley & Sons, Ltd., Chichester, **1994**.
[245] A. L. Allred, E. G. Rochow, *J. Inorg. Nucl. Chem.* **1958**, *5*, 264–268.

more polarizable ($\alpha_{||}$ = 88.9 a.u., see Figure 79) and, moreover, it is able to establish interactions with short equilibrium distances due to the strong orbital contraction.

3.4.4.4. AIM analysis

We have performed the AIM analysis of all As and Sb complexes included in this study. The basis set used in this work is not supported by the AIM program for Bi. In benzene, 1,3,5-trifluorobenzene and hexafluorobenzene complexes, the pnicogen-π is characterized by the presence of six bond and six ring critical points (CP) symmetrically distributed. The bond CPs connect the pnicogen atom with the carbon atoms. For *s*-triazine complexes the interaction is characterized by the presence of three bond and three ring critical points symmetrically distributed. In both series of *s*-triazine complexes (**a** and **b**) the bond CPs connect the pnicogen atom with the carbon atoms of the ring. In all complexes **89–100b**, the interaction is further characterized by the presence of one cage CP connecting the pnicogen atom with the center of the ring, as is common in ion-π and lp-π interactions.[9a,31a] In Figure 81 we show the distribution of critical points in some selected complexes.

The density at the cage critical point has been used as a measure of bond strength in a variety of noncovalent interactions.[238] We have examined if these values can be used as a measure of bond order in the complexes studied here. We have represented in Figure 82 a plot that allows us to analyze the existence of a linear relationship between the interaction energies and the ρ values (gathered in Table 11). As a matter of fact, we have obtained a strong relationship (R^2 = 0.962) between the value of the charge density computed at the cage critical point and the interaction energy. The importance of this relationship should be emphasized, since in the same plot we have combined four different arenes and two pnicogens. Therefore, this relevant representation allows for dealing simultaneously with a great variety of complexes.

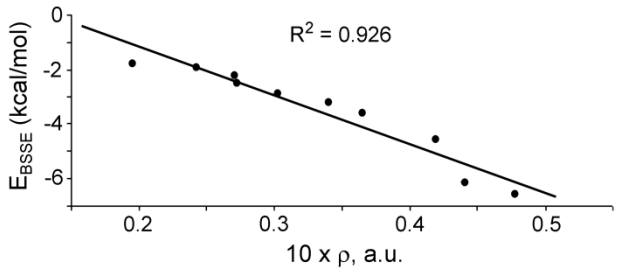

Figure 82. Regression plot of the interaction energy versus the value of the charge density at the cage critical point in As and Sb complexes.

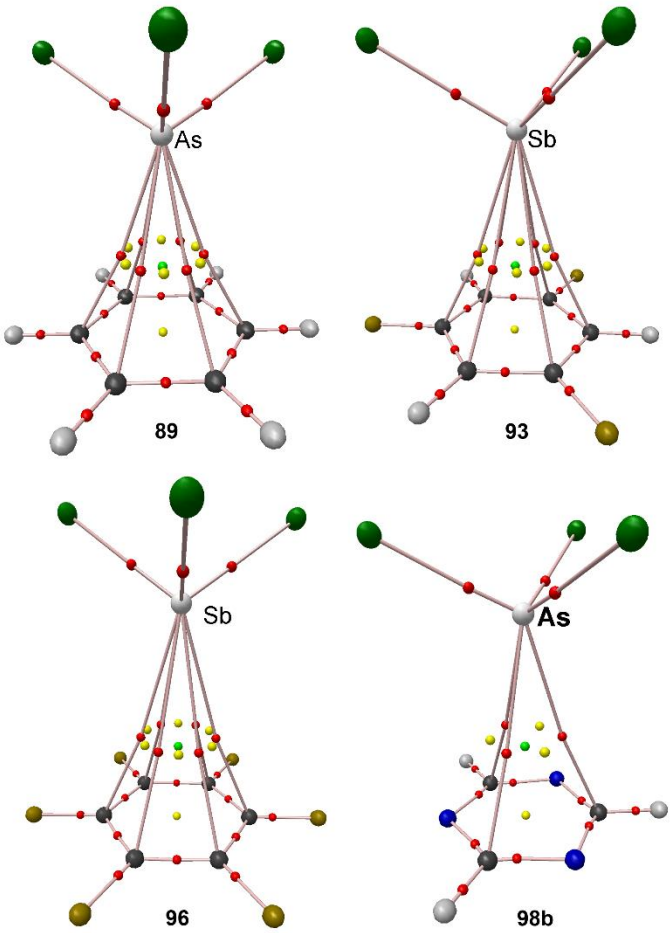

Figure 81. Distribution of critical points in complexes **89**, **93**, **96** and **98b**. The bond, ring and cage critical points are represented by red, yellow and green spheres, respectively. The bond paths connecting the nuclei with bond CPs are also represented.

3.4.4.5. Biological considerations

We have examined the PDB in order to provide experimental evidence of the importance of pnicogen-π interaction in biological systems. We have searched for structures containing trivalent As, Sb and Bi ligands. There are 38 structures for As, three structures for Sb and only one (still unreleased) structure for Bi (3TPH). Interestingly, in some of the protein structures that present trivalent As in the structure, the source of As is a dithiothreitol-mediated reaction of cysteine with the arsenic center of the cacodylate (dimethyl arsinic acid) present in the crystallization buffer.[246] Two representative examples are shown in Figure 83. One of them (on the right side) is a T4 polynucleotide kinase/phosphatase (Pnkp) enzyme that belongs to a family of bifunctional enzymes with 5′-kinase and 3′-phosphatase activities that function in nucleic acid repair.[81] The arsenic adduct is located at 3.7 Å above the planar aromatic TRP213 side chain. A similar reaction of a tryptophan-proximal

[246] a) K. B. Jacobson, J. B. Murphey, B. D. Sarma, *FEBS Lett.* **1972**, *22*, 80–82; b) D. H. H. Tsao, A. H. Maki, *Biochemistry* **1991**, *30*, 4565–4572; c) S. Maignan, J.-P. Guilloteau, Z.-L. Qing, C. Clement-Mella, V. Mikol, *J. Mol. Biol.* **1998**, *282*, 359–368; d) F. Tete-Favier, D. Cobessi, S. Boschi-Muller, S. Azza, G. Branlant, A. Aubry, Structure **2000**, *8*, 1167–1178; e) M. S. Junop, M. Modesti, A. Guarné, R. Ghirlando, M. Gellert, W. Yang, *EMBO J.* **2000**, *19*, 5962–5970.

cysteine with cacodylate has been also reported for EcoRI methyltransferase and Escherichia coli peptide methionine sulphoxide reductase.[246] The other example selected is the human phosphodiesterase 4B2B.[247] In this case the aromatic residue is phenylalanine instead of tryptophan. The interaction distance is 3.75 Å and the As atom is located almost exactly over the center of the benzene ring.

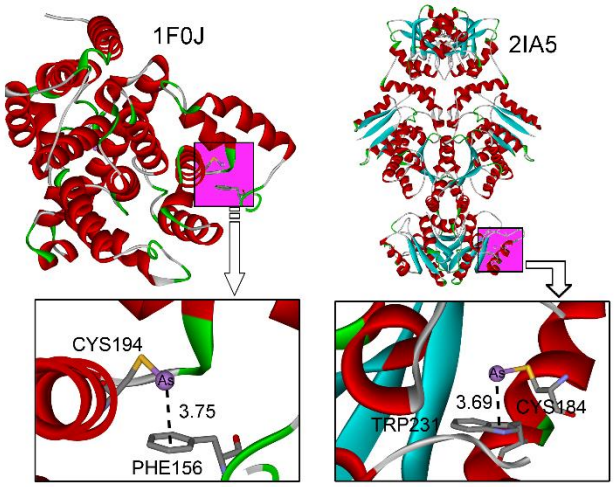

Figure 83. Partial views of the PDB structures 1F0J (left) and 2IA5 (right) exhibiting As-π interactions, which are highlighted and magnified at the bottom of the figure.

More interestingly, a pnicogen-π interaction involving Sb(III) likely participates in the mechanism of inhibition of trypanothione reductase (TR). The current treatment of leishmaniasis relies on antimony based drugs, meglumine antimoniate (Glucantime), and sodium stibogluconate (Pentostam).[82] The human protozoan parasites of the trypanosomatidae family differ from the other eukaryotes in their specific redox metabolism because the glutathione/glutathione reductase system is replaced by the unique trypanothione/trypanothione reductase system. The crystal structures of TR from *Leishmania infantum* and its complex with NADPH and Sb(III) was reported in 2009.[82] The Sb(III) present in the catalytic cleft is coordinated by the two redox-active catalytic cysteine residues (CYS52 and CYS57) and one threonine residue (THR335). Thus, the inhibition mechanism is due to the disulfur brigde breaking caused by the complexation of the Sb(III), which reduces the redox capability of the enzyme. Although not suggested by the original authors, we propose that the pnicogen-π interaction with the FAD cofactor also stabilize the coordination of the Sb(III) to the active site, as indicated in Figure 84. Therefore this interaction helps to the tight binding of the inhibitor to the active site. The Sb-π distance is in good agreement with the theoretical values present in Table 11. Interestingly, Sb(V)-containing compounds are less toxic than their trivalent analogues, although Sb(V) is considered to be a pro-drug that has to be activated by conversion to the trivalent form Sb(III) to exert its action against the parasite.[83]

[247] R. X. Xu, A. M. Hassell, D. Vanderwall, M. H. Lambert, W. D. Holmes, M. A. Luther, W. J. Rocque, M. V. Milburn, Y. Zhao, H. Ke, R. T. Nolte, *Science* **2000**, *288*, 1822–1825.

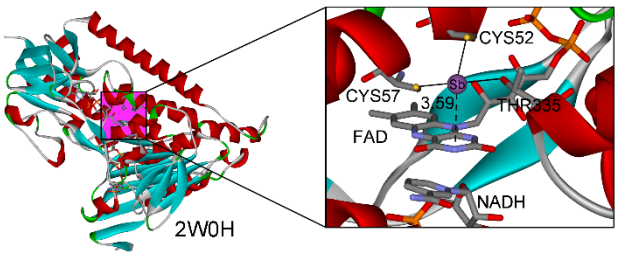

Figure 84. Partial view of the PDB structure 2W0H exhibiting an interesting Sb-π interaction, which is highlighted and magnified at the right side of the figure.

3.4.5. Conclusions

The analysis of the results presented in this manuscript offers some interesting conclusions:
First, the pnicogen-π interaction is stronger in electron-rich than in electron-poor arenes, indicating that the interaction is better described as a traditional Lewis acid to π-base (arene) interaction than as an electron transfer between the pnicogen (lone pair) and the arene. Related to this, the MEP results anticipate that the electrostatic interaction is not favored in electron-deficient arenes, as corroborated by the DFT-D3 calculations. Particularly, in these complexes the interaction is dominated by dispersion forces. Consequently, the dispersion corrected DFT method gives reliable results (comparable to MP2) if the latest developed correction for dispersion is used. The density at the cage critical point that is originated upon complexation of the ECl_3 molecule can be used as a measure of the strenght of the interaction. Finally, the pnicogen-π interaction is also relevant in biological systems and it likely participates in the mechanism of inhibition of Sb-based drugs used to treat Leishmaniasis.

3.4.6. Acknowledgements

We thank CONSOLIDER–Ingenio 2010 (CSD2010-0065) and the MICINN of Spain (project CTQ2011-27512/BQU, FEDER funds) for financial support. DQ thanks the MICINN of Spain for a “Ramon y Cajal” contract. We thank the CESCA for computational facilities.

Chapter 4

Aerogen bonding Interactions

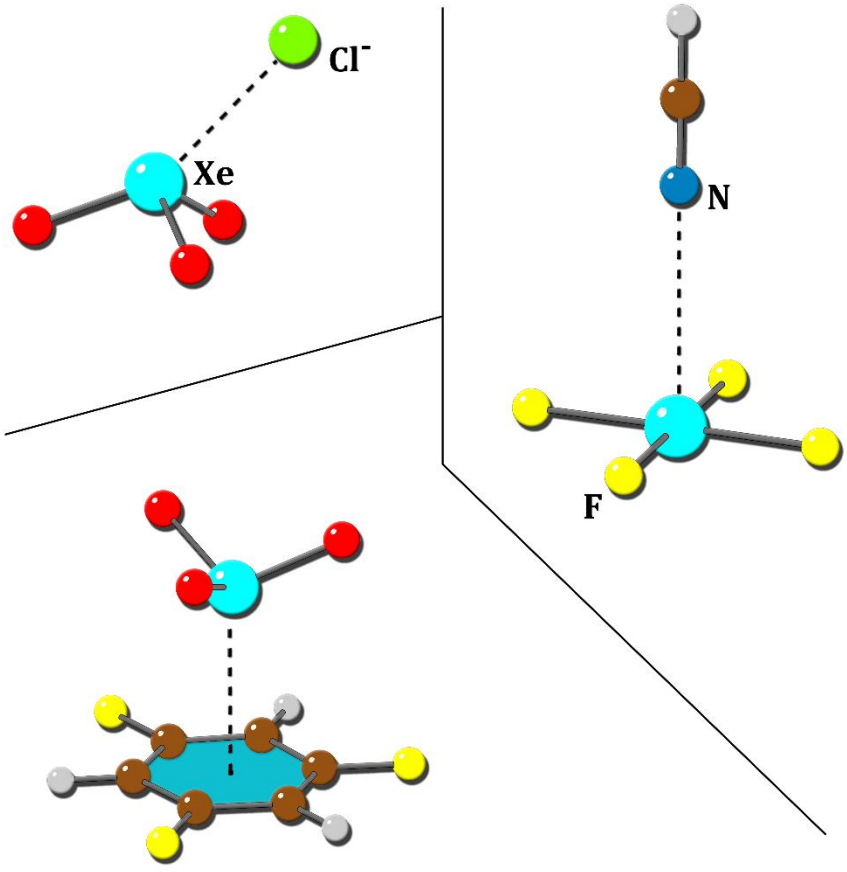

4.1. Preface and Objectives

This chapter is devoted to the study of σ- and π-hole interactions involving aerogen moieties. The chapter is divided into four sections: firstly *section 4.2.* empasses the discovery of a new supramolecular bond between aerogen atoms and electron-rich species. The study was supported by experimental evidences retrieved from the ICSD (Inorganic Crystal Structure Database) involving xenon compounds. Secondly, *section 4.3.* is devoted to the study of π-hole interactions involving Xe(IV) compounds. In this case the structures considered for the study were XeF_4 and $Xe(OTF_4)_5$ derivatives. Finally, *section 4.4.* is devoted to the analysis of the interaction between Xe(IV) and Xe(VI) compounds and aromatic rings of different electronic nature, such as benzene or hexafluorobenzene, thus defining aerogen-π interactions.

The main objectives of the chapter are listed below:

- A study of the physical nature and stability properties of aerogen bonding interactions, using the ICSD as source for experimental evidences.

- Analysing the interaction between π-holes involving Xe(IV) compounds and electron-rich molecules.

- Analysing the interaction between Xe(IV) and Xe(VI) compounds and aromatic moieties of different electronic nature.

4.2. Aerogen bonding interaction: a new supramolecular force?

4.2.1. Abstract

We report evidence of the favorable noncovalent interaction between a covalently bonded atom of Group 18 (known as noble gases or aerogens) and a negative site, for example, a lone pair of a Lewis base or an anion. It involves a region of positive electrostatic potential (σ-hole), therefore it is a totally new and unexplored σ-hole-based interaction, namely aerogen bonding. We demonstrate for the first time the existence of σ-hole regions in aerogen derivatives by means of high level *ab initio* calculations. In addition, several crystal structures retrieved from the Cambridge Structural Database (CSD) give reliability to the calculations. Energetically, aerogen bonds are comparable to hydrogen bonds and other σ-hole based interactions but less directional. They are expected to be important in xenon chemistry.

4.2.2. Introduction

Noncovalent interactions are the main protagonists of supramolecular chemistry and biochemistry controlling the central parts of living systems. An appropriate comprehension of the different noncovalent forces is necessary for the rational design of new drugs and developing improved synthetic receptors capable to function in competitive media.[135] Among many interactions, the hydrogen bond is probably the most studied and analyzed noncovalent interaction.[136] However, σ-hole interactions involving tetrel, pnicogen, chalcogen and halogen atoms have attracted substantial attention in recent years and they are recognized by the scientific community as powerful tools in supramolecular chemistry, crystal engineering and biochemistry.[70,86a,86b,137,157,210] These interactions are moderately strong and directional basically due to the localization of a positive region on the extension of the covalent bonds (σ-hole) in the acceptor molecule.

Usually, the name of the group (halogen, chalcogen etc...) is used to specify the interactions and they are subgroups of a general definition of σ-hole bonding interactions given by Politzer and coworkers.[4c] As far as our knowledge extends, the σ-hole interaction has not been described for group 18 of elements (noble gases or aerogens). This is likely due to the general assumption that these elements are monatomic gases with very low chemical reactivity. As a matter of fact, inertness of noble gases makes them suitable in applications where reactions are not desired.
In this manuscript we propose the term aerogen bonding for describing the unprecedented σ-hole interaction between electron-rich entities (anions or lone pair possessing atoms) and elements belonging to group 18. The energetic features and structural properties of aerogen bonding are discussed and two fascinating X-ray structures are selected to illustrate the existence of this interaction. Obviously, this rare type of bonding is not expected to be an effective and reliable instrument in crystal engineering or supramolecular chemistry; however it is certainly important in terms of gaining knowledge in the molecular and supramolecular sciences.

4.2.3. Theoretical methods

The energies of all complexes included in this study were computed at the RI-MP2/aug-cc-pVTZ level of theory. For fifth row elements the aug-cc-pVTZ-PP basis set was used, which uses a relativistic effective core potential (ECP) to accelerate the calculations and to account for relativistic effects, which cannot be neglected. The calculations have been performed by using the program TURBOMOLE version 6.5.[141] The interaction energies were calculated with correction for the basis set superposition error (BSSE) by using the Boys-Bernardi counterpoise technique.[142] The MEP and NBO calculations have been performed at the MP2/aug-cc-pVTZ level by means of the Gaussian 09 calculation package.[143] The "Atoms in molecules" (AIM) analysis was performed at the MP2/aug-cc-pVTZ level of theory. The calculation of AIM properties was done using the AIMAll program.[181] The minimum nature of the complexes has been checked at the same level by performing frequency calculations.

4.2.4. Results and discussion

The synthesis and crystal structure determination of xenon trioxide was reported in 1963 by Templeton *et al.*[248] The molecule XeO_3 is in the shape of a trigonal pyramid with dimensions similar to those of the isoelectronic iodate ion (see Figure 85). The crystal packing shows that each xenon establishes three noncovalent Xe···O contacts with neighbouring molecules at distances (from 2.8 to 2.9 Å) longer than the sum of the covalent radii of Xe and O (2.03 Å) and shorter than the sum of van der Walls radii (3.68 Å) that can be defined as σ-hole aerogen bonding interactions. In Figure 85 we show the molecular electrostatic potential (MEP) surface computed at the MP2/aug-cc-pVTZ level of theory and a strong and extended σ-hole can be clearly observed. Unexpectedly a very positive potential is found at the position where the lone pair of the Xe(VI) is located, which can be related to the inert pair effect.[249]

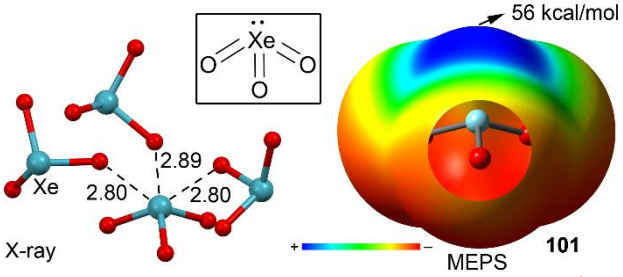

Figure 85. Left: X-ray structure of XeO_3. Right: MEPS of XeO_3. Distances in Å.

The chemistry of Xe(IV) has been recently reviewed[250] and most of the known compounds are salts where purely electrostatic interactions dominate in their solid state structure. However, one neutral and interesting derivative of Xe(IV) is the XeF_2O compound that was synthesized from the co-condensation of water and

[248] D. H. Templeton, A. Zalkin, J. D. Forrester, S. M. Williamson, *J. Am. Chem. Soc.* **1963**, *85*, 816–817.
[249] G. E. Rodgers, *J. Chem. Educ.* **2014**, *91*, 216–224.
[250] J. Haner, G. J. Schrobilgen, *Chem. Rev.* **2015**, *115*, 1255–1295.

XeF_4.[251] Most interestingly, in the presence of CH_3CN, the isolation of $F_2OXe{\cdot}NCCH_3$ is achieved.[252] This structure is the first and unique example of a Xe(IV)-N bond. Two further examples of Xe(IV)-N donor-acceptor bonds have been reported,[253] but involving a positively charged Xe(IV) moiety, i.e., $[C_6F_5XeF_2]^+$. A partial view of the $F_2OXe{\cdot}NCCH_3$ crystal structure is shown in Figure 86.

It can be observed that the $XeOF_2$ moiety is planar showing a T-shaped arrangement of two fluorine atoms and an oxygen double bond domain in the equatorial plane and two mutually trans valence electron lone pairs perpendicular to that plane. The nitrogen electron pair donor atom of CH_3CN interacts with the Xe atom opposite to the Xe=O bond and is coplanar with the $XeOF_2$ moiety. This has been defined as a coordination Xe(IV)-N bond by the original authors.[252]

We also show in Figure 86 the MEP of $XeOF_2$ and $TeOF_2$ for comparison purposes. The MEP surface of trigonal $TeOF_2$ molecule shows a clear π-hole above and below the Te atom. In contrast, the MEP surface of the T-shaped $XeOF_2$ molecule shows a strong σ-hole at the Xe atom in the prolongation of the Xe=O bond due to the existence of two valence lone pairs. Therefore the Xe(IV)–N noncovalent contact observed in the solid state of $F_2OXe{\cdot}NCCH_3$ is a clear example of a σ-hole interaction (aerogen bonding). Interestingly the $XeOF_2$ molecule in the solid state is surrounded by four CH_3CN molecules (see Figure 86), one establishing the aerogen bonding interaction with the Xe and the rest forming O(F)···C noncovalent carbon bonding interactions.[70,137b,157]

We have optimized several complexes of XeO_3 and XeF_2O with two electron donor molecules (see Figure 87) and compared their energetic and geometric features with complexes where lighter aerogens (Ar and Kr, **104**–**107**) are used. Moreover we have also compared the interaction energies of the aerogen complexes to those using halogen, chalcogen, pnicogen and tetrel atoms of the same row as σ-hole donors.

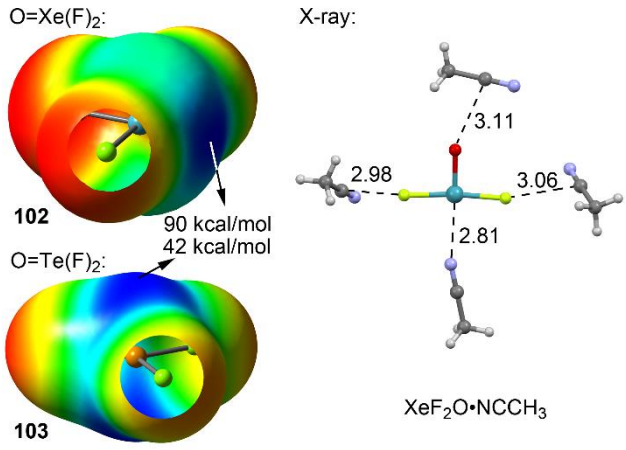

Figure 86. Right: X-ray structure of $XeF_2O{\cdot}CH_3CN$. Distances in Å. Left: MEP of XeF_2O and TeF_2O.

[251] a) J. S. Ogden, J. J. Turner, *Chem. Commun*. **1966**, *19*, 693–694; b) E. Jacob, R. Opferkuch, *Angew. Chem. Int. Ed.* **1976**, *15*, 158–159.
[252] D. S. Brock, V. Bilir, H. P. A. Mercier, G. J. Schrobilgen, *J. Am. Chem. Soc*. **2007**, *129*, 3598–3611.
[253] K. Koppe, J. Haner, H. P. A. Mercier, G. J. Schrobilgen, *Inorg. Chem*. **2014**, *53*, 11640–11661.

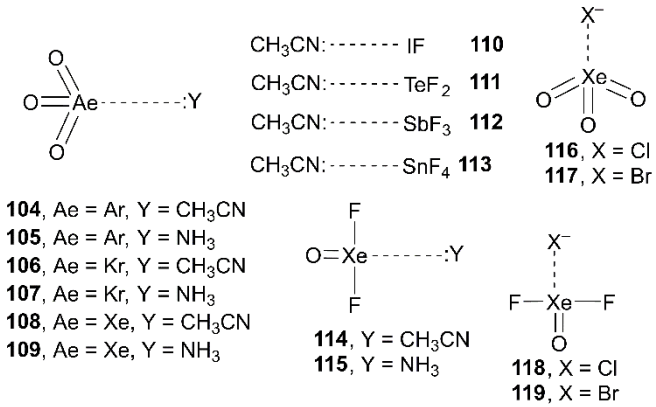

Figure 87. Complexes **104**–**119** studied in this work.

These comparisons allow us, first, to investigate if the aerogen bonding follows the same energetic trend than the rest of σ-hole interactions. That is, the strength of the interaction augments as the bond donor atom is increasingly polarizable (heavier atoms). Secondly, to investigate whether the aerogen bonding is energetically similar to other well-known σ-hole interactions, using elements with similar polarizability values.

The energetic and geometric results of the *ab initio* optimized complexes **104**–**119** are gathered in Table 12 (see Figure S13 in the SI for a representation of the optimized geometries). From the inspection of the results, several interesting points arise. First, in the Ae(VI) complexes **104**–**109**, the interaction energies follow the expected trend for a σ-hole based interaction. That is, the largest interaction energies (in absolute value) are obtained for the heaviest aerogen atom (complexes **108** and **109**). Second, complexes **110**–**113** where elements of the same row are used as σ-hole donors present interaction energies that are larger in absolute value than the one obtained for complex **108** ($O_3Xe\cdots NCCH3$) apart from the pnicogen bonded complex **112**. The most favourable one is the tetrel complex (**113**) that correspond to the strongest σ-hole donor molecule (see Figure 88) followed by the halogen bonded complex **110** also in agreement with the MEP analysis. The strength of chalcogen and pnicogen complexes is comparable to the aerogen bonding complex **108**. Third, the interaction energies of Xe(IV) complexes **114**–**115** are larger in absolute value than those computed for the equivalent Xe(VI) complexes **108**–**109**, in agreement with the electrostatic potential values at the σ-holes (see Figures 85 and 86). Finally, we have also included several complexes with anions (**116**–**119**) and the interaction energies are very large, in line with reported anionic complexes between halides and traditional σ-hole donor atoms.[29]

Table 12. Interaction energies without and with the basis set superposition error (ΔE and ΔE_{CP} in kcal/mol, respectively), and equilibrium distances (R_e, Å) for complexes **104**–**119** at the RI-MP2/aug-cc-pVTZ level of theory. The point group (PG) and imaginary frequencies (N_{Imag}) are also indicated.

Complex	ΔE	ΔE_{CP}	R_e	PG (N_{Imag})
104	–6.6	–6.4	2.934	C_1 (0)
104a	–6.7	–5.9	2.909	C_{3v} (3)
105	–7.1	–6.5	2.853	C_s (0)
105a	–6.4	–5.1	2.978	C_{3v} (2)
106	–8.1	–7.2	2.980	C_s (0)
106a	–7.4	–6.8	3.053	C_{3v} (3)
107	–9.0	–8.3	2.843	C_s (0)
107a	–6.9	–6.5	3.127	C_{3v} (2)
108	–11.6	–9.5	3.142	C_s (0)
108a	–9.2	–8.0	2.960	C_{3v} (3)
109	–10.4	–9.0	2.779	C_s (0)
109a	–8.3	–7.4	3.221	C_{3v} (2)
110	–15.0	–12.2	2.450	C_s (0)
111	–13.1	–10.3	2.535	C_s (0)
112	–10.4	–8.1	2.722	C_s (0)
113	–21.6	–16.6	2.273	C_s (0)
114	–12.1	–10.1	2.798	C_s (0)
115	–14.6	–12.6	2.690	C_1 (0)
116	–39.0	–37.2	2.784	C_s (0)
117	–34.2	–32.6	2.983	C_s (0)
118	–41.9	–40.0	2.697	C_s (0)
119	–37.2	–35.4	2.874	C_s (0)

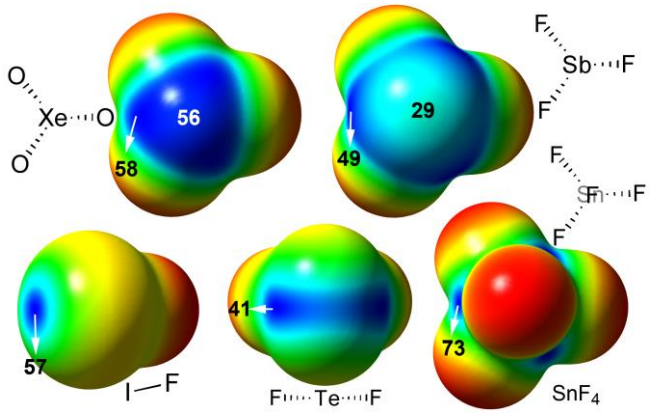

Figure 88. MEP surfaces computed for several σ-hole donor molecules at the MP2/aug-cc-pVTZ level of theory. Some MEP energy values in kcal/mol are indicated.

At this point, it is worth emphasizing the difference observed in the MEP surfaces of XeO_3 and SbF_3 (see Figure 88, top). Both molecules have a lone pair located in the molecular C_{3v} axis and both present positive potential values at the location of the lone pair. However, the MEP of SbF_3 shows three well defined σ-holes located at the extensions of the Sb-F bonds with a MEP value that is 20 kcal/mol more positive than that at the location of the inert lone pair (see Figure 88). In contrast, the MEP surface of XeO_3 shows a negligible difference between the MEP values measured at the σ-hole and lone pair locations. A similar result is observed in the MEP surfaces of

ArO_3 and KrO_3 molecules (see SI, Figure S14). Therefore the aerogen bonding is less directional than the rest of σ-hole bonding interactions. As a matter of fact, we have also optimized complexes **104**–**109** imposing C_{3v} symmetry (lone pair directed to the inert lone pair,[249] complexes denoted as **104a**–**109a** in Table 12) and the interaction energies are comparable.

The geometries of some representative complexes and their corresponding distribution of critical points[238] (see SI for details) are given in Figure 89. It can be observed that the electron-rich atom of the Lewis base (or anion) is positioned at the σ-hole location (extension of the Xe=O covalent bond). All complexes are characterized by the presence of a bond critical point (small red sphere) connecting the Xe atom to the electron-rich atom thus confirming the interaction. The values of the charge density ρ(r) at the bond critical point in the aerogen bonding complexes shown in Figure 89 (values in italics) are similar to those reported for σ-hole interactions of groups 14-17.[70,86a,86b,137,157,210]

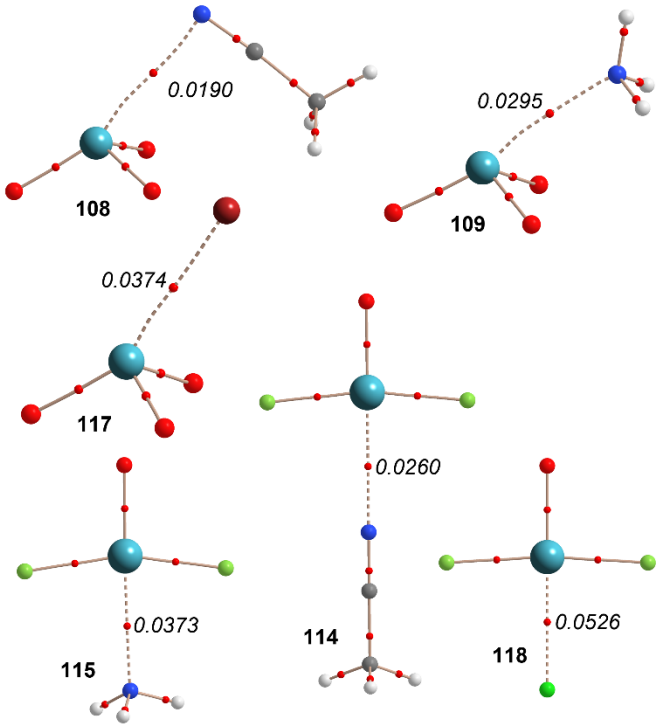

Figure 89. AIM distribution of critical points (red spheres correspond to bond critical points) at the MP2/aug-cc-pVTZ level of theory. The ρ(r) values at the bond critical points are indicated in a.u.

In order to study if orbital contributions are important to explain the aerogen interactions described above, we have performed Natural Bond Orbital (NBO) calculations focusing our attention on the second order perturbation analysis,[206] since it is very useful to study donor acceptor interactions. The results are summarized in Table 13. For Ae(VI) complexes, the orbital contribution is small (~10% of the total interaction energy) for the lighter aerogens and the contribution is important in xenon complexes, especially in complex **109** where the orbital contribution dominates the interaction, in agreement with the short Xe···N distance (2.779 Å).

A very remarkable finding derived from the NBO analysis of AeO_3 complexes with the CH_3CN (**104**, **106** and **108**), is that the electron donor orbital does not corresponds to the lone pair of the N atom; instead it is the π-system of the CN triple bond. This result likely explains the unexpected similar interaction energies obtained for NH_3 and CH_3CN complexes with AeO_3 σ-hole donor molecules. That is, the CH_3CN is a weak Lewis base (sp-hybridized lone pair) and therefore it is expected to have smaller complexation energies than the stronger NH_3 Lewis base (sp^3-hybridized lone pair). The geometry of the optimized complexes (see Figure 89) clearly agrees with the fact that the electron-rich part of the molecule that interacts with the σ-hole is the π-system of the triple bond.

For the Xe(IV) complexes **114** and **115**, the orbital contribution is very large, especially in complex **115** where the concomitant stabilization energy due to the electron donation from the lone pair of N to the antibonding Xe-O orbital (n→σ*) is approximately equal to the interaction energy reported in Table 12, thus representing a major factor in the stabilization. More interestingly, complex **114** (the one observed experimentally) presents two types of donor-acceptor orbital interactions. One corresponds to the expected n→σ* donation with a $E^{(2)}$ = 4.49 kcal/mol, which is considerably smaller than the value obtained for complex **115** due to the larger N-Xe distance in complex **114** and low basicity of the sp-hybridized lone pair. The other one corresponds to a back-bonding donation from one lone pair of xenon to the N-C antibonding orbital. This surprising back-bonding orbital donation is not negligible, since it has a concomitant stabilization energy of $E^{(2)}$ = 2.06 kcal/mol that is approximately 20 % of the total interaction energy.

Table 13. Donor and acceptor NBOs with indication of the second-order interaction energy $E^{(2)}$ (kcal/mol) and type of interaction for aerogen neutral complexes.

Complex	Donor[a]	Acceptor	$E^{(2)}$	Type
104	BD(3) N–C	BD(1)* Ar-O	0.49	π→σ*
105	LP N	BD(1)* Ar-O	0.77	n→σ*
106	BD(3) N–C	BD(1)* Kr-O	0.99	π→σ*
107	LP N	BD(1)* Kr-O	2.22	n→σ*
108	BD(3) N–C	BD(1)* Xe-O	2.23	π→σ*
109	LP N	BD(1)* Xe-O	6.76	n→σ*
114	LP N	BD(1)* Xe-O	4.49	n→σ*
	LP Xe	BD(1)* N-C	2.06	n→σ*
115	LP N	BD(1)* Xe-O	12.32	n→σ*

[a]BD, BD* and LP stand for bonding, anti-bonding and lone pair orbital, respectively.

4.2.5 Conclusions

In conclusion, in this manuscript we report unprecedented σ-hole interactions involving noble gases. We propose the use of aerogen bonding to refer to the noncovalent interaction between atoms of group 18 acting as Lewis acids and any entity with the ability to act as an electron donor (lone pair, anion, etc.). Aerogen bonds have, at least, comparable strength to hydrogen bonds and other σ-hole based interactions, though are less directional. Due to the increasing interest and research on xenon derivatives, this interaction is expected to play an important role in their

solid state chemistry. Moreover, from a pedagogic point of view, this newly defined interaction is certainly of interest, being the ultimate sub-class of σ-hole noncovalent bonding interactions.

4.2.6. Acknowledgements

This work was funded by the MINECO of Spain (CONSOLIDER-Ingenio 2010 project CSD2010-0065 FEDER funds).

4.2.7. Supporting Information

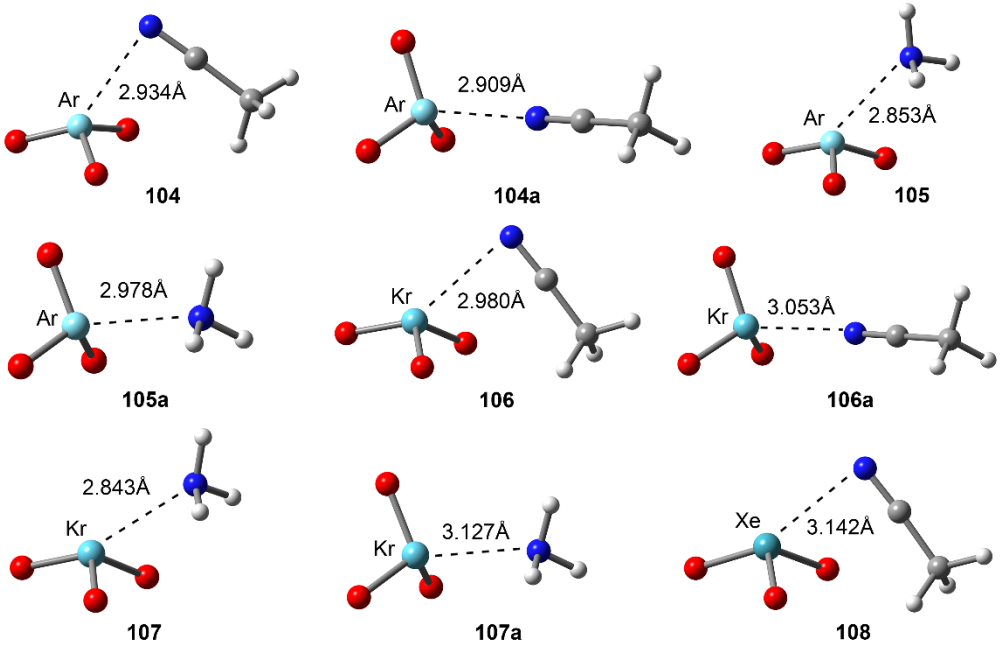

Figure S13. Optimized geometries at the RI-MP2/aug-cc-pVTZ level of theory.

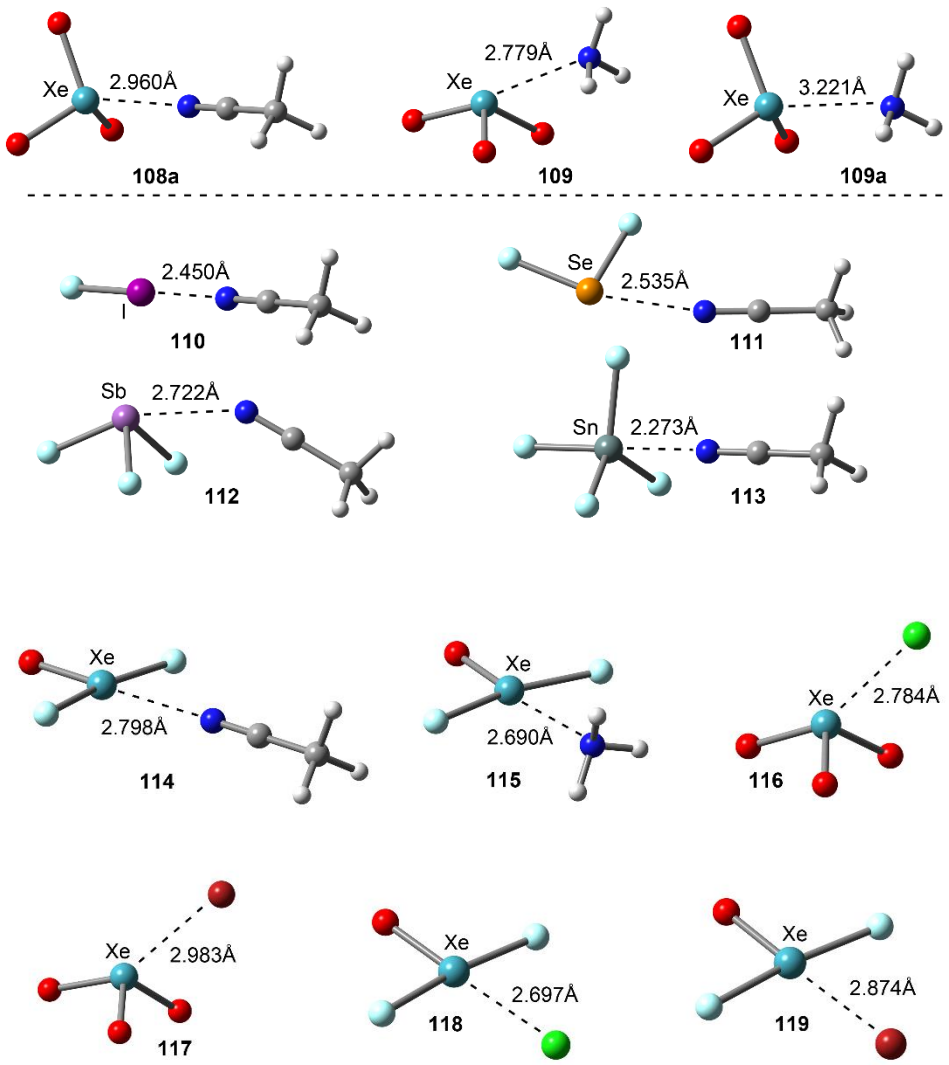

Figure S13 (cont). Optimized geometries at the RI-MP2/aug-cc-pVTZ level of theory.

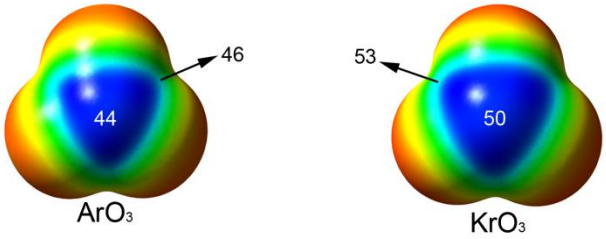

Figure S14. MEP analysis of ArO_3 and KrO_3 molecules

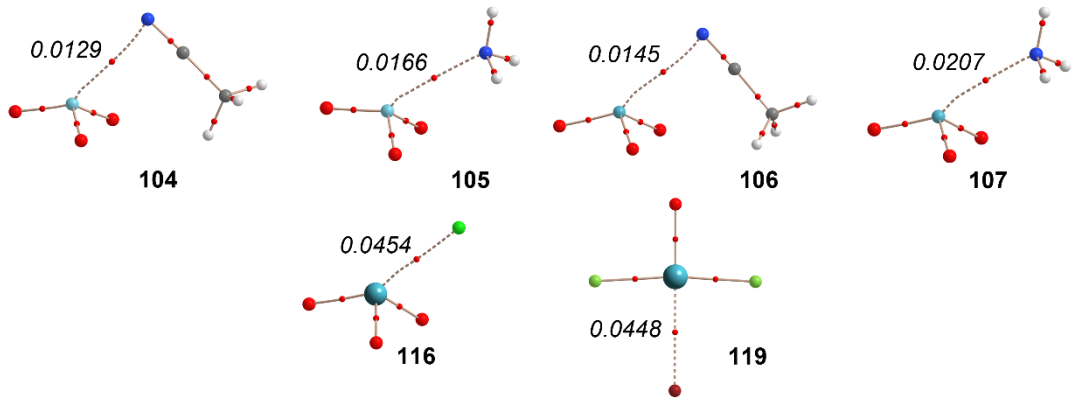

Figure S15. AIM distribution of critical points (red spheres correspond to bond critical points) at the MP2/aug-cc-pVTZ level of theory for complexes **104**–**107**, **116** and **119**. The ρ(r) values at the bond critical point are indicated in a.u.

4.3. π-Hole aerogen bonding interactions.

4.3.1. Abstract

In this manuscript we combine high level *ab initio* calculations (RI-MP2/aug-cc-pVTZ) and the analysis of several crystal structures to demonstrate the existence of π-hole aerogen bonding interactions in Xe(IV) compounds. The ability of XeF_4 and $Xe(OMe)_4$ to interact with electron-rich molecules is rationalized using several computational tools, including molecular electrostatic potential surfaces, energetic and geometric features of the complexes and "Atoms in molecules" (AIM) and Natural Bond Orbital (NBO) analyses. We have found support for the π-hole interaction involving the xenon atom from the solid state architecture of several X-ray structures retrieved from the crystal structural depot. Particularly, π-hole aerogen bonding interactions are quite common in the solid state of Xe(IV) compounds.

4.3.2. Introduction

Many features of modern chemistry and biology are determined by noncovalent interactions.[254] The understanding of many biological functions and drug design develops are basically due to the chemical and physics insights acquired from the theoretical and experimental analysis of host-guest complexes [255] and the concomitant expansion of supramolecular chemistry. Perfect examples are cation-π[233a,256] and anion-π[9a,31] interactions that previously to the evidence of their noticeable role in living systems[13a] they first became apparent in artificial systems. Moreover, σ-hole interactions involving tetrel, pnicogen, chalcogen and halogen atoms are also being recognized by the scientific community as powerful tools in supramolecular chemistry, crystal engineering and biochemistry.[233a,256] The strength of these interactions is moderately strong and they are highly directional due to the localization of a positive region on the extension of the covalent bonds (σ-hole) in the acceptor molecule. Frequently, the name of the group of atoms that provides the σ-hole (from IV to VII)[4c,5a,19a,25b,73b,85,86a,86b,86c,90,157,257] is used to specify the name of the interaction (halogen,[156,207c,258] chalcogen,[208b,259] etc[92] bonding) and they can be considered as subgroups of a general definition of σ-hole bonding interactions given by Politzer and coworkers. Very recently, the σ-hole interaction has been described for group VIII of elements (noble gases or aerogens).[260] This type of interaction is somewhat counterintuitive due to the general assumption that

[254] a) G. V. Oshovsky, D. N. Reinhoudt, W. Verboom, *Angew. Chem. Int. Ed*. **2007**, *46*, 2366–2393; b) J. M. Zayed, N. Nouvel, U. Rauwald, O. A. Scherman, *Chem. Soc. Rev*. **2010**, *39*, 2806–2816.
[255] a) M. Zürcher, F. Diederich, *J. Org. Chem*. **2008**, *73*, 4345–4361; b) D. K. Smith, *J. Chem. Educ*. **2005**, *82*, 393–400; c) D. A. Uhlenheuer, K. Petkau, L. Brunsveld, *Chem. Soc. Rev*. **2010**, *39*, 2817–2826.
[256] N. Zacharias, D. A. Dougherty, *Trends Pharmacol. Sci.* **2002**, *23*, 281–287.
[257] S. Scheiner, *Acc. Chem. Res*. **2013**, *46*, 280–288.
[258] a) P. Metrangolo, G. Resnati, *Chem. Eur. J*. **2001**, *7*, 2511–2519; b) S. J. Grabowski, *Phys. Chem. Chem. Phys*. **2013**, *15*, 7249–7259.
[259] a) P. Sanz, M. Yáñez, O. Mó, *Chem. Eur. J.* **2002**, *8*, 3999–4007; b) P. Sanz, M. Yáñez, O. Mó, *New J. Chem.* **2002**, *26*, 1747–1752.
[260] A. Bauzá, A. Frontera, *Angew. Chem. Int. Ed*. **2015**, *54*, 7340–7343.

these elements are monatomic gases with very low chemical reactivity. This particular case of σ-hole interaction has been termed as aerogen bonding and has been described theoretically and detected in several fascinating X-ray structures.[250]

In addition to the bunch of σ-hole interactions, a rather unexplored group of noncovalent interactions can be classified as π-hole bonding. A π-hole is a region of positive electrostatic potential that is perpendicular to a portion of a molecular framework.[5a] In case that this portion is an electron-deficient aromatic π system the interaction is known either as lone pair-π[8] or anion-π depending on the nature of the electron donor. Other founding π-hole interactions that encompass different molecular frameworks should be emphasized. For example, the identification of π-hole interactions in crystal structures was carried out by Bürgi and Dunitz in a series of studies revealing the trajectory along which a nucleophile attacks the π-hole of a C=O group.[15] Closely related, the ability of guanosine to act as a π-hole was pointed out by Egli and co-workers in 1995, when they studied the crystal structure of Z-DNA.[16] Recently, π-hole interactions have been described in SO_2 and SO_3 moieties,[18a] RNO_2 molecules,[19a,167] XCN, XZO_2 (X = halogen, Z = pnicogen), etc.[20a,20b]

In this manuscript we report an unprecedented theoretical study of π-hole aerogen bonding interaction involving Xe(IV) derivatives [i.e. XeF_4 and $Xe(OMe)_4$]. The energetic features and structural properties of π-hole complexes are discussed and three interesting X-ray structures are selected to illustrate the existence of this interaction. This unique type of bonding is not expected to be an effective instrument in crystal engineering or supramolecular chemistry; however it is certainly important in terms of gaining knowledge in the molecular and supramolecular sciences. The chemistry of Xe(IV) has been recently reviewed[250] and most of the known compounds are salts where purely electrostatic interactions dominate in their solid state structure. However, one neutral and interesting derivative is the xenon tetrafluoride. Its synthesis and crystal structure determination was reported in 1963 by Levy *et al.*[261] and it is the first binary fluoride of xenon that was discovered.[262]

The molecule XeF_4 is in the shape of a square planar and its crystal packing shows that each xenon establishes several noncovalent Xe···F contacts with neighbouring molecules at distances (from 3.20 to 3.56 Å) longer than the sum of the covalent radii of Xe and F (1.97 Å) and shorter than the sum of van der Walls radii (3.63 Å) that can be defined as π-hole aerogen bonding interactions. Similar interactions are also observed in the crystal packing of the molecular addition compound $XeF_4 \cdot XeF_2$.[263] In Figure 90 we also show the molecular electrostatic potential surface (MEP) computed at the MP2/aug-cc-pVTZ level of theory for XeF_4 and a strong and extended π-hole can be clearly observed. Unexpectedly a very positive potential is found at the position where the lone pair of the Xe(IV) is located, which is likely related to the inert electron pair effect.[249] Moreover, the global maximum (highest value of positive electrostatic potential) is not found along the C_4 axis, instead it is located bisecting the angle defined by the F-Xe-F atoms. The location of the MEP

[261] H. A. Levy, J. H. Burns, P. A. Agron, *Science* **1963**, *139*, 1208–1209.
[262] a) N. Barlett, *Proc. Chem. Soc*. **1962**, 218–218; b) K. O. Christe, *Chem. Commun*. **2013**, *49*, 4588–4590.
[263] J. H. Burns, R. D. Ellison, H. A. Levy, *J. Phys. Chem*. **1963**, *67*, 1569–1570.

maximum strongly agrees with the position of the F atoms of the neighbouring molecules in the crystal structure of XeF_4.

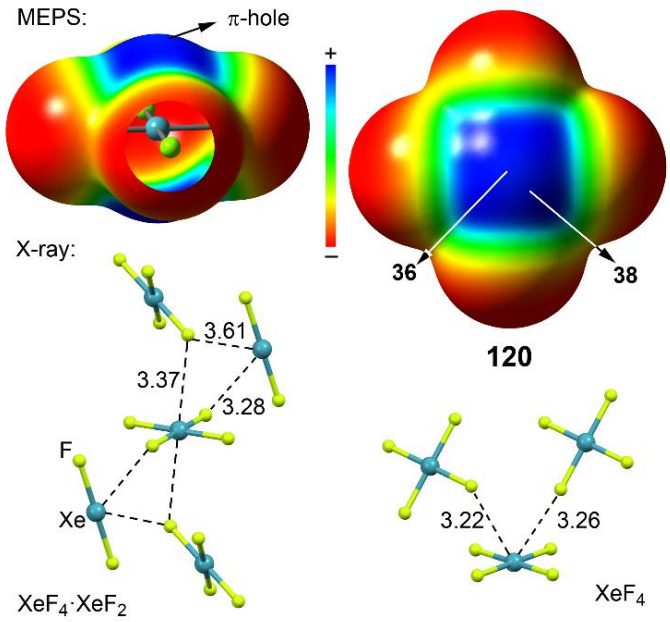

Figure 90. Top: MEP of XeF_4, energies in kcal/mol. Bottom: X-ray structures of XeF_4 and $XeF_4 \cdot XeF_2$. Distances in Å.

Another interesting Xe(IV) derivative is the $Xe(OTeF_5)_4$ compound. [264] Experimentally it shows a good thermal stability (it can be purified by sublimation). A partial view of its crystal structure is shown in Figure 91. The environment around xenon is square planar and two adjacent F_5Te-moieties point up and down in pairs. In its crystal packing, each xenon establishes two symmetrically equivalent noncovalent Xe···F contacts with two neighbouring molecules at 3.31 Å distance giving rise to the formation of an infinite 1D ladder in the solid state. In Figure 91 we also show the MEP calculated for $Xe(OMe)_4$ as a theoretical model. It can be observed a moderately strong π-hole over the Xe atom. The size of the π-hole is smaller than the one computed for XeF_4 due to the presence of the lone pairs of the oxygen atoms pointing above and below the XeO_4 core plane (see red contours in Figure 91). This MEP analysis is useful to rationalize the solid state architecture of $Xe(OTeF_5)_4$.

[264] a) L. Turowsky, K. Seppelt, *Z. Anorg. Allg. Chem*. **1981**, *472*, 7; b) D. Lentz, K. Seppelt, *Angew. Chem. Int. Ed*. **1978**, *17*, 356–361.

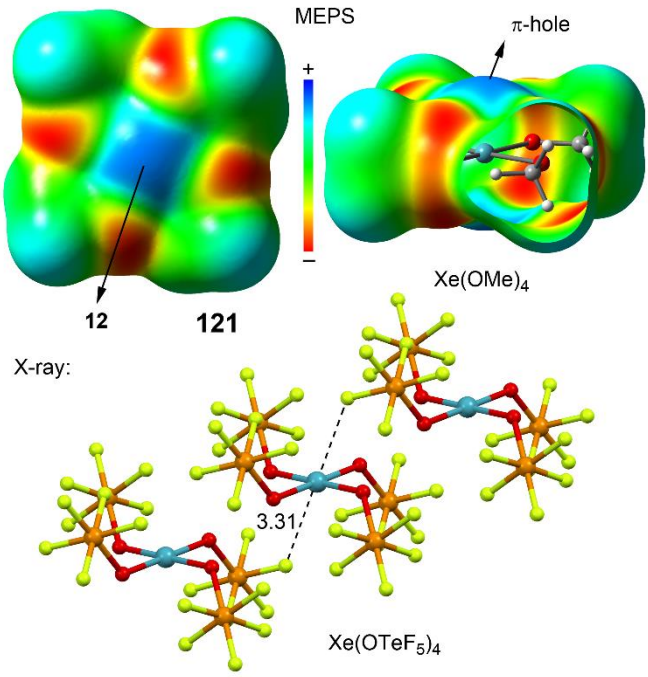

Figure 91. Top: MEP of $Xe(OMe)_4$, energies in kcal/mol. Bottom: X-ray structures of $Xe(OTeF_5)_4$. Distances in Å.

4.3.3. Theoretical methods

The geometries of all complexes were optimized at the RI-MP2/aug-cc-pVTZ level of theory by means of the Turbomole 6.5 software.[141] The interaction energies were calculated with correction for the basis set superposition error (BSSE) by using the Boys-Bernardi counterpoise technique.[142] The symmetry constrain imposed in the optimizations of the complexes is indicated in Table 14. The Bader's "Atoms in molecules" theory has been used to study the aerogen bonding interactions discussed herein by means of the AIMAll calculation package.[181] The MEP surface analysis was performed at the same level of theory and the MEP surface figures have been generated using GaussView. For the $Xe(OCH_3)_4$ complexes, the carbon atoms of the methyl group has been forced to be coplanar with the XeO_4 core in order to avoid the formation of C-H···X hydrogen bonds.

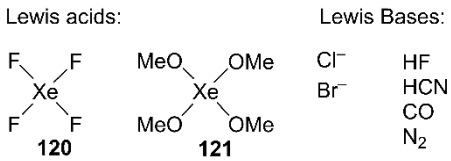

Figure 92. π-Hole donor xenon compounds **120–121** (Lewis acids) and electron-rich molecules (Lewis bases) used in this work.

4.3.4. Results and discussion

We have analysed theoretically the π-hole binding ability of two square planar Xe(IV) derivatives as aerogen bond donors and several electron-rich molecules (see Figure 92), ranging from very weak Lewis bases (N_2) to anions (Cl^- and Br^-).

We have optimized the aerogen bonding complexes **122**–**137**, which are represented in Figure 93 and the resulting interaction energies are summarized in Table 14. For the xenon tetrafluoride (**120**) complexes with anions (**122** and **123**), the interaction energies are large and negative and the equilibrium distances are short (see Figure 94 for the geometries of some representative complexes). In neutral complexes **124**–**128** the interaction energies are modest, ranging from –4.0 to –0.7 kcal/mol. The smallest interaction energy (in absolute value) corresponds to complex **129** where the π-system of the N_2 molecule interacts with the π-hole of **120**. In this complex we have also computed the interaction energy using a larger basis set (aug-cc-pVQZ) and the resulting value is similar (–0.9 kcal/mol) to the one listed in Table 14, giving reliability to the level of theory and confirming the modest but favourable interaction energy of complex **129**.

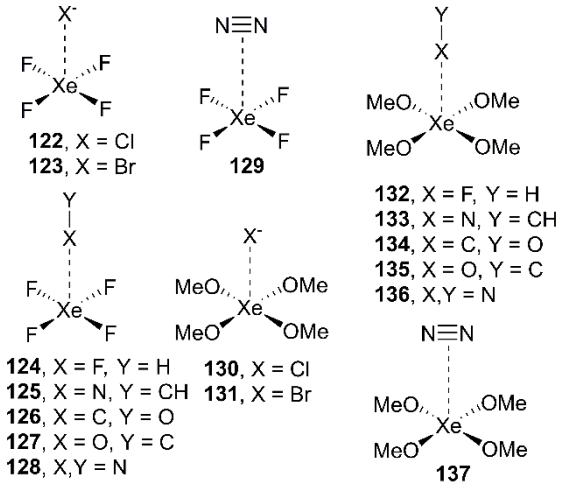

Figure 93. Complexes **122**–**137** studied in this work.

The $Xe(OMe)_4$ complexes with anions present more modest interaction energies in agreement with the magnitude of the π-hole. Unexpectedly, two $Xe(OMe)_4$ neutral complexes (**135** and **137**) are slightly more favourable than the corresponding XeF_4 complexes (**127** and **129**) likely due to additional long-range interactions with the OCH_3 groups. This aspect is further analysed below in the Natural Bond Orbital analysis.

Table 14. Interaction energies with the BSSE correction (E_{BSSE}, kcal/mol) and equilibrium distances (R_e, Å) at the RI-MP2/aug-cc-pVTZ level of theory.

Complex	E_{BSSE}	R_e	$10^2 \times \rho$	$10^2 \times \nabla^2\rho$	Symm.
122	–18.8	3.128	2.47	7.43	C_{4v}
123	–16.3	3.326	2.08	5.52	C_{4v}
124	–2.5	3.122	1.06	5.06	C_{2v}
125	–4.0	3.272	1.17	4.45	C_{2v}
126	–1.8	3.565	0.80	2.70	C_{2v}
127	–0.8	3.417	0.68	2.86	C_{2v}
128	–1.3	3.484	0.72	2.83	C_{2v}
129	–0.7	3.716[a]	0.49	1.76	C_{2v}
130	–12.1	3.237	1.99	6.02	C_2
131	–10.8	3.427	1.71	4.60	C_2
132	–1.2	3.229	0.83	3.85	C_2

Complex	E_{BSSE}	R_e	$10^2 \times \rho$	$10^2 \times \nabla^2\rho$	Symm.
133	–2.1	3.334	1.02	3.84	C_2
134	–1.3	3.567	0.79	2.64	C_2
135	–0.9	3.402	0.70	2.92	C_2
136	–1.2	3.460	0.75	2.93	C_2
137	–1.1	3.574[a]	0.65	2.33	C_2

[a]Measured from the Xe to N≡N centroid.

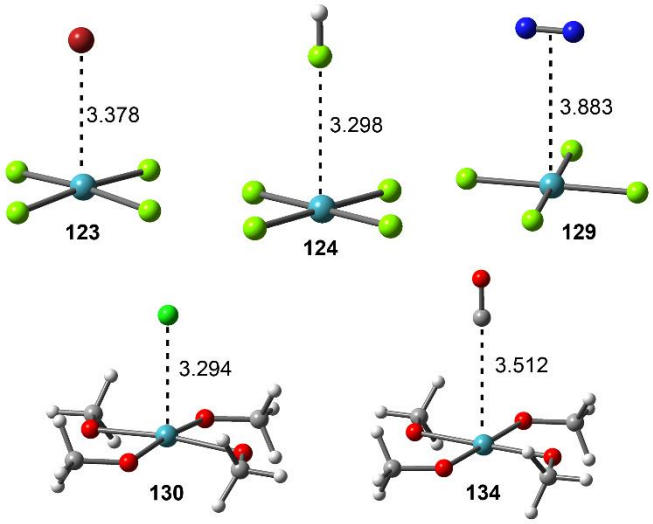

Figure 94. RI-MP2/aug-cc-pVTZ optimized geometries of several aerogen bonding complexes. Distances in Å.

4.3.4.1. Atoms in molecules characterization of π-hole aerogen bonding complexes

We have performed the "Atoms in molecules"[196,238,265] (AIM) analysis of all complexes included in this study. Previous investigations have illustrated that the AIM analysis is useful (especially $\nabla^2\rho$) to explain the phenomenon of aerogen bonding in Xe(II) compounds.[266] In general the complexes are characterized by the presence of a bond critical point (CP) and a bond path connecting the electron-rich atom with xenon. In complexes **129** and **137**, where the electron donor is the π-system of the N_2 molecule, the bond CP that emerges upon complexation connects the xenon atom with the bond CP of the N≡N bond (see complex **137** in Figure 95). We have gathered in Table 14 the values of ρ and $\nabla^2\rho$ at the bond CP that characterizes the aerogen bonding interaction for complexes **122**–**137**.

The density at the bond CP has been used as a measure of bond strength in a variety of noncovalent interactions. We have examined if these values can be also used as a measure of bond order in the complexes studied here. We have represented in Figure 96 a plot where we analyse the existence of a linear relationship between the interaction energies and the ρ values (summarized in Table 14). Remarkably, we

[265] P. L. A. Popelier, *Atoms In Molecules. An Introduction*; Prentice Hall, Harlow, **2000**.
[266] P. J. MacDougall, G. J. Schrobilgen, R. F. W. Bader, *Inorg. Chem.* **1989**, *28*, 763–769.

have obtained a strong relationship with a regression coefficient r = 0.982. It should be emphasized the relevance of this relationship since in the same representation we have included two different π-hole donor molecules (**120** and **121**) and anionic and neutral π-hole acceptors. Therefore it allows for dealing simultaneously with both series complexes and using charged and neutral electron donors in the same representation. These results confirm that ρ at the bond CP is directly related to the strength of the aerogen bonding interaction.

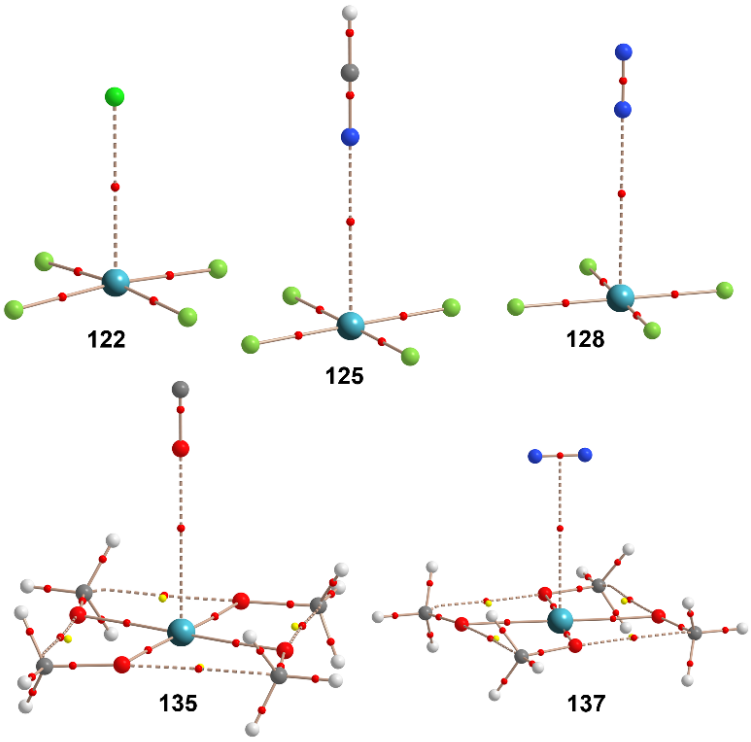

Figure 95. Representation of bond (red) and ring (yellow) critical points in several complexes. The bond paths connecting (3,-1) critical points are also represented.

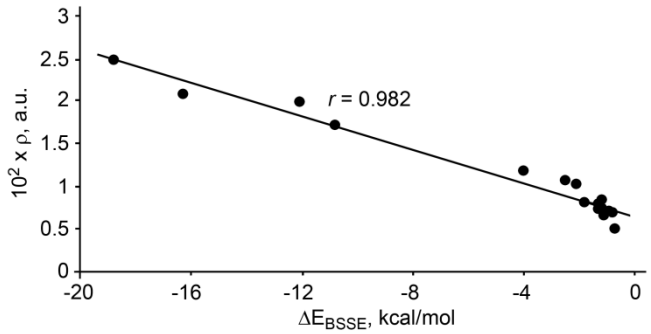

Figure 96. Regression plot of the density (ρ) at the bond CP *versus* the interaction energy (BSSE corrected) for complexes **122**–**137**.

4.3.4.2. NBO analysis

In order to study if orbital contributions are important to explain the aerogen π-hole complexes described above, we have performed Natural Bond Orbital (NBO)

calculations focusing our attention on the second order perturbation analysis, since it is a convenient tool to analyze donor acceptor interactions.[258] The results are summarized in Table 15. For the anionic complexes, the orbital contribution is small compared to the total interaction energy (~20%) and it is basically due to the interaction of a lone pair (LP) of the anion with empty Rydberg orbitals (RY*) of xenon.

Table 15. Donor and acceptor NBOs with indication of the second-order interaction energy $E^{(2)}$ (kcal/mol) and type of interaction for aerogen complexes **122**–**137**. Values in italics correspond to back-bonding contributions

Complex	Donor[a]	Acceptor	$E^{(2)}$	Type
122	LP Cl	RY* Xe	3.84	n→π*
	LP Xe	RY* Cl	*0.27*	n→π*
123	LP Br	RY* Xe	3.12	n→π*
	LP Xe	RY* Br	*0.30*	n→π*
124	BD F–H	RY* Xe	1.00	σ→π*
	LP F	RY* Xe	0.32	n→π*
	LP Xe	RY* F	*0.70*	n→π*
	LP Xe	BD* F–H	*0.35*	n→σ*
125	BD N–C & C–H	RY* Xe	2.07	π/σ→π*
	LP N	RY* Xe	0.32	n→π*
	LP Xe	RY* N	*0.69*	n→π*
	LP Xe	BD* N–C	*1.26*	n→π*
126	BD C–O	RY* Xe	0.13	π→π*
	LP C	RY* Xe	0.42	n→π*
	LP Xe	RY* C	*0.50*	n→π*
	LP Xe	BD* C–O	*0.19*	n→π*
127	BD O–C	RY* Xe	0.49	π→π*
	LP O	RY* Xe	0.29	n→π*
	LP Xe	RY* O	*0.42*	n→π*
	LP Xe	BD* O–C	*0.44*	n→π*
128	BD N–N	RY* Xe	0.48	π→π*
	LP N	RY* Xe	0.34	n→π*
	LP Xe	RY* N	0.92	n→π*
	LP Xe	BD* N–N	*0.33*	n→π*
129	BD N–N	RY* Xe	0.07	π→π*
	LP Xe	RY* N	*0.54*	n→π*
130	LP Cl	RY* Xe	1.83	n→π*
	LP Xe	RY* Cl	*0.10*	n→π*
131	LP Br	RY* Xe	1.69	n→π*
	LP Xe	RY* Br	*0.12*	n→π*
132	BD F–H	RY* Xe	1.49	σ→π*
	LP F	RY* Xe	0.21	n→π*
	LP Xe	RY* F	*0.06*	n→π*
	LP Xe	BD* F–H	*0.45*	n→σ*
133	BD N–C	RY* Xe	0.59	π→π*
	LP N	RY* Xe	0.37	n→π*
	LP Xe	BD* N–C	*1.00*	n→π*
	LP Xe	RY* N	*0.50*	n→π*
	LP O	RY* N	*0.12*	n→π*
134	BD O–C	RY* Xe	0.16	π→π*
	LP C	RY* Xe	0.30	n→π*
	LP Xe	BD* C–O	*0.07*	n→π*
	LP Xe	RY* C	*0.13*	n→π*
	LP O	RY* C	*0.10*	n→π*

Complex	Donor[a]	Acceptor	$E^{(2)}$	Type
135	BD O–C	RY* Xe	0.79	π→π*
	LP O (OC)	RY* Xe	0.54	n→π*
	LP Xe	BD* O–C	*0.52*	n→π*
	LP Xe	RY* O	*0.10*	n→π*
	LP O (OMe)	RY* O	*0.16*	n→π*
136	BD N–N	RY* Xe	0.50	π→π*
	LP N	RY* Xe	0.46	n→π*
	LP Xe	BD* N–N	*0.53*	n→π*
	LP Xe	RY* N	*0.38*	n→π*
	LP O	RY* N	*0.14*	n→π*
137	BD N–N	RY* Xe	0.18	π→π*
	LP Xe	RY* N	*0.22*	n→π*
	LP O	RY* N	*0.18*	n→π*

[a]BD, BD* and LP, RY* stand for bonding, anti-bonding, lone pair and Rydberg orbital, respectively.

Curiously, there is also a very small contribution of a back-bonding donation from one LP of xenon to the RY* orbital of Cl/Br (ranging from 0.10 to 0.32 kcal/mol). In contrast to the anionic complexes where electrostatic effects are dominant, the orbital contribution in the neutral complexes represents a major factor in the stabilization. For instance, in the XeF_4 neutral complexes **124–129** there are four contributions. In two of them the electron-rich molecule act as donor and Xe as acceptor (see Table 15). In the other two (values in italics) the Xe atom acts as donor (back-bonding using its LP). The back-bonding is not dominant in complexes **124** and **125** and the interaction can be classified as an lp→π-hole interaction. Remarkably, the back-bonding becomes more important in complexes **126**–**128** and, consequently, the interaction is almost equally dominated by the donation and back-bonding contributions. Finally, in complex **129** the orbital contribution interaction is governed by the donation from the LP of Xe to the RY* orbitals of N atoms.

The NBO analysis is also helpful to rationalize the stronger binding energies obtained for complexes **132–137** [$Xe(OMe)_4$ with weak Lewis bases] compared to complexes **125–129** (see Table 15), in sharp disagreement to the π-hole MEP values. Complexes **133–137** exhibit two different back-bonding orbital interactions. The first one is equivalent to the aforementioned for XeF_4 complexes (i.e., from the LP of Xe to the anti-bonding orbital of the X-Y interacting molecule or the RY* orbital of interacting X atom, see Table 15). The second one corresponds to an electron donation from the four lone pairs of the oxygen atoms of the OCH_3 groups to the RY* orbital of the interacting atom with concomitant stabilization energies [$E^{(2)}$] that range from 0.10 to 0.18 kcal/mol. The equivalent back-bonding from the F atoms in XeF_4 complexes **126–129** is not observed, thus explaining the similar or even slightly more favourable binding energies observed for complexes **133–137**.

4.3.5. Conclusions

In this manuscript we report unprecedented π-hole interactions involving two square planar Xe(IV) derivatives. We have extended the recently described σ-hole

aerogen bonding interaction (i.e. noncovalent bonding between atoms of group 18 acting as Lewis acids and any entity with the ability to act as an electron donor) to π-hole aerogen bonding. Several X-ray structures illustrate this type of interaction in the solid state. The interaction is strong and dominated by electrostatic effects when the electron donor is an anion. In these complexes the orbital contribution is very small. Conversely, the interaction is modest (ranging from –3.8 to –0.5 kcal/mol) when the electron donor is a weak Lewis base. The AIM analysis demonstrates that the density at the bond critical point can be used as a measure of bond order of the aerogen bond and it linearly correlates with the interaction energy. Finally, the NBO analysis reveals that the back-bonding (from the LPs of Xe and oxygen atoms) is very relevant in some complexes.

4.3.6. Acknowledgements

We thank the DGICYT of Spain (projects CTQ2011-27512/BQU and CONSOLIDER INGENIO 2010 CSD2010-00065, FEDER funds) and the Direcció General de Recerca i Innovació del Govern Balear (project 23/2011, FEDER funds) for financial support.

4.4. Theoretical study on the dual behaviour of XeO_3 and XeF_4 toward aromatic rings: Lone pair-π *vs.* Aerogen-π interactions.

4.4.1. Abstract

In this study several lone pair-π and aerogen-π complexes between XeO_3, XeF_4 and aromatic rings of different electronic nature (benzene, trifluorobenzene and hexafluorobenzene) have been optimized at the RI-MP2/aug-cc-pVTZ level of theory. All complexes were characterized as true minima by frequency analysis calculations. The donor/acceptor role of the ring in the complexes has been analyzed using the NBO computational tool showing a remarkable contribution of orbital interactions to the global stabilization of the aerogen-π complexes. Finally the Bader's AIM analysis of several complexes has been performed in order to further characterize the lp-π and aerogen-π interactions.

4.4.2. Introduction

Supramolecular chemists rely on a depth comprehension of the noncovalent forces, which are the ground pillars of modern chemistry. A proper understanding and intelligent utilization of them is essential in order to achieve progress in fields such as supramolecular chemistry,[1] molecular recognition[161] and materials science.[79a] For instance, interactions involving aromatic rings (i.e. π-π stacking,[234a] cation-π,[233] anion-π,[9b] lp-π[8b] and C-H/π[153b] interactions) are extremely important in many chemical and biological processes,[232b] including molecular sensing,[2] crystal engineering and enzymatic mechanisms.

In this context, the most known supramolecular force that is ubiquitous in many chemical and biological systems is the hydrogen bonding. In recent years, another noncovalent force that shares strength and directionality features with the hydrogen bonding is the halogen bonding interaction. Consequently, a series of studies using the CSD (Cambridge Structural Database) have been carried out in order to shed light into the impact of this interaction in the crystal formation.[3] The interest among the scientific community has grown exponentially due to the recognition of its importance in biological systems and the design of new materials; leading to a plethora of theoretical and experimental studies devoted to this topic.[4a,4b,4c] In addition, apart from the well-established amount of noncovalent forces, an emerging group of so called "unconventional" noncovalent interactions has attracted the interest of scientific community during the past years.[189] It refers to the interaction between group IV to VII bearing compounds (donor) and nucleophiles (acceptor).[5a,5b,157] Frequently, the name of the group of atoms that provides the σ-hole (from IV to VII) is used to specify the name of the interaction, and they can be considered as subgroups of a general definition of σ-hole bonding interactions given by Politzer and coworkers. A great deal of computational studies[6a,6b,6c] has been devoted to these emerging group of interactions, concluding that their strength is moderately strong and they are highly directional due to the localization of a positive potential region on the extension of the covalent bonds (σ-hole) in the

acceptor molecule.[7a,7b,7c,267,7d] The magnitudes of the σ-hole potentials are ruled by the same factors as for the halogens.

Recently, a new supramolecular force has been put into scene, named aerogen bonding,[260,268] which implies an interaction between an aerogen bearing moiety and an electron-rich entity. Very few examples are available in the CSD, due to the low reactivity of the aerogen element series. While its potential practical applications in the field of supramolecular chemistry are very limited, aerogen bonding interactions can be of great importance in xenon chemistry. Very recently, Miao *et al.* have highlighted the possibility of electron-rich arenes to be an important stabilization source of xenon compounds through the establishment of aerogen-π interactions.[268b]

In addition to the group of σ-hole interactions, a rather unexplored group of noncovalent interactions can be classified as π-hole bonding. A π-hole is a region of positive electrostatic potential that is perpendicular to a portion of a molecular framework.[27] In case that this portion is an electron-deficient aromatic π-system the interaction is characterized either as lone pair-π or anion-π depending on the nature of the electron donor. Other previous π-hole interactions that encompass different molecular portions should be remarked. For example, the identification of π-hole interactions in crystal structures was carried out by Burgi and Dunitz in a series of studies revealing the trajectory of a nucleophilic attack to the π-hole of a C=O group.[15a,15b,15c] Moreover, the ability of guanosine to act as a π-hole donor was pointed out by Egli and co-workers in 1995, when they studied the crystal structure of Z-DNA.[16] In addition, Alkorta and coworkers have extensively studied π-hole interactions involving pnicogen atoms in order to rationalize and understand in a deeper way the nature and physical properties of these particular interactions.[109,269] Recently, the study of π-hole interactions has been extended to acyl carbons,[17] SO_n moieties (n = 2,3),[18a,170] RZO_2,[19a,167,270] XCN and XZO_2 molecules (X = halogen, Z = pnicogen), etc.[20a,20b] Finally, it is also worth mentioning the ability of Xe(IV) derivatives to interact as π-hole donors, extending the recently described σ-hole aerogen bonding to π-hole aerogen bonding. In fact, a search performed in the CSD provided experimental evidence to the existence of this type of π-hole interaction in the solid state.[271]

In the present study, our main objective was to evaluate the ability of Xe(VI) and Xe(IV) compounds to establish lone pair-π and aerogen-π interactions. We have used XeO_3 and XeF_4 as either lone pair or σ-/π-hole donors, respectively, and benzene, trifluorobenzene and hexafluorobenzene as π-systems (see Figure 97). For all combinations two types of minima (binding modes) have been found on the potential surface. For the XeO_3 series of complexes, the Xe is pointing to the π-

[267] J. S. Murray, L. Macaveiu, P . Politzer, *J. Comput. Sci.* **2014**, *5*, 590–596.
[268] J. Miao, B. Song, Y Gao *Chem. Asian. J*. **2015**, *10*, 2615–2618.
[269] a) I. Alkorta, J. Elguero, J. E. Del Bene, *J. Phys. Chem. A* **2013**, *117*, 10497–10503; b) S. Mohammad, R. Vahid, C. Trujillo, I. Alkorta, G. Sanchez–Sanz, J. Elguero, *J. Phys. Chem. A* **2012**, *116*, 5199–5206; c) C. Trujillo, G. Sánchez, I. Alkorta, J. Elguero, *New J. Chem.* **2015**, *39*, 6791–6802.
[270] a) S. Roy, A. Bauzá, A. Frontera, R. Banik, A. Purkayastha, M. G. B. Drew, B. M. Reddy, B. Sridhar, S. Kr. Dasa S. Das, *CrystEngComm*, **2015**, *17*, 3912–3916. b) S. Cañellas, A. Bauzá, A. Lancho, A. Garcia-Raso, J. J. Fiol, E. Molins, P. Ballester, A. Frontera, *CrystEngComm*, **2015**, *17*, 5987–5997.
[271] A. Bauzá, A. Frontera, *Phys. Chem. Chem. Phys.* **2015**, *17*, 24748–24753.

system (aerogen-π interaction) in one binding mode, and the lone pairs of the O are pointing to the π-system (lp-π interaction) in the other one. For the XeF_4 complexes, the XeF_4 plane is stacked parallel or T-shaped to the aromatic ring (aerogen-π or lp-π, respectively). The interaction energies of both binding modes have been compared and the physical nature of the interaction analyzed using different computational tools including the Natural Bond Orbital (NBO) analysis, the Symmetry Adapted Perturbational Theory (SAPT) partition scheme and the Bader's theory of "Atoms in molecules" (AIM).

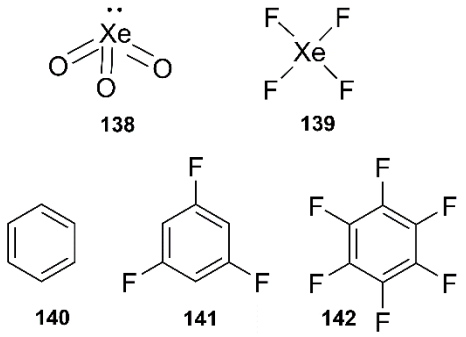

Figure 97. Compounds **138** to **142** used in this study.

4.4.3. Theoretical methods

The geometries and energies of all complexes included in this study were computed at the RI-MP2/aug-cc-pVTZ level of theory. The calculations have been performed by using the program TURBOMOLE version 7.0[141] For the xenon atom the aug-cc-pVTZ-PP basis set was used. The interaction energies were calculated with correction for the basis set superposition error (BSSE) by using the Boys-Bernardi counterpoise technique.[142] The optimization of the molecular geometries has been performed imposing the C_s symmetry point group. Frequency calculations have been performed at the RI-MP2/aug-cc-pVTZ level of theory and in all cases a true minima have been found. The MEPS calculations have been performed at the MP2/aug-cc-pVTZ level by means of the Gaussian 09 software.[143] The partitioning of the interaction energies into the individual electrostatic, induction, dispersion and exchange-repulsion components was carried out with the symmetry adapted intermolecular perturbation theory approach DFT-SAPT at the DF-DFT/aug-cc-pVTZ//RI-MP2/aug-cc-pVTZ level of theory.[198] The Bader's "Atoms in molecules" theory has been used to study the interactions discussed herein by means of the AIMAll calculation package.[181]

4.4.4. Results and discussion

4.4.4.1. MEP study

As a preliminary study, we have computed the MEP (Molecular Electrostatic Potential) surface of compounds **138** to **142**, which are shown in Figure 98. We have also included the quadrupole moment values (Q_{zz}) of the aromatic rings retrieved

from the literature.[33b,240] As it can be observed, the MEP surface of compounds **138** and **139** shows an extended positive potential region located at the xenon atom (σ- and π-hole, respectively) thus expecting a favorable interaction with electron-rich entities. Curiously, the position of the σ-/π-hole coincides with the location of the inert lone pair of Xe(VI) and Xe(IV), respectively.[249]

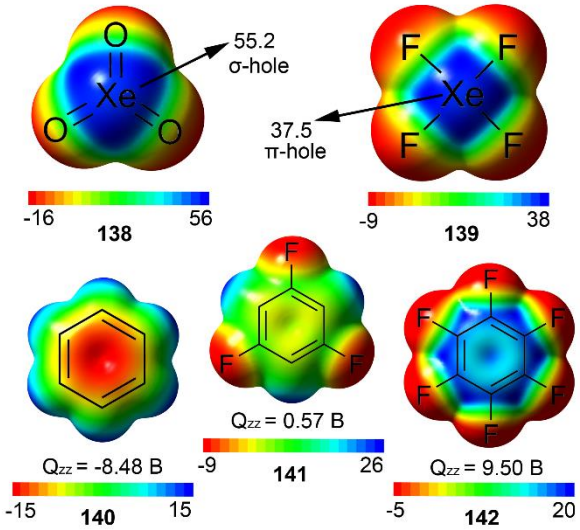

Figure 98. MEPS (Molecular Electrostatic Potential) surface of compounds **138** to **142**. Energy values are in kcal/mol.

It is also remarkable the difference in magnitude observed for both xenon derivatives, much larger in the XeO_3 moiety, thus expecting a stronger binding upon complexation with electron-rich entities. Regarding the aromatic rings, a progressive change from red to blue color in the MEP surface above the ring center is observed as the number of fluorine substituents increases with a concomitant change in the sign of the quadrupole moment from negative to positive. This gradual change of the π-basicity (or π-acidity) of the arene is useful to predict the behavior of the two different interactions considered in this study. Thus, in case of the electron-rich compound **140**, a favorable interaction with electron-poor entities (σ- or π-hole) is expected, thus favoring the aerogen-π interaction. On the other hand, the opposite behavior is expected for compound **142**, since the value of the MEP over the ring center is positive, along with its Q_{zz} value.
Finally, for compound **141** the electrostatic component is not expected to play an important role due to the negligible Q_{zz} and MEP value over the center of the ring. Therefore, other energy components like polarization and dispersion effects are key players in the overall stabilization of the complexes, as further discussed below.

4.4.4.2. Energetic study

The interaction energies and equilibrium distances obtained for complexes **143**–**154** (see Figure 99) studied herein are summarized in Table 16. From the inspection of the results, several interesting conclusions arise. First, in all cases the binding energy values are favorable, ranging between –2 and –12 kcal/mol. Second, for

complexes involving benzene, the most favorable binding mode is the aerogen-π, in agreement with the MEP analysis showed above. Third, lone pair-π interactions are preferred for XeO_3 complexes with hexafluorobenzene. The opposite is observed for XeF_4 complexes, where the aerogen-π interaction is more favored likely for the face-to-face π-stacking nature of this complex. This particular aspect is further analyzed in the NBO and AIM analyses (*vide infra*). Finally, for trifluorobenzene complexes, the aerogen-π interaction is more favored than the lone pair-π for both xenon derivatives, likely due to polarization an dispersion effects (the Xe element is considerably more polarizable than O or F).[191]

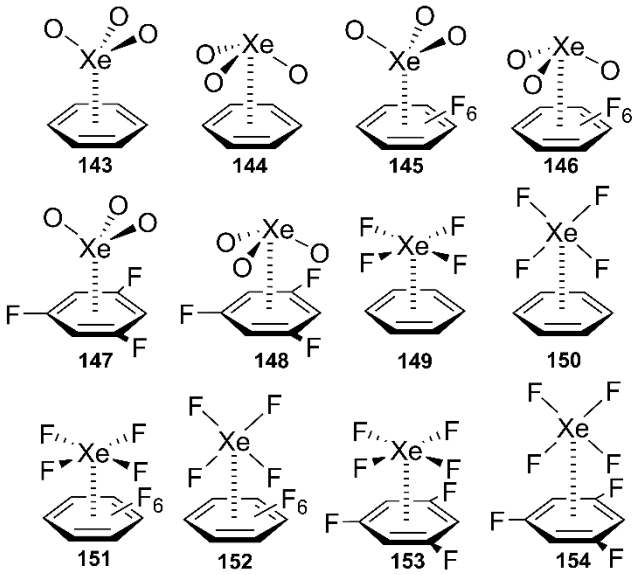

Figure 99. Complexes **143** to **154** used in this study.

The energetically most favorable complex of this study is **143**, which contains XeO_3 and benzene (–12.4 kcal/mol), thus remarking the ability of electron-rich aromatic moieties to stabilize xenon compounds by means of aerogen-π interactions, in agreement with recent results reported by Miao *et al.*[268b] The lone pair-π interaction for this π-system is clearly disfavored due to the electronic nature of the arene and consequently, a weak binding energy value is obtained for complex **144** (–2.5 kcal/mol). In hexafluorobenzene complexes **145** and **146**, the lone pair-π interaction is the preferred, with a binding energy value of –5.1 kcal/mol in **146**. Finally, in the trifluorobenzene complexes **147** and **148**, the aerogen-π is more favored over the lone pair-π interaction.

On the other hand, in the XeF_4 series of complexes, the largest binding energy value corresponds to the aerogen-π complex **149** (–8.8 kcal/mol). In addition, the lone pair-π interaction is not favored in complex **150**, obtaining the lowest energy value of the Xe(VI) series (–1.9 kcal/mol). In complexes involving C_6F_6, the aerogen-π interaction (complex **151**, –3.5 kcal/mol) is slightly more favored than the lone pair-π (complex **152**, –3.1 kcal/mol). This is an unexpected result since the electronic nature of this arene does not favor the interaction with electron-poor entities. In this case orbital effects have a key role in the stabilization of complex **152** as explained in the following NBO analysis. Finally, in complexes **153** and **154** a preference for

the aerogen-π over the lone pair-π interaction is observed, as obtained for the XeO_3 moiety. This issue will be further analyzed in the SAPT analysis (vide infra).

Table 16. Interaction energies of complexes **143** to **154** at the RI-MP2/aug-cc-pVTZ level of theory without and with the BSSE correction (E and E_{BSSE} in kcal/mol, respectively), equilibrium distances (R_e in Å) and value of the density at the cage critical point ($10^2 \times \rho$·, a.u.).

Complex	E	E_{BSSE}	R_e	Complex type	$10^2 \times \rho$
143	−16.6	−12.4	2.904[a]	σ-hole	1.08
144	−4.5	−2.5	3.259[b]	lp-π	0.18
145	−6.2	−2.2	3.061[a]	σ-hole	0.94
146	−8.1	−5.1	3.049[a]	lp-π	0.26
147	−10.7	−6.7	2.979[b]	σ-hole	1.02
148	−6.3	−3.7	3.119[a]	lp-π	0.23
149	−12.9	−8.8	3.045[b]	π-hole	0.91
150	−3.4	−1.9	3.026[a]	lp-π	0.16
151	−8.1	−3.5	3.096[b]	π-hole	0.89
152	−5.3	−3.1	2.905[a]	lp-π	0.21
153	−10.0	−5.7	3.097[a]	π-hole	0.88
154	−4.3	−2.4	2.978[b]	lp-π	0.27

[a]Distances measured from the Xe to the ring centroid
[b]Shortest distance measured from the O/F to the closest carbon atom of the ring

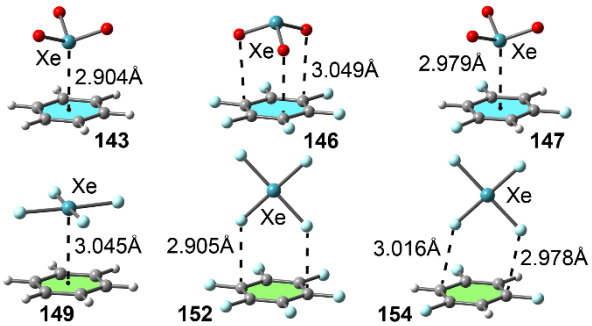

Figure 100. Optimized geometries of some representative complexes at the RI-MP2/aug-cc-pVTZ level of theory.

4.4.4.3. NBO analysis

To study the importance of orbital effects in the aerogen-π and lone pair-π interactions described above, we have performed natural bond orbital (NBO) calculations focusing our attention on the second order perturbation analysis,[206] due to its usefulness to study donor-acceptor interactions. From the analysis of the results (see Table 17) some conclusions can be extracted. First, in XeO_3 aerogen-π complexes (**143**, **145** and **147**) an important contribution from the bonding C-C orbitals (π) of the ring moiety to the antibonding Xe-O orbitals (σ*) of the XeO_3 entity is observed, being the major factor of stabilization in these complexes. This observation confirms the σ-hole nature of the noncovalent interactions in these complexes. It is also worth mentioning the magnitude of this orbital interaction compared to the total interaction energy (~40% for **143** and ~50% for **144**).

Second, in addition to this contribution, the interaction of a bonding C-C orbital (π) of the aromatic moiety with empty Rydberg orbitals (RY*) of xenon also contributes

to the overall stabilization of the complexes. Finally, it is somewhat unexpected the observation of weak back-bonding orbital interactions in these set of complexes (see values in italics), due to the participation of the inert lone pair of Xe and the lone pairs of the O atoms. The back bonding donation from the lone pair of xenon (LP) is to the antibonding C-H orbitals in **143** and antibonding C-F orbitals in **145** and **147**. On the other hand, in complexes **144**, **146** and **148**, characterized as a lone pair-π interaction, the most remarkable contribution comes from the interaction of the oxygen lone pairs of the Xe-O moiety (LP) to the antibonding C-C orbitals (π*) of the benzene ring.

In the XeF_4 series (complexes **149** to **154**) the orbital contribution is smaller than the XeO_3 series (~20% the total interaction energy). A common trend is observed, which is a contribution from the lone pairs of the fluorine atoms (LP) to the antibonding C-C orbitals (π*) of the ring, independently of the type of interaction considered. In addition, the interaction of a bonding C-C orbital (π) of the aromatic moiety with empty Rydberg orbitals (RY*) of xenon also contributes to the final stabilization of complexes **149**, **151** and **153**. This result explains the preference for the aerogen-π interaction over the lone pair-π in complexes **151** and **152**. Finally, no back bonding orbital interactions involving the xenon atom were observed for this set of complexes.

Table 17. Donor and acceptor NBOs with indication of the second-order interaction energy $E^{(2)}$ and type of interaction for aerogen-π and lone pair-π complexes.

Complex	Donor	Acceptor	$E^{(2)}$	Type
143	BD C-C	BD* Xe-O RY*Xe BD* C-H	5.01	π→σ*
	BD C-C	BD* C-C	1.44	n→σ*
	LP Xe		*0.36*	n→σ*
	LP O		*0.36*	π→π*
144	LP O	BD* C-C	0.63	n→π*
	BD C-C	BD* Xe-O	0.30	π→σ*
145	BD C-C	BD* Xe-O	2.17	π→σ*
	BD C-C	RY*Xe BD* C-F	1.16	π→π*
	LP Xe		*0.33*	n→σ*
146	LP O	BD* C-C	0.82	n→π*
	BD C-C	BD* Xe-O	0.21	π→σ*
147	BD C-C	BD* Xe-O RY* Xe	3.48	π→σ*
	BD C-C	BD* C-F	0.98	π→π*
	LP Xe	BD* C-C	*0.27*	n→σ*
	LP O		*0.21*	n→π*
148	LP O	BD*C-C	0.93	n→π*
	BD C-C	BD* Xe-O	0.15	π→σ*
149	LP F	BD* C-C	1.40	n→π*
	BD C-C	RY* Xe	1.16	π→π*
150	LP F	BD* C-C	0.48	n→π*
151	BD C-C	RY* Xe	1.97	π→π*
	LP F	BD* C-C	0.89	n→π*
152	LP F	BD* C-C	0.48	n→π*
153	BD C-C	RY* Xe	1.23	π→π*
	LP F	BD* C-C	1.08	n→π*
154	LP F	BD* C-C	0.51	n→π*

[a]BD, BD* and LP, RY* stand for bonding, anti-bonding, lone pair and Rydberg orbital, respectively.

4.4.4.4. SAPT analysis

In Table 18 we summarize the DF-DFT-SAPT energy values relative to some representative lone pair and aerogen-π complexes. The total SAPT interaction energies for these complexes are similar to those obtained using the RI-MP2/aug-cc-pVTZ level of theory (see Table 16) giving reliability to the partition method. The energetic contributions (Table 18) indicate that aerogen-π complex **143** ($XeO_3\cdots C_6H_6$) is dominated by the electrostatic term in agreement with the MEP analysis. However the contributions of induction and dispersion terms are also important. In the lp-π complex **152** ($XeF_4\cdots C_6F_6$) the electrostatic and dispersion terms are the most important contributions to the total interaction energy. Finally, among the complexes involving the trifluorobenzene ring, (**147**, **148**, **153** and **154**) although both the electrostatic and induction terms are important, in the aerogen-π complexes (**147**, **151** and **153**) the dispersion component plays a key role in the overall stabilization of the complexes, being the most remarkable contributor. This is not observed for the lone pair-π complexes **148**, **152** and **154**, likely due to the higher polarizability of the interacting atom (xenon) in complexes **147**, **151** and **153**.

Table 18. SAPT interaction energies and their partitioning into the electrostatic, induction, dispersion and exchange contributions (E_{total}, E_{ee}, E_{ex}, E_{ind}, E_{disp}, respectively, kcal/mol) at the RI-DFT/aug-cc-pVTZ level of theory using the DF-DFT-SAPT approach.

Compound	E_{ee}	E_{ex}	E_{ind}	E_{disp}	E_{total}
143	−15.6	25.7	−8.7	−10.2	−8.8
147	−8.6	20.2	−6.7	−9.2	−4.3
148	−3.7	9.1	−0.3	−7.0	−1.9
151	−5.1	17.0	−3.9	−10.1	−2.1
152	−3.0	6.9	−0.2	−5.0	−1.2
153	−7.6	17.7	−3.9	−9.8	−3.6
154	−2.2	6.2	−0.1	−4.7	−0.7

4.4.4.5. AIM analysis

We have also used the Bader's theory of "Atoms in molecules" to characterize the lone pair-π and aerogen-π interactions described above by selecting some representative complexes, which are shown in Figure 101. It can be observed that XeO_3 complexes **143** and **146** are characterized by the presence of three bond and three ring critical points (CPs) symmetrically distributed. In the aerogen-π complex **143** the bond CPs connect the xenon atom to three carbon atoms of the ring. In the lp-π complex **146** the bond CPs connect the oxygen atoms to three carbon atoms of the ring moiety In both complexes, the interactions are further characterized by the presence of a cage critical point as is frequent in ion-π and lp-π interactions.[9a,31a]

In the lp-π complex **152** (XeF_4 series) the interaction is characterized by the presence of two bond and two ring CPs symmetrically distributed. The bond CPs connect the fluorine atoms to two carbon atoms of the ring. The aerogen-π complex **153** is characterized by the presence of three bond and three ring critical points (CPs) symmetrically distributed. Very remarkably, the bond CPs connect the Xe

atom to three carbon atoms of the ring. This results unambiguously confirms the aerogen-π nature of the interaction, since the F atoms are not involved in the distribution of CPs and bond paths. Finally, both complexes **152** and **153** are also characterized by the presence of a cage CP (see Figure 101). The value of the Laplacian in all cases is positive, as is common in closed shell calculations.

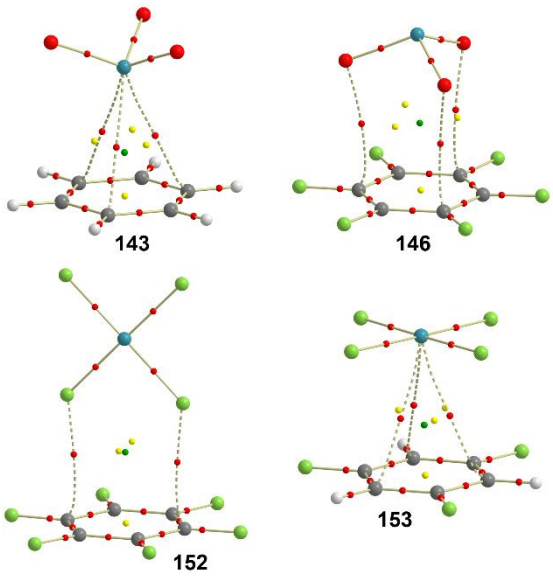

Figure 101. Distribution of critical points and bond paths in complexes **143**, **146**, **152** and **153**. Bond, ring and cage critical points are represented by red, yellow and green spheres, respectively. The bond paths connecting bond critical points are also represented.

4.4.5. Conclusions

The noncovalent complexes between several aromatic rings and two xenon derivatives have been studied using high level *ab initio* calculations and two different binding modes for each combination have been obtained, which are defined as lone pair-π and aerogen-π interactions. Among the π-systems considered the aerogen-π interaction established between the XeO_3 derivative and the benzene ring achieves the largest binding energy value. On the other hand, the lone pair-π interaction is the strongest one in case of the hexafluorobenzene moiety. Moreover, in case of trifluorobenzene where electrostatic effects are negligible, the aerogen-π interaction is more favorable than the lp-π due to the major contribution of the polarization and dispersion terms, as shown in the SAPT analysis. In addition, the NBO analysis showed that orbitals effects are remarkable contributors to the global stabilization of the aerogen-π complexes studied herein. Unexpectedly, in the aerogen-π complexes involving XeO_3 moiety, a weak back-bonding donation from, the inert lone pair of xenon atom to the antibonding orbitals of the aromatic ring was observed. Finally, the Bader's theory of "Atoms in molecules" has been successfully used to characterize both π-interactions discussed herein.

4.4.6. Acknowledgements

We thank the DGICYT of Spain (projects CTQ2014-57393-C2-1-P and CONSOLIDER INGENIO 2010 CSD2010-00065, FEDER funds).

Chapter 5

General conclusions

The research work included in this thesis was focused to the understanding and rationalization of the σ- and π-hole interactions involving tetrel, pnicogen and aerogen bearing compounds. The studies of their physical nature and stability properties are valuable contributions and might be used as a starting point for the preparation of new supramolecular architectures or artificial host-guest systems based on this group of interactions. Another interesting aspect derived from our investigation are the directionality studies performed on both tetrel and pnicogen bonding interactions, which certainly will improve the search criteria in the CSD and PDB databases in order to find relevant examples regarding both interactions. Finally, we have shown the importance of these interactions in fields such as solid state chemistry, atmospheric chemistry and biological systems, which are also key aspects of this PhD thesis.

The main conclusions are listed below:

- Tetrel bonding interactions are energetically favorable and comparable in strength with other "well-known" supramolecular bonds, such as halogen and hydrogen bonding interactions.

- Tetrel bonds are directional, as revealed in the *ab initio*/CSD study. Particularly, when the Tetrel atom is a carbon the interaction is known as carbon bonding, which present similar strength than CH-π interactions.

- Tetrel bonding interactions play an important role in fiels such as CFC chemistry and biological systems, being of great importance in the understanding of new stabilization modes between CFC gases and other atmospheric molecules, such as CO_2 and CO and also in the stabilization of protein-ligand complexes involving HEME group.

- Pnicogen bonding involving the π-hole present in the nitrogen atom of the -NO_2 group have revealed to be highly directional. In addition, the Lewis acid character of the NO_3^- anion has been studied using an exhaustive analysis of the CSD and PDB databases. If the nitrate anion is surrounded by the appropiate chemical context, the charge dumping process reveals a π-hole on the tip of the nitrogen atom, leading to favorable interaction energy values.

- Pnicogen bonds between sp^3 pnicogen derivatives and aromatic rings have been found to be attractive and described as a donor-acceptor interaction favored by an electron-rich π-system that plays the electron donor role. Furthermore, several examples extracted from the PDB database have been analysed, remarking the importance of this interaction in the mechanism of action of drugs used in the treatment of Leishmaniasis disease.

- Aerogen bonding interactions have been proposed as a new σ-hole supramolecular bond, being of great importance in the field of solid state chemistry, particularly in the preparation of Xe(VI) and Xe(IV) derivatives. In addition, a studied performed on Xe(IV) compounds revealed their ability to behave as π-hole bond donors. For both σ- and π-hole interactions several examples have been found in the CSD, giving support to the results retrieved from the calculations.

- The ability of both XeO_3 and XeF_4 moieties to interact with aromatic systems of different electronic nature has been shown, highlighting their dual behaviour as either lp-donor or σ-/π-hole donor.

Chapter 6

Bibliography

[1] H. J. Schneider, *Angew. Chem. Int. Ed.* **2009**, *48*, 3924–3977.

[2] a) J. M. Lehn, *Supramolecular Chemistry Concepts and Perspectives*, Wiley-VCH, Weinheim, **1995**; b) A. S. Mahadevi, G. N. Sastry, *Chem. Rev.* **2016**, *116*, 2775–2825.

[3] P. Murrayrust, W. D. S. Motherwell, *J. Am. Chem. Soc.* **1979**, *101*, 4374–4376.

[4] a) P. Metrangolo, H. Neukirch, T. Pilati, G. Resnati, *Acc. Chem. Res.* **2005**, *38*, 386–395; b) P. Politzer, J. S. Murray, *ChemPhysChem* **2013**, *14*, 278–294; c) P. Politzer, J. S. Murray, T. Clark, *Phys. Chem. Chem. Phys.* **2013**, *15*, 11178–11189; d) L. P. Wolters, P. Schyman, M. J. Pavan, W. L. Jorgensen, F. M. Bickelhaupt, S. Kozuch, *WIREs Comp. Mol. Sci.* **2014**, *4*, 523–540; e) K. El Hage, V. Pandyarajan, N. B. Phillips, B. J. Smith, J. G. Menting, J. Whittaker, M. C. Lawrence, M. Meuwly, M. A. Weiss, *J. Biol. Chem*. **2016**, *291*, 27023–27041; f) P. Politzer, J. S. Murray, T. Clark, *Top. Curr. Chem.*, **2015**, *358*, 19–42.

[5] a) P. Politzer, J. S. Murray, T. Clark, *Phys. Chem. Chem. Phys.* **2010**, *12*, 7748–7757; b) K. E. Riley, J. S. Murray, J. Franfrlík, J. Rezáč, R. J. Solá, M. C. Concha, F. M. Ramos, P. Politzer, *J. Mol. Model.* **2011**, *17*, 3309–3318; c) B. V. Pandiyan, P. Deepa, P. Kolandaivel, *Mol. Phys.* **2016**, *114*, 3629–3642.

[6] a) J. S. Murray, P. Lane, T. Clark, P. Politzer, *J. Mol. Model.* **2007**, *13*, 1033–1038; b) J. S. Murray, P. Lane, P. Politzer, *Int. J. Quantum Chem.* **2007**, *107*, 2286–2292; c) J. S. Murray, P. Lane, P. Politzer, *J. Mol. Model.* **2009**, *15*, 723–729.

[7] a) S. C. Nyburg, C. H. Faerman, *Acta Crystallogr. B* **1985**, *41*, 274–279; b) P. Politzer, K. E. Riley, F. A. Bulat, J. S. Murray, *Comp. Theor. Chem.* **2012**, *998*, 2–8; c) T. N. G. Row, R. Parthasarathy, *J. Am. Chem. Soc.* **1981**, *103*, 477–479; d) N. Ramasubbu, R. Parthasarathy, *Phosphorus Sulfur* **1987**, *31*, 221–229.

[8] a) M. Egli, S. Sarkhel, *Acc. Chem. Res.* **2007**, *40*, 197–205; b) T. J. Mooibroek, P. Gamez, J. Reedijk, *CrystEngComm* **2008**, *10*, 1501–1515.

[9] a) A. Frontera, P. Gamez, M. Mascal, T. J. Mooibroek, J. Reedijk, *Angew. Chem. Int. Ed.* **2011**, *50*, 9564–9583; b) B. L. Schottel, H. T. Chifotides, K. R. Dunbar, *Chem. Soc. Rev.* **2008**, *37*, 68–83; c) C. Caltagirone, P. A. Gale, *Chem. Soc. Rev.* **2009**, *38*, 520–563.

[10] a) P. Gamez, T. J. Mooibroek, S. J. Teat, J. Reedijk, *Acc. Chem. Res.* **2007**, *40*, 435–444; b) B. P. Hay, V. S. Bryantsev, *Chem. Commun.* **2008**, *44*, 2417–2428.

[11] a) D. Quiñonero, C. Garau, C. Rotger, A. Frontera, P. Ballester, A. Costa, P. M. Deyà, *Angew. Chem. Int. Ed.* **2002**, *41*, 3389–3392; b) M. Mascal, A. Armstrong, M. D. Bartberger, *J. Am. Chem. Soc.* **2002**, *124*, 6274–6276; c) I. Alkorta, I. Rozas, J. Elguero, *J. Am. Chem. Soc.* **2002**, *124*, 8593–8598; d) D. Y. Kim, N. J. Singh, K. S. Kim, *J. Chem. Theory Comput.* **2008**, *4*, 1401–1407.

[12] a) B. L. Schottel, J. Bacsa, K. R. Dunbar, *Chem. Commun.* **2005**, *41*, 46–47; b) B. Han, J. Lu, J. K. Kochi, *Cryst. Growth Des.* **2008**, *8*, 1327–1334; c) M. Mascal, I. Yakovlev, E. B. Nikitin, J. C. Fettinger, *Angew. Chem. Int. Ed.* **2007**, *46*, 8782–8784; d) R. J. Götz, A. Robertazzi, I. Mutikainen, U. Turpeinen, P. Gamez, J. Reedijk, *Chem. Commun.* **2008**, *44*, 3384–3386; e) M. Albrecht, M. Müller, O. Mergel, K. Rissanen, A. Valkonen, *Chem. Eur. J.* **2010**, *16*, 5062–5069.

[13] a) C. Estarellas, A. Frontera, D. Quiñonero, P. M. Deyà, *Angew. Chem. Int. Ed.* **2011**, *50*, 415–418; b) S. Chakravarty, Z.-Z. Sheng, B. Iverson, B. Moore, *FEBS Lett.* **2012**, *586*, 4180–4185; c) D. D. Jenkins, J. B. Harris, E. E. Howell, R. J. Hinde, J. Baudry, *J. Comput. Chem.* **2013**, *34*, 518–522.

[14] a) R. E. Dawson, A. Hennig, D. P. Weimann, D. Emery, V. Ravikumar, J. Montenegro, T. Takeuchi, S. Gabutti, M. Mayor, J. Mareda, C. A. Schalley, S. Matile, *Nat. Chem.* **2010**, *2*, 533–538; b) N. Sakai, J. Mareda, E. Vauthey, S. Matile, *Chem. Commun.* **2010**, *46*, 4225–4237.

[15] a) H. B. Burgi, *Inorg. Chem.* **1973**, *12*, 2321–2325; b) H. B. Burgi, J. D. Dunitz, E. Shefter, *J. Am. Chem. Soc.* **1973**, *95*, 5065–5067; c) H. B. Burgi, J. D. Dunitz, J. M. Lehn, G. Wipff, *Tetrahedron* **1974**, *30*, 1563–1572.

[16] M. Egli, R. V. Gessner, *P. Natl. Acad. Sci. USA* **1995**, *92*, 180–184.
[17] P. Sjoberg, P. Politzer, *J. Phys. Chem.* **1990**, *94*, 3959–3961.

[18] a) L. M. Azofra, I. Alkorta, S. Scheiner, *Theor. Chem. Acc.* **2014**, *133*, 1586, 8p; b) M. D. Esrafili, R. Nurazar, *Mol. Phys.* **2016**, *114*, 276–282; c) X. Guo, Y. -W. Liu, Q. -Z. Li, W. -Z. Li, J. -B. Cheng, *Chem. Phys. Lett*. **2015**, *620*, 7–12; d) D. Quiñonero, *Molecules* **2015**, *20*, 11632–11659.

[19] a) A. Bauzá, R. Ramis, A. Frontera, *J. Phys. Chem. A.* **2014**, *118*, 2827–2834; b) D. Quiñonero, A. Bauzá, G. Sánchez-Sanz, C. Trujillo, I. Alkorta, J. Elguero, *New. J. Chem.* **2016**, *40*, 9060–9072.

[20] a) G. Sánchez-Sanz, C. Trujillo, M. Solimannejad, I. Alkorta, J. Elguero, *Phys. Chem. Chem. Phys.* **2013**, *15*, 14310–14318; b) J. E. Del Bene, I. Alkorta, J. Elguero, *J. Phys. Chem. A.* **2013**, *117*, 6893–6903.

[21] a) S. L. Grabowski, *Molecules* **2015**, *20*, 11297–11316; b) S. L. Grabowski, *ChemPhysChem* **2015**, *16*, 1470–1479; c) S. L. Grabowski, *ChemPhysChem*, **2014**, *15*, 2985–2993.

[22] M.-X. Liu, H.-Y. Zhuo, Q.-Z. Li, C. Wen-Zuo, J.-B. Cheng, *J. Mol. Model.* **2016**, *22*, 1–7.

[23] S. Yourdkhani, T. Korona, N. L. Hadipour, J. *Comp. Chem.* **2015**, *36*, 2412–2428.

[24] a) T. Clark, M. Hennemann, J. S. Murray, P. Politzer, *J. Mol. Model.* **2007**, *13*, 291–296; b) T. Brinck, J. S. Murray, P. Politzer, *Int. J. Quantum Chem.* **1992**, *44*, 55–64; c) P. Auffinger, F. A. Hays, E. Westhof, P. S. Ho, *P. Natl. Acad. Sci. USA* **2004**, *101*, 16789–16794; d) P. Politzer, P. Lane, M. C. Concha, Y. Ma, J. S. Murray, *J. Mol. Model.* **2007**, *13*, 305–311.

[25] a) P. Politzer, J. S. Murray, *Practical Aspects of Computational Chemistry*, Springer, Heidelberg, **2009**; b) J. S. Murray, K. E. Riley, P. Politzer, T. Clark, *Aust. J. Chem.* **2010**, *63*, 1598–1607.

[26] a) E. Arunan, G. R. Desiraju, R. A. Klein, J. Sadlej, S. Scheiner, I. Alkorta, D. C. Clary, R. H. Crabtree, J. J. Dannenberg, P. Hobza, H. G. Kjaergaard, A. C. Legon, B. Mennucci, D. J. Nesbitt, *Pure Appl. Chem.* **2011**, *83*, 1637–1641; b) G. R. Desiraju, P. S. Ho, L. Kloo, A. C. Legon, R. Marquardt, P. Metrangolo, P. Politzer, G. Resnati, K. Rissanen, *Pure Appl. Chem.* **2013**, *85*, 1711–1713.

[27] J. S. Murray, P. Lane, T. Clark, K. E. Riley, P. Politzer, *J. Mol. Model.* **2012**, *18*, 541–548.

[28] A. J. Stone, *J. Am. Chem. Soc.* **2013**, *135*, 7005–7009.

[29] A. Bauzá, I. Alkorta, A. Frontera, J. Elguero, *J. Chem. Theory Comput.* **2013**, *9*, 5201–5210.

[30] A. Bondi, *J. Phys. Chem.* **1964**, *68*, 441–451.

[31] a) A. Frontera, D. Quiñonero, P. M. Deyà, *WIREs Comput. Mol. Sci.* **2011**, *1*, 440–459; b) A. Frontera, *Coord. Chem. Rev.* **2013**, *257*, 1716–1727; c) J. J. Fiol, M. Barceló-Oliver, A. Tasada, A. Frontera, À. Terrón, Á. García-Raso, *Coord. Chem. Rev.* **2013**, *257*, 2705–2715.

[32] a) D. Kim, P. Tarakeshwar, K. S. Kim, *J. Phys. Chem. A.* **2004**, *108*, 1250–1258; b) D. Y. Kim, N. J. Singh, J. W. Lee, K. S. Kim, *J. Chem. Theory Comput.* **2008**, *4*, 1162–1169.

[33] a) C. Garau, A. Frontera, D. Quiñonero, P. Ballester, A. Costa, P. M. Deyà, *ChemPhysChem* **2003**, *4*, 1344–1348; b) D. Quiñonero, C. Garau, A. Frontera, P. Ballester, A. Costa, P. M. Deyà, *Chem. Phys. Lett.* **2002**, *359*, 486–492; c) A. Bauzá, P. M. Deyà, A. Frontera, D. Quiñonero, *Phys. Chem. Chem. Phys.* **2014**, *16*, 1322–1326.

[34] S. E. Wheeler, K. N. Houk, *J. Phys. Chem. A.* **2010**, *114*, 8658–8664.

[35] S. E. Wheeler, J. W. G. Bloom, *Chem. Commun.* **2014**, *50*, 11118–11121.

[36] a) C. Garau, D. Quiñonero, A. Frontera, P. Ballester, A. Costa, P. M. Deyà, *Org. Lett.* **2003**, *5*, 2227–2229; b) C. Garau, A. Frontera, D. Quiñonero, P. Ballester, A. Costa, P. M. Deyà, *J. Phys. Chem. A.* **2004**, *108*, 9423–9427.

[37] a) C. Garau, D. Quiñonero, A. Frontera, P. Ballester, A. Costa, P. M. Deyà, *New J. Chem.* **2003**, *27*, 211–214; b) D. Quiñonero, A. Frontera, C. Garau, P. Ballester, A. Costa, P. M. Deyà, *ChemPhysChem* **2006**, *7*, 2487–2491.

[38] a) O. Dumele, B. Schreib, U. Warzok, N. Trapp, C. A. Schalley, F. Diederich, *Angew. Chem. Int. Ed.* **2017**, *56*, 1152–1157; b) F. Pan, N. K. Beyeh, R. H. A. Ras, K. Rissanen, *Cryst. Growth & Des*. **2016**, *16*, 6729–6733; c) S. T. Nguyen, A. L. Rheingold, G. S. Tschumper, D. L. Watkins, Cryst. *Growth & Des.* **2016**, *16*, 6648–6653; d) F. Fernández-Palacio, M. Poutanen, M. Saccone, A. Siiskonen, G. Terraneo, G. Resnati, O. Ikkala, P. Metrangolo, A. Priimagi, *Chem. Mater.* **2016**, *28*, 8314–8321; e) G. Kawaguchi, M. Maesato, T. Komatsu, T. Imakubo, A. Kiswandhi, D. Graf, H. Kitagawa, *Chem. Mater.* **2016**, *28*, 7276–7286; f) P. S. Salini, K. Shinaj, M. Hariharan, Cryst. *Growth & Des.* **2016**, *16*, 5822–5830.

[39] A. Crihfield, J. Hartwell, D. Phelps, R. B. Walsh, J. L. Harris, J. F. Payne, W. T. Pennington, T. W. Hanks, *Cryst. Growth Des.* **2003**, *3*, 313–320.

[40] T. Shirman, J. F. Lamere, L. J. W. Shimon, T. Gupta, J. M. L. Martin, M. E. Van Der Boom, *Cryst. Growth Des.* **2008**, *8*, 3066–3072.

[41] a) R. Gajda, A. Katrusiak, *Acta Crystallogr. B* **2007**, *63*, 896–902; b) C. B. Aakeroy, J. Desper, B. A. Helfrich, P. Metrangolo, T. Pilati, G. Resnati, A. Stevenazzi, *Chem. Commun.* **2007**, *43*, 4236–4238; c) A. K. Przybył, M. J. Kubicki, *Chem. Crystallogr.* **2012**, *42*, 685–690.

[42] T. A. Logothetis, F. Meyer, P. Metrangolo, T. Pilati, G. Resnati, *New J. Chem.* **2004**, *28*, 760–763.

[43] A. C. B. Lucassen, T. Zubkov, L. J. W. Shimon, M. E. Van Der Boom, *CrystEngComm* **2007**, *9*, 538–540.

[44] L. C. Gilday, S. W. Robinson, T. A. Barendt, M. J. Langton, B. R. Mullaney, P. D. Beer, *Chem. Rev.* **2015**, *115*, 7118–7195.

[45] E. Bosch, C. L. Barnes, *Cryst. Growth Des.* **2002**, *2*, 299–302.

[46] S. Samai, K. Biradha, *CrystEngComm* **2009**, *11*, 482–492.

[47] M. J. Bojdys, M. E. Briggs, J. T. A. Jones, D. J. Adams, S. Y. Chong, M. Schmidtmann, A. I. Cooper, *J. Am. Chem. Soc.* **2011**, *133*, 16566–16571.

[48] C. B. Aakeroy, A. Rajbanshi, P. Metrangolo, G. Resnati, M. F. Parisi, J. Desper, T. Pilati, *CrystEngComm* **2012**, *14*, 6366–6368.

[49] X. Pang, H. Wang, X. R. Zhao, W. J. Jin, *Dalton Trans.* **2013**, *42*, 8788–8795.

[50] a) S. Muniappan, S. Lipstman, I. Goldberg, *Chem. Commun.* **2008**, *44*, 1777–1779; b) H. M. Titi, R. Patra, I. Goldberg, *Chem. Eur. J.* **2013**, *19*, 14941–14949.

[51] a) K. Raatikainen, J. Huuskonen, M. Lahtinen, P. Metrangolo, K. Rissanen, *Chem. Commun.* **2009**, *45*, 2160–2162; b) K. Raatikainen, K. Rissanen, *Cryst. Growth Des.* **2010**, *10*, 3638–3646; c) K. Raatikainen, K. Rissanen, *CrystEngComm* **2011**, *13*, 6972–6977.

[52] K. Raatikainen, K. Rissanen, *Chem. Sci.* **2012**, *3*, 1235–1239.

[53] P. Metrangolo, F. Meyer, T. Pilati, D. M. Proserpio, G. Resnati, *Cryst. Growth Des.* **2008**, *8*, 654–659.

[54] N. Houbenov, R. Milani, M. Poutanen, J. Haataja, V. Dichiarante, J. Sainio, J. Ruokolainen, G. Resnati, P. Metrangolo, O. Ikkala, *Nat. Commun.* **2014**, *5*, 4043.

[55] a) D. M. Himmel, K. Das, A. D. Clark, S. H. Hughes, A. Benjahad, S. Oumouch, J. Guillemont, S. Coupa, A. Poncelet, I. Csoka, C. Meyer, K. Andries, C. H. Nguyen, D. S. Grierson, E. J. Arnold, *J. Med. Chem.* **2005**, *48*, 7582–7591; b) A. Benjahad, J. Guillemont, K. Andries, C. H. Nguyen, D. S. Grierson, *Bioorg. Med. Chem. Lett.* **2003**, *13*, 4309–4312.

[56] M. Llinàs-Brunet, M. D. Bailey, N. Goudreau, P. K. Bhardwaj, J. Bordeleau, M. Bös, Y. Bousquet, M. G. Cordingley, J. Duan, P. Forgione, M. Garneau, E. Ghiro, V. Gorys, S. Goulet, T. Halmos, S. H. Kawai, J. Naud, M. -A. Poupart, P. W. J. White, *J. Med. Chem.* **2010**, *53*, 6466–6476.

[57] R. D. Carpenter, A. Natarajan, E. Y. Lau, M. Andrei, D. M. Solano, F. C. Lightstone, S. J. DeNardo, K. S. Lam, M. J. Kurth, *Cancer Res.* **2010**, *70*, 5448–5456.

[58] B. L. Grasberger, T. Lu, C. Schubert, D. J. Parks, T. E. Carver, H. K. Koblish, M. D. Cummings, L. V. LaFrance, K. L. Milkiewicz, R. R. Calvo, D. Maguire, J. Lattanze, C. F. Franks, S. Zhao, K. Ramachandren, G. R. Bylebyl, M. Zhang, C. L. Manthey, E. C. Petrella, M. W. Pantoliano, I. C. Deckman, J. C. Spurlino, A. C. Maroney, B. E. Tomczuk, C. J. Molloy, R. F. Bone, *J. Med. Chem.* **2005**, *48*, 909–912.

[59] D. J. Parks, L. V. LaFrance, R. R. Calvo, K. L. Milkiewicz, V. Gupta, J. Lattanze, K. Ramachandren, T. E. Carver, E. C. Petrella, M. D. Cummings, D. Maguire, B. L. Grasberger, T. Lu, *Bioorg. Med. Chem. Lett.* **2005**, *15*, 765–770.

[60] Z. Xu, Z. Liu, T. Chen, T. Chen, Z. Wang, G. Tian, J. Shi, X. Wang, Y. Lu, X. Yan, G. Wang, H. Jiang, K. Chen, S. Wang, Y. Xu, J. Shen, W. Zhu, *J. Med. Chem.* **2011**, *54*, 5607–5611.

[61] J. Ren, Y. He, W. Chen, T. Chen, G. Wang, Z. Wang, Z. Xu, X. Luo, W. Zhu, H. Jiang, J. Shen, Y. Xu, *J. Med. Chem.* **2014**, *57*, 3588–3593.

[62] a) A. Bauzá, D. Quiñonero, P. M. Deyà, A. Frontera, *CrystEngComm* **2013**, *15*, 3137–3144; b) M. Iwaoka, N. Isozumi, *Molecules* **2012**, *17*, 7266–7283; c) G. Sánchez-Sanz, C. Trujillo, I. Alkorta, J. Elguero, *ChemPhysChem* **2012**, *13*, 496–503; d) P. Sanz, O. Mó, M. Yáñez, *Phys. Chem. Chem. Phys.* **2003**, *5*, 2942–2947; e) M. H. Esseffar, R. Herrero, E. Quintanilla, J. Z. Dávalos, P. Jiménez, J. -L. M. Abboud, M. Yáñez, O. Mó, *Chem. Eur. J.* **2007**, *13*, 1796–1803; f) M. Iwaoka, S. Takemoto, S. Tomoda, *J. Am. Chem. Soc.* **2002**, *124*, 10613–10620; g) L. M. Azofra, S. Scheiner, *J. Chem. Phys.* **2014**, *140*, 034302, 10p; h) J. Fanfrlík, A. Přáda, Z. Padělková, A. Pecina, J. Macháček, M. Lepšík, J. Holub, A. Růžička, D. Hnyk, P. Hobza, *Angew. Chem. Int. Ed.* **2014**, *53*, 10139–10142; i) U. Adhikari, S. Scheiner, *Chem. Phys. Lett.* **2012**, *532*, 31–35.

[63] V. Nziko, S. Scheiner, *J. Phys. Chem. A.* **2014**, *118*, 10849–10856.

[64] a) F. T. Burling, B. M. Goldstein, *J. Am. Chem. Soc.* **1992**, *114*, 2313–2320; b) Y. Nagao, T. Hirata, S. Goto, S. Sano, A. Kakehi, K. Iizuka, M. Shiro, *J. Am. Chem. Soc.* **1998**, *120*, 3104–3110; c) S. Wu, A. Greer, *J. Org. Chem.* **2000**, *65*, 4883–4887.

[65] a) J. C. Taylor, G. D. Markham, *J. Biol. Chem.* **1999**, *274*, 32909–32914; b) W. Brandt, A. Golbraikh, M. Tager, U. Lendeckel, *Eur. J. Biochem.* **1999**, *261*, 89–97.

[66] a) M. Iwaoka, S. Takemoto, M. Okada, S. Tomoda, *Chem. Lett.* **2001**, *30*, 132–133; b) M. Iwaoka, S. Takemoto, M. Okada, S. Tomoda, *Bull. Chem. Soc. Jpn.* **1977**, *99*, 4860–4862.

[67] R. E. Rosenfield, R. Parthasarathy, J. D. Dunitz, *J. Am. Chem. Soc.* **1977**, *99*, 4860–4862.

[68] A. Kucsman, I. Kapovits, 'Nonbonded Sulfur-Oxygen Interaction in Organic Sulfur Compounds', in: *Organic Sulfur Chemistry*, Elsevier, Amsterdam, **1985**, pp. 191–245.

[69] J. T. Goettel, P. Chaudhary, P. Hazendonk, H. P. A. Mercier, M. Gerken, *Chem. Commun.* **2012**, *48*, 9120–9122.

[70] S. Zahn, R. Frank, E. Hey-Hawkins, B. Kirchner, *Chem. Eur. J.* **2011**, *17*, 6034–6038.

[71] B. E. Rocher-Casterline, L. C. Ch'ng, A. K. Mollner, H. Reisler, *J. Chem. Phys.* **2011**, *134*, 211101, 4p.

[72] P. Batail, D. Grandjean, F. Dudragne, C. Michaud, *Acta Crystallogr. B* **1975**, *B34*, 1367–1372.

[73] a) P. Kilian, A. M. Z. Slawin, J. D. Woollins, *Chem. Eur. J.* **2003**, *9*, 215–222; b) M. R. Sundberg, R. Uggla, C. Viñas, F. Teixidor, S. Paavola, R. Kivekäs, *Inorg. Chem. Commun.* **2007**, *10*, 713–716; c) A. C. Marr, M. Nieuwenhuyzen, C. L. Pollock, G. C. Saunders, *Organometallics* **2007**, *26*, 2659–2671; d) C. Ganesamoorthy, M. S. Balakrishna, J. T. Mague, H. M. Tuononen, *Inorg. Chem.* **2008**, *47*, 7035–7047; e) S. Bauer, S. Tschirschwitz, P. Lönnecke, R. Frank, B. Kirchner, M. L. Clarke, E. Hey-Hawkins, *Eur. J. Inorg. Chem.* **2009**, *2009*, 2776–2788; f) M. Bühl, P. Kilian, J. D. Woollins, *ChemPhysChem* **2011**, *12*, 2405–2408.

[74] E. V. Avtomonov, K. Megges, S. Wocadlo, J. Lorberth, *J. Organomet. Chem.* **1996**, *524*, 253–261.

[75] a) S. B. Bushuk, F. H. Carré, D. M. H. Guy, W. E. Douglas, Y. A. Kalvinkovskya, L. G. Klapshina, A. N. Rubinov, A. P. Stupak, B. A. Bushuk, *Polyhedron* **2004**, *23*, 2615–2623; b) S. Tschirschwitz, P. Lönnecke, E. Hey-Hawkins, *Dalton Trans.* **2007**, *37*, 1377–1382.

[76] G. Müller, J. Brand, S. E. Jetter, F. Chemie, U. Konstanz, D. Konstanz, *Z. Naturforsch.* **2001**, *56b*, 1163–1171.

[77] S. Scheiner, *Chem. Phys.* **2011**, *387*, 79–84.

[78] M. M. Watt, M. S. Collins, D. W. Johnson, *Acc. Chem. Res.* **2013**, *46*, 955–966.

[79] a) W. J. Vickaryous, R. Herges, D. W. Johnson, *Angew. Chem. Int. Ed.* **2004**, *43*, 5831–5833; b) W. J. Vickaryous, E. R. Healey, O. B. Berryman, D. W. Johnson, *Inorg. Chem.* **2005**, *44*, 9247–9252; c) V. M. Cangelosi, A. C. Sather, L. N. Zakharov, O. B. Berryman, D. W. Johnson, *Inorg. Chem.* **2007**, *46*, 9278–9284; d) V. M. Cangelosi, L. N. Zakharov, S. A. Fontenot, M. A. Pitt, D. W. Johnson, *Dalton Trans.* **2008**, *37*, 3447–3453; e) V. M. Cangelosi, L. N. Zakharov, J. L. Crossland, B. C. Franklin, D. W. Johnson, *Cryst. Growth Des.* **2010**, *10*, 1471–1473; f) N. R. Lindquist, T. G. Carter, V. M. Cangelosi, L. N. Zakharov, D. W. Johnson, *Chem. Commun.* **2010**, *46*, 3505–3507; g) M. A. Pitt, L. N. Zakharov, K. Vanka, W. H. Thompson, B. B. Laird, D. W. Johnson, *Chem. Commun.* **2008**, *44*, 3936–3938; h) V. M. Cangelosi, M. A. Pitt, W. J. Vickaryous, C. A. Allen, L. N. Zakharov, D. W. Johnson, *Cryst. Growth Des.* **2010**, *10*, 3531–3536; i) W. J. Vickaryous, L. N. Zakharov, D. W. Johnson, *Main Group Chem.* **2006**, *5*, 51–59; j) V. M. Cangelosi, L. N. Zakharov, D. W. Johnson, *Angew. Chem. Int. Ed.* **2010**, *49*, 1248–1251; k) V. M. Cangelosi, T. G. Carter, J. L. Crossland, L. N. Zakharov, D. W. Johnson, *Inorg. Chem.* **2010**, *49*, 9985–9992; l) S. A. Fontenot, V. M. Cangelosi, M. A. W. Pitt, A. C. Sather, L. N. Zakharov, O. B. Berryman, D. W. Johnson, *Dalton Trans.* **2011**, *40*, 12125–12131.

[80] a) W. Frank, J. Schneider, S. Müller-Becker, *J. Chem. Soc. Chem. Commun.* **1993**, 799–800; b) D. Mootz, V. Händler, *Z. Anorg. Allg. Chem.* **1986**, *533*, 23–29.

[81] H. Zhu, P. Smith, L. K. Wang, S. Shuman, *Virology* **2007**, *366*, 126–136.

[82] P. Baiocco, G. Colotti, S. Franceschini, A. Ilari, *J. Med. Chem.* **2009**, *52*, 2603–2612.

[83] L. G. Goodwin, J. E. Page, *Biochem. J.* **1943**, *37*, 198–209.

[84] G. Sánchez-Sanz, C. Trujillo, I. Alkorta, J. Elguero, *Phys. Chem. Chem. Phys.* **2014**, *16*, 15900–15909.

[85] A. Bundhun, P. Ramasami, J. S. Murray, P. Politzer, *J. Mol. Model.* **2013**, *19*, 2739–2746.

[86] a) S. J. Grabowski, *Phys. Chem. Chem. Phys.* **2014**, *16*, 1824–1834; b) A. Bauzá, T. J. Mooibroek, A. Frontera, *Chem. Eur. J.* **2014**, *20*, 10245–10248; c) A. Bauzá, R. Ramis, A. Frontera, *Comp. Theor. Chem.* **2014**, *1038*, 67–70.

[87] I. Alkorta, I. Rozas, J. Elguero, *J. Phys. Chem. A* **2001**, *105*, 743–749.

[88] I. Alkorta, *J. Organomet. Chem.* **2001**, *625*, 148–153.

[89] a) C. J. Levy, R. J. Puddephatt, *J. Am. Chem. Soc.* **1997**, *119*, 10127–10136; b) J. Langer, S. Matejcik, E. Illenberger, *Phys. Chem. Chem. Phys.* **2000**, *2*, 1001–1005; c) J. Mikosch, S. Trippel, C. Eichhorn, R. Otto, U. Lourderaj, J. X. Zhang, W. L. Hase, M. Weidemüller, R. Wester, *Science* **2008**, *319*, 183–186; d) M. Sohail, R. Panisch, A. Bowden, A. R. Bassindale, P. G. Taylor, A. A. Korlyukov, D. E. Arkhipov, L. Male, S. Callear, S. J. Coles, M. B. Hursthouse, R. W. Harrington, W. Clegg, *Dalton Trans.* **2013**, *42*, 10971–10981.

[90] D. Mani, E. Arunan, *Phys. Chem. Chem. Phys.* **2013**, *15*, 14377–14383.

[91] S. P. Thomas, M. S. Pavan, T. N. Guru Row, *Chem. Commun.* **2014**, *50*, 49–51.

[92] Q. Li, X. Guo, X. Yang, W. Li, J. Cheng, H.-B. Li, *Phys. Chem. Chem. Phys.* **2014**, *16*, 11617–11625.

[93] a) X. Dai, D. L. Schulz, C. W. Braun, A. Ugrinov, P. Boudjouk, *Organometallics* **2010**, *29*, 2203–2205; b) X. Dai, S.-B. Choi, C. W. Braun, P. Vaidya, S. Kilina, A. Ugrinov, D. L. Schulz, P. Boudjouk, *Inorg. Chem.* **2011**, *50*, 4047–4053.

[94] J. Tillmann, F. Meyer-Wegner, A. Nadj, J. Becker-Baldus, T. Sinke, M. Bolte, M. C. Holthausen, M. Wagner, H.-W. Lerner, *Inorg. Chem.* **2012**, *51*, 8599–8606.

[95] P. G. Taylor, A. R. Bassindale, Y. El Aziz, M. Pourny, R. Stevenson, M. B. Hursthouse, S. J. Coles, *Dalton Trans.* **2012**, *41*, 2048–2059.

[96] A. R. Bassindale, M. Pourny, P. G. Taylor, M. B. Hursthouse, M. E. Light, *Angew. Chem. Int. Ed.* **2003**, *42*, 3488–3490.

[97] a) G. van de Goor, C. C. Freyhardt, P. Behrens, *Z. Anorg. Allg. Chem.* **1995**, *621*, 311–322; b) P. Caullet, J. L. Guth, J. Hazm, J. M. Lamblin, H. Gies, *Eur. J. Sol. State Inorg.* **1991**, *28*, 345–361.

[98] L. A. Villaescusa, P. Lightfoot, R. E. Morris, *Chem. Commun.* **2002**, *38*, 2220–2221.

[99] X. Yang, *Mater Res. Bul.* **2006**, *41*, 54–66.

[100] a) S. C. A. H. Pierrefixe, S. J. M. van Stralen, J. N. P. van Stralen, C. Fonseca Guerra, F. M. Bickelhaupt, *Angew. Chem. Int. Ed.* **2009**, *48*, 6469–6471; b) S. C. A. H. Pierrefixe, J. Poater, C. Im, F. M. Bickelhaupt, *Chem. Eur. J.* **2008**, *14*, 6901–6911.

[101] E. K. Lermontova, A. A. Selina, S. S. Karlov, A. V. Churakov, J. A. K. Howard, Y. F. Oprunenko, M. Y. Antipin, J. Sundermeyer, G. S. Zaitseva, *J. Organomet. Chem.* **2006**, *691*, 5710–5724.

[102] a) R. R. Holmes, *Chem. Rev.* **1996**, *96*, 927–950; b) G. P. Schiemenz, *Z. Anorg. Allg. Chem.* **2002**, *628*, 2597-2604; c) P. D. Prince, M. J. Bearpark, G. S. McGrady, J. W. Steed, *Dalton Trans.* **2008**, *37*, 271–282; d) P. Gualco, M. Mercy, S. Ladeira, Y. Coppel, L. Maron, A. Amgoune, D. Bourissou, *Chem. Eur. J.* **2010**, *16*, 10808–10817; e) D. Kost, I. Kalikhman, *Acc. Chem. Res.* **2009**, *42*, 303–314; f) W. Levason, G. Reid, W. Zhang, *Coord. Chem. Rev.* **2011**, *255*, 1319–1341.

[103] a) M. Yamashita, Y. Yamamoto, K.-Y. Akiba, D. Hashizume, F. Iwasaki, N. Takagi, S. Nagase, *J. Am. Chem. Soc.* **2005**, *127*, 4354–4371; b) K.-Y. Akiba, Y. Moriyama, M. Mizozoe, H. Inohara, T. Nishii, Y. Yamamoto, M. Minoura, D. Hashizume, F. Iwasaki, N. Takagi, K. Ishimura, S. Nagase, *J. Am. Chem. Soc.* **2005**, *127*, 5893–5901.

[104] a) A. Bauzá, T. J. Mooibroek, A. Frontera, *Phys. Chem. Chem. Phys.* **2014**, *16*, 19192–19197; b) F. H. Allen, *Acta Crystallogr. B* **2002**, *58*, 380–388.

[105] a) P. H. Maccallum, R. Poet, E. J. Milnerwhite, *J. Mol. Biol.* **1995**, *248*, 374–384; b) G. J. Bartlett, A. Choudhary, R. T. Raines, D. N. Woolfson, *Nat. Chem. Biol.* **2010**, *6*, 615–620; c) M. Harder, B. Kuhn, F. Diederich, *ChemMedChem* **2013**, *8*, 397–404.

[106] X. Guo, L. Cao, Q. Li, W. Li, J. Cheng, *J. Mol. Model.* **2014**, *20*, 2493–2498.

[107] M. Mitra, P. Manna, A. Bauzá, P. Ballester, S. K. Seth, S. Ray Choudhury, A. Frontera, S. Mukhopadhyay, *J. Phys. Chem. B* **2014**, *118*, 14713–14726.

[108] S. Khan, S. Chattopadhyay, A. A. Masum, M. M. Islam, M. G. B. Drew, A. Bauzá, A. Frontera, *Polyhedron* **2017**, *123*, 334–343.

[109] J. E. Del Bene, I. Alkorta, J. Elguero, *J. Phys. Chem. A* **2013**, *117*, 11592–11604.

[110] A. Hazari, L. K. Das, R. M. Kadam, A. Bauzá, A. Frontera, A. Ghosh, *Dalton Trans.* **2015**, *44*, 3862–3876.

[111] S. Sarkhel, A. Rich, M. Egli, *J. Am. Chem. Soc.* **2003**, *125*, 8998–8999.

[112] A. Jain, V. Ramanathan, R. Sankararamakrishnan, *Protein Sci.* **2009**, *18*, 595–605.

[113] T. J. Mooibroek, P. Gamez, *CrystEngComm* **2012**, *14*, 1027–1030.

[114] a) C. C. Forbes, A. M. Beatty, B. D. Smith, *Org. Lett.* **2001**, *3*, 3595–3598; b) B. W. Gung, X. Xue, H. J. Reich, *J. Org. Chem.* **2005**, *70*, 7232–7237; c) W. B. Motherwell, J. Moïse, A. E. Aliev, M. Nic, S. J. Coles, P. N. Horton, M. B. Hursthouse, G. Chessari, C. A. Hunter, J. G. Vinter, *Angew. Chem. Int. Ed.* **2007**, *46*, 7823–7826; d) B. W. Gung, Y. Zou, Z. Xu, J. C. Amicangelo, D. G. Irwin, S. Ma, H.-C. Zhou, *J. Org. Chem.* **2008**, *73*, 689–693; e) R. Annunziata, M. Benaglia, F. Cozzi, A. Mazzanti, *Chem. Eur. J.* **2009**, *15*, 4373–4381; f) T. Korenaga, T. Shoji, K. Onoue, T. Sakai, *Chem. Commun.* **2009**, *45*, 4678–4680; g) M. Benaglia, F. Cozzi, M. Mancinelli, A. Mazzanti, *Chem. Eur. J.* **2010**, *16*, 7456–7468.

[115] T. Korenaga, H. Tanaka, T. Ema, T. Sakai, *J. Fluorine Chem.* **2003**, *122*, 201–205.

[116] J. C. Amicangelo, D. G. Irwin, C. J. Lee, N. C. Romano, N. L. Saxton, *J. Phys. Chem. A* **2013**, *117*, 1336–1350.

[117] M. Giese, M. Albrecht, T. Krappitz, M. Peters, V. Gossen, G. Raabe, A. Valkonen, K. Rissanen, *Chem. Commun.* **2012**, *48*, 9983–9985.

[118] A. Bretschneider, D. M. Andrada, S. Dechert, S. Meyer, R. A. Mata, F. Meyer, *Chem. Eur. J.* **2013**, *19*, 16988–17000.

[119] D. X. Wang, M. X. Wang, *J. Am. Chem. Soc.* **2013**, *135*, 892–897.

[120] Q. He, Y. Han, Y. Wang, Z.-T. Huang, D.-X. Wang, *Chem. Eur. J.* **2014**, *20*, 7486–7491.

[121] S. T. Schneebeli, M. Frasconi, Z. Liu, Y. Wu, D. M. Gardner, N. L. Strutt, C. Cheng, R. Carmieli, M. R. Wasielewski, J. F. Stoddart, *Angew. Chem. Int. Ed.* **2013**, *52*, 13100–13104.

[122] H. T. Chifotides, I. D. Giles, K. R. Dunbar, *J. Am. Chem. Soc.* **2013**, *135*, 3039–3055.

[123] P. Ballester, *Acc. Chem. Res.* **2013**, *46*, 874–884.

[124] a) G. Gil-Ramírez, E. C. Escudero-Adán, J. Benet-Buchholz, P. Ballester, *Angew. Chem. Int. Ed.* **2008**, *47*, 4114–4118; b) L. Adriaenssens, G. Gil-Ramírez, A. Frontera, D. Quiñonero, E. C. Escudero-Adán, P. Ballester, *J. Am. Chem. Soc.* **2014**, *136*, 3208–3218.

[125] J. Sabek, L. Adriaenssens, T. Guinovart, E. J. Parra, F. X. Rius, P. Ballester, P. Blondeau, *Chem. Eur. J.* **2015**, *21*, 448–454.

[126] Y. Zhao, Y. Domoto, E. Orentas, C. Beuchat, D. Emery, J. Mareda, N. Sakai, S. Matile, *Angew. Chem. Int. Ed.* **2013**, *52*, 9940–9943.

[127] Y. Zhao, C. Beuchat, Y. Domoto, J. Gajewy, A. Wilson, J. Mareda, N. Sakai, S. Matile, *J. Am. Chem. Soc.* **2014**, *136*, 2101–2111.

[128] Y. Zhao, N. Sakai, S. Matile, *Nat. Commun.* **2014**, *5*, 3911, 5p.

[129] X. Lucas, A. Bauzá, A. Frontera, D. Quiñonero, *Chem. Sci.* **2016**, *7*, 1038–1050.

[130] C. Estarellas, A. Frontera, D. Quiñonero, P. M. Deyà, *Chem. Asian J.* **2011**, *6*, 2316–2318.

[131] A. Bauzá, D. Quiñonero, P. M. Deyà, A. Frontera, *Chem. Asian J.* **2013**, *8*, 2708–2713.

[132] A. Bauzá, D. Quiñonero, P. M. Deyà, A. Frontera, *Chem. Eur. J.* **2014**, *20*, 6985–6990.

[133] I. V. Krieger, J. S. Freundlich, V. B. Gawandi, J. P. Roberts, V. B. Gawandi, Q. Sun, J. L. Owen, M. T. Fraile, S. I. Huss, J.-L. Lavandera, T. R. Ioerger, J. C. Sacchettini, *Chem. Biol.* **2012**, *19*, 1556–1567.

[134] N. Hafezi, J. M. Holcroft, K. J. Hartlieb, E. J. Dale, N. A. Vermeulen, C. L. Stern, A. A. Sarjeant, J. F. Stoddart, *Angew. Chem. Int. Ed.* **2015**, *54*, 456–461.

[135] a) *Encyclopedia of Supramolecular Chemistry*, New York, **2004**; b) K. Ariga, T. Kunitake, *Supramolecular Chemistry-Fundamentals and Applications*, Springer-Verlag, Heidelberg, **2006**; c) *Supramolecular Chemistry: From Molecules to Nanomaterials*, John Wiley & Sons, Chichester, **2012**.

[136] E. Arunan, G. R. Desiraju, R. A. Klein, J. Sadlej, S. Scheiner, I. Alkorta, D. C. Clary, R. H. Crabtree, J. J. Dannenberg, P. Hobza, H. G. Kjaergaard, A. C. Legon, B. Mennucci, D. Nesbitt, *J. Pure Appl. Chem.* **2011**, *83*, 1619–1636.

[137] a) A. Priimagi, G. Cavallo, P. Metrangolo, G. Resnati, *Acc. Chem. Res*. **2013**, *46*, 2686–2695; b) S. Scheiner, *Acc. Chem. Res*. **2013**, *46*, 280–288.

[138] N. W. Mitzel, U. Losehand, *Angew. Chem. Int. Ed.* **1997**, *36*, 2807–2809.

[139] N. W. Mitzel, A. J. Blake, D. W. H. Rankin, *J. Am. Chem. Soc*. **1997**, *119*, 4143–4148.

[140] S.-B. Choi, B.-K. Kim, P. Boudjouk, D. G. Grier, *J. Am. Chem. Soc*. **2001**, *123*, 8117–8118.

[141] R. Ahlrichs, M. Bär, M. Hacer, H. Horn, C. Kömel, *Chem. Phys. Lett.* **1989**, *162*, 165–169.

[142] S. B. Boys, F. Bernardi, *Mol. Phys.* **1970**, *19*, 553–566.

[143] Gaussian 09, Revision B.01, M. J. Frisch, G. W. Trucks, H. B. Schlegel, G. E. Scuseria, M. A. Robb, J. R. Cheeseman, G. Scalmani, V. Barone, B. Mennucci, G. A. Petersson, H. Nakatsuji, M. Caricato, X. Li, H. P. Hratchian, A. F. Izmaylov, J. Bloino, G. Zheng, J. L. Sonnenberg, M. Hada, M. Ehara, K. Toyota, R. Fukuda, J. Hasegawa, M. Ishida, T. Nakajima, Y. Honda, O. Kitao, H. Nakai, T. Vreven, J. A. Montgomery, Jr., J. E. Peralta, F. Ogliaro, M. Bearpark, J. J. Heyd, E. Brothers, K. N. Kudin, V. N. Staroverov, R. Kobayashi, J. Normand, K. Raghavachari, A. Rendell, J. C. Burant, S. S. Iyengar, J. Tomasi, M. Cossi, N. Rega, J. M. Millam, M. Klene, J. E. Knox, J. B. Cross, V. Bakken, C. Adamo, J. Jaramillo, R. Gomperts, R. E. Stratmann, O. Yazyev, A. J. Austin, R. Cammi, C. Pomelli, J. W. Ochterski, R. L. Martin, K. Morokuma, V. G. Zakrzewski, G. A. Voth, P. Salvador, J. J. Dannenberg, S. Dapprich, A. D. Daniels, Ö. Farkas, J. B. Foresman, J. V. Ortiz, J. Cioslowski, D. J. Fox, Gaussian, Inc., Wallingford CT, 2009.

[144] Y. Shao, L.F. Molnar, Y. Jung, J. Kussmann, C. Ochsenfeld, S.T. Brown, A.T.B. Gilbert, L.V. Slipchenko, S.V. Levchenko, D.P. O'Neill, R.A. DiStasio Jr., R.C. Lochan, T. Wang, G.J.O. Beran, N.A. Besley, J.M. Herbert, C.Y. Lin, T. Van Voorhis, S.H. Chien, A. Sodt, R.P. Steele, V.A. Rassolov, P.E. Maslen, P.P. Korambath, R.D. Adamson, B. Austin, J. Baker, E.F.C. Byrd, H. Dachsel, R.J. Doerksen, A. Dreuw, B.D. Dunietz, A.D. Dutoi, T.R. Furlani, S.R. Gwaltney, A. Heyden, S. Hirata, C-P. Hsu, G. Kedziora, R.Z. Khalliulin, P. Klunzinger, A.M. Lee, M.S. Lee, W.Z. Liang, I. Lotan, N. Nair, B. Peters, E.I. Proynov, P.A. Pieniazek, Y.M. Rhee, J. Ritchie, E. Rosta, C.D. Sherrill, A.C. Simmonett, J.E. Subotnik, H.L. Woodcock III,

W. Zhang, A.T. Bell, A.K. Chakraborty, D.M. Chipman, F.J. Keil, A.Warshel, W.J. Hehre, H.F. Schaefer, J. Kong, A.I. Krylov, P.M.W. Gill, M. Head-Gordon, *Phys. Chem. Chem. Phys.* **2006**, *8*, 3172–3191.

[145] I. Kalikhman, O. Girshberg, L. Lameyer, D. Stalke, D. Kost, *J. Am. Chem. Soc*. **2001**, *123*, 4709–4716.

[146] S. Muhammad, A. R. Bassindale, P. G. Taylor, L. Male, S. J. Coles, M. B. Hursthouse, *Organometallics* **2011**, *30*, 564–571.

[147] See CSD refcodes BIDFIE, BIDFOK, CANCUR, IVEPUV, OJUYIB, WAVYAV, WAVYEZ, WAVYID, WAVYOJ, and WIJPUB.

[148] H. J. Schneider, A. Yatsimirski, *Principles and Methods in Supramolecular Chemistry*, Wiley, Chichester, **2000**.

[149] G. R. Desiraju, *Angew. Chem. Int. Ed.* **2011**, *50*, 52–59.

[150] G. R. Desiraju, T. Steiner, *The Weak Hydrogen Bond in Structural Chemistry and Biology*, Oxford Univ. Press, Oxford, **1999**.

[151] J. W. Larson, T. B. McMahon, *Inorg. Chem*. **1984**, *23*, 2029–2033.

[152] a) M. Nishio, Y. Umezawa, J. Fantini, M. S. Weiss, P. Chakrabarti, *Phys. Chem. Chem. Phys*. **2014**, *16*, 12648–12683; b) M. Nishio, Y. Umezawa, K. Honda, S. Tsuboyamad, H. Suezawae, *CrystEngComm* **2009**, *11*, 1757–1788; c) M. Nishio, M. Hirota, Y. Umezawa, *The C–H/π Interaction: Evidence, Nature, Consequences*, Wiley-VCH: New York, **1998**.

[153] a) U. Samanta, D. Pal, P. Chakrabarti, *Proteins* **2000**, *38*, 288–300; b) M. J. Plevin, D. L. Bryce, J. Boisbouvier, *Nature Chem*. **2010**, *2*, 466–471; c) M. Brandl, M. S. Weiss, A. Jabs, J. Sühnel, R. Hilgenfeld, *J. Mol. Biol.* **2001**, *307*, 357–377.

[154] a) F. A. Quiocho, N. K. Vyas, *Nature* **1984**, *310*, 381–386; b) N. K. Vyas, M. N. Vyas, F. A. Quiocho, *Science* **1988**, *242*, 1290–1295; c) M. Nishio, *Phys. Chem. Chem. Phys*. **2011**, *13*, 13873–13900; d) Z. R. Laughrey, S. E. Kiehna, A. J. Riemen, M. L. Waters, *J. Am. Chem. Soc.* **2008**, *130*, 14625–14633; e) N. P. Barwell, A. P. Davis, *J. Org. Chem.* **2011**, *76*, 6548–6557.

[155] a) P. V. Hobza, K. Müller-Dethlefs, *Noncovalent Interactions: Theory and Experiment*, RSC publishing, **2010**; b) *Supramolecular Systems in Biomedical Fields*, RSC publishing, **2013**.

[156] T. Clark, *WIREs Comp. Mol. Sci.* **2013**, *3*, 13–20.

[157] A. Bauzá, T. J. Mooibroek, A. Frontera, *Angew. Chem. Int. Ed.* **2013**, *52*, 12317–12321.

[158] J. A. Pople, M. Head-Gordon, K. Raghavachari, *J. Chem. Phys.* **1987**, *87*, 5968–5975.

[159] a) T. J. Mooibroek, P. Gamez, *CrystEngComm* **2013**, *15*, 1802–1805; b) T. J. Mooibroek, P. Gamez, *CrystEngComm* **2013**, *15*, 4565–4570; c) K. E. Ranaghan, J. E. Hung, G. J. Bartlett, T. J. Mooibroek, J. N. Harvey, D. N. Woolfson, W. A. van der Donk, A. Mulholland, *Chem. Sci*. **2014**, *5*, 2191–2199.

[160] T. J. Mooibroek, P. Gamez, *CrystEngComm* **2012**, *14*, 8462–8467.

[161] C. A. Hunter, J. K. M. Sanders *J. Am. Chem. Soc.* **1990**, *112*, 5525–5534.

[162] S. J. Grabowski, *Chem. Rev.* **2011**, *111*, 2597–2625.

[163] Y. Bai, T. R. Sosnick, L. Mayne, S. W. Englander, *Science* **1995**, *269*, 192–197.

[164] A .C. Legon, D. J. Millen, *Acc. Chem. Res.* **1987**, *20*, 39–46.

[165] G. A. Cavallo, P. Metrangolo, R. Milani, T. Pilati, A. Priimagi, G. Resnati, G. Terraneo, *Chem. Rev.* **2016**, *116*, 2478–2601.

[166] T. Steiner, *Angew. Chem. Int. Ed.* **2002**, *41*, 48–76.

[167] A. Bauzá, T. J. Mooibroek, A. Frontera, *Chem. Commun*. **2015**, *51*, 1491–1493.

[168] A. Bauzá, A. Frontera, T. J. Mooibroek, *Cryst. Growth Des.* **2016**, *16*, 5520–5524.

[169] A. Bauzá, T. J. Mooibroek, A. Frontera, *ChemPhysChem* **2016**, *17*, 1608–1614.

[170] L. M. Azofra, I. Alkorta, S. Scheiner, *Phys. Chem. Chem. Phys.* **2014**, *16*, 18974–18981.

[171] A. Chatterjee, T. Ebina, T. Iwasaki, F. Mizukami, *J. Mol. Struct*. **2003**, *630*, 233–242.

[172] J. E. Lovelock, R. J. Maggs, R. A. Rasmussen, *Nature* **1972**, *237*, 452–453.

[173] B. G. de Oliveira, R. C. M. Ugulino de Araújo, E. S. Leite, M. N. Ramos, *Int. J. Quantum Chem.* **2011**, *111*, 111–116.

[174] K. S. Diao, F. Wang, H. J. Wang, *J. Mol. Struct.* **2009**, *913*, 195–199.

[175] L. Ai, J. Liu, *J. Mol. Model.* **2014**, *20*, 2179, 10p.

[176] K. S. Diao, F. Wang, H. J. Wang, *Environ. Contam. Toxicol.* **2010**, *84*, 170–174.

[177] J. G. Calvert, R. Atkinson, J. A. Kerr, S. Madronich, G. K. Moortgat, T. J. Wallington *et al., The Mechanisms of Atmospheric Oxidation of the Alkenes*, Oxford University Press, New York, **2000**.

[178] a) M. P. Fraser, G. R. Cass, B. R. Simoneit, *Environ. Sci. Technol.* **1998**, *32*, 2051–2060; b) A. C. Aikin, J. R. Herman, E. J. Maier, C. J. McQuillan, *J. Geophys. Res.* **1982**, *87*, 3105–3118; c) Y. Xiaoi, D. J. Jacob, S. Turquety, *J. Geophys. Res.* **2007**, *112*, D12305.

[179] R. Custelcean, J. E. Jackson, *Chem. Rev.* **2001**, *101*, 1963–1980.

[180] K. Remya, C. H. Suresh, *Phys. Chem. Chem. Phys.* **2015**, *17*, 18380–18392.

[181] AIMAll (Version 13.05.06), T. A. Keith, TK Gristmill Software, Overland Park KS, USA, **2013**.

[182] *Computational Chemistry: Reviews of Current Trends*, *Vol. 4*, World Scientific, Singapore, **1996**.

[183] F. Vögtle, *Supramolecular Chemistry: an Introduction*, Wiley, New York, **1993**.

[184] P. D. Beer, P. A. Gale, D. K. Smith, *Supramolecular Chemistry*, Oxford University Press, Oxford, **1999**.

[185] J. W. Steed, J. L. Atwood, *Supramolecular Chemistry*, Wiley, Chichester, **2000**.

[186] H. Destecroix, H. C. M. Renney, T. J. Mooibroek, T. S. Carter, P. F. N. Stewart, M. P. Crump, A. P. Davis, *Angew. Chem. Int. Ed*. **2015**, *54*, 2057–2061.

[187] P. Murray-Rust, W. C. Stallings, C. T. Monti, R. K. Preston, J. P. Glusker, *J. Am. Chem. Soc.* **1983**, *105*, 3206–3214.

[188] N. Ramasubbu, R. Parthasarathy, P. Murray-Rust, *J. Am. Chem. Soc*. **1986**, *108*, 4308–4314.

[189] A. Bauzá, T. J. Mooibroek, A. Frontera, *ChemPhysChem* **2015**, *16*, 2496–2517.

[190] A. Bauzá, T. J. Mooibroek, A. Frontera, *Chem. Rec.* **2016**, 16, 473–487.

[191] A. Bauzá, A. Frontera, *ChemPhysChem* **2015**, *16*, 3108–3113.

[192] A. Bauzá, T. J. Mooibroek, A. Frontera, *Phys. Chem. Chem. Phys*. **2016**, *18*, 1693–1698.

[193] E. C. Escudero-Adán, A. Bauzá, A. Frontera, P. Ballester, *ChemPhysChem* **2015**, *16*, 2530–2533.

[194] M. Solimannejad, M. Orojloo, S. Amani, *J. Mol. Model.* **2015**, *21*, 183, 7p.

[195] M. Marín-Luna, I. Alkorta, J. Elguero, *J. Phys. Chem. A* **2016**, *120*, 648–656.

[196] R. F. W. Bader, *Chem. Rev*. **1991**, *91*, 893–928.

[197] S. Grimme, J. Antony, S. Ehrlich, H. A. Krieg, *J. Chem. Phys.* **2010**, *132*, 154104, 19p.

[198] A. Heβelmann, G. Jansen, *Phys. Chem. Chem. Phys*. **2003**, *5*, 5010–5014.

[199] H. -J. Werner, P. J. Knowles, G. Knizia, F. R. Manby, M. Schütz, *WIREs Comput. Mol. Sci*. **2012**, *2*, 242–253.

[200] MOLPRO, version 2012.1, a package of ab initio programs, H.-J. Werner, P. J. Knowles, G. Knizia, F. R. Manby, M. Schütz, P. Celani, W. Györffy, D. Kats, T. Korona, R. Lindh, A. Mitrushenkov, G. Rauhut, K. R. Shamasundar, T. B. Adler, R. D. Amos, A. Bernhardsson, A. Berning, D. L. Cooper, M. J. O. Deegan, A. J. Dobbyn, F. Eckert, E. Goll, C. Hampel, A. Hesselmann, G. Hetzer, T. Hrenar, G. Jansen, C. Köppl, Y. Liu, A. W. Lloyd, R. A. Mata, A. J. May, S. J. McNicholas, W. Meyer, M. E. Mura, A. Nicklaß, D. P. O'Neill, P. Palmieri, D. Peng, K. Pflüger, R. Pitzer, M. Reiher, T. Shiozaki, H. Stoll, A. J. Stone, R. Tarroni, T. Thorsteinsson, M. Wang.

[201] https://www.ccdc.cam.ac.uk/Community/freeservices/Relibase/ (accessed on 25 January 2016).

[202] P. Asztalos, A. Müller, W. Hölke, H. Sobek, M. G. Rudolph, *Acta Cryst*. **2014**, *D70*, 1832–1843.

[203] J. Drenth, *Biochem*. **1976**, *15*, 3731–3738.

[204] T. S. Thorsen, R. Matt, W. I. Weis, B. K. Kobilka, *Struct*. **2014**, *22*, 1657–1664.

[205] M. Kato, K. Komamura, M. Kitakaze, *Circ. J*. **2006**, *70*, 1658–1660.

[206] F. Weinhold, C. R. Landis, *Valency and Bonding: A Natural Bond Orbital Donor-Acceptor Perspective*, Cambridge University Press, Cambridge, UK, **2005**.

[207] a) *Hydrogen Bonding: New Insights*, Springer, Heidelberg, **2006**; b) M. Erdélyi, *Chem. Soc. Rev*. **2012**, *41*, 3547–3557; c) G. Cavallo, P. Metrangolo, T. Pilati, G. Resnati, M. Sansotera, G. Terraneo, *Chem. Soc. Rev*. **2010**, *39*, 3772–3783.

[208] a) D. B. Werz, R. Gleiter, F. Rominger, *J. Am. Chem. Soc.* **2002**, *124*, 10638–10639; b) P. Sanz, O. Mó, M. Yáñez, *Phys. Chem. Chem. Phys*. **2003**, *5*, 2942–2947.

[209] a) S. Scheiner, *J. Chem. Phys*. **2011**, *134*, 094315, 9p; b) J. E. Del Bene, I. Alkorta, G. Sánchez-Sanz, J. Elguero, *J. Phys. Chem. A* **2012**, *116*, 9205–9213.

[210] A. Bauzá, T. J. Mooibroek, A. Frontera, *Chem. Commun.* **2014**, *50*, 12626–12629.

[211] T. J. Mooibroek, P. Gamez, *CrystEngComm* **2012**, *14*, 3902–3906.

[212] a) R. F. W. Bader, *Atoms in Molecules: A Quantum Theory*, Oxford University Press, USA, **1994**; b) R. F. W. Bader, *Atoms in Molecules. Encyclopaedia of Computational Chemistry*,John Wiley & Sons, Chichester, **1998**, vol. 1, pp. 64–86.

[213] H. J. Schneider, *Supramolecular Systems in Biomedical Fields*, RSC Publishing, Cambridge, **2013**.

[214] P. J. Cragg, *Supramolecular Chemistry: From Biological Inspiration to Biomedical Applications*, Springer, Dordrecht, **2010**.

[215] P. Politzer, J. S. Murray, P. Lane, *Int. J. Quantum Chem.* **2007**, *107*, 3046–3052.

[216] F. Weinhold, R. A. Klein, *Angew. Chem. Int. Ed.* **2014**, *53*, 11214–11217.

[217] A. Bauzá, A. Frontera, T. J. Mooibroek, J. Reedijk, *Crystengcomm* **2015**, *17*, 3768–3771.

[218] C. E. Housecrof, A. G. Sharpe, *Inorganic Chemistry*, Prentice Hall, Harlow, **2005**.

[219] N. Ahmed, I. Geronimo, I. C. Hwang, N. J. Singh, K. S. Kim, *Chem. Eur. J.* **2011**, *17*, 8542–8548.

[220] N. Ahmed, V. Suresh, B. Shirinfar, I. Geronimo, A. Bist, I. C. Hwang, K. S. Kim, *Org. Biomol. Chem.* **2012**, *10*, 2094–2100.

[221] R. F. W. Bader, *Acc. Chem. Res.* **1985**, *18*, 9–15.

[222] C. R. Groom, I. J. Bruno, M. P. Lightfoot, S. C. Ward, *Acta Crystallogr. B72* **2016**, 171–179.

[223] H. M. Berman, J. Westbrook, Z. Feng, G. Gilliland, T. N. Bhat, H. Weissig, I. N. Shindyalov, P. E. Bourne, *Nucleic Acid Res.* **2000**, *28*, 235–242.

[224] Q. Wang, Z. -Y. Fu, X. Li, L. M. Yu, *Acta Crystallogr. E* **2011**, *67*, O1671–U1543.

[225] T. J. Siciliano, M. C. Deblock, K. M. Hindi, S. Durmus, M. J. Panzner, C. A. Tessier, W. J. Youngs *J. Organomet. Chem.* **2011**, *696*, 1066–1071.

[226] G. B. Jameson, E. Blazso, N. Seferiadis, H. R. Oswald *Acta Crystallogr. B* **1982**, 38, 2272–2274.

[227] J. Cheung, W. A. Hendrickson, *Structure* **2009**, *17*, 190–201.

[228] D. Trinschek, M. Jansen, *Angew. Chem. Int. Ed.* **1999**, *38*, 133–135.

[229] M. Jansen, *Angew. Chem. Int. Ed.* **1979**, *18*, 698–698.

[230] P. A. Gale, *Accounts Chem. Res.* **2011**, *44*, 216–226.

[231] H. Valkenier, L. W. Judd, H. Li, S. Hussain, D. N. Sheppard, A. P. Davis, *J. Am. Chem. Soc.* **2014**, *136*, 12507–12512.

[232] a) L. M. Salonen, M. Ellermann, F. Diederich, *Angew. Chem. Int. Ed.* **2011**, *50*, 4808–4842; b) E. A. Meyer, R. K. Castellano, F. Diederich, *Angew. Chem. Int. Ed.* **2003**, *42*, 1210–1250.

[233] a) J. C. Ma, D. A. Dougherty, *Chem. Rev.* **1997**, *97*, 1303–1324; b) P. B. Crowley, A. Golovin, *Proteins* **2005**, *59*, 231–239; c) A. Robertazzi, F. Krull, E. -W. Knapp, P. Gamez, *CrystEngComm*, **2011**, *13*, 3293–3300.

[234] a) K. Muller-Dethlefs, P. Hobza, *Chem. Rev*. **2000**, *100*, 143–168; b) S. K. Burley, G. A. Petsko, *Science* **1985**, *229*, 23–28; c) J. T. Stivers, Y. L. Jiang, *Chem. Rev.* **2003**, *103*, 2729–2759.

[235] A. Schier, H. Schmidbaur, *Organometallics* **2008**, *27*, 2361–2395.

[236] J. Zukerman-Schpector, A. Otero-de-la-Roza, V. Lauña, E. R. T. Tiekink, *Chem. Commun*. **2011**, *47*, 7608–7610.

[237] A. A. Auer, D. Mansfeld, C. Nolde, W. Schneider, M. Schurmann, M. Mehring, *Organometallics* **2009**, *28*, 5405–5411.

[238] R. W. F. Bader, *Atoms in Molecules. A Quantum Theory*, Clarendon, Oxford, **1990**.

[239] F. Biegler-König, J. Schönbohm, D. Bayles, *J. Comput. Chem*. **2001**, *22*, 545–559.

[240] a) M. R. Battaglia , A. D. Buckingham, J. H. Williams, *Chem. Phys. Lett*. **1981**, *78*, 421–423; b) J. Vrbancich, G. L. D. Ritchie, *J. Chem. Soc. Faraday Trans. II* **1979**, *76*, 648–655.

[241] *Biological Chemistry of Arsenic, Antimony and Bismuth*, John Wiley & Sons, Ltd., Chichester, **2010**.

[242] J. S. Thayer, *J. Chem. Ed.* **2005**, *82*, 1721–1729.

[243] W. Kutzelnigg, *Angew. Chem. Int. Ed.* **1984**, *23*, 272–295.

[244] K. C. H. Lange, T. Klapötke, *The Chemistry of Organic Arsenic, Antimony and Bismuth*, John Wiley & Sons, Ltd., Chichester, **1994**.

[245] A. L. Allred, E. G. Rochow, *J. Inorg. Nucl. Chem.* **1958**, *5*, 264–268.

[246] a) K. B. Jacobson, J. B. Murphey, B. D. Sarma, *FEBS Lett*. **1972**, *22*, 80–82; b) D. H. H. Tsao, A. H. Maki, *Biochemistry* **1991**, *30*, 4565–4572; c) S. Maignan, J.-P. Guilloteau, Z.-L. Qing, C. Clement-Mella, V. Mikol, *J. Mol. Biol*. **1998**, *282*, 359–368; d) F. Tete-Favier, D. Cobessi, S. Boschi-Muller, S. Azza, G. Branlant, A. Aubry, Structure **2000**, *8*, 1167–1178; e) M. S. Junop, M. Modesti, A. Guarné, R. Ghirlando, M. Gellert, W. Yang, *EMBO J.* **2000**, *19*, 5962–5970.

[247] R. X. Xu, A. M. Hassell, D. Vanderwall, M. H. Lambert, W. D. Holmes, M. A. Luther, W. J. Rocque, M. V. Milburn, Y. Zhao, H. Ke, R. T. Nolte, *Science* **2000**, *288*, 1822–1825.

[248] D. H. Templeton, A. Zalkin, J. D. Forrester, S. M. Williamson, *J. Am. Chem. Soc*. **1963**, *85*, 816–817.

[249] G. E. Rodgers, *J. Chem. Educ*. **2014**, *91*, 216–224.

[250] J. Haner, G. J. Schrobilgen, *Chem. Rev*. **2015**, *115*, 1255–1295.

[251] a) J. S. Ogden, J. J. Turner, *Chem. Commun*. **1966**, *19*, 693–694; b) E. Jacob, R. Opferkuch, *Angew. Chem. Int. Ed.* **1976**, *15*, 158–159.

[252] D. S. Brock, V. Bilir, H. P. A. Mercier, G. J. Schrobilgen, *J. Am. Chem. Soc*. **2007**, *129*, 3598–3611.

[253] K. Koppe, J. Haner, H. P. A. Mercier, G. J. Schrobilgen, *Inorg. Chem*. **2014**, *53*, 11640–11661.

[254] a) G. V. Oshovsky, D. N. Reinhoudt, W. Verboom, *Angew. Chem. Int. Ed*. **2007**, *46*, 2366–2393; b) J. M. Zayed, N. Nouvel, U. Rauwald, O. A. Scherman, *Chem. Soc. Rev*. **2010**, *39*, 2806–2816.

[255] a) M. Zürcher, F. Diederich, *J. Org. Chem*. **2008**, *73*, 4345–4361; b) D. K. Smith, *J. Chem. Educ*. **2005**, *82*, 393–400; c) D. A. Uhlenheuer, K. Petkau, L. Brunsveld, *Chem. Soc. Rev*. **2010**, *39*, 2817–2826.

[256] N. Zacharias, D. A. Dougherty, *Trends Pharmacol. Sci.* **2002**, *23*, 281–287.

[257] S. Scheiner, *Acc. Chem. Res*. **2013**, *46*, 280–288.

[258] a) P. Metrangolo, G. Resnati, *Chem. Eur. J*. **2001**, *7*, 2511–2519; b) S. J. Grabowski, *Phys. Chem. Chem. Phys*. **2013**, *15*, 7249–7259.

[259] a) P. Sanz, M. Yáñez, O. Mó, *Chem. Eur. J.* **2002**, *8*, 3999–4007; b) P. Sanz, M. Yáñez, O. Mó, *New J. Chem.* **2002**, *26*, 1747–1752.

[260] A. Bauzá, A. Frontera, *Angew. Chem. Int. Ed*. **2015**, *54*, 7340–7343.

[261] H. A. Levy, J. H. Burns, P. A. Agron, *Science* **1963**, *139*, 1208–1209.

[262] a) N. Barlett, *Proc. Chem. Soc*. **1962**, 218–218; b) K. O. Christe, *Chem. Commun*. **2013**, *49*, 4588–4590.

[263] J. H. Burns, R. D. Ellison, H. A. Levy, *J. Phys. Chem*. **1963**, *67*, 1569–1570.

[264] a) L. Turowsky, K. Seppelt, *Z. Anorg. Allg. Chem*. **1981**, *472*, 7; b) D. Lentz, K. Seppelt, *Angew. Chem. Int. Ed*. **1978**, *17*, 356–361.

[265] P. L. A. Popelier, *Atoms In Molecules. An Introduction*; Prentice Hall, Harlow, **2000**.

[266] P. J. MacDougall, G. J. Schrobilgen, R. F. W. Bader, *Inorg. Chem*. **1989**, *28*, 763–769.

[267] J. S. Murray, L. Macaveiu, P . Politzer, *J. Comput. Sci.* **2014**, *5*, 590–596.

[268] J. Miao, B. Song, Y Gao *Chem. Asian. J*. **2015**, *10*, 2615–2618.

[269] a) I. Alkorta, J. Elguero, J. E. Del Bene, *J. Phys. Chem. A* **2013**, *117*, 10497–10503; b) S. Mohammad, R. Vahid, C. Trujillo, I. Alkorta, G. Sanchez–Sanz, J. Elguero, *J. Phys. Chem. A* **2012**, *116*, 5199–5206; c) C. Trujillo, G. Sánchez, I. Alkorta, J. Elguero, *New J. Chem.* **2015**, *39*, 6791–6802.

[270] a) S. Roy, A. Bauzá, A. Frontera, R. Banik, A. Purkayastha, M. G. B. Drew, B. M. Reddy, B. Sridhar, S. Kr. Dasa S. Das, *CrystEngComm*, **2015**, *17*, 3912–3916. b) S. Cañellas, A. Bauzá, A. Lancho, A. Garcia-Raso, J. J. Fiol, E. Molins, P. Ballester, A. Frontera, *CrystEngComm*, **2015**, *17*, 5987–5997.

[271] A. Bauzá, A. Frontera, *Phys. Chem. Chem. Phys.* **2015**, *17*, 24748–24753.

Annex I

Computational methodology

$$H\psi = -(h/i)(\partial\psi/\partial t)$$

A.I.1. Quantum mechanics

Computational Chemistry has become a very important tool in modern chemistry to understand the structure, properties and reactivity of chemicals. Below a brief description of computational methods used during the development of this thesis is summarized. For more extensive treatment general literature is available.[272,273]

Quantum mechanics (QM) is the correct mathematical description of the nuclei and electrons behaviour at an atomic level. QM was born at the beginning of the 20th century[274] and as the application of new quantum concepts to study atomic and molecular systems has a fast and wide acceptance. In its early stages, some semi-empirical approximations were developed as Hückel[275,276,277] and extended-Hückel methods.[278] The microscopic systems, which present corpuscular and wave behaviour, obey the quantum mechanics laws. These were discovered by Heisenberg, Born and Jordan in 1925 and by Schrödinger in 1926. By using Quantum Mechanics the interpretation and prediction of the molecular structure and properties as well as chemical reactivity is possible.

The molecular systems are defined by a wavefunction, which Schrödinger equation accomplishes:

$$H\psi = -(h/i)(\partial\psi/\partial t) \qquad \text{Equation 1A}$$

When the solution to this equation is found without using any empiric data, the methods used are named *ab initio* (from Latin, at the beginning). Equation 1A can only solve one-electron systems in their exact form. However, for multiple electron systems it is always necessary to make approximations to simplify the calculations, which lead to different theoretical methods useful in treating molecular systems. Then, solving the Schrödinger equation in its time-independent form,[279] becomes a milestone equation, under the Born-Oppenheimer approximation. The wavefunction (Ψ) is related to the electron density (ρ) by definition. The electron density is defined as a multiple integral over the spin coordinates of all electrons and moreover one of the spatial variables (Equation 2A).

$$\rho(\vec{r}) = N\int\ldots\int |\psi(\vec{x}_1,\vec{x}_2,\ldots,\vec{x}_N)|^2\, ds_1 d\vec{x}_2\ldots d\vec{x}_N \qquad \text{Equation 2A}$$

The electron density ρ determines the probability of finding one of the N electrons within an infinitesimal element of space with arbitrary spin while other electrons have arbitrary positions and spin in the state represented by the wavefunction Ψ.

---

[272] D. B. Cook, *Handbook of Computational Quantum Chemistry*, Oxford University Press, Oxford, **1998**.
[273] A. Szabo; N. S. Ostlund, *Modern Quantum Chemistry*, McGraw-Hill, New York, **1989**.
[274] C. J. Cramer, *Essentials of Computational Chemistry: Theories and Models*, Wiley, **2004**.
[275] E. Huckel, *Z. Phys. Chem.* **1930**, *60*, 423–456.
[276] E. Huckel, *Z. Phys. Chem.* **1931**, *70*, 204–286.
[277] E. Huckel, *Z. Phys. Chem.* **1932**, *76*, 628–648.
[278] R. Hoffmann, *J. Chem. Phys.* **1963**, *39*, 1397–1412.
[279] E. Schrodinger, *Phys. Rev.* **1926**, *28*, 1049–1070.

A.I.2. *Ab initio* calculations

As mentioned above, for many-body problems there is not a "correct" solution; we therefore require some means to decide whether one proposed wavefunction is "better" than another. The variation theorem provides us with a mechanism for answering this question. The theorem states that the energy calculated from an approximation to the true wavefunction will always be greater than the true energy. Consequently, the better the wavefunction, the lower the energy. The "best" wavefunction is obtained when the energy is a minimum. At the minimum, the first derivative of the energy, δE, will be zero. The Hartree-Fock (HF) equations (Equation 4A) are obtained by imposing this condition on the expression for the energy, subject to the constraint that the molecular orbitals remain orthonormal. The orthonormality condition is written in terms of the overlap integral, S_{ij}, between two orbitals *i* and *j* (see Equation 3A).

$$S_{ij} = \int x_i x_j d_\tau = \delta_{ij} \qquad \text{Equation 3A}$$

$$\delta E - 2\delta \sum_i \sum_j \varepsilon_{ij} S_{ij} = 0 \qquad \text{Equation 4A}$$

The solution of this equation is rather complicated. However, a qualitative picture is possible. The major difference between polyelectronic systems and systems with single electrons is the presence of interactions between the electrons, which are expressed as Coulumb and exchange integrals. Suppose we are given the task of finding the "best" (i. e. lowest energy) wavefunction for a polyelectronic system. We wish to retain the orbital picture of the system. The problem is to find a solution which simultaneously enables all the electronic motions to be taken into account. After the mathematical treatment, we arrive to an equation where each electron has been assumed to move in a "fixed" field comprising the nuclei and the other electrons. This has important implications for the way in which we attempt to find a solution. For any solution that we might find by solving the equation for one electron will naturally affect the solutions for the other electrons in the system. The general strategy is called a self-consistent field (SCF) approach. The SCF method gradually refines the individual electronic solutions that correspond to lower and lower total energies until the point is reached at which the results for all the electrons are unchanged, when they are said to be self-consistent.

The most significant drawback of Hartree-Fock theory is that it fails to adequately represent electron correlation. In the self-consistent field method the electrons are assumed to be moving in an average potential of the other electrons, and so the instantaneous position of an electron is not influenced by the presence of a neighboring electron. In fact, the motions of electrons are correlated and they tend to "avoid" each other more than Hartree-Fock theory would suggest, giving rise to a lower energy. The correlation energy is defined as the difference between the Hartree-Fock energy and the exact energy. Neglecting electron correlation can lead to some clearly anomalous results, especially as the dissociation limit is approaching. The electron correlation is crucial in the study of dispersive effects, which play a major role in intermolecular interactions.

Møller and Plesset proposed an alternative way to tackle the problem of electron correlation. Their method is based upon Rayleigh-Schrödinger perturbation theory, in which the "true" Hamiltonian operator (H) is expressed as the sum of "zeroth-order" Hamiltonian (H^0) and a perturbation (H'). The parameter λ further indicates the smallness of the perturbation (see Equation 5A). In order to calculate higher-order wavefunctions we need to establish the form of the perturbation. This is the difference between the "real" Hamiltonian and the zeroth-order Hamiltonian.

$$H = H^0 + \lambda H' \qquad \text{Equation 5A}$$

On the other hand, the sum of the zeroth-order and first-order energies thus corresponds to the Hartree-Fock energy. To obtain an improvement on the Hartree-Fock energy it is therefore necessary to use Møller-Plesset perturbation theory to at least second order. This level of theory is referred to as MP2. Third- and fourth-order Møller-Plesset calculations (MP3 and MP4) are also available as standard options in many *ab initio* packages. The advantage of many-body perturbation theory is that it is size-independent. However, Møller-Plesset perturbation theory is not variational and can sometimes give energies that are lower than the "true" energy. These calculations are computationally intensive; however, they are the most popular way to incorporate electron correlation into molecular quantum mechanical calculations. Therefore, nowadays the MP2 method[280] is the most popular and simple method that includes electron correlation, by means of the perturbation theory application (in this case, of second order) to the HF determinant. In spite of the high computational cost of the Møller-Plesset (MP2) methodology in comparison with HF theory, other post-HF methods such as Configuration Interactions (CI) or Coupled Cluster (CC) require more computational resources, intractable in medium-large system sizes. The RI-MP2 method (Resolution of the Identity MP2)[281,282] also treats the electron correlation and, thanks to the use of auxiliary basis set to avoid dealing a complete set of two-electron repulsion integrals, is a calculistic methodology that consumes less time and resources than MP2.
It is very normal to use the frozen core (FC) approximation that only estimates the electron correlation energy associated to the valence electrons, since the important chemical changes take place in the valence orbitals while the intern orbitals are practically constant. In general, the calculations performed in this thesis are done using the frozen core approximation.

A.I.3. Density Functional Theory (DFT)

Density Functional Theory (DFT) represents an alternative methodology for evaluating the energy and other properties of a polyelectronic system.[283] Rather than having to work with a complex and non-observable Ψ, DFT uses functional of the electron density (ρ), which is directly related with Ψ, physically observable and

[280] C. Moller, M. S. Plesset, *Phys. Rev.* **1934**, *46*, 0618–0622.
[281] M. Feyereisen, G. Fitzgerald, A. Komornicki, *Chem. Phys. Lett.* **1993**, *208*, 359–363.
[282] O. Vahtras, J. Almlof, M. W. Feyereisen, *Chem. Phys. Lett.* **1993**, *213*, 514–518.
[283] R. G. Parr; W. Yang, *Density Functional Theory of Atoms and Molecules*, Oxford University Press, New York, **1989**.

easy to handle, presenting the basis for DFT. This methodology introduces the electron correlation effects in the Schrödinger equation resolution by means of approximate alternative methods.

The two major theoretical pillars of the DFT were established by Hohenberg and Kohn theorem postulated in 1964.[284] The first Hohenberg-Kohn theorem states that the external potential (e. g. due to the nuclei) is a unique function of the ground state electron density since, in turn, an external potential fixes the Hamiltonian and determines the energy of the system and all other ground state electronic properties. The second theorem states that in any system the ground state functional for energy delivers the lowest energy if and only if the input density is the true ground state density. This theorem is only the extension of variational principles to the density functional theory. In 1965 Prof. Kohn and Prof. Sham suggested an avenue for how the unknown universal functional in DFT can be approached.[285] Their approach consists of reducing the intractable many-body problem of interacting electrons in a static external potential to a tractable problem of non-interacting electrons moving under an effective potential. The typical representation of Kohn-Sham equations is presented in Equation 6A.

$$F[\rho(\vec{r})]\varphi_i(\vec{r}) = \varepsilon_i\varphi_i(\vec{r}) \qquad \text{Equation 6A}$$

$F[\rho(\vec{r})]$ is the Kohn-Sham functional and ε_i is the orbital energy of the corresponding Khon-Sham orbital φ_i. The Kohn-Sham functional can be divided in different parts as presented in the following Equation 7A.

$$F[\rho(\vec{r})] = T_s[\rho(\vec{r})] + J[\rho(\vec{r})] + E_{xc}[\rho(\vec{r})] = T_s[\rho(\vec{r})] + J[\rho(\vec{r})] + (T_c[\rho(\vec{r})] + E_{ncl}[\rho(\vec{r})])$$

Equation 7A

$T_s[\rho(\vec{r})]$ is the kinetic energy in a non-interacting system, $J[\rho(\vec{r})]$ is the classical coulomb interaction and $E_{xc}[\rho(\vec{r})]$ is the exchange-correlation energy. This term is defined as the sum of two terms: the residual part of the true kinetic energy, $T_c[\rho(\vec{r})]$ and the non-classical electrostatic contributions $E_{ncl}[\rho(\vec{r})]$. In other words, the exchange-correlation energy $E_{xc}[\rho(\vec{r})]$ is the functional which contains everything that is unknown or we do not know exactly how to handle. The Kohn-Sham approach moves the search of an unknown universal functional to a search of an unknown universal exchange-correlation functional.

The Kohn-Sham approach establishes the guidelines for the construction of the universal functional. However the unknown exchange-correlation energy has to be approximated. The most relevant approximations are LDA, GGA, meta-GGA and hyper-GGA. These approximations are the first steps on the Jacob's ladder of exchange-correlation functional. This is an imaginary ladder drawn by Perdew[286] that connects the "Hartree world" where there is no exchange or correlation energy

[284] P. Hohenberg, W. Kohn, *Phys. Rev. B* **1964**, *136*, B864–B871.
[285] W. Kohn, L. J. Sham, *Phys. Rev.* **1965**, *140*, 1133–1138.
[286] J. P. Perdew, A. Ruzsinszky, L. A. Constantin, J. W. Sun, G. I. Csonka, *J. Chem. Theory Comput.* **2009**, *5*, 902–908.

with the "Heaven of Chemical Accuracy" where the error in bonding energies is less than one kcal/mol.

The central idea of Local Density Approximation (LDA) is a hypothetical uniformed electron gas. In this system the electrons move around a distribution of positive background charges that make the system electrically neutral. The number of electrons N and the volume of the gas V are considered to approach infinity and the electron density attains a constant value anywhere in V. The LDA functional considered that exchange-correlation has a local effect and only depends on the electron density value in each point in the space. The LDA exchange part is represented by the known exchange energy of one electron in a uniform electron gas at one particular density. There is no analytical expression for the correlation part; moreover there are very accurate Monte-Carlo simulations for a homogeneous electron gas.[287] Even the relative simplicity of LDA functional, acceptable results are achieved, but their moderate accuracy is certainly insufficient for most chemical applications.

In the 80's, the Generalized Gradient Approximation (GGA) methods were developed. They introduced the density gradient ($\nabla\rho$) as well as the electron density (ρ) at each point in space. The corrections from the gradient are added to the local definition of exchange-correlation redefining the $E_{xc}[\rho(\vec{r})]$ functional. Nowadays, there are many GGA functionals based on different formulations of the exchange and correlation parts as Becke-Perdew (BP86),[288] Perdew-Burke-Ernzerhof (PBE),[289] Becke-Lee-Yang-Parr (BLYP),[290] etc.

The corrections introduced by GGA highly improved the results with respect to LDA, achieving an acceptable accuracy. The deviations on bond energies are partially corrected and accordingly the total and bonding energies too. This derives in molecular geometries that are in better agreement with the experimental ones. Although the GGA functionals have problems in the description of "weak" interactions as dispersion,[291] π-stacking,[292] etc., that are completely neglected in their formulation, these functionals are widely used in computational chemistry for systems without relevant "weak" interactions, e.g., many organometallic complexes. The main errors of the previous functionals are found in the exchange part description because it is usually known that the exchange contributions are significantly larger in absolute numbers than the corresponding correlation effects. The hybrid functionals are an approach to minimize this problem with a partial incorporation of the Hartree-Fock exact exchange-energy in the previous functional. There are many hybrid functionals with different percentage of exact exchange (ee). Nowadays, one of the most used hybrid functionals is the B3LYP (20% of ee).[293] It has become a reference in computational chemistry showing remarkable results in a

[287] D. M. Ceperley, B. J. Alder, *Phys. Rev. Lett.* **1980**, *45*, 566–569.
[288] J. P. Perdew, *Phys. Rev. B* **1986**, *33*, 8822–8824.
[289] J. P. Perdew, K. Burke, M. Ernzerhof, *Phys. Rev. Lett.* **1996**, *77*, 3865–3868.
[290] A. D. Becke, *Phys. Rev. A* **1988**, *38*, 3098–3100.
[291] P. Hobza, J. Sponer, T. Reschel, *J. Comput. Chem.* **1995**, *16*, 1315–1325.
[292] X. Y. Ye, Z. H. Li, W. N. Wang, K. N. Fan, W. Xu, Z. Y. Hua, *Chem. Phys. Lett.* **2004**, *397*, 56–61.
[293] P. J. Stephens, F. J. Devlin, C. F. Chabalowski, M. J. Frisch, *J. Phys. Chem.* **1994**, *98*, 11623–11627.

wide variety of properties and reactions. Its exchange part is made up of 80% of Becke, 3-parameters exchange functional and 20% Hartree-Fock exact exchange.[294] The Becke's functional[290,295,296] includes three semi-empirical parameters adjusted in order to minimize the atomization and ionization energies error as well as the proton affinities in the G2 set of molecules. The correlation part is constructed by Lee-Yang-Parr (LYP) correlation functional.[297] Related to this, the M06 suite of functionals, which differ in the amount of the exact exchange included with M06 including 27% of the HF exchange, M06-2X including 54%, and M06-HF including 100% are another example of accurate and efficient hybrid functionals.[298] Particularly, in this thesis the BP86 functional with the empirical dispersion correction 3 (D3) has been used.[197]

A.I.4. Basis set function

One of the inherent approximations for all *ab initio* methods is the introduction of a finite set of basis functions. An exact representation of a molecular orbital can only be achieved using a complete basis set, i.e., infinite, which is practically impossible. Obviously, the bigger the basis set, the better the representation, but the computational cost is larger. Therefore, the idea is to use the smallest basis set possible without compromising the efficiency of the calculation.[299]

Due to computational efficiency, the Gaussian type orbitals (GTO) are the most used basis set in electronic structure calculations. However, due to our computational capabilities, we have been able to perform RI-MP2 calculations with TURBOMOLE programme,[141] using def2-TZVP basis set of Alrichs[300]. In addition, in some studies the double and triple-zeta basis sets of Dunning (aug-cc-pVXZ, X = D, T) have been used.

A.I.5. Basis Set Superposition Error (BSSE)

Suppose we wish to calculate the energy of formation of a bimolecular complex, such as the specific supramolecular system (AB) obtained from the following reaction between A and B:

$$A + B \Leftrightarrow A - B$$

One might expect that this energy value could be obtained by first calculating the energy of a single A and B molecules, then calculating the energy of the dimer (AB), and finally subtracting the energy of the two isolated molecules (the 'reactants')

[294] A. D. Becke, *J. Chem. Phys.* **1993**, *98*, 1372–1377.
[295] A. D. Becke, *J. Chem. Phys.* **1993**, *98*, 5648–5652.
[296] A. D. Becke, *J. Chem. Phys.* **1996**, *104*, 1040–1046.
[297] C. T. Lee, W. T. Yang, R. G. Parr, *Phys. Rev. B* **1988**, *37*, 785–789.
[298] a) Y. Zhao, D. G. Truhlar, *Theor. Chem. Acc.* **2008**, *120*, 215–241; b) Y. Zhao, D. G. Truhlar, *J. Phys. Chem. A* **2006**, *110*, 13126–13130; c) Y. Zhao, D. G. Truhlar, J. *Chem. Phys.* **2006**, *125*, 194101.
[299] D. Feller; E. R. Davidson, *Rev. Comput. Chem.* **1990**, *1*, 1.
[300] A. Schafer, H. Horn, R. Ahlrichs, *J. Chem. Phys.* **1992**, *97*, 2571–2577.

from that of the dimer (the 'products'). Its interaction energy can be obtained according to the Equation 8A:

$$\Delta E_{interac.} = E(AB)^*_{ab} - E(A)_a - E(B)_b \qquad \text{Equation 8A}$$

Where:

- * indicates that the optimized geometry complex is used,
- *a*, *b* and *ab* subscripts mean that the energy calculation have been performed using the basis set of *A*, *B* and *AB*, respectively.

The favourable complexation processes present negative energies, so the more negative the energies, the more favourable the formation of complex.

However, the energy difference obtained by such an approach will invariably be an overestimate of the true value. Ideally, the best solution would be to use a complete basis set (CBS) to avoid this overestimation. Since this solution is not possible, the first condition is to use the same basis set to perform all the calculations and compare interaction energies. The discrepancy arises from a phenomenon known as basis set superposition error (BSSE). As the two A and B molecules approach each other, the energy of the system falls not only because of the favourable intermolecular interactions but also because the basis functions on each molecule provide a better description of the electronic structure around the other molecule. Hence, in a complex, the basis set of one molecule can help to compensate the incomplete basis set of another molecule and vice versa. In this way the energy is artificially greater (more negative) and the interaction energy is overestimated.

It is clear that the BSSE would be expected to be particularly significant when small, inadequate basis sets are used (e.g. the minimal basis STO-nG basis sets) which do not provide for an adequate representation of the electron distribution far from the nuclei, particularly in the region where noncovalent interactions are strongest. The most used method to correct this error is the Counterpoise technique.[142] By this method, the BSSE is estimated as the difference between the energies of the monomers with the regular basis set and the energies calculated with the complete basis set for the entire complex (Equation 8A).

To estimate how much of this energy of complexation is due to the BSSE, it takes four additional energy calculations. Using the basis set *a* for A, and basis set *b* for B, each of the two fragments in the geometry of the complex are calculated with the complete basis set *ab*. For example, the energy of A is calculated in the presence of normal basis set functions *a* and with the basis set functions *b* of fragment B located in the corresponding nuclear positions, but without B nuclei present. These basis set functions located at fixed points of the space is often referred to as ghost orbitals. The energy of fragment A will be lowered due to ghost functions, since the basis set becomes more complete. The correction of *Counterpoise* is defined as shown in Equation 9A.

$$\Delta E_{CP} = E(A)^*_{ab} + E(B)^*_{ab} - E(A)^*_a - E(B)^*_b \qquad \text{Equation 9A}$$

The interaction energy corrected by means of *Counterpoise* technique is expressed as follows in Equation 10A. With the notation used before, the interaction energy can also be written as shown in Equation 11A.

$$\Delta E_{\text{int}erac.}^{BSSE} = \Delta E_{\text{int}erac.} - \Delta E_{CP} \quad \text{Equation 10A}$$

$$\Delta E_{\text{int}erac.}^{BSSE} = E(AB)^*_{ab} - [E(A)^*_{ab} + E(A)_a - E(A)^*_a] - [E(B)^*_{ab} + E(B)_b - E(B)^*_b]$$

Equation 11A

Fortunately, the complexes that present monatomic ions, it holds that $(N)^*_n = E(N)_n$ and the corrected energy calculation is less arduous.

A.I.6. Molecular Electrostatic Potential

The molecular electrostatic potential (MEP)[301] can be defined as the electrostatic component of the interaction energy between the charge distribution of one molecule and a positive point charge (and therefore $Q_B = +1$), and can be calculated from Equation 15A:

$$V_{MEP} = \sum_A \sum_B \frac{Q_B Z_A}{|R_B - R_A|} - \sum_B Q_B \sum_i^{occupied} \sum_\mu \sum_\vartheta c_{\mu i} c_{\vartheta i} \left\langle \varphi_\mu \left| \frac{1}{R_B - r} \right| \varphi_\vartheta \right\rangle \quad \text{Equation 12A}$$

Where:

- Z_A is the atomic number of atom A,
- Q_B is the classical point charge,
- r indicates the electron position,
- R_A indicates the nuclei location of atom A,
- R_B indicates the position of classical atom B,
- φ is the basis set used for molecule A,
- $c_{\mu i}$ is the orbital atomic coefficient μ in the molecular orbital i.

The first term represents the nuclear electrostatic repulsion between the nuclei A and a classical particles while the second corresponds to the electrostatic attraction originated between the electrons of A and the classical particle B. The MEP formalism enables the rigorous calculation of electrostatic interactions between any classical charge and a perturbed molecule, without considering the induction, dispersion or repulsion effects.

[301] E. Scrocco; J. Tomasi, *Top. Curr. Chem.* **1973**, *42*, 95–170.

A.I.7. Atoms in molecules (AIM)

The Bader's theory of "Atoms in molecules" (AIM)[196,238] is an intent to rigorously define the atom and chemical bond from the polielectronic wavefunction. Principally being based on Hellman-Feynman theorem,[302] it shows that all properties of one molecule are determined by the electron density distribution (ρ). Hence, the AIM theory is a formalism that permits defining the atom concepts in molecule, chemical bond, molecular structure and stability, structural change and, moreover, give descriptions of different kinds of bonding and atomic interactions according to the ideas of descriptive chemistry.

An important part of the AIM theory is the topological analysis of ρ, which can give a good description, depending on its gradient vector and stationary points. The ρ gradient ($\nabla\rho$) or trajectory is a vector that is directed in the direction of the greater slope towards the maximum. In a molecule, all the trajectories start at the infinity and finish at a nuclei, without crossing each other. In this way every nucleus acts as an attractor of different trajectories, which is named attractive basin. It has been demonstrated[303] that it can divide a system in regions or quantic subsystems in which all the total system magnitudes are well-defined through zero flux surfaces of $\nabla\rho$. In general, each and every one of the delimited volumes of these surfaces have single atomic nucleus, so are named atomic basin.

The stationary points of the electron density function ($\nabla\rho = 0$) are called critical points (CPs). Their nature is determined by means of the hessian matrix of ρ, whose eigenvalues are named curvatures and their signs determine the kind of CP. A negative curvature indicates that ρ is a maximum in the direction of the associated eigenvector, while being a minimum when it is positive. The rank of a CP, described as ω, is the number of curvatures different from zero. Their classification designed as σ, is the sum of all their algebraic signs. CPs are labelled giving the pair value (ω, σ). The CPs of ω=3 correspond to ρ distributions in molecules with stable nuclear configurations and are the interest of this study. There are four possible types of CP of ω=3.

- (3,–3) is a local maximum of the electron density and corresponds to nuclei.
- (3,–1) is an inflexion point and it is located between both bonded nuclei (BCP).
- (3,+1) is also an inflexion point and occurs as consequence of particular geometric distributions of bonds defining elements in molecular structure. When bonds are disposed in such a way that a ring is formed, a ring CP (RCP) in its interior is generated.
- (3,+3) is a local minimum that is associated to the structural element generated when several rings form a cage and is therefore named cage CP (CCP).

[302] R. P. Feynman, *Phys. Rev.* **1939**, *56*, 340–343.
[303] S. Srebrenik, R. F. W. Bader, *J. Chem. Phys.* **1975**, *63*, 3945–3961.

Due to ρ(r) being a continuous function, the total number of CPs present in the system should satisfy the Poincaré-Hopf relation (Equation 16A):[304]

$$n - b + r - c = 1 \qquad \text{Equation 13A}$$

Where *n*, *b*, *r*, and *c* are the total number of nuclei, bond, ring and cage CPs, respectively.

A.I.8. SAPT (Symmetry Adapted Perturbation Theory)

Symmetry-adapted perturbation theory (SAPT) provides a means of directly computing the noncovalent interaction between two molecules, that is, the interaction energy is determined without computing the total energy of the monomers or dimer. In addition, SAPT provides a decomposition of the interaction energy into physically meaningful components: i.e., electrostatic, exchange, induction, and dispersion terms. In SAPT, the Hamiltonian of the dimer is partitioned into contributions from each monomer and the interaction.

$$H = F_A + W_A + F_B + W_B + V \qquad \text{Equation 14A}$$

Here, the Hamiltonian is written as a sum of the usual monomer Fock operators, *F*, the fluctuation potential of each monomer, *W*, and the interaction potential, *V*. The monomer Fock operators, F_A+F_B, are treated as the zeroth-order Hamiltonian and the interaction energy is evaluated through a perturbative expansion of V, W_A, and W_B. Through first-order in *V*, electrostatic and exchange interactions are included; induction and dispersion first appear at second-order in *V*. For a complete description of SAPT, the reader is referred to the excellent review by Jeziorski, Moszynski, and Szalewicz.[305]

The current applications of SAPT utilize usually a hybrid approach to compute the total interaction energy. That is, the Hartree-Fock interaction energy contains the following SAPT corrections

$$E_{\text{int}}^{HF} = E_{pol} + E_{exch} + E_{ind,resp} + E_{exch-ind,resp} + \ldots \qquad \text{Equation 15A}$$

where the dots stand for the second-order exchange-deformation and the third- and higher-order induction, exchange-induction, and exchange-deformation terms (Equation 18A neglects also very small zeroth-order terms vanishing as S^4 appearing in the Heitler-London interaction energy).
Thus, by using E_{int}^{HF} one sums to infinity certain SAPT components. The difference between E_{int}^{HF} and the sum of computed SAPT corrections is usually small and therefore SAPT corrections can be used to interpret the Hartree-Fock interaction energy as well as in the fitting procedures. The remaining SAPT corrections which

[304] H. Hopf, *Math. Ann.* **1927**, *96*, 225–250.
[305] B. Jeziorski, R. Moszynski, K. Szalewicz, *Chem. Rev.* **1994**, *94*, 1887–1930.

describe correlation effects are added to E_{int}^{HF}. One should mention that the Hartree-Fock interaction energy can be expanded rigorously in powers of *V*.[306] The methods of this expansion are analogous (but not identical) to the symmetry-adapted perturbation theories discussed so far. It has been shown that these HF-SAPT expansions reproduce E_{int}^{HF} to within 2-15% at the second order and 1-5% in the third order. See ref. 302 for a more comprehensive treatment of SAPT.

A.I.9. Natural Bonding Orbitals (NBO)

The concept of "natural'" orbitals was first introduced by Löwdin[307] to describe the unique set of orthonormal 1-electron functions $\theta_i(\vec{r})$ that are *intrinsic* to the N-electron wavefunction ψ(1, 2, ..., N). Mathematically, the θ_i's can be considered as *eigen*orbitals of ψ (or, more precisely, of ψ's first-order reduced density operator), and they are therefore "best possible" (most rapidly convergent, in the mean-squared sense) for describing the electron density $\rho(\vec{r})$ of ψ. Compared to many other choices of orbitals that might be imagined or invented (i. e. the standard atomic orbital (AO) basis functions of electronic structure calculation packages), the natural orbitals are singled out by ψ itself as "natural" for its own description. An important fact that should be remarked is that natural orbitals (like the canonical molecular orbitals of Hartree Fock theory) are necessarily *symmetry adapted*. For instance, supposing that the quantum mechanical system of interest corresponds to two H atoms, A and B,

$$\psi_2 = \psi(H_A, H_B) \qquad \text{Equation 16A}$$

On physical grounds one might expect that the orbital description of ψ_2 is nearly identical to that for the corresponding localized wavefunctions

$$\psi_{1A} = \psi(H_A), \psi_{1B} = \psi(H_B) \qquad \text{Equation 17A}$$

However, due to the fact that ψ_2 must incorporate the superposition symmetry[308] between H_A, H_B (even if these atoms have no interactions of physical significance), the natural orbitals of ψ_2 will be found to differ *qualitatively* from those of ψ_{1A} or ψ_{1B}. This has the unfortunate consequence of making the orbitals look "more delocalized" (and less transferable) than is physically meaningful, obscuring many simplicities of chemical bonding. (Similar spurious mixings occur when the atoms are merely separated by a few links of an alkane chain.) Thus, the natural orbitals as

[306] a) M. Jeziorska, B. Jeziorski, J. Cizek, *Int. J. Quantum. Chem.* **1987**, *32*, 149–164; b) R. Moszynski, T. G. A. Heijmen, B. Jeriorski, *Mol. Phys.* **1996**, *88*, 741–758; c) P. v. R. Schleyer, Encyclopedia of Computational Chemistry, John Wiley & Sons, Chichester, **1998**.
[307] P.-O. Löwdin, *Phys. Rev.* **1955**, *97*, 1474–1489.
[308] F. Weinhold, *J. Chem. Ed.* **1999**, *76*, 1141–1146.

originally defined include bogus "delocalization effects" that have no physical significance.[309]

To remove spurious effects associated with symmetry adaptation, one can formulate[310] a *localized* criterion for orbitals that have the analogous maximum-occupancy (natural) character in localized 1-center and 2-center regions of the molecule. Because the maximum occupancy of an orbital is inherently limited to a pair of electrons[311] by the Pauli exclusion principle, local 1- and 2-center orbitals with occupancies sufficiently close to 2.000 can serve equally well as "true" natural orbitals for describing ψ. As anticipated by G. N. Lewis,[312] localized orbitals of near-double occupancy can be found in the 1- and 2-center regions suggested by the elementary Lewis structure diagram. Such *natural bond orbitals* (NBOs) provide the most accurate possible "natural Lewis structure" picture of ψ, because all orbital details (polarization coefficients, atomic hybrid compositions, etc.) are mathematically chosen to include the highest possible percentage of the electron density. This percentage (denoted %-ρ_L) gives an intrinsic measure of the accuracy of the natural Lewis structure picture, and is often found to be >99% for common organic molecules, dramatic testimony to the profound accuracy of Lewis's concept. The NBOs are one of a sequence of natural localized orbital sets that include natural atomic (NAO), hybrid (NHO), and (semi-)localized molecular orbital (NLMO) sets, intermediate between basis AOs and canonical molecular orbitals (MOs)

$$\text{AOs} \rightarrow \text{NAOs} \rightarrow \text{NHOs} \rightarrow \text{NBOs} \rightarrow \text{NLMOs} \rightarrow \text{MOs}$$

All these natural localized sets are complete and orthonormal, able to exactly describe any property of ψ. Compared to standard AOs, e.g., the NAOs give a much more condensed description of ψ, with only a small number of them (i.e., corresponding to the formal "minimal basis") having appreciable occupancy. Thus, a "minimal" description in terms of core and valence-shell NAOs is often found adequate for chemical purposes, providing a compact representation of ψ that is intimately related to standard valence concepts. The mutual orthogonality[313] of natural localized orbitals may seem to be a conceptual liability, inasmuch as the concept of "orbital overlap" seems to be lost. However, each orthogonal NAO (or NHO, NBO, etc.) can be uniquely associated with a corresponding "pre-orthogonal" PNAO (or PNHO, PNBO, etc.) which remains orthogonal to PNAOs on the same atom but has nonvanishing overlap integrals with those on other atoms. In accordance

[309] More precisely, the transformation from symmetry-adapted to non-symmetry-adapted form corresponds to a unitary transformation of orbitals that merely multiplies ψ by an overall phase factor, and hence has no effect on the energy, density, or other measurable properties.

[310] a) J. P. Foster, F. Weinhold, *J. Am. Chem. Soc.* **1980**, *102*, 7211–7218; b) A. E. Reed, L. A. Curtiss, F. Weinhold, *Chem. Rev.* **1988**, *88*, 899–926; c) F. Weinhold, *Natural Bond Orbital Methods*, in, P. v. R. Schleyer, *Encyclopedia of Computational Chemistry*, John Wiley & Sons, Chichester, **1998**, vol. 3, pp. 1792–1811.

[311] For open-shell systems, electrons of different spin generally occupy different spin-orbitals, and the occupancy limit of each spin-orbital is accordingly reduced to one.

[312] a) G. N. Lewis, *J. Am. Chem. Soc.* **1916**, *38*, 762–785; b) G. N. Lewis, *Valence and the structure of atoms and molecules*, The Chemical Catalog Co., New York, **1923**.

[313] Mutually orthogonality of a set of orbitals is an elementary prerequisite for associating the orbitals with a physical (Hermitian) operator as eigenfunctions. Overlapping orbitals therefore cannot be considered as eigenfunctions of any "system Hamiltonian" of physical significance.

with the Mulliken approximation,[278,314] the corresponding Hamiltonian interaction elements are found to be closely proportional to these overlap integrals. That is, if $\hat{F}$ denotes the effective orbital Hamiltonian (Fock or Kohn-Sham operator), the interaction strength <hA|$\hat{F}$|hB> of bonding NHOs h_A, h_B can be approximated in terms of overlapping PNHOs $\tilde{h}_A, \tilde{h}_B$ as

$$< h_A \mid \hat{F} \mid h_B > \cong k < \tilde{h}_A \mid \tilde{h}_B > \qquad \text{Equation 18A}$$

where *k* is a proportionality constant of order unity. In accordance with the simple bond orbital picture[315] each bonding NBO σ_{AB} can be written in terms of two directed valence hybrids (NHOs) h_A, h_B on atoms A and B, with corresponding polarization coefficients c_A, c_B,

$$\sigma_{AB} = C_A H_A + C_B H_B \qquad \text{Equation 19A}$$

that vary smoothly from covalent ($c_A = c_B$) to ionic ($c_A >> c_B$) limit. Each valence bonding NBO (Equation 22A) must in turn be paired with a corresponding valence *anti*bonding NBO

$$\sigma_{AB}{}^* = C_B h_A - c_A h_B \qquad \text{Equation 20A}$$

to complete the span of the valence space. The "Lewis"-type (donor) NBOs (22A) are thereby complemented by the "non-Lewis"-type (acceptor) NBOs (23A) that are formally empty in an idealized Lewis structure picture. Weak occupancies of the valence antibonds (23A) signal irreducible departures from an idealized localized Lewis structure picture, i.e., true "delocalization effects." The energetic stabilization due to such $\sigma \rightarrow \sigma^*$ donor acceptor interactions can be estimated by 2nd-order perturbation theory, viz., for the $\sigma_i \rightarrow \sigma_j^*$ interaction,

$$\Delta E^{(2)}_{i \rightarrow j^*} = -2 \frac{\left\langle \sigma_i \mid \hat{F} \mid \sigma_j^* \right\rangle^2}{\varepsilon_{j^*} - \varepsilon_i} \qquad \text{Equation 21A}$$

where $\hat{F}$ is the effective orbital Hamiltonian (Fock or Kohn-Sham operator) and $\varepsilon_i = \left\langle \sigma_i \mid \hat{F} \mid \sigma_i \right\rangle$, $\varepsilon_{j^*} = < \sigma_j^* \mid \hat{F} \mid \sigma_j^* >$ are the respective orbital energies of donor and acceptor NBOs. Consideration of valence antibonds (23A) therefore leads to far-reaching extension of elementary Lewis structure concepts to encompass leading delocalization corrections in simple NBO perturbative estimates such as Equation 24A.

As a result of each $\sigma_i \rightarrow \sigma_j^*$ perturbation, the starting NBO acquires a weak antibonding "tail" in the final (doubly occupied) NLMO Ω_i. More generally, each semilocalized NLMO Ω_i can be expressed as a linear combination of the parent

[314] a) R. S. Mulliken, *J. Chem. Phys.* **1944**, *46*, 497; b) J. Hinze, H. H. Jaffe, *J. Am. Chem. Soc.* **1962**, *84*, 540–546.
[315] R. S. Mulliken, *J. Chem. Phys.* **1935**, *3*, 573–585.

Lewis-type NBO σ_i (with coefficient $c_{ii} \cong 1$) and residual weak contributions ($c_{ji} \cong 0$) from non-Lewis (NL) NBOs σ_j^*

$$\Omega_i = c_{ii}\sigma_i + \sum_j^{NL} c_{ji}\sigma_j^* \qquad \text{Equation 22A}$$

that reflect the irreducible physical effect of $\sigma_i \rightarrow \sigma_j^*$ delocalizations. Despite the compact, recognizable forms of NLMOs and their close connection to chemical structure concepts, it is important to recognize that a Slater determinant of doubly occupied NLMOs is *equivalent* to the usual MO wavefunction. Hence, the simplicity of NBO-based expansions such as (25A) is achieved with *no* loss of accuracy in the description of ψ.

A.I.10. Atomic Charges

The charge assigned over the atoms has been a valuable tool for chemists, despite the idea that the atomic charge in a molecule is not really an observable chemical quantity. The atomic charges have been a key concept in the understanding of many types of chemical reactions, and are of great importance in the interpretation of numerous phenomena such as the dipolar moment or chemical shift in NMR. Moreover, they are important parameters in structure-property and structure-activity relations. A lot of schemes have been proposed, both quantum-chemical and empirical, either to assign the electron density distribution between the atoms of a molecule or charges of these atoms. Traditionally, the Mulliken method[316,317] and electrostatic potential have been the most useful in defining atomic charges.

The methods based on the population analysis distribute the electronic density between nuclei, so that every atom has a specific number of electrons (not necessarily integer) associated to it. This partition provides a way to calculate the atomic charge over every nucleus. Nevertheless, no quantum-mechanics operator exists for the atomic charge and the partition scheme is arbitrary.

The Mulliken's population analysis[316,317] is a trivial calculation once it has been reached the consistency in the Self Consistent Field (SCF) that the electronic population needs in every orbital ($P_{\mu\mu}$) and in the overlapping area ($S_{\mu\nu}$), as shown in Equation 23A for the atomic charge over atom A:

$$q_A = Z_A - \sum_{\mu=1}^{K} P_{\mu\mu} - \sum_{\omega=1}^{K} \sum_{\theta=1,\theta\neq\mu}^{K} P_{\mu\theta} S_{\mu\theta} \qquad \text{Equation 23A}$$

Thus, the atomic charge is estimated by subtracting the electronic population in each of the orbitals of the atom from the nuclear charge and the overlapping population is divided equally between the two atoms, regardless differences in the type of atom (coefficient, electronegativity, etc). The Mulliken's population analysis

316 R. S. Mulliken, *J. Chem. Phys.* **1955**, *23*, 1833–1840.
317 R. S. Mulliken, *J. Chem. Phys.* **1962**, *36*, 3428–3439.

is widely used due to its simplicity; however it presents a great dependency upon the basis set used.[318,319]

The electrostatic potential methods determine atomic charges fitting the electrostatic potential to a series of points surrounding the molecule. These points can be chosen in multiple ways, but they should be in a region where it is more important to define the molecular interactions correctly, that is to say below the van der Waals radii of the atoms. Once the electrostatic potential has been calculated (Equation 12A) at these points, by means of mathematical adjustment, the partial atomic charges that best reproduced the potential are derived. This procedure is done through the least-squares fit, that is normally combined with Lagrange multiplier as described in the literature.[320] Related to this, the Merz-Kollman scheme[321] uses the Connolly algorithm[322] to generate five spherical surfaces of points around every atom. These surfaces are found at distances of 1.4, 1.6, 1.8 and 2.0 times the van der Waals atomic radius, all with a density of 1 point/Å^2. The molecular surface is built taking into account the union of all these surfaces for every atom and eliminating the points that are within of multipole of van de Waals radius of any atom.

[318] P. Politzer, R. S. Mulliken, *J. Chem. Phys.* **1971**, *55*, 5135–5137.
[319] D. L. Grier, A. Streitwieser, *J. Am. Chem. Soc.* **1982**, *104*, 3556–3564.
[320] K. B. Wiberg, P. R. Rablen, *J. Comput. Chem.* **1993**, *14*, 1504–1518.
[321] B. H. Besler, K. M. Merz, P. A. Kollman, *J. Comput. Chem.* **1990**, *11*, 431–439.
[322] L. E. Chirlian, M. M. Francl, *J. Comput. Chem.* **1987**, *8*, 894–905.

A.I.11. References

[272] D. B. Cook, *Handbook of Computational Quantum Chemistry*, Oxford University Press, Oxford, **1998**.

[273] A. Szabo; N. S. Ostlund, *Modern Quantum Chemistry*, McGraw-Hill, New York, **1989**.

[274] C. J. Cramer, *Essentials of Computational Chemistry: Theories and Models*, Wiley, **2004**.

[275] E. Huckel, *Z. Phys. Chem.* **1930**, *60*, 423–456.

[276] E. Huckel, *Z. Phys. Chem.* **1931**, *70*, 204–286.

[277] E. Huckel, *Z. Phys. Chem.* **1932**, *76*, 628–648.

[278] R. Hoffmann, *J. Chem. Phys.* **1963**, *39*, 1397–1412.

[279] E. Schrodinger, *Phys. Rev.* **1926**, *28*, 1049–1070.

[280] C. Moller, M. S. Plesset, *Phys. Rev.* **1934**, *46*, 0618–0622.

[281] M. Feyereisen, G. Fitzgerald, A. Komornicki, *Chem. Phys. Lett.* **1993**, *208*, 359–363.

[282] O. Vahtras, J. Almlof, M. W. Feyereisen, *Chem. Phys. Lett.* **1993**, *213*, 514–518.

[283] R. G. Parr; W. Yang, *Density Functional Theory of Atoms and Molecules*, Oxford University Press, New York, **1989**.

[284] P. Hohenberg, W. Kohn, *Phys. Rev. B* **1964**, *136*, B864–B871.

[285] W. Kohn, L. J. Sham, *Phys. Rev.* **1965**, *140*, 1133–1138.

[286] J. P. Perdew, A. Ruzsinszky, L. A. Constantin, J. W. Sun, G. I. Csonka, *J. Chem. Theory Comput.* **2009**, *5*, 902–908.

[287] D. M. Ceperley, B. J. Alder, *Phys. Rev. Lett.* **1980**, *45*, 566–569.

[288] J. P. Perdew, *Phys. Rev. B* **1986**, *33*, 8822–8824.

[289] J. P. Perdew, K. Burke, M. Ernzerhof, *Phys. Rev. Lett.* **1996**, *77*, 3865–3868.

[290] A. D. Becke, *Phys. Rev. A* **1988**, *38*, 3098–3100.

[291] P. Hobza, J. Sponer, T. Reschel, *J. Comput. Chem.* **1995**, *16*, 1315–1325.

[292] X. Y. Ye, Z. H. Li, W. N. Wang, K. N. Fan, W. Xu, Z. Y. Hua, *Chem. Phys. Lett.* **2004**, *397*, 56–61.

[293] P. J. Stephens, F. J. Devlin, C. F. Chabalowski, M. J. Frisch, *J. Phys. Chem.* **1994**, *98*, 11623–11627.

[294] A. D. Becke, *J. Chem. Phys.* **1993**, *98*, 1372–1377.

[295] A. D. Becke, *J. Chem. Phys.* **1993**, *98*, 5648–5652.

[296] A. D. Becke, *J. Chem. Phys.* **1996**, *104*, 1040–1046.

[297] C. T. Lee, W. T. Yang, R. G. Parr, *Phys. Rev. B* **1988**, *37*, 785–789.
[298] a) Y. Zhao, D. G. Truhlar, *Theor. Chem. Acc.* **2008**, *120*, 215–241; b) Y. Zhao, D. G. Truhlar, *J. Phys. Chem. A* **2006**, *110*, 13126–13130; c) Y. Zhao, D. G. Truhlar, J. *Chem. Phys.* **2006**, *125*, 194101.

[299] D. Feller; E. R. Davidson, *Rev. Comput. Chem.* **1990**, *1*, 1.

[300] A. Schafer, H. Horn, R. Ahlrichs, *J. Chem. Phys.* **1992**, *97*, 2571–2577.

[301] E. Scrocco; J. Tomasi, *Top. Curr. Chem.* **1973**, *42*, 95–170.

[302] R. P. Feynman, *Phys. Rev.* **1939**, *56*, 340–343.

[303] S. Srebrenik, R. F. W. Bader, *J. Chem. Phys*. **1975**, *63*, 3945–3961.

[304] H. Hopf, *Math. Ann.* **1927**, *96*, 225–250.

[305] B. Jeziorski, R. Moszynski, K. Szalewicz, *Chem. Rev.* **1994**, *94*, 1887–1930.

[306] a) M. Jeziorska, B. Jeziorski, J. Cizek, *Int. J. Quantum. Chem.* **1987**, *32*, 149–164; b) R. Moszynski, T. G. A. Heijmen, B. Jeriorski, *Mol. Phys.* **1996**, *88*, 741–758; c) P. v. R. Schleyer, Encyclopedia of Computational Chemistry, John Wiley & Sons, Chichester, **1998**.

[307] P.-O. Löwdin, *Phys. Rev.* **1955**, *97*, 1474–1489.

[308] F. Weinhold, *J. Chem. Ed.* **1999**, *76*, 1141–1146.

[309] More precisely, the transformation from symmetry-adapted to non-symmetry-adapted form corresponds to a unitary transformation of orbitals that merely multiplies ψ by an overall phase factor, and hence has no effect on the energy, density, or other measurable properties.

[310] a) J. P. Foster, F. Weinhold, *J. Am. Chem. Soc.* **1980**, *102*, 7211–7218; b) A. E. Reed, L. A. Curtiss, F. Weinhold, *Chem. Rev.* **1988**, *88*, 899–926; c) F. Weinhold, *Natural Bond Orbital Methods*, in, P. v. R. Schleyer, *Encyclopedia of Computational Chemistry*, John Wiley & Sons, Chichester, **1998**, vol. 3, pp. 1792–1811.

[311] For open-shell systems, electrons of different spin generally occupy different spin-orbitals, and the occupancy limit of each spin-orbital is accordingly reduced to one.

[312] a) G. N. Lewis, *J. Am. Chem. Soc.* **1916**, *38*, 762–785; b) G. N. Lewis, *Valence and the structure of atoms and molecules*, The Chemical Catalog Co., New York, **1923**.

[313] Mutually orthogonality of a set of orbitals is an elementary prerequisite for associating the orbitals with a physical (Hermitian) operator as eigenfunctions. Overlapping orbitals therefore cannot be considered as eigenfunctions of any "system Hamiltonian" of physical significance.

[314] a) R. S. Mulliken, *J. Chem. Phys.* **1944**, *46*, 497; b) J. Hinze, H. H. Jaffe, *J. Am. Chem. Soc.* **1962**, *84*, 540–546.

[315] R. S. Mulliken, *J. Chem. Phys.* **1935**, *3*, 573–585.

[316] R. S. Mulliken, *J. Chem. Phys.* **1955**, *23*, 1833–1840.

[317] R. S. Mulliken, *J. Chem. Phys.* **1962**, *36*, 3428–3439.

[318] P. Politzer, R. S. Mulliken, *J. Chem. Phys.* **1971**, *55*, 5135–5137.

[319] D. L. Grier, A. Streitwieser, *J. Am. Chem. Soc.* **1982**, *104*, 3556–3564.

[320] K. B. Wiberg, P. R. Rablen, *J. Comput. Chem.* **1993**, *14*, 1504–1518.

[321] B. H. Besler, K. M. Merz, P. A. Kollman, *J. Comput. Chem.* **1990**, *11*, 431–439.

[322] L. E. Chirlian, M. M. Francl, *J. Comput. Chem.* **1987**, *8*, 894–905.

Annex II

Published articles

Angewandte International Edition Chemie

Supramolecular Chemistry

DOI: 10.1002/anie.201306501

Tetrel-Bonding Interaction: Rediscovered Supramolecular Force?**

*Antonio Bauzá, Tiddo J. Mooibroek, and Antonio Frontera**

Noncovalent bonding interactions are crucial in many chemical and biological phenomena and they have been intensively investigated for many years.[1] The hydrogen bond (AH···D) is probably the most studied and analyzed noncovalent interaction, where A (acceptor) can be basically any atom more electronegative than H and D (donor) can be any entity with the ability to act as an electron donor (lone pair, π system, anion, etc.).[2] Among many interactions, those involving halogen, chalcogen, and pnictogen atoms have attracted considerable attention in recent years and they are increasingly being recognized by scientists and used in supramolecular chemistry, crystal engineering, and biochemistry.[3] These interactions are moderately strong and directional because of the localization of a positive region on the extension of the covalent bonds (σ hole) in the acceptor molecule. This class of interactions has been also observed for the group IV elements. For instance, Si···N contacts have been described in the solid-state structure of $Si(ONMe_2)_4$ and related compounds by Mitzel et al.,[4,5] and Si···halide contacts have been described in perhalocyclohexasilane compounds.[6] Moreover, group IV interactions have been recently included as a subgroup of a general definition of σ-hole-bonding interactions by Politzer and co-workers.[7]

Herein we coin the term tetrel bonding for describing the tendency of heavier tetrel atoms (Tr) to interact with anions or lone-pair-possessing atoms (group IV elements are also referred to as tetrels). The binding features and structural properties of tetrel bonding are discussed, several fascinating X-ray structures are selected to illustrate the importance of this interaction, and a survey of the Cambridge Structure Database (CSD) suggests that the tetrel bonding is common in X-ray structures. The tetrel bonding is expected to be an effective and reliable instrument in crystal engineering, supramolecular chemistry, biochemistry, etc. As far as our knowledge extends, this term has not been used before to describe this interaction, which has been scarcely studied in the literature.

[*] A. Bauzá, Prof. A. Frontera
Departament de Química, Universitat de les Illes Balears
Crta. de Valldemossa km 7.5, 07122 Palma, Baleares (Spain)
E-mail: toni.frontera@uib.es
Dr. T. J. Mooibroek
School of Chemistry, University of Bristol
Cantock's Close, Bristol (UK)

[**] This work was funded by the MINECO of Spain (CONSOLIDER-Ingenio 2010 project CSD2010-0065, and project CTQ2011-27512, FEDER funds) and the Govern Balear (project 23/2011, FEDER funds). T.J.M. acknowledges the School of Chemistry of the University of Bristol (UK).

Supporting information for this article is available on the WWW under http://dx.doi.org/10.1002/anie.201306501.

Recently, Taylor et al.[8] reported that the synthesis of spherosilicates is significantly improved using *n*-butylammonium fluoride (TBAF) as a catalyst. Interestingly, during the reaction work-up a new class of cage compound was obtained showing a fluoride ion perfectly centered within the octasilsesquioxane cage (see Figure 1).[9] Using NMR data the

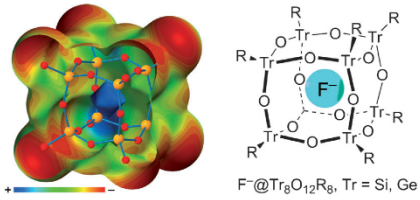

Figure 1. Right: A F^- ion encapsulated inside a $Tr_8O_{12}R_8$ cage. Left: MEPS of $SiO_{12}(OH)_8$ cage.

authors conclude that it essentially resembles a naked uncoordinated fluoride ion. These fluoride-encapsulated octasilsesquioxane cages can be used as small models for studying the environment that exists in zeolites. It is well known that fluoride anions act as templates in zeolite synthesis and also acts as a stabilizing agent for the zeolite building unit by electron-density transfer into the framework of silicon atoms.[10,11] This type of encapsulated compounds has been also reported for germanium-based T8 cages.[12]

We have computed the interaction energies of fluoride complexes with $Tr_8O_{12}(OH)_8$ cages (Tr = Si, Ge, and Sn; see the Supporting Information for computational details). It can be observed that the binding energies are very large and negative, thus indicating a strong interaction. Consistent with related σ-hole-based interactions, the binding energy becomes more favorable toward the heavier tetrels. Since the fluoride establishes eight tetrel bonding interactions simultaneously the charge transfer is very large (>50% of the charge). In terms of energetic features, each individual $F^-\cdots Tr$ interaction ranges from 11 to 15 kcal mol^{-1}. The optimized Si and Ge complexes are shown in Figure 2 and the related X-ray structures retrieved from the CSD are also shown for comparison purposes. The energetic results gathered in Table 1 are in disagreement with experimental results, and suggests that the interaction of F^- with the Si atoms is almost negligible. This conclusion is based on the fact that fluoride ion makes very little difference to the structure. That is, the mean separation between the silicon atoms on opposite vertices of the cube is only slightly shorter in the fluoride encapsulated cage (5.306 Å) than that in the free structure (5.381 Å), and the Si···F separation in these types of fluoride cages is about 2.65 Å, which is much longer than that of a full

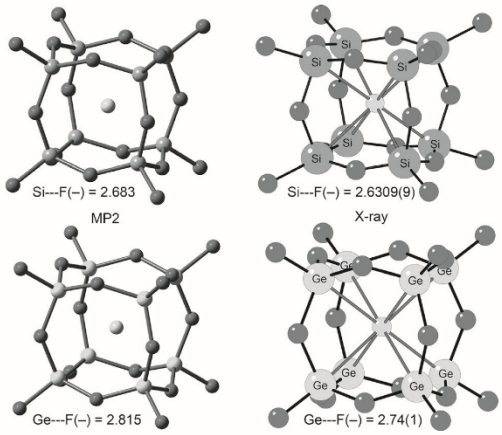

Figure 2. RI-MP2/aug-cc-pVDZ $F^-@Tr_8O_{12}(OH)_8$ optimized complexes and the equivalent X-ray structures. Distances in Å.

Table 1: Interaction energies without and with the basis set superposition error (ΔE and ΔE_{CP}, respectively), and equilibrium distances (R_e) for $F^-@Tr_8O_{12}(OH)_8$ complexes at the RI-MP2/aug-cc-pVDZ level of theory.

Complex	ΔE [kcal mol^{-1}]	ΔE_{CP} [kcal mol^{-1}]	$\Delta E_{CP}/8$ [kcal mol^{-1}]	R_e [Å]
$F^-@Si_8O_{12}(OH)_8$	−98.0	−89.3	−11.2	2.683
$F^-@Ge_8O_{12}(OH)_8$	−116.8	−108.9	−13.6	2.815
$F^-@Sn_8O_{12}(OH)_8$	−124.8	−119.1	−14.8	3.113

Si–F covalent bond (1.709 Å). This assessment is certainly true in terms of covalent bonding (the absence of any measurable Si–F coupling has been used to confirm the low degree of silicon–fluoride interaction). However, in terms of noncovalent bonding, the reported changes on the ^{29}Si and ^{19}F NMR spectra along with structural changes (the Si atoms approximate to the F^- upon binding) are in agreement with a moderately strong noncovalent interaction, as those observed in Table 1. Moreover, the molecular electrostatic potential surface (MEPS) mapped onto the van der Waals surface shows a small region of positive potential in the center of the cage (see Figure 1).

An interesting experimental finding that nicely illustrates the importance of noncovalent tetrel-bonding interactions is the formation of a crystalline chloride-bridged disiloxane.[13] The X-ray structure is shown in Figure 3 (QOMBID, top) and the bifurcated tetrel bond was defined by the original authors as a dative bond to each of the silicon centers. This is confirmed by reference to the Si-Cl distances, 2.887 and 2.731 Å, respectively, which are both substantially longer than normal covalent Si–Cl bonds (2.05 ± 0.03 Å)[13] and significantly shorter than the sum of the corresponding van der Waals radii. Furthermore, in Figure 3 (bottom) we show the X-ray structures of two binuclear pentacoordinate silicon complexes of diketopiperazine. By means of variable-temperature NMR spectroscopy and X-ray crystallography experiments the S_N2 reaction mechanism has been studied for five differently substituted analogous structures (X = F, Cl, OTf, Br, and I).[14] Two extreme cases are shown in Figure 3, wherein a covalent bond (F-Si, OYOMIZ) is observed for a very poor leaving group (F^-) and a tetrel bond (I···Si, OYOMOZ) is clearly formed for a good leaving group (I^-).

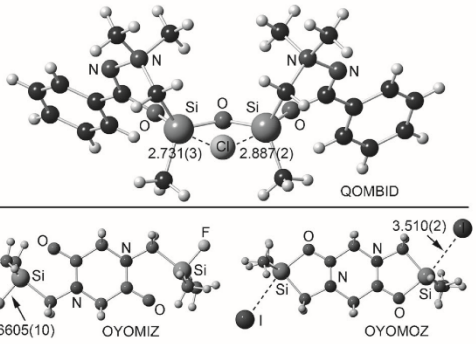

Figure 3. X-ray fragments of CSD structures QOMBID, OYOMIZ, and OYOMOZ. Distances in Å.

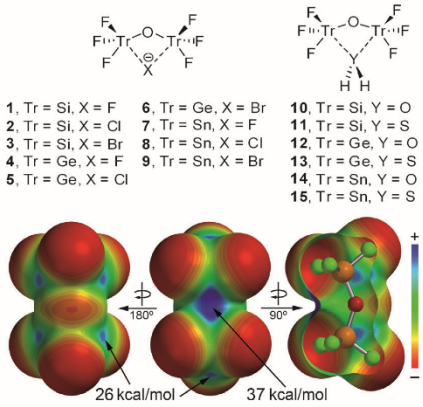

Figure 4. Top: complexes **1**–**15**. Bottom: MEPS of the $F_3Tr\text{-}O\text{-}TrF_3$ molecules.

We have studied computationally the tetrel-bonded complexes of perfluorodisiloxane, as a theoretical model of the experimental structure described above (QOMBID, see Figure 3), with halides. In addition we have extended our study to perfluorodigermoxane and perfluorodistannoxane to analyze the influence of the tetrel atom on the interaction strength. In addition to the anionic donors (F^-, Cl^-, and Br^-) we have also included in the study neutral donor molecules (H_2O and H_2S), as represented in Figure 4 (top). Previous to the optimization of the complexes we calculated the MEP surfaces of the $F_3Tr\text{-}O\text{-}TrF_3$ (Tr = Si, Ge, and Sn) molecules. The three surfaces are very similar and we have only represented the one obtained for $F_3Si\text{-}O\text{-}SiF_3$ in Figure 4

(bottom). The presence of four equivalent σ holes at one side of the molecule (Figure 4, bottom left) and two σ holes at both ends of the molecule (Figure 4, bottom middle) can be observed. These six σ holes are almost isoenergetic. The most positive part of the MEPS is found opposite to the four equivalent σ holes as a consequence of the superposition of two σ holes along the bisectrix of the Si-O-Si angle (obtuse part). The MEP value at this point is 37 kcal mol^{-1} for Si, 41 kcal mol^{-1} for Ge, and 45 kcal mol^{-1} for Sn. Therefore the σ hole becomes more positive toward the heavier tetrels.

The binding energies and equilibrium distances for the anionic complexes **1–9** are gathered in Table 2. The energies are very large in fluoride complexes because of the partial covalent bond as suggested by the very short equilibrium distances. The energetic features of complexes involving Cl^- and Br^- are more modest and comparable to the explanation given above for the $Tr_8O_{12}(OH)_8$ cages. As predicted by the MEPS, the energies are more favorable for the heavier tetrels and the charge transfer is very important (47–66%). It is interesting to note the variation of the Tr-O-Tr angle, which increases upon going from fluoride to bromide and decreases upon going from Si to Sn to facilitate the simultaneous interaction with both tetrel atoms. The strong interaction energies observed for F^- complexes suggest that the observation of this interaction in solution would be difficult for this anion (S_N2 reaction will likely occur), however it would be possible for the higher halides.

Table 2: Interaction energies without and with the BSSE (ΔE and ΔE_{CP}, respectively), equilibrium distances (R_e), Tr-O-Tr angle, and Merz–Kollman charges (Q_{MK}) for the complexes **1–9** at the RI-MP2/aug-cc-pVDZ level of theory.

Complex	ΔE [kcal mol^{-1}]	ΔE_{CP} [kcal mol^{-1}]	R_e [Å]	∡Tr-O-Tr [°]	Q_{MK} [e]
1	−89.7	−83.6	1.917	109.6	−0.43
2	−38.9	−34.0	2.497	125.0	−0.45
3	−28.9	−24.0	2.726	130.1	−0.49
4	−103.9	−96.5	1.994	108.3	−0.48
5	−57.6	−51.5	2.490	119.3	−0.40
6	−47.7	−41.7	2.662	122.3	−0.38
7	−121.0	−115.7	2.147	108.0	−0.53
8	−80.6	−75.4	2.621	117.0	−0.40
9	−72.2	−66.8	2.774	119.3	−0.34

The binding energies and equilibrium distances for the neutral complexes **10–15** are summarized in Table 3. The energies are obviously less favorable than those computed for the anionic complexes because of the different electrostatic nature of the donor atom. The equilibrium distances are longer, and consequently the Tr-O-Tr angle considerably increases with respect to the anionic complexes to facilitate the interaction of the lone pairs of the O/S atoms with the σ holes. The interaction energies of the water complexes are considerably more favorable than the H_2S ones and the equilibrium distances shorter, all of which is in line with the higher basicity of the oxygen atom. The geometries of some representative complexes are shown in Figure 5. In all complexes the $X^-\cdots$Tr-F angle is close to 180°, thus indicating that the interaction is highly directional, which is similar to a halogen-bonding interaction.

Table 3: Interaction energies without and with the BSSE (ΔE and ΔE_{CP}, respectively), equilibrium distances (R_e), and Tr-O-Tr angle for the complexes **10–15** at the RI-MP2/aug-cc-pVDZ level of theory.

Complex	ΔE [kcal mol^{-1}]	ΔE_{CP} [kcal mol^{-1}]	R_e [Å]	∡Tr-O-Tr [°]
10	−9.3	−6.2	2.740	140.5
11	−2.8	−1.1	3.748	147.5
12	−15.2	−9.9	2.487	127.2
13	−3.3	−1.2	3.647	136.8
14	−24.3	−19.1	2.521	121.4
15	−8.3	−4.6	3.159	135.2

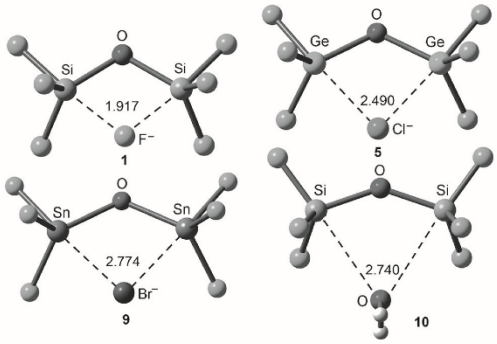

Figure 5. RI-MP2/aug-cc-pVDZ optimized geometries of some representative F_3Tr-O-TrF_3 complexes. Distances in Å.

Finally, we would like to highlight the solid-state structure of tetramethylammonium fluoride octadecasil as it has been elucidated based on powder X-ray diffraction data.[15] The topology is defined by rhombododecahedral [$4^6 6^{12}$] cages, which are linked together by hexahedral [4^6] cages, commonly referred to as double 4-rings (D4R; Figure 6). Interestingly, the octadecasil structure is acting as a ditopic carcerand, wherein the fluoride guest is confined within the D4R unit, thus forming eight tetrel bonds, and the counterion is located

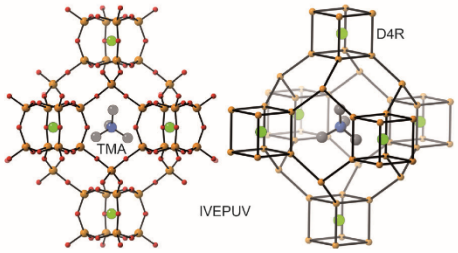

Figure 6. Partial view of the X-ray structure of TMA^+F^--octadecasil, showing D4R units with the guest fluoride, and the [$4^6 6^{12}$] cage with tetramethylammonium ion. For clarity, the oxygen atoms have been omitted in the representation shown in the right.

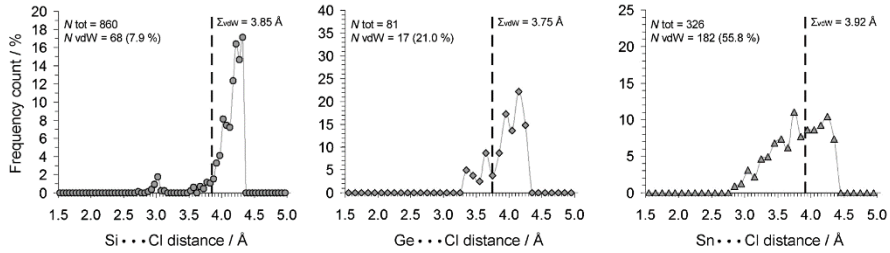

Figure 7. Plots of the frequency count [%] as a function of the $R_3Tr\cdots Cl$ distance [Å] for Tr = Si (a), Ge (b), and Sn (c). The solid lines are added as a guide to the eye and the vertical dashed lines indicate the sum of the van der Waals radii of Tr and Cl. The inset numbers represent the total amount of data (N_{tot}) and the absolute and relative mount of data displaying van der Waals overlap.

in the interior of the rhombododecahedral cages, thus forming a large number of C–H···O interactions. The oxygen atoms of the D4R units are pointing toward the exterior of the cage and concurrently toward the interior of the $[4^66^{12}]$ cage, thereby facilitating both tetrel-bonding interactions in the former and the hydrogen-bonding interactions in the latter.

The Cambridge Structure Database was inspected to assess whether tetrel bonding could be a generally occurring interaction within crystal structures (see the Supporting Information for details). Table 3 lists some numerical data of intermolecular distances (d) between a tetravalent tetrel atom (Tr = Si, Ge, Sn) and an electron-rich atom (El.R. = O^0, F, Cl, Br, I) where $d = \Sigma_{vdWaals\,|\,0.5}$ Å. The amount of data where overlap of van der Waals shells was observed is listed separately and, for comparison, also expressed as percentage of the total amount of data. The fraction of van der Waals overlap seems to increase on the order of Si < Ge < Sn and O ≤ F < Cl ≤ Br < I. The data for $R_4Si\cdots F$ seems to be an exception and manual inspection of the data revealed that about $^1/_3$ of the cases of van der Waals overlap are found within (engineered) cage structures such as the one shown in Figure 1.[16] As a typical example, Figure 7 shows plots of the frequency count versus the intermolecular $R_4Tr\cdots Cl$ distance (comparable plots for the rest of the data given in Table 4 can be found in the Supporting Information and reveal similar features).

For the distances involving $R_4Si\cdots Cl$ (Figure 7, left), the majority of the data is found to be above the $\Sigma_{vdWaals}$ benchmark, yet a small peak centered around 3 Å is observed. Such peaks are also present for the other halides as the interacting atom (not for oxygen; see the Supporting Information). These Si···Hlg data are about 0.8 Å within the sum of the van der Waals radii of the elements involved. This means that these interactions are very significant, yet not as strong as a conventional Si-Hlg bond ($\Sigma_{vdWaals}$-Si-Hlg < 1.76 Å). Such peaks were not found for $R_4Ge\cdots Cl$ (center) and $R_4Sn\cdots Cl$ (Figure 7, right), but the relative amount of overlap of van der Waals shells clearly increases on the order of Si < Ge < Sn. For $R_4Sn\cdots Cl$, more than half of the data actually is found within the $\Sigma_{vdWaals}$ benchmark (3.92 Å) and a number of short distances are found around 3 Å.

The CSD data presented above clearly suggests that noncovalent interactions with the tetravalent tetrel entities investigated are rather common within the CSD (16% of all the data involve overlap of van der Waals shells). It must be stressed that the majority of these data are mere accidental occurrences rather than engineered. Actually, the very short (and relatively rare) Tr···El.R. distances highlighted in this paper imply that the strength of tetrel bonding can be significantly tweaked. Clearly this phenomenon presents an opportunity for (supramolecular) chemists to further explore the potential of this novel interaction.

Table 4: Numerical overview of data retrieved from the Cambridge Stucture Database involving tetravalent tetrel atoms and a charge-neutral oxygen or halogen atom.

	R_4Si		R_4Ge		R_4Sn	
El.R	N_{tot}[a]	N_{vdW}[b]	N_{tot}[a]	N_{vdW}[b]	N_{tot}[a]	N_{vdW}[b]
O^0	3449	118 (5.5%)	626	177 (28%)	678	293 (43%)
F	1030	143 (14%)	48	2 (4.2%)	109	35 (32%)
Cl	860	68 (7.9%)	81	17 (21%)	326	182 (56%)
Br	151	16 (11%)	8	3 (38%)	45	50 (44%)
I	102	28 (28%)	9	4 (44%)	25	16 (64%)

[a] Number of data with intermolecular distances less than or equal to the sum of the van der Waals radii of Tr – El.R. [b] Number of data with intermolecular distances less than or equal to the sum of the van der Waals radii of Tr + El.R. – 0.5 Å. Value within parentheses is the percentage of the van der Waals overlap (N_{vdW}/N_{tot}) × 100.

In conclusion, we propose the use of tetrel bonding to refer to the noncovalent interaction between tetrel atoms acting as Lewis acids and any entity with the ability to act as an electron donor (lone pair, anion, etc.). Tetrel bonds have, as a minimum, comparable strength to hydrogen bonds and other σ-hole-based interactions, they are highly directional, and might serve as a new possible molecular linker. The tetrel-bonding interaction is expected to be involved in new effective and reliable instruments for crystal engineering, supramolecular chemistry, and catalysis.

Received: July 25, 2013
Revised: August 29, 2013
Published online: October 2, 2013

Keywords: ab initio calculations · group 14 elements · noncovalent interactions · silicon · supramolecular chemistry

[1] a) *Encyclopedia of Supramolecular Chemistry* (Eds.: J. L. Atwood, J. W. Steed), Marcel Dekker, New York, **2004**; b) K. Ariga, T. Kunitake in *Supramolecular Chemistry—Fundamentals and Applications*, Springer, Heidelberg, **2006**; c) *Supramolecular Chemistry: From Molecules to Nanomaterials* (Eds.: P. Gale, J. Steed), Wiley, Chichester, **2012**.

[2] E. Arunan, G. R. Desiraju, R. A. Klein, J. Sadlej, S. Scheiner, I. Alkorta, D. C. Clary, R. H. Crabtree, J. J. Dannenberg, P. Hobza, H. G. Kjaergaard, A. C. Legon, B. Mennucci, D. J. Nesbitt, *Pure Appl. Chem.* **2011**, *83*, 1619–1636.

[3] a) A. Priimagi, G. Cavallo, P. Metrangolo, G. Resnati, *Acc. Chem. Res.* **2013**, DOI: 10.1021/ar400103r; b) S. Scheiner, *Acc. Chem. Res.* **2013**, *46*, 280–288; c) S. Zahn, R. Frank, E. Hey-Hawkins, B. Kirchner, *Chem. Eur. J.* **2011**, *17*, 6034–6038.

[4] N. W. Mitzel, U. Losehand, *Angew. Chem.* **1997**, *109*, 2897–2899; *Angew. Chem. Int. Ed. Engl.* **1997**, *36*, 2807–2809.

[5] N. W. Mitzel, A. J. Blake, D. W. H. Rankin, *J. Am. Chem. Soc.* **1997**, *119*, 4143–4148.

[6] S.-B. Choi, B.-K. Kim, P. Boudjouk, D. G. Grier, *J. Am. Chem. Soc.* **2001**, *123*, 8117–8118.

[7] P. Politzer, J. S. Murray, T. Clark, *Phys. Chem. Chem. Phys.* **2013**, *15*, 11178–11189.

[8] P. G. Taylor, A. R. Bassindale, Y. El Aziz, M. Pourny, R. Stevenson, M. B. Hursthouse, S. J. Coles, *Dalton Trans.* **2012**, *41*, 2048–2059.

[9] A. R. Bassindale, M. Pourny, P. G. Taylor, M. B. Hursthouse, M. E. Light, *Angew. Chem.* **2003**, *115*, 3612–3614; *Angew. Chem. Int. Ed.* **2003**, *42*, 3488–3490.

[10] G. van de Goor, C. Freyhardt, P. Behrens, *Z. Anorg. Allg. Chem.* **1995**, *621*, 311–322.

[11] P. Caullet, J. L. Guth, J. Hazm, J. M. Lamblin, H. Gies, *Eur. J. Solid State Inorg. Chem.* **1991**, *28*, 345–361.

[12] L. A. Villaescusa, P. Lightfoot, R. E. Morris, *Chem. Commun.* **2002**, 2220–2221.

[13] I. Kalikhman, O. Girshberg, L. Lameyer, D. Stalke, D. Kost, *J. Am. Chem. Soc.* **2001**, *123*, 4709–4716.

[14] S. Muhammad, A. R. Bassindale, P. G. Taylor, L. Male, S. J. Coles, M. B. Hursthouse, *Organometallics* **2011**, *30*, 564–571.

[15] X. Yang, *Mater. Res. Bull.* **2006**, *41*, 54–66.

[16] See CSD refcodes BIDFIE, BIDFOK, CANCUR, IVEPUV, OJUYIB, WAVYAV, WAVYEZ, WAVYID, WAVYOJ, and WIJPUB.

ChemComm

COMMUNICATION

View Article Online
View Journal | View Issue

Cite this: *Chem. Commun.*, 2014, 50, 12626

Received 20th July 2014,
Accepted 1st September 2014

DOI: 10.1039/c4cc05602g

www.rsc.org/chemcomm

Non-covalent sp^3 carbon bonding with $ArCF_3$ is analogous to CH–π interactions†

Antonio Bauzá,[a] Tiddo J. Mooibroek*[b] and Antonio Frontera*[a]

A combined CSD and *ab initio* study reveals that the interaction between the sp^3 C-atom in *para*-substituted $ArCF_3$ and electron rich atoms is weak (<5 kcal mol^{-1}), somewhat directional, and thus comparable to CH–π interactions.

Supramolecular chemistry and much of biology is concerned with intermolecular attractions that are reversible in the ambient temperature regime.[1] The sharing of a hydrogen atom (H) between a donor (D) and acceptor (A) entity, D–H···A hydrogen bonding,[2] is a particularly well established supramolecular binding motif varying in strength from very weak (~1 kcal mol^{-1})[3] to very strong (~40 kcal mol^{-1}).[4] The bottom of the H-bonding spectrum consists of weakly polarized D–H entities (*e.g.* aliphatic or aromatic CH) and mildly electron rich H-acceptor moieties (*e.g.* π-electrons).[5] While a single interaction is energetically unimpressive, when several weak hydrogen bonds work together they can stabilize protein structures[6] and contribute to the binding of proteins to ligands such as carbohydrates.[7] Over the years, many other weak intermolecular forces have been identified as potentially relevant in (bio)chemical machineries: halogen bonding, π–π stacking, carbonyl–carbonyl, cation–π, anion–π and lone-pair–π interactions.[8] Given this abundance of supramolecular synthons one may wonder what other electron poor/rich entities nature has to offer. Or better yet, which ones we might design ourselves.

Recent theoretical explorations have suggested that the chalcogen, pnicogen and tetrel atoms in their sp^3 hybridized form can be made electron poor enough to accommodate an electron rich guest.[9] Surprisingly few inquiries have been dedicated to study the most abundant of these nuclei, namely R_4C.[10] It has recently been calculated that strong complexes (up to −42.3 kcal mol^{-1}) are formed between electron rich entities and derivatives of small cycloalkane rings containing four cyano groups in the 1,1′,2,2′ positions.[11] Moreover, this interaction was found to be highly directional by means of a thorough statistical evaluation of the Cambridge Structure Database (CSD).

In analogy to strong and weak hydrogen bonding, we wondered if perhaps weak non-covalent bonding with sp^3 hybridized carbon could have some relevance. Our approach was to conduct a rigorous statistical survey of the CSD together with quantum mechanical computations on the RI-MP2/def2-TZVP level of theory. For the present study we considered the sp^3 C-atom in (*para*-substituted) α,α,α-trifluorotoluene and for comparison regular (*para*-substituted) toluene (see Fig. 1).

Both these entities are very common in the CSD. An illustration of the query used to obtain datasets from the CSD is shown in Fig. 1a. An entry was considered a hit when the intermolecular distance (D) between the carbon atom of the $-CX_3$ moiety (X = F, H) and any electron rich atom (red, El.R. = N, P, As, O, S, Se, Te, F, Cl, Br, I or At) was ≤5 Å. These data are thus located within a sphere with a radius of 5 Å, centred on the sp^3 C-atom. The distance d signifies the spatial separation between El.R. and an imaginary plane that is perpendicular to the aryl ring plane and runs through the sp^3 C-atom. Using D, d, and Pythagoras's theorem, the parallel displacement parameter r could be computed. The angle α between the aryl ring, the sp^3 C-atom and El.R. was measured as well.

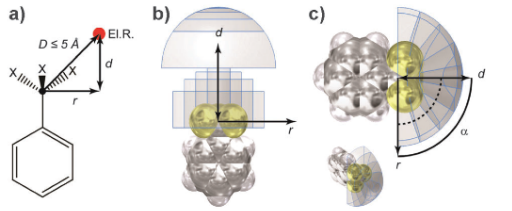

Fig. 1 (a) Query used to inspect the CSD for intermolecular interactions between an electron rich atom (El.R., N, P, As, O, S, Se, Te, F, Cl, Br, I or At) and (*para*-substituted) $-C_6H_4-CX_3$, where X = F, or H; (b and c) illustrations of the method used to assess directionality with X = F as example.

[a] *Department of Chemistry, Universitat de les Illes Balears, Crta. De Valldemossa km 7.5, 07122 Palma, Baleares, Spain. E-mail: toni.frontera@uib.es; Fax: +34 971 173426*

[b] *School of Chemistry of the University of Bristol, Cantock's Close, BS8 1TS Bristol, UK. E-mail: chtjm@bristol.ac.uk*

† Electronic supplementary information (ESI) available: Fig. S1 and S2, computational details and energy values. See DOI: 10.1039/c4cc05602g

Illustrated in Fig. 1b and c is the method used to assess directionality. This method has been very successful in establishing the directional character of other weak intermolecular interactions.[12]

The parameter $P(x)$ signifies the distribution of the data along some metric parameter x, that has been corrected for the volume occupied by the host and for a random scattering of data. When $P \neq 1$, a non-accidental clustering of data is established and $P > 1$ is indicative of an attractive interaction. For this study, P has been made dependant on both r and α (see Fig. 1a and b). The data for $P(r)$ was limited to data with $\alpha \geq 90^\circ$, so that the hits are located within a hemisphere centred at CX_3. The data for $P(\alpha)$ was limited to data contained within spherical cones that were truncated 2 Å above and below the aryl ring plane (Fig. 1c only illustrates bodies with α in between 90 and 180°). As an example eqn (1) details how $P(r)$ was obtained.‡

The *P versus r* plots for $PhCH_3$ (empty circles) and $PhCF_3$ (black circles) are shown in Fig. 2. For both central groups, $P > 1$ at longer r-values ($r \approx 3.6$ Å for $PhCH_3$ and 4.2 Å for $PhCF_3$), indicating hydrogen bonding to the H-atoms *ortho* to the CX_3 moiety (and possibly also halogen bonding to F). At intermediate r-values P is below unity, indicating a relative depletion of data. Interestingly, with $r \leq 1.0$–0.5 Å the P-values seem to increase slightly to about 1 for $PhCH_3$ and above 1 for $PhCF_3$. These data indicate that the interaction between El.R. and both $PhCX_3$ groups is slightly directional linearly (*i.e.* α close to 180°), but much more so when X = F. A very similar pattern emerges from the *P versus* α plots shown in Fig. 3.

That is; $P \geq 1$ around $\alpha \approx 90$–100° (hydrogen and perhaps halogen bonding); and $P \geq 1$ at $\alpha > 150^\circ$ (some linear directionality of the $PhCX_3\cdots$El.R. interaction). It was further assessed how exactly the data is distributed within the data characterized by $r \leq 1$ Å. Thus, the cumulative hit fraction was plotted as a function of the van der Waals corrected $PhX_3C\cdots$El.R. distance, as is shown in Fig. 4. From these data it is clear that hardly any overlap of van der Waals shells is present between El.R. and the sp^3 C-atom in $PhCF_3$ (0.42%, black circles). For $PhCH_3$ this is 6.62% (open circles). Both these values can be considered as very low and comparable to weak CH–π interactions where typically <10% van der Waals overlap is observed.[13] It can be noted however that the feature for $PhCF_3$ is much steeper than that for $PhCH_3$, meaning that the data for $PhCF_3$ is grouped more.

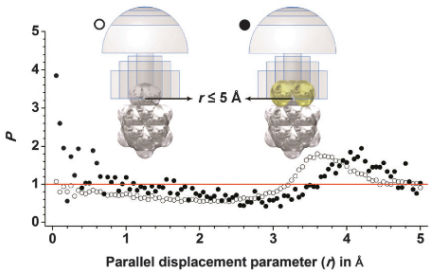

Fig. 2 Directionality plots of *P vs. r* for $PhCX_3\cdots$El.R. with X = H (○, N_{tot} = 88 305) and X = F (●, N_{tot} = 4631). Data used were limited to $\alpha \geq 90^\circ$.

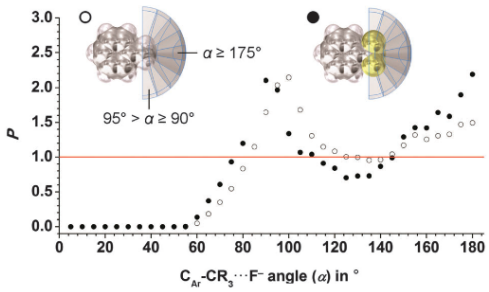

Fig. 3 Directionality plots of *P vs.* α for $PhCX_3\cdots$El.R. with X = H (○, N_{tot} = 53 232) and X = F (●, N_{tot} = 3037). Data used are were limited to data 2 Å above or below the aryl plane.

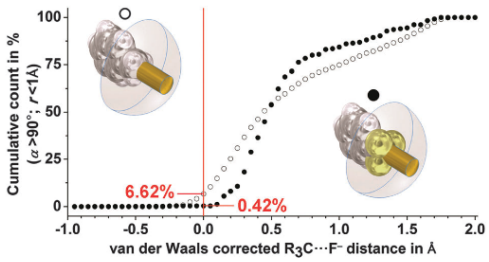

Fig. 4 Assessment of overlapping van der Waals shells for data with $\alpha \geq 90^\circ$ and $r \leq 1$ Å in $PhCX_3\cdots$El.R. pairs with X = H (○, N_{tot} = 2888) and X = F (●, N_{tot} = 236).

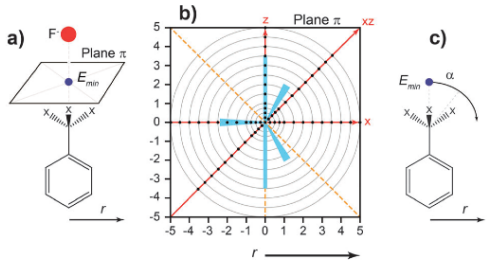

Fig. 5 Illustrations of geometries calculates. See text for details.

In order to relate the above findings from crystal structure data to energetic values, the association of a F^- anion with $PhCX_3$ was examined in some detail on the MP2/def2-TZVP level of theory, as is illustrated in Fig. 5 (see ESI† for details).

First, the energetic minimum (E_{min}, blue dot in Fig. 5a) along the ArC–CX_3 bond was computed for both central groups. To mimic the crystallographic data obtained as a function of r, the F^- anion was then moved away from this origin within the xz-plane π (see Fig. 5a and b). The concentric grey circles in Fig. 5b represent the r increments used, and the black dots denote the geometry of actual calculations. These computations

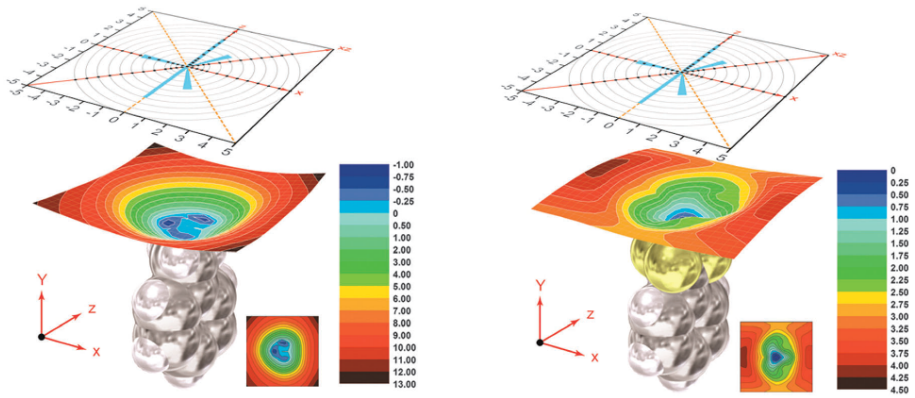

Fig. 6 Illustrations of energy landscapes derived from the calculated energies (RI-MP2/def2-TZVP) by moving F⁻ in the plane π (see Fig. 5b) above $PhCH_3$ (left) or $PhCF_3$ (right). Color codes are relative to E_{min} (along the *y*-axis), which is −11 kcal mol^{-1} for $[PhCH_3\cdots F]^-$ and −0.6 kcal mol^{-1} for $[PhCF_3\cdots F]^-$.

were located on the *x*, *z*, and *xz*-axes that are represented by a solid red line. The data along the rest of the *x*, *z*, and *xz*-axes (orange stripped lines) were obtained by virtue of symmetry. The datasets thus obtained represent the energy landscape of plane π, which can be expressed as $E(r)$. In an attempt to simulate the CSD data as a function of α, the F^- anion was moved away from the origin with regular α-intervals, while keeping the F^- anion in-plane with the aryl ring and keeping the sp^3 C$\cdots$F$^-$ distance constant (to avoid the $PhCF_3$ complexes to converge with unreasonably large F$\cdots$F$^-$ distances). These data can thus be expressed as $E(\alpha)$.

In Fig. 6 the energy landscapes are shown computed at the RI-MP2/def2-TZVP level of theory, which were obtained for the $[PhCX_3\cdots F]^-$ molecule pairs within the *xz*-plane centred at E_{min} for X = H (left) and X = F (right). The colour codes represent values relative to E_{min}. For the $[PhCH_3\cdots F]^-$ pair, E_{min} = −11 kcal mol^{-1} (D = 2.77 Å), positioning the F^- anion directly above the CH_3 hydrogens seems most favourable, and the computed energy is above E_{min} only at r > 1.5 Å. For the $[PhCF_3\cdots F]^-$ interaction, E_{min} = −0.6 kcal mol^{-1} (D = 3.06 Å; −0.8 kcal mol^{-1} at the CCSD(T)/def2-TZVP level of theory) and moving the F^- anion away from this small minimum is energetically unfavourable in all directions and at all values for r. This is also reflected in the $E(r)$ plots shown in Fig. S1 (ESI†) (where E is the average energy computed at a certain r-value, see also Fig. 5b). From the $E(\alpha)$ plots shown in Fig. 7, it is clear that the F^- anions prefer to interact with the H-atoms *ortho* to the CX_3 groups (*i.e.* around α = 80°).

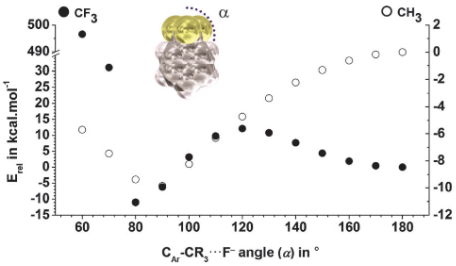

Fig. 7 E_{rel} *vs.* α plots of computed geometries for the interaction of F with $PhCH_3$ (open circles) $PhCF_3$ (black circles).

At smaller α-values steric repulsion takes over and the energies become large and positive. Apparently, the sp^3 H-atoms in $PhCH_3$ provide a smooth electropositive surface so that the transition from α = 190° to 90° is without a barrier. In contrast, the electronegative belts around the F-atoms create a small energetic hill in moving from the local minimum at α = 180° to the one in α = 80°. These computations imply that there is no real energy-well above $PhCH_3$, while there is a small but very narrow energy-well above $PhCF_3$ (*i.e.* the interaction is weak but directional). Introducing electron withdrawing substituents in the *para*-position of $PhCF_3$ significantly increased the interacting energy with F^-: from −2.3 kcal mol^{-1} for *p*-fluoro- to −6.6 kcal mol^{-1} for *p*-nitro substitution (F < CF_3 < CN < NO_2, see Fig. S2 for the whole set of energies, ESI†).

Electron rich entities (El.R.) seem to have a preference for interacting with the aromatic H-atoms of (*para*-substituted) $PhCH_3$ or $PhCF_3$ entities. However, the interaction with the aliphatic H-atoms in $PhCH_3$ or the small electropositive region in between the three F-atoms in $PhCF_3$ is energetically favourable as well: E_{min} = −11 and −0.6 kcal mol^{-1} respectively with El.R. = F^- (and up to −6.6 kcal mol^{-1} with *p*-NO_2PhCF_3). For the larger $PhCH_3\cdots F^-$ interaction, distortion from the linear conformation seems to go without energy penalty. This suggests that this conformation is not at the bottom of an energy-well; hence this type of interaction is hardly directional, as indeed observed in our CSD analysis. In contrast, the small $PhCF_3\cdots F^-$ interaction is located in a very narrow energy-well and any distortion from linearity thus comes with an energy penalty. As a result, this interaction is more directional, as confirmed by our analysis of the CSD.

The estimated −0.6 to −6.6 kcal mol^{-1} for an $[ArCF_3\cdots F]^-$ interaction is comparable to weak CH–π interactions, which are

generally accepted as a small but important supramolecular interaction.[5] Moreover, $-CF_3$ groups are commonplace and moreover widely used in medicinal chemistry. This implies that non-covalent carbon bonding might turn out to be as abundant and functionally relevant as weak CH–π interactions.

Notes and references

‡

$$P(r) = \frac{N_r}{N_{\text{total}}} \Big/ \frac{V_r^{\text{free}}}{V_{\text{total}}^{\text{free}}} \quad (1)$$

N_r = the number of hits in between two r-values; N_{total} = the total number of hits; V_r^{free} = the volume of a 5 Å high and wide hemisphere in between two r-values minus the volume of the host in between these two r-values (hence the free volume); $V_{\text{total}}^{\text{free}}$ is the volume of a 5 Å high and wide hemisphere minus the volume of the host in that hemisphere.

1 H. J. Schneider, *Angew. Chem., Int. Ed.*, 2009, **48**, 3924–3977; H. J. Schneider and A. Yatsimirski, *Principles and Methods in Supramolecular Chemistry*, Wiley, Chichester, 2000.
2 G. R. Desiraju, *Angew. Chem., Int. Ed.*, 2011, **50**, 52–59.
3 G. R. Desiraju and T. Steiner, *The Weak Hydrogen Bond in Structural Chemistry and Biology*, Oxford Univ. Press, Oxford, 1999.
4 J. W. Larson and T. B. McMahon, *Inorg. Chem.*, 1984, **23**, 2029–2033.
5 M. Nishio, Y. Umezawa, J. Fantini, M. S. Weiss and P. Chakrabarti, *Phys. Chem. Chem. Phys.*, 2014, **16**, 12648–12683; M. Nishio, Y. Umezawa, K. Honda, S. Tsuboyamad and H. Suezawae, *CrystEngComm*, 2009, **11**, 1757–1788; M. Nishio, M. Hirota and Y. Umezawa, *The C–H/π interaction: Evidence, nature, consequences*, Wiley-VCH, New York, 1998.
6 U. Samanta, D. Pal and P. Chakrabarti, *Proteins*, 2000, **38**, 288–300; M. J. Plevin, D. L. Bryce and J. Boisbouvier, *Nat. Chem.*, 2010, **2**, 466–471; M. Brandl, M. S. Weiss, A. Jabs, J. Sühnel and R. Hilgenfeld, *J. Mol. Biol.*, 2001, **307**, 357–377.
7 F. A. Quiocho and N. K. Vyas, *Nature*, 1984, **310**, 381–386; N. K. Vyas, M. N. Vyas and F. A. Quiocho, *Science*, 1988, **242**, 1290–1295; M. Nishio, *Phys. Chem. Chem. Phys.*, 2011, **13**, 13873–13900; Z. R. Laughrey, S. E. Kiehna, A. J. Riemen and M. L. Waters, *J. Am. Chem. Soc.*, 2008, **130**, 14625–14633; N. P. Barwell and A. P. Davis, *J. Org. Chem.*, 2011, **76**, 6548–6557.
8 P. V. Hobza and K. Müller-Dethlefs, *Non-covalent Interactions: Theory and Experiment*, RSC publishing, 2010; *Supramolecular Systems in Biomedical Fields*, ed. H. J. Schneider, RSC publishing, 2013.
9 P. Politzer, J. S. Murray and T. Clark, *Phys. Chem. Chem. Phys.*, 2013, **15**, 11178–11189; J. S. Murray, K. E. Riley, P. Politzer and T. Clark, *Aust. J. Chem.*, 2010, **63**, 1598–1607; T. Clark, *Wiley Interdiscip. Rev.: Comput. Mol. Sci.*, 2013, **3**, 13–20; P. Politzer, J. S. Murray and T. Clark, *Phys. Chem. Chem. Phys.*, 2010, **12**, 7748–7757; A. Bundhun, P. Ramasami, J. S. Murray and P. Politzer, *J. Mol. Model.*, 2013, **19**, 2739–2746; A. Bauzá, T. J. Mooibroek and A. Frontera, *Angew. Chem., Int. Ed.*, 2013, **52**, 12317–12321; S. J. Grabowski, *Phys. Chem. Chem. Phys.*, 2014, **16**, 1824–1834.
10 D. Mani and E. Arunan, *Phys. Chem. Chem. Phys.*, 2013, **15**, 14377–14383; S. P. Thomas, M. S. Pavan and T. N. G. Row, *Chem. Commun.*, 2014, **50**, 49.
11 A. Bauzá, T. J. Mooibroek and A. Frontera, *Chem. – Eur. J.*, 2014, **20**, 10245–10248.
12 T. J. Mooibroek and P. Gamez, *CrystEngComm*, 2013, **15**, 1802–1805; T. J. Mooibroek and P. Gamez, *CrystEngComm*, 2013, **15**, 4565–4570; K. E. Ranaghan, J. E. Hung, G. J. Bartlett, T. J. Mooibroek, J. N. Harvey, D. N. Woolfson, W. A. van der Donk and A. Mulholland, *Chem. Sci.*, 2014, **5**, 2191–2199.
13 T. J. Mooibroek and P. Gamez, *CrystEngComm*, 2012, **14**, 8462–8467.

PCCP

PAPER

View Article Online
View Journal | View Issue

Cite this: *Phys. Chem. Chem. Phys.*, 2016, 18, 32155

Theoretical study on σ- and π-hole carbon···carbon bonding interactions: implications in CFC chemistry†

Antonio Bauzá and Antonio Frontera*

Received 19th September 2016,
Accepted 1st November 2016

DOI: 10.1039/c6cp06449c

www.rsc.org/pccp

In this manuscript the ability of CO_2 and several CFCs to establish noncovalent carbon···carbon interactions (termed as noncovalent carbon···carbon bonding) with atmospheric gases CO, ethene and ethyne has been studied at the RI-MP2/def2-TZVPD level of theory. We have used several CFCs ($CFCl_3$, CF_3Cl, CF_2Cl_2 and CH_3F) and the CO_2 molecule as σ- and π-hole carbon bond donors (electron poor carbon atoms). As electron rich moieties we have used CO, ethene and ethyne (electron rich carbon atom bearing molecules). We have also used Bader's theory of "atoms in molecules" to further analyse and characterize the noncovalent interactions described herein. Finally, we have analyzed possible cooperativity effects between the noncovalent carbon···carbon bonding and hydrogen bonding interactions in the case of ethyne.

Introduction

Noncovalent interactions are recognized as key players in modern chemistry.[1] Actually, supramolecular chemists rely on their proper comprehension and rationalization in order to achieve progress in fields such as, molecular recognition[2,3] and materials science.[4] Hydrogen bonding and, more recently, halogen bonding are examples of well-known σ-hole interactions that play an important role in many chemical and biological environments.[5,6] For instance, hydrogen bonding interactions are main driving forces in enzyme chemistry and protein folding.[7] Consequently, both noncovalent forces have been widely studied from theoretical and experimental perspectives.[8,9] Their similarities in both strength and directionality features stimulated a series of studies using the Cambridge Structural Database (CSD) in order to shed light on the impact of these interactions in crystal structures.[10,11] Related to this, σ-hole interactions involving elements of Groups IV–VI have also earned recognition among the scientific society as an important addition to the family of well-established directional non-covalent interactions.[12–14] Recently, it was demonstrated that atoms of Groups IV–VI (from tetrels to chalcogens) when covalently bonded are able to establish attractive interactions with electron rich entities through their positive electrostatic potential regions, which are attributed to the anisotropies of the electronic density distribution on the extensions of their covalent bonds.[15–18] It was also shown that the factors that rule the σ-hole potentials are the same across Groups IV–VI.

As a natural consequence of the scientific curiosity over the σ-hole chemistry a novel and relatively unexplored group of non-covalent interactions emerged, called π-hole bonding. A π-hole is a region of positive electrostatic potential that is perpendicular to a portion of a molecular framework.[19] Two pioneering works that exemplify the impact of π-hole interactions in chemical and biological systems should be emphasized. Firstly, Bürgi and Dunitz studied the trajectory along which a nucleophile attacks the π-hole of a C=O group[20–22] and, secondly, Egli and co-workers studied and rationalized the ability of guanosine to behave as a π-hole donor in the crystal structure of Z-DNA.[23] More recently, the study of π-hole interactions has been extended to acyl carbons[24] and other entities involving pnicogen[25–29] and chalcogen bearing compounds.[30,31]

Haloalkanes were widely used in industry as refrigerant agents, propellants and cleaning solvents until the 1970s.[32] Related to this, chlorofluorocarbons (CFCs) are a family of haloalkane compounds mostly formed by hydrocarbons, particularly alkanes, covalently bonded with halogens such as chlorine or fluorine. Nowadays, they are well known to play a key role in the depletion process of the ozone layer, which is a vital natural defense against the incoming UV radiation.[33] Several theoretical studies have been devoted to analyse the interaction between CFCs and ozone, carbon dioxide and nitrogen oxide molecules, as well as sulphur containing compounds.[34–36] While CFCs are considered as an important source of carbon atoms,[37] it is intriguing whether they can undergo carbon bonding interactions with other atmospheric gases, such as carbon monoxide or ethene and ethyne molecules.[38,39] In this regard, we propose to coin the term dicarbon bond, since both

Department of Chemistry Universitat de les Illes Balears, Crta. de Valldemossa km 7.5, 07122 Palma, Baleares, Spain. E-mail: toni.frontera@uib.es; Fax: +34 971 173426

† Electronic supplementary information (ESI) available. See DOI: 10.1039/c6cp06449c

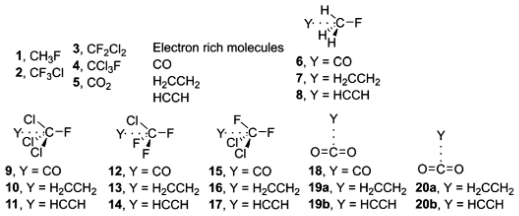

Fig. 1 Compounds **1–5** and complexes **6–20** used in this study. For complexes **19** and **20** two possible orientations were considered; parallel (denoted as a) and perpendicular (denoted as b).

the electron donor and acceptor belong are carbon atoms, thus resembling the concept of the dihydrogen bond.[40] The concept of carbon–carbon interactions involving sp and sp^2 carbons has been previously studied by Remya and coworkers.[41]

In this study, our purpose is to investigate the ability of CFCs and CO_2 moieties to establish σ- and π-hole noncovalent carbon···carbon bonding interactions. In order to achieve this goal, we have used several CFCs ($CFCl_3$, CCl_3F, CH_3F and CF_2Cl_2) as σ-hole carbon bond donor entities. We have used CO, ethene and ethyne as electron rich moieties (see Fig. 1). Particularly, in CO_2 π-hole complexes, we have explored two different orientations (parallel and perpendicular) between both donor and acceptor molecules. Finally, we have also used Bader's theory of "atoms in molecules" to further describe and rationalize the interactions described above.

Theoretical methods

The energies of all complexes included in this study were computed at the RI-MP2/def2-TZVPD level of theory by means of the program TURBOMOLE version 7.0.[42] Single point calculations at the CCSD(T)/def2-TZVP level of theory have been performed in order to give reliability to the RI-MP2 method. The MEP (molecular electrostatic potential) calculations have been performed at the MP2/def2-TZVP level of theory by means of the Gaussian09 calculation package.[43] Frequency calculations have been performed at the RI-MP2/def2TZVPD level of theory and in all cases a true minima have been found. Moreover, all carbon···carbon complexes correspond to global minima apart from complex **8** that is a local minimum. The global minimum corresponds to an H-bonded complex CH_3F···HCCH. Bader's "Atoms in molecules" theory has been used to study the interactions discussed herein by means of the AIMall calculation package.[44] The calculations for wavefunction analyses were carried out at the MP2/def2-TZVP level of theory.

Results and discussion

MEPS study

As a preliminary study, we have computed the molecular electrostatic potential (MEP) surface of compounds **1** to **5** (see Fig. 2). As it can be observed, for compounds **1** to **4** the MEP surface showed the presence of a positive potential area located

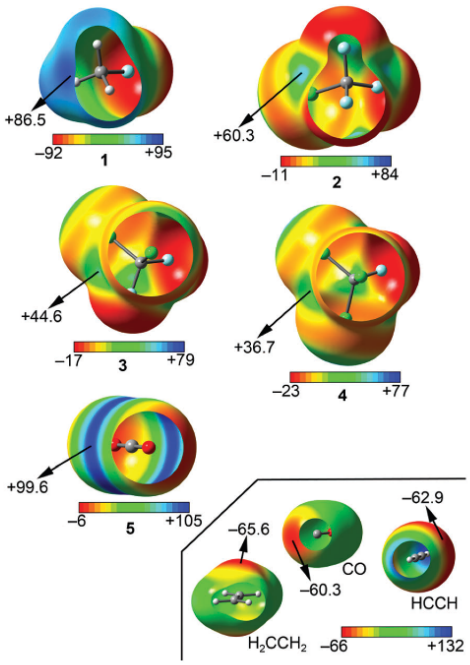

Fig. 2 MEP (molecular electrostatic potential) surfaces for compounds **1** to **5**. Energy values in kJ mol^{-1}.

at the outermost region of the carbon atom, opposite to the C–X bond (σ-hole). Consequently, an attractive interaction with electron rich entities is expected. In addition, the MEP value of the σ-hole is more positive for compounds **1** and **2**, thus expecting a stronger binding upon complexation from an electrostatic perspective. Moreover, the MEP values become less positive ongoing from compound **2** to **4**, due to the difference in electronegativity between chlorine and fluorine atoms. In the case of compound **5**, a positive potential region is observed on the tip of the carbon atom, perpendicularly located over the molecular plane (π-hole). The MEP value obtained is the most positive among compounds **1** to **5**, thus expecting a stronger binding for π-complexes over the σ-hole set. Finally, among the electron donors, the most negative MEP value corresponds to the ethene molecule, thus expecting a slightly stronger binding over the other CO and ethyne molecules.

Energetic study

The interaction energies and equilibrium distances obtained for complexes **6** to **20** (see Fig. 3) studied herein are summarized in Table 1. The examination of the results indicates that the interaction energy values are weak but attractive in all cases, ranging from −11 to −4 kJ mol^{-1}. Among the σ-hole complexes studied (**6–17**) the $CFCl_3$ and CF_2Cl_2 ones (**9–11** and **15–17**, respectively) present stronger interaction energies, conversely to the MEP analysis that shows more positive values at the σ-hole of CH_3F and CF_3Cl molecules likely due to the greater

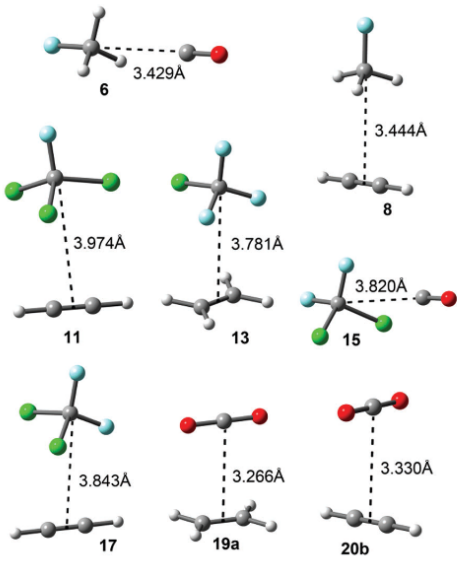

Fig. 3 Optimized geometries of some representative complexes at the RI-MP2/def2-TZVPD level of theory.

Table 1 Interaction energies (ΔE, kJ mol^{-1}), equilibrium distances (R, Å) and symmetry point groups used (Symm.) at the RI-MP2/def2-TZVPD level of theory for complexes **6** to **20**

Complex	ΔE^a	R^b	Symm.
6 (OC:CH_3F)	−4.3	3.429	C_{3v}
7 (H_2CCH_2:CH_3F)	−7.0 (−6.7)	3.452	C_s
8 (HCCH:CH_3F)	−6.2	3.444	C_s
9 (OC:CCl_3F)	−4.8 (−4.3)	3.922	C_{3v}
10 (H_2CCH_2:CCl_3F)	−10.8	3.937	C_s
11 (HCCH:CCl_3F)	−8.6	3.974	C_s
12 (OC:$CClF_3$)	−4.1 (−4.0)	3.748	C_s
13 (H_2CCH_2:$CClF_3$)	−7.6	3.781	C_s
14 (HCCH:$CClF_3$)	−6.3 (−5.5)	3.802	C_s
15 (OC:CCl_2F_2)	−4.5	3.820	C_s
16 (H_2CCH_2:CCl_2F_2)	−9.4 (−8.2)	3.830	C_s
17 (HCCH:CCl_2F_2)	−7.8	3.843	C_s
18 (OC:CO_2)	−5.4	3.240	C_{2v}
19a (H_2CCH_2:CO_2)	−9.2	3.266	C_{2v}
19b (H_2CCH_2:CO_2)	−8.8	3.252	C_{2v}
20a (HCCH:CO_2)	−9.8	3.210	C_{2v}
20b (HCCH:CO_2)	−6.1	3.330	C_{2v}

[a] Values in parentheses correspond to the CCSD(T)/def2-TZVPD level of theory. [b] For complexes involving ethene and ethyne distances were measured from the C–C bond centroid.

polarizability of chlorine *vs.* fluorine. Moreover, $CFCl_3$ and CF_2Cl_2 complexes present larger equilibrium distance values than those involving CH_3F and CF_3Cl molecules. On the other hand, for CH_3F and CF_3Cl complexes (**6–8** and **12–14**, respectively) comparable interaction energy values were obtained. For π-complexes involving CO_2 (**18** to **20b**) the binding energy values are similar to those obtained for CCl_3F and CF_2Cl_2 complexes. For some complexes we have computed the interaction energies at a higher level of theory in order to validate the computational method used herein. The values in parentheses summarized in Table 1 correspond to the interaction energies at the CCSD(T)/def2-TZVPD level of theory, which are in good agreement with the MP2 values.

The σ-hole CFC complexes with ethene (**7**, **10**, **13**, **16**) are more favourable than the complexes with ethyne, in agreement with the MEP values shown in Fig. 2, which indicate that ethene is slightly more π-basic than ethyne. In addition, complexes involving the CO molecule achieved the lowest binding energy values of the set, also in agreement with the MEP analysis. For π-hole complexes **18** to **20** the parallel orientation presents larger binding energy values than the perpendicular one, likely due to a major overlap between the π-systems of CO_2 and ethene/ethyne molecules. Moreover, the $CO_2\cdots$ethene π-hole complexes **19a,b** are more favourable than the ethyne ones (**20a,b**).

AIM analysis

We have used Bader's theory of "atoms in molecules" to characterize the noncovalent carbon···carbon bond complexes described above. The distribution of critical points (CPs) and bond paths for some representative complexes is shown in Fig. 4. For σ-hole complexes involving the CH_3F moiety (**6** to **8**) the presence of a bond CP (red sphere) and bond path (dashed line) connecting both carbon atoms can be noted. In addition, in the case of complex **7** two symmetrically distributed bond CPs connect the π-system of ethene (both C atoms) to the carbon atom of the CH_3F moiety, consequently a supramolecular ring is formed and a ring CP is created. On the other hand, for complexes involving the CO_2 moiety (**18**, **19b** and **20b**)

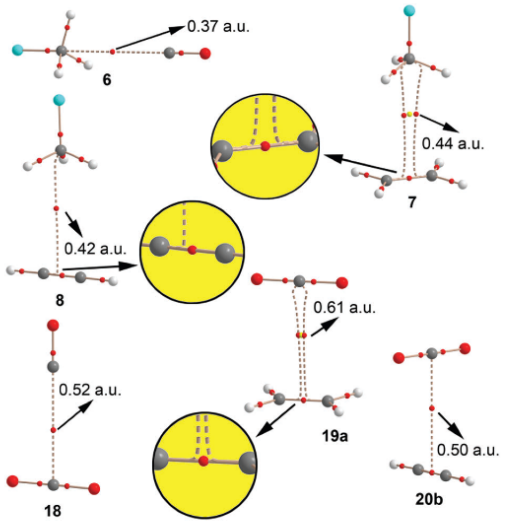

Fig. 4 Distribution of critical points and bond paths in complexes **6**, **7**, **8**, **18**, **19a** and **20b**. Bond and ring critical points are represented by red and yellow spheres, respectively. The bond paths connecting bond critical points are also represented. The value of the density at the bond critical point ($\rho \times 10^2$) is also indicated.

the interaction is characterized by the presence of a bond CP and bond path connecting the carbon atom of CO_2 to either the carbon atom of CO or the bond critical point of the CC bond of ethene/ethyne. Moreover, in complex **19a** where the CO_2 and the ethene portions are disposed in parallel, the presence of two symmetrically distributed bond CPs connecting both C atoms of the ethene to the central C atom of CO_2 can be noted, forming a supramolecular ring and its corresponding ring CP. The values of the Laplacian are all positive, as in common in closed shell calculations. Finally, additional AIM analyses are included in the ESI† (see Fig. S1). In these complexes the bond paths that characterize the interaction connect the carbon atoms of the electron rich molecules to the halogen atoms of the CFCs.

Noncovalent carbon···carbon bonding *vs.* H-bonding

This manuscript is devoted to the ability of CFCs to establish noncovalent carbon···carbon bonding with other atmospheric gases. It should be mentioned that the most favourable binding mode between CH_3F and ethyne is the formation of a hydrogen-bonded complex by means of a HCC–H···FCH_3 interaction. The interaction energy of the global minimum is −8.8 kJ mol^{-1} while the carbon···carbon complex **8** is −6.2 kJ mol^{-1}. We have also analysed possible cooperativity effects between both interactions. Particularly, we have computed the binding energies of ethyne interacting with two CH_3F molecules either forming two H-bonds (ΔE_1, complex **21**) or two noncovalent carbon···carbon bonds (ΔE_2, complex **22**), see Fig. 5. It can be observed that the H-bonding complex is approximately 5 kJ mol^{-1} more favourable than the noncovalent carbon···carbon complex. More interestingly, the H-bonded complex **21** has enhanced the ability to interact with additional CH_3F molecules forming noncovalent carbon···carbon bonding interactions (ΔE_3 = −19.8 kJ mol^{-1}) to form complex **23**. Similarly, the noncovalent carbon···carbon bonded complex **22** forms stronger H-bonding interactions (ΔE_4 = −24.7 kJ mol^{-1}) than ethyne alone (ΔE_1 = −16.5 kJ mol^{-1}). Therefore, strong cooperativity effects are found between both interactions in the formation of complex **23**. This mutual influence between the interactions is further confirmed by the AIM analysis. The charge density at the bond CP is usually related to the interaction strength.[45] It can be observed that the values of $\rho(r)$ at the bond CPs that characterize the H-bonding and noncovalent carbon···carbon bonding interactions in complex **23** are greater than the corresponding values in complexes **21** and **22**, thus confirming the mutual reinforcement of both interactions, in agreement with the energetic study (Fig. 5).

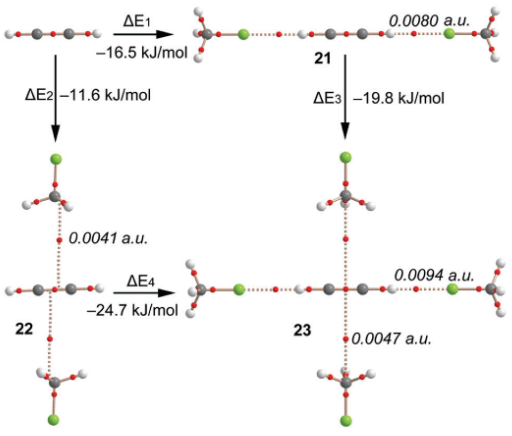

Fig. 5 Distribution of critical points and bond paths in complexes **21–23**, along with the binding energies. The value of the density at the bond critical point is also indicated in italics.

Conclusions

The results reported in this manuscript highlight the ability of CFCs and CO_2 molecules to establish weak interactions (noncovalent carbon···carbon bonds) with CO, ethene and ethyne molecules acting as electron donors, which are present in the higher layers of the atmosphere. The results presented herein provide new insights into how these molecules interact with each other and may be important in the field of atmospheric chemistry. We have successfully used Bader's theory of "atoms in molecules" to characterize the noncovalent carbon···carbon bond complexes described above. Finally, favourable cooperativity effects between noncovalent carbon···carbon and hydrogen bonding interactions have been demonstrated energetically using the AIM theory.

Acknowledgements

A. B. and A. F. thank the DGICYT of Spain (projects CTQ2014-57393-C2-1-P and CONSOLIDER INGENIO 2010 CSD2010-00065, FEDER funds). We thank the CTI (UIB) for computational facilities.

References

1 C. A. Hunter and J. K. M. Sanders, *J. Am. Chem. Soc.*, 1990, **112**, 5525.
2 H. J. Schneider, *Angew. Chem., Int. Ed.*, 2009, **48**, 3924.
3 C. A. Hunter and J. K. M. Sanders, *J. Am. Chem. Soc.*, 1990, **112**, 5525.
4 W. J. Vickaryous, R. Herges and D. W. Jonhson, *Angew. Chem., Int. Ed.*, 2004, **43**, 5831.
5 S. J. Grabowski, *Chem. Rev.*, 2011, **111**, 2597.
6 P. Murrayrust and W. D. S. Motherwell, *J. Am. Chem. Soc.*, 1979, **101**, 4374.
7 Y. Bai, T. R. Sosnick, L. Mayne and S. W. Englander, *Science*, 1995, **269**, 192.
8 A. C. Legon and D. J. Millen, *Acc. Chem. Res.*, 1987, **20**, 39.
9 P. Metrangolo, H. Neukirch, T. Pilati and G. Resnati, *Acc. Chem. Res.*, 2005, **38**, 386.
10 G. A. Cavallo, P. Metrangolo, R. Milani, T. Pilati, A. Priimagi, G. Resnati and G. Terraneo, *Chem. Rev.*, 2016, **116**, 2478.
11 T. Steiner, *Angew. Chem., Int. Ed.*, 2002, **41**, 48.

12 P. Politzer, J. S. Murray and T. Clark, *Phys. Chem. Chem. Phys.*, 2010, **12**, 7748.
13 K. E. Riley, J. S. Murray, J. Franfrlík, J. Rezáč, R. J. Solá, M. C. Concha, F. M. Ramos and P. Politzer, *J. Mol. Model.*, 2011, **17**, 3309.
14 A. Bauzá, T. J. Mooibroek and A. Frontera, *Angew. Chem., Int. Ed.*, 2013, **52**, 12317.
15 S. C. Nyburg and C. H. Faerman, *Acta Crystallogr., Sect. B: Struct. Sci.*, 1985, **41**, 274.
16 P. Politzer, K. E. Riley, F. A. Bulat and J. S. Murray, *Comput. Theor. Chem.*, 2012, **998**, 2.
17 T. N. G. Row and R. Parthasarathy, *J. Am. Chem. Soc.*, 1981, **103**, 477.
18 N. Ramasubbu and R. Parthasarathy, *Phosphorus Sulfur Relat. Elem.*, 1987, **31**, 221.
19 J. S. Murray, P. Lane, T. Clark, K. E. Riley and P. Politzer, *J. Mol. Model.*, 2012, **18**, 541.
20 H. B. Burgi, *Inorg. Chem.*, 1973, **12**, 2321.
21 H. B. Burgi, J. D. Dunitz and E. Shefter, *J. Am. Chem. Soc.*, 1973, **95**, 5065.
22 H. B. Burgi, J. D. Dunitz, J. M. Lehn and G. Wipff, *Tetrahedron*, 1974, **30**, 1563.
23 M. Egli and R. V. Gessner, *Proc. Natl. Acad. Sci. U. S. A.*, 1995, **92**, 180.
24 P. Sjoberg and P. Politzer, *J. Phys. Chem.*, 1990, **94**, 3959.
25 A. Bauzá, R. Ramis and A. Frontera, *J. Phys. Chem. A*, 2014, **118**, 2827.
26 A. Bauzá, T. J. Mooibroek and A. Frontera, *Chem. Commun.*, 2015, **51**, 1491.
27 A. Bauzá, A. Frontera and T. J. Mooibroek, *Cryst. Growth Des.*, 2016, **16**, 5520.
28 A. Bauzá, T. J. Mooibroek and A. Frontera, *Chem. Commun.*, 2015, **51**, 1491.
29 A. Bauzá, T. J. Mooibroek and A. Frontera, *ChemPhysChem*, 2016, **17**, 1608.
30 L. M. Azofra, I. Alkorta and S. Scheiner, *Theor. Chem. Acc.*, 2014, **133**, 1586.
31 L. M. Azofra, I. Alkorta and S. Scheiner, *Phys. Chem. Chem. Phys.*, 2014, **16**, 18974.
32 A. Chatterjee, T. Ebina, T. Iwasaki and F. Mizukami, *J. Mol. Struct.*, 2003, **630**, 233.
33 J. E. Lovelock, R. J. Maggs and R. A. Rasmussen, *Nature*, 1972, **237**, 452.
34 B. G. de Oliveira, R. C. M. Ugulino de Araújo, E. S. Leite and M. N. Ramos, *Int. J. Quantum Chem.*, 2011, **111**, 111.
35 K. S. Diao, F. Wang and H. J. Wang, *J. Mol. Struct.*, 2009, **913**, 195.
36 L. Ai and J. Liu, *J. Mol. Model.*, 2014, **20**, 2179.
37 K. S. Diao, F. Wang and H. J. Wang, *Bull. Environ. Contam. Toxicol.*, 2010, **84**, 170.
38 J. G. Calvert, R. Atkinson, J. A. Kerr, S. Madronich, G. K. Moortgat and T. J. Wallington, *et al.*, The Mechanisms of Atmospheric Oxidation of the Alkenes, Oxford University Press, New York, 2000.
39 (*a*) M. P. Fraser, G. R. Cass and B. R. Simoneit, *Environ. Sci. Technol.*, 1998, **32**, 2051; (*b*) A. C. Aikin, J. R. Herman, E. J. Maier and C. J. McQuillan, *J. Geophys. Res.*, 1982, **87**, 3105; (*c*) Y. Xiaoi, D. J. Jacob and S. Turquety, *J. Geophys. Res.*, 2007, **112**, D12305.
40 R. Custelcean and J. E. Jackson, *Chem. Rev.*, 2001, **101**, 1963.
41 K. Remya and C. H. Suresh, *Phys. Chem. Chem. Phys.*, 2015, **17**, 18380.
42 R. Ahlrichs, M. Bär, M. Hacer, H. Horn and C. Kömel, *Chem. Phys. Lett.*, 1989, **162**, 165.
43 M. J. Frisch, G. W. Trucks, H. B. Schlegel, G. E. Scuseria, M. A. Robb, J. R. Cheeseman, G. Scalmani, V. Barone, B. Mennucci, G. A. Petersson, H. Nakatsuji, M. Caricato, X. Li, H. P. Hratchian, A. F. Izmaylov, J. Bloino, G. Zheng, J. L. Sonnenberg, M. Hada, M. Ehara, K. Toyota, R. Fukuda, J. Hasegawa, M. Ishida, T. Nakajima, Y. Honda, O. Kitao, H. Nakai, T. Vreven, J. A. Montgomery, Jr., J. E. Peralta, F. Ogliaro, M. Bearpark, J. J. Heyd, E. Brothers, K. N. Kudin, V. N. Staroverov, R. Kobayashi, J. Normand, K. Raghavachari, A. Rendell, J. C. Burant, S. S. Iyengar, J. Tomasi, M. Cossi, N. Rega, J. M. Millam, M. Klene, J. E. Knox, J. B. Cross, V. Bakken, C. Adamo, J. Jaramillo, R. Gomperts, R. E. Stratmann, O. Yazyev, A. J. Austin, R. Cammi, C. Pomelli, J. W. Ochterski, R. L. Martin, K. Morokuma, V. G. Zakrzewski, G. A. Voth, P. Salvador, J. J. Dannenberg, S. Dapprich, A. D. Daniels, Ö. Farkas, J. B. Foresman, J. V. Ortiz, J. Cioslowski and D. J. Fox, *Gaussian 09, Revision B.01*, Gaussian, Inc., Wallingford CT, 2009.
44 T. A. Keith, *AIMAll (Version 13.05.06)*, TK Gristmill Software, Overland Park KS, USA, 2013.
45 J. Leszczynski, in *Computational Chemistry: Reviews of Current Trends*, ed. J. Leszczynski, World Scientific, Singapore, 1996, vol. 4.

crystals

MDPI

Article

$RCH_3\cdots O$ Interactions in Biological Systems: Are They Trifurcated H-Bonds or Noncovalent Carbon Bonds?

Antonio Bauzá and Antonio Frontera *

Department of Chemistry, Universitat de les Illes Balears, Crta de Valldemossa km 7.5, 07122 Palma de Mallorca (Baleares), Spain; antonio.bauza@uib.es
* Correspondence: toni.frontera@uib.es; Tel.: +34-971-173426

Academic Editor: Sławomir J. Grabowski
Received: 26 January 2016; Accepted: 14 March 2016; Published: 17 March 2016

Abstract: In this manuscript, we combine high-level *ab initio* calculations on some model systems (XCH_3 σ-hole/H-bond donors) and a Protein Data Bank (PDB) survey to distinguish between trifurcated H-bonds and noncovalent carbon bonds in $XCH_3\cdots O$ complexes (X = any atom or group). Recently, it has been demonstrated both experimentally and theoretically the importance of noncovalent carbon bonds in the solid state. When an electron-rich atom interacts with a methyl group, the role of the methyl group is commonly viewed as a weak H-bond donor. However, if the electron-rich atom is located equidistant from the three H atoms, the directionality of each individual H-bond in the trifurcated binding mode is poor. Therefore, the $XCH_3\cdots O$ interaction could be also defined as a tetrel bond ($C\cdots O$ interaction). In this manuscript, we shed light into this matter and demonstrate the importance of $XCH_3\cdots O$ noncovalent carbon bonding interactions in two relevant protein-substrate complexes retrieved from the PDB.

Keywords: H-bonding; tetrel bonding; PDB search; *ab initio* calculations

1. Introduction

Supramolecular chemistry is a multidisciplinary field of research that develops very fast and has a deep impact [1,2] in the scientific community. Undoubtedly, the comprehension of the great deal of noncovalent forces, which are the basis of highly specific recognition, is crucial for the chemists working in this discipline. For instance, interactions between hosts and guests govern the creation of assemblies with high affinities even in highly competitive media [3–6]. For this reason, the correct description and understanding of noncovalent interactions between molecules is essential for being successful in this field of research. In general, strong and highly directional interactions, such as hydrogen bonding and σ-hole bonding [7–17], and less directional forces like ion pairing are used for this purpose.

The allocation of a hydrogen atom between a donor (D) and acceptor (A) moiety, $D–H\cdots A$ hydrogen bonding [18] is a particularly well studied and established supramolecular interaction ranging in strength from very weak (~1 kcal/mol) [19] to very strong (~40 kcal/mol) [20]. The weakest H-bonding interactions are established between weakly polarized D–H bonds (e.g., aliphatic CH) and mildly electron-rich H-acceptor moieties (e.g., alkene π-electrons) [21–23]. While a single interaction is energetically insignificant, when several weak H-bonds coexist they can stabilize protein structures [24–26] and contribute to the binding of proteins to carbohydrates [27–31]. Apart from this weak bonding interaction, recent theoretical explorations have suggested that pnicogen and tetrel atoms in their sp^3 hybridized form can act as electron poor entities suitable to accommodate an electron-rich guest [16,32–37]. Surprisingly few studies have been dedicated to studying the most

abundant of these atoms, namely, the carbon atom. As a matter of fact, it has recently been reported that strong complexes are formed between electron-rich entities and 1,1,2,2-tetracyanocyclopropane [38–40]. Moreover, the ability of the carbon atom in a methyl group or in an aliphatic chain (sp^3 hybridized) to participate in σ-hole interactions (as a σ-hole donor, *i.e.* electron acceptor) has been explored by Mani and Arunan [41]. They demonstrated that the carbon atom in fact could act as an electrophilic center which can non-covalently bond with electron-rich entities leading to noncovalent carbon bonding, following a nomenclature analogous to other σ-hole interactions [7–17]. The theoretical predictions were confirmed experimentally by Guru Row's group [42], thus validating the existence of this type of bonding by means of X-ray charge density analysis. Electron density topologies in two prototypical crystal structures with potential carbon bonding motifs (R_3N^+–$CH_3\cdots$O/Cl) were reported and revealed two distinct features of bond paths. That is, for the X-ray structure with the R_3N^+–$CH_3\cdots$ Cl motif, the bond path revealed a C–H$\cdots$Cl hydrogen bond and for the other motif the bond path connected the electron-rich oxygen atom with the –CH_3 carbon atom; remarkably, no other bond paths connected the oxygen atom to the C–H hydrogen atoms. More recently, cooperativity effects involving carbon bonding interactions, and other noncovalent interactions have been analyzed in several theoretical studies [43–45].

The presence of methyl groups is abundant in many biologically relevant ligands and electron-rich O atoms are ubiquitous in proteins. Therefore, we wondered if perhaps weak non-covalent bonding with sp^3 hybridized carbon could have some relevance in ligand-protein complexes. Our approach was to conduct a rigorous statistical survey of the PDB together with quantum mechanical computations on the RI-MP2/aug-cc-pVTZ level of theory on some model systems. For the present theoretical study, we considered the sp^3 C-atom in several exemplifying molecules (**1**–**3**, see Figure 1) and computed their complexes with the electron-rich O atom of two molecules (formaldehyde and HO^-). In addition, using Bader's theory of "atoms in molecules" [46], we analyzed the bond path connecting the O atom with the CH_3 group in several complexes with the purpose of differentiating the H-bonding from the carbon bonding. From the PDB search, we analyzed the impact of the X–$CH_3\cdots$O interactions in biologically relevant protein-ligand complexes.

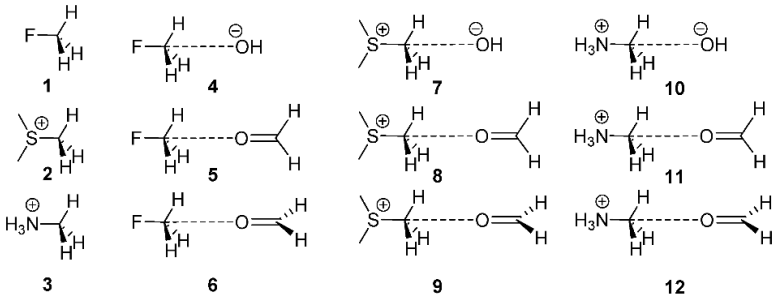

Figure 1. Compounds and complexes **1**–**12** studied in this work.

2. Results and Discussion

2.1. Preliminary MEP Analysis

We firstly computed the molecular electrostatic potential (MEP) mapped onto the van der Waals surface in very simple compounds (XCH_3) to explore the existence/absence of a σ-hole in the carbon atom (along the extension of the X–C bond) and to compare its electrostatic potential to that measured along the C–H bonds of the methyl group. In particular we computed the MEP surfaces of fluoromethane, dimethylether, dimethylthioether, dimethylformamide (DMF), acetonitrile, and methylamine, and the results are shown in Figure 2. In fluoromethane and dimethylether, an evident

σ-hole is observed (see Figure 2a,b) in the C atom with a MEP value that is comparable to that observed in the H atoms. Therefore, either the carbon or the hydrogen bonding interactions should be equally favored, at least electrostatically, in both molecules. For the DMF and acetonitrile molecules, a perfectly defined σ-hole is not observed; however, both molecules present a significantly positive value of MEP at the C atom. Finally, the methylamine and dimethylthioether molecules (see Figure 2d,e) do not present a σ-hole at the C atom, although the electrostatic potential is slightly positive. Consequently, both molecules are better H-bond donors than carbon bond donors in terms of electrostatic effects.

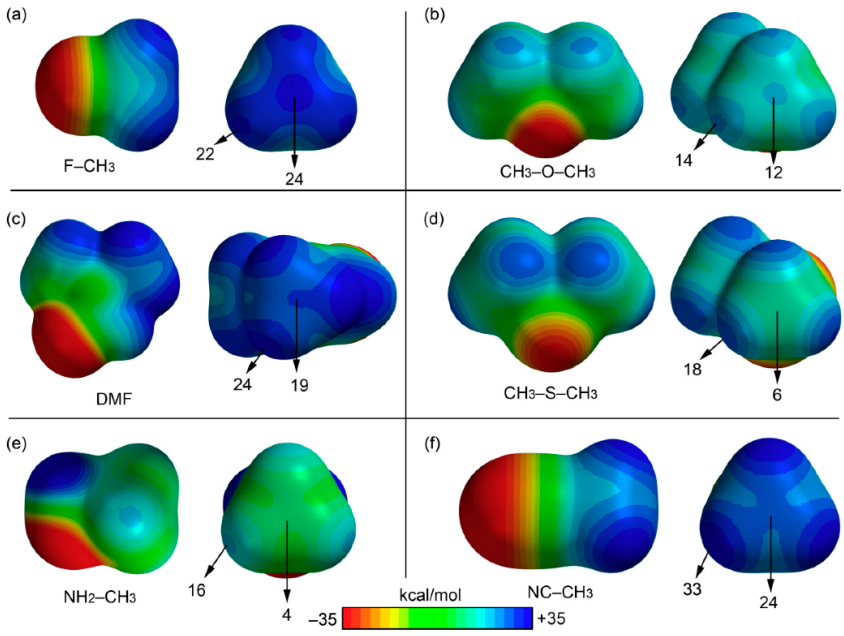

Figure 2. MEP surfaces of fluoromethane (**a**); dimethylether (**b**); DMF (**c**); dimethylthioether (**d**); methylamine (**e**); and acetonitrile (**f**). The MEP values at selected points are indicated.

2.2. Energetic and Geometric Results

Table 1 reports the interaction energies and equilibrium distances of the optimized complexes **4**–**12** (see Figures 1 and 3) computed at the RI-MP2/aug-cc-pVTZ level of theory. In complexes **7** and **10**, where the OH^- anion interacts with charged carbon bond donors, the noncovalent complex was not found; instead, a nucleophilic S_N2 reaction occurs in the optimization. In formaldehyde complexes, we studied the influence of the orientation of the lone pairs of the O atom on the interaction energy and equilibrium distance. At this point, it should be noted that we used two charged carbon bond donors for the following reasons. First, the utilization of trimethylsulfonium was chosen to mimic the SAM cofactor (important in methyl transfer enzymatic processes). Second, we used methanaminium because, at physiological conditions, the amine groups are likely protonated.

From the inspection of the results summarized in Table 1 and Figure 3, several points are worth discussing. First, in the fluoromethane complexes, the interaction energy with the charged OH^- guest is large and negative (−12.9 kcal/mol), modest for the complex with the neutral formaldehyde guest (−1.9 kcal/mol). Interestingly, the carbon bonding complexes (or trifurcated H-bonded) were found to be minima on the potential hypersurface. Moreover, the orientation of the oxygen lone pairs in the formaldehyde in its complexes with fluoromethane does not influence either the interaction energy or the equilibrium distance (complexes **5** and **6**). Second, the trimethylsulfonium and methanaminium

complexes with neutral formaldehyde present large interaction energies, being more favorable with the protonated amine. Third, the interaction energies are identical for both orientations of formaldehyde; however, in the case of trimethylsulfonium, the C···O equilibrium distance is longer in complex **8** than in **9** and the S–C···O angle is smaller (172.0° in **8** and 178.6° in **9**, see Figure 3b). This behavior is not observed in methanaminium complexes **11** and **12,** and both present almost identical geometric and energetic features.

Table 1. Interaction energies (BSSE corrected, ΔE_{BSSE}, kcal/mol) and equilibrium distances (R_1 and R_2, Å) for complexes **4-12** at the RI-MP2/aug-cc-pVTZ level of theory.

Complex	ΔE_{BSSE}	R_1 (C···O)	R_2 (C···H)
4	−12.9	2.654	2.521
5	−1.9	2.993	2.829
6	−1.9	2.993	2.830
7	_ [1]	_ [1]	_ [1]
8	−8.5	2.822	2.502
9	−8.5	2.803	2.665
10	_ [1]	_ [1]	_ [1]
11	−9.7	2.746	2.600
12	−9.7	2.746	2.614

[1] S_N2 attack.

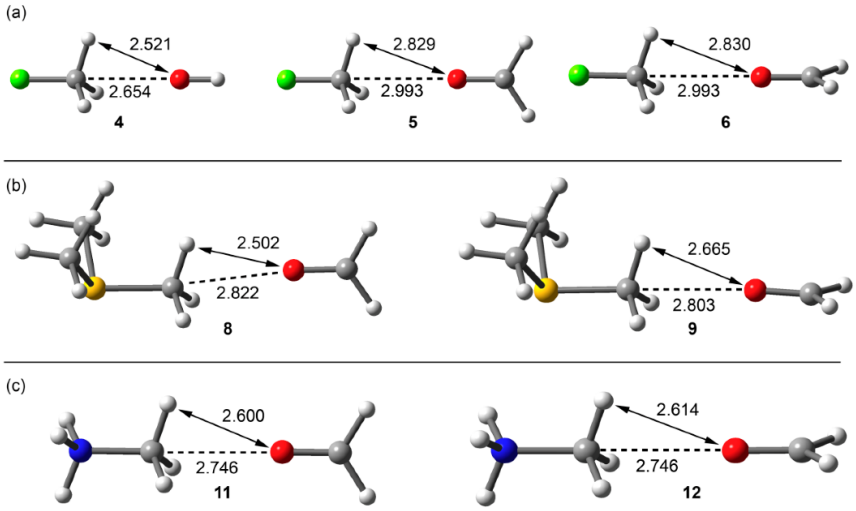

Figure 3. RI-MP2/aug-cc-pVTZ optimized complexes of fluoromethane (**a**); trimethylsulfonium (**b**); and methanaminium (**c**). Distances in Å.

2.3. *AIM Analysis*

We used Bader's theory of "atoms in molecules" (AIM) to characterize the noncovalent bonds in complexes **4**–**12** and to differentiate the type of interaction (carbon or hydrogen bonding). A bond critical point (CP) and a bond path connecting two atoms is unambiguous evidence of interaction. The AIM distribution of critical points and bond paths computed for the complexes is shown in Figure 4. In all CH_3F complexes (Figure 4a), the interaction is characterized by the presence of a bond CP that connects the O atom with the carbon atom, thus confirming the carbon bonding nature of this interaction. The value of ρ at the bond CP that emerges upon complexation is larger in complex **4**

than in either complex **5** or **6**, in agreement with the interaction energies and equilibrium distances. In trimethylsulfonium complex **9**, where the S–C···O angle is close to 180°, the AIM analysis shows a bond CP and bond path unambiguously connecting the C and O atoms. In complex **8**, where the S–C···O angle is 172°, the bond path presents a different trajectory and, at first sight, seems to connect the O atom of formaldehyde to the C–H bond critical point. However, a closer look reveals that the bond path suddenly deviates when it reaches the C–H bond critical point and finally connects to the C atom. The distribution in methanaminium complexes **11** and **12** (see Figure 4c) clearly shows a bond CP and bond path connecting the C and O atoms, thus confirming the carbon bonding nature of the interaction. In all cases, the Laplacian of ρ at the bond CP that connects the O and C atoms is positive, as is common in closed shell interactions. Interestingly, for the whole series of complexes, the value of ρ strongly correlates with the interaction energies. Therefore, the value of ρ can be used as a measure of bond order in this type of noncovalent bonding.

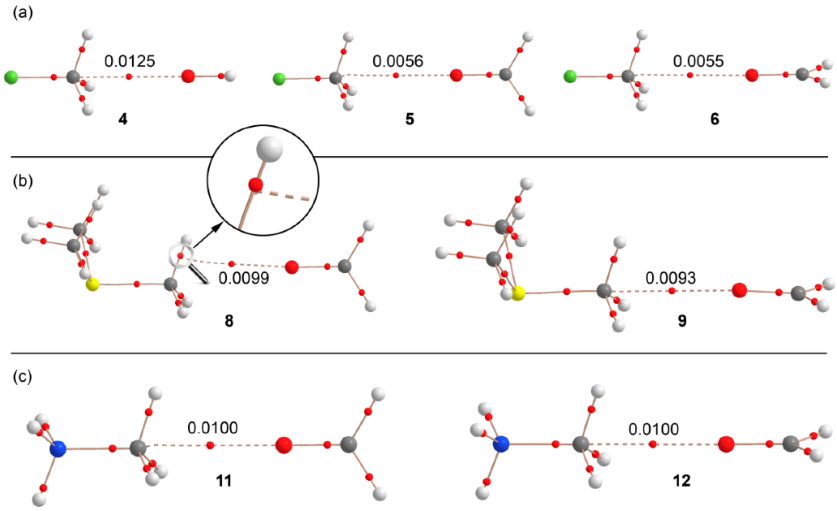

Figure 4. Distribution of critical points (red spheres) and bond paths for complexes of fluoromethane (**a**); trimethylsulfonium (**b**); and methanaminium (**c**) at the RI-MP2/aug-cc-pVTZ level of theory. The value of the charge density (ρ) at the bond critical points that emerge upon complexation are indicated in a.u.

We also analyzed the effect of the X–C···O angle on the interaction to find the value that causes a change from carbon bonding to hydrogen bonding. For this study, we progressively changed the F–C···O angle (α) starting from 180° and moving the O atom in two opposite directions (see Figure 5a): (i) toward a single H atom (α < 180° values) and (ii) toward the middle of two H atoms (α > 180° values). In each point, we optimized the geometry and simply froze the angle to the desired value. Moreover, we analyzed the distribution of critical points in order to find the value of α where the interaction changes from carbon to hydrogen bonding. If the OH^- moves to a single C–H bond (Figure 5b), the interaction rapidly changes from carbon bonding to hydrogen bonding; therefore, the critical angle is close to 170°. This result agrees with the behavior observed for complex **8** (see Figure 4) that presents an S–C···O angle of 172°, and the bond path trajectory reveals that it is in the borderline between both interactions. When the OH^- moves to the opposite direction (toward the middle of two C–H bonds), the behavior is different: For α = 190° a bond path connects the C and O atoms similarly to fully optimized complex **4**. Curiously, and for α = 200° and 210°, two bond paths connect the C and

O atoms, forming a bifurcated carbon bonding. As a consequence, a ring CP (yellow sphere) is also generated. Finally, at 220°, the carbon bonding changes to a bifurcated H-bonding interaction.

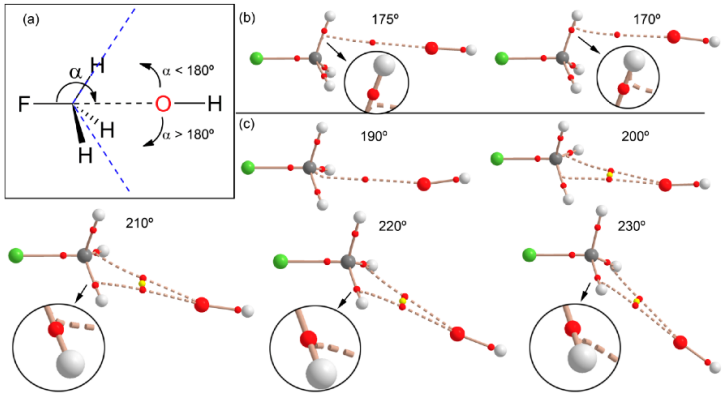

Figure 5. (**a**) Schematic representation of the angle and both directions; (**b**) distribution of critical points (red spheres) and bond paths for complexes of fluoromethane with OH^- using F–C···O angles <180° at the RI-MP2/aug-cc-pVTZ level of theory; (**c**) same as (**b**) but using angles $\alpha > 180°$.

This analysis is useful for defining the search criteria of carbon bonding complexes in X-ray structure databases (CSD, PDB, *etc.*). Since the H atoms bonded to C are usually not experimentally located, there is some uncertainty regarding their real position in the CH_3 group. Therefore, it is recommended that a tight criterion regarding the X–C···O angle (*i.e.*, $\alpha > 170°$) is used when searching for this type of noncovalent carbon bonding X-ray structures.

2.4. PDB Search

We explored the PDB in order to prove the importance of carbon bonding interactions in biologically relevant molecules. The following criteria were used for the search: (i) The CH_3 donor group belongs to the ligand and the O atom is part of the protein; (ii) C···O distance (d) is shorter than 3.2 Å and the X–C···O angle (A) >170°; (iii) only X-ray solid state structures are considered (no NMR resolved); and (iv) a resolution factor <10 Å. The search was performed using the freely available Relibase software [47]. As a result, we found 459 protein-ligand complexes exhibiting this type of bonding (see ESI for the full list of hits and their geometrical features, Table S1). The histograms plots for the angle and distance are represented in Figure 6. The importance of this result should be emphasized since we found a large number of hits, taking into consideration the tight geometric criteria used and that only one electron-rich element was used in the search (O). Therefore, carbon bonding interaction in general has a bright future in this field and will likely become a prominent player for explaining some biological processes, either controlling or fine-tuning the binding of substrates to enzymes.

In the original manuscripts where the protein-ligand complexes were reported, the X–CH_3···O interaction was either overlooked or considered as an H-bonding by the original authors. We selected two examples from this search to further illustrate the importance of this interaction. For the first example [48], we selected a very well resolved X-ray structure (PDB ID: 4NSY, resolution 1.1 Å. see Figure 7a) that is a covalent complex between a trypsin-type serine protease (lysyl endoproteinase, LysC) and its inhibitor N^{α}-p-tosyl-lysyl chloromethylketone (TLCK). Chloromethyl ketones such as TLCK (Figure 7b) are well-known covalent inhibitors of cysteine and serine proteases [49]. Two covalent bonds are formed with serine proteases, each one to the active-site serine and histidine. Similarly, in the LysC enzyme, the TLCK inhibitor is attacked by SER194 and by nucleophilic substitution of the Cl atom

by HIS57. This covalently bonded inhibitor interacts with the other subunit by means of a noncovalent carbon bonding interaction (see Figure 7a). We constructed a model to energetically evaluate this interaction. We substituted the SER193 and HIS47 that are covalently bonded to the inhibitor by C–H bonds in order to keep the size of the system computationally approachable. The model also includes the alanine residue and part of the peptide backbone (see Figure 7c). The interaction energy is −1.8 kcal/mol that is similar to that obtained for neutral complexes **5** and **6** (see Table 1). Remarkably, the distribution of CPs shows a bond critical point and a bond path connecting the O atom of the amide group to the carbon atom of the inhibitor, thus confirming the existence of the carbon bonding interaction in 4NSY.

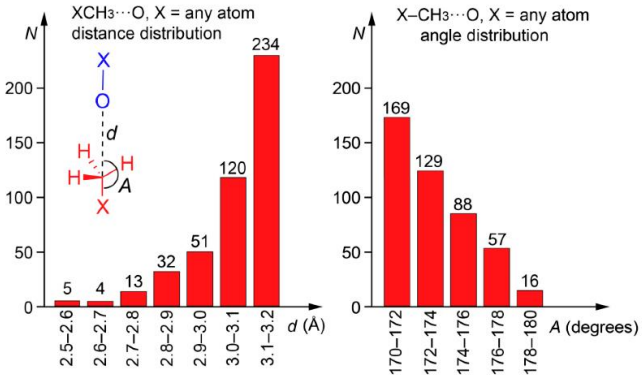

Figure 6. Histograms obtained directly from the Relibase software. Distance distribution is shown on the left and the angle distribution on the right of the figure. Inset figure: definition of *d* and A parameters; the protein is represented in blue and the ligand in red.

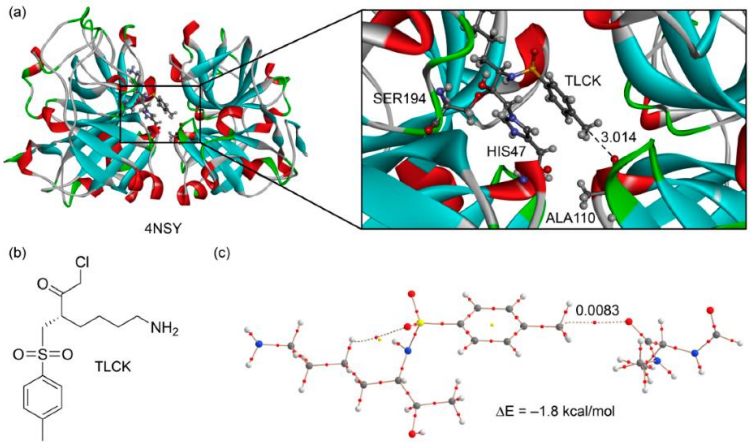

Figure 7. (**a**) X-ray structure of 4NSY with indication of the carbon bonding interaction (distance in Å); (**b**) chemical drawing of the TLCK; (**c**) AIM distribution of critical points of a model derived from the X-ray coordinates.

The second example we selected [50] corresponds to the structure of a M3 muscarinic acetylcholine receptor bound to tiotropium (PDB ID: 4U14, resolution 2.5 Å. see Figure 8a). Tiotropium is a

muscarinic receptor antagonist (anticholinergic bronchodilator) used in the management of chronic obstructive pulmonary disease [51]. The presence of a dimethylammonium group in the structure ensures their ability to form electrostatically assisted carbon (or hydrogen) bonding interactions using the R_3N^+–CH_3 groups. As a matter of fact, an aspartate residue of the active site is very close to a carbon atom belonging to one of both methyl groups (2.935 Å) with an almost linear N–C···O angle (177.4°). We used a theoretical model derived from the crystallographic coordinates that includes the antagonist and the aspartate bonded to a fragment of the peptide backbone. The AIM analysis confirms the existence of a carbon bonding interaction (see bond path in Figure 8a). The ASP147 residue is likely deprotonated in the X-ray structure, since both C–O distances are very similar (1.248 and 1.250 Å). In any case, we evaluated the interaction energy considering both possibilities. The interaction energy of the carbon bonding complex using the protonated ASP147 is –9.0 kcal/mol. Moreover, the value of the density at the bond critical point is ρ = 0.0093 a.u. These values strongly agree with those previous ones computed for methanaminium (see Table 1 and Figure 4 (complexes **11** and **12**)). Considering the deprotonated ASP147, the interaction energy is very large (−73.9 kcal/mol) due to the strong electrostatic contribution. Therefore, this charge-assisted carbon bonding interaction has a strong influence on the binding of tiotropium in the muscarinic acetylcholine receptor.

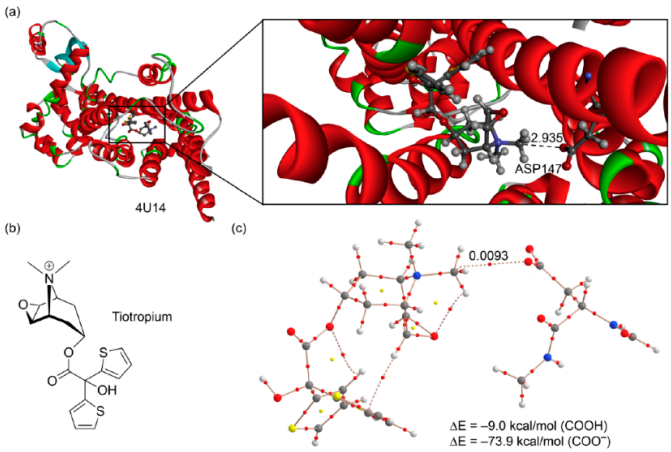

Figure 8. (**a**) X-ray structure of 4U14 with indication of the carbon bonding interaction (distance in Å); (**b**) chemical drawing of the tiotropium antagonist; (**c**) AIM distribution of critical points of a model retrieved from the X-ray coordinates.

2.5. NBO Analysis

To find out whether orbital effects are important to explain the carbon bonding interactions described above, we performed natural bond orbital (NBO) calculations focusing our attention on the second order perturbation analysis, due to its usefulness for studying donor-acceptor interactions [52]. We carried out the NBO calculations for complex **4** and for the theoretical model used to characterize the interaction in the PDB ID 4U14 (see Figure 8c). The results of the second order perturbation analysis are summarized in Table 2. For complex **4**, we found an important orbital contribution that consists in the interaction of the lone pair orbital (LP) of the donor with the C–F antibonding orbital (BD*) of the acceptor. This interaction is significant (3.5 kcal/mol) since it accounts for approximately 27% of the total interaction energy and further confirms that the interaction in complex **4** is with the σ-hole of the carbon atom. Moreover, the expected LP→BD*(C–H) orbital contribution that is typical of a hydrogen bond is less than 0.1 kcal/mol. Similarly, in the PDB 4U14, we found an interesting LP(O)→BD*(C–N)

contribution that is 2.0 kcal/mol and that the LP(O)→BD*(C–H) interaction is less than 0.1 kcal/mol, in sharp agreement with the AIM analysis commented above.

Table 2. Donor and acceptor NBOs with indication of the second-order interaction energy $E^{(2)}$ and donor and acceptor orbitals for complexes **4** and PDB ID 4U14. Energy values are in kcal/mol.

Complex	Donor [1]	Acceptor	$E^{(2)}$
4	LP (O)	BD* (C–H)	<0.1
	LP(O)	BD* (C–F)	3.5
4U14	LP (O)	BD* (C–H)	<0.1
	LP(O)	BD* (C–N)	2.0

[1] LP stands for lone pair orbital and BD* for antibonding orbital.

2.6. SAPT Analysis

In Table 3, we summarize the DF-DFT-SAPT energy values relative to some of the carbon bonding complexes showed above in order to show the relative importance of the electrostatic contribution to the total interaction energies, especially those involving charged carbon bonding donors. The total SAPT interaction energies for these three complexes are similar to those obtained using the RI-MP2/aug-cc-pVTZ level of theory (see Table 1), attributing reliability to the partition method and the level of theory used to compute the SAPT. The energetic contributions (Table 3) indicate that the cationic complexes **9** and **12** are clearly dominated by the electrostatic term. Moreover, the contributions of induction and dispersion terms are also important. In the neutral complex **6**, the electrostatic and dispersion terms equally contribute to the total interaction energy.

Table 3. SAPT interaction energies (E_{total}, kcal/mol) and their partitioning into the electrostatic, exchange, induction, dispersion, and contributions (E_{ee}, E_{ex}, E_{ind}, E_{disp}, respectively, kcal/mol) at the RI-DFT/aug-cc-pVTZ level of theory using the DF-DFT-SAPT approach.

Complex	E_{ee}	E_{ex}	E_{ind}	E_{disp}	E_{total}
6	–1.8	2.1	–0.2	–1.6	–1.5
9	–8.3	4.4	–1.3	–2.4	–7.6
12	–9.5	4.8	–1.7	–2.3	–8.7

To further demonstrate the importance of electrostatic forces in the interaction energies of compounds **9** and **12**, we computed the carbon bonding interaction of their equivalent neutral complexes where methylamine and dimethylthioether are used as carbon bond donors. The results are gathered in Figure 9, and it can be observed that the interaction energies are very small (–0.7 kcal/mol for **13** and −1.1 kcal/mol for **14**), in agreement with the MEP surfaces of methylamine and dimethylthioether shown in Figure 2. Moreover, the localization of the minima corresponding to the carbon bonding complexes **13** and **14** (see Figure 9) on the potential surface is worth emphasizing, since the MEP value at the H-atoms is considerably more positive than that at the C atom in both neutral molecules.

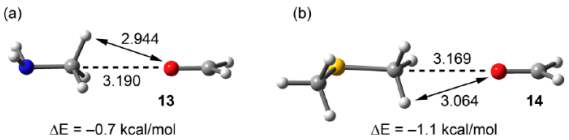

Figure 9. RI-MP2/aug-cc-pVTZ optimized complexes end interaction energies of methylamine (**a**) and dimethylthioether (**b**). Distances in Å.

3. Theoretical Methods

The geometries of the complexes studied herein have been fully optimized at the RI-MP2/aug-cc-pVTZ level of theory. Cartesian coordinates of the optimized complexes are given in the supplementary material file (Tables S2–S8). The calculations have been performed by using the program TURBOMOLE version 7.0 [53]. The interaction energies were calculated with correction for the basis set superposition error (BSSE) by using the Boys–Bernardi counterpoise technique [54]. The C_s symmetry point group has been used in the optimization of the complexes. The minimum nature of the complexes has been confirmed by carrying out frequency calculations. For the theoretical analysis of the noncovalent interactions present in PDB structures 4NSY and 4U14, the BP86-D3/aug-cc-pVTZ level of theory was used; the position of the hydrogen atoms present in these structures was optimized prior to the evaluation of the binding energy values. For the hereoatoms we used the crystallographic coordinates, we used the DFT-D functional with the latest available correction for dispersion (D3) [55]. Bader's "atoms in molecules" theory was used to study the interactions discussed herein by means of the AIMall calculation package [56]. Finally, the partitioning of the interaction energies into the individual electrostatic, induction, dispersion, and exchange-repulsion components was carried out with the symmetry adapted intermolecular perturbation theory approach DFT-SAPT at the BP86/aug-cc-pVTZ level of theory using the aug-cc-pVQZ basis set for the MP2 density fitting [57] by means of the MOLPRO program [58,59].

4. Conclusions

In this manuscript, we analyzed the dual ability of the methyl group (XCH_3) to act as either H-bond or carbon bond donor in complexes with electron-rich oxygen atoms by means of high-level *ab initio* calculations and using Bader's theory of atoms in molecules. For X–C$\cdots$O complexes exhibiting angles close to linearity, a carbon bonding interaction instead of H-bonding is established as confirmed by AIM and NBO analyses. The importance of electrostatic and dispersion contributions to the interaction energy of the carbon bonding complexes was shown using the SAPT partition scheme. We demonstrated the importance of latter interactions in biological systems by examining the PDB and illustrated this in two selected examples. Since $-CH_3$ groups are commonplace, non-covalent carbon bonding involving this group might turn out to be as functionally relevant as other σ-hole and hydrogen bonding interactions.

Supplementary Materials: The following are available online at http://www.mdpi.com/2073-4352/6/3/26/s1. Table S1: Results from the PDB search. Distances in Å. Angles in degrees. Table S2: Cartesian coordinates of the complexes **4**. Table S3: Cartesian coordinates of the complexes **5**. Table S4: Cartesian coordinates of the complexes **6**. Table S5: Cartesian coordinates of the complexes **8**. Table S6: Cartesian coordinates of the complexes **9**. Table S7: Cartesian coordinates of the complexes **11**. Table S8: Cartesian coordinates of the complexes **12**.

Acknowledgments: We thank CONSOLIDER-Ingenio 2010 (project CSD2010-0065) and the MICINN of Spain (project CTQ2014-57393-C2-1-P FEDER funds). We thank the CTI for computational facilities.

Author Contributions: Antonio Bauzá and Antonio Frontera conceived and designed the calculations; Antonio Bauzá and Antonio Frontera analyzed the data; Antonio Frontera wrote the paper.

Conflicts of Interest: The authors declare no conflict of interest. The founding sponsors had no role in the design of the study, in the collection, analyses, or interpretation of data, in the writing of the manuscript, or in the decision to publish the results.

Abbreviations

The following abbreviations are used in this manuscript:

AIM	Atoms in molecules
DMF	Dimethylformamide
MEP	Molecular electrostatic potential

MP2	Second order Moller-Plesset
SAM	S-Adenosyl methionine
PDB	Protein Databank
CSD	Cambridge Structural Database
CP	Critical point
LysC	lysyl endoproteinase
TLCK	N^{α}-p-tosyl-lysyl chloromethylketone
ASP	Aspartate
HIS	Histidine
SER	Serine
NBO	Natural Bond Orbital
SAPT	Symmetry adapted perturbation theory

References

1. Schneider, H.J. Binding mechanisms in supramolecular complexes. *Angew. Chem. Int. Ed.* **2009**, *48*, 3924–3977. [CrossRef] [PubMed]
2. Schneider, H.J.; Yatsimirski, A. *Principles and Methods in Supramolecular Chemistry*; Wiley: Chichester, UK, 2000.
3. Lehn, J.M. *Supramolecular Chemistry Concepts and Perspectives*; Wiley–VCH: Weinheim, Germany, 1995.
4. Vögtle, F. *Supramolecular Chemistry: An Introduction*; Wiley: New York, NY, USA, 1993.
5. Beer, P.D.; Gale, P.A.; Smith, D.K. *Supramolecular Chemistry*; Oxford University Press: Oxford, UK, 1999.
6. Steed, J.W.; Atwood, J.L. *Supramolecular Chemistry*; Wiley: Chichester, UK, 2000.
7. Destecroix, H.; Renney, H.C.M.; Mooibroek, T.J.; Carter, T.S.; Stewart, P.F.N.; Crump, M.P.; Davis, A.P. Affinity enhancement by dendritic side chains in synthetic carbohydrate receptors. *Angew. Chem. Int. Ed.* **2015**, *54*, 2057–2061. [CrossRef] [PubMed]
8. Murray-Rust, P.; Motherwell, W.D.S. Computer retrieval and analysis of molecular geometry. 4. Intermolecular interactions. *J. Am. Chem. Soc.* **1979**, *101*, 4374–4376. [CrossRef]
9. Murray-Rust, P.; Stallings, W.C.; Monti, C.T.; Preston, R.K.; Glusker, J.P. Intermolecular interactions of the carbon-fluorine bond: The crystallographic environment of fluorinated carboxylic acids and related structures. *J. Am. Chem. Soc.* **1983**, *105*, 3206–3214. [CrossRef]
10. Ramasubbu, N.; Parthasarathy, R.; Murray-Rust, P. Angular preferences of intermolecular forces around halogen centers: Preferred directions of approach of electrophiles and nucleophiles around carbon-halogen bond. *J. Am. Chem. Soc.* **1986**, *108*, 4308–4314. [CrossRef]
11. Metrangolo, P.; Neukirch, H.; Pilati, T.; Resnati, G. Halogen bonding based recognition processes: A world parallel to hydrogen bonding. *Acc. Chem. Res.* **2005**, *38*, 386–395. [CrossRef] [PubMed]
12. Politzer, P.; Murray, J.S. Halogen bonding: An interim discussion. *ChemPhysChem* **2013**, *14*, 278–294. [CrossRef] [PubMed]
13. Bauzá, A.; Mooibroek, T.J.; Frontera, A. The Bright Future of Unconventional σ/π-Hole Interactions. *ChemPhysChem* **2015**, *16*, 2496–2517. [CrossRef] [PubMed]
14. Politzer, P.; Murray, J.S.; Clark, T. Halogen bonding: An electrostatically-driven highly directional noncovalent interaction. *Phys. Chem. Chem. Phys.* **2010**, *12*, 7748–7757. [CrossRef] [PubMed]
15. Bauzá, A.; Mooibroek, T.J.; Frontera, A. Tetrel Bonding Interactions. *Chem. Rec.* **2016**, *16*, 473–487. [CrossRef] [PubMed]
16. Bauzá, A.; Mooibroek, T.J.; Frontera, A. Tetrel-bonding interaction: Rediscovered supramolecular force? *Angew. Chem. Int. Ed.* **2013**, *52*, 12317–12321. [CrossRef] [PubMed]
17. Bauzá, A.; Frontera, A. Competition between halogen bonding and π-hole interactions involving various donors: the role of dispersion effects. *ChemPhysChem* **2015**, *16*, 3108–3113.
18. Desiraju, G.R. A bond by any other name. *Angew. Chem. Int. Ed.* **2011**, *50*, 52–59. [CrossRef] [PubMed]
19. Desiraju, G.R.; Steiner, T. *The Weak Hydrogen Bond in Structural Chemistry and Biology*; Oxford University Press: Oxford, UK, 1999.

20. Larson, J.W.; McMahon, T.B. Gas-phase bihalide and pseudobihalide ions. An ion cyclotron resonance determination of hydrogen bond energies in XHY- species (X, Y = F, Cl, Br, CN). *Inorg. Chem.* **1984**, *23*, 2029–2033. [CrossRef]
21. Nishio, M.; Umezawa, Y.; Fantini, J.; Weiss, M.S.; Chakrabarti, P. CH–π hydrogen bonds in biological macromolecules. *Phys. Chem. Chem. Phys.* **2014**, *16*, 12648–12683. [CrossRef] [PubMed]
22. Nishio, M.; Umezawa, Y.; Honda, K.; Tsuboyamad, S.; Suezawae, H. CH/π hydrogen bonds in organic and organometallic chemistry. *CrystEngComm* **2009**, *11*, 1757–1788. [CrossRef]
23. Nishio, M.; Hirota, M.; Umezawa, Y. *The C–H/π Interaction: Evidence, Nature, Consequences*; Wiley: New York, NY, USA, 1998.
24. Samanta, U.; Pal, D.; Chakrabarti, P. Environment of tryptophan side chains in proteins. *Proteins* **2000**, *38*, 288–300. [CrossRef]
25. Plevin, M.J.; Bryce, D.L.; Boisbouvier, J. Direct detection of CH/π interactions in proteins. *Nat. Chem.* **2010**, *2*, 466–471. [CrossRef] [PubMed]
26. Brandl, M.; Weiss, M.M.S.; Jabs, A.; Sühnel, J.; Hilgenfeld, R. C-H...pi-interactions in proteins. *J. Mol. Biol.* **2001**, *307*, 357–377. [CrossRef] [PubMed]
27. Quiocho, F.A.; Vyas, N.K. Novel stereospecificity of the L-arabinose-binding protein. *Nature* **1984**, *310*, 381–386. [CrossRef] [PubMed]
28. Vyas, N.K.; Vyas, M.N.; Quiocho, F.A. Sugar and signal-transducer binding sites of the *Escherichia coli* galactose chemoreceptor protein. *Science* **1988**, *242*, 1290–1295. [CrossRef] [PubMed]
29. Nishio, M. The CH/π hydrogen bond in chemistry. Conformation, supramolecules, optical resolution and interactions involving carbohydrates. *Phys. Chem. Chem. Phys.* **2011**, *13*, 13873–13900. [CrossRef] [PubMed]
30. Laughrey, Z.R.; Kiehna, S.E.; Riemen, A.J.; Waters, M.L. Carbohydrate−π Interactions: what are they worth? *J. Am. Chem. Soc.* **2008**, *130*, 14625–14633. [CrossRef] [PubMed]
31. Barwell, N.P.; Davis, A.P. Substituent effects in synthetic lectins—Exploring the role of CH−π interactions in carbohydrate recognition. *J. Org. Chem.* **2011**, *76*, 6548–6557. [CrossRef] [PubMed]
32. Politzer, P.; Murray, J.S.; Clark, T. Halogen bonding and other σ-hole interactions: A perspective. *Phys. Chem. Chem. Phys.* **2013**, *15*, 11178–11189. [CrossRef] [PubMed]
33. Murray, J.S.; Riley, K.E.; Politzer, P.; Clark, T. Directional weak intermolecular interactions: σ-hole bonding. *Aust. J. Chem.* **2010**, *63*, 1598–1607. [CrossRef]
34. Clark, T. σ-Holes. *Wiley Interdiscip. Rev. Comput. Mol. Sci.* **2013**, *3*, 13–20. [CrossRef]
35. Bauzá, A.; Mooibroek, T.J.; Frontera, A. σ-Hole opposite to a lone pair: unconventional pnicogen bonding interactions between ZF_3 (Z = N, P, As and Sb). *ChemPhysChem* **2016**, *17*. [CrossRef]
36. Bundhun, A.; Ramasami, P.; Murray, J.S.; Politzer, P. Trends in σ-hole strengths and interactions of F_3MX molecules (M = C, Si, Ge and X = F, Cl, Br, I). *J. Mol. Model.* **2013**, *19*, 2739–2746. [CrossRef] [PubMed]
37. Grabowski, S.J. Tetrel bond–σ-hole bond as a preliminary stage of the SN_2 reaction. *Phys. Chem. Chem. Phys.* **2014**, *16*, 1824–1834. [CrossRef] [PubMed]
38. Bauzá, A.; Mooibroek, T.J.; Frontera, A. Small cycloalkane $(CN)_2C$–$C(CN)_2$ Structures Are Highly Directional Non-covalent Carbon-Bond Donors. *Chem. Eur. J.* **2014**, *20*, 10245–10248.
39. Bauzá, A.; Mooibroek, T.J.; Frontera, A. 1,1,2,2-Tetracyanocyclopropane (TCCP) as supramolecular synthon. *Phys. Chem. Chem. Phys.* **2016**, *18*, 1693–1698. [CrossRef] [PubMed]
40. Escudero-Adán, E.C.; Bauzá, A.; Frontera, A.; Ballester, P. Nature of noncovalent carbon-bonding interactions derived from experimental charge-density analysis. *ChemPhysChem* **2015**, *16*, 2530–2533. [CrossRef] [PubMed]
41. Mani, D.; Arunan, E. The X–C···Y (X = O/F, Y = O/S/F/Cl/Br/N/P) 'carbon bond' and hydrophobic interactions. *Phys. Chem. Chem. Phys.* **2013**, *15*, 14377–14383. [CrossRef] [PubMed]
42. Thomas, S.P.; Pavan, M.S.; Row, T.N.G. Experimental evidence for 'carbon bonding' in the solid state from charge density analysis. *Chem. Commun.* **2014**, *50*, 49–51. [CrossRef] [PubMed]
43. Solimannejad, M.; Orojloo, M.; Amani, S. Effect of cooperativity in lithium bonding on the strength of halogen bonding and tetrel bonding: $(LiCN)_n\cdots ClYF_3$ and $(LiCN)_n\cdots YF_3Cl$ (Y = C, Si and n = 1–5) complexes as a working model. *J. Mol. Model.* **2015**, *21*, 183. [CrossRef] [PubMed]
44. Marín-Luna, M.; Alkorta, I.; Elguero, J. Cooperativity in Tetrel Bonds. *J. Phys. Chem. A* **2016**, *120*, 648–656. [CrossRef] [PubMed]

45. Guo, X.; Liu, Y.-W.; Li, Q.-Z.; Li, W.-Z.; Cheng, J.-B. Competition and cooperativity between tetrel bond and chalcogen bond in complexes involving F2CX (X = Se and Te). *Chem. Phys. Lett.* **2015**, *620*, 7–12. [CrossRef]
46. Bader, R.F.W. A quantum theory of molecular structure and its applications. *Chem. Rev.* **1991**, *91*, 893–928. [CrossRef]
47. Relibase. Available online: https://www.ccdc.cam.ac.uk/Community/freeservices/Relibase/ (accessed on 25 January 2016).
48. Asztalos, P.; Müller, A.; Hölke, W.; Sobek, H.; Rudolph, M.G. Atomic resolution structure of a lysine-specific endoproteinase from Lysobacter enzymogenes suggests a hydroxyl group bound to the oxyanion hole. *Acta Crystallogr. Sect. D—Biol. Crystallogr.* **2014**, *70*, 1832–1843. [CrossRef] [PubMed]
49. Drenth, J. Binding of chloromethyl ketone substrate analogues to crystalline papain. *Biochemistry* **1976**, *15*, 3731–3738. [CrossRef] [PubMed]
50. Thorsen, T.S.; Matt, R.; Weis, W.I.; Kobilka, B.K. Modified T4 Lysozyme Fusion Proteins Facilitate G Protein-Coupled Receptor Crystallogenesis. *Structure* **2014**, *22*, 1657–1664. [CrossRef] [PubMed]
51. Kato, M.; Komamura, K.; Kitakaze, M. Tiotropium, a novel muscarinic M3 receptor antagonist, improved symptoms of chronic obstructive pulmonary disease complicated by chronic heart failure. *Circ. J.* **2006**, *70*, 1658–1660. [CrossRef] [PubMed]
52. Weinhold, F.; Landis, C.R. *Valency and Bonding: A Natural Bond Orbital Donor-Acceptor Perspective*; Cambridge University Press: Cambridge, UK, 2005.
53. Ahlrichs, R.; Bär, M.; Hacer, M.; Horn, H.; Kömel, C. Electronic structure calculations on workstation computers: the program system TURBOMOLE. *Chem. Phys. Lett.* **1989**, *162*, 165–169. [CrossRef]
54. Boys, S.B.; Bernardi, F. The calculation of small molecular interactions by the differences of separate total energies. Some procedures with reduced errors. *Mol. Phys.* **1970**, *19*, 553–566. [CrossRef]
55. Grimme, S.; Antony, J.; Ehrlich, S.; Krieg, H.A. Consistent and accurate *ab initio* parametrization of density functional dispersion correction (DFT-D) for the 94 elements H-Pu. *J. Chem. Phys.* **2010**, *132*, 154104–154119. [CrossRef] [PubMed]
56. Todd, A.; Keith, T.K. *AIMAll*; Version 13.05.06; Gristmill Software: Overland Park, KS, USA, 2013.
57. Heßelmann, A.; Jansen, G. The helium dimer potential from a combined density functional theory and symmetry-adapted perturbation theory approach using an exact exchange–correlation potential. *Phys. Chem. Chem. Phys.* **2003**, *5*, 5010–5014. [CrossRef]
58. Werner, H.-J.; Knowles, P.J.; Knizia, G.; Manby, F.R.; Schütz, M. Molpro: A general-purpose quantum chemistry program package. *WIREs Comput. Mol. Sci.* **2012**, *2*, 242–253. [CrossRef]
59. Werner, H.-J.; Knowles, P.J.; Knizia, G.; Manby, F.R.; Schütz, M.; Celani, P.; Korona, T.; Lindh, R.; Mitrushenkov, A.; Rauhut, G.; *et al.* MOLPRO, Version 2012.1; a Package of ab Initio Programs. Available online: https://www.molpro.net/info/authors (accessed on 15 March 2016).

ChemComm

COMMUNICATION

View Article Online
View Journal | View Issue

Directionality of π-holes in nitro compounds†

Antonio Bauzá,[a] Tiddo J. Mooibroek*[b] and Antonio Frontera*[a]

Cite this: *Chem. Commun.*, 2015, **51**, 1491

Received 15th November 2014,
Accepted 1st December 2014

DOI: 10.1039/c4cc09132a

www.rsc.org/chemcomm

A statistical survey of the Cambridge Structural Database reveals that the interaction between the π-holes of nitro groups and electron-rich atoms is somewhat directional. High-level *ab initio* computations indicate energies up to −6.6 kcal mol^{-1}.

Intermolecular interactions determine how molecules interact with one another, and are thus fundamental to inquiries in areas like supramolecular chemistry and molecular biology.[1] It is well-appreciated that even weak interactions (*e.g.*, hydrogen bonding involving C–H) can bear functional relevance, especially when several such forces work in concert.[2] This begs the question what weak interactions can be identified as possibly functionally relevant.

Hydrogen (H) and halogen (Hlg) bonds are by far the best established intermolecular forces.[3] The regions of electropositive potential on R–H and R–Hlg (Fig. 1a and b, phenol and bromobenzene, respectively) can be described as unpopulated σ* antibonding orbitals along the R–H/Hlg vector.[7b,c] These 'σ-holes' have also been identified on atoms that belong to the oxygen, nitrogen and carbon families, and their binding to electron-rich entities is referred to as chalcogen-,[4] pnicogen-,[5] and tetrel-bonding,[6] respectively.

In analogy to the σ-hole, a π-hole can be seen as an electropositive potential located on an unpopulated π*-orbital. The best-known π-hole interactions involve carbonyl compounds (*e.g.*, *p*-quinone, as shown in Fig. 1c): Bürgi and Dunitz[7] uncovered the trajectory along which a nucleophile attacks the π-hole of a carbonyls' C-atom, and π-hole interactions involving amides are known to persist in protein structures.[8] Aromatic rings bearing electron withdrawing substituents, such as hexafluorobenzene (Fig. 1d), can also function as π-holes.[9] Interactions involving such π acidic aromatic rings are generally referred to as anion- or lone pair-π interactions.[10]

A recent theoretical study revealed that a π-hole can also be found on a nitro group.[11] Association of this π-hole with electron-rich entities (ElR, *e.g.*, H_2O and Cl^-) was estimated to vary in strength between −0.5 and −27.9 kcal mol^{-1}. Fig. 1e and f illustrate the π-holes in nitromethane and nitrobenzene, respectively. One might thus wonder if the '$NO_2^{\pi}\cdots$ElR' interaction bears any functional relevance. The first step towards answering this question is to establish whether this intermolecular force is actually directional. Analysis of the data compiled within the Cambridge Structural Database (CSD)[12] has proven to be an exquisite tool for revealing the directional nature of traditional and non-canonical intermolecular forces. We thus set out to evaluate the CSD using a methodology that is particularly apt for ascertaining the directional character of weak intermolecular forces.[9]

Aliphatic and aromatic C–NO_2 compounds that are abundant within the CSD were considered: there are 900 crystallographic information files (CIFs) containing nitromethane, and 14 227 CIFs containing an aromatic nitro compound where the NO_2 moiety is flanked by two *ortho*-H's (this allows the NO_2 and C_6H_2 moieties to be relatively coplanar). Fig. 2a illustrates the query used to obtain initial datasets from the CSD.

An entry was considered a hit when the intermolecular distance (*D*) between the C–N centroid (blue) and any electron-rich atom (red, ElR = N, P, As, O, S, Se, Te, F, Cl, Br, I or At) was ≤5 Å. The initial dataset was thus confined within a sphere with a radius of 5 Å, centred on the C–N centroid. The spatial separation (*d*) between ElR and the CNO_2 plane was also retrieved from the CSD. The *xy* coordinates relative to this plane were determined as described elsewhere.[13] By virtue of Pythagoras's theorem, the parallel displacement parameter *r* could be derived

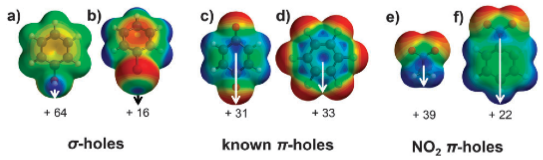

Fig. 1 Some σ-and π-holes with their electropositive potential in kcal mol^{-1} (MP2/6-311+G**).

[a] *Department of Chemistry, Universitat de les Illes Balears, Crta. de Valldemossa km 7.5, 07122 Palma (Baleares), Spain. E-mail: toni.frontera@uib.es; Fax: +34 971 173426*
[b] *School of Chemistry of the University of Bristol, Cantock's Close, BS8 1TS, Bristol, UK. E-mail: chtjm@bristol.ac.uk*

† Electronic supplementary information (ESI) available. See DOI: 10.1039/c4cc09132a

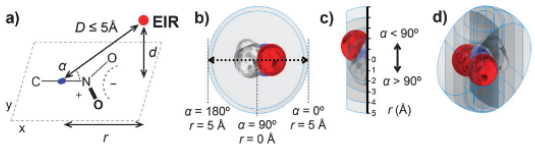

Fig. 2 Illustrations of the method used to analyse directionality of intermolecular interactions between an electron-rich atom (ElR., N, P, As, O, S, Se, Te, F, Cl, Br, I or At) and a nitro group (in this illustration nitromethane).

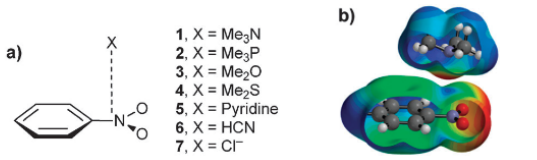

Fig. 4 (a) Complexes **1–7** studied in this work. (b) A pictorial representation of the complementarity of the MEP surfaces of nitrobenzene and trimethylamine.

from D and d. The $CN^{centroid}$–N–ElR angle (α) was measured as well.

For this study, only the data characterized by $y = \pm 2$ Å were considered, which are therefore located within the 4 Å wide spherical segment, as illustrated in Fig. 2b–d. The data can thus be characterized by the parallel displacement (r) within this spherical segment, either towards the NO_2 group ($\alpha < 90°$) or towards the other atoms attached to C ($\alpha > 90°$). To analyse directionality, we applied a method described in detail elsewhere.[9,13,14] This method entails computing the parameter $P(r)$,‡ which signifies the distribution of the data along r that is corrected for the volume occupied by the host and for a random scattering of data. When $P \neq 1$, non-accidental clustering of data is established and $P > 1$ is indicative of an attractive interaction.

The P *versus* r plots for CH_3NO_2 (black circles) and $C_6H_2NO_2$ (open circles) are shown on the left hand side of Fig. 3. For both 'hosts', $P > 1$ around $r = 0$, indicating some directionality of the π-hole. The P-values of 2–3 are similar to those observed for $C–H\cdots\pi^{phenyl}$ hydrogen bonding.[15] In the case of CH_3NO_2, the observed clustering is spread out over the region ranging from $r = -1$ to +1 Å. It is likely that CH···ElR hydrogen bonding also contributes to the observed distribution. The clustering observed for aromatic NO_2 is spread out over the region from $r = 0$ to +1 Å, and hydrogen bonding cannot contribute in this case. It was further assessed how exactly the data are distributed within the data characterized by $-1 > r < 1$ Å. Thus, the relative hit fraction was plotted as a function of the van der Waals corrected $CN^{centroid}\cdots$ElR distance, as shown on the right hand side of Fig. 3. For both central groups, roughly 20% van der Waals overlap is present. These two plots together indeed show that a nitro moiety can be a directional π-hole donor.

We have theoretically analysed (see the ESI† for details) several representative complexes between electron-rich moieties and nitrobenzene (Fig. 4a; a similar study with nitromethane is reported elsewhere).[11] The interaction energies and some geometric features of the complexes are summarized in Table 1. The interaction energies are similar for nearly all complexes ranging from −2.3 to −6.6 kcal mol^{-1} and the most favourable one corresponds to chloride complex **7**. The π-hole in nitrobenzene is located along the C–N bond and close to the nitrogen atom (see Fig. 1f and 4b). We have included both ElR···N and ElR···C distances (denoted as D_N and D_C, respectively) in Table 1. All complexes exhibit similar D_N and D_C distances and in all cases the electron-rich atom is located over the C–N bond, in agreement with results of the MEP analysis. The interaction energy is modest in complex **6** due to the low basicity of the sp-hybridized nitrogen atom of the HCN molecule.

Table 1 BSSE corrected interaction energies (E, kcal mol^{-1}) and equilibrium distances from the electron-rich atom to the N (D_N) and C (D_C) atoms of the C–NO_2 moiety (in Å) of complexes **1–7** at the RI-MP2/def2-TZVPD//PB86-D3/def2-TZVPD level of theory

Complex	E	D_N	D_C
1	−6.2	2.770	2.932
2	−4.3	3.636	3.547
3	−4.4	2.825	2.931
4	−4.7	3.416	3.448
5	−4.7	2.956	3.001
6	−2.3	3.181	3.191
7	−6.6	3.204	3.047

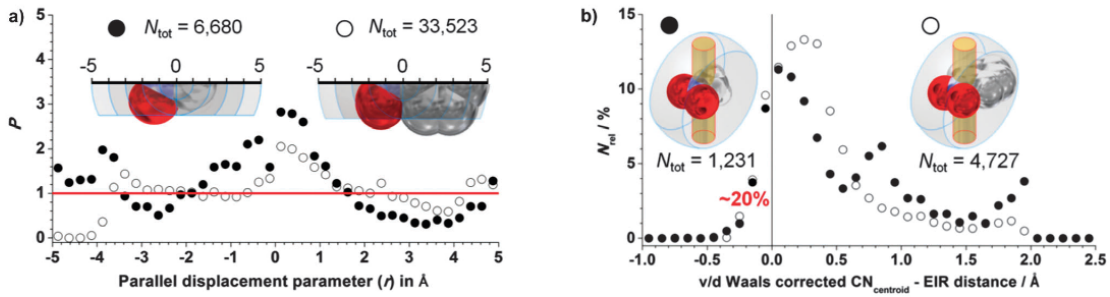

Fig. 3 Analysis of the directional nature of CNO_2 π-holes. Left: directionality plots of P *vs.* r for $CH_3NO_2\cdots$ElR (●, N_{tot} = 6 680) and $C_6H_2NO_2\cdots$ElR (○, N_{tot} = 33 523) of the data characterized by $D \leq 5$ Å and $y \pm 2$ Å; right: $N_{relative}$ *vs.* v/d Waals corrected $CN_{centroid}$–ELR distance (assuming $(^{vdW}C + {}^{vdW}N)/2$ = 1.625 Å) for $CH_3NO_2\cdots$ElR (●, N_{tot} = 1 231) and $C_6H_2NO_2\cdots$ElR (○, N_{tot} = 4 727) of the data characterized by $D \leq 5$ Å and $r \pm 1$ Å.

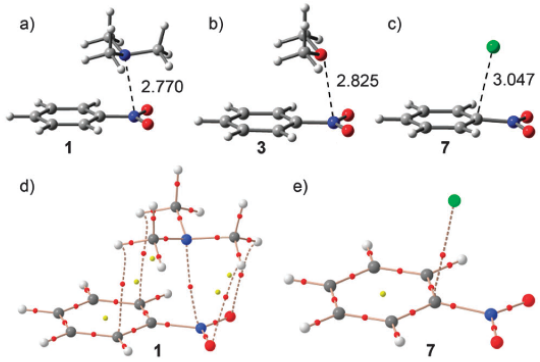

Fig. 5 (a–c) Optimized π-hole complexes **1**, **3** and **7** studied in this work. (d and e) Distribution of critical points in complexes **1** and **7** (bond and ring critical points are represented by red and yellow spheres, respectively). Bond paths connecting bond critical points are represented.

The optimized geometries of some complexes are shown in Fig. 5, including the "atoms-in-molecules"[16] (AIM) distribution of critical points computed for complexes **1** (lone pair donor ElR) and **5** (anionic ElR). The optimized geometries and critical point distribution for the rest of the complexes are included in the ESI.‡ It can be clearly observed in Fig. 5 and Fig. S1 (ESI†) that the position of the ElR atom of the interacting molecule coincides with the location of the π-hole in all complexes, indicating that the interaction is basically electrostatic in nature. The AIM analysis of **1** is complicated since it shows five bond critical points symmetrically distributed. One bond critical point ($\rho = 1.54 \times 10^2$ a.u.) connects both nitrogen atoms characterizing and confirming the π-hole interaction. In addition, two bond critical points ($\rho = 0.62 \times 10^2$ a.u.), which connect two hydrogen atoms of trimethylamine to two carbon atoms of the ring, reveal the presence of two C–H/π interactions. Moreover, two additional bond critical points ($\rho = 0.70 \times 10^2$ a.u.) connecting two hydrogen atoms to the oxygen atoms of the nitro group, reveal the presence of two C–H···O interactions. The charge density computed at the bond critical point that connects both nitrogen atoms is considerably greater than the ones measured at the other bond critical points (1.54×10^2 *vs.* $\sim 0.66 \times 10^2$). Therefore, the complexation is dominated by the π-hole interaction with some contribution of the other two interactions. In complex **7**, the distribution shows a single bond critical point that connects Cl^- to the carbon atom, instead of the nitrogen atom, confirming the interaction.

In conclusion, we have demonstrated that the nitro groups in nitromethane and nitrobenzene are able to interact favourably with electron-rich molecules by means of the π-hole that is located above and below the C–N bond. The interaction is characterized by the presence of a bond critical point that connects the ElR atom to the C–N bond. More importantly, the statistical survey of the CSD study reveals that the interaction between the π-holes of nitro-groups and electron-rich atoms is directional. Nitro groups are widespread amongst small organic molecules and to date the protein data bank (PDB) contains 380 ligands that bear an $-NO_2$ moiety. It is thus reasonable to anticipate an experimental study unveiling the functional relevance of this novel π-hole interaction.

AB and AF thank MINECO of Spain (projects CTQ2011-27512/BQU and CSD2010-00065, FEDER funds) for financial support.

Notes and references

‡ $$P(r) = \frac{N_r}{N_{\text{total}}} \Big/ \frac{V_r^{\text{free}}}{V_{\text{total}}^{\text{free}}}$$

N_r = the number of hits in between two *r*-values; N_{total} = the total number of hits; V_r^{free} = the volume in between two *r*-values minus the volume of the host in between these two *r*-values (hence, the free volume), as found within a 4 Å wide symmetrical spherical segment of a sphere with a 5 Å radius; $V_{\text{total}}^{\text{free}}$ is the volume of a 4 Å wide symmetrical spherical segment of a sphere with a 5 Å radius minus the volume of the host in that body. Models of the central groups were constructed using averages of interatomic distances and angles and assuming generally accepted van der Waals radii. All volumes were computed using Autodesk® Inventor® Professional.

1 (*a*) H. J. Schneider, *Angew. Chem., Int. Ed.*, 2009, **48**, 3924–3977; (*b*) H. J. Schneider and A. Yatsimirski, *Principles and methods in supramolecular chemistry*, Wiley, Chichester, 2000.
2 (*a*) T. Steiner, *Angew. Chem., Int. Ed.*, 2002, **41**, 48–76; (*b*) M. Brandl, M. S. Weiss, A. Jabs, J. Suhnel and R. Hilgenfeld, *J. Mol. Biol.*, 2001, **307**, 357–377.
3 (*a*) *Hydrogen Bonding: New Insights*, ed. S. Grabowski, Springer, Heidelberg, 2006; (*b*) M. Erdélyi, *Chem. Soc. Rev.*, 2012, **41**, 3547; (*c*) E. Parisini, P. Metrangolo, T. Pilati, G. Resnati and G. Terraneo, *Chem. Soc. Rev.*, 2010, **39**, 3772.
4 (*a*) M. Iwaoka, S. Takemoto and S. Tomoda, *J. Am. Chem. Soc.*, 2002, **124**, 10613–10620; (*b*) D. B. Werz, R. Gleiter and F. Rominger, *J. Am. Chem. Soc.*, 2002, **124**, 10638–10639; (*c*) P. Sanz, O. Mó and M. Yáñez, *Phys. Chem. Chem. Phys.*, 2003, **5**, 2942–2947.
5 (*a*) S. Zahn, R. Frank, E. Hey-Hawkins and B. Kirchner, *Chem. – Eur. J.*, 2011, **17**, 6034–6038; (*b*) S. Scheiner, *J. Chem. Phys.*, 2011, **134**, 094315; (*c*) J. E. Del Bene, I. Alkorta, G. Sánchez-Sanz and J. Elguero, *J. Phys. Chem. A*, 2012, **116**, 9205–9213; (*d*) P. Kilian, A. M. Z. Slawin and J. D. Woollins, *Chem. – Eur. J.*, 2003, **9**, 215–222.
6 (*a*) A. Bauzá, T. J. Mooibroek and A. Frontera, *Angew. Chem., Int. Ed.*, 2013, **52**, 12317–12321; (*b*) S. J. Grabowski, *Phys. Chem. Chem. Phys.*, 2014, **16**, 1824–1834; (*c*) A. Bauzá, T. J. Mooibroek and A. Frontera, *Chem. – Eur. J.*, 2014, **20**, 10245–10248; (*d*) A. Bauzá, T. J. Mooibroek and A. Frontera, *Chem. Commun.*, 2014, **50**, 12626–12629.
7 (*a*) H. B. Burgi, *Inorg. Chem.*, 1973, **12**, 2321–2325; (*b*) H. B. Burgi, J. D. Dunitz and E. Shefter, *J. Am. Chem. Soc.*, 1973, **95**, 5065–5067; (*c*) H. B. Burgi, J. D. Dunitz, J. M. Lehn and G. Wipff, *Tetrahedron*, 1974, **30**, 1563–1572.
8 (*a*) P. H. Maccallum, R. Poet and E. J. Milnerwhite, *J. Mol. Biol.*, 1995, **248**, 374–384; (*b*) G. J. Bartlett, A. Choudhary, R. T. Raines and D. N. Woolfson, *Nat. Chem. Biol.*, 2010, **6**, 615–620; (*c*) M. Harder, B. Kuhn and F. Diederich, *ChemMedChem*, 2013, **8**, 397–404.
9 (*a*) T. J. Mooibroek and P. Gamez, *CrystEngComm*, 2012, **14**, 3902–3906; (*b*) T. J. Mooibroek and P. Gamez, *CrystEngComm*, 2012, **14**, 1027–1030.
10 A. Frontera, P. Gamez, M. Mascal, T. J. Mooibroek and J. Reedijk, *Angew. Chem., Int. Ed.*, 2011, **50**, 9564–9583.
11 A. Bauza, R. Ramis and A. Frontera, *J. Phys. Chem. A*, 2014, **118**, 2827–2834.
12 F. H. Allen, *Acta Crystallogr., Sect. B: Struct. Sci.*, 2002, **58**, 380–388.
13 K. E. Ranaghan, J. E. Hung, G. J. Bartlett, T. J. Mooibroek, J. N. Harvey, D. N. Woolfson, W. A. van der Donk and A. Mulholland, *Chem. Sci.*, 2014, **5**, 2191–2199.
14 (*a*) T. J. Mooibroek and P. Gamez, *CrystEngComm*, 2013, **15**, 1802–1805; (*b*) T. J. Mooibroek and P. Gamez, *CrystEngComm*, 2013, **15**, 4565–4570.
15 T. J. Mooibroek and P. Gamez, *CrystEngComm*, 2012, **14**, 8462–8467.
16 (*a*) R. F. W. Bader, *Atoms in Molecules: A Quantum Theory*, Oxford University Press, USA, 1994; (*b*) R. F. W. Bader, *Chem. Rev.*, 1991, **91**, 893–928; (*c*) R. F. W. Bader, *Atoms in Molecules*, Encyclopaedia of Computational Chemistry, 1998, vol. 1, pp. 64–86.

View Article Online / Journal Homepage / Table of Contents for this issue
Dynamic Article Links

PCCP

Cite this: *Phys. Chem. Chem. Phys.*, 2012, **14**, 14061–14066

www.rsc.org/pccp

PAPER

Pnicogen–π complexes: theoretical study and biological implications†

Antonio Bauzá, David Quiñonero, Pere M. Deyà and Antonio Frontera*

Received 1st August 2012, Accepted 31st August 2012
DOI: 10.1039/c2cp42672b

The energetic and geometric features of pnicogen–π complexes involving different types of aromatic rings (benzene, trifluorobenzene, hexafluorobenzene and *s*-triazine) and the heavier pnicogenes (ECl_3, E = As, Sb, Bi) are investigated using theoretical methods (*ab initio* and DFT-D3). We have analyzed how the interaction energy is affected by the π-acidity of the aromatic moieties and the pnicogen used. In addition, we have found several examples in the Protein Databank where pnicogen–π interactions are present. This likely indicates the potential use of this interaction in the design and synthesis of potential inhibitors of enzymatic reactions. Moreover, in order to know the reliability of the latest version of dispersion termed corrected DFT-D3, we have also compared the energies obtained using the *ab initio* MP2 method with those obtained using BP86-D3. We have also computed and analyzed the dispersion contribution to the total interaction energy in order to know if it is crucial for the favourable binding. This allows a better understanding of the physical nature of the interaction. Finally, we have used the Bader's theory of "atoms-in-molecules" to demonstrate that the electron density computed at the bond critical point that emerges upon complexation can be used as a measure of bond order in this noncovalent interaction.

1. Introduction

The rational use of noncovalent interactions is crucial in modern chemistry[1] and, among others, interactions involving aromatic rings are extremely important in many fields.[2] For instance, ion–π,[3,4] π–π stacking,[5] lp–π[6] and C–H/π[7] interactions participate in important chemical and biological processes including molecular recognition, crystal engineering and enzymatic mechanisms. In addition, the importance of the π-interaction of arenes with heavier pnicogenes (As, Sb and Bi) has also been known for a long time, but its study in the context of supramolecular chemistry is more recent.[8] As a matter of fact, the important work developed by Johnson's group in the last few years highlights the potential use of this weak interaction to control self-assembly processes that yield to the formation of macrocycles.[9]

Mainly using X-ray analysis,[9,10] it has been demonstrated that post-transition metals with stereochemically active lone pairs, such as heavier pnicogenes in low oxidation states, produce stable arene complexes. For instance the binding enthalpies between $SbCl_3$ and neutral aromatic rings have been recently measured, ranging 5–10 kcal mol^{-1}. These values are in the typical range of non-covalent weak interactions.[11] The attractive origin of this interaction can be explained using two opposite points of view, which have been proposed in the literature. On one hand, it can be described as an electrostatic interaction between a Lewis acid (main group metalloid) and a π-base (arene ring) interaction.[11] These donor(π)–acceptor(As) orbital interactions are also known as "Menshutkin complexes". On the other hand, the interaction can be also described as an electron transfer between the pnicogen atom and the arene. In the latter description the interaction is identical to a lp–π interaction, which generally occurs between an arene and a Lewis base. This description has been recently proposed for supramolecular architectures based on As–π interactions.[12] It should be also noted that Auer *et al.* have demonstrated that dispersion forces are important in this type of interaction since standard DFT methods are not well suited for the quantitative description of the bonding between bismuth and arenes.[13]

The aim of this study is to investigate the geometric and energetic features of pnicogen π complexes between aromatic moieties and ECl_3 neutral molecules. In order to shed light on the nature of the interaction, we have used four different arenes, ranging from electron rich to electron poor. In cases where the origin of the interaction is the Lewis acidity of the pnicogen, the formation of the complexes should be favoured in electron rich arenes. In contrast, if the interaction is equivalent to an lp π interaction, the formation of the complexes should be favoured in electron poor arenes. In addition, as previous works demonstrate that dispersion is important in this interaction, the

Departament de Química, Universitat de les Illes Balears, 07122 Palma de Mallorca, Spain. E-mail: toni.frontera@uib.es; Fax: +34 971173426; Tel: −34 971173498

† Electronic supplementary information (ESI) available: Cartesian coordinates of all compounds and complexes. See DOI: 10.1039/c2cp42672b

latest version of dispersion, termed corrected DFT-D3, has been used to carry out the calculations and the geometries and energies have been compared to those obtained using the *ab initio* MP2 method. Furthermore, the "atoms in molecules" (AIM)[14] analysis allows us to demonstrate that the electron density at the cage critical points that characterize the pnicogen bond can be used as a measure of bond order. Finally, we have analyzed the protein database (PDB) in order to provide evidence of the importance of pnicogen–π complexes in some biological systems.

2. Theoretical methods

The geometry of all the complexes included in this study was optimized at the BP86-D3/def2-TZVPD level of theory and imposing the C_{3v} symmetry point group within the program TURBOMOLE version 5.10.[15] For comparison purposes some complexes have been also computed at the MP2/def2-TZVPD. The interaction energies were calculated with correction for the basis set superposition error (BSSE) by using the Boys–Bernardi counterpoise technique.[16] The calculation of the wavefunction to perform the "atoms-in-molecules" (AIM) analysis was computed at the same level of theory. The calculation of AIM properties was done using the AIM2000 program.[17]

3. Results and discussion

3.1. Preliminary considerations

In Fig. 1 the Molecular Electrostatic Potential (MEP) surfaces of the arenes are represented including the values of quadrupole moments (Q_{zz}) retrieved from the literature.[18] On going from benzene to hexafluorobenzene, it can be observed a progressive change from red to blue colour above the ring and a change in the sign of the quadrupole moment from negative to positive. This gradual change of the π-basicity (or π-acidity) of the arene is useful to analyze the physical nature of the pnicogen–π interaction, as is explained below. We have also included *s*-triazine in this study, because, notwithstanding it has a Q_{zz} value like trifluorobenzene, it presents a peculiar distribution of the MEP above the ring that facilitates a dual behaviour. That is, depending on the relative orientation of the ECl_3 molecule with respect to the position of the aromatic nitrogen atoms, one of the proposed mechanisms of binding will be favoured. Therefore it is a good candidate for analyzing the physical nature of the pnicogen–π interaction. In addition, the use of an heteroaromatic ring allows us to compare the strength of the interaction with respect to carboaromatic rings. The MEP surface obtained for the three ECl_3 molecules (in Fig. 1 only the $AsCl_3$ is indicated as a model) is identical and the MEP value at the position of the lone pair is positive, indicating the presence of a σ-hole at this position, resembling the heavier halogens. Therefore, from this preliminary result, based only on electrostatic considerations, in the pnicogen–π interaction the ECl_3 acts as a Lewis acid and it cannot be defined as an lp–π interaction.

In previous studies, it has been argued that the polarization of the π-cloud of the arene induced by the permanent dipole of the ECl_3 molecule is important.[12] Moreover, it has been also proposed that dispersion effects are important in this type of interaction,[13] mostly to explain the fact that the heavier pnicogenes have more favourable interaction energies. Another possibility can be related to the polarization of the ECl_3 molecule, since the heavier pnicogenes are more polarisable, as is indicated by the molecular polarizabilities computed for $AsCl_3$, $SbCl_3$ and $BiCl_3$ (see Fig. 1). This issue is further analyzed below.

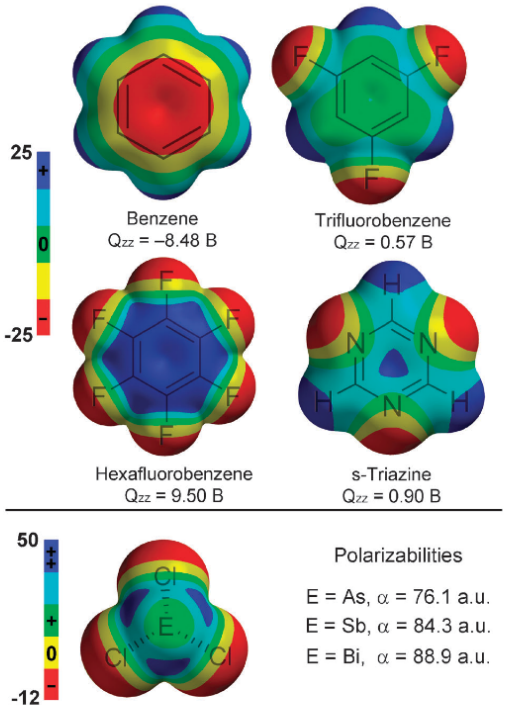

Fig. 1 Top: MEP surfaces of benzene, trifluorobenzene and hexafluorobenzene. Down, MEP surface of $AsCl_3$ as a model of the ECl_3 molecule and molecular polarizabilities.

3.2. Energetic and geometric results

In Table 1 we summarize the binding energies without and with the basis set superposition error (BSSE) correction and equilibrium distances (R_e) for complexes **1–9** (see Fig. 2) at the BP86-D3/def2-TZVPD level of theory. For trifluorobenzene, we have studied two different orientations, one with the chloride atoms of the ECl_3 molecule located above the aromatic C–H bonds and the other above the C–F bonds. The computed interaction energies are identical for both orientations; therefore only one set is included in Table 1. As aforementioned, for *s*-triazine complexes we have also computed two orientations, one denoted as "**a**" where the chloride atoms of the ECl_3 molecule are located above the aromatic C–H bonds (see Fig. 2), and the other denoted as "**b**" where the chloride atoms are located above the aromatic nitrogen atoms.

From the results gathered in Table 1, some interesting issues arise. First, the computed interaction energies obtained for benzene

Table 1 Interaction energies without and with the BSSE correction (E and E_{BSSE}, kcal mol^{-1}), dispersion energy (E_{disp}, kcal mol^{-1}) equilibrium distances (R_e, Å), and the charge density at the cage CP (ρ, a.u.) at the BP86-D3/def2-TZVPD level of theory for complexes **1–12**

Complex	E	E_{BSSE}[a]	E_{disp}	R_e	10^2 ρ
1 (BEN + $AsCl_3$)	−7.1 (−9.9)	−6.5 (−6.9)	−5.2	3.210	0.478
2 (BEN + $SbCl_3$)	−6.4	−6.1	−3.6	3.446	0.440
3 (BEN + $BiCl_3$)	−8.7	−8.4	−3.8	3.328	—
4 (TFB + $AsCl_3$)	−5.2 (−7.8)	−4.6 (−4.7)	−5.1	3.285	0.420
5 (TFB + $SbCl_3$)	−3.9	−3.6	−3.6	3.552	0.365
6 (TFB + $BiCl_3$)	−4.9	−4.6	−4.0	3.474	
7 (HFB + $AsCl_3$)	−3.8 (−6.4)	−3.2 (−3.4)	−5.0	3.383	0.340
8 (HFB + $SbCl_3$)	−2.1	−1.8	−3.2	3.851	0.195
9 (HFB + $BiCl_3$)	−2.2	−1.9	−3.7	3.860	—
10a (TAZ + $AsCl_3$)	−3.3 (−5.7)	−2.9 (−3.4)	−4.1	3.459	0.303
11a (TAZ + $SbCl_3$)	−2.6	−2.2	−3.1	3.713	0.271
12a (TAZ + $BiCl_3$)	−3.3	−2.9	−3.5	3.667	
10b (TAZ + $AsCl_3$)	−2.9 (−5.2)	−2.5 (−3.0)	−3.9	3.412	0.272
11b (TAZ + $SbCl_3$)	−2.3	−1.9	−3.0	3.663	0.243
12b (TAZ + $BiCl_3$)	−2.8	−2.3	−3.4	3.607	—

[a] Values in parenthesis are computed at the MP2/def2-TZVPD level of theory.

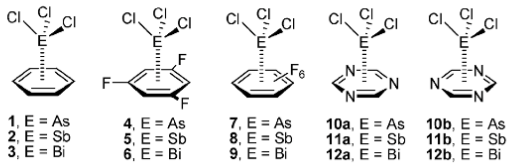

Fig. 2 Pnicogen–π bonding complexes **1–12**.

complexes are more favourable than the rest of arenes, indicating that electron rich arenes favour the pnicogen–π interaction. The interaction strength progressively decreases as the quadrupole of the arene becomes more positive. In line with the energetic results, the equilibrium distances are shorter for benzene complexes than for the rest of arenes. This result clearly corroborates the postulation derived from the MEP results (*vide supra*). That is, the pnicogen–π interaction is better described as an electron donation from the arene to the ECl_3 molecule that acts as a Lewis acid. Second, in agreement with previous calculations, the interaction energy of the heaviest pnicogen with benzene (complex **3**) is the most favourable. Moreover, for *s*-triazine and 1,3,5-trifluorobenzene complexes, As and Bi complexes give very similar interaction energies. This likely means that the strengthening of the interaction observed in complex **3** (−8.4 kcal mol^{-1}, $Cl_3Bi\cdots BEN$) is due to electrostatic effects. This is confirmed by the small interaction energy obtained for complex **9** (−1.9 kcal mol^{-1}, $Cl_3Bi\cdots HFB$), which is significantly more positive than complex **7** (−3.2 kcal mol^{-1}, $Cl_3As\cdots HFB$). In HFB complexes, the possible lp·π nature of the interaction may be enhanced because the arene is π-acidic. It is well-known that strong relativistic effects occur in bismuth.[19] Accordingly, the energies of all of the *n*s orbitals in bismuth are substantially lower than those of arsenic and antimony. The p-orbital energies are also lower but the difference is smaller than that of the s-orbitals.[20] The lower energy of the valence 6s orbital implies that the $6s^2$ lone pair of electrons is less readily available for bonding, making bismuth(III) a significantly weaker Lewis base than the lighter pnicogens,[21] and therefore the lp–π interaction would be considerably unfavoured with respect to As, in agreement with the interaction energies of complexes **7** and **9**. Apart from complex **9**, the equilibrium distances obtained for $BiCl_3$ complexes are shorter than $SbCl_3$ complexes. The Bi atom has a smaller atomic radius than Sb due to a double effect: the orbital contraction due to relativistic effects[22] and the further contraction caused by the less effective screening provided by occupied f-orbitals.[23]

The results obtained for *s*-triazine complexes support the idea that the ECl_3 molecule acts as a Lewis acid in the pnicogen–π interaction. The best fitting of both MEP surfaces (*s*-triazine and the ECl_3 molecule) shown in Fig. 1 is achieved if the chlorine atoms lie over the C H bonds. The results gathered in Table 1 confirm this issue, since the "**a**" complexes are more favourable than "**b**" complexes.

Finally, we have also included in Table 1 the interaction energies computed using the *ab initio* MP2/def2-TZVPD level of theory for $AsCl_3$ complexes. It can be observed a very good agreement between the energetic results computed at MP2 and BP86-D3 levels of theory. This result gives reliability to the DFT method in combination with latest dispersion correction developed by Grimme *et al.*[24]

3.3. Dispersion effects

It has been previously described in the literature the importance of dispersion in the pnicogen–π interaction involving bismuth. In fact, the density functional theory (without dispersion correction) is not well suited for the quantitative description of the bonding between pnicogen and arenes, since for several functionals a very shallow minimum is found.[13] We have examined dispersion effects in the systems reported herein. The dispersion contribution is included in Table 1. It can be observed that the dispersion is very important in all complexes, especially in those involving π-acidic arenes, since it overcomes the unfavourable electrostatic interaction. It has been also proposed that the higher ability of heaviest pnicogen to interact with benzene is due to dispersion effects. However the results reported herein do not agree with this explanation, since the dispersion contribution is higher in $AsCl_3$ complex **1** than in either $SbCl_3$ or $BiCl_3$ complexes **2** or **3**. Therefore a likely explanation for the higher ability of Bi to form pnicogen π complexes is that it is more polarisable (α = 88.9 a.u., see Fig. 1) and, moreover, it is able to establish interactions with short equilibrium distances due to the strong orbital contraction.

3.4. AIM analysis

We have performed the AIM analysis of all As and Sb complexes included in this study. The basis set used in this work is not supported by the AIM program for Bi. In benzene, 1,3,5-trifluorobenzene and hexafluorobenzene complexes, the pnicogen–π is characterized by the presence of six bond and six ring critical points (CP) symmetrically distributed. The bond CPs connect the pnicogen atom with the carbon atoms. For *s*-triazine complexes the interaction is characterized by the presence of three bond and three ring critical points symmetrically distributed. In both series of *s*-triazine complexes (**a** and **b**) the

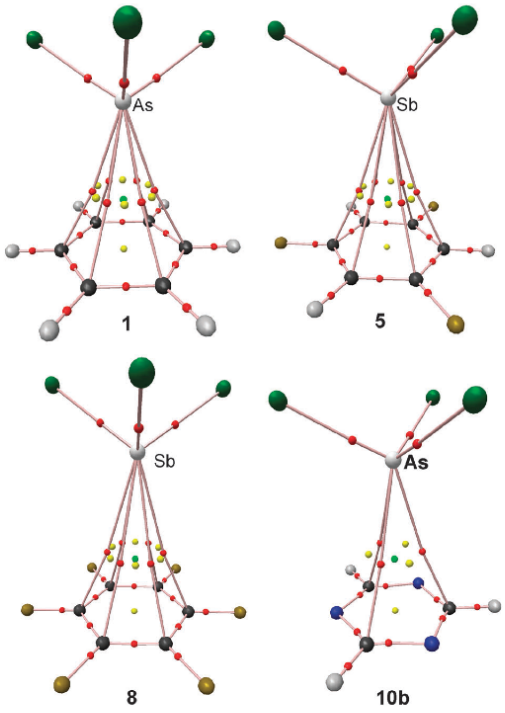

Fig. 3 Distribution of critical points in complexes **1**, **5**, **8** and **10a**. The bond, ring and cage critical points are represented by red, yellow and green spheres, respectively. The bond paths connecting the nuclei with bond CPs are also represented.

bond CPs connect the pnicogen atom with the carbon atoms of the ring. In all complexes **1–12b**, the interaction is further characterized by the presence of one cage CP connecting the pnicogen atom with the center of the ring, as is common in ion π and lp π interactions.[25] In Fig. 3 we show the distribution of critical points in some selected complexes. The density at the cage critical point has been used as a measure of bond strength in a variety of noncovalent interactions.[14] We have examined if these values can be used as a measure of bond order in the complexes studied here. We have represented in Fig. 4 a plot that allows us to analyze the existence of a linear relationship between the interaction energies and the ρ values (gathered in Table 1). As a matter of fact, we have obtained a strong

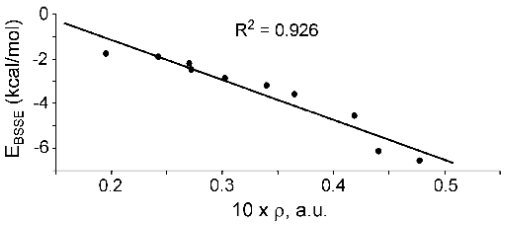

Fig. 4 Regression plot of the interaction energy *versus* the value of the charge density at the cage critical point in As and Sb complexes.

relationship ($R^2 = 0.962$) between the value of the charge density computed at the cage critical point and the interaction energy. The importance of this relationship should be emphasized, since in the same plot we have combined four different arenes and two pnicogens. Therefore, this relevant representation allows for dealing simultaneously with a great variety of complexes.

3.5. Biological considerations

We have examined the PDB in order to provide experimental evidence of the importance of pnicogen–π interaction in biological systems. We have searched for structures containing trivalent As, Sb and Bi ligands. There are 38 structures for As, three structures for Sb and only one (still unreleased) structure for Bi (3TPH). Interestingly, in some of the protein structures that present trivalent As in the structure, the source of As is a dithiothreitol-mediated reaction of cysteine with the arsenic center of the cacodylate (dimethyl arsenic acid) present in the crystallization buffer.[26] Two representative examples are shown in Fig. 5. One of them (on the right side) is a T4 polynucleotide kinase/phosphatase (Pnkp) enzyme that belongs to a family of bifunctional enzymes with 5′-kinase and 3′-phosphatase activities that function in nucleic acid repair.[27] The arsenic adduct is located at 3.7 Å above the planar aromatic Trp213 side chain. A similar reaction of a tryptophan-proximal cysteine with cacodylate has been also reported for *Eco*RI methyltransferase and *Escherichia coli* peptide methionine sulphoxide reductase.[26] The other example selected is the human phosphodiesterase 4B2B.[28] In this case the aromatic residue is phenylalanine instead of tryptophan. The interaction distance is 3.75 Å and the As atom is located almost exactly over the center of the benzene ring.

More interestingly, a pnicogen–π interaction involving Sb(III) likely participates in the mechanism of inhibition of trypanothione reductase (TR). The current treatment of leishmaniasis relies on antimony based drugs, meglumine antimoniate (Glucantime), and sodium stibogluconate (Pentostam).[29] The human protozoan parasites of the trypanosomatidae family differ from the other eukaryotes in their specific redox metabolism because the

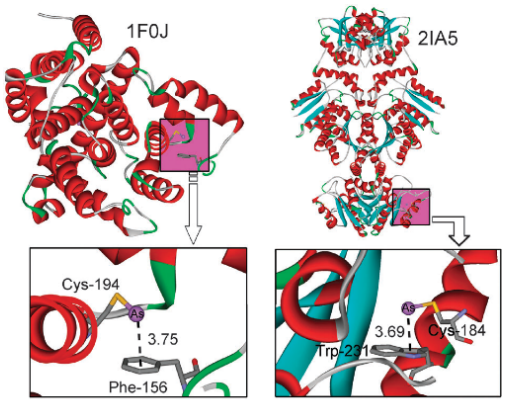

Fig. 5 Partial views of the PDB structures 1F0J (left) and 2IA5 (right) exhibiting As–π interactions, which are highlighted and magnified at the bottom of the figure.

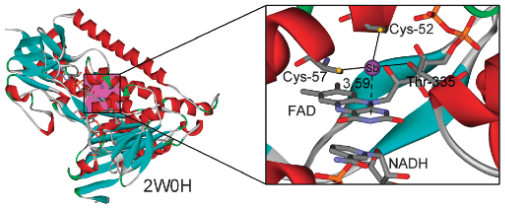

Fig. 6 Partial view of the PDB structure 2W0H exhibiting an interesting Sb–π interaction, which is highlighted and magnified at the right side of the figure.

glutathione–glutathione reductase system is replaced by the unique trypanothione trypanothione reductase system. The crystal structures TR from *Leishmania infantum* and its complex with NADPH and Sb(III) was reported in 2009.[29] The Sb(III) present in the catalytic cleft is coordinated by the two redox-active catalytic cysteine residues (Cys-52 and Cys-57) and one threonine residue (Thr-335). Thus, the inhibition mechanism is due to the disulfur brigde breaking caused by the complexation of the Sb(III), which reduce the redox capability of the enzyme. Although not suggested by the original authors, we propose that the pnicogen–π interaction with the FAD cofactor also stabilize the coordination of the Sb(III) to the active site, as indicated in Fig. 6. Therefore this interaction helps to the tight binding of the inhibitor to the active site. The Sb–π distance is in good agreement with the theoretical values present in Table 1. Interestingly, Sb(V)-containing compounds are less toxic than their trivalent analogues, although Sb(V) is considered to be a pro-drug that has to be activated by conversion to the trivalent form Sb(III) to exert its action against the parasite.[30]

4. Conclusions

The analysis of the results presented in this manuscript offers some interesting conclusions:

1. The pnicogen–π interaction is stronger in electron rich than in electron poor arenes, indicating that the interaction is better described as a traditional Lewis acid to π-base (arene) interaction than as an electron transfer between the pnicogen (lone pair) and the arene.

2. The MEP results anticipate that the electrostatic interaction is not favored in electron-deficient arenes, as corroborated by the DFT-D3 calculations. In these complexes the interaction is dominated by dispersion forces.

3. The dispersion corrected DFT method gives reliable results (comparable to MP2) if the latest developed correction for dispersion is used

4. The density at the cage critical point that is originated upon complexation of the ECl_3 molecule can be used as a measure of the strength of the interaction.

5. The pnicogen π interaction is also relevant in biological systems and it likely participates in the mechanism of inhibition of Sb-based drugs used to treat leishmaniasis.

Acknowledgements

We thank CONSOLIDER–Ingenio 2010 (CSD2010-0065) and the MICINN of Spain (project CTQ2011-27512/BQU, FEDER funds) for financial support. D.Q. thanks the MICINN of Spain for a "Ramon y Cajal" contract. We thank the CESCA for computational facilities.

Notes and references

1 H. J. Schneider, *Angew. Chem., Int. Ed.*, 2009, **48**, 3924–3977.
2 L. M. Salonen, M. Ellermann and F. Diederich, *Angew. Chem., Int. Ed.*, 2011, **50**, 4808–4842; E. A. Meyer, R. K. Castellano and F. Diederich, *Angew. Chem., Int. Ed.*, 2003, **42**, 1210–1250.
3 J. C. Ma and D. A. Dougherty, *Chem. Rev.*, 1997, **97**, 1303–1324; P. B. Crowley and A. Golovin, *Proteins: Struct., Funct., Genet.*, 2005, **59**, 231–239.
4 B. L. Schottel, H. T. Chifotides and K. R. Dunbar, *Chem. Soc. Rev.*, 2008, **37**, 68–83; C. Caltagirone and P. A. Gale, *Chem. Soc. Rev.*, 2009, **38**, 520–563; A. Frontera, D. Quiñonero and P. M. Deyà, *Wiley Interdiscip Rev.: Comput. Mol. Sci.*, 2011, **1**, 440–459; P. Gamez, T. J. Mooibroek, S. J. Teat and J. Reedijk, *Acc. Chem. Res.*, 2007, **40**, 435–444; A. Robertazzi, F. Krull, E.-W. Knapp and P. Gamez, *CrystEngComm*, 2011, **13**, 3293–3300.
5 K. Muller-Dethlefs and P. Hobza, *Chem. Rev.*, 2000, **100**, 143–168; S. K. Burley and G. A. Petsko, *Science*, 1985, **229**, 23–28; J. T. Stivers and Y. L. Jiang, *Chem. Rev.*, 2003, **103**, 2729–2759.
6 T. J. Mooibroek, P. Gamez and J. Reedijk, *CrystEngComm*, 2008, **10**, 1501–1515.
7 M. J. Plevin, D. L. Bryce and J. Boisbouvier, *Nat. Chem.*, 2010, **2**, 466–471.
8 M. M. Watt, M. S. Collins and D. W. Johnson, *Acc. Chem. Res.*, DOI: 10.1021/ar300100g.
9 W. J. Vickaryous, R. Herges and D. W. Johnson, *Angew. Chem., Int. Ed.*, 2004, **43**, 5831–5833; W. J. Vickaryous, E. Rather Healy, O. B. Berryman and D. W. Johnson, *Inorg. Chem.*, 2005, **44**, 9247–9252; V. M. Cangelosi, A. C. Sather, Z. N. Zakharov, O. B. Berryman and D. W. Johnson, *Inorg. Chem.*, 2007, **46**, 9278–9284; V. M. Cangelosi, L. N. Zakharov, S. A. Fontenot, M. A. Pitt and D. W. Johnson, *Dalton Trans.*, 2008, 3447–3453; V. M. Cangelosi, L. N. Zakharov, J. L. Crossland, B. C. Franklin and D. W. Johnson, *Cryst. Growth Des.*, 2010, **10**, 1471–1473; N. R. Lindquist, T. G. Carter, V. M. Cangelosi, L. N. Zakharov and D. W. Johnson, *Chem. Commun.*, 2010, **46**, 3505–3507; M. A. Pitt, L. N. Zakharov, K. Vanka, W. H. Thompson, B. B. Laird and D. W. Johnson, *Chem. Commun.*, 2008, 2936–2938; V. M. Cangelosi, M. A. Pitt, W. J. Vickaryous, C. A. Allen, L. N. Zakharov and D. W. Johnson, *Cryst. Growth Des.*, 2010, **10**, 3531–3536; W. J. Vickaryous, L. N. Zakharov and D. W. Johnson, *Main Group Chem.*, 2006, **5**, 51–59; V. M. Cangelosi, L. N. Zakharov and D. W. Johnson, *Angew. Chem., Int. Ed.*, 2010, **49**, 1248–1251; V. M. Cangelosi, T. G. Carter, J. L. Crossland, L. N. Zakharov and D. W. Johnson, *Inorg. Chem.*, 2010, **49**, 9985–9992; S. A. Fontenot, V. M. Cangelosi, M. A. W. Pitt, A. C. Sather, L. N. Zakharov, O. B. Berryman and D. W. Johnson, *Dalton Trans.*, 2011, **40**, 12125–12131.
10 W. Frank, J. Schneider and S. Müller-Becker, *J. Chem. Soc., Chem. Commun.*, 1993, 799–800; D. Mootz and V. Händler, *Z. Anorg. Allg. Chem.*, 1986, **533**, 23–29.
11 A. Schier and H. Schmidbaur, *Organometallics*, 2008, **27**, 2361–2395.
12 J. Zukerman-Schpector, A. Otero-de-la-Roza, V. Lauña and E. R. T. Tiekink, *Chem. Commun.*, 2011, **47**, 7608–7610.
13 A. A. Auer, D. Mansfeld, C. Nolde, W. Schneider, M. Schurmann and M. Mehring, *Organometallics*, 2009, **28**, 5405–5411.
14 R. W. F. Bader, *Atoms in Molecules. A Quantum Theory*, Clarendon, Oxford, 1990.
15 R. Ahlrichs, M. Bär, M. Hacer, H. Horn and C. Kömel, *Chem. Phys. Lett.*, 1989, **162**, 165–169.
16 S. B. Boys and F. Bernardy, *Mol. Phys.*, 1970, **19**, 553–566.
17 F. Biegler-König, J. Schönbohm and D. Bayles, *J. Comput. Chem.*, 2001, **22**, 545–559.
18 M. R. Battaglia, A. D. Buckingham and J. H. Williams, *Chem. Phys. Lett.*, 1981, **78**, 421–423; J. Vrbancich and G. L. D. Ritchie, *J. Chem. Soc., Faraday Trans. 2*, 1979, **76**, 648–655; D. Quiñonero,

C. Garau, A. Frontera, P. Ballester, A. Costa and P. M. Deyà, *Chem. Phys. Lett.*, 2002, **359**, 486–492.
19 *Biological Chemistry of Arsenic, Antimony and Bismuth*, ed. H. Sun, John Wiley & Sons, Ltd, Chichester, U.K., 2010.
20 J. S. Thayer, *J. Chem. Educ.*, 2005, **82**, 1721–1729.
21 W. Kutzelnigg, *Angew. Chem., Int. Ed. Engl.*, 1984, **23**, 272–295.
22 K. C. H. Lange and T. Klapötke, in: *The Chemistry of Organic Arsenic, Antimony and Bismuth*, ed. S. Patai, John Wiley & Sons, Ltd, Chichester, U.K., 1994.
23 A. L. Allred and E. G. Rochow, *J. Inorg. Nucl. Chem.*, 1958, **5**, 264–268.
24 S. Grimme, J. Antony, S. Ehrlich and H. Krieg, *J. Chem. Phys.*, 2010, **132**, 154104.
25 A. Frontera, P. Gamez, M. Mascal, T. J. Mooibroek and J. Reedijk, *Angew. Chem., Int. Ed.*, 2011, **50**, 9564–9583; A. Frontera, D. Quiñonero and P. M. Deyà, *Wiley Interdiscip Rev.: Comput. Mol. Sci.*, 2011, **1**, 440–459.
26 K. B. Jacobson, J. B. Murphey and B. D. Sarma, *FEBS Lett.*, 1972, **22**, 80–82; D. H. H. Tsao and A. H. Maki, *Biochemistry*, 1991, **30**, 4565–4572; S. Maignan, J.-P. Guilloteau, Z.-L. Qing, C. Clement-Mella and V. Mikol, *J. Mol. Biol.*, 1998, **282**, 359–368; F. Tete-Favier, D. Cobessi, S. Boschi-Muller, S. Azza, G. Branlant and A. Aubry, *Structure (London)*, 2000, **8**, 1167–1178; M. S. Junop, M. Modesti, A. Guarné, R. Ghirlando, M. Gellert and W. Yang, *EMBO J.*, 2000, **19**, 5962–5970.
27 H. Zhu, P. Smith, L. K. Wang and S. Shuman, *Virology*, 2007, **366**, 126–136.
28 R. X. Xu, A. M. Hassell, D. Vanderwall, M. H. Lambert, W. D. Holmes, M. A. Luther, W. J. Rocque, M. V. Milburn, Y. Zhao, H. Ke and R. T. Nolte, *Science*, 2000, **288**, 1822–1825.
29 P. Baiocco, G. Colotti, S. Franceschini and A. Ilari, *J. Med. Chem.*, 2009, **52**, 2603–2612.
30 L. G. Goodwin and J. E. Page, *Biochem. J.*, 1943, **37**, 198.

Angewandte Communications

Aerogen Bonding

International Edition: DOI: 10.1002/anie.201502571
German Edition: DOI: 10.1002/ange.201502571

Aerogen Bonding Interaction: A New Supramolecular Force?**

*Antonio Bauzá and Antonio Frontera**

Abstract: *We report evidence of the favorable noncovalent interaction between a covalently bonded atom of Group 18 (known as noble gases or aerogens) and a negative site, for example, a lone pair of a Lewis base or an anion. It involves a region of positive electrostatic potential (σ-hole), therefore it is a totally new and unexplored σ-hole-based interaction, namely aerogen bonding. We demonstrate for the first time the existence of σ-hole regions in aerogen derivatives by means of high-level ab initio calculations. In addition, several crystal structures retrieved from the Cambridge Structural Database (CSD) give reliability to the calculations. Energetically, aerogen bonds are comparable to hydrogen bonds and other σ-hole-based interactions but less directional. They are expected to be important in xenon chemistry.*

Noncovalent interactions are the main protagonists of supramolecular chemistry and biochemistry controlling the central parts of living systems. An appropriate comprehension of the different noncovalent forces is necessary for the rational design of new drugs and developing improved synthetic receptors capable to function in competitive media.[1] Among many interactions, the hydrogen bond is probably the most studied and analyzed noncovalent interaction.[2] However, σ-hole interactions involving tetrel, pnicogen, chalcogen, and halogen atoms have attracted substantial attention in recent years and they are recognized by the scientific community as powerful tools in supramolecular chemistry, crystal engineering, and biochemistry.[3] These interactions are moderately strong and directional basically due to the localization of a positive region on the extension of the covalent bonds (σ-hole) in the acceptor molecule. Usually, the name of the group (halogen, chalcogen, etc.) is used to specify the interactions and they are subgroups of a general definition of σ-hole bonding interactions given by Politzer and co-workers.[4] As far as our knowledge extends, the σ-hole interaction has not been described for Group 18 elements (noble gases or aerogens). This is likely due to the general assumption that these elements are monatomic gases with very low chemical reactivity. As a matter of fact, inertness of noble gases makes them suitable in applications in which reactions are not desired.

In this manuscript we propose the term "aerogen bonding" for describing the unprecedented σ-hole interaction between electron-rich entities (anions or lone pair possessing atoms) and elements belonging to Group 18. The energetic features and structural properties of aerogen bonding are discussed and two fascinating X-ray structures are selected to illustrate the existence of this interaction. Obviously, this rare type of bonding is not expected to be an effective and reliable instrument in crystal engineering or supramolecular chemistry; however, it is certainly important in terms of gaining knowledge in the molecular and supramolecular sciences.

The synthesis and crystal structure determination of xenon trioxide was reported in 1963 by Templeton et al.[5] The molecule XeO_3 is in the shape of a trigonal pyramid with dimensions similar to those of the isoelectronic iodate ion (Figure 1). The crystal packing shows that each xenon

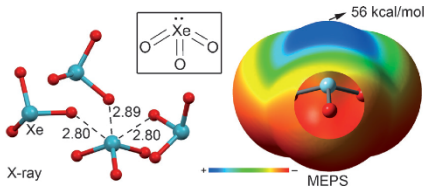

Figure 1. X-ray structure of XeO_3 (left) and MEPS of XeO_3 (right; distances in Å).

establishes three noncovalent Xe···O contacts with neighboring molecules at distances (from 2.8 to 2.9 Å) longer than the sum of the covalent radii of Xe and O (2.03 Å) and shorter than the sum of van der Waals radii (3.68 Å) that can be defined as σ-hole aerogen bonding interactions. In Figure 1 we show the molecular electrostatic potential surface (MEPS) computed at the MP2/aug-cc-pVTZ level of theory and a strong and extended σ-hole can be clearly observed. Unexpectedly a very positive potential is found at the position where the lone pair of the Xe^{VI} is located, which can be related to the inert pair effect.[6]

The chemistry of Xe^{IV} has been recently reviewed[7] and most of the known compounds are salts in which purely electrostatic interactions dominate in their solid state structure. However, one neutral and interesting derivative of Xe^{IV} is the XeF_2O compound that was synthesized from the co-condensation of water and XeF_4.[8] Most interestingly, in the presence of CH_3CN, the isolation of $F_2OXe{\cdot}NCCH_3$ is achieved.[9] This structure is the first and unique example of a Xe^{IV}–N bond. Two further examples of Xe^{IV}–N donor–acceptor bonds have been reported,[10] but involve a positively charged Xe^{IV} moiety, i.e., $[C_6F_5XeF_2]^+$. A partial view of the $F_2OXe{\cdot}NCCH_3$ crystal structure is shown in Figure 2. It can be observed that the $XeOF_2$ moiety is planar showing a T-

[*] A. Bauzá, Prof. A. Frontera
Departament de Química, Universitat de les Illes Balears
Crta. de Valldemossa km 7.5, 07122 Palma, Baleares (Spain)
E-mail: toni.frontera@uib.es

[**] This work was funded by the MINECO of Spain (CONSOLIDER-Ingenio 2010 project CSD2010-0065 FEDER funds).

Supporting information for this article is available on the WWW under http://dx.doi.org/10.1002/anie.201502571.

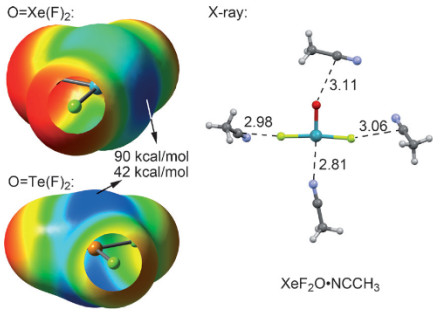

Figure 2. MEPS of XeF_2O and TeF_2O (left). X-ray structure of $XeF_2O{\cdot}CH_3CN$ (right; distances in Å).

shaped arrangement of two fluorine atoms and an oxygen double bond domain in the equatorial plane and two mutually *trans* valence electron lone pairs perpendicular to that plane. The nitrogen electron pair donor atom of CH_3CN interacts with the Xe atom opposite to the Xe=O bond and is coplanar with the $XeOF_2$ moiety. This has been defined as a coordination Xe^{IV}–N bond by the original authors.[9] We also show in Figure 2 the MEPS of $XeOF_2$ and $TeOF_2$ for comparison purposes. The MEP surface of the trigonal $TeOF_2$ molecule shows a clear π-hole above and below the Te atom. In contrast, the MEP surface of the T-shaped $XeOF_2$ molecule shows a strong σ-hole at the Xe atom in the prolongation of the Xe=O bond due to the existence of two valence lone pairs. Therefore the Xe^{IV}–N noncovalent contact observed in the solid state of $F_2OXe{\cdot}NCCH_3$ is a clear example of a σ-hole interaction (aerogen bonding). Interestingly, the $XeOF_2$ molecule in the solid state is surrounded by four CH_3CN molecules (Figure 2), one establishing the aerogen bonding interaction with the Xe and the rest forming O(F)···C noncovalent carbon bonding interactions.[3b–d]

We have optimized several complexes of XeO_3 and XeF_2O with two electron donor molecules (Figure 3) and compared their energetic and geometric features with complexes in which lighter aerogens (Ar and Kr, **1–4**) are used. The computational details are included in the Supporting Information (SI). Moreover, we also compare the interaction energies of the aerogen complexes to those using halogen, chalcogen, pnicogen, and tetrel atoms of the same row as σ-hole donors. These comparisons allow us, first, to investigate if the aerogen bonding follows the same energetic trend than the rest of σ-hole interactions. That is, the strength of the interaction augments as the bond donor atom is increasingly polarizable (heavier atoms). Secondly, to investigate whether the aerogen bonding is energetically similar to other well-known σ-hole interactions, using elements with similar polarizability values.

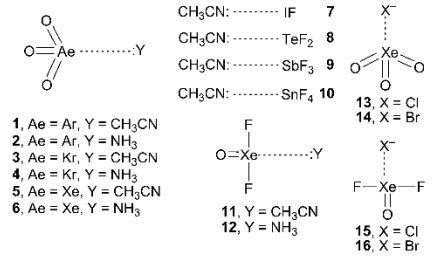

Figure 3. Complexes **1–16** studied in this work.

The energetic and geometric results of the ab initio optimized complexes **1–16** are gathered in Table 1 (see Figure S1 in the SI for a representation of the optimized geometries). From the inspection of the results, several interesting points arise. First, in the Ae^{VI} complexes **1–6**, the interaction energies follow the expected trend for a σ-hole-based interaction. That is, the largest interaction energies (in absolute value) are obtained for the heaviest aerogen atom (complexes **5** and **6**). Second, complexes **7–10**, in which elements of the same row are used as σ-hole donors present interaction energies that are larger in absolute value than the one obtained for complex **5** ($O_3Xe{\cdots}NCCH_3$) apart from the pnicogen-bonded complex **9**. The most favorable one is the tetrel complex (**10**) that correspond to the strongest σ-hole donor molecule (Figure 4) followed by the halogen-bonded complex **7** also in agreement with the MEP analysis. The strength of chalcogen and pnicogen complexes is comparable to the aerogen bonding complex **5**. Third, the interaction energies of Xe^{IV} complexes **11–12** are larger in absolute value than those computed for the equivalent Xe^{VI} complexes **5–6**, in agreement with the electrostatic potential values at the σ-holes (Figures 1 and 2). Finally, we have also included several complexes with anions (**13–16**) and the interaction energies

Table 1: Interaction energies without and with the basis set superposition error (ΔE and ΔE_{CP}, respectively), and equilibrium distances (R_e) for complexes **1–16** at the RI-MP2/aug-cc-pVTZ level of theory. The point group (PG) and imaginary frequencies (NImag) are also indicated.

Complex	ΔE [kcal mol^{-1}]	ΔE_{CP} [kcal mol^{-1}]	R_e [Å]	PG (NImag)
1	−6.6	−6.4	2.934	C_1 (0)
1a	−6.7	−5.9	2.909	C_{3v} (3)
2	−7.1	−6.5	2.853	C_s (0)
2a	−6.4	−5.1	2.978	C_{3v} (2)
3	−8.1	−7.2	2.980	C_s (0)
3a	−7.4	−6.8	3.053	C_{3v} (3)
4	−9.0	−8.3	2.843	C_s (0)
4a	−6.9	−6.5	3.127	C_{3v} (2)
5	−11.6	−9.5	3.142	C_s (0)
5a	−9.2	−8.0	2.960	C_{3v} (3)
6	−10.4	−9.0	2.779	C_s (0)
6a	−8.3	−7.4	3.221	C_{3v} (2)
7	−15.0	−12.2	2.450	C_s (0)
8	−13.1	−10.3	2.535	C_s (0)
9	−10.4	−8.1	2.722	C_s (0)
10	−21.6	−16.6	2.273	C_s (0)
11	−12.1	−10.1	2.798	C_s (0)
12	−14.6	−12.6	2.690	C_1 (0)
13	−39.0	−37.2	2.784	C_s (0)
14	−34.2	−32.6	2.983	C_s (0)
15	−41.9	−40.0	2.697	C_s (0)
16	−37.2	−35.4	2.874	C_s (0)

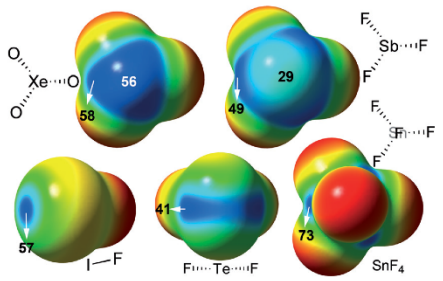

Figure 4. MEP surfaces computed for several σ-hole donor molecules at the MP2/aug-cc-pVTZ level of theory. Some MEP energy values in kcal mol^{-1} are indicated.

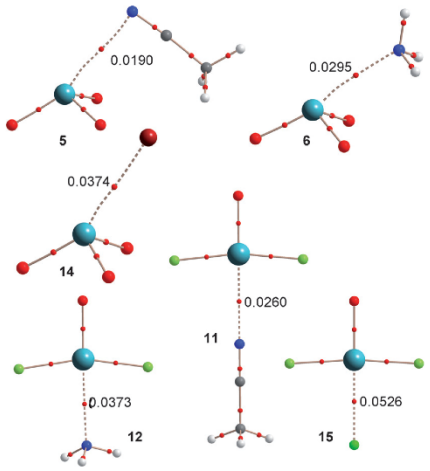

Figure 5. AIM distribution of critical points (red spheres correspond to bond critical points) at the MP2/aug-cc-pVTZ level of theory. The $\rho(r)$ values at the bond critical points are indicated in atomic units (a.u.).

are very large, in line with reported anionic complexes between halides and traditional σ-hole donor atoms.[11]

At this point, it is worth emphasizing the difference observed in the MEP surfaces of XeO_3 and SbF_3 (Figure 3, top). Both molecules have a lone pair located in the molecular C_{3v} axis and both present positive potential values at the location of the lone pair. However, the MEPS of SbF_3 shows three well-defined σ-holes located at the extensions of the Sb–F bonds with a MEP value that is 20 kcal mol^{-1} more positive than that at the location of the inert lone pair (Figure 4). In contrast, the MEP surface of XeO_3 shows a negligible difference between the MEP values measured at the σ-hole and lone pair locations. Similar result is observed in the MEP surfaces of ArO_3 and KrO_3 molecules (Figure S2). Therefore the aerogen bonding is less directional than the rest of the σ-hole bonding interactions. As a matter of fact, we have also optimized complexes **1–6** imposing C_{3v} symmetry (lone pair directed to the inert lone pair,[6] complexes denoted as **1a–6a** in Table 1) and the interaction energies are comparable. The geometries of some representative complexes and their corresponding distribution of critical points[12] (see SI for details) are given in Figure 5. It can be observed that the electron-rich atom of the Lewis acid (or anion) is positioned at the σ-hole location (extension of the Xe=O covalent bond). All complexes are characterized by the presence of a bond critical point (small red sphere) connecting the Xe atom to the electron-rich atom thus confirming the interaction. The values of the charge density $\rho(r)$ at the bond critical point in the aerogen bonding complexes shown in Figure 5 (values in italics) are similar to those reported for σ-hole interactions of groups 14–17.[3]

To study if orbital contributions are important to explain the aerogen interactions described above, we have performed natural bond orbital (NBO) calculations focusing our attention on the second order perturbation analysis,[13] because it is very useful to study donor–acceptor interactions.[13] The results are summarized in Table 2. For Ae^{VI} complexes, the orbital contribution is small (≈10% of the total interaction energy) for the lighter aerogens and the contribution is important in xenon complexes, especially in complex **6**, in which the orbital contribution dominates the interaction, in agreement with the short Xe···N distance (2.779 Å). A very

Table 2: Donor and acceptor NBOs with indication of the second-order interaction energy $E^{(2)}$ and type of interaction for aerogen neutral complexes.

Complex	Donor[a]	Acceptor	$E^{(2)}$ [kcal mol^{-1}]	Type
1	BD(3) N-C	BD(1)* Ar-O	0.49	π→σ*
2	LP N	BD(1)* Ar-O	0.77	n→σ*
3	BD(3) N-C	BD(1)* Kr-O	0.99	π→σ*
4	LP N	BD(1)* Kr-O	2.22	n→σ*
5	BD(3) N-C	BD(1)* Xe-O	2.23	π→σ*
6	LP N	BD(1)* Xe-O	6.76	n→σ*
11	LP N	BD(1)* Xe-O	4.49	n→σ*
	LP Xe	BD(1)* N-C	2.06	n→σ*
12	LP N	BD(1)* Xe-O	12.32	n→σ*

[a] BD, BD*, and LP stand for bonding, anti-bonding, and lone pair orbital, respectively.

remarkable finding derived from the NBO analysis is that in the AeO_3 complexes with CH_3CN (**1**, **3**, and **5**), the electron donor orbital does not correspond to the lone pair of the N atom; instead it is the π-system of the CN triple bond. This result likely explains the unexpected similar interaction energies obtained for NH_3 and CH_3CN complexes with AeO_3 σ-hole donor molecules. That is, the CH_3CN is a weak Lewis base (sp-hybridized lone pair) and therefore it is expected to have smaller complexation energies than the stronger NH_3 Lewis base (sp^3-hybridized lone pair). The geometry of the optimized complexes (Figure 5) clearly agrees with the fact that the electron-rich part of the molecule that interacts with the σ-hole is the π-system of the triple bond. For the Xe^{IV} complexes **11** and **12**, the orbital contribution is very large, especially in complex **12** in which the concomitant stabilization energy due to the electron donation from the lone pair of N to the antibonding Xe–O orbital (n→σ*) is approximately equal to the interaction

energy reported in Table 1, thus representing a major factor in the stabilization. More interestingly, complex **11** (the one observed experimentally) presents two types of donor–acceptor orbital interactions. One corresponds to the expected $n \rightarrow \sigma^*$ donation with a $E^{(2)} = 4.49$ kcal mol^{-1}, which is considerably smaller than the value obtained for complex **12** due to the larger N–Xe distance in complex **11** and low basicity of the sp-hybridized lone pair. The other one corresponds to a back-bonding donation from one lone pair of Xenon to the N–C antibonding orbital. This surprising back-bonding orbital donation is not negligible, because it has a concomitant stabilization energy of $E^{(2)} = 2.06$ kcal mol^{-1} that is approximately 20% of the total interaction energy.

In conclusion, in this manuscript we report unprecedented σ-hole interactions involving noble gases. We propose the use of aerogen bonding to refer to the noncovalent interaction between atoms of Group 18 acting as Lewis acids and any entity with the ability to act as an electron donor (lone pair, anion, etc.). Aerogen bonds have, at least, comparable strength to hydrogen bonds and other σ-hole-based interactions, though are less directional. Due to the increasing interest and research on xenon derivatives, this interaction is expected to play an important role in their solid-state chemistry. Moreover, from a pedagogic point of view, this newly defined interaction is certainly of interest, being the ultimate subclass of σ-hole noncovalent bonding interactions.

Keywords: ab initio calculations · aerogens · noncovalent interactions · supramolecular chemistry · xenon

How to cite: *Angew. Chem. Int. Ed.* **2015**, *54*, 7340–7343
Angew. Chem. **2015**, *127*, 7448–7451

[1] a) *Encyclopedia of Supramolecular Chemistry* (Eds.: J. L. Atwood, J. W. Steed), Marcel Dekker, New York, **2004**; b) K. Ariga, T. Kunitake in *Supramolecular Chemistry—Fundamentals and Applications*, Springer, Heidelberg, **2006**; c) *Supramolecular Chemistry: From Molecules to Nanomaterials* (Eds.: P. Gale, J. Steed), Wiley, Chichester, **2012**.

[2] E. Arunan, G. R. Desiraju, R. A. Klein, J. Sadlej, S. Scheiner, I. Alkorta, D. C. Clary, R. H. Crabtree, J. J. Dannenberg, P. Hobza, H. G. Kjaergaard, A. C. Legon, B. Mennucci, D. J. Nesbitt, *Pure Appl. Chem.* **2011**, *83*, 1619–1636.

[3] a) A. Priimagi, G. Cavallo, P. Metrangolo, G. Resnati, *Acc. Chem. Res.* **2013**, *46*, 2686–2695; b) S. Scheiner, *Acc. Chem. Res.* **2013**, *46*, 280–288; c) S. Zahn, R. Frank, E. Hey-Hawkins, B. Kirchner, *Chem. Eur. J.* **2011**, *17*, 6034–6038; d) A. Bauzá, T. J. Mooibroek, A. Frontera, *Angew. Chem. Int. Ed.* **2013**, *52*, 12317–12321; *Angew. Chem.* **2013**, *125*, 12543–12547; e) S. J. Grabowski, *Phys. Chem. Chem. Phys.* **2014**, *16*, 1824–1834; f) A. Bauzá, T. J. Mooibroek, A. Frontera, *Chem. Eur. J.* **2014**, *20*, 10245–10248; g) A. Bauzá, T. J. Mooibroek, A. Frontera, *Chem. Commun.* **2014**, *50*, 12626–12629.

[4] P. Politzer, J. S. Murray, T. Clark, *Phys. Chem. Chem. Phys.* **2013**, *15*, 11178–11189.

[5] D. H. Templeton, A. Zalkin, J. D. Forrester, S. M. Williamson, *J. Am. Chem. Soc.* **1963**, *85*, 817–817.

[6] G. E. Rodgers, *J. Chem. Educ.* **2014**, *91*, 216–224.

[7] J. Haner, G. J. Schrobilgen, *Chem. Rev.* **2015**, *115*, 1255–1295.

[8] a) J. S. Ogden, J. J. Turner, *Chem. Commun.* **1966**, *19*, 693–694; b) E. Jacob, R. Opferkuch, *Angew. Chem. Int. Ed. Engl.* **1976**, *15*, 158–159; *Angew. Chem.* **1976**, *88*, 190–190.

[9] D. S. Brock, V. Bilir, H. P. A. Mercier, G. J. Schrobilgen, *J. Am. Chem. Soc.* **2007**, *129*, 3598–3611.

[10] K. Koppe, J. Haner, H. P. A. Mercier, G. J. Schrobilgen, *Inorg. Chem.* **2014**, *53*, 11640–11661.

[11] A. Bauzá, I. Alkorta, A. Frontera, J. Elguero, *J. Chem. Theory Comput.* **2013**, *9*, 5201–5210.

[12] R. F. W. Bader, *Atoms in Molecules: A Quantum Theory*, Oxford University Press, London, **1990**.

[13] F. Weinhold, C. R. Landis, *Valency and Bonding: A Natural Bond Orbital Donor-Acceptor Perspective*, Cambridge University Press, Cambridge, UK, **2005**.

Received: March 19, 2015
Published online: May 7, 2015

PCCP

PAPER

View Article Online
View Journal | View Issue

π-Hole aerogen bonding interactions†

Antonio Bauzá and Antonio Frontera*

Cite this: *Phys. Chem. Chem. Phys.*, 2015, **17**, 24748

Received 5th June 2015,
Accepted 30th July 2015

DOI: 10.1039/c5cp03272e

www.rsc.org/pccp

In this manuscript we combine high level *ab initio* calculations (RI-MP2/aug-cc-pVTZ) and the analysis of several crystal structures to demonstrate the existence of π-hole aerogen bonding interactions in Xe(IV) compounds. The ability of XeF_4 and $Xe(OMe)_4$ to interact with electron rich molecules is rationalized using several computational tools, including molecular electrostatic potential surfaces, energetic and geometric features of the complexes and "atoms in molecules" (AIM) and Natural Bond Orbital (NBO) analyses. We have found support for the π-hole interaction involving the xenon atom from the solid state architecture of several X-ray structures retrieved from the crystal structural depot. Particularly, π-hole aerogen bonding interactions are quite common in the solid state of Xe(IV) compounds.

Introduction

Many features of modern chemistry and biology are determined by non-covalent interactions.[1] The understanding of many biological functions and drug design develops basically due to the chemical and physics insights acquired from the theoretical and experimental analysis of host–guest complexes[2] and the concomitant expansion of supramolecular chemistry. Perfect examples are cation–π[3] and anion–π[4] interactions, which before evidence of their noticeable role in living systems,[5] first became apparent in artificial systems. Moreover, σ-hole interactions involving tetrel, pnicogen, chalcogen and halogen atoms are also being recognized by the scientific community as powerful tools in supramolecular chemistry, crystal engineering and biochemistry.[3] The strength of these interactions is moderately strong and they are highly directional due to the localization of a positive region on the extension of the covalent bonds (σ-hole) in the acceptor molecule. Frequently, the name of the group of atoms that provides the σ-hole (from IV to VII)[6–11] is used to specify the name of the interaction (halogen,[12,13] chalcogen,[14] *etc.*[15] bonding), and they can be considered as subgroups of a general definition of σ-hole bonding interactions given by Politzer and coworkers.[6] Very recently, the σ-hole interaction has been described for group VIII of elements (noble gases or aerogens).[16] This type of interaction is somewhat counterintuitive due to the general assumption that these elements are monatomic gases with very low chemical reactivity. This particular case of σ-hole interaction has been termed aerogen bonding and has been described theoretically and detected in several fascinating X-ray structures.[17]

In addition to the group of σ-hole interactions, a rather unexplored group of noncovalent interactions can be classified as π-hole bonding. A π-hole is a region of positive electrostatic potential that is perpendicular to a portion of a molecular framework.[18] In case that this portion is an electron deficient aromatic π system the interaction is known either as lone pair–π[19] or anion–π[4] depending on the nature of the electron donor. Other founding π-hole interactions that encompass different molecular frameworks should be emphasized. For example, the identification of π-hole interactions in crystal structures was carried out by Bürgi and Dunitz in a series of studies revealing the trajectory along which a nucleophile attacks the π-hole of a C=O group.[20] Closely related, the ability of guanosine to act as a π-hole was pointed out by Egli and co-workers in 1995, when they studied the crystal structure of Z-DNA.[21] Recently, π-hole interactions have been described in SO_2 and SO_3 moieties,[22] RNO_2 molecules,[23] XCN, XZO_2 (X = halogen, Z = pnictogen), *etc.*[24]

In this manuscript we report an unprecedented theoretical study of π-hole aerogen bonding interactions involving Xe(IV) derivatives [*i.e.* XeF_4 and $Xe(OMe)_4$]. The energetic features and structural properties of π-hole complexes are discussed and three interesting X-ray structures are selected to illustrate the existence of this interaction. This unique type of bonding is not expected to be an effective instrument in crystal engineering or supramolecular chemistry; however it is certainly important in terms of gaining knowledge in the molecular and supramolecular sciences. The chemistry of Xe(IV) has been recently reviewed[17] and most of the known compounds are salts where purely electrostatic interactions dominate in their solid state structure. However, one neutral and interesting derivative is the xenon tetrafluoride. Its synthesis and crystal structure determination were reported in 1963 by Levy *et al.*[25] and it is the first binary fluoride of xenon that

Departament de Química, Universitat de les Illes Balears, Crta. de Valldemossa km 7.5, 07122 Palma de Mallorca, Baleares, Spain. E-mail: toni.frontera@uib.es; Tel: +34 971173498

† Electronic supplementary information (ESI) available: Cartesian coordinates of all optimized complexes and CSD search details. See DOI: 10.1039/c5cp03272e

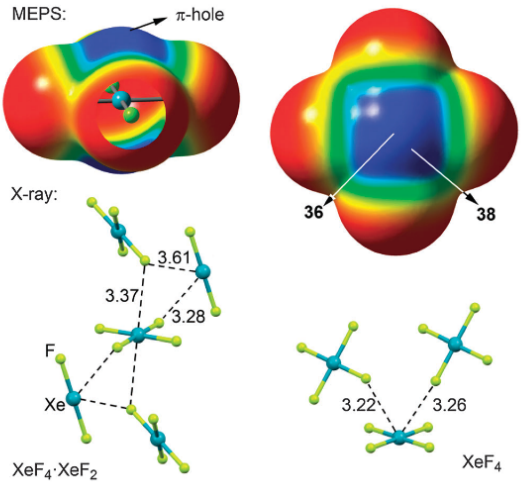

Fig. 1 Top: MEPS of XeF_4, energies in kcal mol $^{-1}$. Bottom: X-ray structures of XeF_4 and $XeF_4{\cdot}XeF_2$, distances in Å.

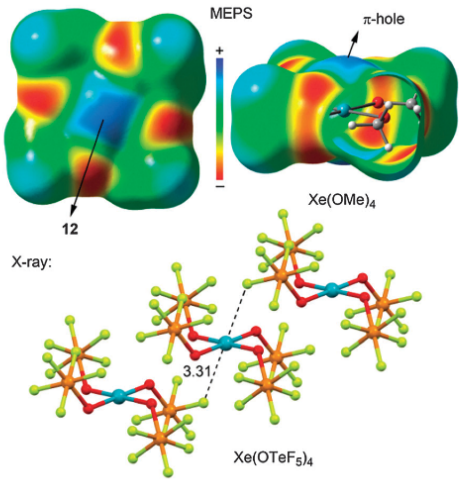

Fig. 2 Top: MEPS of $Xe(OMe)_4$, energies in kcal mol $^{-1}$. Bottom: X-ray structure of $Xe(OTeF_5)_4$, distances in Å.

was discovered.[26] The molecule XeF_4 is in the square planar shape and its crystal packing shows that each xenon establishes several noncovalent Xe···F contacts with neighbouring molecules at distances (from 3.20 to 3.56 Å) longer than the sum of the covalent radii of Xe and F (1.97 Å) and shorter than the sum of van der Waals radii (3.63 Å) that can be defined as π-hole aerogen bonding interactions. Similar interactions are also observed in the crystal packing of the molecular addition compound $XeF_4{\cdot}XeF_2$.[27] In Fig. 1 we also show the molecular electrostatic potential surface (MEPS) computed at the MP2/aug-cc-pVTZ level of theory for XeF_4 and a strong and extended π-hole can be clearly observed. Unexpectedly a very positive potential is found at the position where the lone pair of the Xe(IV) is located, which is likely related to the inert electron pair effect.[28] Moreover, the global maximum (highest value of positive electrostatic potential) is not found along the C_4 axis, instead it is located bisecting the angle defined by the F–Xe–F atoms. The location of the MEP maximum strongly agrees with the position of the F atoms of the neighbouring molecules in the crystal structure of XeF_4.

Another interesting Xe(IV) derivative is the compound $Xe(OTeF_5)_4$.[29] Experimentally it shows a good thermal stability (it can be purified by sublimation). A partial view of its crystal structure is shown in Fig. 2. The environment around xenon is square planar and two adjacent F_5Te-moieties point up and down in pairs. In its crystal packing, each xenon establishes two symmetrically equivalent noncovalent Xe···F contacts with two neighbouring molecules at a distance of 3.31 Å, giving rise to the formation of an infinite 1D ladder in the solid state. In Fig. 2 we also show the MEPS calculated for $Xe(OMe)_4$ as a theoretical model. It can be observed a moderately strong π-hole over the Xe atom. The size of the π-hole is smaller than the one computed for XeF_4 due to the presence of the lone pairs of the oxygen atoms pointing above and below the XeO_4 core plane (see red contours in Fig. 2). This MEP analysis is useful to rationalize the solid state architecture of $Xe(OTeF_5)_4$.

Results and discussion

We have analysed theoretically the π-hole binding ability of two square planar Xe(IV) derivatives as aerogen bond donors and several electron rich molecules (see Scheme 1), ranging from very weak Lewis bases (N_2) to anions (Cl^- and Br^-).

We have optimized the aerogen bonding complexes **3–18**, which are represented in Fig. 3 and the resulting interaction energies are summarized in Table 1. For the xenon tetrafluoride

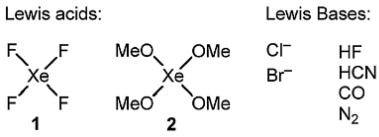

Scheme 1 π-Hole donor xenon compounds **1–2** (Lewis acids) and electron rich molecules (Lewis bases) used in this work.

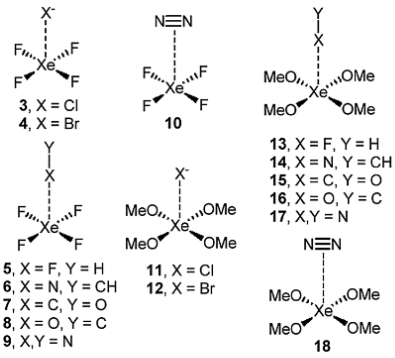

Fig. 3 Complexes **3–18** studied in this work.

Table 1 Interaction energies with the BSSE correction (E_{BSSE}, kcal mol^{-1}) and equilibrium distances (R_e, Å) at the RI-MP2/aug-cc-pVTZ level of theory

Complex	E_{BSSE}	R_e	$10^2 \times \rho$	$10^2 \times \nabla^2\rho$	Symm.
3	−18.8	3.128	2.47	7.43	C_{4v}
4	−16.3	3.326	2.08	5.52	C_{4v}
5	−2.5	3.122	1.06	5.06	C_{2v}
6	−4.0	3.272	1.17	4.45	C_{2v}
7	−1.8	3.565	0.80	2.70	C_{2v}
8	−0.8	3.417	0.68	2.86	C_{2v}
9	−1.3	3.484	0.72	2.83	C_{2v}
10	−0.7	3.716[a]	0.49	1.76	C_{2v}
11	−12.1	3.237	1.99	6.02	C_2
12	−10.8	3.427	1.71	4.60	C_2
13	−1.2	3.229	0.83	3.85	C_2
14	−2.1	3.334	1.02	3.84	C_2
15	−1.3	3.567	0.79	2.64	C_2
16	−0.9	3.402	0.70	2.92	C_2
17	−1.2	3.460	0.75	2.93	C_2
18	−1.1	3.574[a]	0.65	2.33	C_2

[a] Measured from the Xe to N≡N centroid.

(**1**) complexes with anions (**3** and **4**), the interaction energies are large and negative and the equilibrium distances are short (see Fig. 4 for the geometries of some representative complexes). In neutral complexes **5**–**10** the interaction energies are modest, ranging from −4.0 to −0.7 kcal mol^{-1}. The smallest interaction energy (in absolute value) corresponds to complex **10** where the π-system of the N_2 molecule interacts with the π-hole of **1**. In this complex we have also computed the interaction energy using a larger basis set (aug-cc-pVQZ) and the resulting value is similar (−0.9 kcal mol^{-1}) to the one listed in Table 1, giving reliability to the level of theory and confirming the modest but favourable interaction energy of complex **10**. The $Xe(OMe)_4$ complexes with anions present more modest interaction energies in agreement with the magnitude of the π-hole. Unexpectedly, two $Xe(OMe)_4$ neutral complexes (**16** and **18**) are slightly more favourable than the corresponding XeF_4 complexes (**8** and **10**) likely due to additional long-range interactions with the OCH_3 groups. This aspect is further analysed below in the natural bond orbital analysis.

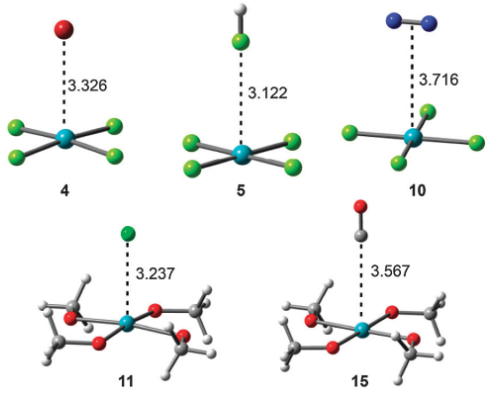

Fig. 4 RI-MP2/aug-cc-pVTZ optimized geometries of several aerogen bonding complexes, distances in Å.

Atoms-in-molecules characterization of π-hole aerogen bonding complexes

We have performed the atoms-in-molecules[30] (AIM) analysis of all complexes included in this study. Previous investigations have illustrated that the AIM analysis is useful (especially $\nabla^2\rho$) to explain the phenomenon of aerogen bonding in Xe(II) compounds.[31] In general the complexes are characterized by the presence of a bond critical point (CP) and a bond path connecting the electron rich atom with xenon. In complexes **10** and **18**, where the electron donor is the π-system of the N_2 molecule, the bond CP that emerges upon complexation connects the xenon atom with the bond CP of the N≡N bond (see complex **18** in Fig. 5). We have gathered in Table 1 the values of ρ and $\nabla^2\rho$ at the bond CP that characterizes the aerogen bonding interaction for complexes **3**–**18**. The density at the bond CP has been used as a measure of bond strength in a variety of noncovalent interactions.[30] We have examined if these values can be also used as a measure of bond order in the complexes studied here. We have represented in Fig. 6 a plot where we analyse the existence

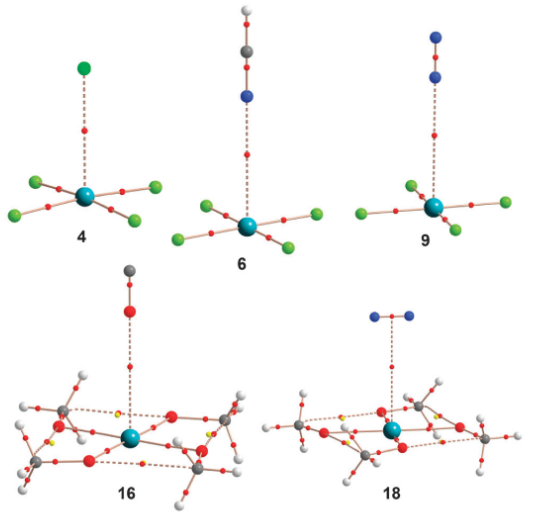

Fig. 5 Representation of bond (red) and ring (yellow) critical points in several complexes. The bond paths connecting (3, −1) critical points are also represented.

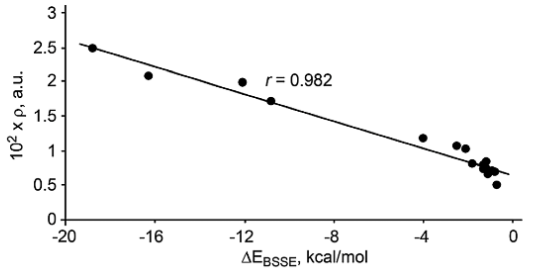

Fig. 6 Regression plot of the density (ρ) at the bond CP *versus* the interaction energy (BSSE corrected) for complexes **3**–**18**.

Table 2 Donor and acceptor NBOs with indication of the second-order interaction energy $E^{(2)}$ (kcal mol^{-1}) and type of interaction for aerogen complexes **3–18**. Values in italics correspond to back-bonding contributions

Complex	Donor[a]	Acceptor	$E^{(2)}$	Type
3	LP Cl	RY* Xe	3.84	n → π*
	LP Xe	RY* Cl	*0.27*	n → π*
4	LP Br	RY* Xe	3.12	n → π*
	LP Xe	RY* Br	*0.30*	n → π*
5	BD F–H	RY* Xe	1.00	σ → π*
	LP F	RY* Xe	0.32	n → π*
	LP Xe	RY* F	*0.70*	n → π*
	LP Xe	BD* F–H	*0.35*	n → σ*
6	BD N–C & C–H	RY* Xe	2.07	π/σ → π*
	LP N	RY* Xe	0.32	n → π*
	LP Xe	RY* N	*0.69*	n → π*
	LP Xe	BD* N–C	*1.26*	n → π*
7	BD C–O	RY* Xe	0.13	π → π*
	LP C	RY* Xe	0.42	n → π*
	LP Xe	RY* C	*0.50*	n → π*
	LP Xe	BD* C–O	*0.19*	n → π*
8	BD O–C	RY* Xe	0.49	π → π*
	LP O	RY* Xe	0.29	n → π*
	LP Xe	RY* O	*0.42*	n → π*
	LP Xe	BD* O–C	*0.44*	n → π*
9	BD N–N	RY* Xe	0.48	π → π*
	LP N	RY* Xe	0.34	n → π*
	LP Xe	RY* N	*0.92*	n → π*
	LP Xe	BD* N–N	*0.33*	n → π*
10	BD N–N	RY* Xe	0.07	π → π*
	LP Xe	RY* N	*0.54*	n → π*
11	LP Cl	RY* Xe	1.83	n → π*
	LP Xe	RY* Cl	*0.10*	n → π*
12	LP Br	RY* Xe	1.69	n → π*
	LP Xe	RY* Br	*0.12*	n → π*
13	BD F–H	RY* Xe	1.49	σ → π*
	LP F	RY* Xe	0.21	n → π*
	LP Xe	RY* F	*0.06*	n → π*
	LP Xe	BD* F–H	*0.45*	n → σ*
14	BD N–C	RY* Xe	0.59	π → π*
	LP N	RY* Xe	0.37	n → π*
	LP Xe	BD* N–C	*1.00*	n → π*
	LP Xe	RY* N	*0.50*	n → π*
	LP O	RY* N	*0.12*	n → π*
15	BD O–C	RY* Xe	0.16	π → π*
	LP C	RY* Xe	0.30	n → π*
	LP Xe	BD* C–O	*0.07*	n → π*
	LP Xe	RY* C	*0.13*	n → π*
	LP O	RY* C	*0.10*	n → π*
16	BD O–C	RY* Xe	0.79	π → π*
	LP O (OC)	RY* Xe	0.54	n → π*
	LP Xe	BD* O–C	*0.52*	n → π*
	LP Xe	RY* O	*0.10*	n → π*
	LP O (OMe)	RY* O	*0.16*	n → π*
17	BD N–N	RY* Xe	0.50	π → π*
	LP N	RY* Xe	0.46	n → π*
	LP Xe	BD* N–N	*0.53*	n → π*
	LP Xe	RY* N	*0.38*	n → π*
	LP O	RY* N	*0.14*	n → π*
18	BD N–N	RY* Xe	0.18	π → π*
	LP Xe	RY* N	*0.22*	n → π*
	LP O	RY* N	*0.18*	n → π*

[a] BD, BD* and LP, RY* stand for bonding, anti-bonding, lone pair and Rydberg orbital, respectively.

of a linear relationship between the interaction energies and the ρ values (summarized in Table 1). Remarkably, we have obtained a strong relationship with a regression coefficient $r = 0.982$. The relevance of this relationship should be emphasized since in the same representation we have included two different π-hole donor molecules (**1** and **2**) and anionic and neutral π-hole acceptors. Therefore it allows for dealing simultaneously with both series of complexes and using charged and neutral electron donors in the same representation. These results confirm that ρ at the bond CP is directly related to the strength of the aerogen bonding interaction.

NBO analysis

In order to study if orbital contributions are important to explain the aerogen π-hole complexes described above, we have performed Natural Bond Orbital (NBO) calculations focusing our attention on the second order perturbation analysis, since it is a convenient tool to analyze donor acceptor interactions.[13] The results are summarized in Table 2. For the anionic complexes, the orbital contribution is modest compared to the total interaction energy (~20%) and it is basically due to the interaction of a lone pair (LP) of the anion with empty Rydberg orbitals (RY*) of xenon. Curiously, there is also a very small contribution of a back-bonding donation from one LP of xenon to the RY* orbital of Cl/Br (ranging from 0.10 to 0.32 kcal mol^{-1}). In contrast to the anionic complexes where electrostatic effects are dominant, the orbital contribution in the neutral complexes represents a major factor in the stabilization. For instance, in the XeF_4 neutral complexes **5–9** there are four contributions. In two of them the electron rich molecule acts as donor and Xe as acceptor (see Table 2). In the other two (values in italics) the Xe atom acts as donor (back-bonding using its LP). The back-bonding is not dominant in complexes **5** and **6** and the interaction can be classified as an LP→π-hole interaction. Remarkably, the back-bonding becomes more important in complexes **7–9** and, consequently, the interaction is almost equally dominated by the donation and back-bonding contributions. Finally, in complex **10** the orbital contribution interaction is governed by the donation from the LP of Xe to the RY* orbitals of N atoms. The NBO analysis is also helpful to rationalize the similar (or even stronger in two complexes, *vide supra*) binding energies obtained for complexes **14–18** [$Xe(OMe)_4$ with weak Lewis bases] compared to complexes **6–10** (see Table 1), in sharp disagreement to the π-hole MEP values given in Fig. 1 and 2. Complexes **14–18** exhibit two different back-bonding orbital interactions. The first one is equivalent to the aforementioned one for XeF_4 complexes (*i.e.*, from the LP of Xe to the anti-bonding orbital of the X–Y interacting molecule or the RY* orbital of interacting X atom, see Table 2). The second

one corresponds to an electron donation from the four lone pairs of the oxygen atoms of the OCH_3 groups to the RY* orbital of the interacting atom with concomitant stabilization energies [$E^{(2)}$] that range from 0.10 to 0.18 kcal mol^{-1}. The equivalent back-bonding from the F atoms in XeF_4 complexes **6–10** is not observed, thus explaining the similar or even slightly more favourable binding energies observed for complexes **14–18**.

Conclusions

In this manuscript we report unprecedented π-hole interactions involving two square planar Xe(IV) derivatives. We have extended the recently described σ-hole aerogen bonding interaction (*i.e.* noncovalent bonding between atoms of group 18 acting as Lewis acids and any entity with the ability to act as an electron donor) to π-hole aerogen bonding. Several X-ray structures illustrate this type of interaction in the solid state. The interaction is strong and dominated by electrostatic effects when the electron donor is an anion. In these complexes the orbital contribution is very small. Conversely, the interaction is modest (ranging from −3.8 to −0.5 kcal mol^{-1}) when the electron donor is a weak Lewis base. The AIM analysis demonstrates that the density at the bond critical point can be used as a measure of bond order of the aerogen bond and it linearly correlates with the interaction energy. Finally, the NBO analysis reveals that the back-bonding (from the LPs of Xe and oxygen atoms) is very relevant in some complexes.

Theoretical methods

The geometries of all complexes were optimized at the RI-MP2/aug-cc-pVTZ level of theory by means of the Turbomole 6.5 software.[32] For the xenon atom the aug-cc-pVTZ-PP basis set was used. The interaction energies were calculated with correction for the basis set superposition error (BSSE) by using the Boys–Bernardi counterpoise technique.[33] The symmetry constraint imposed in the optimizations of the complexes is indicated in the tables. Bader's "atoms in molecules" theory has been used to study the aerogen bonding interactions discussed herein by means of the AIMall calculation package.[34] The MEP surface analysis was performed at the same level of theory and the MEPS figures were generated using GaussView. For the $Xe(OCH_3)_4$ complexes, the carbon atoms of the methyl group were forced to be coplanar with the XeO_4 core in order to avoid the formation of C–H···X hydrogen bonds.

Acknowledgements

We thank the DGICYT of Spain (projects CTQ2011-27512/BQU and CONSOLIDER INGENIO 2010 CSD2010-00065, FEDER funds) and the Direcció General de Recerca i Innovació del Govern Balear (project 23/2011, FEDER funds) for financial support.

Notes and references

1 G. V. Oshovsky, D. N. Reinhoudt and W. Verboom, *Angew. Chem., Int. Ed.*, 2007, **46**, 2366–2393; J. M. Zayed, N. Nouvel, U. Rauwald and O. A. Scherman, *Chem. Soc. Rev.*, 2010, **39**, 2806–2816.
2 M. Zürcher and F. Diederich, *J. Org. Chem.*, 2008, **73**, 4345–4361; D. K. Smith, *J. Chem. Educ.*, 2005, **82**, 393–400; D. A. Uhlenheuer, K. Petkau and L. Brunsveld, *Chem. Soc. Rev.*, 2010, **39**, 2817–2826.
3 J. C. Ma and D. A. Dougherty, *Chem. Rev.*, 1997, **97**, 1303–1324; N. Zacharias and D. A. Dougherty, *Trends Pharmacol. Sci.*, 2002, **23**, 281–287.
4 A. Frontera, P. Gamez, M. Mascal, T. J. Mooibroek and J. Reedijk, *Angew. Chem., Int. Ed.*, 2011, **50**, 9564–9583; A. Frontera, *Coord. Chem. Rev.*, 2013, **257**, 1716–1727; J. J. Fiol, M. Barceló-Oliver, A. Tasada, A. Frontera, À. Terrón and Á. García-Raso, *Coord. Chem. Rev.*, 2013, **257**, 2705–2715; A. Frontera, D. Quiñonero and P. M. Deyà, *Wiley Interdiscip. Rev.: Comput. Mol. Sci.*, 2011, **1**, 440–459.
5 C. Estarellas, A. Frontera, D. Quiñonero and P. M. Deyà, *Angew. Chem., Int. Ed.*, 2011, **50**, 415–418.
6 J. S. Murray, K. E. Riley, P. Politzer and T. Clark, *Aust. J. Chem.*, 2010, **63**, 1598–1607; P. Politzer, J. S. Murray and T. Clark, *Phys. Chem. Chem. Phys.*, 2013, **15**, 11178–11189.
7 M. R. Sundberg, R. Uggla, C. Viñas, F. Teixidor, S. Paavola and R. Kivekäs, *Inorg. Chem. Commun.*, 2007, **10**, 713–716; S. Scheiner, *Acc. Chem. Res.*, 2013, **46**, 280–288; A. Bauzá, R. Ramis and A. Frontera, *J. Phys. Chem. A*, 2014, **118**, 2827–2834.
8 P. Politzer, J. S. Murray and T. Clark, *Phys. Chem. Chem. Phys.*, 2010, **12**, 7748–7757.
9 A. Bundhun, P. Ramasami, J. S. Murray and P. Politzer, *J. Mol. Model.*, 2013, **19**, 2739–2746.
10 D. Mani and E. Arunan, *Phys. Chem. Chem. Phys.*, 2013, **15**, 14377–14383.
11 A. Bauzá, T. J. Mooibroek and A. Frontera, *Angew. Chem., Int. Ed.*, 2013, **52**, 12317–12321; S. J. Grabowski, *Phys. Chem. Chem. Phys.*, 2014, **16**, 1824–1834; A. Bauzá, R. Ramis and A. Frontera, *Comput. Theor. Chem.*, 2014, **1038**, 67–70; A. Bauzá, T. J. Mooibroek and A. Frontera, *Chem. – Eur. J.*, 2014, **20**, 10245–10248; E. C. Escudero-Adán, A. Bauzá, A. Frontera and P. Ballester, *ChemPhysChem*, 2015, **16**, DOI: 10.1002/cphc.201500437; A. Bauzá, T. J Mooibroek and A. Frontera, *ChemPhysChem*, 2015, **16**, DOI: 10.1002/cphc.201500314.
12 T. Clark, *Wiley Interdiscip. Rev.: Comput. Mol. Sci.*, 2013, **3**, 13–20.
13 P. Metrangolo and G. Resnati, *Chem. – Eur. J.*, 2001, **7**, 2511–2519; G. Cavallo, P. Metrangolo, T. Pilati, G. Resnati, M. Sansotera and G. Terraneo, *Chem. Soc. Rev.*, 2010, **39**, 3772–3783; S. J. Grabowski, *Phys. Chem. Chem. Phys.*, 2013, **15**, 7249–7259.
14 P. Sanz, M. Yáñez and O. Mó, *Chem. – Eur. J.*, 2002, **8**, 3999–4007; P. Sanz, M. Yáñez and O. Mó, *New J. Chem.*, 2002, **26**, 1747–1752; P. Sanz, M. Yáñez and O. Mó, *Phys. Chem. Chem. Phys.*, 2003, **5**, 2942–2947.
15 Q. Li, X. Guo, X. Yang, W. Li, J. Cheng and H.-B. Li, *Phys. Chem. Chem. Phys.*, 2014, **16**, 11617–11625.
16 A. Bauzá and A. Frontera, *Angew. Chem., Int. Ed.*, 2015, **54**, 7340–7343.

17 J. Haner and G. J. Schrobilgen, *Chem. Rev.*, 2015, **115**, 1255–1295 and references cited therein.
18 P. Politzer, J. S. Murray and T. Clark, *Phys. Chem. Chem. Phys.*, 2010, **12**, 7748–7757.
19 M. Egli and S. Sarkhel, *Acc. Chem. Res.*, 2007, **40**, 197–205; T. J. Mooibroek, P. Gamez and J. Reedijk, *CrystEngComm*, 2008, **10**, 1501–1515.
20 H. B. Bürgi, *Inorg. Chem.*, 1973, **12**, 2321–2325; H. B. Bürgi, J. D. Dunitz and E. Shefter, *J. Am. Chem. Soc.*, 1973, **95**, 5065–5067; H. B. Bürgi, J. D. Dunitz, J. M. Lehn and G. Wipff, *Tetrahedron*, 1974, **30**, 1563–1572.
21 M. Egli and R. V. Gessner, *Proc. Natl. Acad. Sci. U. S. A.*, 1995, **92**, 180–184.
22 L. M. Azofra, I. Alkorta and S. Scheiner, *Theor. Chem. Acc.*, 2014, **133**, 1586.
23 (*a*) A. Bauza, R. Ramis and A. Frontera, *J. Phys. Chem. A*, 2014, **118**, 2827–2834; (*b*) A. Bauzá, T. J. Mooibroek and A. Frontera, *Chem. Commun.*, 2015, **51**, 1491–1493.
24 (*a*) G. Sánchez-Sanz, C. Trujillo, M. Solimannejad, I. Alkorta and J. Elguero, *Phys. Chem. Chem. Phys.*, 2013, **15**, 14310–14318; (*b*) J. E. Del Bene, I. Alkorta and J. Elguero, *J. Phys. Chem. A*, 2013, **117**, 6893–6903.
25 H. A. Levy, J. H. Burns and P. A. Agron, *Science*, 1963, **139**, 1208.
26 N. Barlett, *Proc. Chem. Soc.*, 1962, 218; K. O. Christe, *Chem. Commun.*, 2013, **49**, 4588–4590.
27 J. H. Burns, R. D. Ellison and H. A. Levy, *J. Phys. Chem.*, 1963, **67**, 1569.
28 G. E. Rodgers, *J. Chem. Educ.*, 2014, **91**, 216–224 and references cited therein.
29 L. Turowsky and K. Seppelt, *Z. Anorg. Allg. Chem.*, 1981, **472**, 7; D. Lentz and K. Seppelt, *Angew. Chem., Int. Ed.*, 1978, **17**, 356.
30 R. F. W. Bader, *Chem. Rev.*, 1991, **91**, 893–928; R. F. W. Bader, *Atoms in Molecules, A Quantum Theory*, Oxford University Press, Oxford, UK, 1990; P. L. A. Popelier, *Atoms in Molecules. An Introduction*, Prentice Hall, Harlow, England, 2000.
31 P. J. MacDougall, G. J. Schrobilgen and R. F. W. Bader, *Inorg. Chem.*, 1989, **28**, 763–769.
32 R. Ahlrichs, M. Bär, M. Hacer, H. Horn and C. Kömel, *Chem. Phys. Lett.*, 1989, **162**, 165–169.
33 S. B. Boys and F. Bernardi, *Mol. Phys.*, 1970, **19**, 553–566.
34 T. A. Keith, *AIMAll (Version 13.05.06)*, TK Gristmill Software, Overland Park KS, USA, 2013.

ChemPubSoc Europe

DOI: 10.1002/cphc.201500757

CHEMPHYSCHEM Articles

Theoretical Study on the Dual Behavior of XeO_3 and XeF_4 toward Aromatic Rings: Lone Pair–π versus Aerogen–π Interactions

Antonio Bauzá and Antonio Frontera*[a]

In this study, several lone pair–π and aerogen–π complexes between XeO_3 and XeF_4 and aromatic rings with different electronic natures (benzene, trifluorobenzene, and hexafluorobenzene) are optimized at the RI-MP2/aug-cc-pVTZ level of theory. All complexes are characterized as true minima by frequency analysis calculations. The donor/acceptor role of the ring in the complexes is analyzed using the natural bond orbital computational tool, showing a remarkable contribution of orbital interactions to the global stabilization of the aerogen–π complexes. Finally, Bader's AIM analysis of several complexes is performed to further characterize the lone pair–π and aerogen–π interactions.

1. Introduction

Supramolecular chemists rely on a deep comprehension of the noncovalent forces that are the pillars of modern chemistry. A proper understanding and the intelligent utilization of them is essential to achieve progress in fields such as supramolecular chemistry,[1] molecular recognition,[2] and materials science.[3] For instance, interactions involving aromatic rings [i.e. π–π stacking,[4] cation–π,[5] anion–π,[6] lone pair–π,[7] and C–H–π[8] interactions] are extremely important in many chemical and biological processes, including molecular sensing,[9] crystal engineering, and enzymatic mechanisms.[10] In this context, the best known supramolecular force, which is ubiquitous in many chemical and biological systems, is hydrogen bonding. In recent years, another noncovalent force that has been found to have similar strength and directionality features to hydrogen bonding is the halogen bonding. Consequently, a series of studies using the Cambridge Structural Database (CSD) have been carried out to shed light into the impact of this interaction on crystal formation.[11] The interest of the scientific community has grown exponentially, owing to the recognition of its importance in biological systems and the design of new materials; this has led to a plethora of theoretical and experimental studies devoted to this topic.[12–14] In addition, apart from the many well-established noncovalent forces, an emerging group of so-called "unconventional" noncovalent interactions has attracted the interest of the scientific community during the past years.[15] This group involves to the interactions between group IV–VII bearing compounds (donor) and nucleophiles (acceptor).[16–18] Frequently, the name of the group of atoms that provides the σ hole (from IV to VII) is used to name the interaction, and they can be considered as subgroups of general σ-hole bonding interactions as defined by Politzer and co-workers. A great number of computational studies[19–21] has been devoted to this emerging group of interactions, concluding that their strength is moderately strong and they are highly directional, owing to the localization of a positive potential region on the extension of the covalent bonds (σ hole) in the acceptor molecule.[22–25] The magnitudes of the σ-hole potentials are determined by the same factors as for the halogens. Recently, a new supramolecular force named aerogen bonding[26a] has emerged onto the scene; this interaction is between an aerogen-bearing moiety and an electron-rich entity. Very few examples are available in the CSD, owing to the low reactivity of the aerogen element series. Although its potential practical applications in the field of supramolecular chemistry are limited, aerogen-bonding interactions could be of great importance in xenon chemistry. Recently, Miao et al. highlighted the potential of electron-rich arenes as an important stabilization source for xenon compounds through the establishment of aerogen–π interactions.[26b]

In addition to σ-hole interactions, a rather unexplored group of noncovalent interactions can be classified as π-hole bonding. A π hole is a region of positive electrostatic potential that is perpendicular to a portion of a molecular framework.[27] When this portion is an electron-deficient aromatic π-system, the interaction is characterized either as lone pair–π or anion–π, depending on the nature of the electron donor. Other π-hole interactions that encompass different molecular portions should also be mentioned. For example, Burgi, Dunitz, and co-workers identified π-hole interactions in crystal structures in a series of studies, which revealed the trajectory of a nucleophilic attack to the π hole of a C=O group.[28–30] Moreover, the ability of guanosine to act as a π-hole donor was pointed out by Egli and Gessner in 1995, when they studied the crystal structure of Z-DNA.[31] In addition, Alkorta and co-workers have extensively studied π-hole interactions involving pnicogen atoms to rationalize and obtain a deeper understanding of the

[a] A. Bauzá, Prof. A. Frontera
Departament de Química, Universitat de les Illes Balears
Crta. de Valldemossa km 7.5, 07122 Palma de Mallorca, Baleares (Spain)
E-mail: toni.frontera@uib.es

Supporting Information for this article is available on the WWW under http://dx.doi.org/10.1002/cphc.201500757.

nature and physical properties of these particular interactions.[32] Recently, the study of π-hole interactions has been extended to acyl C atoms,[33] SO_n moieties ($n=2,3$),[34,35] RZO_2,[36,37] XCN, and XZO_2 molecules (X = halogen, Z = pnicogen), and so forth.[38,39]

Finally, it is also worth mentioning the ability of Xe^{IV} derivatives to act as π-hole donors, extending the recently described σ-hole aerogen bonding to π-hole aerogen bonding. In fact, a search performed in the CSD provided experimental evidence of the existence of this type of π-hole interaction in the solid state.[40]

In the present study, our main objective was to evaluate the ability of Xe^{VI} and Xe^{IV} compounds to establish lone pair–π and aerogen–π interactions. We used XeO_3 and XeF_4 as either lone pair or σ-/π-hole donors, respectively, and benzene, trifluorobenzene, and hexafluorobenzene as the π systems. For all combinations, two types of minima (binding modes) were found on the potential surface. For the XeO_3 series of complexes, the Xe atom points toward the π system (aerogen–π interaction) in one binding mode, and the lone pairs of the O atom point toward the π system (lone pair–π interaction) in the other mode. For the XeF_4 complexes, the XeF_4 plane is stacked parallel or perpendicular to the aromatic ring (aerogen–π or lone pair–π, respectively). The interaction energies of both binding modes have been compared and the physical nature of the interaction analyzed using different computational tools, including the natural bond orbital (NBO) analysis, the symmetry adapted perturbational theory (SAPT) partition scheme, and Bader's theory of atoms-in-molecules (AIM).

2. Results and Discussion

2.1. MEPS Study

As a preliminary study, for compounds **1**–**5** (Figure 1), we computed the molecular electrostatic potential surface (MEPS), which are shown in Figure 2. We have also included the quadrupole moment values (Q_{zz}) of the aromatic rings, as obtained from the literature.[41] The MEPSs of compounds **1** and **2** show an extended positive potential region located at the Xe atom (σ- and π-hole, respectively), thus, a favorable interaction with electron-rich entities is expected. Curiously, the position of the σ/π hole coincides with the location of the inert lone pair of

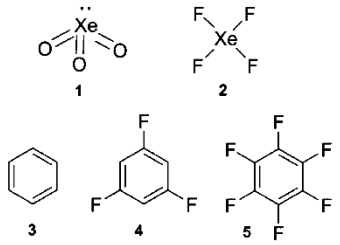

Figure 1. Compounds 1–5.

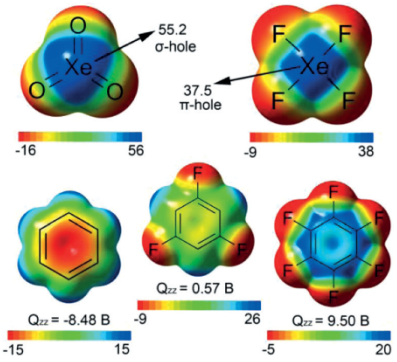

Figure 2. MEPS of compounds **1**–**5**. Energy values are in kcal mol^{-1}.

Xe^{VI} and Xe^{IV}, respectively.[42] Also remarkable, is the difference in the magnitude of the MEP for both Xe derivatives, with it being much larger for the XeO_3 moiety, thus a stronger binding upon complexation with electron-rich entities is expected. Regarding the aromatic rings, a progressive change from red to blue in the MEPS above the ring center is observed as the number of F substituents increases with a concomitant change in the sign of the quadrupole moment from negative to positive. This gradual change of the π basicity (or π acidity) of the arene is useful to predict the behavior of the two different interactions considered in this study. Thus, in the case of the electron-rich compound **3**, a favorable interaction with electron-poor entities (σ or π hole) is expected, thus, favoring the aerogen–π interaction. The opposite behavior is expected for compound **5**, as the value of the MEP over the ring center is positive, along with its Q_{zz} value. Finally, the electrostatic component is not expected to play an important role for compound **4**, owing to the negligible Q_{zz} and MEP values over the center of the ring. Therefore, other energy components, such as polarization and dispersion effects, are key players in the overall stabilization of the complexes, as discussed further in Section 2.4.

2.2. Energetic Study

The interaction energies and equilibrium distances obtained for complexes **6**–**17** (Figure 3) studied herein are summarized in Table 1 (see also Figure 4). From an inspection of the results, several interesting conclusions arise. First, in all cases the binding-energy values are favorable, ranging between −2 and −12 kcal mol^{-1}. Second, for complexes involving benzene, the most favorable binding mode is the aerogen–π, which is in agreement with the MEPS analysis shown in Section 2.1. Third, lone pair–π interactions are preferred for XeO_3 complexes with hexafluorobenzene. The opposite is observed for XeF_4 complexes, where the aerogen–π interaction is more favored, likely because of the face-to-face π-stacking nature of this complex. This particular aspect was further analyzed in the NBO and AIM analyses (Sections 2.3 and 2.5). Finally, for trifluorobenzene

ChemPubSoc Europe

CHEMPHYSCHEM Articles

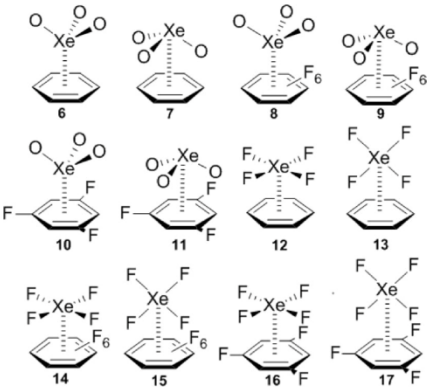

Figure 3. Complexes **6**–**17**.

Table 1. Interaction energies of complexes **6**–**17** at the RI-MP2/aug-cc-pVTZ level of theory without and with the BSSE correction (E and E_{BSSE} in kcal mol^{-1}, respectively), equilibrium distances (R_e in Å) and value of the density at the cage critical point (ρ, a.u.).

E	E_{BSSE}	R_e	Complex type	$10^2\times\rho$
−16.6	−12.4	2.904[a]	σ-hole	1.08
−4.5	−2.5	3.259[b]	lone pair–π	0.18
−6.2	−2.2	3.061[a]	σ-hole	0.94
−8.1	−5.1	3.049[a]	lone pair–π	0.26
−10.7	−6.7	2.979[b]	σ-hole	1.02
−6.3	−3.7	3.119[a]	lone pair–π	0.23
−12.9	−8.8	3.045[b]	π-hole	0.91
−3.4	−1.9	3.026[a]	lone pair–π	0.16
−8.1	−3.5	3.096[b]	π-hole	0.89
−5.3	−3.1	2.905[a]	lone pair–π	0.21
−10.0	−5.7	3.097[a]	π-hole	0.88
−4.3	−2.4	2.978[b]	lone pair–π	0.27

[a] Distances measured from the Xe atom to the ring centroid. [b] Shortest distance measured from the O/F atom to the closest C atom of the ring.

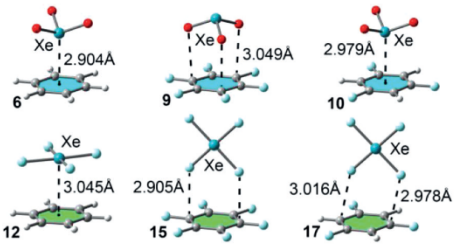

Figure 4. Optimized geometries of some representative complexes at the RI-MP2/aug-cc-pVTZ level of theory.

complexes, the aerogen–π interaction is more favored than the lone pair–π for both Xe derivatives, likely owing to polarization and dispersion effects (the Xe element is considerably more polarizable than either O or F).[43]

The energetically most favorable complex of this study is **6**, which contains XeO_3 and benzene (−12.4 kcal mol^{-1}), thus indicating the ability of electron-rich aromatic moieties to stabilize Xe compounds by means of aerogen–π interactions, in agreement with recent results reported by Miao et al.[26b] The lone pair–π interaction for this π-system is clearly disfavored, owing to the electronic nature of the arene, and consequently, a weak binding-energy value is obtained for complex **7** (−2.5 kcal mol^{-1}). In hexafluorobenzene complexes **8** and **9**, the lone pair–π interaction is the preferred, with a binding-energy value of −5.1 kcal mol^{-1} for **9**. Finally, in the trifluorobenzene complexes **10** and **11**, the aerogen–π interaction is favored over the lone pair–π interaction.

In contrast, in the XeF_4 series of complexes, the largest binding energy value corresponds to the aerogen–π complex **12** (−8.8 kcal mol^{-1}). In addition, the lone pair-π interaction is not favored in complex **13**, obtaining the lowest energy value of the Xe^{VI} series (−1.9 kcal mol^{-1}). In complexes involving C_6F_6, the aerogen–π interaction (**14**; −3.5 kcal mol^{-1}) is slightly more favored than the lone pair–π interaction (**15**; −3.1 kcal mol^{-1}). This is an unexpected result, as the electronic nature of this arene does not favor interactions with electron-poor entities. In this case, orbital effects play a key role in the stabilization of complex **14**, as explained in the following NBO analysis (Section 2.3). Finally, in complexes **16** and **17,** a preference for the aerogen–π over the lone pair–π interaction is observed, as obtained for the XeO_3 moiety. This issue will be further analyzed in the SAPT analysis (Section 2.4).

2.3. NBO Analysis

To study the importance of orbital effects in the aerogen–π and lone pair–π interactions described in Section 2.2, we performed natural bond orbital (NBO) calculations, focusing our attention on the second-order perturbation analysis,[44] owing to its suitability to study donor–acceptor interactions. From the analysis of the results (see Table 2) some conclusions can be extracted. First, in XeO_3 aerogen–π complexes (**6**, **8**, and **10**) an important contribution from the bonding C–C orbitals (π) of the ring moiety to the antibonding Xe–O orbitals (σ*) of the XeO_3 entity is observed, which is the major factor of stabilization in these complexes. This observation confirms the σ-hole nature of the noncovalent interactions in these complexes. It is also worth mentioning the magnitude of this orbital interaction compared with the total interaction energy (≈40% for **6** and ≈50% for **10**). Second, in addition to this contribution, the interaction of a bonding C–C orbital (π) of the aromatic moiety with empty Rydberg orbitals (RY*) of Xe also contributes to the overall stabilization of the complexes. Finally, somewhat unexpectedly, weak back-bonding orbital interactions was observed in these set of complexes (see values in italics, Table 2), due to the participation of the inert lone pair of Xe and the lone pairs of the O atoms. The back -bonding donation from the lone pair of Xe (LP) is to the antibonding C–H orbitals in **6** and antibonding C–F orbitals in **8** and **10**. In contrast, in complexes **7**, **9**, and **11**, characterized as a lone pair-π interaction, the most remarkable contribution comes from the

Table 2. Donor and acceptor NBOs with the second-order interaction energy $E^{(2)}$ [kcal mol^{-1}] and type of interaction for aerogen–π and lone pair–π complexes.[a]

Complex	*Donor*	Acceptor	E^2	*Type*
6	BD C–C	BD* Xe–O	5.01	π→σ*
	BD C–C	RY*Xe	1.44	n→σ*
	LP Xe	*BD* C–H*	*0.36*	*n→σ**
	LP O	*BD* C–C*	*0.36*	*π→π**
7	LP O	BD* C–C	0.63	n→π*
	BD C–C	BD* Xe–O	0.30	π→σ*
8	BD C–C	BD* Xe-O	2.17	π→σ*
	BD C–C	RY*Xe	1.16	π→π*
	LP Xe	*BD* C–F*	*0.33*	*n→σ**
9	LP O	BD* C–C	0.82	n→π*
	BD C–C	BD* Xe–O	0.21	π→σ*
10	BD C–C	BD* Xe–O	3.48	π→σ*
	BD C–C	RY* Xe	0.98	π→π*
	LP Xe	*BD* C–F*	*0.27*	*n→σ**
	LP O	*BD* C–C*	*0.21*	*n→π**
11	LP O	BD*C–C	0.93	n→π*
	BD C–C	BD* Xe–O	0.15	π→σ*
12	LP F	BD* C–C	1.40	n→π*
	BD C–C	RY* Xe	1.16	π→π*
13	LP F	BD* C–C	0.48	n→π*
14	BD C–C	RY* Xe	1.97	π→π*
	LP F	BD* C–C	0.89	n→π*
15	LP F	BD* C–C	0.48	n→π*
16	BD C–C	RY* Xe	1.23	π→π*
	LP F	BD* C–C	1.08	n→π*
17	LP F	BD* C–C	0.51	n→π*

[a] BD, BD* and LP, RY* stand for bonding, antibonding, lone pair,and Rydberg orbital, respectively. Weak back-bonding orbital interactions are shown in italics.

interaction of the O lone pairs of the Xe–O moiety (LP) to the antibonding C–C orbitals (π*) of the benzene ring.

In the XeF_4 series (complexes **12**–**17**), the orbital contribution is smaller than in the XeO_3 series (≈20% of the total interaction energy). A common trend is observed, which is a contribution from the lone pairs of the F atoms (LP) to the antibonding C–C orbitals (π*) of the ring, independent of the type of interaction considered. In addition, the interaction of a bonding C–C orbital (π) of the aromatic moiety with empty Rydberg orbitals (RY*) of Xe also contributes to the final stabilization of complexes **12**, **14**, and **16**. This result explains the preference for the aerogen–π interaction over the lone pair–π interaction in complexes **14** and **15**. Finally, no back-bonding orbital interactions involving the Xe atom were observed for this set of complexes.

2.4. SAPT Analysis

In Table 3, we summarize the DF-DFT-SAPT energy values relative to some representative lone pair and aerogen–π complexes. The total SAPT interaction energies for these complexes are similar to those obtained using the RI-MP2/aug-cc-pVTZ level of theory (see Table 1), giving reliability to the partition method. The energetic contributions (Table 3) indicate that aerogen–π complex **6** (XeO_3···C_6H_6) is dominated by the electrostatic term, which is in agreement with the MEPS analysis.

Table 3. SAPT interaction energies (E_{total}) and their partitioning into the electrostatic, exchange, induction, and dispersion contributions (E_{cc}, E_{ex}, E_{ind}, and E_{disp}, respectively; kcal mol^{-1}) at the RI-DFT/aug-cc-pVTZ level of theory using the DF-DFT-SAPT approach.

Compound	E_{cc}	E_{ex}	E_{ind}	E_{disp}	E_{total}
6	−15.6	25.7	−8.7	−10.2	−8.8
10	−8.6	20.2	−6.7	−9.2	−4.3
11	−3.7	9.1	−0.3	−7.0	−1.9
14	−5.1	17.0	−3.9	−10.1	−2.1
15	−3.0	6.9	−0.2	−5.0	−1.2
16	−7.6	17.7	−3.9	−9.8	−3.6
17	−2.2	6.2	−0.1	−4.7	−0.7

However, the contributions of induction and dispersion terms are also important. In the lone pair–π complex **15** (XeF_4···C_6F_6) the electrostatic and dispersion terms are the most important contributions to the total interaction energy. Finally, for the complexes involving the trifluorobenzene ring, (**10**, **11**, **16**, and **17**) although both the electrostatic and induction terms are important, in the aerogen–π complexes (**10**, **14**, and **16**) the dispersion component plays a key role in the overall stabilization of the complexes, being the most remarkable contributor. This is not observed for the lone pair–π complexes **11**, **15**, and **17**, likely owing to the higher polarizability of the interacting atom (Xe) in complexes **10**, **14**, and **16**.

2.5. AIM Analysis

We also used the Bader's theory of AIM to characterize the lone pair–π and aerogen–π interactions described in Section 2.2 by selecting some representative complexes (see Figure 5). XeO_3 complexes **6** and **9** are characterized by the presence of three bond and three ring critical points (CPs) that are symmetrically distributed. In the aerogen–π complex **6,** the bond CPs connect the Xe to three C atoms of the ring. In the

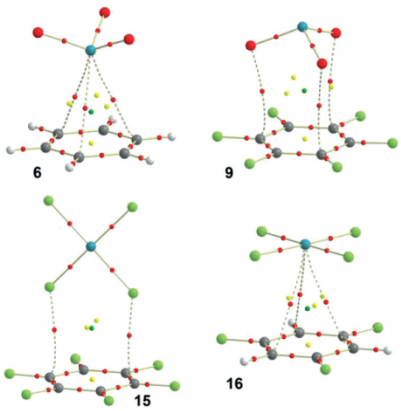

Figure 5. Distribution of CPs and bond paths in complexes **6**, **9**, **15**, and **16**. Bond, ring, and cage CPs are represented by red, yellow, and green spheres, respectively. The bond paths connecting bond CPs are also represented.

ChemPubSoc Europe

CHEMPHYSCHEM Articles

lone pair–π complex **9**, the bond CPs connect the O atoms to three C atoms of the ring moiety In both complexes, the interactions are further characterized by the presence of a cage CP, as is frequent in ion–π and lone pair–π interactions.[45] In the lone pair–π complex **15** (XeF_4 series), the interaction is characterized by the presence of two bond and two ring CPs that are symmetrically distributed. The bond CPs connect the F atoms to two C atoms of the ring. The aerogen–π complex **16** is characterized by the presence of three bond and three ring critical points (CPs) that are symmetrically distributed. Remarkably, the bond CPs connect the Xe atom to three C atoms of the ring. These results unambiguously confirm the aerogen–π nature of the interaction, as the F atoms are not involved in the distribution of CPs and bond paths. Finally, both complexes **15** and **16** are also characterized by the presence of a cage CP (see Figure 5). The value of the Laplacian in all cases is positive, as is common in closed shell calculations.

3. Conclusions

The noncovalent complexes between several aromatic rings and two Xe derivatives were studied using high-level ab initio calculations and two different binding modes were obtained for each combination; these are defined as lone pair–π and aerogen–π interactions. Among the π systems considered the aerogen–π interaction established between the XeO_3 derivative and the benzene ring achieves the largest binding energy value. In contrast, the lone pair–π interaction is the strongest one for the hexafluorobenzene moiety. Moreover, in the case of trifluorobenzene, where electrostatic effects are negligible, the aerogen–π interaction is more favorable than the lone pair–π interaction, owing to the major contribution of the polarization and dispersion terms, as shown in the SAPT analysis. In addition, the NBO analysis showed that orbitals effects are significant contributors to the global stabilization of the aerogen–π complexes studied herein. Unexpectedly, in the aerogen–π complexes involving the XeO_3 moiety, a weak back-bonding donation from the inert lone pair of the Xe atom to the antibonding orbitals of the aromatic ring was observed. Finally, Bader's atoms-in-molecules theory was successfully used to characterize both π interactions discussed herein.

Theoretical Methods

The geometries and energies of all complexes included in this study were computed at the RI-MP2/aug-cc-pVTZ level of theory. The calculations have been performed by using the program TURBOMOLE version 7.0[46] For the Xe atom, the aug-cc-pVTZ-PP basis set was used. The interaction energies were calculated with corrections for the basis set superposition error (BSSE) by using the Boys–Bernardi counterpoise technique.[47] The optimization of the molecular geometries was performed, imposing the C_s symmetry point group. Frequency calculations were performed at the RI-MP2/aug-cc-pVTZ level of theory, and in all cases a true minima was found. The MEPS calculations were performed at the MP2/aug-cc-pVTZ level by means of the Gaussian 09 software.[48] The partitioning of the interaction energies into the individual electrostatic, induction, dispersion, and exchange-repulsion components was carried out with the SAPT approach DFT-SAPT[49] at the DF-BP86/aug-cc-pVTZ//RI-MP2/aug-cc-pVTZ level of theory using the MOLPRO 2012 software.[50] Bader's AIM theory has been used to study the interactions discussed herein by means of the AIMall calculation package.[51]

Acknowledgements

We thank the Dirección General de Investigación Científica y Técnica (DGICYT) of Spain (projects CTQ2014-57393-C2-1-P and CONSOLIDER INGENIO 2010 CSD2010-00065, FEDER funds).

Keywords: ab initio calculations · molecular recognition · noncovalent interactions · pi interactions · supramolecular chemistry

[1] H. J. Schneider, *Angew. Chem. Int. Ed.* **2009**, *48*, 3924 – 3977; *Angew. Chem.* **2009**, *121*, 3982 – 4036.
[2] C. A. Hunter, J. K. M. Sanders, *J. Am. Chem. Soc.* **1990**, *112*, 5525 – 5534.
[3] W. J. Vickaryous, R. Herges, D. W. Jonhson, *Angew. Chem. Int. Ed.* **2004**, *43*, 5831 – 5833; *Angew. Chem.* **2004**, *116*, 5955 – 5957.
[4] K. Müller-Dethlefs, P. Hobza, *Chem. Rev.* **2000**, *100*, 143 – 168.
[5] J. C. Ma, D. A. Dougherty, *Chem. Rev.* **1997**, *97*, 1303 – 1324.
[6] B. L. Schottel, H. T. Chifotides, K. R. Dunbar, *Chem. Soc. Rev.* **2008**, *37*, 68 – 83.
[7] T. J. Mooibroek, P. Gamez, J. Reedijk, *CrystEngComm* **2008**, *10*, 1501 – 1515.
[8] M. J. Plevin, D. L. Bryce, J. Boisbouvier, *Nat. Chem.* **2010**, *2*, 466 – 471.
[9] J. M. Lehn in *Supramolecular chemistry concepts and perspectives*, Wiley-VCH, Weinheim, **1995**.
[10] E. A. Meyer, R. K. Castellano, F. Diederich, *Angew. Chem. Int. Ed.* **2003**, *42*, 1210 – 1250; *Angew. Chem.* **2003**, *115*, 1244 – 1287.
[11] P. Murray-Rust, W. D. S. Motherwell, *J. Am. Chem. Soc.* **1979**, *101*, 4374 – 4376.
[12] P. Metrangolo, H. Neukirch, T. Pilati, G. Resnati, *Acc. Chem. Res.* **2005**, *38*, 386 – 395.
[13] P. Politzer, J. S. Murray, *ChemPhysChem* **2013**, *14*, 278 – 294.
[14] P. Politzer, J. S. Murray, T. Clark, *Phys. Chem. Chem. Phys.* **2013**, *15*, 11178 – 11189.
[15] A. Bauzá, T. J. Mooibroek, A. Frontera, *ChemPhysChem* **2015**, DOI: 10.1002/cphc.201500314.
[16] P. Politzer, J. S. Murray, T. Clark, *Phys. Chem. Chem. Phys.* **2010**, *12*, 7748 – 7757.
[17] K. E. Riley, J. S. Murray, J. Franfrlík, J. Rezáč, R. J. Solá, M. C. Concha, F. M. Ramos, P. Politzer, *J. Mol. Model.* **2011**, *17*, 3309 – 3318.
[18] A. Bauzá, T. J. Mooibroek, A. Frontera, *Angew. Chem. Int. Ed.* **2013**, *52*, 12317 – 12321; *Angew. Chem.* **2013**, *125*, 12543 – 12547.
[19] J. S. Murray, P. Lane, T. Clark, P. Politzer, *J. Mol. Model.* **2007**, *13*, 1033 – 1038.
[20] J. S. Murray, P. Lane, P. Politzer, *Int. J. Quantum Chem.* **2007**, *107*, 2286 – 2292.
[21] J. S. Murray, P. Lane, P. Politzer, *J. Mol. Model.* **2009**, *15*, 723 – 729.
[22] S. C. Nyburg, C. H. Faerman, *Acta Crystallogr. Sect. B* **1985**, *41*, 274 – 279.
[23] a) P. Politzer, K. E. Riley, F. A. Bulat, J. S. Murray, *Comput. Theor. Chem.* **2012**, *998*, 2 – 8; b) J. S. Murray, L. Macaveiu, P. Politzer, *J. Comput. Sci.* **2014**, *5*, 590 – 596.
[24] T. N. G. Row, R. Parthasarathy, *J. Am. Chem. Soc.* **1981**, *103*, 477 – 479.
[25] N. Ramasubbu, R. Parthasarathy, *Phosphorus Sulfur Silicon Relat. Elem.* **1987**, *31*, 221 – 229.
[26] a) A. Bauzá, A. Frontera, *Angew. Chem. Int. Ed.* **2015**, *54*, 7340 – 7343; *Angew. Chem.* **2015**, *127*, 7448 – 7451; b) J. Miao, B. Song, Y Gao *Chem. Asian. J.* DOI: 10.1002/asia.201500785.
[27] J. S. Murray, P. Lane, T. Clark, K. E. Riley,, P. Politzer, *J. Mol. Model.* **2012**, *18*, 541 – 548.
[28] H. B. Burgi, *Inorg. Chem.* **1973**, *12*, 2321 – 2325.

ChemPubSoc Europe

CHEMPHYSCHEM Articles

[29] H. B. Burgi, J. D. Dunitz, E. Shefter, *J. Am. Chem. Soc.* **1973**, *95*, 5065–5067.
[30] H. B. Burgi, J. D. Dunitz, J. M. Lehn, G. Wipff, *Tetrahedron* **1974**, *30*, 1563–1572.
[31] M. Egli, R. V. Gessner, *Proc. Natl. Acad. Sci. USA* **1995**, *92*, 180–184.
[32] a) J. E. Del Bene, I. Alkorta, J. Elguero, *J. Phys. Chem. A* **2013**, *117*, 11592–11604; b) I. Alkorta, J. Elguero, J. E. Del Bene, *J. Phys. Chem. A* **2013**, *117*, 10497–10503; c) S. Mohammad, R. Vahid, C. Trujillo, I. Alkorta, G. Sanchez-Sanz, J. Elguero, *J. Phys. Chem. A* **2012**, *116*, 5199–5206; d) C. Trujillo, G. Sánchez, I. Alkorta, J. Elguero, *New J. Chem.* **2015**, *39*, 6791–6802.
[33] P. Sjoberg, P. Politzer, *J. Phys. Chem.* **1990**, *94*, 3959–3961.
[34] L. M. Azofra, I. Alkorta, S. Scheiner, *Theor. Chem. Acc.* **2014**, *133*, 1586–1588.
[35] L. M. Azofra, I. Alkorta, S. Scheiner, *Phys. Chem. Chem. Phys.* **2014**, *16*, 18974–18981.
[36] A. Bauzá, R. Ramis, A. Frontera, *J. Phys. Chem. A* **2014**, *118*, 2827–2834.
[37] a) A. Bauzá, T. J. Mooibroek, A. Frontera, *Chem. Commun.* **2015**, *51*, 1491–1493; b) S. Roy, A. Bauzá, A. Frontera, R. Banik, A. Purkayastha, M. G. B. Drew, B. M. Reddy, B. Sridhar, S. Kr. Dasa, S. Das, *CrystEngComm* **2015**, *17*, 3912–3916; c) S. Cañellas, A. Bauzá, A. Lancho, A. Garcia-Raso, J. J. Fiol, E. Molins, P. Ballester, A. Frontera, *CrystEngComm* **2015**, *17*, 5987–5997.
[38] G. Sánchez-Sanz, C. Trujillo, M. Solimannejad, I. Alkorta, J. Elguero, *Phys. Chem. Chem. Phys.* **2013**, *15*, 14310–14318.
[39] J. E. Del Bene, I. Alkorta, J. Elguero, *J. Phys. Chem. A* **2013**, *117*, 6893–6903.
[40] A. Bauzá, A. Frontera, *Phys. Chem. Chem. Phys.* **2015**, DOI: 10.1039/C5CP03272E.
[41] a) M. R. Battaglia, A. D. Buckingham, J. H. Williams, *Chem. Phys. Lett.* **1981**, *78*, 421–423; b) J. Vrbancich, G. L. D. Ritchie, *J. Chem. Soc. Faraday Trans. 2* **1980**, *76*, 648–655; c) D. Quiñonero, C. Garau, A. Frontera, P. Ballester, A. Costa, P. M. Deyà, *Chem. Phys. Lett.* **2002**, *359*, 486–492.
[42] G. E. Rodgers, *J. Chem. Educ.* **2014**, *91*, 216–224.
[43] A. Bauzá, A. Frontera, *ChemPhysChem* **2015**, DOI: 10.1002/cphc.201500542.
[44] F. Weinhold, C. R. Landis, *Valency and Bonding: A Natural Bond Orbital Donor-Acceptor Perspective*, Cambridge University Press, Cambridge, **2005**.
[45] a) A. Frontera, P. Gamez, M. Mascal, T. J. Mooibroek, J. Reedijk, *Angew. Chem. Int. Ed.* **2011**, *50*, 9564–9583; *Angew. Chem.* **2011**, *123*, 9736–9756; b) A. Frontera, D. Quiñonero, P. M. Deyà, *WIREs Comput. Mol. Sci.* **2011**, *1*, 440–459.
[46] R. Ahlrichs, M. Bär, M. Hacer, H. Horn, C. Kömel, *Chem. Phys. Lett.* **1989**, *162*, 165–169.
[47] S. B. Boys, F. Bernardy, *Mol. Phys.* **1970**, *19*, 553–566.
[48] Gaussian 09, Revision B.01, M. J. Frisch, G. W. Trucks, H. B. Schlegel, G. E. Scuseria, M. A. Robb, J. R. Cheeseman, G. Scalmani, V. Barone, B. Mennucci, G. A. Petersson, H. Nakatsuji, M. Caricato, X. Li, H. P. Hratchian, A. F. Izmaylov, J. Bloino, G. Zheng, J. L. Sonnenberg, M. Hada, M. Ehara, K. Toyota, R. Fukuda, J. Hasegawa, M. Ishida, T. Nakajima, Y. Honda, O. Kitao, H. Nakai, T. Vreven, J. A. Montgomery, Jr., J. E. Peralta, F. Ogliaro, M. Bearpark, J. J. Heyd, E. Brothers, K. N. Kudin, V. N. Staroverov, R. Kobayashi, J. Normand, K. Raghavachari, A. Rendell, J. C. Burant, S. S. Iyengar, J. Tomasi, M. Cossi, N. Rega, J. M. Millam, M. Klene, J. E. Knox, J. B. Cross, V. Bakken, C. Adamo, J. Jaramillo, R. Gomperts, R. E. Stratmann, O. Yazyev, A. J. Austin, R. Cammi, C. Pomelli, J. W. Ochterski, R. L. Martin, K. Morokuma, V. G. Zakrzewski, G. A. Voth, P. Salvador, J. J. Dannenberg, S. Dapprich, A. D. Daniels, Ö. Farkas, J. B. Foresman, J. V. Ortiz, J. Cioslowski, and D. J. Fox, Gaussian, Inc., Wallingford CT, 2009.
[49] a) A. Heßelmann, G. Jansen, *Phys. Chem. Chem. Phys.* **2003**, *5*, 5010–5014; b) H.-J. Werner, P. J. Knowles, G. Knizia, F. R. Manby, M. Schütz, *WIREs Comput. Mol. Sci.* **2012**, *2*, 242–253.
[50] MOLPRO, version 2012.1, H.-J. Werner, P. J. Knowles, G. Knizia, F. R. Manby, M. Schütz, P. Celani, T. Korona, R. Lindh, A. Mitrushenkov, G. Rauhut, K. R. Shamasundar, T. B. Adler, R. D. Amos, A. Bernhardsson, A. Berning, D. L. Cooper, M. J. O. Deegan, A. J. Dobbyn, F. Eckert, E. Goll, C. Hampel, A. Hesselmann, G. Hetzer, T. Hrenar, G. Jansen, C. Köppl, Y. Liu, A. W. Lloyd, R. A. Mata, A. J. May, S. J. McNicholas, W. Meyer, M. E. Mura, A. Nicklass, D. P. O'Neill, P. Palmieri, D. Peng, K. Pflüger, R. Pitzer, M. Reiher, T. Shiozaki, H. Stoll, A. J. Stone, R. Tarroni, T. Thorsteinsson, M. Wang, see http://www.molpro.net.
[51] AIMAll (Version 13.05.06), Todd A. Keith, TK Gristmill Software, Overland Park KS, USA, 2013.

Manuscript received: September 2, 2015
Accepted Article published: September 11, 2015
Final Article published: October 2, 2015